

# NISTIR 8271 DRAFT SUPPLEMENT

## Face Recognition Vendor Test (FRVT) Part 2: Identification

Patrick Grother  
Mei Ngan  
Kayee Hanaoka  
*Information Access Division  
Information Technology Laboratory*

This document is a draft supplement of [NIST Interagency Report 8271](#)

2021/09/21



# NISTIR 8271 DRAFT SUPPLEMENT

## Face Recognition Vendor Test (FRVT) Part 2: Identification

Patrick Grother  
Mei Ngan  
Kayee Hanaoka  
*Information Access Division  
Information Technology Laboratory*

This document is a draft supplement of [NIST Interagency Report 8271](#)

June 2021



U.S. Department of Commerce  
*Wynn Coggins, Acting Secretary*

National Institute of Standards and Technology  
*James Altoff, Under Secretary of Commerce for Standards and Technology and Director, acting*

## RELEASE NOTES

**2021-09-21:** The 1:N track of the FRVT remains open. Three news items:

- ▷ This document is the tenth draft update to [NIST Interagency Report 8271](#). It includes results for algorithms recently submitted by six first-time developers: Cubox, Fincore, HyperVerge, Qnap Security, Staqu Technologies, and Tripleize (Aize, 3-ize).
- ▷ It includes results also for four returning developers: Cognitec Systems, Incode Technologies, Innovatrics, Neurotechnology, and Rank One Computing.

**2021-08-02:** The 1:N track of the FRVT remains open. Three news items:

- ▷ This document is the ninth draft update to [NIST Interagency Report 8271](#). It includes results for algorithms recently submitted by eight participants: Cyberlink Corp, NEC Corp, N-Tech Lab, Realnetworks Inc., Sensetime Group, Veridas Digital, Viettel Group, and Vigilant Solutions.
- ▷ Algorithms submitted since July 24 will be included in the next update scheduled for September 9, 2021.
- ▷ A new report, NIST Interagency Report 8381 - FRVT Part 7: Identification for Paperless Travel and Immigration, has been released [[PDF](#), [webpage](#)]. It documents the use of FRVT 1:N algorithms in positive access control and immigration status update travel applications where the enrolled population size is as low as 420 people for aircraft boarding, and 42 000 for an airport security line. These population sizes are much smaller than those used in the main [1:N evaluation](#). Going forward, we will update the report and webpage with results for new algorithms.

**2021-07-07:** The 1:N track of the FRVT remains open. One update:

- ▷ This document is the eighth draft update to [NIST Interagency Report 8271](#). It include results for an algorithm from one participant: Kakao Enterprises.

**2021-06-22:** The 1:N track of the FRVT remains open. Three updates:

- ▷ This is the seventh draft of the update to [NIST Interagency Report 8271](#). It includes results for algorithms from three new participants: Line Corporation, Rendip, and Samsung S1 Corp.
- ▷ We have also added results for algorithms from five returning developers: Imagus Technology, Kneron, Tevian, Visidon, and Xforward AI Technology.
- ▷ The algorithm-specific report cards (examples: [1](#), [2](#), and [3](#)) now include figures showing how low threshold values can be used to reduce candidate list lengths for human review, while (usually) elevating miss rates (FNIR) only modestly. The reports also feature some minor additions and clarifications.

**2021-03-26:** The 1:N track of the FRVT remains open. Three updates:

- ▷ This is the sixth draft of the update to [NIST Interagency Report 8271](#). It includes results for algorithms from three returning developers: Neurotechnology, Guangzhou Pixel Solutions, and Tech5 SA.
- ▷ We have added results on the webpage and in the report for a new ageing dataset in which border crossing photos are searched against a gallery of border crossing photos collected between 10 and 15 years prior to the mated search photos. See section [2](#) for a description of the images. Table [1](#) has a new entry describing the experiment.
- ▷ We will mostly discontinue running the mugshot ageing test, reserving it for algorithms that show high accuracy on the new border-crossing set.

**2021-03-26:** Regarding the fifth draft of the update to [NIST Interagency Report 8271](#):

- ▷ In addition have added results for first algorithms from two new participants: Viettel Group and Veridas Digital Authentication Solutions.

- ▷ We have added results for algorithms from two returning developers: Idemia and Cognitec Systems.
- ▷ In addition to the report, the [results page](#) and its hyperlinked [report cards](#) have been updated.

**2021-02-08:** Regarding the fourth draft of the update to [NIST Interagency Report 8271](#):

- ▷ We have added results for eight algorithms submitted by eight developers: Cyberlink, Dermalog, Imagus, Paravision, Sensetime, Trueface, Vigilant Solutions, and X-Forward AI. With the exception of Trueface, all of these developers have participated previously.
- ▷ We anticipate updating this report again in the first week of March 2021.
- ▷ The main [results page](#) has been revised with tabs for the investigative and lights-out identification tables, and a new tab dedicated to speed and resource consumption.
- ▷ The report cards (example [here](#)) hyperlinked from the [results page](#) have been revised to improve content and format.

**2020-12-14:** Regarding third draft of the update to [NIST Interagency Report 8271](#):

- ▷ We have added results for fifteen algorithms submitted by thirteen developers. The four first-time participants are: Acer, Akurat Satu Indonesia, Canon, and Xforward AI Technology. The ten returning developers are: AllGoVision, Cyberlink Corp, Dahua Technology, Deepglint, Guangzhou Pixel Solutions, IIT Vision, Innovatrics, Rank One Computing, Scanovate, Sensetime Group, Synesis, and VisionLabs.
- ▷ We have added two new datasets to the evaluation: First a set of “visa-border” photos, representing search of an airport immigration lane photo against a database of closely ISO standard portraits; second a “visa-kiosk” set representing search of a photo collected in a registered traveller kiosk against the same ISO portrait gallery. The images are described in section 2.1.
- ▷ As in previous reports, we include results for searching mugshots against a mugshot gallery containing a single image of each of 12 million people. However we have suspending running searches against a gallery in which multiple lifetime photos per person are present, because this is computationally expensive. We retain a  $N = 3$  million search test dedicated to ageing in which mugshots taken up to 18 years after the first photograph are searched - see Table 6.
- ▷ Tables containing computational resource information, Table 2 . . . , now include duration of the finalization step, in which search algorithms can, at their option, build fast-search data structures.
- ▷ We have linked revised per-algorithm PDF report cards from the main [results page](#).
- ▷ We have regenerated all figures and tables to drop algorithms submitted before June 2018. Results for prior algorithms appear in [archived editions](#) of this report.
- ▷ Going forward, we anticipate producing more frequent updates to this report. Developers may submit one algorithm to this evaluation every four calendar months.

**2020-03-24:** Regarding the second draft of the update to [NIST Interagency Report 8271](#):

- ▷ Adds results for three algorithms from three developers, Dermalog, Innovatrics, and Synesis.
- ▷ Adds Table 6 on ageing showing the increase in false negative rates with time elapsed between two photos. Some of the results were contained in graphs in prior editions of this report, but the table adds results for some newly submitted algorithms.
- ▷ Adjusts frontal mugshot results (for recent and lifetime consolidated galleries) to include the effect of removing some images that should not have been included in image test sets. These images were mostly profile views, images of tattoos containing faces, images of faces on tee shirts, and images of photographs on walls behind the intended subject. This affects many tables and reduces false negative identification rates for all algorithms. The reduction is larger for “recent” enrollments than for “lifetime consolidated” ones with the consequence that accuracy on recent images is now superior.

**2020-02-26:** Regarding the first draft of the update to [NIST Interagency Report 8271](#):

- ▷ Adds results for 38 algorithms from 31 different developers, eleven of whom are entirely new to the 1:N track of FRVT. These are Allgovision, Cyberlink, Deepsea Tencent, Farbar F8, Imperial College London, Intsys MSU, Kedacom, Kneron, Pixelall, and Scanovate.

## DISCLAIMER

Specific hardware and software products identified in this report were used in order to perform the evaluations described in this document. In no case does identification of any commercial product, trade name, or vendor, imply recommendation or endorsement by the National Institute of Standards and Technology, nor does it imply that the products and equipment identified are necessarily the best available for the purpose.

## INSTITUTIONAL REVIEW BOARD

The National Institute of Standards and Technology's Research Protections Office reviewed the protocol for this project and determined it is not human subjects research as defined in Department of Commerce Regulations, 15 CFR 27, also known as the Common Rule for the Protection of Human Subjects (45 CFR 46, Subpart A).

## ACKNOWLEDGMENTS

The authors are grateful for the support and collaboration of the the Department of Homeland Security's Science & Technology Directorate (S&T), Office of Biometric Identity Management (OBIM), and Customs and Border Protection (CBP).

Additionally, the authors are grateful to staff in the NIST Biometrics Research Laboratory for infrastructure supporting rapid evaluation of algorithms.

## Executive Summary

This document is a draft revision of the September 2019 report [NIST Interagency Report 8271](#). That report gave extensive documentation of face recognition applied to mugshots. This report extends that by adding more two more challenging datasets containing images with serious departures from canonical frontal image standards. The report also adds results for algorithms submitted to NIST since in 2019 and 2020. The algorithms, which implement one-to-many identification of faces appearing in two-dimensional images, are prototypes from the research and development laboratories of mostly commercial suppliers, and are submitted to NIST as compiled black-box libraries implementing a NIST-specified C++ test interface. The report therefore does not describe how algorithms operate. The report lists accuracy results alongside developer names and will therefore be useful for comparison of face recognition algorithms and assessment of absolute capability. The report is accompanied by a [webpage](#) with sortable results.

The evaluation uses six datasets: frontal mugshots, profile view mugshots, desktop webcam photos, visa-like immigration application photos, immigration lane photos, and registered traveler kiosk photos. These datasets are sequestered at NIST, meaning that developers do not have access to them for training or testing. This aspect is important because face recognition algorithms are very often deployed without the developer having access to the customers image data. A possible exception to this would be in a cloud-based application where the operational image data is uploaded to a cloud operated by a face recognition developer.

The major result in NIST IR 8271 was that massive gains in accuracy have been achieved in the years 2013 to 2018 and these far exceed improvements made in the prior period, 2010 to 2013. While the industry gains were broad - at least 30 developers' algorithms outperformed the most accurate algorithm from late 2013, there remains a wide range of capability. While this report shows accuracy gains only over the period 2018-2020, the most accurate algorithm reported here is substantially more accurate than anything reported in NIST IR 8271. This is evidence that face recognition development continues apace, and that FRVT reports are but a snapshot of contemporary capability.

From discussion with developers, the accuracy gains stem from the adoption of deep convolutional neural networks. As such, face recognition has undergone an industrial revolution, with algorithms increasingly tolerant of poorly illuminated and other low quality images, and poorly posed subjects. One related result is that a few algorithms correctly match side-view photographs to galleries of frontal photos, with search accuracy approaching that of the best c. 2010 algorithms operating on purely frontal images. The capability to recognize under a 90-degree change in viewpoint - pose invariance - has been a long-sought milestone in face recognition research.

With good quality portrait photos, the most accurate algorithms will find matching entries, when present, in galleries containing 12 million individuals, with rank one miss rates of approaching 0.1%. The remaining errors are in large part attributable to long-run ageing, facial injury and poor image quality. Given this impressive achievement - close to perfect recognition - an advocate might claim that cooperative face recognition is a solved problem, a statement that can be refuted with the following context and caveats:

- ▷ **Mugshots vs. less constrained captures:** The low error rates reported here are attained using mostly excellent cooperative live-capture mugshot images collected with an attendant present. Recognition in other circumstances, particularly those without a dedicated photographic environment and human or automated quality control checks, will lead to declines in accuracy. This is documented here for side-view images, poorer quality webcam images, and, particularly, for newly introduced ATM-style kiosk photos that were not originally intended for automated face recognition. In this case, recognition error rates are much higher, often in excess of 20% even with the more accurate algorithms which variously remain intolerant of face cropping (at image edge) and of large downward head pitch.
- ▷ **Algorithm accuracy spectrum:** Recognition accuracy is very strongly dependent on the algorithm and, more

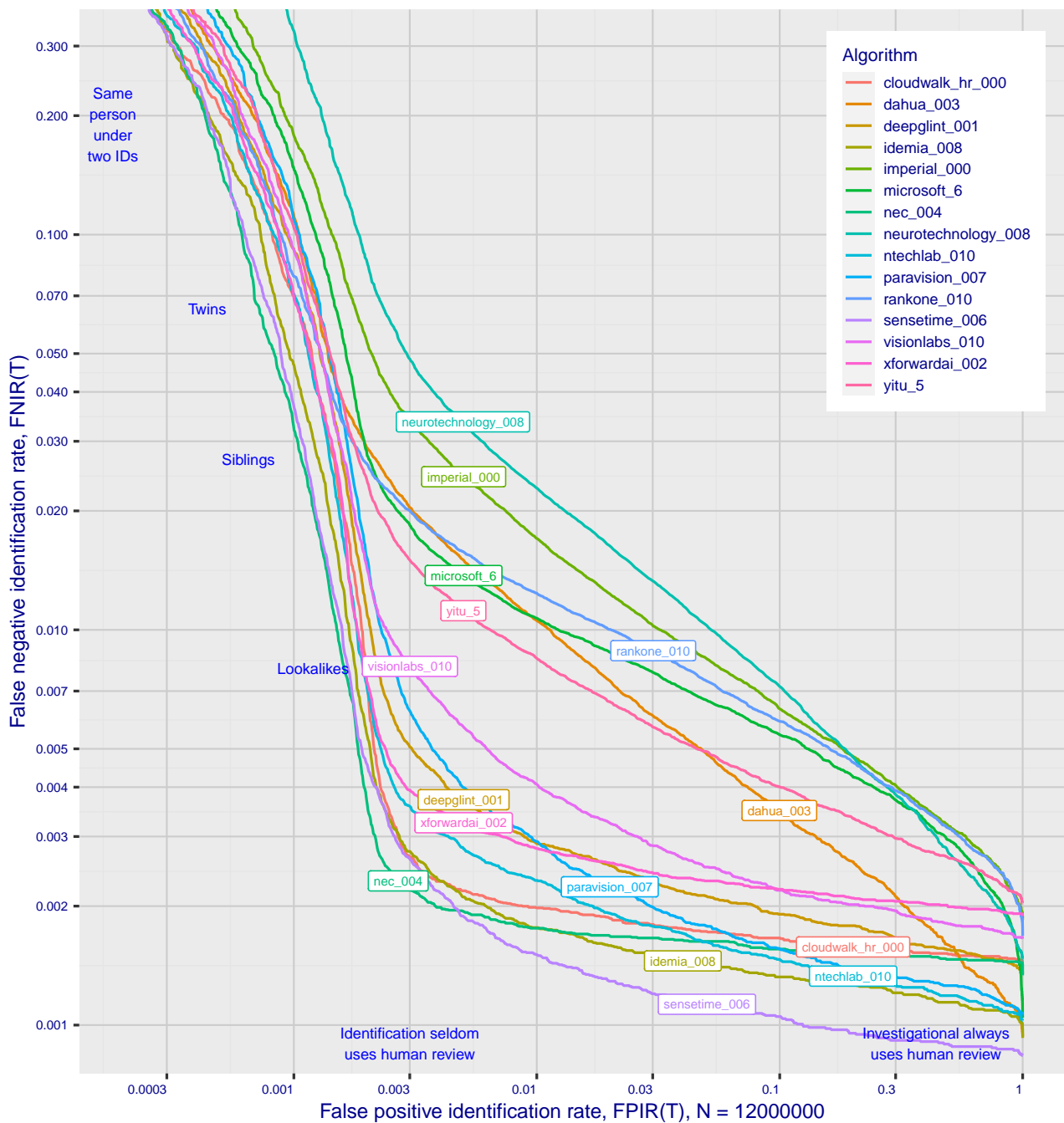


Figure 1: Identification miss rates across the false positive range.  $N = 12$  million individuals are enrolled with one recent image.

generally, on the developer of the algorithm. False negative error rates in a particular scenario range from a few tenths of one percent to beyond fifty percent. This is tabulated exhaustively later: For example Table 9 shows accuracy across datasets. Figure 1 here compares algorithms on mugshot searches in a consolidated gallery of 12 million subjects and 12 million photos. Many algorithms do not achieve the low error rates noted above, and while many of those may still be useful and valuable to end-users, only the most accurate excel on poor quality images and those collected long after the initial enrollment sample.

▷ **Versioning:** While results for up to ten algorithms from each developer are reported here, the intra-provider

accuracy variations are usually smaller than the inter-provider variations. That said different versions give an order of magnitude fewer misses. Some developers demonstrate speed-accuracy tradeoffs<sup>1</sup>. See Figs. 18, 19.

- ▷ **Low similarity scores:** In thousands of mugshot cases the correct gallery image is returned at rank 1 but its similarity score is nevertheless low, below some operationally required score threshold. This is not so important when face recognition is used for “lead generation” in investigational applications because human reviewers are specifically required to review potentially long candidate lists and the threshold is effectively 0. In applications where search volumes are higher and labor is not available to review the results from searches, a higher threshold must be applied. This reduces the length of candidate lists and false positive identification rates at the expense of increased false negative miss rates. The tradeoff between the two error rates is reported extensively later.
- ▷ **Population size:** As the number of enrolled subjects grows, some mates are displaced from rank one, decreasing accuracy. As tabulated later for N up to 12 million, false negative rates generally rise slowly with population size. This enables use of face recognition in very large populations. However in most positive and negative identification applications<sup>2</sup>, a score threshold is set to limit the rate at which non-mate searches produce false positives. This has the consequence that some mated searches will report the mate below threshold, i.e. a miss, even if it is at rank 1. The utility of this is that many non-mated searches will return no candidate identities at all. As the error-tradeoff characteristic shows, investigational miss rates on the right side are very low but then rise steadily (in the center region) as threshold is increased to support “lights-out” applications, and ultimately rise quickly (left side) as discussed below. Thus, if we demand that just one in one thousand non-mate searches produce any false positives, the most accurate algorithms there (Sensetime-004 and NEC-3) would fail on between 3 and 5% of mated searches. Even though the graph shows results for the most accurate algorithms, all but two would fail to find the mate in more than 8% of mated searches. While the two most accurate algorithms produce a relatively flat error tradeoff until the threshold is raised to limit false positives to about 1 in 400 non-mated searches<sup>3</sup>.

Thereafter, as the threshold is raised to further reduce false positives, miss rates rise rapidly. This means that low false positive identification rates are inaccessible with these algorithms, a result that does not apply for ten-finger identification algorithms. The rapid rise occurs because the lower mate scores are mixed with very high non-mate scores, the low scores from poor image quality and ageing, the high non-mates from the presence of lookalikes persons (doppelgangers), twins (discussed next) and, ultimately, the presence of a few unconsolidated subjects i.e. persons present under multiple IDs.

- ▷ **False negatives from ageing:** A large source of error in long-run applications where subjects are not re-enrolled on a set schedule is ageing. Changes in facial appearance increase with the time elapsed between photographs. These will depress similarity scores and eventually cause false negatives. All faces age and while this usually proceeds in a graceful and progressive manner, drug use can accelerate this [28]. Elective surgery may be effective in delaying it although this has not been formally quantified with face recognition. As ageing is essentially unavoidable, it can only be mitigated by scheduled re-capture, as in passport re-issuance. To quantify ageing effects, we used the more accurate algorithms to enroll the earliest image of 3.1 million adults and then search

<sup>1</sup>For example, NEC-0 prepares templates much faster than NEC-2 but gives twenty times more misses. Dermalog-5 executes a template search much more quickly than Dermalog-6 but is also much less accurate.

<sup>2</sup>In a positive identification application such as a registered traveler system, a user is making an implicit claim to be enrolled in the system - most users will be. In a negative application, such as with deportees, the implicit claim is that the subject is not enrolled - most will not be.

<sup>3</sup>The gallery size here is 12 million people, one image per person. Given 331 201 non-mated searches, an exhaustive implementation of one-too-many search would execute almost 4 trillion comparisons. At a false positive identification rate of 0.0025 the number of false positives is, to first order, 828 corresponding to single-comparison false match rate of  $828 / 4 \text{ trillion} = 2.1 \times 10^{-10}$  i.e. about 1 in 5 billion. Strictly this FMR computation is meaningful only for algorithms that implement 1:N search using N 1:1 comparisons, which is not always the case.

with 10.3 million newer photos taken up to 18 years after the initial enrollment photo. Figure 2 puts ageing into context by contrasting it with the increase in false negatives that occurs when the number of individuals in an enrollment database becomes larger and the chance of a false positive increases such that higher thresholds may become necessary<sup>4</sup>.

The Figure shows, from top to bottom, increases in false negative identification rates (FNIR) with the algorithm being tested. This applies to increases due to  $N$  on the left side, and increases due to ageing on the right side. The relative spacing of the dots shows that for all algorithms the dependency of FNIR on  $N$  (up to 12 million) is considerably less than on  $\Delta T$  (up to 18 years).

In the inset table, accuracy is seen to degrade progressively with time, as mate scores decline and non-mates displace mates from rank 1 position. More accurate algorithms tend to be less sensitive to ageing. The more accurate algorithms give fewer errors after 18 years of ageing than middle tier algorithms give after four. Note also we do not quantify an ageing rate - more formal methods [2] borrowed from the longitudinal analysis literature have been published for doing so (given suitable repeated measures data). See Figures 60, 80 and 90.

---

<sup>4</sup>Some algorithms implement strategies to automatically adjust scores to account for increased population size. This relieves the system owner of having to increase thresholds as  $N$  increases.

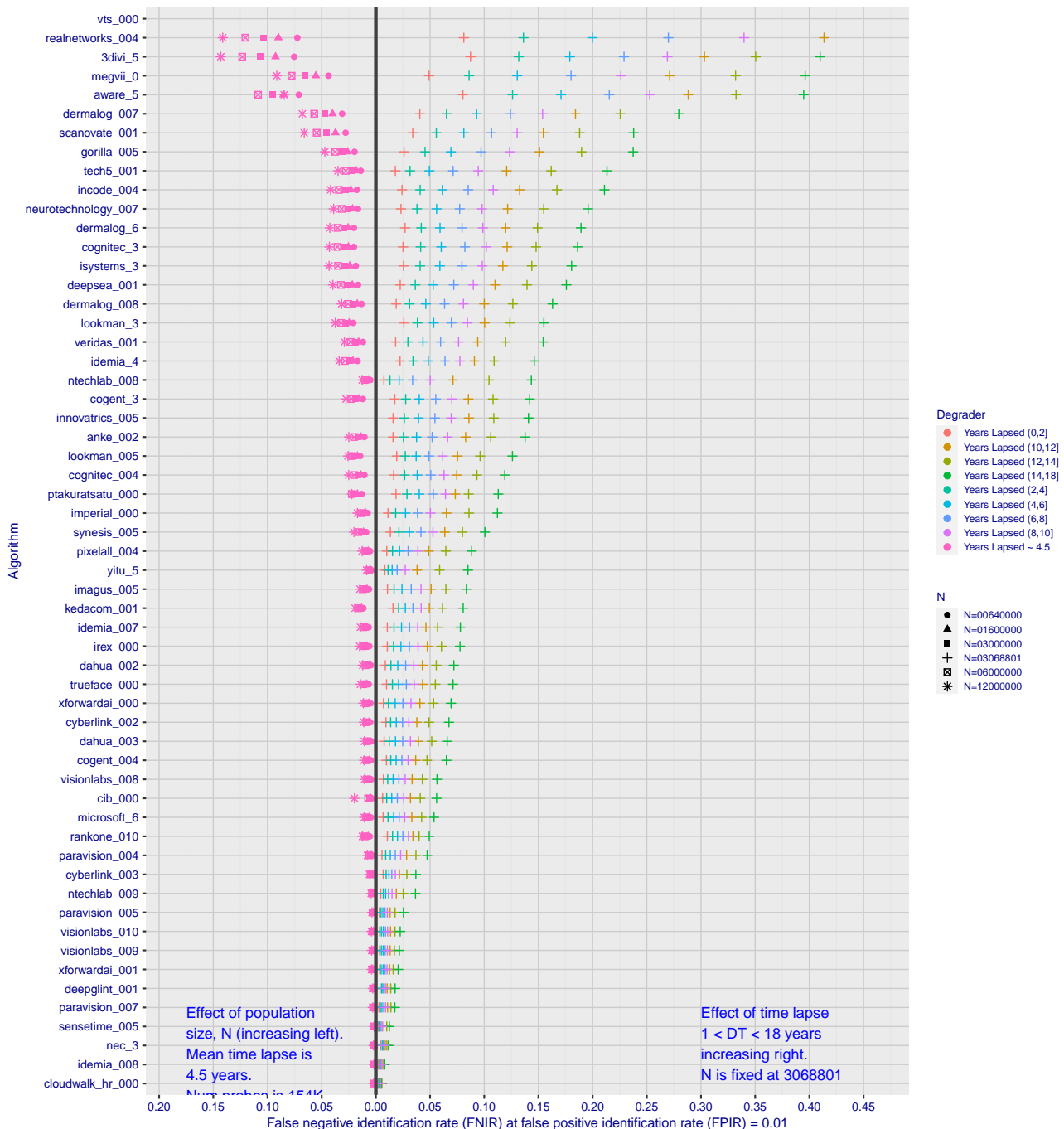


Figure 2: Identification miss rates as a function of enrolled population size,  $N$ , and time-lapse,  $\Delta T$ .

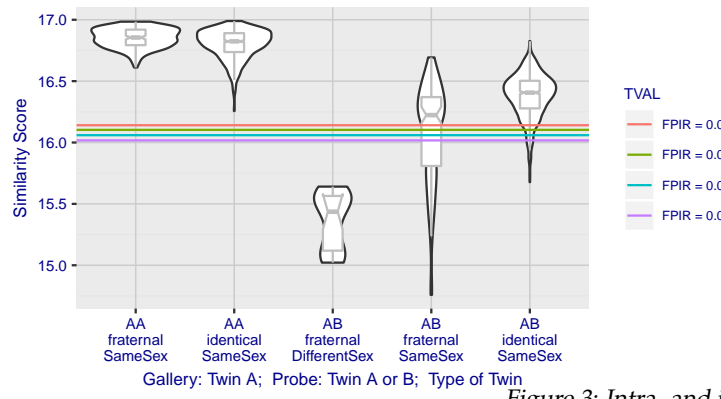


Figure 3: Intra- and inter-twin scores

▷ **False positives from twins:** By enrolling 640 000 mugshots, adding photos of one twin, and then searching photos of those subjects and their twin the inset figure shows, for one typical algorithm, the similarity is generally greater when searching twins against themselves (A) than when searching twins against their sibling (B) but very often still above even stringent thresholds i.e. those corresponding to one in one thousand searches producing a false positive. Thus twins will very often produce a high-scoring non-match on a candidate list and a false alarm in an online identification system. The plot of Fig. 3 shows that fraternal twins are sometimes correctly rejected at those thresholds - including most different sex twins (at center). Figure ?? shows substantially similar behavior for all algorithms tested. In an investigative search, a twin would typically appear at rank 1, or rank 2 if their sibling happened to also be the gallery. Twins (and triplets etc.) constituted 3.3% of all live births [17] in recent years<sup>5</sup>, and because that number is higher today than when the individuals in current adult databases were born, the false positives that arise from twins are now, and will increasingly be, an operational problem. Relative to the United States, twins are born with considerable regional variation. For example they are much less common in East Asia, and much more common in Sub-Saharan Africa [21].

The presence of twins in the mugshot database is inevitable given its size, around 12.3 million people. As this is not an insignificant sample of the domestic United States population, people with other familial ties will be present also. The data was collected over an extended period and because location information is not available, we are unable to estimate the proportion of the domestic population that is present in the dataset. However, if we assume twins are neither more or less disposed to arrest than the general population, we can estimate that hundreds of thousands of individuals in the dataset are twins. This will affect false positive rates because we randomly set aside 331 201 individuals for nonmate searches, and some proportion of those will be twins with siblings in the gallery.

▷ **Database integrity:** An operational error rate should be added to all false negative rates in this report reflecting the proportion of images in a real database that are un-matchable. Such anomalies arise from images that: do not contain a face; include multiple persons; cannot be decoded; are rotated by 90° or 180°; depict a face on clothing; and others introduced by a long tail of various clerical errors. While the mugshot trials in this report have been constructed to minimize such effects, they are a real problem in actual operations.

This report is being updated continuously as new algorithms are submitted to FRVT, and run on new datasets. Participation in the [one-to-many identification track](#) is independent of participation in the [one-to-one verification track](#) of FRVT.

<sup>5</sup>See the CDC's National Vital Statistics Report for 2017: [https://www.cdc.gov/nchs/data/nvsr/nvsr67/nvsr67\\_08-508.pdf](https://www.cdc.gov/nchs/data/nvsr/nvsr67/nvsr67_08-508.pdf)

## Scope and Context

**Audience:** This report is intended for developers, integrators, end users, policy makers and others who have some familiarity with biometrics applications. The methods and metrics documented here will be of interest to organizations engaged in tests of face recognition algorithms. Some of these have been incorporated in the ISO/IEC 19795 Part 1 Biometric Testing and Reporting Framework standard, now nearing publication.

**Prior benchmarks:** Automated face recognition accuracy has improved massively in the two decades since initial commercialization of the various technologies. NIST has tracked that improvement through its conduct of regular independent, free, open, and public evaluations. These have fostered improvements in the state of the art. This report serves as an update to the [NIST Interagency Report 8271](#) on performance of face identification algorithms, published in September 2019.

**Demographics:** In December 2019, NIST published a first report on demographic dependencies in face recognition, [NIST Interagency Report 8280](#) that documented age, sex and race differentials in one-to-one and one-to-many false positive and false negative rates.

**Scope:** NIST IR 8271 documented recognition results for four databases containing in excess of 30.2 million still photographs of 14.4 million individuals. That constituted the largest public and independent evaluation of face recognition ever conducted. It includes results for accuracy, speed, investigative vs. identification applications, scalability to large populations, use of multiple images per person, images of cooperative and non-cooperative subjects.

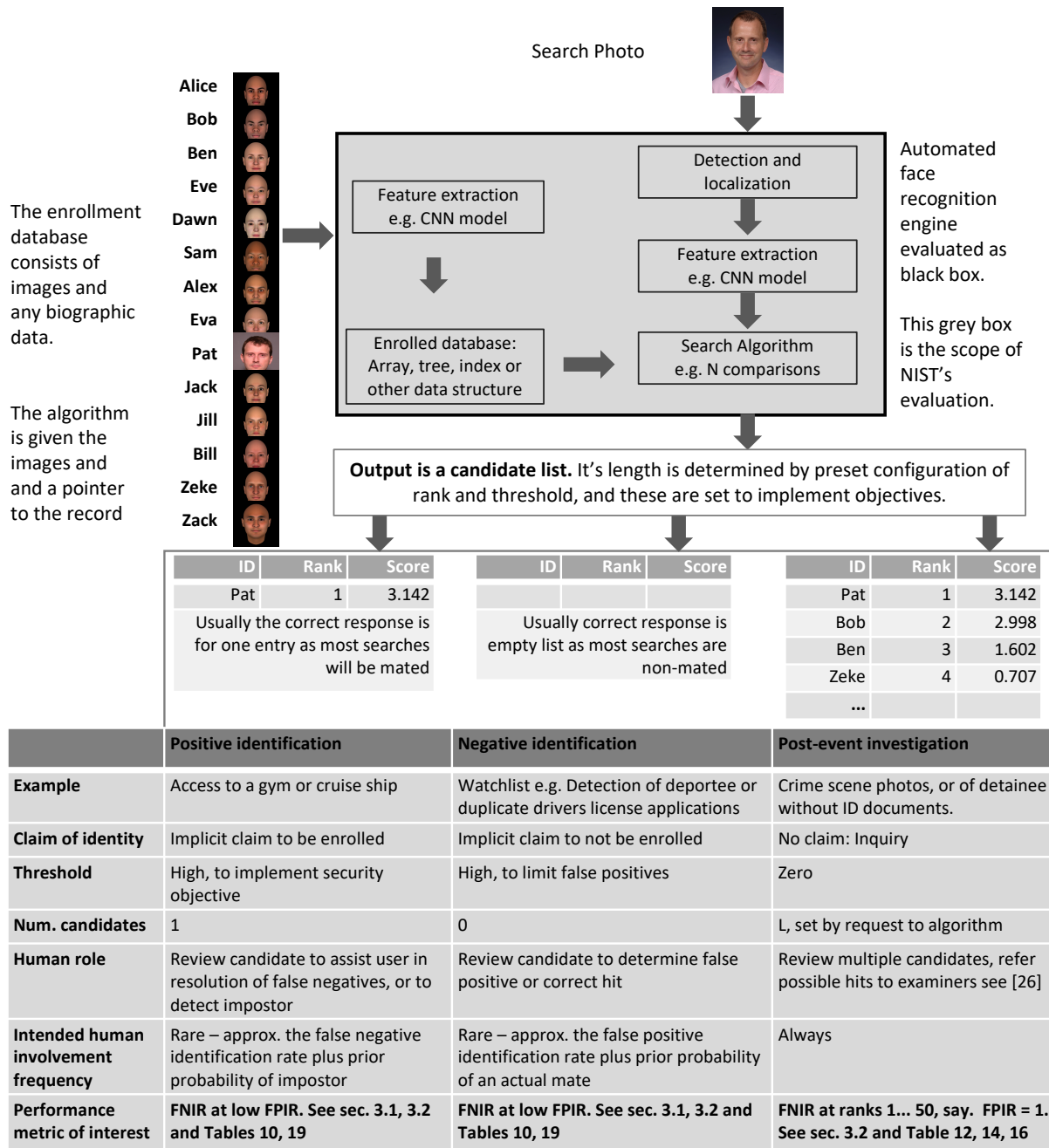
The report also includes results for ageing, recognition of twins, and recognition of profile-view images against frontal galleries. It otherwise does not address causes of recognition failure, neither image-specific problems nor subject-specific factors including demographics. Separate reports on demographic dependencies in face recognition will be published in the future. Additionally out of scope are: performance of live [human-in-the-loop transactional systems](#) like automated border control gates; human recognition accuracy as used in forensic applications; and recognition of persons in video sequences (which NIST evaluated separately [9]). Some of those applications share core matching technologies that *are* tested in this report.

**Images:** Five kinds of images are employed; these are either compared with images of the same kind, or against others from different capture environments as follows. The primary dataset is a set of law enforcement mugshot images (Fig. 5) which are enrolled and then searched with three kinds of images: other mugshots (i.e. within-domain); profile-view photographs (90 degree cross-view); and lower quality webcam images (Fig. 6) collected in similar detention operations (cross-domain). Additionally we compare high quality visa-like photos collected in immigration offices, with: medium quality border crossing images collected in primary immigration lanes; poor quality images collected in ATM-like registered traveller kiosks.

**Participation and industry coverage:** The report includes performance figures for prototype algorithms from the research laboratories of commercial developers and a few universities. This represents a substantial majority of the face recognition industry, but only a tiny minority of the academic community. Participation was open worldwide. While there is no charge for participation, developers incur some software engineering expense in implementing their algorithms behind the NIST application programming interface (API). The test is a black-box test where the function of the algorithm, and the intellectual property associated with it, is hidden inside pre-compiled libraries.

**Recent technology development:** Most face recognition research with deep convolutional neural networks (CNNs) has been aimed at achieving invariance to pose, illumination and expression variations that characterize photojournalism and social media images. The initial research [18, 22] employed large numbers of images of relatively few ( $\sim 10^4$ ) individuals to learn invariance. Inevitably much larger populations ( $\sim 10^7$ ) were employed for training [11, 20] but the benchmark, Labeled Faces in the Wild with (essentially) an equal error rate metric [12], represents an easy task,

one-to-one verification at very high false match rates. While a larger scale identification benchmark duly followed, Megaface [15], its primary metric, rank one hit rate, contrasts with the high threshold discrimination task required in most large-population applications of face recognition, namely credential de-duplication, and background checks. There, identification in galleries containing up to  $10^8$  individuals must be performed using a) very few images per individual and b) stringent thresholds to afford very low false positive identification rates. This track of FRVT was launched to measure the capability of the new technologies, including in these two cases. FRVT has included open-set identification tests since 2002, reporting both false negative and positive identification rates [7].



**Performance metrics for applications:** This report documents the performance of one-to-many face recognition algorithms. The word "performance" here refers to recognition accuracy and computational resource usage, as measured

by executing those algorithms on massive sequestered datasets.

This report includes extensive tabulation of recognition error rates germane to the main use-cases for face search technology. The Figure below, inspired by the Figure 1 in [23] differentiates different applications of the technolgy. The last row directs readers to the main tables relevant to those applications, respectively threshold-based and rank-based metrics that are special cases of the metrics given in section 3. The terms negative identification and positive identification are taken from the ISO/IEC 2382-37:2017 standardized biometrics vocabulary.

The algorithms are specifically configured for these applications by setting thresholds and candidate list lengths. Both rank-based metrics and threshold-based metrics include tradeoffs. In investigation, overall accuracy will be reduced if labor is only available to review a few candidates from the automated system. Note that when a fixed number of candidates are returned, the false positive identification rate of the automated face recognition engine will be 100%, because a probe image of anyone not enrolled will still return candidates. In identification applications where false positives must be limited to satisfy reviewer labor availability or a security objective, higher false negative rates are implied. This report includes extensive quantification of this threshold-based tradeoff.

See Sec. 3

**Template diversity:** The FRVT is designed to evaluate black-box technologies with the consequence that the templates that hold features extracted from face images are entirely proprietary opaque binary data that embed considerable intellectual property of the developer. Despite migration to CNN-based technologies there is no consensus on the optimal feature vector dimension. This is evidenced by template sizes ranging from below 100 bytes to more than four kilobytes. This diversity of approaches, suggests there is no prospect of a standard template something that would require a common feature set to be extracted from faces. Interoperability in automated face recognition remains solidly based on images and documentary standards for those, in particular the ICAO portrait [27] specification deriving from the ISO/IEC 19794-5 Token frontal [24] standard, which are similar to certain ANSI/NIST Type 10 [26] formats.

**Training:** The algorithms submitted to NIST have been developed using image datasets that developers do not disclose. The development will often include application of machine learning techniques and will additionally involve iterative training and testing cycles. NIST itself does not perform any training and does not refine or alter the algorithm in any way. Thus the model, data files, and libraries that define an algorithm are fixed for the duration of the tests. This reflects typical operational reality where recognition software, once installed, is fixed and constant until upgraded. This situation persists because on-site training of algorithms on customer data is atypical essentially because training is not a turnkey process.

**Automated search and human review:** Virtually all applications using automated face search require human review of the outputs at some frequency: Always for investigational applications; rarely in positive identification applications, after rejection (false or otherwise); and rarely in negative identification applications, after an alarm (false or otherwise). The human role is usually to compare a reference image with the query image or the live-subject if present, to render either a definitive decision on “exclusion” (different subjects), or “identification” (same subject), or a declaration that one or both images have “no value” and that no decision can be made. Note that automated face recognition algorithms are not built to do exclusion - low scores from a face comparison arise from different faces *and* poor quality images of the same face.

Human reviewers make recognition errors [5, 19, 25] and are sensitive to image acquisition and quality. Accurate human review is supported by high resolution - as specified in the Type 50, 51 acquisition profiles of the ANSI/NIST Type 10 record [26], and by multiple non-frontal views as specified in the same standard. These often afford views of the ear. Organizations involved in image collection should consider supporting human adjudication by collecting high-resolution frontal and non-frontal views, preparing low resolution versions for automated face recognition [24], and retaining both for any subsequent resolution of candidate matches. Along these lines, the ISO/IEC Joint Technical

Committee 1 subcommittee 37 on biometrics has just initiated projects on image quality assessment and face-aware capture.

## Release Notes

**FRVT Activities:** Since February 2017, NIST has been evaluating one-to-one verification algorithms on an ongoing basis. NIST then restarted FRVT's one-to-many track in February 2018, inviting participants to send up to prototype algorithms. Both tracks allows developers to submit updated algorithms to NIST at any time but no more frequently than four calendar months. This more closely aligns development and evaluation schedules. Results are posted to the web within a few weeks of submission. Details and full report are linked from the [Ongoing FRVT site](#).

**FRVT Reports:** The results of the FRVT appear in the series NIST Interagency Reports tabulated below. The reports were developed separately and released on different schedules. In prior years NIST has mostly reported FRVT results as a single report; this had the disadvantage that results from completed sub-studies were not published until all other studies were complete.

Date	Link	Title	No.
2014-03-20	<a href="#">PDF</a>	FRVT Performance of Automated Age Estimation Algorithms	7995
2015-04-20	<a href="#">PDF</a>	Face Recognition Vendor Test (FRVT) Performance of Automated Gender Classification Algorithms	8052
2014-05-21	<a href="#">PDF</a>	FRVT Performance of face identification algorithms	8009
2017-03-07	<a href="#">PDF</a>	Face In Video Evaluation (FIVE) Face Recognition of Non-Cooperative Subjects	8173
2017-11-23	<a href="#">PDF</a>	The 2017 IARPA Face Recognition Prize Challenge (FRPC)	8197
2018-11-27	<a href="#">PDF</a>	Face Recognition Vendor Test - Part 2: Identification	8271
2019-09-11	<a href="#">PDF</a>	Face Recognition Vendor Test - Part 2: Identification	8271
2019-12-11	<a href="#">PDF</a>	Face Recognition Vendor Test - Part 3: Demographic Effects	8280
2020-01-03	<a href="#">WWW</a>	Face Recognition Vendor Test (FRVT) - Part 1 Verification	Draft

Details appear on pages linked from <https://www.nist.gov/programs-projects/face-projects>.

**Appendices:** This report is accompanied by appendices which present exhaustive results on a per-algorithm basis. These are machine-generated and are included because the authors believe that visualization of such data is broadly informative and vital to understanding the context of the report.

**Typesetting:** Virtually all of the tabulated content in this report was produced automatically. This involved the use of scripting tools to generate directly type-settable L<sup>A</sup>T<sub>E</sub>X content. This improves timeliness, flexibility, maintainability, and reduces transcription errors.

**Graphics:** Many of the Figures in this report were produced using the **ggplot2** package running under **R**, the capabilities of which extend beyond those evident in this document.

# Contents

<b>Release Notes</b>	<b>1</b>
<b>Disclaimer</b>	<b>4</b>
<b>Institutional Review Board</b>	<b>4</b>
<b>Acknowledgments</b>	<b>4</b>
<b>Executive Summary</b>	<b>5</b>
<b>Scope and Context</b>	<b>11</b>
<b>Release Notes</b>	<b>15</b>
<b>1 Introduction</b>	<b>17</b>
<b>2 Evaluation datasets</b>	<b>18</b>
<b>3 Performance metrics</b>	<b>24</b>
<b>4 Results</b>	<b>40</b>
<b>Appendices</b>	<b>74</b>
<b>A Accuracy on large-population FRVT 2018 mugshots</b>	<b>74</b>
<b>B Effect of time-lapse: Accuracy after face ageing</b>	<b>119</b>
<b>C Effect of enrolling multiple images</b>	<b>212</b>
<b>D Accuracy with poor quality webcam images</b>	<b>219</b>
<b>E Accuracy for profile-view to frontal recognition</b>	<b>229</b>
<b>F Search duration</b>	<b>233</b>
<b>G Gallery Insertion Timing</b>	<b>240</b>

# 1 Introduction

One-to-many identification represents the largest market for face recognition technology. Algorithms are used across the world in a diverse range of biometric applications: detection of duplicates in databases, detection of fraudulent applications for credentials such as passports and driving licenses, token-less access control, surveillance, social media tagging, lookalike discovery, criminal investigation, and forensic clustering.

This report contains a breadth of performance measurements relevant to many applications. Performance here refers to accuracy and resource consumption. In most applications, the core accuracy of a facial recognition algorithm is the most important performance variable. Resource consumption will be important also as it drives the amount of hardware, power, and cooling necessary to accommodate high volume workflows. Algorithms consume processing time, they require computer memory, and their static template data requires storage space. This report documents these variables.

## 1.1 Open-set searches

FRVT tested open-set identification algorithms. Real-world applications are almost always “open-set”, meaning that some searches have an enrolled mate, but some do not. For example, some subjects have truly not been issued a visa or drivers license before; some law enforcement searches are from first-time arrestees<sup>6</sup>. In an “open-set” application, algorithms make no prior assumption about whether or not to return a high-scoring result, and for a mated search, the ideal behaviour is that the search produces the correct mate at high score and first rank. For a non-mate search, the ideal behavior is that the search produces zero high-scoring candidates.

Many academic benchmarks execute only closed-set searches. The proportion of mates found in the rank one position is the default accuracy metric. This hit rate metric ignores the score with which a mate is found; weak hits count as much as strong hits. This ignores the real-world imperative that in many applications it is necessary to elevate a threshold to reduce the number of false positives.

---

<sup>6</sup>Operationally closed-set applications are rare because it is usually not the case that all searches have an enrolled mate. One counter-example, however, is a cruise ship in which all passengers are enrolled and all searches should produce exactly one identity. Another example is forensic identification of dental records from an aircraft crash.

## 2 Evaluation datasets

This report documents accuracy for four kinds of images - mugshots, webcam, profiles and wild - as described in the following sections.

### 2.1 Immigration-related images

This report includes benchmark tests sharing a common enrollment of high quality frontal portrait images collected while subject make applications for various immigration benefits. We then search that with two kinds of images, webcam images collected during in-bound immigration and also images collected from registered travelers using a ATM-style kiosk. These are described below and depicted in Figure 4.



Figure 4: Example photos.

- ▷ **Application reference photos:** The images are collected in an attended interview setting using dedicated capture equipment and lighting. The images, at size 300x300 pixels, are smaller than normally indicated by ISO. The images are all high-quality frontal portraits collected in immigration offices and with a white background. As such, potential quality related drivers of high false match rates (such as blur) can be expected to be absent. The images are encoded as ISO/IEC 10918-1 i.e. JPEG. Older images had a compression ration of about 16:1, while newer images, since 2010, are more lightly compressed at 4:1. When these images are provided as input into the algorithm, they are labeled with the type "iso". This report enrols 1 600 000 application images, one per person.
- ▷ **Border crossing photos:** Most images are have width 320 and height 240 pixels. They are JPEG compressed at 16:1 i.e. filesize just below 15KB. The images present challenges for face recognition in that subjects often exhibit non-zero yaw and pitch (associated with the rotational degrees of freedom of the camera mount), low contrast (due to varying and intense background lights), and poor spatial resolution (due to inexpensive cameras). There are often subjects standing in the background, usually at very low resolution (see Figure 4b). In such cases, algorithms should detect all faces and determine which is the largest and most centered. When these images are provided as input into the algorithm, they are labeled with the type "wild".
- ▷ **Kiosk photos:** These photos were collected from subjects whose attention was focused on interaction with an immigration kiosk. They images were not intended for use with automated face recognition. The camera is situated above a display which the user touches, and is triggered either without directing the subject to look at it, or without waiting for the subject to comply. The images are therefore characterized by pitch-down pose, sometimes exceeding 45 degrees, as in Figure 4c. Yaw-angle variation is mild, with most images close to frontal. The images

have width 320 pixels and height 240 pixels and therefore tall individuals are sometimes cropped. This is often just above the eyes and can occur at the nose or mouth. Conversely, short individuals are sometimes cropped such that only the top part of the face is visible. In a quite small number of cases, there other subjects standing just behind the primary subject such that algorithms should detect all faces and determine which is the largest and most centered. Background ceiling lighting is often visible and this sometimes leads to under-exposure of the face. When these images are provided as input into the algorithm, they are labeled with the type "wild".

## 2.2 Law enforcement images

The main mugshot dataset used is referred to as the FRVT 2018 set. This set was collected over the period 2002 to 2017 in routine United States law enforcement operations. This set yields three subsets

- ▷ **Mugshots:** Mugshots comprise about 86% of the database. They have reasonable compliance with the ANSI/NIST ITL1-2011 Type 10 standard's subject acquisition profiles levels 10-20 for frontal images [26]. The most common departure from the standard's requirements is the presence of mild pose variations around frontal - the images of Figure 5 are typical. The images vary in size, with many being 480x600 pixels with JPEG compression applied to produce filesizes of between 18 and 36KB with many images outside this range, implying that about 0.5 bits are being encoded per pixel. When these images are provided as input into the algorithm, they are labeled with the type "mugshot".

Example images appear in Fig. 5

[NIST Interagency Report 8238](#) includes a comparison of this set of mugshots with the smaller and easier sets of mugshots used in tests run in 2010 and 2014.

- ▷ **Profile images:** Profile-view images have been collected in law enforcement for more than 100 years, as human capability is improved with orthogonal information. The profile images used in this report were collected during the same session as the frontal mugshot photograph, in the same standardized photographic setup. These would not therefore be used with automated face recognition. A small subset, 200 000 images, were set aside for testing. When these images are provided as input into the algorithm, they are labeled with the type "wild".

Example images appear in Fig. 7

- ▷ **Webcam images:** The remaining 14% of the images were collected using an inexpensive webcam attached to a flexible operator-directed mount. These images are all of size 240x240 pixels, that are in considerable violation of most quality-related clauses of all face recognition standards. As evident in the figure, the most common defects are non-frontal pose (associated with the rotational degrees of freedom of the camera mount), low contrast (due to varying and intense background lights), and poor spatial resolution (due to inexpensive camera optics) - see examples in Fig 6. The images are overly JPEG compressed, to between 4 and 7KB, implying that only 0.5 to 1 bits are being encoded per color pixel. When these images are provided as input into the algorithm, they are labeled with the type "wild".

Example images appear in Fig. 6

These are drawn from NIST Special Database 32 which may be downloaded [here](#).

These images were partitioned in galleries and probesets for the various experiment listed in Table 1.

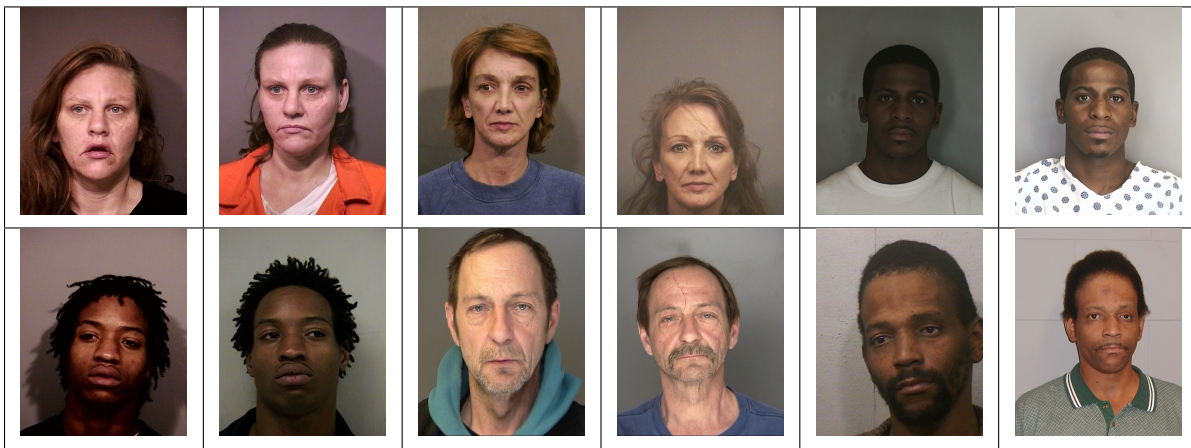


Figure 5: Six mated mugshot pairs representative of the FRVT-2014 (LEO) and FRVT-2018 datasets. The images are collected live, i.e. not scanned from paper. Image source: NIST Special Database 32 the Multiple Encounter Deceased Subjects dataset.



Figure 6: Twelve webcam images representative of probes against the FRVT-2018 mugshot gallery. The first eight images are four mated pairs. Such images present challenges to recognition including pose, non-uniform illumination, low contrast, compression, cropping, and low spatial sampling rate. Image source: NIST Special Database 32 the Multiple Encounter Deceased Subjects dataset.



Figure 7: **[Profile views]** The three images are a frontal enrollment, subsequent frontal probe, and same-session ninety degree profile view. While collection of both frontal and profile views has been typical in law enforcement for more than a century, the recognition of profile to frontal views has essentially been impossible. However, reasonably high accuracy results is now possible - see section E.

Image				
Encounter	1	...	$K_i - 1$	$K_i$
Capture Time	$T_1$	...	$T_{K_i - 1}$	$T_{K_i}$
Role RECENT	Not used	Not used	Enrolled	Search
Role LIFETIME	Enrolled	Enrolled	Enrolled	Search

Figure 8: Depiction of the “recent” and “lifetime” enrollment types. Image source: NIST Special Database 32

## 2.3 Enrollment strategies

Many operational applications include collection and enrollment of biometric data from subjects on more than one occasion. This might be done on a regular basis, as might occur in credential (re-)issuance, or irregularly, as might happen in a criminal recidivist situation [4]. The number of images per person will depend on the application area. In civil identity credentialing (e.g. passports, driver’s licenses), the images will be acquired approximately uniformly over time (e.g. ten years for a passport). While the distribution of dates for such images of a person might be assumed uniform, a number of factors might undermine this assumption<sup>7</sup>. In criminal applications, the number of images would depend on the number of arrests. The distribution of dates for arrest records for a person (i.e. the recidivism distribution) has been modeled using the exponential distribution but is recognized to be more complicated<sup>8</sup>.

In any case, the 2010 NIST evaluation of face recognition showed that considerable accuracy benefits accrue with retention and use of *all* historical images [6].

To this end, the FRVT API document provides  $K \geq 1$  images of an individual to the enrollment software. The software is tasked with producing a single proprietary undocumented “black-box” template<sup>9</sup> from the  $K$  images. This affords the algorithm an ability to generate a *model* of the individual, rather than to simply extract features from each image on a sequential basis.

As depicted in Figure 8, the  $i$ -th individual in the FRVT 2018 dataset has  $K_i$  images. These are labelled as  $x_k$  for  $k = 1 \dots K_i$  in chronological order of capture date. To measure the utility of having multiple enrollment images, this report evaluates three kinds of enrollment:

- ▷ **Recent:** Only the second most recent image,  $x_{K_i - 1}$  is enrolled. This strategy of enrollment mimics the operational policy of retaining the imagery from the most recent encounter. This might be done operationally to ameliorate the effects of face ageing. Obviously retaining only the most recent image should only be done if the identity of the person is trusted to be correct. For example, in an access control situation retention of the most recent successful *authentication* image would be hazardous if it could be a false positive.
- ▷ **Lifetime-consolidated:** All but the most recent image are enrolled,  $x_1 \dots x_{K_i - 1}$ . This subject-centric strategy might be adopted if quality variations exist where an older image might be more suitable for matching, despite the ageing effect.

<sup>7</sup>For example, a person might skip applying for a passport for one cycle, letting it expire. In addition, a person might submit identical images (from the same photography session) to consecutive passport applications at five year intervals.

<sup>8</sup>A number of distributions have been considered to model recidivism, see for example [3].

<sup>9</sup>There are no formal face template standards. Template standards only exist for fingerprint minutiae - see ISO/IEC 19794-2:2011.

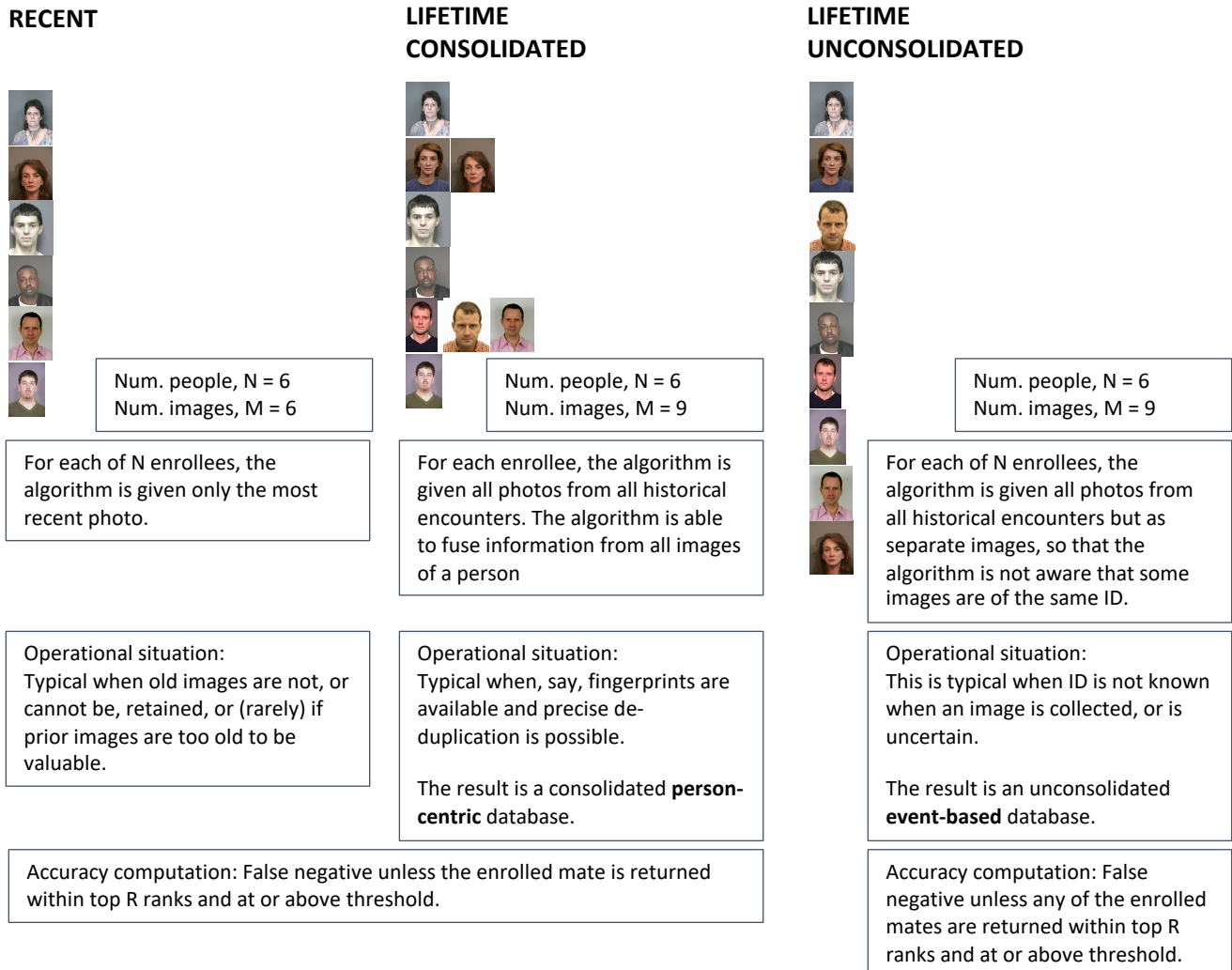


**Figure 9: Enrollment strategies.** The figure shows the three kinds of enrollment databases examined in this report. Image source: NIST Special Database 32

	ENROLLMENT				SEARCH			
	TYPE SEE SECTION 2.3	POPULATION FILTER	N-SUBJECTS	N-IMAGES	MATE N-SUBJECTS	NON-MATE N-IMAGES	N-SUBJECTS	N-IMAGES
<b>Mugshot trials from enrollment of single images</b>								
1	RECENT	NATURAL	640 000	640 000	154 549	154 549	331 254	331 254
2	RECENT	NATURAL	1 600 000	1 600 000				
3	RECENT	NATURAL	3 000 000	3 000 000				
4	RECENT	NATURAL	6 000 000	6 000 000				
5	RECENT	NATURAL	12 000 000	12 000 000				
<b>Cross-domain</b>								
13	MUGSHOTS AS ON ROW 2				82 106 WEBCAM	82 106 WEBCAM	331 254 WEBCAM	331 254 WEBCAM
<b>Cross-view</b>								
14	MUGSHOTS AS ON ROW 2				100 000 PROFILE	100 000 PROFILE	100 000 PROFILE	100 000 PROFILE
<b>Mugshot ageing</b>								
17	OLDEST	NATURAL	3 068 801	3 068 801	2 853 221	10 951 064	0	0
<b>Border crossing ageing</b>								
17	OLDEST	NATURAL	1 600 000	1 600 000	1 922 437	1 922 437	1 920 000	1 920 000
<b>Visa-border</b>								
19	PRIOR	NATURAL	1 600 000 VISA	1 600 000 VISA	80 000 BORDER	80 000 BORDER	80 000 BORDER	80 000 BORDER
20	VISA AS ON ROW 18				21 016 BORDER	21 016 BORDER	21 016 BORDER	21 016 BORDER

**Table 1: Enrollment and search sets.** Each row summarizes one identification trial. Unless stated otherwise, all entries refer to mugshot images. The term “natural” means that subjects were selected without heed to demographics, i.e. in the distribution native to this dataset. The probe images were collected in a different calendar year to the enrollment image. Missing values in rows 2-12 are the same as in row 1.

▷ **Lifetime-unconsolidated:** Again all but the most recent image are enrolled  $x_1 \dots x_{K_i-1}$  but now separately, with different identifiers, such that the algorithm is not aware that the images are from the same face. This kind of event- or encounter-centric enrollment is very common when operational constraints preclude reliable consolidation of the historical encounters into a single identity. This aspect also prevents the recognition algorithm from a) building a holistic model of identity (as is common in speaker recognition systems) and b) implementing fusion, for example template-level fusion of feature vectors, or post-search score-level fusion. The result is that searches will typically yield more than one image of a person in the top ranks. This has consequences for appropriate metrics, as detailed in section 3.2.1

NIST first evaluated this kind of enrollment in mid 2018, and the results tables include some comparison of accuracy available from all three enrollment styles.

In all cases, the most recent image,  $x_{K_i}$ , is reserved as the search image. For the 1.6 million subject enrollment partition of the FRVT 2018 data,  $1 \leq K_i \leq 33$  with  $K_i = 1$  in 80.1% of the individuals,  $K_i = 2$  in 13.4%,  $K_i = 3$  in 3.7%,  $K_i = 4$  in 1.4%,  $K_i = 5$  in 0.6%,  $K_i = 6$  in 0.3%, and  $K_i > 6$  is 0.2% for everyone else. This distribution is substantially dependent on United States recidivism rates.

We did not evaluate the case of retaining only the highest quality image, since automated quality assessment is out of scope for this report. We do not anticipate that such strategies will prove beneficial when the quality assessment apparatus is imperfect and unvalidated.

### 3 Performance metrics

This section gives specific definitions for accuracy and timing metrics. Tests of open-set biometric algorithms must quantify frequency of two error conditions:

- ▷ **False positives:** Type I errors occur when search data from a person who has never been seen before is incorrectly associated with one or more enrollees' data.
- ▷ **Misses:** Type II errors arise when a search of an enrolled person's biometric does not return the correct identity.

Many practitioners prefer to talk about "hit rates" instead of "miss rates" - the first is simply one minus the other as detailed below. Sections 3.1 and 3.2 define metrics for the Type I and Type II performance variables.

Additionally, because recognition algorithms sometimes fail to produce a template from an image, or fail to execute a one-to-many search, the occurrence of such events must be recorded. Further because algorithms might elect to not produce a template from, for example, a poor quality image, these failure rates must be combined with the recognition error rates to support algorithm comparison. This is addressed in section 3.5.

Finally, section 3.7 discusses measurement of computation duration, and section 3.8 addresses the uncertainty associated with various measurements. Template size measurement is included with the results.

#### 3.1 Quantifying false positives

It is typical for a search to be conducted into an enrolled population of  $N$  identities, and for the algorithm to be configured to return the closest  $L$  candidate identities. These candidates are ranked by their score, in descending order, with all scores required to be greater than or equal to zero. A human analyst might examine either all  $L$  candidates, or just the top  $R \leq L$  identities, or only those with score greater than threshold,  $T$ . The workload associated with such examination is discussed later, in 3.6.

False alarm performance is quantified in two related ways. These express how many searches produces false positives, and then, how many false positives are produced in a search.

**False positive identification rate:** The first quantity, FPIR, is the proportion of non-mate searches that produce an adverse outcome:

$$\text{FPIR}(N, T) = \frac{\text{Num. non-mate searches where one or more enrolled candidates are returned with score at or above threshold}}{\text{Num. non-mate searches attempted.}} \quad (1)$$

Under this definition, FPIR can be computed from the highest non-mate candidate produced in a search - it is not necessary to consider candidates at rank 2 and above. FPIR is the primary measure of Type I errors in this report.

**Selectivity:** However, note that in any given search, several non-mate may be returned above threshold. In order to quantify such events, a second quantity, selectivity (SEL), is defined as the *number* of non-mates returned on a candidate list, averaged over all searches.

$$\text{SEL}(N, T) = \frac{\text{Num. non-mate enrolled candidates returned with score at or above threshold}}{\text{Num. non-mate searches attempted.}} \quad (2)$$

where  $0 \leq \text{SEL}(N, T) \leq L$ . Both of these metrics are useful operationally. FPIR is useful for targeting how often an

adverse false positive outcome can occur, while SEL as a number is related to workload associated with adjudicating candidate lists. The relationship between the two quantities is complicated - it depends on whether an algorithm concentrates the false alarms in the results of a few searches or whether it disburses them across many. This was detailed in FRVT 2014, NISTIR 8009. It has not yet been detailed in FRVT 2018.

### 3.2 Quantifying hits and misses

If  $L$  candidates are returned in a search, a shorter candidate list can be prepared by taking the top  $R \leq L$  candidates for which the score is above some threshold,  $T \geq 0$ . This reduction of the candidate list is done because thresholds may be applied, and only short lists might be reviewed (according to policy or labor availability, for example). It is useful then to state accuracy in terms of  $R$  and  $T$ , so we define a “miss rate” with the general name **false negative identification rate** (FNIR), as follows:

$$\text{FNIR}(N, R, T) = \frac{\text{Num. mate searches with enrolled mate found outside top } R \text{ ranks or score below threshold}}{\text{Num. mate searches attempted.}} \quad (3)$$

This formulation is simple for evaluation in that it does not distinguish between causes of misses. Thus a mate that is not reported on a candidate list is treated the same as a miss arising from face finding failure, algorithm intolerance of poor quality, or software crashes. Thus if the algorithm fails to produce a candidate list, either because the search failed, or because a search template was not made, the result is regarded as a miss, adding to FNIR.

*Hit rates, and true positive identification rates:* While FNIR states the “miss rate” as how often the correct candidate is either not above threshold or not at good rank, many communities prefer to talk of “hit rates”. This is simply the **true positive identification rate**(TPIR) which is the complement of FNIR giving a positive statement of how often mated searches are successful:

$$\text{TPIR}(N, R, T) = 1 - \text{FNIR}(N, R, T) \quad (4)$$

This report does not report true positive “hit” rates, preferring false negative miss rates for two reasons. First, costs rise linearly with error rates. For example, if we double FNIR in an access control system, then we double user inconvenience and delay. If we express that as decrease of TPIR from, say 98.5% to 97%, then we mentally have to invert the scale to see a doubling in costs. More subtly, readers don’t perceive differences in numbers near 100% well, becoming inured to the “high nineties” effect where numbers close to 100 are perceived indifferently.

**Reliability** is a corresponding term, typically being identical to TPIR, and often cited in automated (fingerprint) identification system (AFIS) evaluations.

An important special case is the **cumulative match characteristic**(CMC) which summarizes accuracy of mated-searches only. It ignores similarity scores by relaxing the threshold requirement, and just reports the fraction of mated searches returning the mate at rank  $R$  or better.

$$\text{CMC}(N, R) = 1 - \text{FNIR}(N, R, 0) \quad (5)$$

We primarily cite the complement of this quantity,  $\text{FNIR}(N, R, 0)$ , the fraction of mates *not* in the top  $R$  ranks.

The **rank one hit rate** is the fraction of mated searches yielding the correct candidate at best rank, i.e.  $\text{CMC}(N, 1)$ . While this quantity is the most common summary indicator of an algorithm’s efficacy, it is not dependent on similarity scores, so it does not distinguish between strong (high scoring) and weak hits. It also ignores that an adjudicating reviewer is often willing to look at many candidates.

### 3.2.1 False negative rates for unconsolidated galleries

As detailed in section 2.3 a common type of gallery, here referred to as the lifetime unconsolidate type, is populated with all images of an individual without any association between them. That is, the gallery construction algorithm is not provided with any ID labels that would support processing of a person's images jointly. This contrasts with the lifetime consolidate type where an algorithm may explicitly fuse features from multiple images of a person, or select a best image. In such cases, where the number of enrolled images is a random variable, we define two false negative rates as follows.

The first demands that the algorithm place any of the  $K_i$  mates in the top  $R \geq 1$  ranks. The proportion of searches for which this does not occur forms a false negative identification rate:

$$\text{FNIR}_{\text{any}}(N, R, T) = 1 - \frac{\text{Num. mate searches where any enrolled mate is found in the top } R \text{ ranks and at-or-above threshold}}{\text{Num. mate searches attempted.}} \quad (6)$$

The second demands that the algorithm place all  $K_i$  mates in the top  $R \geq K_i$  ranks. The proportion of searches for which this does not occur forms a false negative identification rate:

$$\text{FNIR}_{\text{all}}(N, R, T) = 1 - \frac{\text{Num. mate searches where all enrolled mates are found in the top } R \text{ ranks and at-or-above threshold}}{\text{Num. mate searches attempted.}} \quad (7)$$

Placing all mates in the top ranks is a more difficult task than correctly retrieving any image, so it holds that:  $\text{FNIR}_{\text{all}} \geq \text{FNIR}_{\text{any}}$ . This is evident in the results presented for November 2018 algorithms in Tables starting at ??.

The information retrieval community might prefer to compute and plot *precision* and *recall*; this is a valid approach, but we advance the two metrics above because they relate to our normal definition of consolidated FNIR, and they cover the two extreme use-cases of wanting any hit vs. all hits.

## 3.3 DET interpretation

In biometrics, a false negative occurs when an algorithm fails to match two samples of one person – a Type II error. Correspondingly, a false positive occurs when samples from two persons are improperly associated – a Type I error.

Matches are declared by a biometric system when the native comparison score from the recognition algorithm meets some threshold. Comparison scores can be either similarity scores, in which case higher values indicate that the samples are more likely to come from the same person, or dissimilarity scores, in which case higher values indicate different people. Similarity scores are traditionally computed by fingerprint and face recognition algorithms, while dissimilarities are used in iris recognition. In some cases, the dissimilarity score is a distance possessing metric properties. In any case, scores can be either mate scores, coming from a comparison of one person's samples, or nonmate scores, coming from comparison of different persons' samples.

The words "genuine" or "authentic" are synonyms for mate, and the word "impostor" is used as a synonym for non-mate. The words "mate" and "nonmate" are traditionally used in identification applications (such as law enforcement search, or background checks) while genuine and impostor are used in verification applications (such as access control).

An error tradeoff characteristic represents the tradeoff between Type II and Type I classification errors. For identification this plots false negative vs. false positive identification rates i.e. FNIR vs. FPIR parametrically with T. Such plots

are often called detection error tradeoff (DET) characteristics or receiver operating characteristic (ROC). These serve the same function – to show error tradeoff – but differ, for example, in plotting the complement of an error rate (e.g.  $TPIR = 1 - FNIR$ ) and in transforming the axes, most commonly using logarithms, to show multiple decades of FPIR. More rarely, the function might be the inverse of the Gaussian cumulative distribution function.

The slides of Figures 10 through 15 discuss presentation and interpretation of DETs used in this document for reporting face identification accuracy. Further detail is provided in formal biometrics testing standards, see the various parts of ISO/IEC 19795 Biometrics Testing and Reporting. More terms, including and beyond those to do with accuracy, appear in ISO/IEC 2382-37 Information technology – Vocabulary – Part 37: Harmonized biometric vocabulary.

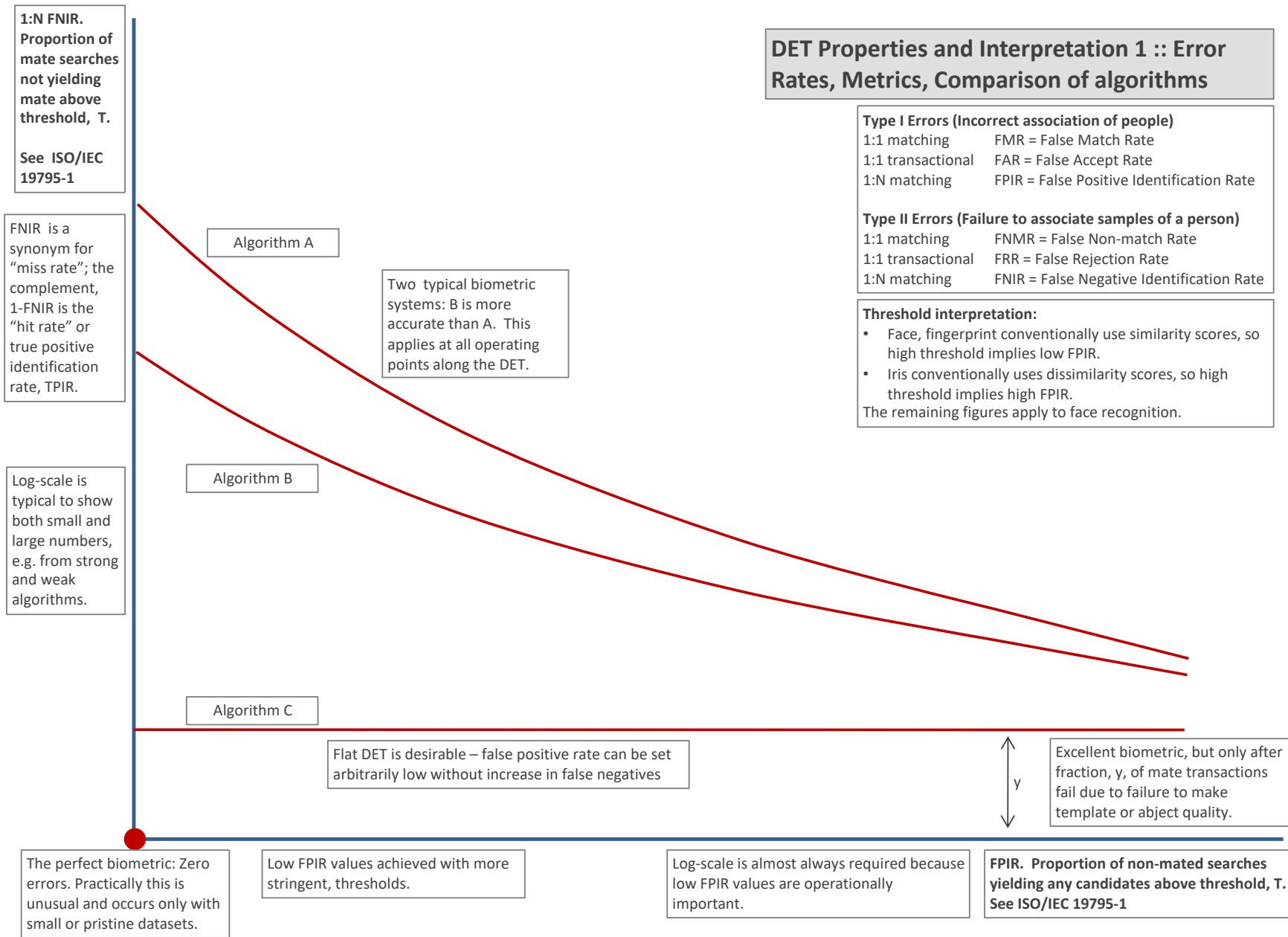


Figure 10: DET as the primary performance reporting mechanism.

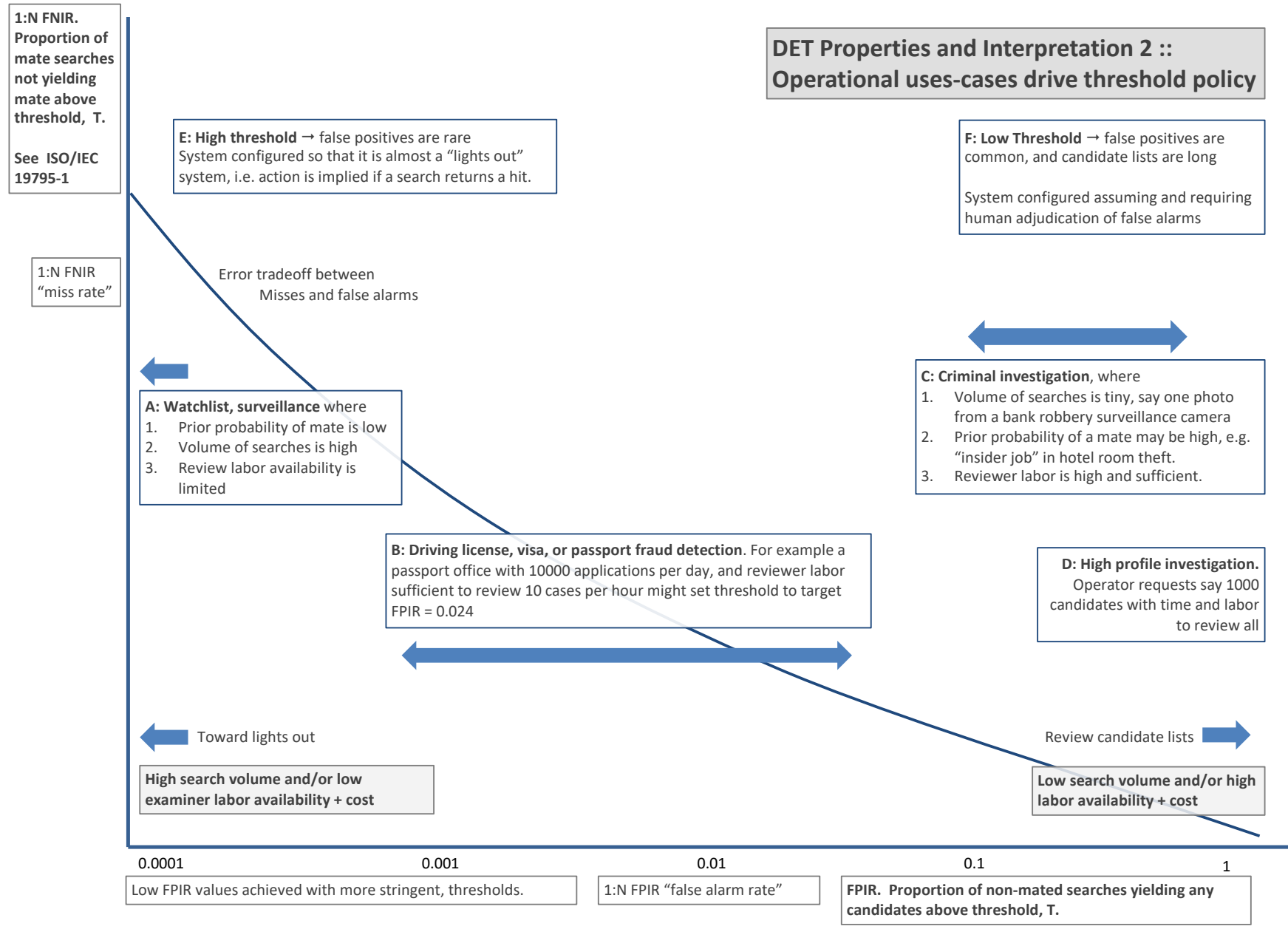
2021 / 09 / 21  
09:55:08FNIR(N, R, T) = False neg. identification rate  
FPIR(N, T) = False pos. identification rate  
N = Num. enrolled subjects  
R = Num. candidates examinedT = Threshold  
T = 0 → Investigation  
T > 0 → Identification

Figure 11: DET as the primary performance reporting mechanism.

2021/09/21  
09:55:08

$\text{FNIR}(N, R, T) =$  False neg. identification rate  
 $\text{FPIR}(N, T) =$  False pos. identification rate

$N$  = Num. enrolled subjects  
 $R$  = Num. candidates examined

$T$  = Threshold

$T = 0 \rightarrow$  Investigation  
 $T > 0 \rightarrow$  Identification

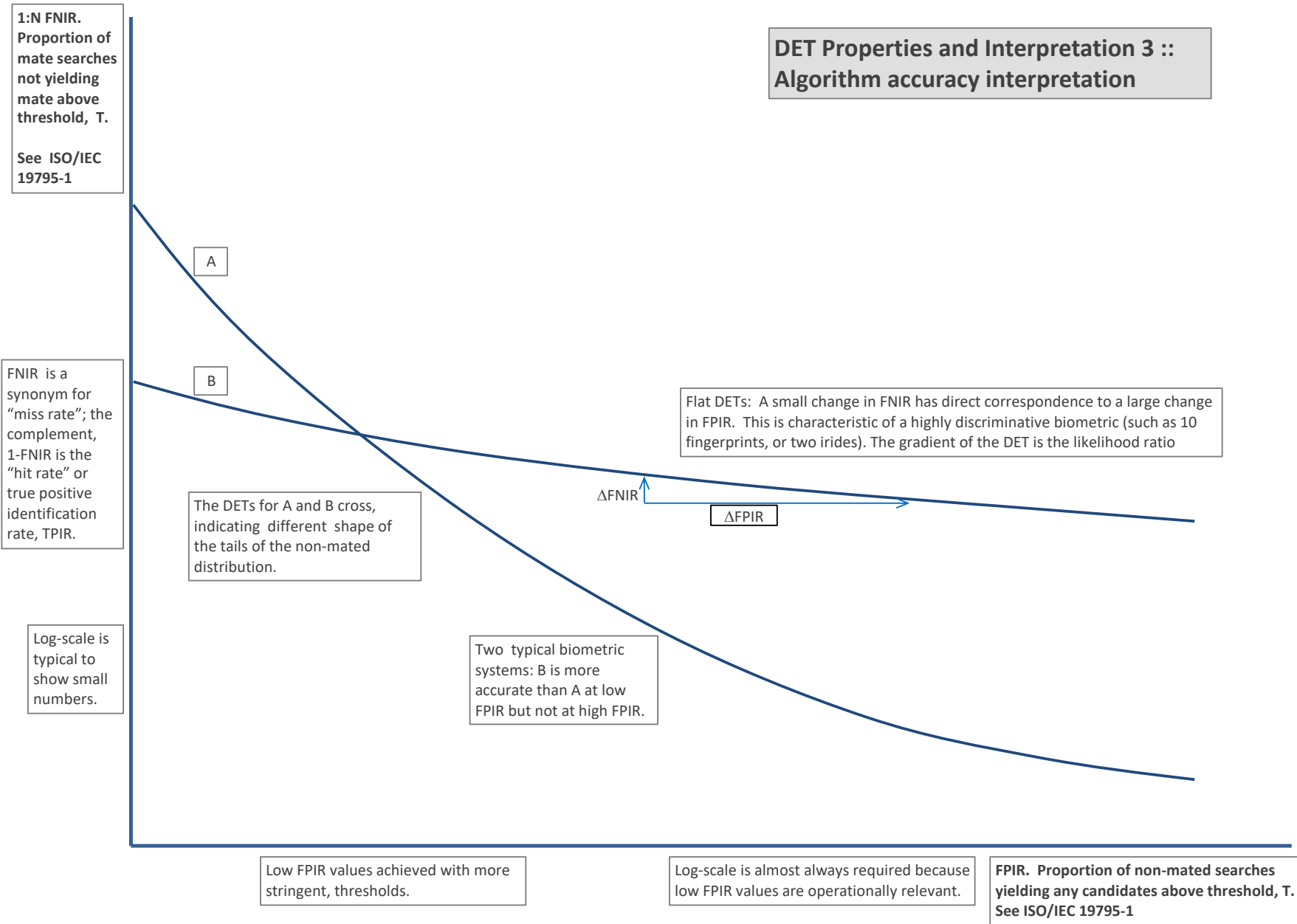


Figure 12: DET as the primary performance reporting mechanism.

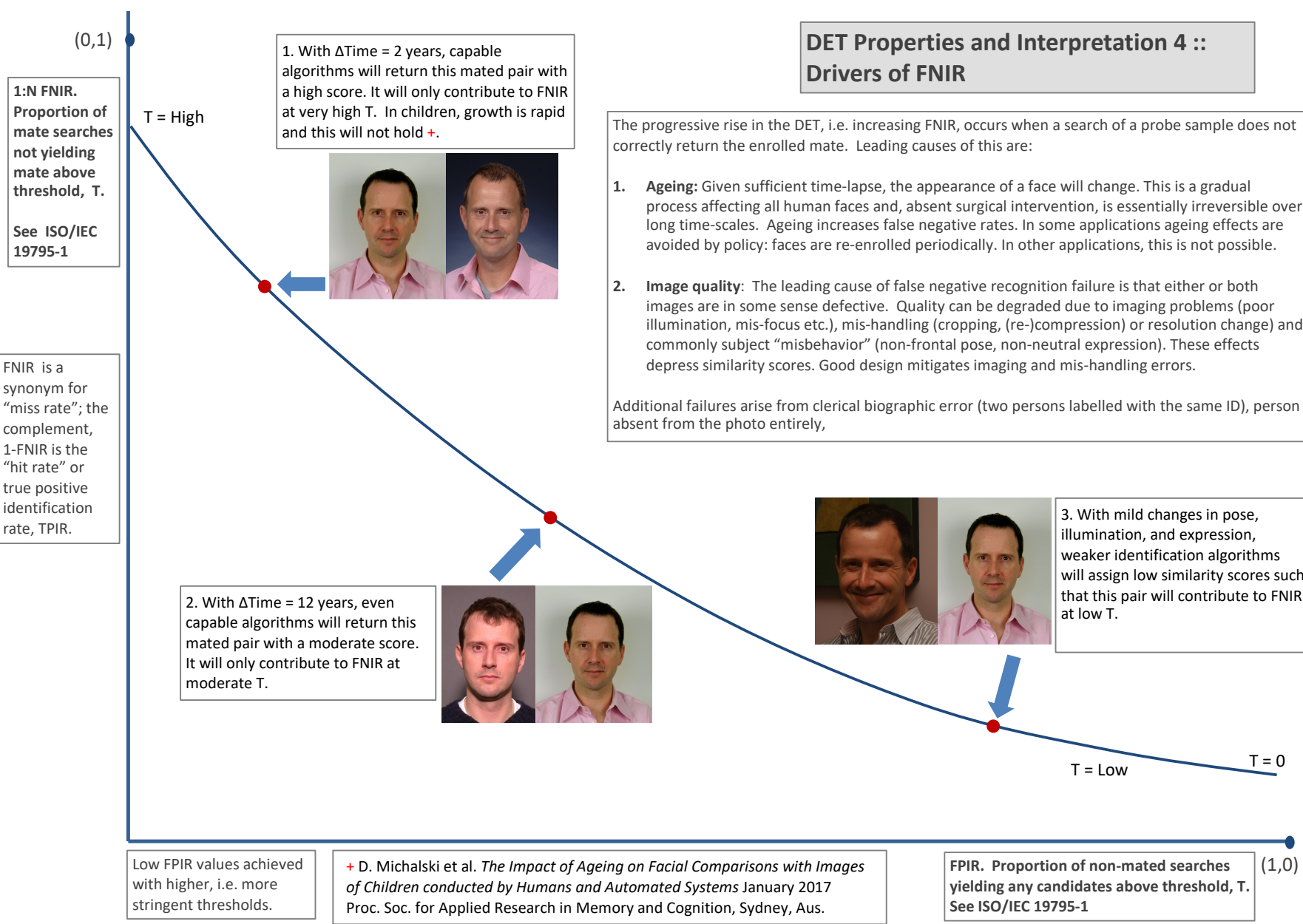
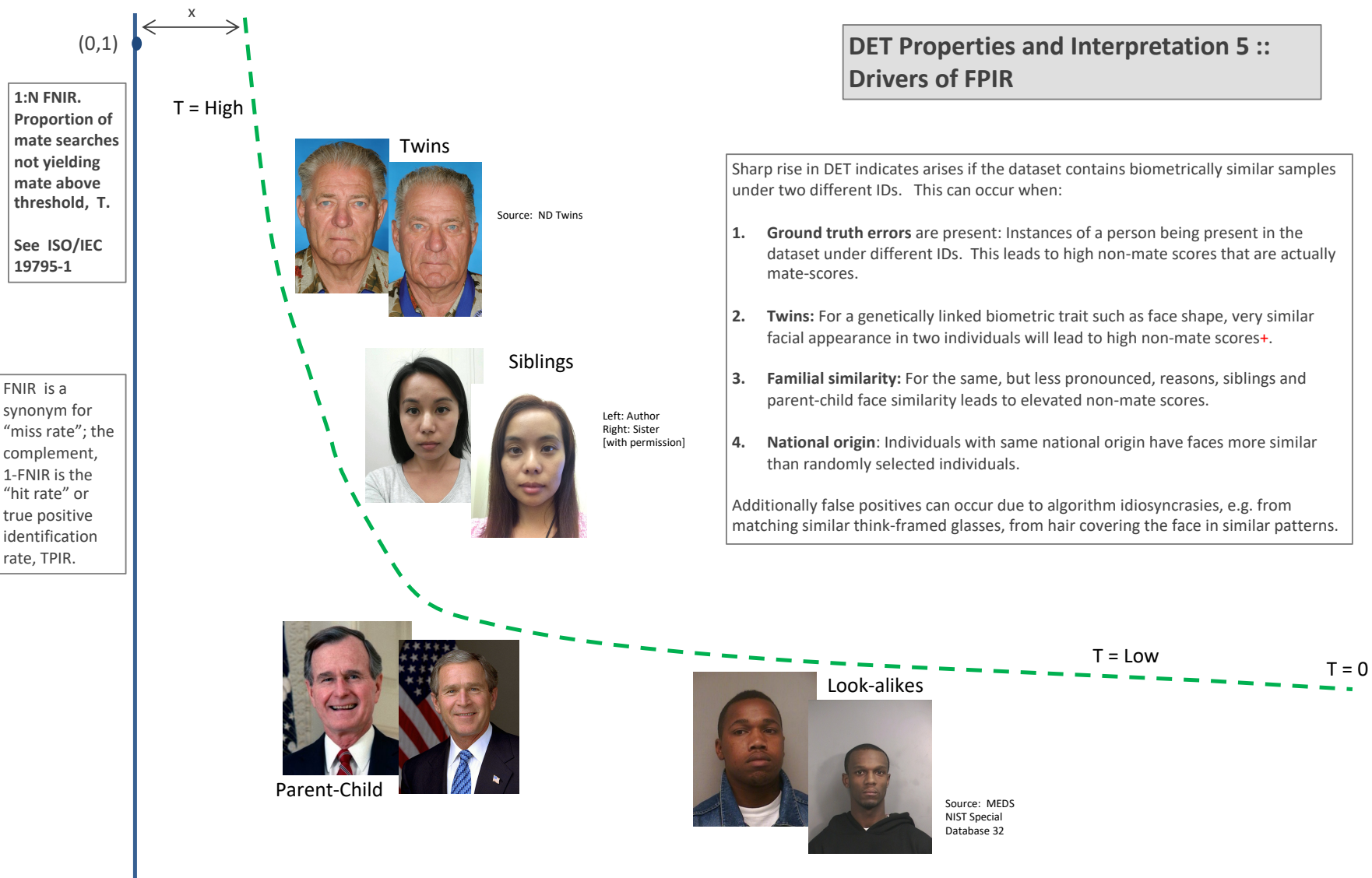


Figure 13: DET as the primary performance reporting mechanism.



Low FPIR values achieved with higher, i.e. more stringent thresholds.

+ NOTE: While most algorithms will not recognize twins correctly, there is at least one face recognition algorithm that can correctly distinguish twins [US Patent: [US7369685B2](#)].

**FPIR**. Proportion of non-mated searches yielding any candidates above threshold, T.  
See ISO/IEC 19795-1

Figure 14: DET as the primary performance reporting mechanism.

2021/09/21  
09:55:08

$\text{FNIR}(N, R, T) =$  False neg. identification rate  
 $\text{FPIR}(N, T) =$  False pos. identification rate

$N$  = Num. enrolled subjects  
 $R$  = Num. candidates examined

$T$  = Threshold

$T = 0 \rightarrow$  Investigation  
 $T > 0 \rightarrow$  Identification

**1:N FNIR.**  
Proportion of mate searches not yielding mate above threshold,  $T$ .  
See ISO/IEC 19795-1

Algorithm X,  
Condition 1

Algorithm X,  
Condition 2

If system X is used with images of different properties, say from different imaging systems, or from different populations, generally both FNIR and FPIR will change. The dotted line joins points of the same threshold. Horizontal (vertical) lines indicate change in FPIR (FNIR) only. Two cases concerning population size are shown below (A and B), for the blue curves.

FNIR is a synonym for "miss rate"; the complement, 1-FNIR is the "hit rate" or true positive identification rate, TPIR.

Log-scale is typical to show small numbers.

Algorithm Y,  
Condition 1

Algorithm Y,  
Condition 2

If DETs are computed for two categories (men and women) or (cameras A and B) or (indoor vs. outdoor), generally the Type I and Type II errors will differ and the line of constant threshold will be neither horizontal nor vertical.

The ideal situation in most applications is that a fixed threshold yields a fixed FPIR so that system owners see no change in false alarms across populations or conditions.

Low FPIR values achieved with higher, i.e. more stringent, thresholds.

Log-scale is often required because low FPIR values are operationally relevant.

**FPIR.** Proportion of non-mated searches yielding any candidates above threshold,  $T$ . See ISO/IEC 19795-1

Figure 15: DET as the primary performance reporting mechanism.

## DET Properties and Interpretation 7 :: Effect of enrolled population size.

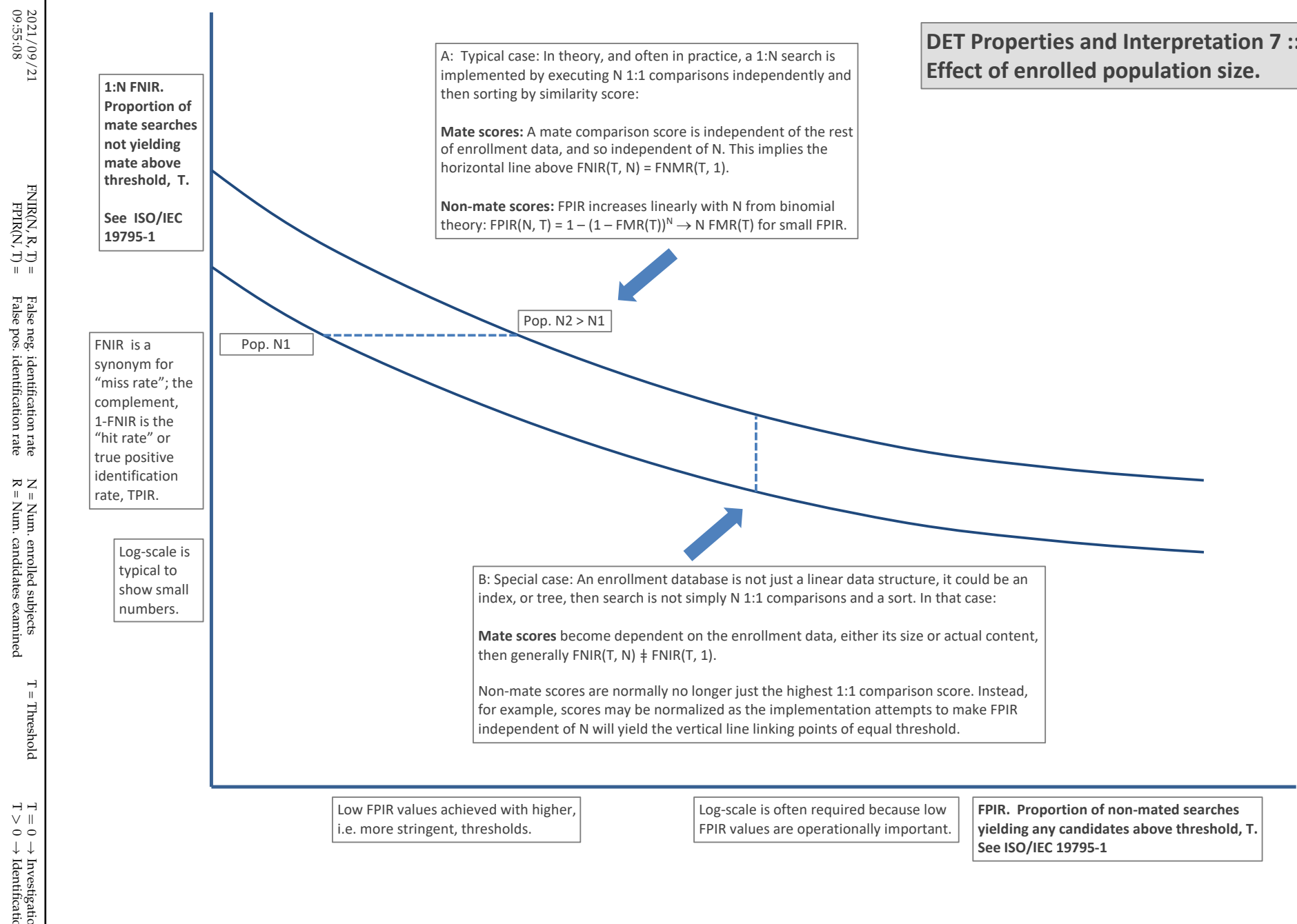


Figure 16: DET as the primary performance reporting mechanism.

## DET Properties and Interpretation 8 :: Non-ideal tests, datasets or systems

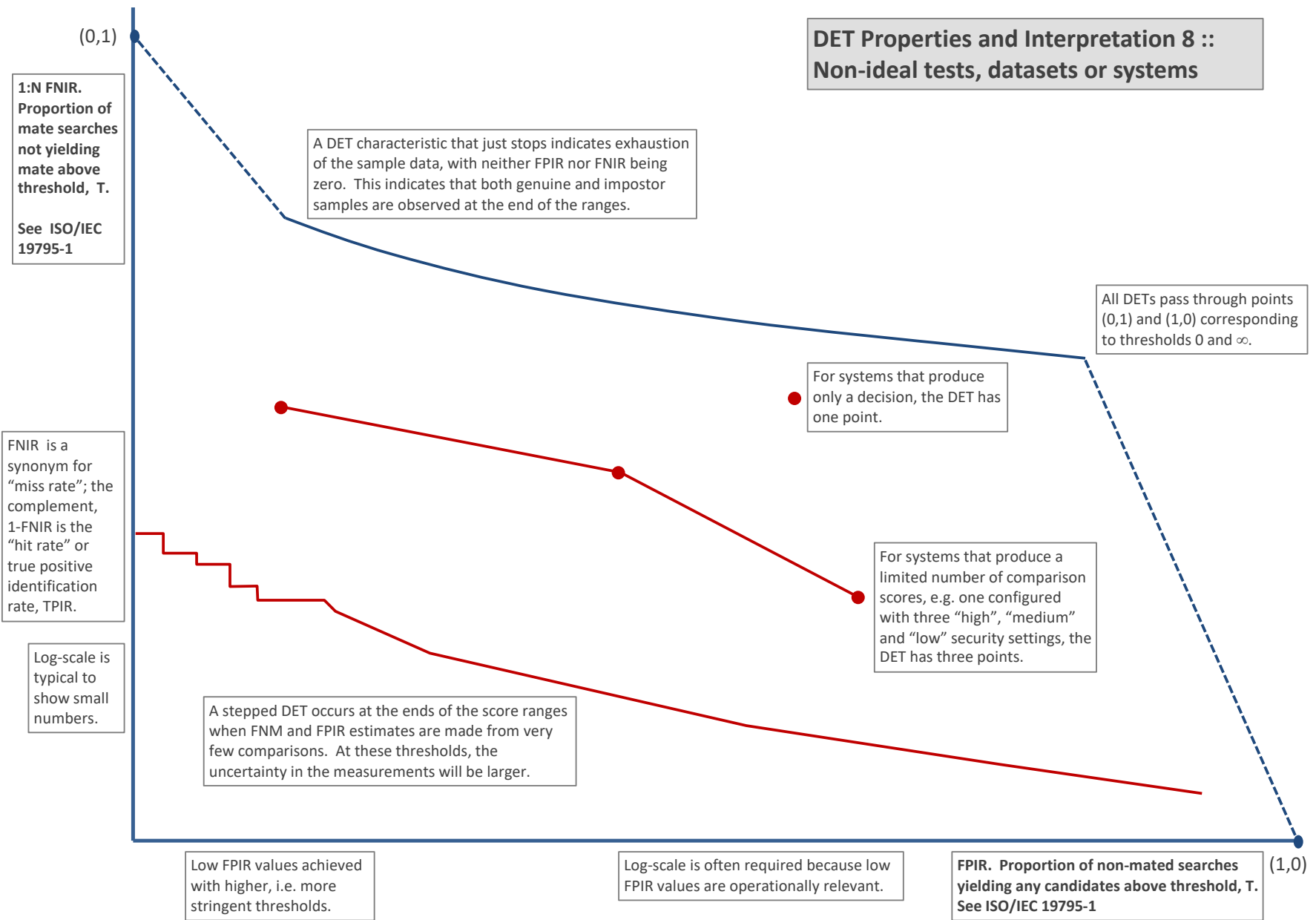


Figure 17: DET as the primary performance reporting mechanism.

### 3.4 Best practice testing requires execution of searches with and without mates

FRVT embeds 1:N searches of two kinds: Those for which there is an enrolled mate, and those for which there is not. The respective numbers for these types of searches appear in Table 1. However, it is common to conduct only mated searches<sup>10</sup>. The cumulative match characteristic is computed from candidate lists produced in mated searches. Even if the CMC is the only metric of interest, the actual trials executed in a test should nevertheless include searches for which no mate exists. As detailed in Table 1 the FRVT reserved disjoint populations of subjects for executing true non-mate searches.

### 3.5 Failure to extract features

During enrollment some algorithms fail to convert a face image to a template. The proportion of failures is the failure-to-enroll rate, denoted by FTE. Similarly, some search images are not converted to templates. The corresponding proportion is termed failure-to-extract, denoted by FTX.

We do not report FTX because we assume that the same underlying algorithm is used for template generation for enrollment and search.

Failure to extract rates are incorporated into FNIR and FPIR measurements as follows.

- ▷ **Enrollment templates:** Any failed enrollment is regarded as producing a zero length template. Algorithms are required by the API [10] to transparently process zero length templates. The effect of template generation failure on search accuracy depends on whether subsequent searches are mated, or non-mated: Mated searches will fail giving elevated FNIR; non-mated searches will not produce false positives so, to first order, FPIR will be reduced by a factor of  $1 - \text{FTE}$ .
- ▷ **Search templates and 1:N search:** In cases where the algorithm fails to produce a search template from input imagery, the result is taken to be a candidate list whose entries have no hypothesized identities and zero score. The effect of template generation failure on search accuracy depends on whether searches are mated, or non-mated: Mated searches will fail giving elevated FNIR; Non-mated searches will not produce false positives, so FPIR will be reduced. Thus given a measurement of false negative and positive rates made over only those where failures-to-extract did not occur, those rates - call them  $\text{FNIR}^\dagger$  and  $\text{FPIR}^\dagger$  - could be adjusted by an explicit measurement of FTX as follows

$$\text{FNIR} = \text{FTX} + (1 - \text{FTX})\text{FNIR}^\dagger \quad (8)$$

$$\text{FPIR} = (1 - \text{FTX})\text{FPIR}^\dagger \quad (9)$$

This approach is the correct treatment for positive-identification applications such as access control where cooperative users are enrolled and make attempts at recognition. This approach is not appropriate to negative identification applications, such as visa fraud detection, in which hostile individuals may attempt to evade detection by submitting poor quality samples. In those cases, template generation failures should be investigated as though a false alarm had occurred.

<sup>10</sup>For example, the [Megaface benchmark](#). This is bad practice for several reasons: First, if a developer knows, or can reasonably assume, that a mate always exists, then unrealistic gaming of the test is possible. A second reason is that it does not put FPIR on equal footing with FNIR and that matters because in most applications, not all searches have mates - not everyone has been previously enrolled in a driving license issuance or a criminal justice system - so addressing between-class separation becomes necessary.

### 3.6 Fixed length candidate lists, threshold independent workload

Suppose an automated face identification algorithm returns  $L$  candidates, and a human reviewer is retained to examine up to  $R$  candidates, where  $R \leq L$  might be set by policy, preference or labor availability. For now, assume also that the reviewer is not provided with, or ignores, similarity scores, and thresholds are not applied. Given the algorithm typically places mates at low (good) ranks, the number of candidates a reviewer can be expected to review can be derived as follows. Note that the reviewer will:

- ▷ Always inspect the first ranked image Frac. reviewed = 1
- ▷ Then inspect those candidates where mate not confirmed at rank 1 Frac. reviewed = 1-CMC(1)
- ▷ Then inspect those candidates where mate not confirmed at rank 1 or 2 Frac. reviewed = 1-CMC(2)

etc. Thus if the reviewer will stop after a maximum of  $R$  candidates, the expected number of candidate reviews is

$$M(R) = 1 + (1 - CMC(1)) + (1 - CMC(2)) + \dots + (1 - CMC(R - 1)) \quad (10)$$

$$= R - \sum_{r=1}^{R-1} CMC(r) \quad (11)$$

A recognition algorithm that front-loads the cumulative match characteristic will offer reduced workload for the reviewer. This workload is defined only over the searches for which a mate exists. In the cases where there truly is no mate, the reviewer would review all  $R$  candidates. Thus, if the proportion of searches for which a mate does exist is  $\beta$ , which in the law enforcement context would be the recidivism rate [3], the full expression for workload becomes:

$$M(R) = \beta \left( R - \sum_{r=1}^{R-1} CMC(r) \right) + (1 - \beta)R \quad (12)$$

$$= R - \beta \sum_{r=1}^{R-1} CMC(r) \quad (13)$$

### 3.7 Timing measurement

Algorithms were submitted to NIST as implementations of the application programming interface(API) specified by NIST in the Evaluation Plan [10]. The API includes functions for initialization, template generation, finalization, search, gallery insert, and gallery delete. Two template generation functions are required, one for the preparation of an enrollment template, and one for a search template.

In NIST's test harness, all functions were wrapped by calls to the C++ std::chrono::high\_resolution\_clock which on the dedicated timing machine counts 1ns clock ticks. Precision is somewhat worse than that however.

## 3.8 Uncertainty estimation

### 3.8.1 Random error

This study leverages operational datasets for measurement of recognition error rates. This affords several advantages. First, large numbers of searches are conducted (see Table 1) giving precision to the measurements. Moreover, for the two mugshot datasets, these do not involve reuse of individuals so binomial statistics can be expected to apply to recognition error counts. In that case, an observed count of a particular recognition outcome (i.e. a false negative or false positive) in  $M$  trials will sustain 95% confidence that the actual error rate is no larger than some value.

As an example, the minimum number of mugshot searches conducted in this report is  $M = 154\,549$ , and for an observed FNIR around 0.002, the measurement supports a conclusion that the actual FNIR is no higher than 0.00228 at 99% confidence level. On the false positive side, we tabulate FNIR at FPIR values as low as 0.001. Given estimates based on 331 254 non-mate trials, the actual FPIR values will be below 0.00115 at 99% confidence. In conclusion, large scale evaluation, without reuse of subjects, supports tight uncertainty bounds on the measured error rates.

### 3.8.2 Systematic error

The FRVT 2018 dataset includes anomalies discovered as a result of inspecting images involved in recognition failures from the most accurate algorithms. Two kinds of failure occur: False negatives (which, for the purpose here, include failures to make templates) and false positives.

**False negative errors:** We reviewed 600 false negative pairs for which either or both of the leading two algorithms did not put the correct mate in the top 50 candidates. Given 154 549 searches, this number represents 0.39% of the total, resulting in  $\text{FNIR} \sim 0.0039$ . Of the 600 pairs:

- ▷ **A: Poor quality:** About 20% of the pairs included images of very low quality, often greyscale, low resolution, blurred, low contrast, partially cropped, interlaced, or noisy scans of paper images. Additionally, in a few cases, the face is injured or occluded by bandages or heavy cosmetics.
- ▷ **B: Ground truth identity label bugs:** About 15% of the pairs are not actually mated. We only assigned this outcome when a pair is clearly not mated.
- ▷ **C: Profile views:** About 35% included an image of a profile (side) view of the face, or, more rarely, an image that was rotated 90 degrees in-plane (roll).
- ▷ **D: Tattoos:** About 30% included an image of a tattoo that contained a face image. These arise from mis-labelling in the parent dataset metadata.
- ▷ **E: Ageing:** There is considerable time-lapse between the two captures.

All these estimates are approximate. Of these, the tattoo and mislabelled images can never be matched. These constitute an accuracy floor in the sample implying that FNIR cannot be below 0.0018<sup>11</sup>. The profile-views, low-quality images, and images with considerable ageing can, in principle, be successfully matched - indeed some algorithms do so - so are not part of the accuracy floor.

<sup>11</sup>This value is the sum of two partial false negative rates:  $\text{FNIR}_B = 0.15 * 0.0039$  plus  $\text{FNIR}_D = 0.3 * 0.0039$

For the microsoft-4 algorithm the lowest miss rate from (recent entry in Table 21) is  $\text{FNIR}(640\,000, 50, 0) = 0.0018$ . This is close to the value estimated from the inspection of misses. It is below the 0.0039 figure because the algorithm does match some profile and poor quality images, that the yitu-2 algorithm does not.

For many tables (e.g. Table 21), the FNIR values obtained for the FRVT-2018 mugshots could be corrected by reducing them by 0.0018. The best values would then be indistinct from zero. The results in this report *were not* adjusted to account for this systematic error.

**False positive errors:** As shown in Figure 1 and discussed in Figure 14 many of the DET characteristics in this report exhibit a pronounced turn upward at low false positive rates. The shape can be caused by identity labelling errors in the ground truth of a dataset, specifically persons present in the database under two IDs such that some proportion of non-mate pairs are actually mated. To look for such possibilities, we merged the highest 1000 non-mate pairs produced by three different algorithms which resulted in 1839 unique pairs. This constitutes 0.56% of all non-mate searches. We assert that it is *very* difficult for human reviewers to assign the pairs into the following three categories: twins; doppelgangers; or ground-truth errors (instances of the same person under two IDs). Given this difficulty we made no attempt to correct any possible ground truth errors except by removing 57 pairs in the following categories:

- ▷ **A: Profile views:** Thirteen pairs included one or two profile-view images. As described in Figure 165, these can cause false positives.
- ▷ **B: Same-session photographs:** For twelve pairs, the images were identical or trivially altered (e.g. cropped) versions of the same photo. These were present under a different ID likely due to some clerical or procedural mistake.
- ▷ **C: Tattoos of faces:** There were fourteen instances of tattoo photographs that contained faces causing false matches.
- ▷ **D: T-shirt faces:** There were six instances of T-shirt photographs (of Bob Marley and Che Guevara) being detected instead of the face and causing false positives.
- ▷ **E: Background faces:** There were twelve instances of one subject appearing in the background of two otherwise correct portrait photos.

Note we did not remove any images where there was a chance that the pair was actually a different person.

In any case, the results in this report have not been adjusted for this systematic error.

## 4 Results

This section gives extensive results for algorithms submitted to FRVT 2018. Three page “report cards” for each algorithm are contained in a [separate supplement](#). Performance metrics were described in section 3. The main results are summarized in tabular form with more exhaustive data included as DET, CMC and related graphs in appendices as follows:

- ▷ The three tables 2-4 list algorithms alongside full developer names, acceptance date, size of the provided configuration data, template size and generation time, and search duration data.
  - The **template generation duration** is most important to applications that require fast response. For example, an eGate taking more than two seconds to produce a template might be unacceptable. Note that GPUs may be of utility in expediting this operation for some algorithms, though at additional expense. Two additional factors should be considered<sup>1213</sup>.
  - The **search duration** is the time taken for a search of a search template into a gallery of  $N$  enrollment templates. This performance variable, together with the volume of searches, is influential on the amount of hardware needed to sustain an operational deployment. This is measured here with the algorithm running on a single core of a contemporary CPU. Search is most simply implemented as  $N$  computations of a distance metric followed by a sort operation to find the closest enrollments. However, considerable optimization of this process is possible, up to and including fast-search algorithms that, by various means, avoid computation of all  $N$  distances.
  - The **template size** is the size of the extracted feature vector (or vectors) and any needed header information. Large template sizes may be influential on bus or network bandwidth, storage requirements, and on search duration. While the template itself is an opaque data blob, the feature dimensionality might be estimated by assuming a four-bytes-per-float encoding. There is a wide range of encodings. For the more accurate algorithm, sizes range from 256 bytes to about 2KB bytes, indicating essentially no consensus on face modeling and template design.
  - The **template size multiplier** column shows how, given  $k$  input images, the size of the template grows. Most implementations internally extract features from each image and concatenate them, and implement some score-level fusion logic during search. Other implementations, including many of the most accurate algorithms, produce templates whose size does not grow with  $k$ . This could be achieved via selection of the best quality image - but this is not optimal in handling ageing where the oldest image could be the best quality. Another mechanism would be feature-level fusion where information is fused from all  $k$  inputs. In any case, as a black-box test, the fusion scheme is proprietary and unknown.
  - The size of the **configuration data** is the total size of all files resident in a vendor-provided directory that contains arbitrary read-only files such as parameters, recognition models (e.g caffe). Generally a large value for this quantity may prohibit the use of the algorithm on a resource-constrained device.

<sup>12</sup>The FRVT 2018 API prohibited threading, so some gains from parallelism may be available on multiple-cores or multiple processors, if the feature extraction code could be distributed across them.

<sup>13</sup>Note also that factors of two or more may be realizable by exploiting modern vector processing instructions on CPUs. It is not clear in our measurements whether all developers exploited Intel’s AVX2 instructions, for example. Our machine was so equipped, but we insisted that the same compiled library should also run on older machines lacking that instruction. The more sophisticated implementations may have detected AVX2 presence and branched accordingly. The less sophisticated may be defaulted to the reduced instruction set. Readers should see the FRVT 2018 API document for the specific chip details.

▷ Tables 21-22 report core rank-based accuracy for mugshot images. The population size is limited to  $N = 1.6$  million identities because this is the largest gallery size on which all algorithms were executed. Notable observations from these tables are as follows:

- **Accuracy gains since 2018:** NIST Interagency Report 8238 documented massive gains over those reported in the FRVT 2014 report, NIST Interagency Report 8009. Further gains are documented in this report. Comparing the most accurate algorithm in November 2018, NEC-3, the value of  $\text{FNIR}(N, L, T)$  reduced from 0.0031 to 0.0024 for the Sensetime-004 algorithm with  $N = 12$  million recent images. The tables show broader gains: many developers have made advances since 2018 with between two and five-fold reduction in errors.
  - **Wide range in accuracy:** The rank-1 miss rates vary from  $\text{FNIR}(N, 1, 0) = 0.0012$  for sensetime-004 up to about 0.5 for the very fast but inaccurate microfocus-x algorithms. Among the developers who are superior to NEC in 2013, the range is from 0.002 to 0.035 for camvi-3. This large accuracy range is consistent with the buyer-beware maxim, and indicates that face recognition software is far from being commoditized.
- ▷ Tables 25-26 report threshold-based error rates,  $\text{FNIR}(N, L, T)$ , for  $N = 1.6$  million for mugshot-mugshot accuracy on FRVT 2014, FRVT 2018, and also (in pink) mugshot-webcam accuracy using FRVT 2018 enrollments. Notable observations from these tables are as follows:
- **Order of magnitude accuracy gains since 2014:** As with rank-based results, the gains in accuracy are substantial, though somewhat reduced. At  $\text{FPIR} = 0.01$ , the best improvement over NEC in 2014 is a 27 fold reduction in  $\text{FNIR}$  using the NEC\_2 algorithm. At  $\text{FPIR} = 0.001$ , the largest gain is a six-fold reduction in  $\text{FNIR}$  via the NEC\_3 algorithm.
  - **Broad gains across the industry:** About 19 companies realize accuracy better than the NEC benchmark from 2014. This is somewhat lower than the 28 developers who succeeded on the rank-1 metric. This may be due to the ubiquity of, and emphasis on, the rank-1 metric in many published algorithm development papers.
  - **Webcam images:** Searches of webcam images give  $\text{FNIR}(N, T)$  values around 2 to 3 times higher than mugshot searches. Notably the leading developers with mugshots are approximately the same with poorer quality webcams. But some developers e.g. Camvi, Megvii, TongYi, and Neurotechnology do improve their relative rankings on webcams, perhaps indicating their algorithms were tailored to less constrained images.
- ▷ Tables 15, 18, 19 and show, respectively, high-threshold, rank 1, and rank 50 FNIR values for all algorithms performing searches into five different gallery sizes,  $N = 640\,000$ ,  $N = 1\,600\,000$ ,  $N = 3\,000\,000$ ,  $N = 6\,000\,000$  and  $12\,000\,000$ . The  $\text{FPIR} = 0.001$  table is included to inform high-volume duplicate detection applications. The Rank-1 table is included as a primary accuracy indicator. The Rank-50 table is included to inform agencies who routinely produce 50 candidates for human-review. The notable results are:

- **Slow growth in rank-based miss rates:**  $\text{FNIR}(N, R)$  generally grows as a power law,  $aN^b$ . From the straight lines of many graphs of Figure 20 this is clearly a reasonable model for most, but not all, algorithms. The coefficient  $a$  can be interpreted as  $\text{FNIR}$  in a gallery of size 1. The more important coefficient  $b$  indicates scalability, and often,  $b \ll 1$ , implies very benign growth in  $\text{FNIR}$ . The coefficients of the models appear in the Tables 18 and 19.
- **Slow growth in threshold-based miss rates:**  $\text{FNIR}(N, T)$  also generally grows as a power law,  $aN^b$  except at the high threshold values corresponding to low  $\text{FPIR}$  values. This is visible in the plots of Figure 36 which

show straight lines except for  $FPIR = 0.001$ , which increase more rapidly with  $N$  above 3 000 000. Each trace in those figures shows  $FNIR(N, T)$  at fixed  $FPIR$  with both  $N$  and  $T$  varying. Thus at large  $N$ , it is usually necessary to elevate  $T$  to maintain fixed  $FPIR$ . This causes increased  $FNIR$ . Why that would no-longer obey a power-law is not known. However, if we expect large galleries to contain individuals with familial relations to the non-mate search images - in the most extreme case, twins - then suppression of false positives becomes more difficult. This is discussed in the Figures starting at Fig. 10

▷ Figure ?? shows false positives from twins against their enrolled siblings, broken out by type of twin: fraternal or identical. The Figure is based on the enrollment of 104 single images on one of a pair of twins, and then the search of 2354 second images. Note that the dataset is heavily skewed towards identical twins which is not representative of the true population. There is also a skew towards same sex fraternal twin pairs compared to different sex fraternal twin pairs again not representative of the true population.

The notable results are:

- For all algorithms tested, the 1087 mated searches (Twin A vs. Twin A) produce scores almost always above typical operational thresholds, with (not shown) matches at rank 1. The images are of good quality, so this is the result expected from the rest of this report.
- For the 1066 identical twin searches (AB), almost all produce the twin at rank 1, with a few producing the mate at further down the candidate lists rank and low score.
- For the 169 fraternal searches (AB) from same sex pairs, most algorithms give a large number of very high scores, implying false positives at all thresholds. However, there are long tails containing lower scores that are correctly below threshold. In general, scores that are higher in this distribution are all rank 1 whereas the lower scores have much higher ranks.
- (Not shown) Of the 169, there are 24 fraternal searches (AB) involving different sex twins. Here most algorithms correctly report scores well below the lowest threshold, and usually not on the candidate list at all.

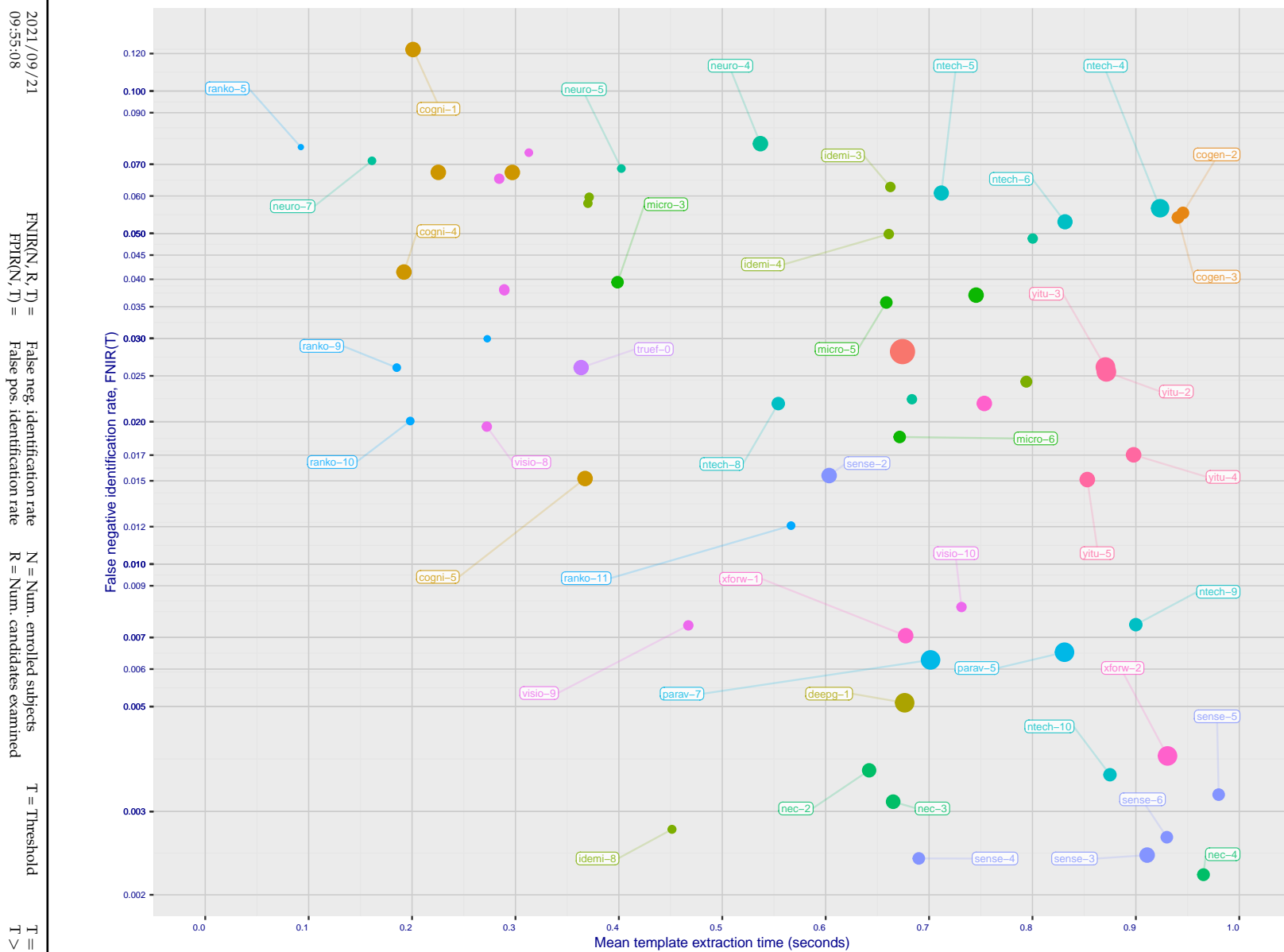


Figure 18: [Mugshot Dataset] Speed-accuracy tradeoff. For developers of the more accurate algorithms the plot shows the tradeoff of high-threshold recognition miss-rates, FNIR( $N, N, T$ ) for FPIR( $N, T$ ) = 0.003, and template generation time. Developers are coded by color. Template size is encoded by the size of the circle. Some labels are quite distant from the respective point, to avoid superposing text. Without any other influences, the assumption would be that taking time to localize the face, and extract features, would lead to better accuracy. The most notable result, for NEC, is that their slower algorithms are much more accurate than the version that extract features in fewer than 90 milliseconds.

2021/09  
09:55:08

$\text{FNI}(N, K, T) =$	False neg. identification rate
$\text{FPIR}(N, T) =$	False pos. identification rate

$N = \text{Num. enrollees}$   
 $R = \text{Num. candida}$

$N$  = Num. enroled subjects  
 $R$  = Num. candidates examined  
 $I$  = Inresitoc

$I = 0 \rightarrow$  investigation  
 $T > 0 \rightarrow$  identification

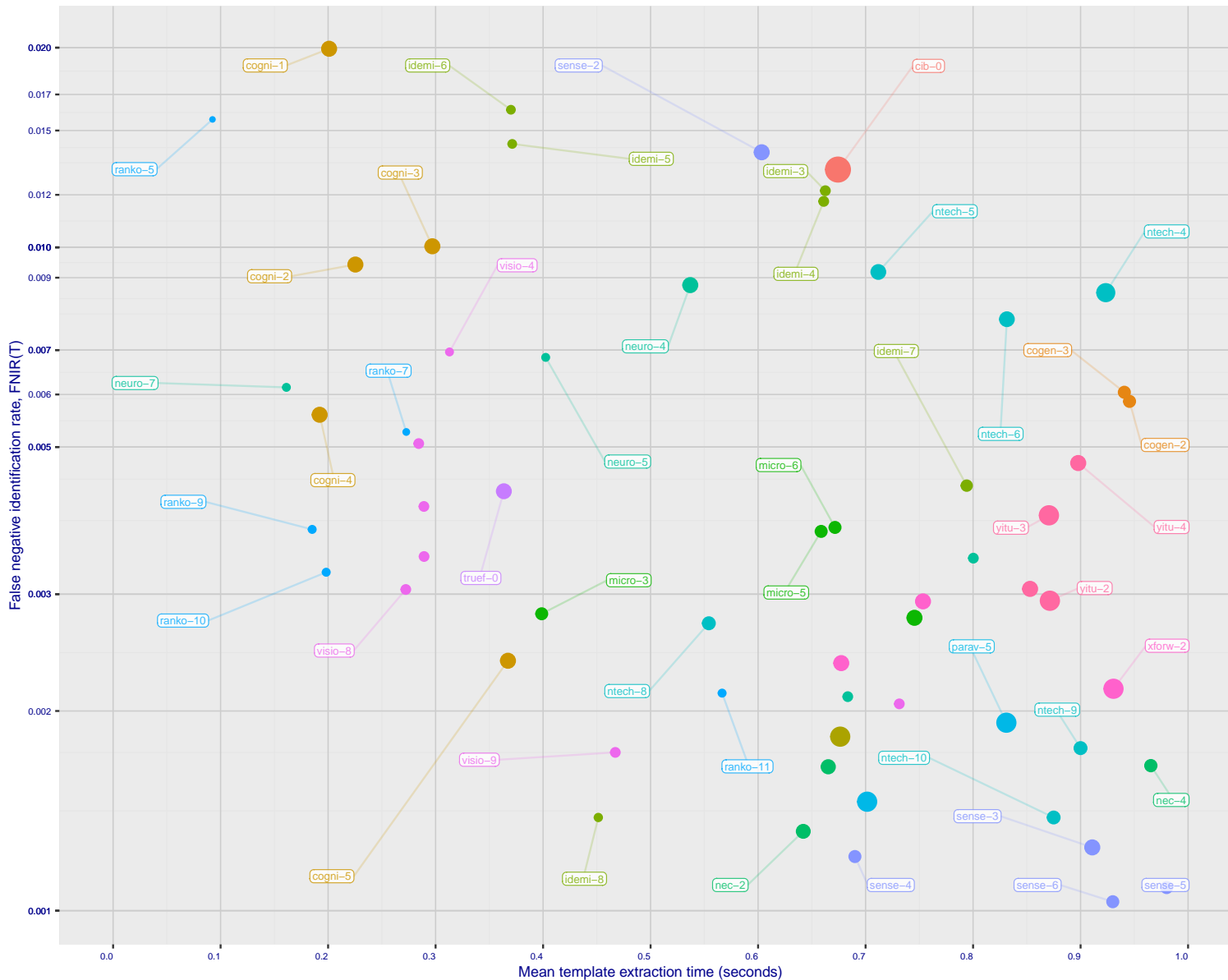


Figure 19: **[Mugshot Dataset] Speed-accuracy tradeoff.** For developers of the more accurate algorithms the plot shows the tradeoff of rank-one recognition miss-rates, FNIR( $N$ , 1, 0), and template generation time. Developers are coded by color. Template size is encoded by the size of the circle. Some labels are quite distant from the respective point, to avoid superposing text. Without any other influences, the assumption would be that taking time to localize the face, and extract features, would lead to better accuracy. This occurs for NEC with their slower algorithm being much accurate than the version that extract features in fewer than 90 milliseconds.

	DEVELOPER	SHORT	SEQ.	VALIDATION	CONFIG <sup>1</sup>		LIB <sup>1</sup>	TEMPLATE GENERATION			FINALIZE <sup>2</sup>		SEARCH DURATION <sup>5</sup>						POWER LAW ( $\mu$ s)							
					FULL NAME	NAME	NUM.	DATE	DATA (MB)	DATA (MB)	SIZE (B)	MULT <sup>3</sup>	TIME (ms) <sup>4</sup>	TIME (s)	L=1	L=50	L=50	L=50	L=50	N=1.6M	N=1.6M	N=3M	N=6M	N=12M		
1	3Divi	3divi	5	2018-10-26	186	51	164	4096	k	90	638	131	28	(76)	538	(70)	537	(70)	1377	(67)	2614	(63)	5530	108	0.07N <sup>1.1</sup>	
2	3Divi	3divi	6	2018-10-26	187	51	30	528	k	91	640	23	5	(11)	33	(12)	33	-	-	-	-	-	-	-	-	
3	Acer Incorporated	acer	000	2020-08-12	35	67	24	512	-	-	15	198	14	4	(52)	295	(53)	295	(43)	623	(61)	2302	(56)	4915	135	0.00N <sup>1.3</sup>
4	Akurat Satu Indonesia	ptakuratsatu	000	2020-10-23	0	572	36	538	-	-	165	905	172	28633	(6)	15	(6)	16	(6)	17	(5)	17	(4)	17	3	6827.74N <sup>0.1</sup>
5	Alchera Inc	alchera	2	2018-10-30	7	14	123	2048	k	6	114	156	63	(143)	2923	(146)	2929	-	-	-	-	-	-	-	-	
6	Alchera Inc	alchera	3	2018-10-30	251	14	78	2048	k	74	531	157	63	(144)	2955	(147)	2956	(125)	6546	(126)	15013	(126)	35262	130	0.10N <sup>1.2</sup>	
7	Alvia / Innovation Sys	isystems	3	2018-10-30	350	784	76	2048	1	-	141	825	108	16	(65)	385	(63)	389	(56)	679	(59)	1822	(81)	9348	136	0.00N <sup>1.3</sup>
8	AllGoVision	allgovision	000	2019-07-30	168	150	104	2048	k	-	47	404	61	12	(147)	3226	(150)	3193	(123)	6129	(123)	12449	(123)	25835	58	1.40N <sup>1.0</sup>
9	AllGoVision	allgovision	001	2020-07-14	283	126	95	2048	-	-	129	777	67	13	(146)	3174	(149)	3183	(122)	6073	(121)	12284	(122)	25701	56	1.42N <sup>1.0</sup>
10	Anke Investments	anke	0	2018-10-30	779	27	144	2072	k	52	429	103	16	(87)	675	(92)	748	(75)	1483	(74)	2968	(68)	6148	79	0.21N <sup>1.1</sup>	
11	Anke Investments	anke	1	2018-10-30	779	27	143	2072	k	53	430	97	15	(92)	707	(95)	769	-	-	-	-	-	-	-	-	
12	Anke Investments	anke	002	2019-06-27	341	401	138	2056	k	86	623	76	13	(86)	624	(87)	682	(67)	1306	(63)	2403	(60)	5082	50	0.30N <sup>1.0</sup>	
13	Aware	aware	5	2018-10-30	368	27	152	3100	k	135	792	140	34	(15)	95	(19)	98	(18)	203	(16)	371	(12)	252	13	4.13N <sup>0.7</sup>	
14	Aware	aware	6	2018-10-30	368	27	12	124	k	134	789	2	2	(30)	158	(30)	162	-	-	-	-	-	-	-	-	
15	Ayonix	ayonix	1	2018-10-29	74	2	51	1036	k	2	12	56	11	(48)	279	(49)	279	-	-	-	-	-	-	-	-	
16	Ayonix	ayonix	2	2018-10-30	74	2	50	1036	1	1	11	82	14	(47)	279	(47)	276	(38)	535	(33)	1087	(33)	2284	65	0.11N <sup>1.0</sup>	
17	Camvi Technologies	camvitech	4	2018-10-30	233	220	44	1024	1	106	686	138	31	(12)	33	(11)	32	(10)	38	(9)	40	(7)	48	4	8492.66N <sup>0.1</sup>	
18	Camvi Technologies	camvitech	5	2018-10-30	257	220	42	1024	1	125	751	136	31	(10)	31	(9)	30	-	-	-	-	-	-	-	-	
19	Canon Inc	cib	000	2020-10-19	426	127	174	8196	-	100	674	160	113	(148)	3589	(152)	3604	(126)	6738	(124)	13495	(124)	27114	24	2.33N <sup>1.0</sup>	
20	Cloudwalk - Hengrui AI Technology	hr	000	2021-02-10	501	392	75	2048	-	164	905	95	15	(49)	282	(47)	276	(37)	539	(40)	1268	(46)	3177	112	0.03N <sup>1.1</sup>	
21	Cognitec Systems GmbH	cognitec	2	2018-10-30	463	26	133	2052	k	-	18	225	126	27	(130)	1733	(132)	1763	(112)	3660	(110)	7279	(108)	1895	54	0.83N <sup>1.0</sup>
22	Cognitec Systems GmbH	cognitec	3	2018-10-30	465	26	132	2052	k	-	28	297	101	16	(129)	1719	(133)	1791	(111)	3638	(109)	7277	(112)	14904	71	0.66N <sup>1.0</sup>
23	Cognitec Systems GmbH	cognitec	004	2021-03-08	384	60	128	2052	-	13	192	74	13	(128)	1673	(130)	1727	(103)	2904	(101)	5801	(99)	11707	21	1.15N <sup>1.0</sup>	
24	Cognitec Systems GmbH	cognitec	005	2021-07-30	460	61	129	2052	-	35	367	43	9	(123)	1556	(124)	1551	(105)	2916	(108)	6561	(109)	13958	85	0.38N <sup>1.1</sup>	
25	Cubox	cubox	000	2021-08-24	529	298	101	2048	-	167	917	49	10	(149)	3646	(146)	4076	(126)	7605	(127)	15871	-	78	1.16N <sup>1.1</sup>		
26	Cyberlink Corp	cyberlink	000	2019-06-12	217	93	130	2052	1	94	654	134	30	(89)	696	(89)	701	(71)	1379	(68)	2639	(70)	6214	67	0.28N <sup>1.0</sup>	
27	Cyberlink Corp	cyberlink	001	2019-10-07	459	102	131	2052	1	50	423	132	28	(90)	698	(89)	700	(69)	1350	(99)	5524	(102)	12031	134	0.00N <sup>1.3</sup>	
28	Cyberlink Corp	cyberlink	002	2020-07-31	333	109	169	4140	-	120	724	164	875	(120)	1353	(151)	3198	(124)	6138	(120)	12205	(106)	13106	15	16.71N <sup>0.8</sup>	
29	Cyberlink Corp	cyberlink	003	2021-01-05	333	100	172	6212	-	109	691	143	35	(71)	488	(90)	723	(72)	1415	(72)	2886	(64)	5643	94	0.12N <sup>1.1</sup>	
30	Cyberlink Corp	cyberlink	004	2021-07-16	371	100	171	6212	-	122	728	122	23	(72)	492	(75)	504	(55)	923	(45)	1448	(48)	3350	18	0.73N <sup>0.9</sup>	
31	Dahua Technology Co Ltd	dahua	0	2018-10-29	276	167	102	2048	k	40	374	120	22	-	(45)	258	-	-	-	-	-	-	-	-		
32	Dahua Technology Co Ltd	dahua	1	2018-10-29	276	167	112	2048	k	36	369	128	28	-	(44)	257	(41)	602	(38)	1202	(44)	3007	119	0.02N <sup>1.2</sup>		
33	Dahua Technology Co Ltd	dahua	002	2019-12-02	607	137	85	2048	k	105	685	115	19	(40)	243	(46)	269	(63)	1189	(73)	2950	(73)	6732	140	0.00N <sup>1.5</sup>	
34	Dahua Technology Co Ltd	dahua	003	2020-11-18	889	154	86	2048	-	119	723	108	18	(50)	283	(49)	249	(32)	468	(31)	935	(30)	1871	20	0.16N <sup>1.0</sup>	
35	Deepglint	deepglint	001	2019-11-15	448	265	154	4096	-	102	676	141	35	(88)	677	(122)	1495	(29)	1724	(70)	2747	(71)	6246	14	25.27N <sup>0.8</sup>	
36	Dermalog	dermalog	5	2018-10-26	0	440	128	1	-	73	528	163	3155	(1)	0	(1)	0	(1)	0	(1)	0	(1)	0	5	66.21N <sup>0.2</sup>	
37	Dermalog	dermalog	6	2018-10-26	0	453	11	256	1	70	507	3	2	(27)	142	(27)	144	(23)	269	(22)	531	(21)	1294	72	0.05N <sup>1.0</sup>	
38	Dermalog	dermalog	007	2020-02-12	0	424	12	18	1	49	410	1	1	(20)	98	(17)	96	(20)	18	(18)	429	(18)	1013	101	0.01N <sup>1.1</sup>	
39	Dermalog	dermalog	008	2021-01-25	0	531	25	512	-	37	370	16	4	(57)	335	(40)	246	(31)	462	(30)	924	(29)	1849	28	0.15N <sup>1.0</sup>	
40	FarBar Inc	f8	001	2019-10-03	266	19	116	2048	k	139	810	79	14	-	-	-	-	-	-	-	-	-	-	-		
41	Fincore Ltd	fincore	000	2021-08-18	250	224	108	2048	-	63	475	38	9	(81)	562	(80)	560	-	-	-	-	-	-	-	-	
42	Gorilla Technology	gorilla	2	2018-10-29	91	1252	56	1132	k	32	338	124	24	(28)	145	(24)	146	(24)	293	(23)	612	(25)	1509	99	0.02N <sup>1.1</sup>	
43	Gorilla Technology	gorilla	3	2018-10-26	94	1252	145	2156	k	76	559	168	12020	-	(130)	2047	-	-	-	-	-	-	-	-		
44	Gorilla Technology	gorilla	004	2020-01-06	182	1244	146	2192	k	42	388	145	41	(51)	286	(52)	285	(64)	1191	(64)	2416	(59)	5036	133	0.00N <sup>1.3</sup>	
45	Gorilla Technology	gorilla	005	2021-02-22	306	1420	173	6288	-	65	483	197	78	(98)	802	(99)	799	(76)	1514	(82)	4454	(77)	8820	121	0.05N <sup>1.2</sup>	
46	Guangzhou Pixel Solutions Co Ltd	pixelall	002	2019-07-01	0	165	149	2560	k	12	190	94	15	(18)	1296	(19)	1334	(96)	2526	(91)	5136	(95)	11045	66	0.52N <sup>1.0</sup>	
47	Guangzhou Pixel Solutions Co Ltd	pixelall	003	2019-11-05	0	690	148	2560	k	113	703	121	22	(15)	1273	(16)	1307	(93)	2474	(92)	5198	(96)	11141	73	0.46N <sup>1.0</sup>	
48	Guangzhou Pixel Solutions Co Ltd	pixelall	004	2020-07-02	0	538	150	2560	k	54	449	107	17	(14)	1259	(15)	1300	(92)	2465	(97)	5492	(97)	11443	84	0.34N <sup>1.1</sup>	
49	Guangzhou Pixel Solutions Co Ltd	pixelall	005	2021-03-23	0	717</td																				

DEVELOPER	SHORT	SEQ.	VALIDATION	CONFIG <sup>1</sup>	LIB <sup>1</sup>	TEMPLATE GENERATION	FINALIZE <sup>2</sup>	SEARCH DURATION <sup>3</sup> MILLISEC						POWER LAW						
								DATA (MB)	DATA (MB)	SIZE (B)	MULT <sup>3</sup>	TIME (MS) <sup>4</sup>	TIME (S)	L=1	L=50	L=50	L=50	L=50	POWER LAW	
FULL NAME	NAME	NUM.	DATE					N=1.6M	N=1.6M	N=1.6M	N=3M	N=6M	N=12M	( $\mu$ s)						
53	Idemia	5	2018-10-29	417	48	<sup>20</sup> 352	1	<sup>39</sup> 371	<sup>22</sup> 5	<sup>24</sup> 137	<sup>25</sup> 138	<sup>29</sup> 437	<sup>27</sup> 724	<sup>26</sup> 1630	<sup>12</sup> 0.01N <sup>1.2</sup>					
54	Idemia	6	2018-10-29	417	48	<sup>21</sup> 352	1	<sup>38</sup> 370	<sup>20</sup> 4	<sup>25</sup> 137	<sup>24</sup> 138	<sup>30</sup> 442	<sup>29</sup> 827	<sup>27</sup> 1646	<sup>12</sup> 0.01N <sup>1.2</sup>					
55	Idemia	007	2020-01-17	738	113	<sup>40</sup> 860	1	<sup>136</sup> 794	<sup>80</sup> 14	<sup>29</sup> 151	<sup>29</sup> 152	<sup>46</sup> 683	<sup>47</sup> 1481	<sup>45</sup> 3022	<sup>13</sup> 0.00N <sup>1.4</sup>					
56	Idemia	008	2021-03-15	378	65	<sup>19</sup> 300	-	<sup>56</sup> 451	<sup>12</sup> 3	<sup>23</sup> 132	<sup>23</sup> 131	<sup>21</sup> 247	<sup>20</sup> 501	<sup>19</sup> 1013	<sup>40</sup> 0.07N <sup>1.0</sup>					
57	Imagus Technology Pty Ltd	005	2021-01-15	222	311	<sup>100</sup> 2048	-	<sup>133</sup> 786	<sup>78</sup> 14	<sup>39</sup> 236	<sup>35</sup> 313	<sup>44</sup> 651	<sup>43</sup> 1361	<sup>34</sup> 2461	<sup>10</sup> 0.03N <sup>1.1</sup>					
58	Imagus Technology Pty Ltd	006	2021-05-27	248	369	<sup>90</sup> 2048	-	<sup>163</sup> 904	<sup>45</sup> 9	<sup>35</sup> 317	<sup>33</sup> 234	<sup>41</sup> 499	<sup>41</sup> 1273	<sup>37</sup> 2727	<sup>12</sup> 0.01N <sup>1.2</sup>					
59	Imperial College London	imperial	000	2019-08-28	461	15	<sup>120</sup> 2048	1	<sup>78</sup> 577	<sup>66</sup> 13	<sup>60</sup> 360	<sup>62</sup> 379	<sup>72</sup> 1626	<sup>29</sup> 4057	<sup>93</sup> 10291	<sup>14</sup> 0.00N <sup>1.5</sup>				
60	Incode Technologies Inc	incode	2	2018-10-29	71	31	<sup>105</sup> 2048	1	<sup>27</sup> 289	<sup>95</sup> 15	<sup>68</sup> 411	<sup>64</sup> 404	-	-	-					
61	Incode Technologies Inc	incode	3	2018-10-29	133	31	<sup>80</sup> 2048	1	<sup>111</sup> 697	<sup>89</sup> 15	<sup>67</sup> 408	<sup>61</sup> 412	<sup>51</sup> 847	<sup>48</sup> 1608	<sup>54</sup> 4486	<sup>10</sup> 0.05N <sup>1.1</sup>				
62	Incode Technologies Inc	incode	004	2019-06-24	254	50	<sup>77</sup> 2048	1	<sup>62</sup> 475	<sup>59</sup> 12	<sup>61</sup> 365	<sup>51</sup> 378	<sup>74</sup> 1482	<sup>50</sup> 1660	<sup>43</sup> 2954	<sup>8</sup> 0.12N <sup>1.1</sup>				
63	Incode Technologies Inc	incode	005	2021-07-29	259	21	<sup>121</sup> 2048	-	<sup>67</sup> 500	<sup>48</sup> 10	<sup>54</sup> 316	<sup>71</sup> 454	<sup>54</sup> 890	<sup>56</sup> 1843	<sup>51</sup> 3640	<sup>9</sup> 0.07N <sup>1.1</sup>				
64	Innovatrics	innovatrics	4	2018-10-30	0	400	<sup>54</sup> 1076	k	<sup>43</sup> 399	<sup>165</sup> 8	<sup>109</sup> 002	<sup>5</sup> 8	<sup>4</sup> 11	<sup>2</sup> 9	<sup>13</sup> 9	<sup>9</sup> 668.38N <sup>0.2</sup>				
65	Innovatrics	innovatrics	005	2019-09-30	0	455	<sup>34</sup> 538	1	<sup>143</sup> 827	<sup>167</sup> 11897	<sup>4</sup> 8	<sup>5</sup> 8	<sup>3</sup> 9	<sup>2</sup> 9	<sup>1</sup> 4055.65N <sup>0.1</sup>					
66	Innovatrics	innovatrics	007	2021-08-16	175	58	<sup>35</sup> 538	-	<sup>130</sup> 777	<sup>81</sup> 14	<sup>19</sup> 97	<sup>20</sup> 100	<sup>16</sup> 188	<sup>17</sup> 378	<sup>16</sup> 788	<sup>19</sup> 0.09N <sup>1.0</sup>				
67	IrexAI	irex	000	2021-02-09	724	46	<sup>151</sup> 3080	-	<sup>148</sup> 844	<sup>19</sup> 19	<sup>65</sup> 616	<sup>83</sup> 600	<sup>60</sup> 1120	<sup>66</sup> 2477	<sup>66</sup> 5863	<sup>88</sup> 0.13N <sup>1.1</sup>				
68	Kakao Enterprise	kakao	000	2021-06-23	404	124	<sup>134</sup> 2052	-	<sup>146</sup> 835	<sup>33</sup> 8	<sup>38</sup> 213	<sup>37</sup> 215	<sup>34</sup> 510	<sup>32</sup> 971	<sup>31</sup> 1955	<sup>9</sup> 0.05N <sup>1.1</sup>				
69	Kedacom International Pte	kedacom	001	2019-09-16	239	36	<sup>18</sup> 292	1	<sup>69</sup> 507	<sup>42</sup> 4	<sup>94</sup> 764	<sup>93</sup> 760	<sup>82</sup> 1940	<sup>75</sup> 2983	<sup>72</sup> 6223	<sup>6</sup> 0.31N <sup>1.0</sup>				
70	Kneron	kneron	000	2020-03-03	366	13	<sup>119</sup> 2048	k	<sup>72</sup> 523	<sup>21</sup> 13	<sup>140</sup> 2535	<sup>143</sup> 2506	<sup>120</sup> 4752	<sup>118</sup> 9696	<sup>121</sup> 20926	<sup>70</sup> 0.95N <sup>1.0</sup>				
71	Kneron	kneron	001	2021-06-10	270	69	<sup>93</sup> 2048	-	<sup>61</sup> 472	<sup>39</sup> 9	<sup>141</sup> 2690	<sup>145</sup> 2642	-	-	-					
72	Line Corporation	line	000	2021-06-02	138	397	<sup>122</sup> 2048	-	<sup>64</sup> 481	<sup>34</sup> 8	<sup>155</sup> 5433	<sup>159</sup> 5418	<sup>131</sup> 10144	-	-	<sup>23</sup> 3.65N <sup>1.0</sup>				
73	Lomonosov Moscow State University	intsyssmu	000	2019-08-19	375	168	<sup>89</sup> 2048	1	<sup>84</sup> 614	<sup>72</sup> 13	<sup>69</sup> 430	<sup>69</sup> 431	<sup>53</sup> 860	<sup>51</sup> 1730	<sup>62</sup> 5353	<sup>117</sup> 0.03N <sup>1.1</sup>				
74	Lookman Electroplast Industries	lookman	3	2018-10-28	203	24	<sup>17</sup> 292	1	<sup>31</sup> 336	<sup>11</sup> 3	<sup>93</sup> 739	<sup>91</sup> 745	<sup>72</sup> 1394	<sup>71</sup> 2817	<sup>70</sup> 6286	<sup>97</sup> 0.13N <sup>1.1</sup>				
75	Lookman Electroplast Industries	lookman	4	2018-10-28	184	24	<sup>37</sup> 548	1	<sup>29</sup> 320	<sup>19</sup> 4	<sup>102</sup> 981	<sup>103</sup> 998	-	-	-					
76	Lookman Electroplast Industries	lookman	005	2019-09-16	239	36	<sup>38</sup> 548	1	<sup>68</sup> 506	<sup>15</sup> 4	<sup>103</sup> 1005	<sup>104</sup> 1008	<sup>97</sup> 2597	<sup>96</sup> 5446	<sup>78</sup> 8939	<sup>95</sup> 0.19N <sup>1.1</sup>				
77	Megvii/Face++	megvii	1	2018-10-28	1703	41	<sup>157</sup> 4096	1	<sup>88</sup> 631	<sup>32</sup> 752	<sup>67</sup> 552	<sup>81</sup> 561	<sup>66</sup> 1222	<sup>62</sup> 2321	<sup>67</sup> 5968	<sup>102</sup> 0.08N <sup>1.1</sup>				
78	Megvii/Face++	megvii	2	2018-10-28	1735	42	<sup>158</sup> 4096	1	<sup>89</sup> 635	<sup>31</sup> 753	<sup>78</sup> 553	<sup>78</sup> 558	-	-	-					
79	MicroFocus	microfocus	5	2018-10-29	94	26	<sup>12</sup> 256	k	<sup>22</sup> 262	<sup>7</sup> 2	<sup>35</sup> 182	<sup>34</sup> 186	<sup>27</sup> 354	<sup>26</sup> 708	<sup>23</sup> 1425	<sup>37</sup> 0.11N <sup>1.0</sup>				
80	MicroFocus	microfocus	6	2018-10-29	94	26	<sup>8</sup> 256	k	<sup>21</sup> 262	<sup>9</sup> 2	<sup>36</sup> 183	<sup>33</sup> 186	-	-	-					
81	Microsoft	microsoft	5	2018-10-29	381	155	<sup>41</sup> 1024	1	<sup>95</sup> 658	<sup>57</sup> 11	<sup>124</sup> 1606	<sup>127</sup> 1673	<sup>108</sup> 3076	<sup>105</sup> 6302	<sup>107</sup> 13160	<sup>49</sup> 0.79N <sup>1.0</sup>				
82	Microsoft	microsoft	6	2018-10-29	478	155	<sup>43</sup> 1024	1	<sup>98</sup> 671	<sup>93</sup> 15	<sup>126</sup> 1642	<sup>126</sup> 1618	<sup>113</sup> 3710	<sup>106</sup> 6401	<sup>105</sup> 12892	<sup>62</sup> 0.68N <sup>1.0</sup>				
83	N-Tech Lab	ntech	5	2018-10-30	1685	113	<sup>73</sup> 1940	k	<sup>117</sup> 711	<sup>151</sup> 55	<sup>42</sup> 243	<sup>42</sup> 246	<sup>36</sup> 538	<sup>34</sup> 1100	<sup>40</sup> 2867	<sup>11</sup> 0.02N <sup>1.1</sup>				
84	N-Tech Lab	ntech	6	2018-10-30	1686	117	<sup>72</sup> 1940	k	<sup>145</sup> 831	<sup>155</sup> 63	<sup>41</sup> 243	<sup>41</sup> 246	<sup>38</sup> 546	<sup>35</sup> 1104	<sup>41</sup> 2873	<sup>11</sup> 0.02N <sup>1.1</sup>				
85	N-Tech Lab	ntechlab	007	2019-06-25	2450	51	<sup>153</sup> 3348	k	<sup>137</sup> 795	<sup>157</sup> 73	<sup>64</sup> 393	<sup>68</sup> 427	<sup>49</sup> 780	<sup>54</sup> 1768	<sup>50</sup> 3499	<sup>68</sup> 0.16N <sup>1.0</sup>				
86	N-Tech Lab	ntechlab	008	2020-01-06	1111	51	<sup>59</sup> 1300	k	<sup>75</sup> 554	<sup>144</sup> 36	<sup>34</sup> 179	<sup>31</sup> 184	<sup>26</sup> 341	<sup>25</sup> 683	<sup>22</sup> 1395	<sup>38</sup> 0.11N <sup>1.0</sup>				
87	N-Tech Lab	ntechlab	009	2021-03-01	1208	42	<sup>58</sup> 1300	-	<sup>162</sup> 899	<sup>142</sup> 25	<sup>33</sup> 178	<sup>32</sup> 184	<sup>25</sup> 336	<sup>24</sup> 676	<sup>26</sup> 1704	<sup>83</sup> 0.05N <sup>1.1</sup>				
88	N-Tech Lab	ntechlab	010	2021-06-24	351	213	<sup>57</sup> 1280	-	<sup>154</sup> 874	<sup>24</sup> 6	<sup>70</sup> 440	<sup>70</sup> 435	<sup>50</sup> 821	<sup>49</sup> 1645	<sup>47</sup> 3337	<sup>44</sup> 0.22N <sup>1.0</sup>				
89	NEC	nec	2	2018-10-30	705	35	<sup>68</sup> 1616	k	<sup>92</sup> 642	<sup>111</sup> 18	<sup>65</sup> 405	<sup>66</sup> 409	<sup>58</sup> 1072	<sup>52</sup> 1755	<sup>53</sup> 4255	<sup>10</sup> 0.06N <sup>1.1</sup>				
90	NEC	nec	3	2018-10-30	774	110	<sup>69</sup> 1712	k	<sup>96</sup> 665	<sup>117</sup> 21	<sup>3</sup> 7	<sup>3</sup> 7	<sup>5</sup> 14	<sup>8</sup> 40	<sup>8</sup> 82	<sup>12</sup> 0.00N <sup>1.2</sup>				
91	NEC	nec	004	2021-07-19	971	63	<sup>55</sup> 1104	-	<sup>174</sup> 965	<sup>26</sup> 7	<sup>38</sup> 349	<sup>38</sup> 351	<sup>45</sup> 662	<sup>42</sup> 1330	<sup>36</sup> 2685	<sup>38</sup> 0.20N <sup>1.0</sup>				
92	Neurotechnology	neurotech	5	2018-10-30	266	53	<sup>256</sup> k	<sup>44</sup> 402	<sup>82</sup> 9	<sup>97</sup> 835	<sup>98</sup> 839	<sup>78</sup> 1690	<sup>76</sup> 3219	<sup>79</sup> 8955	<sup>89</sup> 0.19N <sup>1.1</sup>					
93	Neurotechnology	neurotech	6	2018-10-30	564	53	<sup>13</sup> 256	k	<sup>121</sup> 726	<sup>6</sup> 2	<sup>98</sup> 839	<sup>99</sup> 842	-	-	-					
94	Neurotechnology	neurotech	007	2019-10-03	57	51	<sup>10</sup> 256	k	<sup>76</sup> 161	<sup>5</sup> 2	<sup>107</sup> 1118	<sup>108</sup> 1110	<sup>86</sup> 2143	<sup>81</sup> 4397	<sup>80</sup> 9045	<sup>46</sup> 0.55N <sup>1.0</sup>				
95	Neurotechnology	neurotechnology	008	2021-03-22	355	49	<sup>32</sup> 514	-	<sup>138</sup> 800	<sup>18</sup> 4	<sup>110</sup> 1167	<sup>111</sup> 1149	<sup>88</sup> 2266	<sup>85</sup> 4573	<sup>86</sup> 9586	<sup>52</sup> 0.55N <sup>1.0</sup>				
96	Neurotechnology	neurotechnology	009	2021-09-01	246	82	<sup>20</sup> 513	-	<sup>104</sup> 683	<sup>10</sup> 3	<sup>105</sup> 1035	<sup>106</sup> 1049	<sup>84</sup> 1977	<sup>80</sup> 4270	<sup>79</sup> 8756	<sup>77</sup> 0.32N <sup>1.1</sup>				
97	Newland Computer Co Ltd	newland	2	2018-10-30	96	27	<sup>84</sup> 2048	-	<sup>151</sup> 855	<sup>95</sup> 15	<sup>165</sup> 8741	<sup>170</sup> 8854	<sup>142</sup> 17892	<sup>139</sup> 39356	-	<sup>10</sup> 1.32N <sup>1.1</sup>				
98	Nobilis	nobilis	1	2018-10-3																

	DEVELOPER	SHORT	SEQ.	VALIDATION	CONFIG <sup>1</sup>	LIB <sup>1</sup>	TEMPLATE GENERATION	FINALIZE <sup>2</sup>	SEARCH DURATION <sup>5</sup> MILLISEC						
									DATA (MB)	DATA (MB)	SIZE (B)	MULT <sup>3</sup>	TIME (MS) <sup>4</sup>	TIME (S)	POWER LAW
	FULL NAME	NAME	NUM.	DATE					N=1.6M	N=1.6M	N=1.6M	N=3M	N=6M	N=12M	( $\mu$ s)
105	Qnap Security	qnap	000	2021-07-28	182	15	105 2048	-	57 457	41 9	(112) 1231	(131) 1763	-	-	-
106	Quantasoft	quantasoft	1	2018-10-30	276	452	97 2048	k	41 385	25 6	(166) 15422	(171) 14858	(140) 14717	-	(116) 18323
107	Rank One Computing	rankone	4	2018-10-09	0	101	1 85	k	36	27 7	(21) 101	(21) 101	(17) 190	-	22 0.07N <sup>1.0</sup>
108	Rank One Computing	rankone	5	2018-10-24	0	101	5 133	k	4 92	28 7	(26) 140	(26) 144	(22) 266	(21) 525	(20) 1049
109	Rank One Computing	rankone	006	2019-06-03	0	133	6 165	k	20 245	32 8	-	-	-	-	20 0.11N <sup>1.0</sup>
110	Rank One Computing	rankone	007	2019-11-12	0	137	7 165	k	24 272	30 7	(22) 116	(19) 215	(19) 439	(17) 877	36 0.07N <sup>1.0</sup>
111	Rank One Computing	rankone	009	2020-06-26	0	105	14 260	k	11 185	54 11	(16) 95	(18) 96	(14) 181	(14) 362	(15) 727
112	Rank One Computing	rankone	010	2020-11-05	0	135	15 261	-	14 198	50 10	(17) 95	(15) 95	(13) 178	(13) 357	(14) 714
113	Rank One Computing	rankone	011	2021-08-27	0	175	16 261	-	77 566	35 8	(18) 96	(16) 95	(15) 183	(15) 370	(13) 714
114	Realnetworks Inc	realnetworks	2	2018-10-30	105	104	165 4104	k	19 241	129 28	(132) 2008	(137) 2048	(115) 4194	(114) 8642	(113) 15035
115	Realnetworks Inc	realnetworks	003	2019-06-12	93	102	71 1848	k	10 173	65 13	(109) 1145	(109) 1132	(85) 2142	(93) 5241	(94) 10495
116	Realnetworks Inc	realnetworks	004	2019-10-17	94	102	70 1848	1	9 171	53 11	(108) 1143	(110) 1137	(87) 2149	(87) 4740	(89) 9693
117	Realnetworks Inc	realnetworks	005	2021-06-23	168	209	136 2056	-	30 332	37 9	(127) 1654	(125) 1616	(107) 3030	(103) 6068	(103) 12134
118	Remark Holdings	remarkai	000	2019-06-12	234	1092	96 2048	k	93 650	64 12	(159) 5776	(161) 5703	(133) 11604	(138) 32133	(137) 91436
119	Remark Holdings	remarkai	0	2018-10-30	187	847	81 2048	k	79 593	84 14	(158) 5685	(162) 5723	-	-	-
120	Remark Holdings	remarkai	1	2018-10-30	187	847	108 2048	k	51 427	88 14	(157) 5680	(163) 5761	(136) 12475	(136) 28726	(135) 59618
121	Rendip	rendip	000	2021-05-21	0	416	115 2048	-	159 890	42 9	(43) 249	(59) 368	(48) 697	(46) 1452	(42) 2926
122	Samsung S1 Corp	s1	000	2021-06-03	257	196	156 4096	-	152 865	116 20	(163) 6715	(168) 6794	(139) 13032	(135) 26372	(134) 55723
123	Scanova Ltd	scanova	000	2020-01-15	250	446	118 2048	-	114 705	86 14	(122) 1419	(121) 1412	(106) 3008	(109) 11616	(101) 12012
124	Scanova Ltd	scanova	001	2020-09-10	250	446	82 2048	-	101 675	70 13	(119) 1321	(120) 1320	(94) 2502	(90) 5047	(91) 10163
125	Sensetime Group	sensetime	0	2018-10-30	525	6	167 4104	k	110 693	146 41	(73) 498	(72) 501	(65) 1212	(58) 2281	(50) 5032
126	Sensetime Group	sensetime	1	2018-10-30	525	6	166 4104	k	87 628	151 48	(75) 516	(73) 502	(61) 1146	(60) 2301	(55) 4765
127	Sensetime Group	sensetime	002	2019-06-03	523	6	139 2056	k	82 603	105 18	(59) 359	(60) 370	(80) 1897	(83) 4508	(85) 9543
128	Sensetime Group	sensetime	003	2019-12-02	769	76	137 2056	1	166 910	113 19	(153) 4885	(158) 4989	(135) 12325	(132) 24712	(130) 49445
129	Sensetime Group	sensetime	004	2020-08-10	456	29	46 1032	-	108 690	63 12	(138) 2490	(141) 2477	(119) 4654	(117) 9402	(120) 19651
130	Sensetime Group	sensetime	005	2020-12-17	631	39	48 1032	-	175 980	52 11	(136) 2459	(135) 3939	(127) 7398	(125) 14768	(119) 19016
131	Sensetime Group	sensetime	006	2021-07-26	526	54	47 1032	-	168 929	31 7	(135) 2414	(140) 2422	(117) 4527	(115) 9128	(117) 18640
132	Shaman Software	shaman	6	2018-10-26	0	200	113 2048	k	115 706	85 14	(84) 603	(84) 612	-	-	-
133	Shaman Software	shaman	7	2018-10-26	0	200	117 2048	k	116 707	87 14	(83) 602	(85) 614	(62) 1187	(65) 2448	(61) 5083
134	Shanghai Yitu Technology	yitu	4	2018-10-30	2119	136	141 2070	1	161 897	145 45	(117) 1288	(113) 1203	(91) 2440	(94) 5241	(88) 9671
135	Shanghai Yitu Technology	yitu	5	2018-10-30	2043	136	142 2070	1	150 853	148 44	(113) 1237	(112) 1199	(95) 2513	(89) 5013	(87) 9620
136	Smilart	smilart	4	2018-10-30	65	89	25 512	k	8 167	17 4	(167) 16137	(172) 15633	-	-	-
137	Smilart	smilart	5	2018-10-30	562	89	111 2048	k	85 450	84 14	-	-	-	-	-
138	StaQu Technologies	staqu	000	2021-08-30	1018	690	162 4096	-	142 826	129 24	(150) 4950	(157) 4933	-	-	-
139	Synesis	synesis	003	2019-07-04	143	17	98 2048	k	17 211	60 12	(74) 507	(74) 502	(89) 2297	(84) 4564	(83) 9452
140	Synesis	synesis	3	2018-10-30	237	150	163 4096	k	5 99	137 29	(95) 789	(97) 801	(83) 1941	(78) 3888	(76) 8810
141	Synesis	synesis	005	2020-09-08	494	24	168 4104	-	127 756	123 24	(100) 877	(100) 865	(109) 3182	(86) 4658	(90) 9750
142	Tech5 SA	tech5	001	2019-08-19	1394	116	62 1536	k	158 887	47 10	(62) 383	(94) 766	(106) 2767	(104) 6149	(69) 6178
143	Tech5 SA	tech5	002	2021-04-07	727	112	31 513	-	171 940	15 4	(152) 4682	(167) 6689	(137) 12541	(133) 25145	(132) 50239
144	Tencent Deepsea Lab	deepsea	001	2019-07-29	250	323	91 2048	1	124 737	62 12	(104) 1021	(105) 1020	(102) 2774	(100) 5767	(104) 12341
145	Tevian	tevian	5	2018-10-30	773	15	83 2048	1	48 405	92 15	(66) 405	(68) 408	(82) 854	(83) 1757	(49) 3380
146	Tevian	tevian	006	2021-04-16	769	19	49 1032	-	80 597	46 10	(53) 295	(54) 295	(40) 578	(37) 1187	(39) 2741
147	Thales	cogent	2	2018-10-30	681	39	53 1043	k	172 945	127 27	(133) 2017	(138) 2144	(118) 4298	(113) 8472	(115) 16429
148	Thales	cogent	3	2018-10-30	681	39	52 1043	k	170 940	44 9	(111) 1230	(117) 1311	(100) 2687	(95) 5398	(92) 10184
149	Thales	cogent	004	2021-02-10	1376	59	135 2053	-	173 947	77 14	(142) 2903	(134) 1911	(110) 3566	(111) 7498	(114) 16370
150	TigerIT Americas LLC	tiger	2	2018-10-29	416	518	124 2052	k	59 461	96 15	(131) 1816	(135) 1911	(121) 3833	(112) 7526	(111) 14820
151	TigerIT Americas LLC	tiger	3	2018-10-30	416	518	125 2052	k	58 461	174 37431	(37) 191	(35) 189	-	-	-
152	Toshiba	toshiba	0	2018-10-30	961	105	67 1548	k	156 876	58 12	(162) 6153	(164) 6236	(134) 12221	(134) 25355	(131) 49448
153	Toshiba	toshiba	1	2018-10-30	961	105	140 2060	k	155 875	175 44701	(161) 6007	(165) 6355	-	-	-
154	Tripleize	aize	001	2021-08-06	262	150	79 2048	-	45 402	40 9	(149) 3087	(148) 3080	-	-	-
155	Trueface.ai	trueface	000	2021-01-27	247	119	74 2000	-	33 363	68 13	(44) 271	(57) 327	(42) 614	(39) 1239	(35) 2678
156	Veridas Digital Authentication Solutions S.L.	veridas	001	2021-03-05	347	875	87 2048	-	153 872	69 13	(156) 5493	(160) 5469	(132) 10350	(130) 20655	(127) 41264

**Notes**

1 Configuration size does not capture static data present in libraries. Libraries are included but the size also includes any ancillary libraries for image processing (e.g. openCV) or numerical computation (e.g. blas).

2 Finalization is the processing of converting  $N = 1600000$  templates into a searchable data structure an operation which can be a simple copy, or the building of an index or tree, for example. The duration of the operation may be data dependent, and may not be linear in the number of input templates.3 This multiplier expresses the increase in template size when  $k$  images are passed to the template generation function.

4 All durations are measured on Intel®Xeon®CPU E5-2630 v4 @ 2.0GHz processors. Estimates are made by wrapping the API function call in calls to std::chrono::high\_resolution\_clock which on the machine in (3) counts 1ns clock ticks. Precision is somewhat worse than that however.

5 Search durations are measured as in the prior note. The power-law model in the final column mostly fits the empirical results in Figure 166. However in certain cases the model is not correct and should not be used numerically.

2021 / 09 / 21  
09:55:08FNIR(N, R, T) = False neg. identification rate  
FPIR(N, T) = False pos. identification rateN = Num. enrolled subjects  
R = Num. candidates examinedT = Threshold  
T ∨ 0 → Investigation

Table 4: Summary of algorithms and properties included in this report. The blue superscripts give ranking for the quantity in that column. Missing search durations, denoted by “-”, are absent because those runs were not executed, usually because we did not run on the larger galleries. Caution: The power-law model is sometimes an incorrect model. It is included here only to show broad sublinear behavior, which is flagged in green. The models should not be used for prediction.

	DEVELOPER FULL NAME	SHORT NAME	SEQ. NUM.	VALIDATION DATE	CONFIG <sup>1</sup> DATA (MB)	LIB <sup>1</sup> DATA (MB)	TEMPLATE GENERATION			FINALIZE <sup>2</sup> TIME (S)	SEARCH DURATION <sup>5</sup> MILLISEC						POWER LAW ( $\mu$ s)							
							SIZE (B)	MULT <sup>3</sup>	TIME (MS) <sup>4</sup>		L=1		L=50		L=50									
											N=1.6M	N=1.6M	N=1.6M	N=3M	N=6M	N=12M								
157	Veridas Digital Authentication Solutions S.L.	veridas	002	2021-07-06	347	870	103	2048	-	157	877	51	10	(56)	322	(56)	325	(47)	685	(44)	1365	(38)	2730	810.09N <sup>1.1</sup>
158	Viettel Group	vts	000	2021-03-12	250	257	94	2048	-	66	492	162	2295	(2)	4	(2)	4	(2)	6	(4)	11	-	-	120.61N <sup>0.6</sup>
159	Viettel Group	vts	001	2021-07-16	352	600	99	2048	-	160	891	119	21	(137)	2477	(142)	2487	(118)	4644	(116)	9313	(118)	18713	321.53N <sup>1.0</sup>
160	Vigilant Solutions	vigilant	5	2018-10-30	335	122	66	1544	k	128	762	112	19	-	(129)	1720	-	-	-	-	-	-	-	
161	Vigilant Solutions	vigilant	6	2018-10-30	337	122	65	1544	k	140	816	118	21	-	(128)	1713	-	-	-	-	-	-	-	
162	Vigilant Solutions	vigilantsolutions	007	2021-01-08	340	51	63	1544	-	85	616	106	16	(121)	1354	(120)	1352	(104)	2911	(102)	5966	(98)	11466	910.27N <sup>1.1</sup>
163	Vigilant Solutions	vigilantsolutions	008	2021-07-23	340	51	64	1544	-	48	403	73	13	(106)	1062	(107)	1061	(90)	2330	(98)	5520	(84)	9499	110.11N <sup>1.1</sup>
164	Visidon	visidon	1	2018-10-30	166	42	127	2052	k	97	667	98	15	(180)	4370	(156)	4472	(129)	8454	(128)	17262	(125)	34288	412.40N <sup>1.0</sup>
165	Visidon	vd	002	2021-05-18	248	42	128	2052	-	10	687	39	9	(134)	2089	(139)	2336	-	-	-	-	-	-	
166	VisionLabs	visionlabs	6	2018-10-30	360	17	29	512	1	28	289	171	20290	(13)	36	(13)	36	(11)	39	(10)	44	(8)	53	83211.93N <sup>0.2</sup>
167	VisionLabs	visionlabs	7	2018-10-30	360	17	27	512	1	28	289	173	34666	(14)	63	(14)	63	(12)	72	(12)	80	(10)	115	102076.32N <sup>0.2</sup>
168	VisionLabs	visionlabs	008	2019-06-18	348	17	28	512	1	23	272	169	12747	(8)	23	(7)	24	(7)	26	(6)	29	(5)	33	62539.61N <sup>0.2</sup>
169	VisionLabs	visionlabs	009	2020-08-04	689	20	26	512	-	69	467	170	13245	(9)	23	(8)	29	(8)	34	(11)	61	(11)	145	118.88N <sup>0.6</sup>
170	VisionLabs	visionlabs	010	2021-02-05	1042	20	23	512	-	123	731	166	11837	(7)	21	(10)	32	(9)	36	(7)	39	(6)	43	73183.79N <sup>0.2</sup>
171	Vocord	vocord	5	2018-10-30	1035	185	39	768	k	131	780	20	7	(31)	158	(36)	204	(28)	383	(28)	767	(24)	1466	340.12N <sup>1.0</sup>
172	Vocord	vocord	6	2018-10-30	1035	185	175	10240	k	132	785	161	243	(32)	170	(38)	216	-	-	-	-	-	-	
173	Xforward AI Technology	xforwardai	000	2020-07-24	236	171	92	2048	-	126	753	75	13	(151)	4603	(169)	7647	(141)	15723	(131)	23900	(133)	53729	110.56N <sup>1.1</sup>
174	Xforward AI Technology	xforwardai	001	2021-01-21	332	50	114	2048	-	103	677	104	16	(160)	5887	(155)	4384	(130)	8798	(129)	18553	(118)	48993	110.32N <sup>1.1</sup>
175	Xforward AI Technology	xforwardai	002	2021-05-24	691	50	155	4096	-	169	930	110	18	(164)	6957	(166)	6400	(138)	12659	(137)	31077	(136)	65158	1160.52N <sup>1.1</sup>

## Notes

- 1 Configuration size does not capture static data present in libraries. Libraries are included but the size also includes any ancillary libraries for image processing (e.g. openCV) or numerical computation (e.g. blas).
- 2 Finalization is the processing of converting N = 1600000 templates into a searchable data structure an operation which can be a simple copy, or the building of an index or tree, for example. The duration of the operation may be data dependent, and may not be linear in the number of input templates.
- 3 This multiplier expresses the increase in template size when k images are passed to the template generation function.
- 4 All durations are measured on Intel®Xeon®CPU E5-2630 v4 @ 2.20GHz processors. Estimates are made by wrapping the API function call in calls to std::chrono::high\_resolution\_clock which on the machine in (3) counts 1ns clock ticks. Precision is somewhat worse than that however.
- 5 Search durations are measured as in the prior note. The power-law model in the final column mostly fits the empirical results in Figure 166. However in certain cases the model is not correct and should not be used numerically.

Table 5: Summary of algorithms and properties included in this report. The blue superscripts give ranking for the quantity in that column. Missing search durations, denoted by “-”, are absent because those runs were not executed, usually because we did not run on the larger galleries. Caution: The power-law model is sometimes an incorrect model. It is included here only to show broad sublinear behavior, which is flagged in green. The models should not be used for prediction.

#	ALGORITHM	INVESTIGATION, FNIR(N, R = 1, T = 0)								IDENTIFICATION, FNIR(N, R = L, T ≥ 0) FOR FPIR = 0.001								
		(0, 2]	(2, 4]	(4, 6]	(6, 8]	(8, 10]	(10, 12]	(12, 14]	(14, 18]	(0, 2]	(2, 4]	(4, 6]	(6, 8]	(8, 10]	(10, 12]	(12, 14]	(14, 18]	
1	3DIVI-005	<sup>92</sup> 0.0207	<sup>92</sup> 0.0304	<sup>92</sup> 0.0415	<sup>92</sup> 0.0533	<sup>92</sup> 0.0646	<sup>92</sup> 0.0735	<sup>92</sup> 0.0884	<sup>92</sup> 0.1148	<sup>96</sup> 0.1580	<sup>93</sup> 0.2316	<sup>93</sup> 0.3033	<sup>93</sup> 0.3740	<sup>93</sup> 0.4285	<sup>93</sup> 0.4742	<sup>94</sup> 0.5329	<sup>92</sup> 0.5975	
2	ANKE-000	<sup>90</sup> 0.0162	<sup>90</sup> 0.0245	<sup>90</sup> 0.0333	<sup>90</sup> 0.0428	<sup>90</sup> 0.0515	<sup>90</sup> 0.0615	<sup>90</sup> 0.0780	<sup>89</sup> 0.1028	<sup>91</sup> 0.1132	<sup>91</sup> 0.1761	<sup>91</sup> 0.2402	<sup>90</sup> 0.3057	<sup>90</sup> 0.3640	<sup>90</sup> 0.4200	<sup>90</sup> 0.4928	<sup>90</sup> 0.5680	
3	ANKE-002	<sup>47</sup> 0.0055	<sup>48</sup> 0.0074	<sup>45</sup> 0.0090	<sup>44</sup> 0.0103	<sup>43</sup> 0.0116	<sup>45</sup> 0.0135	<sup>45</sup> 0.0162	<sup>42</sup> 0.0202	<sup>49</sup> 0.0329	<sup>49</sup> 0.0560	<sup>51</sup> 0.0843	<sup>50</sup> 0.1169	<sup>50</sup> 0.1481	<sup>52</sup> 0.1820	<sup>51</sup> 0.2280	<sup>51</sup> 0.2831	
4	AWARE-005	<sup>101</sup> 0.0328	<sup>101</sup> 0.0519	<sup>101</sup> 0.0712	<sup>99</sup> 0.0910	<sup>99</sup> 0.1078	<sup>99</sup> 0.1235	<sup>99</sup> 0.1457	<sup>99</sup> 0.1831	<sup>101</sup> 0.3605	<sup>102</sup> 0.4949	<sup>102</sup> 0.5948	<sup>102</sup> 0.6783	<sup>103</sup> 0.7393	<sup>103</sup> 0.7905	<sup>103</sup> 0.8408	<sup>104</sup> 0.8831	
5	AWARE-006	<sup>105</sup> 0.0702	<sup>105</sup> 0.1110	<sup>106</sup> 0.1502	<sup>108</sup> 0.1899	<sup>105</sup> 0.2253	<sup>106</sup> 0.2614	<sup>105</sup> 0.3045	<sup>105</sup> 0.3659									
6	AYONIX-002	<sup>108</sup> 0.3360	<sup>109</sup> 0.4389	<sup>109</sup> 0.5144	<sup>109</sup> 0.5814	<sup>109</sup> 0.6340	<sup>108</sup> 0.6818	<sup>109</sup> 0.7297	<sup>110</sup> 0.7774	<sup>108</sup> 0.8288	<sup>106</sup> 0.9013	<sup>106</sup> 0.9375	<sup>106</sup> 0.9603	<sup>106</sup> 0.9744	<sup>107</sup> 0.9837	<sup>107</sup> 0.9893	<sup>107</sup> 0.9927	
7	CAMVI-004	<sup>104</sup> 0.0623	<sup>104</sup> 0.0944	<sup>104</sup> 0.1243	<sup>104</sup> 0.1548	<sup>105</sup> 0.1812	<sup>105</sup> 0.2056	<sup>103</sup> 0.2344	<sup>101</sup> 0.2672	<sup>86</sup> 0.0810	<sup>86</sup> 0.1267	<sup>83</sup> 0.1721	<sup>81</sup> 0.2203	<sup>81</sup> 0.2619	<sup>80</sup> 0.3040	<sup>80</sup> 0.3543	<sup>76</sup> 0.4124	
8	CAMVI-005	<sup>106</sup> 0.0849	<sup>106</sup> 0.1255	<sup>106</sup> 0.1631	<sup>106</sup> 0.1989	<sup>108</sup> 0.2298	<sup>108</sup> 0.2585	<sup>104</sup> 0.2915	<sup>104</sup> 0.3246									
9	CIB-000	<sup>17</sup> 0.0019	<sup>17</sup> 0.0030	<sup>12</sup> 0.0037	<sup>12</sup> 0.0044	<sup>13</sup> 0.0049	<sup>15</sup> 0.0057	<sup>13</sup> 0.0069	<sup>13</sup> 0.0062	<sup>20</sup> 0.0139	<sup>21</sup> 0.0240	<sup>22</sup> 0.0373	<sup>23</sup> 0.0525	<sup>23</sup> 0.0859	<sup>21</sup> 0.1109	<sup>21</sup> 0.1454		
10	CLOUDWALK-HR-000	<sup>77</sup> 0.0019	<sup>4</sup> 0.0024	<sup>5</sup> 0.0029	<sup>4</sup> 0.0032	<sup>3</sup> 0.0032	<sup>3</sup> 0.0036	<sup>1</sup> 0.0041	<sup>1</sup> 0.0020	<sup>1</sup> 0.0029	<sup>1</sup> 0.0041	<sup>1</sup> 0.0054	<sup>1</sup> 0.0064	<sup>1</sup> 0.0073	<sup>1</sup> 0.0085	<sup>1</sup> 0.0102	<sup>1</sup> 0.0112	
11	COGENT-000	<sup>8</sup> 0.0128	<sup>86</sup> 0.0184	<sup>88</sup> 0.0250	<sup>87</sup> 0.0327	<sup>87</sup> 0.0407	<sup>86</sup> 0.0488	<sup>85</sup> 0.0611	<sup>81</sup> 0.0794	<sup>72</sup> 0.0559	<sup>73</sup> 0.0923	<sup>72</sup> 0.1342	<sup>71</sup> 0.1812	<sup>71</sup> 0.2243	<sup>70</sup> 0.2675	<sup>69</sup> 0.3240	<sup>73</sup> 0.3992	
12	COGENT-001	<sup>85</sup> 0.0128	<sup>8</sup> 0.0184	<sup>87</sup> 0.0250	<sup>88</sup> 0.0327	<sup>88</sup> 0.0407	<sup>87</sup> 0.0488	<sup>86</sup> 0.0611	<sup>85</sup> 0.0794	<sup>73</sup> 0.0559	<sup>74</sup> 0.0923	<sup>71</sup> 0.1342	<sup>72</sup> 0.1812	<sup>71</sup> 0.2243	<sup>69</sup> 0.2675	<sup>68</sup> 0.3240	<sup>72</sup> 0.3992	
13	COGENT-002	<sup>61</sup> 0.0081	<sup>61</sup> 0.0105	<sup>58</sup> 0.0123	<sup>59</sup> 0.0137	<sup>57</sup> 0.0157	<sup>57</sup> 0.0175	<sup>55</sup> 0.0215	<sup>56</sup> 0.0280	<sup>64</sup> 0.0499	<sup>63</sup> 0.0823	<sup>62</sup> 0.1207	<sup>61</sup> 0.1639	<sup>62</sup> 0.2037	<sup>61</sup> 0.2432	<sup>63</sup> 0.2972	<sup>63</sup> 0.3638	
14	COGENT-003	<sup>66</sup> 0.0082	<sup>62</sup> 0.0108	<sup>60</sup> 0.0128	<sup>62</sup> 0.0145	<sup>61</sup> 0.0168	<sup>63</sup> 0.0191	<sup>64</sup> 0.0239	<sup>61</sup> 0.0312	<sup>75</sup> 0.0582	<sup>75</sup> 0.0971	<sup>75</sup> 0.1417	<sup>71</sup> 0.1918	<sup>73</sup> 0.2380	<sup>76</sup> 0.2836	<sup>78</sup> 0.3440	<sup>79</sup> 0.4207	
15	COGENT-004	<sup>5</sup> 0.0066	<sup>48</sup> 0.0080	<sup>40</sup> 0.0085	<sup>34</sup> 0.0080	<sup>26</sup> 0.0092	<sup>27</sup> 0.0106	<sup>30</sup> 0.0130	<sup>38</sup> 0.0410	<sup>60</sup> 0.0720	<sup>60</sup> 0.1099	<sup>60</sup> 0.1539	<sup>59</sup> 0.1974	<sup>62</sup> 0.2443	<sup>63</sup> 0.3043	<sup>65</sup> 0.3757		
16	COGNITEC-000	<sup>100</sup> 0.0265	<sup>99</sup> 0.0423	<sup>98</sup> 0.0588	<sup>98</sup> 0.0757	<sup>97</sup> 0.0894	<sup>97</sup> 0.1014	<sup>97</sup> 0.1169	<sup>98</sup> 0.1381	<sup>95</sup> 0.1522	<sup>94</sup> 0.2330	<sup>91</sup> 0.3051	<sup>93</sup> 0.3751	<sup>91</sup> 0.4300	<sup>93</sup> 0.4779	<sup>93</sup> 0.5307	<sup>91</sup> 0.5913	
17	COGNITEC-001	<sup>88</sup> 0.0149	<sup>89</sup> 0.0228	<sup>89</sup> 0.0312	<sup>89</sup> 0.0399	<sup>89</sup> 0.0479	<sup>89</sup> 0.0546	<sup>88</sup> 0.0656	<sup>86</sup> 0.0806	<sup>88</sup> 0.0963	<sup>88</sup> 0.1562	<sup>88</sup> 0.2157	<sup>88</sup> 0.2771	<sup>88</sup> 0.3287	<sup>87</sup> 0.3771	<sup>86</sup> 0.4343	<sup>86</sup> 0.4959	
18	COGNITEC-002	<sup>7</sup> 0.0101	<sup>73</sup> 0.0138	<sup>76</sup> 0.0170	<sup>76</sup> 0.0201	<sup>76</sup> 0.0237	<sup>75</sup> 0.0264	<sup>73</sup> 0.0309	<sup>70</sup> 0.0389	<sup>67</sup> 0.0517	<sup>66</sup> 0.0879	<sup>67</sup> 0.1269	<sup>69</sup> 0.1707	<sup>69</sup> 0.2098	<sup>63</sup> 0.2463	<sup>61</sup> 0.2919	<sup>61</sup> 0.3535	
19	COGNITEC-003	<sup>73</sup> 0.0104	<sup>76</sup> 0.0140	<sup>77</sup> 0.0174	<sup>77</sup> 0.0205	<sup>77</sup> 0.0238	<sup>76</sup> 0.0266	<sup>74</sup> 0.0311	<sup>74</sup> 0.0401	<sup>66</sup> 0.0504	<sup>65</sup> 0.0855	<sup>64</sup> 0.1235	<sup>64</sup> 0.1662	<sup>63</sup> 0.2045	<sup>60</sup> 0.2403	<sup>60</sup> 0.2854	<sup>59</sup> 0.3451	
20	COGNITEC-004	<sup>5</sup> 0.0073	<sup>56</sup> 0.0099	<sup>57</sup> 0.0118	<sup>54</sup> 0.0130	<sup>54</sup> 0.0147	<sup>56</sup> 0.0163	<sup>52</sup> 0.0189	<sup>51</sup> 0.0239	<sup>48</sup> 0.0325	<sup>48</sup> 0.0548	<sup>47</sup> 0.0798	<sup>47</sup> 0.1074	<sup>47</sup> 0.1325	<sup>46</sup> 0.1591	<sup>43</sup> 0.1952	<sup>42</sup> 0.2414	
21	CYBERLINK-002	<sup>45</sup> 0.0055	<sup>48</sup> 0.0068	<sup>36</sup> 0.0075	<sup>30</sup> 0.0078	<sup>27</sup> 0.0084	<sup>27</sup> 0.0094	<sup>28</sup> 0.0107	<sup>26</sup> 0.0114	<sup>27</sup> 0.0180	<sup>28</sup> 0.0302	<sup>28</sup> 0.0460	<sup>28</sup> 0.0643	<sup>28</sup> 0.0837	<sup>28</sup> 0.1058	<sup>27</sup> 0.1370	<sup>27</sup> 0.1787	
22	CYBERLINK-003	<sup>3</sup> 0.0041	<sup>29</sup> 0.0052	<sup>22</sup> 0.0057	<sup>20</sup> 0.0058	<sup>20</sup> 0.0061	<sup>20</sup> 0.0068	<sup>18</sup> 0.0078	<sup>15</sup> 0.0078	<sup>15</sup> 0.0109	<sup>15</sup> 0.0175	<sup>16</sup> 0.0259	<sup>16</sup> 0.0356	<sup>16</sup> 0.0468	<sup>16</sup> 0.0594	<sup>17</sup> 0.0787		
23	DAHUA-002	<sup>26</sup> 0.0035	<sup>23</sup> 0.0047	<sup>23</sup> 0.0058	<sup>22</sup> 0.0067	<sup>23</sup> 0.0074	<sup>22</sup> 0.0082	<sup>24</sup> 0.0100	<sup>24</sup> 0.0108	<sup>25</sup> 0.0169	<sup>27</sup> 0.0294	<sup>26</sup> 0.0449	<sup>26</sup> 0.0635	<sup>25</sup> 0.0817	<sup>26</sup> 0.1013	<sup>23</sup> 0.1638		
24	DAHUA-003	<sup>1</sup> 0.0026	<sup>16</sup> 0.0036	<sup>16</sup> 0.0043	<sup>16</sup> 0.0050	<sup>15</sup> 0.0065	<sup>15</sup> 0.0062	<sup>18</sup> 0.0080	<sup>16</sup> 0.0073	<sup>24</sup> 0.0160	<sup>25</sup> 0.0280	<sup>24</sup> 0.0432	<sup>24</sup> 0.0615	<sup>24</sup> 0.0794	<sup>24</sup> 0.0987	<sup>23</sup> 0.1270	<sup>22</sup> 0.1587	
25	DEEPCLOUDT-001	<sup>14</sup> 0.0024	<sup>13</sup> 0.0032	<sup>11</sup> 0.0037	<sup>10</sup> 0.0040	<sup>11</sup> 0.0043	<sup>11</sup> 0.0060	<sup>11</sup> 0.0052	<sup>9</sup> 0.0058	<sup>7</sup> 0.0087	<sup>8</sup> 0.0119	<sup>8</sup> 0.0155	<sup>8</sup> 0.0199	<sup>9</sup> 0.0249	<sup>8</sup> 0.0338	<sup>8</sup> 0.0463		
26	DEEPESEA-001	<sup>6</sup> 0.0081	<sup>69</sup> 0.0116	<sup>68</sup> 0.0149	<sup>71</sup> 0.0182	<sup>71</sup> 0.0216	<sup>74</sup> 0.0260	<sup>76</sup> 0.0332	<sup>78</sup> 0.0432	<sup>61</sup> 0.0458	<sup>61</sup> 0.0752	<sup>59</sup> 0.1086	<sup>56</sup> 0.1482	<sup>58</sup> 0.2186	<sup>58</sup> 0.2663	<sup>57</sup> 0.3213		
27	DERMALOG-006	<sup>7</sup> 0.0113	<sup>77</sup> 0.0142	<sup>73</sup> 0.0163	<sup>72</sup> 0.0183	<sup>69</sup> 0.0200	<sup>68</sup> 0.0218	<sup>66</sup> 0.0251	<sup>64</sup> 0.0329	<sup>70</sup> 0.0545	<sup>68</sup> 0.0889	<sup>68</sup> 0.1271	<sup>67</sup> 0.1697	<sup>65</sup> 0.2090	<sup>64</sup> 0.2498	<sup>64</sup> 0.3028	<sup>64</sup> 0.3670	
28	DERMALOG-007	<sup>83</sup> 0.0125	<sup>83</sup> 0.0170	<sup>83</sup> 0.0214	<sup>83</sup> 0.0264	<sup>82</sup> 0.0309	<sup>81</sup> 0.0356	<sup>82</sup> 0.0432	<sup>82</sup> 0.0579	<sup>87</sup> 0.0910	<sup>87</sup> 0.1453	<sup>87</sup> 0.2009	<sup>82</sup> 0.2602	<sup>81</sup> 0.3134	<sup>86</sup> 0.3649	<sup>86</sup> 0.5007		
29	DERMALOG-008	<sup>4</sup> 0.0057	<sup>47</sup> 0.0077	<sup>49</sup> 0.0095	<sup>49</sup> 0.0110	<sup>48</sup> 0.0128	<sup>49</sup> 0.0148	<sup>49</sup> 0.0180	<sup>50</sup> 0.0223	<sup>65</sup> 0.0501	<sup>64</sup> 0.0850	<sup>63</sup> 0.1247	<sup>62</sup> 0.1692	<sup>62</sup> 0.2105	<sup>62</sup> 0.2541	<sup>66</sup> 0.3102	<sup>66</sup> 0.3762	
30	GORILLA-002	<sup>95</sup> 0.0213	<sup>95</sup> 0.0359	<sup>96</sup> 0.0528	<sup>97</sup> 0.0716	<sup>98</sup> 0.0895	<sup>98</sup> 0.1088	<sup>98</sup> 0.1367	<sup>98</sup> 0.1765	<sup>98</sup> 0.1828	<sup>99</sup> 0.2787	<sup>99</sup> 0.3654	<sup>99</sup> 0.4485	<sup>99</sup> 0.5168	<sup>97</sup> 0.5823	<sup>97</sup> 0.6508	<sup>97</sup> 0.7180	
31	GORILLA-005	<sup>3</sup> 0.0044	<sup>42</sup> 0.0070	<sup>53</sup> 0.0102	<sup>57</sup> 0.0136	<sup>62</sup> 0.0170	<sup>66</sup> 0.0204	<sup>69</sup> 0.0272	<sup>74</sup> 0.0566	<sup>76</sup> 0.0973	<sup>77</sup> 0.1432	<sup>77</sup> 0.1937	<sup>78</sup> 0.2398	<sup>78</sup> 0.2862	<sup>77</sup> 0.3437	<sup>77</sup> 0.4150		
32	IDEMIA-003	<sup>76</sup> 0.0110	<sup>81</sup> 0.0151	<sup>81</sup> 0.0196	<sup>80</sup> 0.0238	<sup>79</sup> 0.0281	<sup>79</sup> 0.0313	<sup>78</sup> 0.0368	<sup>78</sup> 0.0504	<sup>82</sup> 0.0717	<sup>81</sup> 0.1147	<sup>81</sup> 0.1614	<sup>81</sup> 0.2113	<sup>80</sup> 0.2553	<sup>79</sup> 0.3537	<sup>80</sup> 0.4334		
33	IDEMIA-004	<sup>7</sup> 0.0107	<sup>79</sup> 0.0148	<sup>80</sup> 0.0192	<sup>79</sup> 0.0233	<sup>78</sup> 0.0277	<sup>78</sup> 0.0312	<sup>78</sup> 0.0367	<sup>78</sup> 0.0512	<sup>83</sup> 0.0737	<sup>80</sup> 0.0587	<sup>81</sup> 0.0833	<sup>80</sup> 0.1100	<sup>81</sup> 0.1340	<sup>81</sup> 0.1580	<sup>42</sup> 0.1911	<sup>43</sup> 0.2482	
34	IDEMIA-005	<sup>79</sup> 0.0118	<sup>82</sup> 0.0167	<sup>80</sup> 0.0218	<sup>84</sup> 0.0270	<sup>83</sup> 0.0317	<sup>82</sup> 0.0357	<sup>81</sup> 0.0425	<sup>81</sup> 0.0579	<sup>60</sup> 0.0440	<sup>59</sup> 0.0689	<sup>58</sup> 0.0964	<sup>54</sup> 0.1254	<sup>53</sup> 0.1513	<sup>51</sup> 0.1762	<sup>46</sup> 0.2113	<sup>46</sup> 0.2698	
35	IDEMIA-006	<sup>8</sup> 0.0124	<sup>84</sup> 0.0171	<sup>84</sup> 0.0218	<sup>82</sup> 0.0263	<sup>81</sup> 0.0302	<sup>80</sup> 0.0321	<sup>77</sup> 0.0356	<sup>77</sup> 0.0471	<sup>47</sup> 0.0409	<sup>46</sup> 0.0620</td							

MISS RATES		INVESTIGATION, FNIR(N, R = 1, T = 0)								IDENTIFICATION, FNIR(N, R = L, T ≥ 0) FOR FPIR = 0.001							
#	ALGORITHM	(0, 2]	(2, 4]	(4, 6]	(6, 8]	(8, 10]	(10, 12]	(12, 14]	(14, 18]	(0, 2]	(2, 4]	(4, 6]	(6, 8]	(8, 10]	(10, 12]	(12, 14]	(14, 18]
45	ISYSTEMS-002	70.0101	70.0135	70.0169	70.0197	70.0228	70.0256	70.0304	70.0398	85.0779	85.01258	80.01759	80.02299	80.02758	80.03204	84.03763	82.04401
46	ISYSTEMS-003	70.0089	64.0115	64.0139	64.0158	65.0177	65.0198	61.0234	58.0303	79.0647	79.01056	79.01502	79.01986	78.02402	74.02819	73.03351	71.03976
47	KEDACOM-001	70.0116	70.0130	62.0135	55.0133	52.0135	45.0141	39.0151	30.0176	36.0241	36.0360	34.00513	29.00689	27.00866	29.01060	25.01327	25.01694
48	LOOKMAN-003	81.0123	78.0144	72.0158	65.0168	66.0178	61.0188	54.0212	51.0260	59.0438	57.00687	56.00978	56.01296	55.01581	51.01879	53.02294	50.02756
49	LOOKMAN-005	80.0118	72.0134	65.0142	61.0144	56.0150	55.0160	49.0176	48.0213	46.0310	44.0480	41.0698	41.00954	41.01216	41.01491	41.01890	41.02381
50	MICROFOCUS-005	110.04269	110.05527	110.06355	111.07024	110.07503	110.07876	111.08234	112.08601	106.08338	107.09113	107.09468	107.09667	107.09771	106.09836	106.09880	106.09924
51	MICROSOFT-003	21.0034	27.0050	28.0064	31.0078	33.0092	31.0107	34.0135	35.0166	45.0288	45.0503	45.0763	48.01067	48.01359	48.01680	47.02116	45.02644
52	MICROSOFT-004	21.0032	22.0047	24.0060	27.0075	30.0087	30.0103	33.0131	35.0159	42.0268	43.0470	44.0716	43.01007	43.01291	42.01610	45.02052	44.02590
53	MICROSOFT-005	17.0031	29.0047	30.0066	38.0084	38.0103	42.0131	44.0164	49.0185	38.0243	39.0432	39.0658	39.00913	41.01172	38.01476	40.01874	38.02272
54	MICROSOFT-006	22.0032	26.0049	29.0065	37.0081	37.0096	37.0117	36.0144	34.0160	19.0134	19.0233	20.0346	18.00462	17.00578	18.00713	18.00903	18.01156
55	NEC-000	99.0195	94.0316	94.0445	94.0581	93.0699	94.0817	94.0998	94.1237	84.0759	84.1245	84.1729	84.2240	84.2671	83.3117	81.3639	81.4348
56	NEC-001	99.0246	97.0382	95.0524	95.0672	96.0793	96.0904	95.1076	95.1317	89.0109	89.1623	89.2214	89.2834	89.3341	89.3844	89.4440	88.5183
57	NEC-002	23.0033	19.0041	15.0043	13.0044	11.0045	10.0049	10.0056	7.0041	12.0066	8.0090	7.0111	7.0131	6.0149	6.0171	7.0207	7.0267
58	NEC-003	27.0036	21.0046	19.0051	19.0055	19.0059	16.0067	15.0077	17.0073	6.0056	6.0076	6.0091	5.00105	5.0019	5.00137	4.00162	4.00209
59	NEUROTECHNOLOGY-003	96.0234	96.0379	97.0549	96.0682	95.0720	93.0747	93.0886	91.1066	104.06802	104.0817	105.08920	105.09355	105.09594	105.09738	105.09828	105.09885
60	NEUROTECHNOLOGY-004	71.0014	73.0134	71.0156	68.0173	67.0195	67.0212	65.0245	62.0320	78.0642	77.01015	76.01426	71.01881	71.02299	72.02722	71.03269	70.03943
61	NEUROTECHNOLOGY-005	69.0089	66.0116	63.0136	63.0152	64.0173	64.0196	60.0233	59.0306	71.0556	71.09013	69.01315	69.01766	69.02192	68.02617	67.03174	67.03843
62	NEUROTECHNOLOGY-007	61.0078	66.0103	59.0124	60.0140	58.0161	58.0185	59.0225	58.0290	77.0641	80.01069	78.0154	80.02075	81.02572	82.03081	83.03713	83.04421
63	NOBLIS-002	107.01520	107.02419	107.03296	108.04114	108.04856	108.05528	108.06061	108.06532	108.09984	108.09996	108.09998	108.09999	108.09999	108.00000	110.00000	110.00000
64	NTechLab-003	69.0078	71.0131	82.0202	85.0295	86.0405	88.0543	89.0761	90.1035	63.0491	67.0881	74.1384	70.1985	80.2594	80.3270	85.4065	85.4891
65	NTechLab-004	59.0068	63.0110	74.0167	81.0239	84.0330	85.0447	87.0641	88.0891	85.0379	88.0688	61.1108	61.1629	68.2192	72.2846	82.3657	84.4524
66	NTechLab-006	44.0056	50.0095	67.0148	78.0218	80.0301	83.0413	84.0591	89.0814	51.0349	55.0636	58.1023	59.1506	61.2024	62.2617	74.3374	76.4185
67	NTechLab-007	39.0044	36.0066	44.0089	52.0118	55.0150	62.0189	67.0255	69.0342	40.0256	41.0450	45.0705	41.01012	45.01334	49.1692	48.2170	47.2752
68	NTechLab-008	17.0025	18.0038	21.0052	26.0074	39.0104	47.0146	63.0236	68.0348	21.0143	23.0267	27.0459	32.0733	37.01062	37.01469	44.2044	47.2698
69	NTechLab-009	10.0022	12.0031	13.0038	14.0045	15.0055	18.0067	20.0088	22.0100	14.0073	14.0117	14.0170	14.0238	17.0319	15.0419	15.0577	15.0833
70	PARAVISION-002	48.0058	53.0083	55.0111	58.0137	60.0162	60.0187	59.0229	57.0295								
71	PARAVISION-003	39.0048	36.0067	46.0090	47.0109	49.0128	48.0148	48.0178	49.0219	52.0354	53.0618	54.0931	55.1290	56.1625	56.1964	56.2408	53.2924
72	PARAVISION-004	13.0024	14.0032	14.0040	15.0047	14.0053	14.0061	14.0073	15.0072	16.0118	18.0209	19.0327	19.0465	19.0613	19.0779	19.01008	19.01285
73	PARAVISION-005	7.0021	10.0028	10.0035	11.0041	12.0046	12.0054	12.0067	13.0070	8.0057	9.0093	9.0144	10.0207	11.0278	12.0368	13.0508	13.0715
74	PARAVISION-007	4.0019	5.0025	4.0029	6.0033	6.0036	6.0042	6.0049	4.0030	7.0057	10.0094	11.0144	10.0206	11.0275	11.0357	11.0485	11.0652
75	PIXELALL-002	6.0085	6.0019	6.0047	6.0172	6.0198	6.0225	6.0270	6.0349	92.01193	92.01900	92.02601	92.0332	92.03955	92.04565	92.05268	93.06030
76	PIXELALL-003	41.0050	37.0063	34.0072	29.0077	28.0085	28.0095	29.0113	27.0119	39.0248	38.04018	38.0622	38.0861	39.1104	39.1364	35.01723	34.02167
77	PIXELALL-004	40.0049	35.0063	35.0072	32.0079	31.0089	32.0103	32.0127	31.0146	33.0211	35.0360	37.0553	37.0792	34.1045	34.1317	34.1700	37.2246
78	PTAKURATSATU-000	49.0061	50.0082	50.0097	48.0109	44.0120	41.0131	37.0146	39.0180	34.0375	32.0596	30.0842	30.1116	45.1357	44.1553	38.1820	40.2326
79	RANKONE-002	94.0212	93.0313	93.0431	93.0562	94.0712	95.0881	96.1130	97.1543	90.1111	90.1707	90.2305	90.2968	91.3645	91.5172	94.6110	
80	RANKONE-004	103.00424	102.00643	102.00875	105.01127	102.01364	105.01597	100.1914	100.2378	99.1855	98.2681	99.3431	99.4155	99.4785	99.5350	99.55980	99.6722
81	RANKONE-005	87.0136	88.0192	86.0246	86.0303	85.0362	84.0422	83.0521	83.0694	76.0582	79.0910	66.1260	63.1645	61.2005	59.2353	59.2816	60.3522
82	RANKONE-007	67.0078	59.0099	56.0113	53.0123	53.0139	54.0156	53.0191	52.0242	37.0242	37.0376	36.0542	31.0737	31.0935	31.1130	29.1416	29.1811
83	RANKONE-009	43.0054	44.0072	41.0085	42.0098	42.0113	40.0130	45.0169	49.0220	32.0208	33.0345	32.0504	31.0706	31.0930	32.1174	33.1504	32.2002
84	RANKONE-010	37.0047	33.0061	33.0070	28.0076	29.0087	29.0098	30.0113	28.0120	26.0177	24.0269	21.0368	21.0479	17.0590	17.0688	17.0803	16.0991
85	REALNETWORKS-002	102.00381	103.00687	103.01062	103.01495	104.01963	104.02513	108.03206	108.03927	108.02153	108.03323	109.04444	109.05485	101.06355	101.07132	102.07855	102.08437
86	REALNETWORKS-003	99.0245	10.0437	10.0686	10.0975	10.01312	10.01719	10.02294	10.02907	93.0468	95.02370	96.3313	97.04269	97.5142	97.5979	10.06815	10.7567
87	REALNETWORKS-004	97.0244	99.0428	99.0663	100.0939	100.01251	101.01634	101.02170	102.02785	94.01484	96.02377	95.3303	97.04249	97.51016	98.05924	99.06758	99.7534
88	SCANOVATE-001	6.0079	6.0117	70.0151	73.0185	73.0221	73.0259	75.0321	75.04047	83.0727	83.01169	82.01650	82.02115	79.02528	76.02925	76.03437	75.04084

T = 0 → Investigation

T &gt; 0 → Identification

2021 / 09 / 21

09:55:08

FNIR(N, R, T) = False neg. identification rate

N = Num. enrolled subjects

R = Num. candidates examined

MISS RATES		INVESTIGATION, FNIR(N, R = 1, T = 0)								IDENTIFICATION, FNIR(N, R = L, T ≥ 0) FOR FPIR = 0.001							
#	ALGORITHM	(0, 2]	(2, 4]	(4, 6]	(6, 8]	(8, 10]	(10, 12]	(12, 14]	(14, 18]	(0, 2]	(2, 4]	(4, 6]	(6, 8]	(8, 10]	(10, 12]	(12, 14]	(14, 18]
89	SENSETIME-002	<sup>91</sup> 0.0186	<sup>87</sup> 0.0191	<sup>79</sup> 0.0183	<sup>70</sup> 0.0179	<sup>6</sup> 0.0173	<sup>43</sup> 0.0133	<sup>21</sup> 0.0089	<sup>12</sup> 0.0059	<sup>36</sup> 0.0220	<sup>26</sup> 0.0236	<sup>15</sup> 0.0237	<sup>15</sup> 0.0240	<sup>9</sup> 0.0245	<sup>7</sup> 0.0219	<sup>8</sup> 0.0195	<sup>7</sup> 0.0222
90	SENSETIME-003	<sup>8</sup> 0.0021	<sup>9</sup> 0.0028	<sup>8</sup> 0.0031	<sup>5</sup> 0.0033	<sup>4</sup> 0.0035	<sup>5</sup> 0.0040	<sup>5</sup> 0.0047	<sup>5</sup> 0.0033	<sup>8</sup> 0.0046	<sup>5</sup> 0.0064	<sup>4</sup> 0.0076	<sup>3</sup> 0.0086	<sup>3</sup> 0.0101	<sup>2</sup> 0.0122	<sup>3</sup> 0.0155	<sup>3</sup> 0.0196
91	SENSETIME-004	<sup>2</sup> 0.0016	<sup>2</sup> 0.0022	<sup>4</sup> 0.0025	<sup>2</sup> 0.0028	<sup>2</sup> 0.0030	<sup>2</sup> 0.0035	<sup>3</sup> 0.0043	<sup>2</sup> 0.0025	<sup>3</sup> 0.0036	<sup>3</sup> 0.0052	<sup>2</sup> 0.0066	<sup>2</sup> 0.0081	<sup>2</sup> 0.0099	<sup>4</sup> 0.0126	<sup>3</sup> 0.0169	<sup>4</sup> 0.0230
92	SENSETIME-005	<sup>1</sup> 0.0015	<sup>1</sup> 0.0020	<sup>1</sup> 0.0024	<sup>1</sup> 0.0026	<sup>1</sup> 0.0029	<sup>1</sup> 0.0035	<sup>2</sup> 0.0043	<sup>3</sup> 0.0028	<sup>4</sup> 0.0036	<sup>4</sup> 0.0059	<sup>5</sup> 0.0089	<sup>6</sup> 0.0128	<sup>7</sup> 0.0177	<sup>8</sup> 0.0240	<sup>9</sup> 0.0345	<sup>9</sup> 0.0493
93	SLAT-002	<sup>11</sup> 0.8309	<sup>11</sup> 0.8310	<sup>11</sup> 0.8311	<sup>112</sup> 0.8306	<sup>112</sup> 0.8296	<sup>112</sup> 0.8302	<sup>11</sup> 0.8300	<sup>11</sup> 0.8301	<sup>10</sup> 0.8340	<sup>16</sup> 0.8368	<sup>10</sup> 0.8404	<sup>10</sup> 0.8445	<sup>10</sup> 0.8480	<sup>10</sup> 0.8532	<sup>10</sup> 0.8595	<sup>10</sup> 0.8691
94	SYNESIS-003	<sup>84</sup> 0.0125	<sup>80</sup> 0.0151	<sup>78</sup> 0.0174	<sup>75</sup> 0.0199	<sup>74</sup> 0.0223	<sup>70</sup> 0.0240	<sup>70</sup> 0.0279	<sup>80</sup> 0.0331	<sup>80</sup> 0.0658	<sup>78</sup> 0.1052	<sup>78</sup> 0.1483	<sup>77</sup> 0.1968	<sup>77</sup> 0.2399	<sup>75</sup> 0.2834	<sup>75</sup> 0.3405	<sup>74</sup> 0.4046
95	SYNESIS-005	<sup>35</sup> 0.0044	<sup>32</sup> 0.0058	<sup>32</sup> 0.0070	<sup>38</sup> 0.0088	<sup>38</sup> 0.0091	<sup>31</sup> 0.0103	<sup>31</sup> 0.0125	<sup>32</sup> 0.0152	<sup>41</sup> 0.0262	<sup>40</sup> 0.0444	<sup>40</sup> 0.0666	<sup>40</sup> 0.0923	<sup>39</sup> 0.1156	<sup>36</sup> 0.1399	<sup>38</sup> 0.1736	<sup>35</sup> 0.2185
96	TECH5-001	<sup>52</sup> 0.0061	<sup>56</sup> 0.0093	<sup>61</sup> 0.0128	<sup>66</sup> 0.0171	<sup>72</sup> 0.0221	<sup>77</sup> 0.0289	<sup>80</sup> 0.0412	<sup>80</sup> 0.0560	<sup>81</sup> 0.0660	<sup>82</sup> 0.1156	<sup>85</sup> 0.1733	<sup>86</sup> 0.2385	<sup>86</sup> 0.2998	<sup>86</sup> 0.3629	<sup>89</sup> 0.4424	<sup>89</sup> 0.5284
97	TOSHIBA-001	<sup>68</sup> 0.0086	<sup>69</sup> 0.0119	<sup>69</sup> 0.0150	<sup>69</sup> 0.0178	<sup>70</sup> 0.0209	<sup>71</sup> 0.0241	<sup>71</sup> 0.0292	<sup>70</sup> 0.0365								
98	TRUEFACE-000	<sup>31</sup> 0.0043	<sup>31</sup> 0.0057	<sup>25</sup> 0.0061	<sup>23</sup> 0.0067	<sup>29</sup> 0.0073	<sup>29</sup> 0.0084	<sup>23</sup> 0.0097	<sup>21</sup> 0.0099	<sup>36</sup> 0.0200	<sup>32</sup> 0.0338	<sup>33</sup> 0.0504	<sup>30</sup> 0.0705	<sup>30</sup> 0.0904	<sup>31</sup> 0.1112	<sup>28</sup> 0.1401	<sup>28</sup> 0.1792
99	VERIDAS-001	<sup>53</sup> 0.0063	<sup>51</sup> 0.0083	<sup>51</sup> 0.0099	<sup>51</sup> 0.0113	<sup>51</sup> 0.0132	<sup>49</sup> 0.0148	<sup>50</sup> 0.0184	<sup>47</sup> 0.0219	<sup>56</sup> 0.0403	<sup>56</sup> 0.0684	<sup>57</sup> 0.1012	<sup>57</sup> 0.1386	<sup>57</sup> 0.1741	<sup>57</sup> 0.2113	<sup>57</sup> 0.2611	<sup>58</sup> 0.3233
100	VISIONLABS-004	<sup>38</sup> 0.0048	<sup>41</sup> 0.0069	<sup>47</sup> 0.0091	<sup>50</sup> 0.0111	<sup>50</sup> 0.0130	<sup>52</sup> 0.0152	<sup>51</sup> 0.0187	<sup>53</sup> 0.0242	<sup>69</sup> 0.0540	<sup>72</sup> 0.0916	<sup>73</sup> 0.1358	<sup>73</sup> 0.1855	<sup>74</sup> 0.2303	<sup>73</sup> 0.2745	<sup>72</sup> 0.3312	<sup>68</sup> 0.3913
101	VISIONLABS-005	<sup>34</sup> 0.0044	<sup>34</sup> 0.0063	<sup>38</sup> 0.0081	<sup>41</sup> 0.0095	<sup>41</sup> 0.0109	<sup>39</sup> 0.0125	<sup>40</sup> 0.0151	<sup>41</sup> 0.0187	<sup>62</sup> 0.0479	<sup>62</sup> 0.0812	<sup>63</sup> 0.1212	<sup>65</sup> 0.1664	<sup>64</sup> 0.2078	<sup>64</sup> 0.2473	<sup>63</sup> 0.2999	<sup>62</sup> 0.3577
102	VISIONLABS-006	<sup>25</sup> 0.0035	<sup>25</sup> 0.0048	<sup>27</sup> 0.0061	<sup>25</sup> 0.0069	<sup>29</sup> 0.0077	<sup>29</sup> 0.0087	<sup>26</sup> 0.0105	<sup>29</sup> 0.0120	<sup>41</sup> 0.0273	<sup>42</sup> 0.0465	<sup>42</sup> 0.0702	<sup>42</sup> 0.0970	<sup>42</sup> 0.1228	<sup>40</sup> 0.1486	<sup>39</sup> 0.1847	<sup>39</sup> 0.2295
103	VISIONLABS-008	<sup>18</sup> 0.0028	<sup>17</sup> 0.0037	<sup>18</sup> 0.0047	<sup>18</sup> 0.0053	<sup>18</sup> 0.0058	<sup>17</sup> 0.0067	<sup>19</sup> 0.0081	<sup>20</sup> 0.0085	<sup>22</sup> 0.0143	<sup>22</sup> 0.0241	<sup>23</sup> 0.0373	<sup>22</sup> 0.0519	<sup>22</sup> 0.0677	<sup>20</sup> 0.0850	<sup>20</sup> 0.1104	<sup>20</sup> 0.1444
104	VISIONLABS-009	<sup>7</sup> 0.0020	<sup>7</sup> 0.0026	<sup>7</sup> 0.0030	<sup>7</sup> 0.0034	<sup>8</sup> 0.0038	<sup>8</sup> 0.0044	<sup>9</sup> 0.0052	<sup>9</sup> 0.0046	<sup>11</sup> 0.0065	<sup>12</sup> 0.0105	<sup>12</sup> 0.0156	<sup>12</sup> 0.0217	<sup>13</sup> 0.0289	<sup>13</sup> 0.0368	<sup>12</sup> 0.0499	<sup>12</sup> 0.0681
105	VISIONLABS-010	<sup>6</sup> 0.0020	<sup>6</sup> 0.0025	<sup>6</sup> 0.0030	<sup>8</sup> 0.0034	<sup>7</sup> 0.0036	<sup>7</sup> 0.0043	<sup>7</sup> 0.0051	<sup>10</sup> 0.0047	<sup>13</sup> 0.0069	<sup>13</sup> 0.0113	<sup>13</sup> 0.0170	<sup>13</sup> 0.0238	<sup>14</sup> 0.0316	<sup>14</sup> 0.0411	<sup>14</sup> 0.0557	<sup>14</sup> 0.0740
106	VTS-000	<sup>11</sup> 0.5878	<sup>111</sup> 0.6312	<sup>111</sup> 0.6602	<sup>110</sup> 0.6863	<sup>110</sup> 0.7073	<sup>110</sup> 0.7246	<sup>110</sup> 0.7458	<sup>110</sup> 0.7747	<sup>103</sup> 0.5929	<sup>103</sup> 0.6397	<sup>103</sup> 0.6729	<sup>103</sup> 0.7034	<sup>102</sup> 0.7279	<sup>102</sup> 0.7493	<sup>101</sup> 0.7739	<sup>101</sup> 0.8076
107	XFORWARDAI-000	<sup>17</sup> 0.0027	<sup>15</sup> 0.0034	<sup>17</sup> 0.0044	<sup>17</sup> 0.0052	<sup>17</sup> 0.0058	<sup>19</sup> 0.0067	<sup>17</sup> 0.0079	<sup>18</sup> 0.0076	<sup>23</sup> 0.0157	<sup>26</sup> 0.0281	<sup>25</sup> 0.0443	<sup>26</sup> 0.0635	<sup>27</sup> 0.0834	<sup>27</sup> 0.1050	<sup>26</sup> 0.1330	<sup>26</sup> 0.1714
108	XFORWARDAI-001	<sup>12</sup> 0.0023	<sup>8</sup> 0.0028	<sup>7</sup> 0.0034	<sup>7</sup> 0.0037	<sup>7</sup> 0.0045	<sup>8</sup> 0.0052	<sup>8</sup> 0.0043	<sup>10</sup> 0.0060	<sup>11</sup> 0.0096	<sup>10</sup> 0.0144	<sup>9</sup> 0.0200	<sup>10</sup> 0.0260	<sup>10</sup> 0.0334	<sup>10</sup> 0.0435	<sup>10</sup> 0.0586	
109	YITU-002	<sup>55</sup> 0.0066	<sup>52</sup> 0.0083	<sup>48</sup> 0.0094	<sup>45</sup> 0.0101	<sup>45</sup> 0.0121	<sup>51</sup> 0.0150	<sup>50</sup> 0.0223	<sup>63</sup> 0.0328	<sup>28</sup> 0.0189	<sup>29</sup> 0.0317	<sup>30</sup> 0.0494	<sup>34</sup> 0.0750	<sup>36</sup> 0.1066	<sup>42</sup> 0.1494	<sup>49</sup> 0.2171	<sup>55</sup> 0.2958
110	YITU-003	<sup>38</sup> 0.0072	<sup>35</sup> 0.0089	<sup>32</sup> 0.0100	<sup>40</sup> 0.0107	<sup>40</sup> 0.0125	<sup>50</sup> 0.0153	<sup>58</sup> 0.0226	<sup>66</sup> 0.0334	<sup>28</sup> 0.0194	<sup>36</sup> 0.0321	<sup>31</sup> 0.0500	<sup>36</sup> 0.0756	<sup>37</sup> 0.1071	<sup>45</sup> 0.1500	<sup>50</sup> 0.2177	<sup>55</sup> 0.2964
111	YITU-004	<sup>50</sup> 0.0061	<sup>46</sup> 0.0075	<sup>39</sup> 0.0081	<sup>36</sup> 0.0081	<sup>36</sup> 0.0092	<sup>39</sup> 0.0107	<sup>42</sup> 0.0154	<sup>44</sup> 0.0207	<sup>18</sup> 0.0125	<sup>17</sup> 0.0204	<sup>18</sup> 0.0314	<sup>20</sup> 0.0469	<sup>21</sup> 0.0671	<sup>23</sup> 0.0955	<sup>31</sup> 0.1421	<sup>35</sup> 0.2006
112	YITU-005	<sup>56</sup> 0.0067	<sup>49</sup> 0.0080	<sup>42</sup> 0.0087	<sup>39</sup> 0.0085	<sup>36</sup> 0.0094	<sup>39</sup> 0.0108	<sup>41</sup> 0.0151	<sup>43</sup> 0.0204	<sup>17</sup> 0.0124	<sup>16</sup> 0.0198	<sup>17</sup> 0.0308	<sup>17</sup> 0.0462	<sup>20</sup> 0.0667	<sup>22</sup> 0.0953	<sup>30</sup> 0.1418	<sup>31</sup> 0.1930

Table 8: **Accuracy for the FRVT 2018 mugshot sets under ageing.** The second row shows the time lapse between gallery and subsequent probe images, in years. The first two columns identify the algorithm. The next 8 values give rank-based FNIR with  $R = 1$ ,  $T = 0$  and  $FPIR = 1$ . All these are relevant to investigational uses where candidates from all searches would need human review. The second 8 values give threshold-based FNIR with  $T \geq 0$ ,  $FPIR = 0.001$  and no rank criterion. The shaded cells indicate the three most accurate algorithms for that elapsed time. The gallery size is 3068801. The total number of searches is 10951064.

2021 / 09 / 21

09:55:08

FNIR(N, R, T) =

False neg. identification rate

FPIR(N, R, T) =

False pos. identification rate

N = Num. enrolled subjects

R = Num. candidates examined

T = Threshold

 $T = 0 \rightarrow$  Investigation $T > 0 \rightarrow$  Identification

#	ALGORITHM	INVESTIGATION MODE						IDENTIFICATION MODE						FAILURE TO EXTRACT FEATURES						FEATURES									
		RANK ONE MISS RATE, FNIR(N, 0, 1)						HIGH T → FPIR = 0.001, FNIR(N, T, L)						N=1.6M						FEATURES									
		GALLERY		MUGSHOT	MUGSHOT	MUGSHOT	VISA	BORDER	BOR <sub>L</sub> 10YR	KIOSK	MUGSHOT	MUGSHOT	MUGSHOT	VISA	BORDER	BOR <sub>L</sub> 10YR	KIOSK	MUGSHOT	MUGSHOT	MUGSHOT	VISA	BORDER	BOR <sub>L</sub> 10YR	KIOSK					
1	3DIVI-003	21	0.083	207	0.206	139	0.141	145	0.474	209	0.400	207	0.626	147	0.605	111	0.821	0.002	0.005										
2	3DIVI-004	172	0.018	181	0.062	122	0.035	126	0.279	181	0.169	187	0.343	123	0.277	96	0.607	0.002	0.005										
3	3DIVI-005	173	0.018	180	0.062	149	0.930	157	0.821	127	0.279	178	0.166	185	0.339	110	0.996	146	0.864	98	0.597	0.002	0.005	0.442					
4	3DIVI-006	183	0.024	188	0.074	124	0.047	135	0.312	180	0.168	186	0.342	123	0.283	99	0.615	0.002	0.005										
5	ACER-000	15	0.011	145	0.036	130	0.827	108	0.025	111	0.209	17	0.146	163	0.246	71	0.981	118	0.201	84	0.490	0.000	0.000	0.042					
6	AIZE-001	115	0.006	110	0.022	98	0.683	99	0.016	47	0.050	95	0.165	134	0.077	124	0.143	91	0.994	94	0.101	48	0.364	69	0.387	0.001	0.001	0.047	0.000
7	ALCHERA-000	16	0.016	168	0.047	137	0.870	128	0.046	132	0.292	168	0.138	151	0.216	125	0.999	115	0.176	11	0.803	0.006	0.014	0.328					
8	ALCHERA-001	237	0.987	233	1.000	159	1.000	190	1.000	234	0.999	235	1.000	227	1.000	161	1.000	206	1.000	0.006	0.013	0.324							
9	ALCHERA-002	212	0.095	204	0.166	162	0.954	154	0.668	143	0.446	214	0.486	204	0.591	147	1.000	145	0.827	113	0.811	0.001	0.002	0.106					
10	ALCHERA-003	148	0.010	143	0.035	106	0.741	108	0.016	109	0.206	177	0.155	162	0.239	134	0.999	112	0.172	81	0.464	0.001	0.002	0.106					
11	ALLGOVISION-000	155	0.011	139	0.033	140	0.894	105	0.021	129	0.282	146	0.088	140	0.166	86	0.990	97	0.117	90	0.526	0.002	0.003	0.122					
12	ALLGOVISION-001	15	0.009	153	0.038	94	0.661	108	0.021	121	0.241	158	0.102	155	0.221	77	0.986	105	0.150	85	0.491	0.001	0.001	0.042					
13	ANKE-000	163	0.013	148	0.038	152	0.931	160	1.000	168	1.000	156	0.117	154	0.220	92	0.994	201	1.000	185	1.000	0.000	0.001	0.080					
14	ANKE-001	164	0.013	149	0.038	157	0.946	237	1.000	233	1.000	168	0.119	153	0.220	97	0.994	186	1.000	205	1.000	0.000	0.001	0.080					
15	ANKE-002	74	0.003	76	0.016	73	0.522	51	0.005	66	0.119	78	0.032	67	0.079	48	0.948	51	0.034	45	0.245	0.001	0.001	0.049					
16	AWARE-003	19	0.031	193	0.090	174	0.966	145	0.316	131	0.290	161	0.128	179	0.298	75	0.984	135	0.428	91	0.530	0.004	0.003	0.874					
17	AWARE-004	206	0.068	206	0.176	181	0.976	137	0.122	141	0.414	194	0.269	200	0.509	148	1.000	129	0.397	114	0.816	0.003	0.003	0.776					
18	AWARE-005	19	0.031	182	0.067	182	0.978	128	0.048	134	0.308	206	0.364	160	0.253	152	1.000	122	0.255	12	0.916	0.001	0.002	0.189					
19	AWARE-006	208	0.070	200	0.128	184	0.983	139	0.111	142	0.421	198	0.276	190	0.398	143	0.999	122	0.368	106	0.749	0.001	0.002	0.189					
20	AYONIX-000	231	0.450	228	0.685	193	0.996	153	0.607	156	0.867	223	0.811	222	0.939	117	0.998	150	0.954	134	0.982	0.010	0.031	0.939					
21	AYONIX-001	226	0.341	221	0.527	188	0.993	159	0.994	154	0.778	228	0.824	217	0.920	141	0.999	154	0.999	131	0.969	0.010	0.031	0.939					
22	AYONIX-002	227	0.341	222	0.527	189	0.993	149	0.464	153	0.778	224	0.824	218	0.920	139	0.999	141	0.915	130	0.969	0.010	0.031	0.939					
23	CAMVI-003	202	0.052	194	0.090	142	0.911	138	0.093	138	0.360	128	0.071	117	0.132	56	0.970	96	0.114	74	0.402	0.006	0.013	0.675					
24	CAMVI-004	209	0.047	189	0.077	108	0.744	132	0.072	133	0.296	130	0.072	119	0.136	93	0.999	101	0.100	110	0.787	0.000	0.000	0.000					
25	CAMVI-005	208	0.065	198	0.103	110	0.746	139	0.098	137	0.341	139	0.099	147	0.179	146	1.000	108	0.156	14	0.999	0.000	0.000	0.000					
26	CIB-000	24	0.002	10	0.008	16	0.100	10	0.002	15	0.011	6	0.069	33	0.012	32	0.045	158	1.000	29	0.017	22	0.141	121	0.894	0.000	0.000	0.000	0.000
27	CLOUDWALK-HR-000	21	0.001	21	0.010	5	0.064	8	0.002	4	0.006	2	0.057	8	0.002	6	0.013	1	0.133	3	0.005	3	0.033	4	0.099	0.001	0.000	0.042	0.000
28	COGENT-000	149	0.010	166	0.046	172	0.965					106	0.053	120	0.140	103	0.995												
29	COGENT-001	159	0.010	165	0.046	173	0.965					10	0.053	121	0.140	102	0.995												
30	COGENT-002	88	0.004	101	0.020	147	0.925					94	0.044	91	0.098	114	0.998												
31	COGENT-003	99	0.004	105	0.021	156	0.939					96	0.046	85	0.095	115	0.998												
32	COGENT-004	47	0.002	51	0.013	146	0.922	44	0.004	28	0.019	61	0.113	79	0.033	38	0.051	112	0.997	36	0.022	20	0.126	79	0.456	0.000	0.000	0.000	0.000
33	COGNITEC-000	182	0.025	177	0.059	170	0.964					176	0.161	189	0.303	88	0.992												
34	COGNITEC-001	158	0.012	141	0.034	164	0.958					159	0.102	159	0.230	224	1.000												
35	COGNITEC-002	114	0.006	126	0.025	159	0.949					109	0.053	146	0.178	157	1.000												
36	COGNITEC-003	117	0.006	125	0.025	151	0.930					108	0.053	138	0.162	159	1.000												
37	COGNITEC-004	81	0.003	75	0.016	127	0.813	92	0.013	50	0.057	84	0.143	77	0.031	89	0.097	83	0.990	82	0.068	44	0.316	52	0.288	0.002	0.001	0.635	0.006
38	COGNITEC-005	31	0.002	26	0.010	103	0.713	108	0.021	45	0.037	63	0.115	29	0.010	30	0.041	214	1.000	58	0.041	29	0.157	20	0.179	0.002	0.001	0.614	0.017
39	CUBOX-000	16	0.001	24	0.010	2	0.058	6	0.002	2	0.004	1	0.049	11	0.003	12	0.019	2	0.068	7	0.004	2	0.028	1	0.073	0.001	0.000	0.042	0.000
40	CYBERLINK-000	9	0.004	99	0.020	104	0.717	75	0.007			78	0.134	118	0.056	102	0.116	105	0.995	80	0.063	6	0.339	0.001	0.001	0.063			
41	CYBERLINK-001	86	0.004	88	0.018	105	0.731	70	0.007			77	0.133	110	0.054	99	0.109	101	0.995	77	0.062	100	0.652	0.000	0.000	0.040			
42	CYBERLINK-002	6	0.003	42	0.012	86	0.577	44	0.004			54	0.107	41	0.015	44	0.053	82	0.988	3	0.024	3	0.288	0.001	0.000	0.042			
43	CYBERLINK-003	28	0.002	16	0.009	65	0.474	29	0.003	16	0.012	25	0.082	29	0.008	25	0.035	59	0.972	20	0.012								

#	ALGORITHM	INVESTIGATION MODE						IDENTIFICATION MODE						FAILURE TO EXTRACT FEATURES						
		RANK ONE MISS RATE, FNIR(N, 0, 1)						HIGH T → FPIR = .001, FNIR(N, T, L)												
		N=1.6M						N=1.6M												
	GALLERY	MUGSHOT	MUGSHOT	MUGSHOT	VISA	BORDER	VISA	MUGSHOT	MUGSHOT	MUGSHOT	VISA	BORDER	VISA	MUGSHOT	MUGSHOT	MUGSHOT	VISA	BORDER	KIOSK	
	PROBE	MUGSHOT	WEBCAM	PROFILE	BORDER	BOR <sub>2</sub> 10YR	KIOSK	MUGSHOT	WEBCAM	PROFILE	BORDER	BOR <sub>2</sub> 10YR	KIOSK	MUGSHOT	WEBCAM	PROFILE	BOR <sub>2</sub> 10YR	KIOSK		
47	DAHUA-002	<sup>30</sup> 0.002	<sup>41</sup> 0.012	<sup>44</sup> 0.304	<sup>25</sup> 0.003	<sup>20</sup> 0.084	<sup>42</sup> 0.015	<sup>30</sup> 0.046	<sup>23</sup> 0.638	<sup>26</sup> 0.017	<sup>25</sup> 0.159	<sup>0.001</sup>	<sup>0.000</sup>	<sup>0.099</sup>						
48	DAHUA-003	<sup>10</sup> 0.001	<sup>7</sup> 0.007	<sup>30</sup> 0.206	<sup>9</sup> 0.002	<sup>12</sup> 0.009	<sup>10</sup> 0.073	<sup>38</sup> 0.014	<sup>29</sup> 0.041	<sup>19</sup> 0.579	<sup>21</sup> 0.013	<sup>13</sup> 0.081	<sup>16</sup> 0.134	<sup>0.000</sup>	<sup>0.000</sup>	<sup>0.000</sup>	<sup>0.000</sup>	<sup>0.000</sup>	<sup>0.000</sup>	
49	DEEPLINT-001	<sup>10</sup> 0.001	<sup>6</sup> 0.007	<sup>29</sup> 0.200	<sup>17</sup> 0.002	<sup>11</sup> 0.073	<sup>15</sup> 0.003	<sup>7</sup> 0.014	<sup>144</sup> 1.000	<sup>8</sup> 0.006	<sup>25</sup> 0.159	<sup>0.000</sup>	<sup>0.000</sup>	<sup>0.038</sup>						
50	DEEPEA-001	<sup>97</sup> 0.004	<sup>73</sup> 0.016	<sup>128</sup> 0.814	<sup>81</sup> 0.010	<sup>83</sup> 0.140	<sup>97</sup> 0.046	<sup>92</sup> 0.101	<sup>76</sup> 0.985	<sup>86</sup> 0.077	<sup>62</sup> 0.326	<sup>0.000</sup>	<sup>0.001</sup>	<sup>0.047</sup>						
51	DERMALOG-003	<sup>210</sup> 0.126	<sup>209</sup> 0.217	<sup>144</sup> 0.296	<sup>140</sup> 0.560	<sup>215</sup> 0.482	<sup>207</sup> 0.655	<sup>144</sup> 0.677	<sup>117</sup> 0.870	<sup>0.002</sup>	<sup>0.002</sup>	<sup>0.103</sup>								
52	DERMALOG-004	<sup>215</sup> 0.125	<sup>208</sup> 0.215	<sup>150</sup> 0.930	<sup>138</sup> 0.135	<sup>144</sup> 0.467	<sup>212</sup> 0.480	<sup>210</sup> 0.657	<sup>106</sup> 0.995	<sup>140</sup> 0.603	<sup>118</sup> 0.856	<sup>0.001</sup>	<sup>0.002</sup>	<sup>0.107</sup>						
53	DERMALOG-005	<sup>16</sup> 0.015	<sup>147</sup> 0.037	<sup>101</sup> 0.701	<sup>145</sup> 0.242	<sup>149</sup> 0.384	<sup>148</sup> 0.088	<sup>13</sup> 0.154	<sup>85</sup> 0.990	<sup>125</sup> 0.300	<sup>96</sup> 0.614	<sup>0.001</sup>	<sup>0.002</sup>	<sup>0.102</sup>						
54	DERMALOG-006	<sup>134</sup> 0.008	<sup>124</sup> 0.024	<sup>92</sup> 0.619	<sup>82</sup> 0.010	<sup>91</sup> 0.155	<sup>104</sup> 0.052	<sup>95</sup> 0.105	<sup>70</sup> 0.981	<sup>75</sup> 0.059	<sup>61</sup> 0.318	<sup>0.003</sup>	<sup>0.006</sup>	<sup>0.181</sup>						
55	DERMALOG-007	<sup>146</sup> 0.009	<sup>129</sup> 0.027	<sup>96</sup> 0.675	<sup>96</sup> 0.014	<sup>97</sup> 0.170	<sup>143</sup> 0.086	<sup>124</sup> 0.152	<sup>94</sup> 0.990	<sup>92</sup> 0.099	<sup>91</sup> 0.557	<sup>0.001</sup>	<sup>0.002</sup>	<sup>0.102</sup>						
56	DERMALOG-008	<sup>73</sup> 0.003	<sup>66</sup> 0.015	<sup>71</sup> 0.516	<sup>68</sup> 0.007	<sup>43</sup> 0.029	<sup>82</sup> 0.139	<sup>96</sup> 0.045	<sup>82</sup> 0.094	<sup>178</sup> 1.000	<sup>72</sup> 0.057	<sup>48</sup> 0.382	<sup>127</sup> 0.940	<sup>0.000</sup>	<sup>0.000</sup>	<sup>0.002</sup>	<sup>0.000</sup>	<sup>0.000</sup>	<sup>0.000</sup>	
57	EYEDEA-003	<sup>210</sup> 0.080	<sup>202</sup> 0.148	<sup>168</sup> 0.960	<sup>135</sup> 0.101	<sup>139</sup> 0.379	<sup>204</sup> 0.388	<sup>202</sup> 0.543	<sup>98</sup> 0.994	<sup>138</sup> 0.570	<sup>111</sup> 0.792	<sup>0.001</sup>	<sup>0.003</sup>	<sup>0.161</sup>						
58	F-001	<sup>160</sup> 0.012	<sup>95</sup> 0.669	<sup>170</sup> 1.000	<sup>161</sup> 1.000	<sup>171</sup> 0.166	<sup>124</sup> 0.998	<sup>124</sup> 0.998	<sup>124</sup> 0.998	<sup>124</sup> 0.998	<sup>124</sup> 0.998	<sup>124</sup> 0.998	<sup>124</sup> 0.998	<sup>124</sup> 0.998	<sup>124</sup> 0.998	<sup>124</sup> 0.998	<sup>124</sup> 0.998	<sup>124</sup> 0.998	<sup>124</sup> 0.998	
59	FINCORE-000	<sup>152</sup> 0.011	<sup>142</sup> 0.034	<sup>115</sup> 0.767	<sup>116</sup> 0.032	<sup>53</sup> 0.117	<sup>106</sup> 0.191	<sup>160</sup> 0.134	<sup>152</sup> 0.217	<sup>154</sup> 1.000	<sup>114</sup> 0.187	<sup>51</sup> 0.598	<sup>80</sup> 0.458	<sup>0.000</sup>	<sup>0.001</sup>	<sup>0.043</sup>	<sup>0.000</sup>	<sup>0.000</sup>	<sup>0.000</sup>	
60	GLORY-000	<sup>22</sup> 0.178	<sup>215</sup> 0.320	<sup>192</sup> 0.994	<sup>142</sup> 0.228	<sup>159</sup> 0.678	<sup>205</sup> 0.367	<sup>207</sup> 0.547	<sup>180</sup> 0.995	<sup>134</sup> 0.453	<sup>117</sup> 0.839	<sup>0.011</sup>	<sup>0.013</sup>	<sup>0.985</sup>						
61	GLORY-001	<sup>217</sup> 0.127	<sup>212</sup> 0.267	<sup>187</sup> 0.992	<sup>141</sup> 0.178	<sup>149</sup> 0.594	<sup>196</sup> 0.305	<sup>201</sup> 0.537	<sup>89</sup> 0.993	<sup>131</sup> 0.408	<sup>115</sup> 0.819	<sup>0.011</sup>	<sup>0.013</sup>	<sup>0.988</sup>						
62	GORILLA-001	<sup>203</sup> 0.060	<sup>195</sup> 0.095	<sup>154</sup> 0.936	<sup>130</sup> 0.069	<sup>135</sup> 0.329	<sup>208</sup> 0.406	<sup>198</sup> 0.453	<sup>175</sup> 1.000	<sup>135</sup> 0.468	<sup>238</sup> 1.000	<sup>0.001</sup>	<sup>0.001</sup>	<sup>0.069</sup>						
63	GORILLA-002	<sup>179</sup> 0.020	<sup>162</sup> 0.044	<sup>111</sup> 0.753	<sup>110</sup> 0.027	<sup>116</sup> 0.214	<sup>184</sup> 0.188	<sup>123</sup> 0.268	<sup>177</sup> 1.000	<sup>121</sup> 0.250	<sup>145</sup> 1.000	<sup>0.001</sup>	<sup>0.001</sup>	<sup>0.069</sup>						
64	GORILLA-003	<sup>19</sup> 0.036	<sup>184</sup> 0.070	<sup>129</sup> 0.821	<sup>125</sup> 0.048	<sup>126</sup> 0.265	<sup>198</sup> 0.318	<sup>194</sup> 0.434	<sup>127</sup> 1.000	<sup>130</sup> 0.407	<sup>217</sup> 1.000	<sup>0.001</sup>	<sup>0.001</sup>	<sup>0.069</sup>						
65	GORILLA-004	<sup>119</sup> 0.006	<sup>121</sup> 0.024	<sup>100</sup> 0.697	<sup>87</sup> 0.012	<sup>94</sup> 0.162	<sup>148</sup> 0.089	<sup>137</sup> 0.160	<sup>80</sup> 0.959	<sup>102</sup> 0.135	<sup>76</sup> 0.438	<sup>0.000</sup>	<sup>0.001</sup>	<sup>0.042</sup>						
66	GORILLA-005	<sup>8</sup> 0.003	<sup>38</sup> 0.018	<sup>31</sup> 0.209	<sup>62</sup> 0.006	<sup>60</sup> 0.124	<sup>115</sup> 0.058	<sup>124</sup> 0.142	<sup>26</sup> 0.909	<sup>90</sup> 0.088	<sup>61</sup> 0.315	<sup>0.000</sup>	<sup>0.000</sup>	<sup>0.040</sup>						
67	HIK-003	<sup>157</sup> 0.012	<sup>132</sup> 0.027	<sup>99</sup> 0.689	<sup>88</sup> 0.012	<sup>88</sup> 0.151	<sup>153</sup> 0.103	<sup>133</sup> 0.158	<sup>54</sup> 0.969	<sup>105</sup> 0.142	<sup>78</sup> 0.445	<sup>0.000</sup>	<sup>0.000</sup>	<sup>0.048</sup>						
68	HIK-004	<sup>15</sup> 0.011	<sup>130</sup> 0.027	<sup>107</sup> 0.743	<sup>86</sup> 0.012	<sup>90</sup> 0.152	<sup>149</sup> 0.099	<sup>131</sup> 0.153	<sup>61</sup> 0.976	<sup>103</sup> 0.137	<sup>77</sup> 0.434	<sup>0.000</sup>	<sup>0.000</sup>	<sup>0.048</sup>						
69	HIK-005	<sup>102</sup> 0.005	<sup>78</sup> 0.017	<sup>77</sup> 0.535	<sup>72</sup> 0.007	<sup>58</sup> 0.111	<sup>91</sup> 0.044	<sup>66</sup> 0.077	<sup>142</sup> 0.999	<sup>81</sup> 0.068	<sup>92</sup> 0.541	<sup>0.000</sup>	<sup>0.000</sup>	<sup>0.000</sup>						
70	HIK-006	<sup>10</sup> 0.005	<sup>77</sup> 0.017	<sup>78</sup> 0.535	<sup>72</sup> 0.007	<sup>59</sup> 0.047	<sup>74</sup> 0.086	<sup>172</sup> 1.000	<sup>73</sup> 0.000	<sup>124</sup> 0.998	<sup>124</sup> 0.998	<sup>124</sup> 0.998	<sup>124</sup> 0.998	<sup>124</sup> 0.998	<sup>124</sup> 0.998	<sup>124</sup> 0.998	<sup>124</sup> 0.998	<sup>124</sup> 0.998	<sup>124</sup> 0.998	
71	HYPERVERGE-001	<sup>10</sup> 0.001	<sup>34</sup> 0.011	<sup>7</sup> 0.067	<sup>3</sup> 0.002	<sup>3</sup> 0.007	<sup>8</sup> 0.061	<sup>16</sup> 0.004	<sup>22</sup> 0.031	<sup>5</sup> 0.220	<sup>11</sup> 0.007	<sup>9</sup> 0.053	<sup>7</sup> 0.101	<sup>0.001</sup>	<sup>0.000</sup>	<sup>0.041</sup>	<sup>0.000</sup>	<sup>0.000</sup>	<sup>0.000</sup>	
72	IDEMIA-003	<sup>125</sup> 0.007	<sup>140</sup> 0.034	<sup>163</sup> 0.958	<sup>102</sup> 0.018	<sup>113</sup> 0.210	<sup>100</sup> 0.047	<sup>139</sup> 0.165	<sup>98</sup> 0.123	<sup>109</sup> 0.766	<sup>0.000</sup>	<sup>0.000</sup>	<sup>0.041</sup>							
73	IDEMIA-004	<sup>12</sup> 0.007	<sup>138</sup> 0.032	<sup>158</sup> 0.947	<sup>101</sup> 0.018	<sup>112</sup> 0.210	<sup>87</sup> 0.037	<sup>105</sup> 0.118	<sup>60</sup> 0.973	<sup>99</sup> 0.123	<sup>108</sup> 0.766	<sup>0.000</sup>	<sup>0.000</sup>	<sup>0.041</sup>						
74	IDEMIA-005	<sup>133</sup> 0.008	<sup>154</sup> 0.039	<sup>161</sup> 0.954	<sup>107</sup> 0.021	<sup>117</sup> 0.217	<sup>93</sup> 0.044	<sup>128</sup> 0.150	<sup>65</sup> 0.978	<sup>100</sup> 0.130	<sup>120</sup> 0.879	<sup>0.000</sup>	<sup>0.000</sup>	<sup>0.041</sup>						
75	IDEMIA-006	<sup>14</sup> 0.010	<sup>186</sup> 0.072	<sup>176</sup> 0.969	<sup>112</sup> 0.030	<sup>125</sup> 0.253	<sup>96</sup> 0.043	<sup>15</sup> 0.226	<sup>72</sup> 0.982	<sup>106</sup> 0.144	<sup>104</sup> 0.733	<sup>0.000</sup>	<sup>0.000</sup>	<sup>0.041</sup>						
76	IDEMIA-007	<sup>67</sup> 0.003	<sup>70</sup> 0.015	<sup>218</sup> 1.000	<sup>63</sup> 0.006	<sup>44</sup> 0.036	<sup>74</sup> 0.131	<sup>49</sup> 0.018	<sup>46</sup> 0.055	<sup>190</sup> 1.000	<sup>68</sup> 0.052	<sup>31</sup> 0.182	<sup>156</sup> 1.000	<sup>0.000</sup>	<sup>0.000</sup>	<sup>0.040</sup>	<sup>0.000</sup>	<sup>0.000</sup>	<sup>0.000</sup>	
77	IDEMIA-008	<sup>0.001</sup>	<sup>3</sup> 0.007	<sup>12</sup> 0.079	<sup>4</sup> 0.001	<sup>7</sup> 0.007	<sup>10</sup> 0.075	<sup>3</sup> 0.002	<sup>3</sup> 0.013	<sup>4</sup> 0.204	<sup>4</sup> 0.005	<sup>3</sup> 0.036	<sup>7</sup> 0.106	<sup>0.000</sup>	<sup>0.000</sup>	<sup>0.040</sup>	<sup>0.000</sup>	<sup>0.000</sup>	<sup>0.000</sup>	
78	IMAGUS-002	<sup>223</sup> 0.220	<sup>213</sup> 0.301	<sup>186</sup> 0.988	<sup>222</sup> 0.749	<sup>214</sup> 0.816	<sup>169</sup> 1.000	<sup>222</sup> 0.807	<sup>219</sup> 0.909	<sup>161</sup> 1.000	<sup>204</sup> 0.995	<sup>0.004</sup>	<sup>0.008</sup>	<sup>0.550</sup>						
79	IMAGUS-003	<sup>228</sup> 0.356	<sup>219</sup> 0.513	<sup>190</sup> 0.993	<sup>222</sup> 0.807	<sup>219</sup> 0.909	<sup>161</sup> 1.000	<sup>222</sup> 0.807	<sup>219</sup> 0.909	<sup>161</sup> 1.000	<sup>204</sup> 0.995	<sup>0.004</sup>	<sup>0.008</sup>	<sup>0.550</sup>						
80	IMAGUS-005	<sup>41</sup> 0.002	<sup>43</sup> 0.012	<sup>46</sup> 0.319	<sup>61</sup> 0.006	<sup>30</sup> 0.022	<sup>76</sup> 0.132	<sup>52</sup> 0.018	<sup>51</sup> 0.066	<sup>37</sup> 0.838	<sup>41</sup> 0.029	<sup>29</sup> 0.161	<sup>40</sup> 0.231	<sup>0.000</sup>	<sup>0.000</sup>	<sup>0.000</sup>	<sup>0.000</sup>	<sup>0.000</sup>	<sup>0.000</sup>	
81	IMAGUS-006	<sup>49</sup> 0.002	<sup>55</sup> 0.014	<sup>43</sup> 0.293	<sup>43</sup> 0.004	<sup>29</sup> 0.019	<sup>59</sup> 0.112	<sup>54</sup> 0.019	<sup>57</sup> 0.069	<sup>44</sup> 0.897	<sup>40</sup> 0.028	<sup>29</sup> 0.161	<sup>47</sup> 0.260	<sup>0.000</sup>	<sup>0.000</sup>	<sup>0.000</sup>	<sup>0.000</sup>	<sup>0.000</sup>	<sup>0.000</sup>	
82	IMPERIAL-000	<sup>6</sup> 0.002	<sup>67</sup> 0.015	<sup>42</sup> 0.280	<sup>49</sup> 0.004	<sup>39</sup> 0.097	<sup>65</sup> 0.026	<sup>50</sup> 0.068	<sup>28</sup> 0.999	<sup>59</sup> 0.042	<sup>44</sup> 0.245	<sup>0.000</sup>	<sup>0.000</sup>	<sup>0.000</sup>						
83	INCODE-000	<sup>201</sup> 0.049	<sup>197</sup> 0.100	<sup>160</sup> 0.951	<sup>197</sup> 0.310	<sup>192</sup> 0.420	<sup>121</sup> 0.998	<sup>197</sup> 0.310	<sup>191</sup> 0.420	<sup>121</sup> 0.998	<sup>197</sup> 0.310	<sup>0.001</sup>	<sup>0.004</sup>	<sup>0.173</sup>						
84	INCODE-001	<sup>17</sup> 0.017	<sup>16</sup> 0.046	<sup>146</sup> 0.762	<sup>17</sup> 0.005	<sup>187</sup> 0.212	<sup>17</sup> 0.296	<sup>168</sup> 1.000	<sup>187</sup> 0.212	<sup>17</sup> 0.296	<sup>168</sup> 1.000	<sup>0.001</sup>	<sup>0.004</sup>	<sup>0.173</sup>						
85	INCODE-002	<sup>174</sup> 0.018	<sup>169</sup> 0.048	<sup>132</sup> 0.843	<sup>173</sup> 0.184	<sup>174</sup> 0.269	<sup>90</sup> 0.993	<sup>173</sup> 0.184	<sup>174</sup> 0.269	<sup>90</sup> 0.993	<sup>173</sup> 0.184	<sup>0.000</sup>	<sup>0.001</sup>	<sup>0.066</sup>						
86	INCODE-003	<sup>16</sup> 0.013	<sup>156</sup> 0.040	<sup>113</sup> 0.764	<sup>17</sup> 0.005	<sup>178</sup> 0.167	<sup>174</sup> 0.264	<sup>140</sup> 0.999	<sup>178</sup> 0.167	<sup>174</sup> 0.264	<sup>140</sup> 0.999	<sup>0.000</sup>	<sup>0.001</sup>	<sup>0.066</sup>						
87	INCODE-004	<sup>87</sup> 0.004	<sup>8</sup>																	

Table 10: **Miss rates by dataset**: At left, rank 1 miss rates relevant to investigations; at right, with threshold set to target  $FPIR = 0.01$  for higher volume, low prior, uses. Yellow indicates most accurate algorithm. Throughout blue superscripts indicate the rank of the algorithm for that column.

2021/09/21  
09:55:08

$\text{FNIR}(N, R, I) =$  False neg. identification rate  
 $\text{FPIR}(N, T) =$  False pos. identification rate

R = Num. candidates examined

T = Threshold

$T = 0 \rightarrow$  Investigation  
 $T > 0 \rightarrow$  Identification

#	ALGORITHM	INVESTIGATION MODE						IDENTIFICATION MODE						FAILURE TO EXTRACT FEATURES						
		RANK ONE MISS RATE, FNIR(N, 0, 1)						HIGH T → FPIR = 0.001, FNIR(N, T, L)						N=1.6M						
		N=1.6M			N=1.6M			N=1.6M			N=1.6M			N=1.6M			N=1.6M			
		MUGSHOT	MUGSHOT	MUGSHOT	VISA	BORDER	VISA	MUGSHOT	MUGSHOT	MUGSHOT	VISA	BORDER	VISA	MUGSHOT	MUGSHOT	MUGSHOT	VISA	BORDER	KIOSK	
93	PROBE	MUGSHOT	WEBCAM	PROFILE	BORDER	BOR;10YR	KIOSK	MUGSHOT	WEBCAM	PROFILE	BORDER	BOR;10YR	KIOSK	MUGSHOT	WEBCAM	PROFILE	BORDER	BOR;10YR	KIOSK	
94	INNOVATRICS-007	<sup>34</sup> 0.002	<sup>36</sup> 0.011	<sup>31</sup> 0.248	<sup>19</sup> 0.002	<sup>22</sup> 0.013	<sup>15</sup> 0.077	<sup>34</sup> 0.013	<sup>39</sup> 0.051	<sup>22</sup> 0.743	<sup>27</sup> 0.017	<sup>15</sup> 0.093	<sup>19</sup> 0.154	0.000	0.001	0.041	0.000	0.000	0.000	
95	INTSYSMSU-000	<sup>218</sup> 0.146	<sup>119</sup> 0.023	<sup>81</sup> 0.562	<sup>131</sup> 0.002	<sup>75</sup> 0.132	<sup>232</sup> 0.998	<sup>227</sup> 1.000	<sup>150</sup> 1.000	<sup>159</sup> 0.999	<sup>143</sup> 0.999	0.000	0.000	0.050	0.000	0.000	0.000	0.000	0.000	
96	IREX-000	<sup>98</sup> 0.004	<sup>17</sup> 0.010	<sup>97</sup> 0.681	<sup>16</sup> 0.002	<sup>17</sup> 0.012	<sup>23</sup> 0.082	<sup>73</sup> 0.028	<sup>50</sup> 0.060	<sup>49</sup> 0.957	<sup>62</sup> 0.044	<sup>43</sup> 0.302	<sup>22</sup> 0.170	0.000	0.000	0.042	0.000	0.000	0.000	
97	ISYSTEMS-002	<sup>120</sup> 0.006	<sup>127</sup> 0.026	<sup>131</sup> 0.844				<sup>136</sup> 0.078	<sup>113</sup> 0.126	<sup>111</sup> 0.998				0.002	0.002	0.142				
98	ISYSTEMS-003	<sup>108</sup> 0.005	<sup>116</sup> 0.023	<sup>117</sup> 0.791				<sup>128</sup> 0.059	<sup>98</sup> 0.107	<sup>151</sup> 1.000				0.002	0.002	0.142				
99	KAKAO-000	<sup>20</sup> 0.001	<sup>29</sup> 0.011	<sup>15</sup> 0.119	<sup>21</sup> 0.002	<sup>19</sup> 0.013	<sup>18</sup> 0.078	<sup>44</sup> 0.015	<sup>47</sup> 0.056	<sup>15</sup> 0.468	<sup>31</sup> 0.019	<sup>21</sup> 0.141	<sup>21</sup> 0.158	0.000	0.000	0.041	0.000	0.000	0.000	
100	KNERON-000	<sup>115</sup> 0.006	<sup>131</sup> 0.027	<sup>81</sup> 0.552	<sup>11</sup> 0.028	<sup>107</sup> 0.195								0.000	0.000	0.000				
101	KNERON-001	<sup>189</sup> 0.030	<sup>227</sup> 0.621	<sup>37</sup> 0.237	<sup>140</sup> 0.144	<sup>54</sup> 0.207	<sup>128</sup> 0.280							0.000	0.000	0.000	0.000	0.000	0.000	
102	LINE-000	<sup>54</sup> 0.002	<sup>56</sup> 0.014	<sup>31</sup> 0.223	<sup>34</sup> 0.005	<sup>41</sup> 0.029	<sup>51</sup> 0.107	<sup>76</sup> 0.031	<sup>86</sup> 0.095		<sup>63</sup> 0.046	<sup>41</sup> 0.278	<sup>172</sup> 1.000	0.000	0.000	0.000	0.000	0.000	0.000	
103	LOOKMAN-003	<sup>138</sup> 0.009	<sup>152</sup> 0.038	<sup>121</sup> 0.035			<sup>120</sup> 0.239	<sup>92</sup> 0.044	<sup>101</sup> 0.112	<sup>89</sup> 0.084		<sup>65</sup> 0.355	0.000	0.000						
104	LOOKMAN-004	<sup>140</sup> 0.009	<sup>155</sup> 0.039	<sup>180</sup> 0.973				<sup>95</sup> 0.045	<sup>97</sup> 0.105	<sup>62</sup> 0.977				0.000	0.000	0.000				
105	LOOKMAN-005	<sup>132</sup> 0.008	<sup>146</sup> 0.036	<sup>179</sup> 0.972	<sup>120</sup> 0.035		<sup>119</sup> 0.237	<sup>75</sup> 0.030	<sup>73</sup> 0.086	<sup>64</sup> 0.978	<sup>78</sup> 0.062		<sup>57</sup> 0.308	0.000	0.000	0.000				
106	MEGVII-001	<sup>158</sup> 0.012	<sup>85</sup> 0.017	<sup>189</sup> 1.000				<sup>131</sup> 0.072	<sup>90</sup> 0.097					0.002	0.000					
107	MEGVII-002	<sup>159</sup> 0.012	<sup>87</sup> 0.017	<sup>62</sup> 0.450	<sup>204</sup> 1.000			<sup>135</sup> 0.077	<sup>88</sup> 0.096	<sup>123</sup> 0.998				0.002	0.000	0.033				
108	MICROFOCUS-003	<sup>235</sup> 0.594	<sup>231</sup> 0.781	<sup>158</sup> 0.708			<sup>158</sup> 0.907	<sup>228</sup> 0.931	<sup>226</sup> 0.979		<sup>152</sup> 0.982		<sup>138</sup> 0.991	0.001	0.005					
109	MICROFOCUS-004	<sup>233</sup> 0.576	<sup>230</sup> 0.758		<sup>155</sup> 0.701		<sup>157</sup> 0.904	<sup>233</sup> 0.999	<sup>224</sup> 0.975		<sup>153</sup> 0.974		<sup>136</sup> 0.989	0.001	0.005					
110	MICROFOCUS-005	<sup>229</sup> 0.424	<sup>225</sup> 0.601		<sup>151</sup> 0.494		<sup>152</sup> 0.777	<sup>226</sup> 0.835	<sup>220</sup> 0.928		<sup>148</sup> 0.935		<sup>135</sup> 0.985	0.001	0.005					
111	MICROFOCUS-006	<sup>230</sup> 0.427	<sup>224</sup> 0.583		<sup>150</sup> 0.490		<sup>155</sup> 0.782	<sup>230</sup> 0.978	<sup>219</sup> 0.923		<sup>148</sup> 0.923		<sup>132</sup> 0.971	0.001	0.005					
112	MICROSOFT-003	<sup>29</sup> 0.002	<sup>46</sup> 0.012		<sup>40</sup> 0.004		<sup>56</sup> 0.109	<sup>71</sup> 0.028	<sup>80</sup> 0.091		<sup>53</sup> 0.036		<sup>42</sup> 0.233	0.000	0.001					
113	MICROSOFT-004	<sup>22</sup> 0.001	<sup>45</sup> 0.012		<sup>34</sup> 0.004		<sup>57</sup> 0.109	<sup>66</sup> 0.026	<sup>75</sup> 0.087		<sup>49</sup> 0.033		<sup>38</sup> 0.222	0.000	0.001					
114	MICROSOFT-005	<sup>42</sup> 0.002	<sup>33</sup> 0.011	<sup>22</sup> 0.144	<sup>29</sup> 0.003		<sup>40</sup> 0.099	<sup>64</sup> 0.026	<sup>59</sup> 0.070	<sup>20</sup> 0.587	<sup>38</sup> 0.027		<sup>30</sup> 0.180	0.000	0.001	0.049				
115	MICROSOFT-006	<sup>46</sup> 0.002	<sup>40</sup> 0.011	<sup>27</sup> 0.150	<sup>38</sup> 0.004		<sup>42</sup> 0.100	<sup>20</sup> 0.012	<sup>27</sup> 0.037	<sup>8</sup> 0.386	<sup>49</sup> 0.032		<sup>28</sup> 0.178	0.000	0.001	0.049				
116	NEC-000	<sup>171</sup> 0.017	<sup>160</sup> 0.041	<sup>167</sup> 0.959	<sup>108</sup> 0.025		<sup>122</sup> 0.243	<sup>138</sup> 0.079	<sup>122</sup> 0.140	<sup>66</sup> 0.979		<sup>83</sup> 0.474	0.001	0.002	0.890					
117	NEC-001	<sup>180</sup> 0.021	<sup>173</sup> 0.056	<sup>171</sup> 0.967	<sup>11</sup> 0.033		<sup>125</sup> 0.277	<sup>150</sup> 0.106	<sup>149</sup> 0.197	<sup>79</sup> 0.986	<sup>101</sup> 0.133		<sup>82</sup> 0.468	0.005	0.003	0.934				
118	NEC-002	<sup>5</sup> 0.001	<sup>15</sup> 0.009	<sup>51</sup> 0.363	<sup>35</sup> 0.003		<sup>64</sup> 0.117	<sup>10</sup> 0.003	<sup>13</sup> 0.020	<sup>138</sup> 0.999	<sup>13</sup> 0.008		<sup>102</sup> 0.676	0.000	0.001	0.041				
119	NEC-003	<sup>13</sup> 0.001	<sup>22</sup> 0.010	<sup>51</sup> 0.352	<sup>27</sup> 0.004	<sup>18</sup> 0.013	<sup>67</sup> 0.120	<sup>8</sup> 0.002	<sup>11</sup> 0.017	<sup>34</sup> 0.824	<sup>16</sup> 0.008	<sup>6</sup> 0.036	<sup>101</sup> 0.668	0.000	0.001	0.041	<sup>0.001</sup>	<sup>0.001</sup>	<sup>0.001</sup>	
120	NEC-004	<sup>17</sup> 0.001	<sup>14</sup> 0.009	<sup>79</sup> 0.538	<sup>28</sup> 0.003	<sup>9</sup> 0.007	<sup>13</sup> 0.075	<sup>3</sup> 0.002	<sup>4</sup> 0.013	<sup>22</sup> 0.622	<sup>3</sup> 0.004	<sup>1</sup> 0.019	<sup>6</sup> 0.100	0.000	0.001	0.041				
121	NEUROTECHNOLOGY-003	<sup>181</sup> 0.022	<sup>161</sup> 0.042	<sup>167</sup> 0.961				<sup>219</sup> 0.636	<sup>172</sup> 0.266	<sup>182</sup> 1.000				0.000	0.001	0.131				
122	NEUROTECHNOLOGY-004	<sup>110</sup> 0.006	<sup>98</sup> 0.020	<sup>17</sup> 0.970				<sup>125</sup> 0.063	<sup>103</sup> 0.117	<sup>95</sup> 0.994				0.000	0.001	0.131				
123	NEUROTECHNOLOGY-005	<sup>96</sup> 0.004	<sup>123</sup> 0.024	<sup>139</sup> 0.893				<sup>113</sup> 0.054	<sup>115</sup> 0.130	<sup>116</sup> 0.998				0.000	0.000	0.030				
124	NEUROTECHNOLOGY-006	<sup>175</sup> 0.018	<sup>164</sup> 0.045	<sup>96</sup> 0.606				<sup>193</sup> 0.249	<sup>191</sup> 0.418					0.000	0.000					
125	NEUROTECHNOLOGY-007	<sup>91</sup> 0.004	<sup>104</sup> 0.021	<sup>120</sup> 0.796	<sup>80</sup> 0.009		<sup>103</sup> 0.180	<sup>124</sup> 0.062	<sup>143</sup> 0.173	<sup>156</sup> 1.000	<sup>126</sup> 0.339		<sup>165</sup> 1.000	0.001	0.001	0.041				
126	NEUROTECHNOLOGY-008	<sup>53</sup> 0.002	<sup>61</sup> 0.014	<sup>61</sup> 0.457	<sup>43</sup> 0.004	<sup>32</sup> 0.023	<sup>44</sup> 0.101	<sup>108</sup> 0.053	<sup>69</sup> 0.080	<sup>167</sup> 1.000	<sup>53</sup> 0.035	<sup>42</sup> 0.293	<sup>35</sup> 0.203	0.000	0.001	0.052	<sup>0.001</sup>	<sup>0.001</sup>	<sup>0.001</sup>	
127	NEUROTECHNOLOGY-009	<sup>18</sup> 0.001	<sup>30</sup> 0.011	<sup>29</sup> 0.179	<sup>12</sup> 0.002	<sup>21</sup> 0.013	<sup>19</sup> 0.079		<sup>45</sup> 0.015	<sup>42</sup> 0.052	<sup>21</sup> 0.588	<sup>32</sup> 0.020	<sup>25</sup> 0.153	<sup>24</sup> 0.165	0.001	0.000	0.046			
128	NEWLAND-002	<sup>209</sup> 0.079	<sup>199</sup> 0.117	<sup>153</sup> 0.936				<sup>210</sup> 0.438	<sup>197</sup> 0.466	<sup>131</sup> 0.999				0.007	<sup>0.012</sup>	0.200				
129	NOBLIS-001	<sup>225</sup> 0.249	<sup>220</sup> 0.522	<sup>19</sup> 0.993				<sup>235</sup> 1.000	<sup>233</sup> 1.000	<sup>174</sup> 1.000				0.000	0.000	0.000				
130	NOBLIS-002	<sup>221</sup> 0.179	<sup>217</sup> 0.392	<sup>183</sup> 0.982				<sup>231</sup> 0.997	<sup>239</sup> 1.000	<sup>166</sup> 1.000				0.000	0.000	0.000				
131	NTECHLAB-003	<sup>116</sup> 0.006	<sup>113</sup> 0.023	<sup>67</sup> 0.504				<sup>111</sup> 0.054	<sup>104</sup> 0.118	<sup>36</sup> 0.837				0.000	0.000	0.040				
132	NTECHLAB-004	<sup>105</sup> 0.005	<sup>94</sup> 0.019	<sup>61</sup> 0.506	<sup>27</sup> 0.008		<sup>71</sup> 0.129	<sup>88</sup> 0.041	<sup>96</sup> 0.105	<sup>35</sup> 0.833	<sup>70</sup> 0.053		<sup>49</sup> 0.263	0.000	0.000	0.040				
133	NTECHLAB-005	<sup>103</sup> 0.005	<sup>90</sup> 0.018	<sup>51</sup> 0.367	<sup>28</sup> 0.008		<sup>65</sup> 0.118	<sup>89</sup> 0.042	<sup>94</sup> 0.102	<sup>36</sup> 0.771	<sup>81</sup> 0.073		<sup>54</sup> 0.294	0.000	0.000	0.040				
134	NTECHLAB-006	<sup>95</sup> 0.004	<sup>82</sup> 0.017	<sup>52</sup> 0.347	<sup>74</sup> 0.007		<sup>62</sup> 0.113	<sup>83</sup> 0.037	<sup>83</sup> 0.094	<sup>29</sup> 0.754	<sup>73</sup> 0.057		<sup>48</sup> 0.260	0.000	0.000	0.040				
135	NTECHLAB-007	<sup>69</sup> 0.003	<sup>47</sup> 0.012	<sup>41</sup> 0.326	<sup>48</sup> 0.004		<sup>52</sup> 0.107	<sup>63</sup> 0.026	<sup>55</sup> 0.067	<sup>28</sup> 0.750	<sup>47</sup> 0.032		<sup>39</sup> 0.223	0.000	0.000	0.042				
136	NTECHLAB-008	<sup>35</sup> 0.002	<sup>18</sup> 0.010	<sup>20</sup> 0.157	<sup></sup>															

#	ALGORITHM	INVESTIGATION MODE										IDENTIFICATION MODE										FAILURE TO EXTRACT FEATURES											
		RANK ONE MISS RATE, FNIR(N, 0, 1)					N=1.6M					HIGH T → FPIR = 0.001, FNIR(N, T, L)					N=1.6M																
		GALLERY	MUGSHOT	MUGSHOT	MUGSHOT	VISA	BORDER	BOR <sub>2</sub> 10YR	KIOSK	VISA	MUGSHOT	MUGSHOT	MUGSHOT	VISA	BORDER	BOR <sub>2</sub> 10YR	KIOSK	MUGSHOT	MUGSHOT	MUGSHOT	VISA	BORDER	KIOSK	MUGSHOT	MUGSHOT	MUGSHOT	VISA	BORDER	KIOSK				
139	PARAVISION-000	176	0.019	151	0.038	76	0.534	14	0.423	147	0.529	14	0.089	141	0.170	133	0.999	13	0.470	126	0.926	0.000	0.000	0.000	0.000	0.000	0.000	0.000	0.000	0.000			
140	PARAVISION-001	89	0.004	102	0.020	48	0.329	147	0.414	146	0.484	101	0.049	114	0.128	126	0.999	133	0.444	105	0.739	0.000	0.000	0.000	0.000	0.000	0.000	0.000	0.000	0.000			
141	PARAVISION-002	94	0.004	107	0.022	50	0.335	9	0.015	99	0.175	102	0.050	107	0.119	73	0.983	8	0.080	86	0.497	0.000	0.000	0.032	0.000	0.000	0.000	0.000	0.000	0.000			
142	PARAVISION-003	79	0.003	95	0.019	39	0.252	98	0.015	96	0.167	81	0.035	87	0.096	96	0.994	74	0.058	35	0.296	0.000	0.000	0.032	0.000	0.000	0.000	0.000	0.000	0.000			
143	PARAVISION-004	30	0.002	27	0.010	17	0.104	9	0.006	60	0.112	28	0.010	173	1.000	30	0.018	122	0.908	0.000	0.000	0.032	0.000	0.000	0.000	0.000	0.000	0.000					
144	PARAVISION-005	26	0.002	19	0.010	11	0.079	71	0.007	50	0.106	15	0.004	15	0.024	67	0.980	17	0.011	14	0.132	0.000	0.000	0.038	0.000	0.000	0.000	0.000	0.000	0.000			
145	PARAVISION-007	9	0.001	9	0.008	6	0.066	53	0.005	13	0.010	43	0.101	14	0.004	16	0.025	176	1.000	19	0.113	238	1.000	0.000	0.000	0.000	0.000	0.000	0.000	0.000	0.000		
146	PIXELALL-002	100	0.005	109	0.022	123	0.810	84	0.011	104	0.187	154	0.105	189	0.388	163	1.000	130	0.602	157	1.000	0.000	0.000	0.000	0.000	0.000	0.000	0.000	0.000	0.000			
147	PIXELALL-003	52	0.002	60	0.014	70	0.515	67	0.006	87	0.151	88	0.022	62	0.073	145	1.000	56	0.037	93	0.554	0.000	0.000	0.000	0.000	0.000	0.000	0.000	0.000	0.000			
148	PIXELALL-004	50	0.002	64	0.015	74	0.523	59	0.005	89	0.152	81	0.018	68	0.079	160	1.000	6	0.051	139	0.994	0.000	0.000	0.000	0.000	0.000	0.000	0.000	0.000				
149	PIXELALL-005	43	0.002	32	0.011	41	0.264	87	0.012	38	0.028	85	0.146	32	0.012	37	0.050	170	1.000	39	0.027	34	0.203	144	1.000	0.000	0.000	0.000	0.000	0.000			
150	P-TAKURATSU-000	78	0.003	81	0.017	89	0.605	59	0.005	36	0.027	49	0.105	82	0.037	112	0.124	46	0.924	6	0.046	36	0.206	41	0.232	0.000	0.001	0.039	0.000	0.000	0.000		
151	QNAP-000	130	0.008	134	0.027	72	0.522	94	0.013	48	0.054	92	0.158	165	0.129	161	0.238	181	1.000	115	0.191	80	0.539	141	0.998	0.001	0.000	0.054	0.000	0.000	0.000	0.000	0.000
152	QUANTASOFT-001	222	0.218	229	0.727								22	0.639																			
153	RANKONE-002	178	0.019	188	0.071								159	0.118	168	0.261																	
154	RANKONE-003	177	0.019	183	0.068								158	0.118	167	0.255																	
155	RANKONE-004	198	0.041	201	0.141								185	0.193	193	0.426																	
156	RANKONE-005	144	0.009	159	0.041	185	0.986						12	0.059	144	0.173	118	0.998													0.489		
157	RANKONE-006	107	0.005	121	0.797								84	0.037	63	0.977															0.167		
158	RANKONE-007	83	0.003	93	0.019	119	0.796						60	0.022	84	0.095	53	0.967											0.001	0.001	0.102		
159	RANKONE-009	61	0.002	49	0.013	80	0.549	58	0.006	79	0.134	48	0.018	64	0.076	55	0.969	78	0.062	63	0.328	0.000	0.000	0.000	0.000	0.000	0.000	0.000	0.000	0.000			
160	RANKONE-010	35	0.002	20	0.010	56	0.374	52	0.005	35	0.027	69	0.126	37	0.014	48	0.058	32	0.802	69	0.052	37	0.208	46	0.259	0.000	0.000	0.000	0.000	0.000	0.000		
161	RANKONE-011	23	0.002	38	0.011	34	0.223	36	0.004	27	0.019	26	0.082	25	0.009	35	0.048			30	0.182	133	0.977	0.000	0.000	0.000	0.000	0.000	0.000	0.000	0.000		
162	REALNETWORKS-000	196	0.040	192	0.078								196	0.234	183	0.319														0.001	0.000		
163	REALNETWORKS-001	197	0.040	191	0.078								19	0.234	184	0.319													0.001	0.000			
164	REALNETWORKS-002	193	0.039	190	0.078								189	0.231	182	0.315													0.001	0.000			
165	REALNETWORKS-003	184	0.024	179	0.062	116	0.771	115	0.031		110	0.209	17	0.159	171	0.266	122	0.998	110	0.164	87	0.500	0.001	0.000	0.009								
166	REALNETWORKS-004	182	0.024	176	0.059	121	0.797	114	0.031		115	0.213	174	0.158	169	0.263	135	0.999	111	0.170	97	0.613	0.001	0.000	0.009								
167	REALNETWORKS-005	57	0.002	52	0.013	61	0.433	46	0.004	31	0.023	46	0.102	20	0.028	63	0.074	57	0.971	54	0.037	38	0.223	37	0.215	0.000	0.000	0.006	0.000	0.000	0.000		
168	REMARKAI-000	85	0.003	91	0.018	99	0.660	76	0.008		86	0.148	114	0.055	108	0.120	132	0.999	83	0.069	103	0.717	0.000	0.000	0.000								
169	REMARKAI-001	137	0.009	137	0.030								163	0.128	150	0.203												0.000	0.001				
170	REMARKAI-002	135	0.008	136	0.029	123	0.802						162	0.124	148	0.196	87	0.991										0.000	0.001	0.017			
171	RENDIP-000	27	0.002	65	0.015	60	0.424	64	0.006	37	0.028	29	0.084	31	0.012	49	0.059	43	0.894	34	0.022	32	0.185	25	0.167	0.000	0.000	0.041	0.000	0.000	0.000		
172	S1-000	63	0.002	80	0.017	40	0.258	59	0.005	34	0.025	32	0.090	72	0.028	72	0.085	179	1.000	6	0.047	107	1.000	219	1.000	0.000	0.000	0.040	0.000	0.000	0.000		
173	SCANOVATE-000	106	0.005	163	0.045	81	0.560	119	0.035		114	0.211	128	0.067	164	0.240	48	0.893	119	0.215	71	0.400	0.000	0.001	0.057								
174	SCANOVATE-001	109	0.005	157	0.040	88	0.585	113	0.031		102	0.178	139	0.081	158	0.227	45	0.911	116	0.192	74	0.404	0.000	0.001	0.044								
175	SENSETIME-000	59	0.002	72	0.016	79	0.528						56	0.021	52	0.063	238	1.000									0.004	0.000	0.042				
176	SENSETIME-001	60	0.002	71	0.016								59	0.022	53	0.064											0.004	0.000					
177	SENSETIME-002	165	0.014	96	0.020	57	0.384	83	0.011		47	0.104	40	0.015	20	0.028	93	0.994	48	0.032	89	0.523	0.009	0.000	0.040								
178	SENSETIME-003	4	0.001	4	0.007	24	0.150</																										

#	ALGORITHM	INVESTIGATION MODE										IDENTIFICATION MODE										FAILURE TO EXTRACT FEATURES											
		RANK ONE MISS RATE, FNIR(N, 0, 1)										HIGH T → FPIR = 0.001, FNIR(N, T, L)										N=1.6M											
		N=1.6M					N=1.6M					N=1.6M					N=1.6M					N=1.6M					N=1.6M						
		GALLERY	MUGSHOT	MUGSHOT	MUGSHOT	VISA	BORDER	BOR <sub>L</sub> 10YR	KIOSK	MUGSHOT	MUGSHOT	MUGSHOT	VISA	BORDER	BOR <sub>L</sub> 10YR	KIOSK	MUGSHOT	MUGSHOT	WEBCAM	PROFILE	BORDER	BOR <sub>L</sub> 10YR	KIOSK	MUGSHOT	MUGSHOT	WEBCAM	PROFILE	BORDER	BOR <sub>L</sub> 10YR	KIOSK			
185	SHAMAN-007	194 0.040	174 0.057	186 0.333	147 0.004	141 0.099	46 0.018	188 0.365	148 0.031	170 0.141	163 0.240	126 0.065	111 0.123	51 0.960	85 0.075	59 0.314	0.020	0.010															
186	SIAT-001	37 0.002	216 0.333	47 0.004		41 0.099	46 0.018	188 0.365	48 0.031	170 0.141	163 0.240	216 0.582	208 0.646																				
187	SIAT-002	38 0.002	218 0.446	146 0.348		45 0.102	57 0.022	198 0.478	128 0.372	128 0.100	125 0.923	125 0.923	128 0.372	128 0.923																			
188	SMILART-004	236 0.965	232 0.974					229 0.968	225 0.976																								
189	SMILART-005																																
190	STAQU-000	127 0.007	100 0.020	91 0.613	103 0.020	49 0.055	93 0.159	122 0.062	195 0.443	153 1.000	137 0.535	53 0.961	151 1.000	0.000	0.000	0.000	0.000	0.000	0.000	0.000	0.000	0.000	0.000	0.000	0.000	0.000	0.000	0.000	0.000	0.000			
191	SYNESIS-003	169 0.016	117 0.023	131 0.827	90 0.013	81 0.136	126 0.065	111 0.123	51 0.960	85 0.075	59 0.314	0.000	0.001	0.063																			
192	SYNESIS-003	219 0.170	210 0.235																														
193	SYNESIS-005	136 0.009	50 0.013	109 0.744	31 0.003	34 0.092	62 0.025	60 0.072	74 0.984	48 0.032	36 0.214	0.001	0.000	0.135																			
194	TECH5-001	93 0.004	79 0.017	87 0.584	69 0.007	53 0.107	116 0.057	221 0.935	180 1.000	120 0.244	140 0.994	0.000	0.000	0.006																			
195	TECH5-002	70 0.003	31 0.011	47 0.312	30 0.003	42 0.029	31 0.089	69 0.027	38 0.070	35 0.039	35 0.205	77 0.440	0.001	0.000	0.041	0.000	0.000	0.000	0.000	0.000	0.000	0.000	0.000	0.000	0.000	0.000	0.000	0.000	0.000				
196	TEVIAN-003	166 0.015	170 0.052							182 0.177	178 0.298																						
197	TEVIAN-004	153 0.011	150 0.038							157 0.117	145 0.176																						
198	TEVIAN-005	128 0.007	135 0.028	64 0.467					144 0.087	125 0.144	52 0.962																						
199	TEVIAN-006	64 0.002	35 0.011	13 0.123	25 0.003	24 0.013	9 0.071	26 0.010	23 0.032	9 0.425	21 0.016	14 0.093	128 0.951	0.001	0.000	0.062	0.000	0.000	0.000	0.000	0.000	0.000	0.000	0.000	0.000	0.000	0.000	0.000	0.000	0.000			
200	TIGER-000	204 0.062	196 0.095						206 0.390	199 0.500																							
201	TIGER-002	112 0.006	114 0.023	62 0.514					141 0.086	135 0.158	130 0.999																						
202	TIGER-003	111 0.006	115 0.023						140 0.086	134 0.158																							
203	TONGYITRANS-000	123 0.007	112 0.022						133 0.074	100 0.112																							
204	TONGYITRANS-001	124 0.007	111 0.022						127 0.066	93 0.101																							
205	TOSHIBA-000	99 0.004	106 0.022	114 0.766					123 0.062	105 0.118	104 0.995																						
206	TOSHIBA-001	104 0.005	108 0.022						118 0.058	81 0.092																							
207	TRUEFACE-000	82 0.003	51 0.014	36 0.230	73 0.007	33 0.024	35 0.092	50 0.018	51 0.062	39 0.882	42 0.030	33 0.194	33 0.188	0.001	0.001	0.047	0.000	0.000	0.000	0.000	0.000	0.000	0.000	0.000	0.000	0.000	0.000	0.000	0.000	0.000	0.000		
208	VD-000	232 0.474	223 0.551						227 0.917	223 0.946																							
209	VD-001	188 0.028	171 0.053						186 0.201	175 0.281																							
210	VD-002	145 0.010	133 0.027	138 0.893	93 0.013	46 0.050	100 0.176	137 0.079	127 0.148	50 0.996	91 0.095	46 0.367	67 0.372	0.004	0.003	0.156	0.000	0.000	0.000	0.000	0.000	0.000	0.000	0.000	0.000	0.000	0.000	0.000	0.000	0.000	0.000		
211	VERIDAS-001	73 0.003	58 0.014	82 0.550	65 0.006	39 0.028	72 0.131	86 0.037	71 0.082	81 0.987	60 0.044	39 0.266	51 0.264	0.000	0.002	0.093	0.001	0.001	0.001	0.001	0.001	0.000	0.000	0.000	0.000	0.000	0.000	0.000	0.000	0.000	0.000		
212	VERIDAS-002	72 0.003	59 0.014	81 0.550	66 0.006	40 0.028	73 0.131	85 0.037	70 0.082	80 0.987	61 0.044	40 0.266	50 0.264	0.000	0.002	0.093	0.001	0.001	0.001	0.001	0.001	0.000	0.000	0.000	0.000	0.000	0.000	0.000	0.000	0.000	0.000		
213	VIGILANTSOLUTIONS-003	207 0.069	203 0.151	166 0.958					209 0.408	211 0.660	129 0.999																						
214	VIGILANTSOLUTIONS-004	214 0.125	211 0.244	171 0.965					215 0.549	215 0.817	108 0.996																						
215	VIGILANTSOLUTIONS-005	141 0.009		144 0.920					205 0.388		171 1.000																						
216	VIGILANTSOLUTIONS-006	147 0.010		144 0.921					209 0.353		162 1.000																						
217	VIGILANTSOLUTIONS-007	84 0.003	83 0.017	144 0.925	91 0.013	51 0.068	98 0.175	74 0.028	76 0.088	108 0.996	88 0.081	47 0.371	70 0.391	0.000	0.001	0.127	0.000	0.000	0.000	0.000	0.000	0.000	0.000	0.000	0.000	0.000	0.000	0.000	0.000	0.000	0.000		
218	VIGILANTSOLUTIONS-008	77 0.003	84 0.017	143 0.913	95 0.014	52 0.072	101 0.178	55 0.021	65 0.077	129 0.999	95 0.104	49 0.398	88 0.511	0.000	0.001	0.127	0.000	0.000	0.000	0.000	0.000	0.000	0.000	0.000	0.000	0.000	0.000	0.000	0.000	0.000	0.000		
219	VISIONLABS-004	71 0.003	97 0.020	51 0.343					117 0.058	136 0.159	41 0.890																						
220	VISIONLABS-005	62 0.002	92 0.019	49 0.334					103 0.050	126 0.147	40 0.888																						
221	VISIONLABS-006	41 0.002	69 0.015	31 0.211	29 0.004	38 0.096	68 0.027	79 0.090	24 0.672																								
222	VISIONLABS-007	36 0.002	68 0.015	32 0.211	25 0.004	37 0.095	67 0.027	78 0.090	25 0.672	44 0.031	32 0.185	0.001	0.001	0.051																			
223	VISIONLABS-008	48 0.002	54 0.014	21 0.141	13 0.002	21 0.081	25 0.013	41 0.051	15 0.481	25 0.017	18 0.151	0.001	0.000	0.075																			

#	ALGORITHM	INVESTIGATION MODE						IDENTIFICATION MODE						FAILURE TO EXTRACT FEATURES					
		RANK ONE MISS RATE, FNIR(N, 0, 1)						HIGH T → FPIR = 0.001, FNIR(N, T, L)											
		N=1.6M						N=1.6M											
	GALLERY	MUGSHOT	MUGSHOT	MUGSHOT	VISA	BORDER	VISA	MUGSHOT	MUGSHOT	MUGSHOT	VISA	BORDER	VISA	MUGSHOT	MUGSHOT	MUGSHOT	VISA	BORDER	KIOSK
	PROBE	MUGSHOT	WEBCAM	PROFILE	BORDER	BOR <sub>i</sub> 10YR	KIOSK	MUGSHOT	WEBCAM	PROFILE	BORDER	BOR <sub>i</sub> 10YR	KIOSK	MUGSHOT	WEBCAM	PROFILE	BORDER	BOR <sub>i</sub> 10YR	KIOSK
231	VTS-001	<sup>25</sup> 0.002	<sup>21</sup> 0.010	<sup>27</sup> 0.167	<sup>60</sup> 0.006	<sup>26</sup> 0.018	<sup>17</sup> 0.077	<sup>36</sup> 0.013	<sup>40</sup> 0.051	<sup>34</sup> 0.994	<sup>35</sup> 0.022	<sup>25</sup> 0.141	<sup>34</sup> 0.192	0.000	0.000	0.040	0.000	0.000	0.000
232	XFORWARDAI-000	<sup>56</sup> 0.002	<sup>5</sup> 0.014	<sup>14</sup> 0.089	<sup>41</sup> 0.004	<sup>25</sup> 0.015	<sup>36</sup> 0.094	<sup>43</sup> 0.015	<sup>45</sup> 0.053	<sup>11</sup> 0.440	<sup>33</sup> 0.021	<sup>27</sup> 0.159	<sup>26</sup> 0.169	0.000	0.000	0.000	0.000	0.000	0.000
233	XFORWARDAI-001	<sup>51</sup> 0.002	<sup>48</sup> 0.013	<sup>8</sup> 0.067	<sup>27</sup> 0.003	<sup>11</sup> 0.009	<sup>24</sup> 0.082	<sup>18</sup> 0.005	<sup>21</sup> 0.028	<sup>12</sup> 0.448	<sup>15</sup> 0.008	<sup>12</sup> 0.062	<sup>13</sup> 0.123	0.000	0.000	0.000	0.000	0.000	0.000
234	XFORWARDAI-002	<sup>45</sup> 0.002	<sup>41</sup> 0.012	<sup>3</sup> 0.059	<sup>20</sup> 0.002	<sup>6</sup> 0.007	<sup>16</sup> 0.077	<sup>12</sup> 0.003	<sup>10</sup> 0.525	<sup>6</sup> 0.005	<sup>7</sup> 0.041	<sup>5</sup> 0.099	0.000	0.000	0.000	0.000	0.000	0.000	0.000
235	YISHENG-001	<sup>187</sup> 0.027	<sup>178</sup> 0.060		<sup>128</sup> 0.058		<sup>130</sup> 0.287	<sup>199</sup> 0.346	<sup>212</sup> 0.808		<sup>143</sup> 0.666		<sup>124</sup> 0.919		0.002	0.005			
236	YITU-002	<sup>40</sup> 0.002	<sup>21</sup> 0.010					<sup>47</sup> 0.018	<sup>36</sup> 0.049						0.000	0.000			
237	YITU-003	<sup>76</sup> 0.003	<sup>71</sup> 0.016					<sup>53</sup> 0.019	<sup>45</sup> 0.052						0.003	0.001			
238	YITU-004	<sup>11</sup> 0.001	<sup>17</sup> 0.008	<sup>136</sup> 0.866				<sup>24</sup> 0.010	<sup>18</sup> 0.027	<sup>47</sup> 0.936					0.000	0.000	0.000		
239	YITU-005	<sup>58</sup> 0.002	<sup>63</sup> 0.014					<sup>27</sup> 0.010	<sup>24</sup> 0.032						0.003	0.001			

Table 14: **Miss rates by dataset:** At left, rank 1 miss rates relevant to investigations; at right, with threshold set to target FPIR = 0.01 for higher volume, low prior, uses. Yellow indicates most accurate algorithm. Throughout blue superscripts indicate the rank of the algorithm for that column.

2021 / 09 / 21  
09:55:08FNIR(N, R, T) = False neg. identification rate  
FPIR(N, T) = False pos. identification rateN = Num. enrolled subjects  
R = Num. candidates examined

T = Threshold

T = 0 → Investigation  
T > 0 → Identification

#	ALGORITHM	MISSES BELOW THRESHOLD, T		ENROL MOST RECENT				
		FNIR(N, T > 0, R > L)		DATASET: FRVT 2018 MUGSHOTS				
		N=0.64M	N=1.6M	N=3.0M	N=6.0M	N=12.0M		
1	3DIVI-005	<sup>178</sup> 0.1358	<sup>178</sup> 0.1664	<sup>153</sup> 0.1915	<sup>145</sup> 0.2370	<sup>139</sup> 0.3054		
2	ACER-000	<sup>172</sup> 0.1185	<sup>171</sup> 0.1455	<sup>148</sup> 0.1714	<sup>139</sup> 0.2074	<sup>132</sup> 0.2537		
3	ALCHERA-003	<sup>170</sup> 0.1176	<sup>172</sup> 0.1553	<sup>149</sup> 0.1853	<sup>146</sup> 0.2409	<sup>134</sup> 0.3553		
4	ALLGOVISION-000	<sup>145</sup> 0.0688	<sup>146</sup> 0.0881	<sup>131</sup> 0.1084	<sup>124</sup> 0.1389	<sup>112</sup> 0.2129		
5	ALLGOVISION-001	<sup>151</sup> 0.0785	<sup>152</sup> 0.1017	<sup>138</sup> 0.1218	<sup>131</sup> 0.1584	<sup>117</sup> 0.2273		
6	ANKE-000	<sup>157</sup> 0.0942	<sup>156</sup> 0.1169	<sup>143</sup> 0.1404	<sup>136</sup> 0.1776	<sup>133</sup> 0.2559		
7	ANKE-002	<sup>78</sup> 0.0229	<sup>78</sup> 0.0318	<sup>79</sup> 0.0406	<sup>75</sup> 0.0605	<sup>6</sup> 0.1466		
8	AWARE-003	<sup>167</sup> 0.1098	<sup>164</sup> 0.1283	<sup>144</sup> 0.1447	<sup>134</sup> 0.1768	<sup>124</sup> 0.2364		
9	AWARE-005	<sup>20</sup> 0.3389	<sup>202</sup> 0.3643	<sup>16</sup> 0.3993	<sup>154</sup> 0.4526	<sup>13</sup> 0.2531		
10	AYONIX-002	<sup>224</sup> 0.7862	<sup>224</sup> 0.8242	<sup>168</sup> 0.8508	<sup>159</sup> 0.8704	<sup>155</sup> 0.8939		
11	CAMVI-004	<sup>105</sup> 0.0367	<sup>130</sup> 0.0716	<sup>128</sup> 0.0983	<sup>148</sup> 0.2508	<sup>130</sup> 0.2701		
12	CIB-000	<sup>31</sup> 0.0086	<sup>33</sup> 0.0125	<sup>33</sup> 0.0160	<sup>40</sup> 0.0303	<sup>33</sup> 0.1251		
13	CLOUDWALK-HR-000	<sup>7</sup> 0.0019	<sup>6</sup> 0.0020	<sup>8</sup> 0.0023	<sup>8</sup> 0.0072	<sup>1</sup> 0.0701		
14	COGENT-000	<sup>119</sup> 0.0430	<sup>106</sup> 0.0527	<sup>107</sup> 0.0695	<sup>110</sup> 0.1133	<sup>102</sup> 0.1960		
15	COGENT-001	<sup>12</sup> 0.0430	<sup>107</sup> 0.0527	<sup>108</sup> 0.0695	<sup>109</sup> 0.1133	<sup>10</sup> 0.1960		
16	COGENT-002	<sup>90</sup> 0.0322	<sup>94</sup> 0.0444	<sup>94</sup> 0.0610	<sup>107</sup> 0.1116	<sup>114</sup> 0.2180		
17	COGENT-003	<sup>91</sup> 0.0328	<sup>98</sup> 0.0463	<sup>108</sup> 0.0683	<sup>117</sup> 0.1294	<sup>126</sup> 0.2445		
18	COGENT-004	<sup>75</sup> 0.0210	<sup>79</sup> 0.0331	<sup>89</sup> 0.0527	<sup>112</sup> 0.1138	<sup>111</sup> 0.2119		
19	COGNITEC-000	<sup>180</sup> 0.1377	<sup>176</sup> 0.1606	<sup>158</sup> 0.1870	<sup>141</sup> 0.2176	<sup>138</sup> 0.2831		
20	COGNITEC-001	<sup>15</sup> 0.0807	<sup>151</sup> 0.1017	<sup>137</sup> 0.1214	<sup>127</sup> 0.1513	<sup>117</sup> 0.2238		
21	COGNITEC-002	<sup>113</sup> 0.0406	<sup>109</sup> 0.0531	<sup>101</sup> 0.0666	<sup>95</sup> 0.0935	<sup>97</sup> 0.1874		
22	COGNITEC-003	<sup>11</sup> 0.0400	<sup>105</sup> 0.0526	<sup>97</sup> 0.0650	<sup>91</sup> 0.0895	<sup>90</sup> 0.1772		
23	COGNITEC-004	<sup>77</sup> 0.0222	<sup>77</sup> 0.0313	<sup>78</sup> 0.0388	<sup>71</sup> 0.0540	<sup>37</sup> 0.1103		
24	COGNITEC-005	<sup>24</sup> 0.0063	<sup>25</sup> 0.0096	<sup>28</sup> 0.0144	<sup>35</sup> 0.0287	<sup>24</sup> 0.0967		
25	CYBERLINK-000	<sup>115</sup> 0.0414	<sup>118</sup> 0.0565	<sup>112</sup> 0.0707	<sup>103</sup> 0.1031	<sup>108</sup> 0.2050		
26	CYBERLINK-001	<sup>107</sup> 0.0392	<sup>110</sup> 0.0536	<sup>108</sup> 0.0695	<sup>109</sup> 0.0973	<sup>9</sup> 0.1794		
27	CYBERLINK-002	<sup>38</sup> 0.0105	<sup>41</sup> 0.0148	<sup>48</sup> 0.0202	<sup>36</sup> 0.0399	<sup>34</sup> 0.1255		
28	CYBERLINK-003	<sup>22</sup> 0.0056	<sup>22</sup> 0.0077	<sup>21</sup> 0.0100	<sup>24</sup> 0.0235	<sup>30</sup> 0.1237		
29	CYBERLINK-004	<sup>21</sup> 0.0051	<sup>21</sup> 0.0071	<sup>22</sup> 0.0102	<sup>20</sup> 0.0199	<sup>30</sup> 0.1269		
30	DAHUA-001	<sup>134</sup> 0.0569	<sup>132</sup> 0.0727	<sup>129</sup> 0.0878	<sup>113</sup> 0.1148	<sup>96</sup> 0.1867		
31	DAHUA-002	<sup>4</sup> 0.0108	<sup>42</sup> 0.0151	<sup>41</sup> 0.0191	<sup>37</sup> 0.0291	<sup>4</sup> 0.1153		
32	DAHUA-003	<sup>36</sup> 0.0100	<sup>38</sup> 0.0139	<sup>39</sup> 0.0180	<sup>38</sup> 0.0296	<sup>39</sup> 0.1130		
33	DEEPLINT-001	<sup>13</sup> 0.0027	<sup>15</sup> 0.0033	<sup>15</sup> 0.0043	<sup>14</sup> 0.0121	<sup>2</sup> 0.0922		
34	DEEPSEA-001	<sup>99</sup> 0.0347	<sup>97</sup> 0.0462	<sup>93</sup> 0.0586	<sup>89</sup> 0.0802	<sup>88</sup> 0.1708		
35	DERMALOG-005	<sup>14</sup> 0.0700	<sup>145</sup> 0.0880	<sup>138</sup> 0.1144	<sup>130</sup> 0.1578	<sup>12</sup> 0.2451		
36	DERMALOG-006	<sup>108</sup> 0.0395	<sup>104</sup> 0.0517	<sup>98</sup> 0.0659	<sup>99</sup> 0.0973	<sup>89</sup> 0.1745		
37	DERMALOG-007	<sup>146</sup> 0.0691	<sup>145</sup> 0.0863	<sup>132</sup> 0.1107	<sup>126</sup> 0.1504	<sup>122</sup> 0.2299		
38	DERMALOG-008	<sup>95</sup> 0.0338	<sup>96</sup> 0.0455	<sup>96</sup> 0.0626	<sup>104</sup> 0.1060	<sup>120</sup> 0.2276		
39	GORILLA-002	<sup>184</sup> 0.1539	<sup>184</sup> 0.1880	<sup>156</sup> 0.2184	<sup>149</sup> 0.2596	<sup>146</sup> 0.3398		
40	GORILLA-004	<sup>148</sup> 0.0699	<sup>148</sup> 0.0892	<sup>128</sup> 0.1048	<sup>122</sup> 0.1370	<sup>10</sup> 0.1969		
41	GORILLA-005	<sup>124</sup> 0.0453	<sup>119</sup> 0.0583	<sup>111</sup> 0.0704	<sup>101</sup> 0.0974	<sup>68</sup> 0.1474		
42	HIK-003	<sup>154</sup> 0.0828	<sup>153</sup> 0.1028	<sup>136</sup> 0.1202	<sup>129</sup> 0.1525	<sup>12</sup> 0.2480		
43	HIK-004	<sup>152</sup> 0.0796	<sup>149</sup> 0.0988	<sup>134</sup> 0.1147	<sup>125</sup> 0.1474	<sup>130</sup> 0.2483		
44	HIK-005	<sup>88</sup> 0.0312	<sup>91</sup> 0.0436	<sup>96</sup> 0.0560	<sup>93</sup> 0.0911	<sup>11</sup> 0.2129		
45	HYPERVERGE-001	<sup>16</sup> 0.0033	<sup>16</sup> 0.0045	<sup>16</sup> 0.0059	<sup>12</sup> 0.0117	<sup>18</sup> 0.0872		
46	IDEMIA-003	<sup>9</sup> 0.0346	<sup>100</sup> 0.0471	<sup>121</sup> 0.0892	<sup>131</sup> 0.2789	<sup>15</sup> 0.4311		
47	IDEMIA-004	<sup>87</sup> 0.0300	<sup>87</sup> 0.0373	<sup>81</sup> 0.0447	<sup>76</sup> 0.0617	<sup>86</sup> 0.1635		
48	IDEMIA-005	<sup>102</sup> 0.0360	<sup>93</sup> 0.0440	<sup>98</sup> 0.0537	<sup>88</sup> 0.0764	<sup>90</sup> 0.1915		
49	IDEMIA-006	<sup>100</sup> 0.0351	<sup>90</sup> 0.0433	<sup>88</sup> 0.0525	<sup>85</sup> 0.0734	<sup>115</sup> 0.2201		
50	IDEMIA-007	<sup>50</sup> 0.0136	<sup>49</sup> 0.0181	<sup>46</sup> 0.0228	<sup>49</sup> 0.0357	<sup>65</sup> 0.1402		
51	IDEMIA-008	<sup>1</sup> 0.0016	<sup>5</sup> 0.0019	<sup>8</sup> 0.0024	<sup>4</sup> 0.0053	<sup>1</sup> 0.0470		
52	IMAGUS-005	<sup>51</sup> 0.0137	<sup>52</sup> 0.0185	<sup>51</sup> 0.0237	<sup>50</sup> 0.0368	<sup>33</sup> 0.1067		
53	IMAGUS-006	<sup>52</sup> 0.0137	<sup>54</sup> 0.0190	<sup>51</sup> 0.0244	<sup>54</sup> 0.0396	<sup>4</sup> 0.1159		
54	IMPERIAL-000	<sup>65</sup> 0.0187	<sup>65</sup> 0.0259	<sup>72</sup> 0.0358	<sup>84</sup> 0.0733	<sup>92</sup> 0.1794		
55	INCODE-003	<sup>17</sup> 0.1324	<sup>179</sup> 0.1672	<sup>151</sup> 0.1961	<sup>144</sup> 0.2345	<sup>14</sup> 0.3123		
56	INCODE-004	<sup>112</sup> 0.0403	<sup>112</sup> 0.0538	<sup>107</sup> 0.0662	<sup>94</sup> 0.0917	<sup>83</sup> 0.1619		
57	INCODE-005	<sup>28</sup> 0.0083	<sup>29</sup> 0.0113	<sup>29</sup> 0.0145	<sup>27</sup> 0.0247	<sup>28</sup> 0.0912		
58	INNOVATRICS-007	<sup>34</sup> 0.0093	<sup>34</sup> 0.0125	<sup>32</sup> 0.0159	<sup>28</sup> 0.0259	<sup>34</sup> 0.1092		
59	INTSYSMSU-000	<sup>23</sup> 0.9982	<sup>232</sup> 0.9984	<sup>174</sup> 0.9985	<sup>162</sup> 0.9987	<sup>159</sup> 0.9988		
60	IREX-000	<sup>69</sup> 0.0190	<sup>73</sup> 0.0280	<sup>76</sup> 0.0391	<sup>80</sup> 0.0677	<sup>71</sup> 0.1479		
61	ISYSTEMS-002	<sup>136</sup> 0.0584	<sup>136</sup> 0.0783	<sup>125</sup> 0.0973	<sup>123</sup> 0.1373	<sup>12</sup> 0.2295		
62	ISYSTEMS-003	<sup>122</sup> 0.0438	<sup>120</sup> 0.0590	<sup>118</sup> 0.0807	<sup>115</sup> 0.1259	<sup>125</sup> 0.2357		
63	KAKAO-000	<sup>4</sup> 0.0109	<sup>44</sup> 0.0151	<sup>48</sup> 0.0196	<sup>44</sup> 0.0324	<sup>28</sup> 0.1010		
64	KEDACOM-001	<sup>62</sup> 0.0181	<sup>61</sup> 0.0227	<sup>58</sup> 0.0265	<sup>59</sup> 0.0422	<sup>62</sup> 0.1340		
65	LOOKMAN-003	<sup>98</sup> 0.0346	<sup>92</sup> 0.0437	<sup>86</sup> 0.0514	<sup>83</sup> 0.0724	<sup>84</sup> 0.1620		
66	LOOKMAN-005	<sup>79</sup> 0.0240	<sup>75</sup> 0.0301	<sup>71</sup> 0.0356	<sup>65</sup> 0.0512	<sup>61</sup> 0.1334		
67	MEGVI-001	<sup>132</sup> 0.0562	<sup>131</sup> 0.0722	<sup>117</sup> 0.0872	<sup>119</sup> 0.1309	<sup>13</sup> 0.2713		
68	MICROFOCUS-005	<sup>231</sup> 0.9732	<sup>226</sup> 0.8354	<sup>168</sup> 0.8555	<sup>163</sup> 0.8755	<sup>156</sup> 0.8954		
69	MICROSOFT-003	<sup>71</sup> 0.0198	<sup>71</sup> 0.0278	<sup>70</sup> 0.0356	<sup>70</sup> 0.0538	<sup>71</sup> 0.1539		
70	MICROSOFT-004	<sup>64</sup> 0.0185	<sup>66</sup> 0.0259	<sup>68</sup> 0.0333	<sup>66</sup> 0.0517	<sup>75</sup> 0.1510		
71	MICROSOFT-005	<sup>63</sup> 0.0181	<sup>64</sup> 0.0256	<sup>64</sup> 0.0320	<sup>64</sup> 0.0512	<sup>72</sup> 0.1491		
72	MICROSOFT-006	<sup>33</sup> 0.0091	<sup>30</sup> 0.0120	<sup>34</sup> 0.0162	<sup>39</sup> 0.0301	<sup>72</sup> 0.1482		

**Table 15: Identification-mode: Effect of N on FNIR at high threshold.** Values are threshold-based miss rates i.e. FNIR at FPIR = 0.001 for five enrollment population sizes, N. The right six columns apply for enrollment of one image. Missing entries usually apply because another algorithm from the same developer was run instead. Some developers are missing because less accurate algorithms were not run on galleries with  $N \geq 3\,000\,000$ . Throughout blue superscripts indicate the rank of the algorithm for that column.

#	ALGORITHM	MISSES BELOW THRESHOLD, T		ENROL MOST RECENT					
		FNIR(N, T > 0, R > L)		DATASET: FRVT 2018 MUGSHOTS					
		N=0.64M	N=1.6M	N=3.0M	N=6.0M	N=12.0M			
73	NEC-000	<sup>140</sup> 0.0637	<sup>138</sup> 0.0789	<sup>124</sup> 0.0933	<sup>114</sup> 0.1163	<sup>100</sup> 0.1941			
74	NEC-001	<sup>155</sup> 0.0863	<sup>155</sup> 0.1055	<sup>139</sup> 0.1249	<sup>128</sup> 0.1519	<sup>118</sup> 0.2253			
75	NEC-002	<sup>10</sup> 0.0020	<sup>10</sup> 0.0026	<sup>16</sup> 0.0033	<sup>16</sup> 0.0135	<sup>10</sup> 0.0653			
76	NEC-003	<sup>10</sup> 0.0021	<sup>8</sup> 0.0024	<sup>7</sup> 0.0028	<sup>6</sup> 0.0059	<sup>8</sup> 0.0540			
77	NEC-004	<sup>10</sup> 0.0017	<sup>3</sup> 0.0018	<sup>1</sup> 0.0020	<sup>1</sup> 0.0037	<sup>1</sup> 0.0329			
78	NEUROTECHNOLOGY-003	<sup>218</sup> 0.5698	<sup>219</sup> 0.6362	<sup>167</sup> 0.7035	<sup>158</sup> 0.7602	<sup>154</sup> 0.8224			
79	NEUROTECHNOLOGY-004	<sup>126</sup> 0.466	<sup>125</sup> 0.0629	<sup>113</sup> 0.0779	<sup>111</sup> 0.1135	<sup>110</sup> 0.2102			
80	NEUROTECHNOLOGY-005	<sup>109</sup> 0.0396	<sup>113</sup> 0.0538	<sup>108</sup> 0.0675	<sup>98</sup> 0.0950	<sup>104</sup> 0.1966			
81	NEUROTECHNOLOGY-007	<sup>121</sup> 0.0436	<sup>124</sup> 0.0623	<sup>115</sup> 0.0802	<sup>120</sup> 0.1320	<sup>125</sup> 0.2393			
82	NEUROTECHNOLOGY-008	<sup>90</sup> 0.0339	<sup>108</sup> 0.0530	<sup>122</sup> 0.0893	<sup>135</sup> 0.1769	<sup>144</sup> 0.3288			
83	NEUROTECHNOLOGY-009	<sup>42</sup> 0.0108	<sup>45</sup> 0.0152	<sup>44</sup> 0.0196	<sup>42</sup> 0.0324	<sup>36</sup> 0.1102			
84	NTECHLAB-003	<sup>11</sup> 0.0421	<sup>111</sup> 0.0537	<sup>108</sup> 0.0674	<sup>92</sup> 0.0907	<sup>81</sup> 0.1582			
85	NTECHLAB-004	<sup>89</sup> 0.0312	<sup>88</sup> 0.0405	<sup>87</sup> 0.0519	<sup>82</sup> 0.0722	<sup>74</sup> 0.1503			
86	NTECHLAB-005	<sup>92</sup> 0.0334	<sup>89</sup> 0.0424	<sup>91</sup> 0.0537	<sup>87</sup> 0.0760	<sup>79</sup> 0.1543			
87	NTECHLAB-006	<sup>85</sup> 0.0288	<sup>83</sup> 0.0367	<sup>84</sup> 0.0471	<sup>79</sup> 0.0670	<sup>76</sup> 0.1523			
88	NTECHLAB-007	<sup>66</sup> 0.0188	<sup>63</sup> 0.0256	<sup>62</sup> 0.0317	<sup>63</sup> 0.0495	<sup>60</sup> 0.1306			
89	NTECHLAB-008	<sup>40</sup> 0.0107	<sup>39</sup> 0.0145	<sup>40</sup> 0.0187	<sup>34</sup> 0.0286	<sup>27</sup> 0.0995			
90	NTECHLAB-009	<sup>19</sup> 0.0037	<sup>19</sup> 0.0049	<sup>19</sup> 0.0062	<sup>15</sup> 0.0125	<sup>14</sup> 0.0735			
91	NTECHLAB-010	<sup>8</sup> 0.0020	<sup>9</sup> 0.0025	<sup>8</sup> 0.0030	<sup>9</sup> 0.0077	<sup>13</sup> 0.0710			
92	PARAVISION-003	<sup>81</sup> 0.0260	<sup>81</sup> 0.0351	<sup>82</sup> 0.0447	<sup>78</sup> 0.0657	<sup>85</sup> 0.1630			
93	PARAVISION-004	<sup>26</sup> 0.0074	<sup>28</sup> 0.0101	<sup>27</sup> 0.0136	<sup>31</sup> 0.0267	<sup>35</sup> 0.1256			
94	PARAVISION-005	<sup>15</sup> 0.0032	<sup>15</sup> 0.0041	<sup>15</sup> 0.0057	<sup>19</sup> 0.0174	<sup>28</sup> 0.1037			
95	PARAVISION-007	<sup>14</sup> 0.0030	<sup>14</sup> 0.0040	<sup>14</sup> 0.0055	<sup>21</sup> 0.0211	<sup>30</sup> 0.1097			
96	PIXELALL-002	<sup>150</sup> 0.0716	<sup>154</sup> 0.1052	<sup>146</sup> 0.1475	<sup>147</sup> 0.2489	<sup>149</sup> 0.3904			
97	PIXELALL-003	<sup>58</sup> 0.0158	<sup>58</sup> 0.0218	<sup>61</sup> 0.0288	<sup>60</sup> 0.0474	<sup>43</sup> 0.1138			
98	PIXELALL-004	<sup>46</sup> 0.0129	<sup>51</sup> 0.0183	<sup>50</sup> 0.0245	<sup>51</sup> 0.0378	<sup>63</sup> 0.1375			
99	PIXELALL-005	<sup>32</sup> 0.0087	<sup>32</sup> 0.0121	<sup>36</sup> 0.0171	<sup>26</sup> 0.0250	<sup>30</sup> 0.1052			
100	PTAKURATSATU-000	<sup>82</sup> 0.0275	<sup>82</sup> 0.0366	<sup>81</sup> 0.0458	<sup>68</sup> 0.0523	<sup>77</sup> 0.0523			
101	QUANTASOFT-001	<sup>220</sup> 0.6387	<sup>220</sup> 0.6387	<sup>164</sup> 0.6387		<sup>152</sup> 0.6387			
102	RANKONE-002	<sup>163</sup> 0.0973	<sup>159</sup> 0.1175	<sup>148</sup> 0.1359	<sup>132</sup> 0.1718	<sup>131</sup> 0.2613			
103	RANKONE-003	<sup>162</sup> 0.0973	<sup>158</sup> 0.1175	<sup>141</sup> 0.1359	<sup>133</sup> 0.1718	<sup>135</sup> 0.2613			
104	RANKONE-005	<sup>12</sup> 0.0473	<sup>121</sup> 0.0592	<sup>108</sup> 0.0700	<sup>96</sup> 0.0944	<sup>106</sup> 0.1998			
105	RANKONE-007	<sup>60</sup> 0.0168	<sup>60</sup> 0.0222	<sup>56</sup> 0.0266	<sup>53</sup> 0.0381	<sup>40</sup> 0.1132			
106	RANKONE-009	<sup>4</sup> 0.0132	<sup>48</sup> 0.0177	<sup>46</sup> 0.0230	<sup>46</sup> 0.0344	<sup>22</sup> 0.0921			
107	RANKONE-010	<sup>29</sup> 0.0106	<sup>37</sup> 0.0136	<sup>37</sup> 0.0174	<sup>30</sup> 0.0265	<sup>16</sup> 0.0785			
108	RANKONE-011	<sup>23</sup> 0.0063	<sup>25</sup> 0.0087	<sup>24</sup> 0.0115	<sup>32</sup> 0.0269	<sup>42</sup> 0.1135			
109	REALNETWORKS-002	<sup>190</sup> 0.1943	<sup>189</sup> 0.2314	<sup>159</sup> 0.2656	<sup>153</sup> 0.3134	<sup>143</sup> 0.3208			
110	REALNETWORKS-003	<sup>176</sup> 0.1300	<sup>175</sup> 0.1594	<sup>151</sup> 0.1858	<sup>142</sup> 0.2246	<sup>140</sup> 0.3076			
111	REALNETWORKS-004	<sup>175</sup> 0.1279	<sup>174</sup> 0.1581	<sup>159</sup> 0.1857	<sup>143</sup> 0.2329	<sup>142</sup> 0.3179			
112	REALNETWORKS-005	<sup>72</sup> 0.0202	<sup>70</sup> 0.0277	<sup>69</sup> 0.0355	<sup>74</sup> 0.0560	<sup>66</sup> 0.1431			
113	REMARKAI-000	<sup>11</sup> 0.0406	<sup>114</sup> 0.0552	<sup>108</sup> 0.0676	<sup>102</sup> 0.1028	<sup>10</sup> 0.2003			
114	RENDIP-000	<sup>30</sup> 0.0085	<sup>31</sup> 0.0121	<sup>31</sup> 0.0156	<sup>33</sup> 0.0277	<sup>48</sup> 0.1182			
115	S1-000	<sup>74</sup> 0.0204	<sup>72</sup> 0.0279	<sup>77</sup> 0.0382	<sup>77</sup> 0.0630	<sup>81</sup> 0.1707			
116	SCANOVATE-000	<sup>128</sup> 0.0498	<sup>128</sup> 0.0667	<sup>116</sup> 0.0804	<sup>106</sup> 0.1097	<sup>38</sup> 0.1109			
117	SCANOVATE-001	<sup>13</sup> 0.0630	<sup>139</sup> 0.0815	<sup>12</sup> 0.0993	<sup>116</sup> 0.1292	<sup>103</sup> 0.1960			
118	SENSETIME-000	<sup>57</sup> 0.0158	<sup>56</sup> 0.0208	<sup>59</sup> 0.0270	<sup>55</sup> 0.0398	<sup>49</sup> 0.1232			
119	SENSETIME-001	<sup>30</sup> 0.0161	<sup>59</sup> 0.0219	<sup>69</sup> 0.0277	<sup>58</sup> 0.0420	<sup>38</sup> 0.1304			
120	SENSETIME-002	<sup>34</sup> 0.0146	<sup>40</sup> 0.0148	<sup>36</sup> 0.0153	<sup>23</sup> 0.0234	<sup>10</sup> 0.0657			
121	SENSETIME-003	<sup>3</sup> 0.0016	<sup>4</sup> 0.0018	<sup>3</sup> 0.0021	<sup>5</sup> 0.0054	<sup>4</sup> 0.0451			
122	SENSETIME-004	<sup>2</sup> 0.0015	<sup>1</sup> 0.0018	<sup>2</sup> 0.0021	<sup>2</sup> 0.0040	<sup>2</sup> 0.0354			
123	SENSETIME-005	<sup>4</sup> 0.0016	<sup>7</sup> 0.0022	<sup>9</sup> 0.0031	<sup>11</sup> 0.0089	<sup>5</sup> 0.0454			
124	SENSETIME-006	<sup>1</sup> 0.0014	<sup>2</sup> 0.0018	<sup>2</sup> 0.0023	<sup>3</sup> 0.0047	<sup>3</sup> 0.0372			
125	SHAMAN-007	<sup>174</sup> 0.1212	<sup>170</sup> 0.1413	<sup>147</sup> 0.1587	<sup>137</sup> 0.1879	<sup>128</sup> 0.2460			
126	SIAT-001	<sup>40</sup> 0.0136	<sup>46</sup> 0.0176	<sup>48</sup> 0.0230	<sup>45</sup> 0.0344	<sup>27</sup> 0.1035			
127	SIAT-002	<sup>56</sup> 0.0154	<sup>57</sup> 0.0216	<sup>59</sup> 0.0273	<sup>57</sup> 0.0404	<sup>57</sup> 0.1283			
128	SYNESIS-003	<sup>12</sup> 0.0499	<sup>126</sup> 0.0652	<sup>117</sup> 0.0804	<sup>105</sup> 0.1095	<sup>99</sup> 0.1916			
129	SYNESIS-003	<sup>216</sup> 0.5341	<sup>218</sup> 0.5821	<sup>163</sup> 0.6113	<sup>157</sup> 0.6479	<sup>153</sup> 0.6822			
130	SYNESIS-005	<sup>6</sup> 0.0181	<sup>62</sup> 0.0248	<sup>69</sup> 0.0319	<sup>67</sup> 0.0518	<sup>80</sup> 0.1580			
131	TECH5-001	<sup>116</sup> 0.0420	<sup>116</sup> 0.0574	<sup>123</sup> 0.0911	<sup>140</sup> 0.2106	<sup>148</sup> 0.3725			
132	TECH5-002	<sup>20</sup> 0.0194	<sup>69</sup> 0.0269	<sup>68</sup> 0.0346	<sup>69</sup> 0.0537	<sup>82</sup> 0.1607			
133	TEVIAN-005	<sup>14</sup> 0.0692	<sup>144</sup> 0.0873	<sup>130</sup> 0.1066	<sup>118</sup> 0.1301	<sup>91</sup> 0.1840			
134	TEVIAN-006	<sup>28</sup> 0.0078	<sup>26</sup> 0.0098	<sup>25</sup> 0.0130	<sup>29</sup> 0.0261	<sup>59</sup> 0.1305			
135	TIGER-002	<sup>142</sup> 0.0647	<sup>141</sup> 0.0861	<sup>128</sup> 0.1036	<sup>121</sup> 0.1332	<sup>116</sup> 0.2231			
136	TOSHIBA-000	<sup>125</sup> 0.0460	<sup>123</sup> 0.0620	<sup>114</sup> 0.0780	<sup>108</sup> 0.1117	<sup>109</sup> 0.2082			
137	TRUEFACE-000	<sup>48</sup> 0.0134	<sup>50</sup> 0.0182	<sup>57</sup> 0.0238	<sup>52</sup> 0.0380	<sup>61</sup> 0.1385			
138	VD-001	<sup>186</sup> 0.1642	<sup>186</sup> 0.2015	<sup>158</sup> 0.2351	<sup>150</sup> 0.2736	<sup>145</sup> 0.3293			
139	VERIDAS-001	<sup>83</sup> 0.0278	<sup>86</sup> 0.0373	<sup>87</sup> 0.0373	<sup>86</sup> 0.0753	<sup>78</sup> 0.1541			
140	VERIDAS-002	<sup>84</sup> 0.0278	<sup>85</sup> 0.0373	<sup>82</sup> 0.0373	<sup>62</sup> 0.0491	<sup>15</sup> 0.0753			
141	VIGILANTSOLUTIONS-008	<sup>35</sup> 0.0146	<sup>35</sup> 0.0205	<sup>57</sup> 0.0269	<sup>61</sup> 0.0489	<sup>4</sup> 0.1164			
142	VISIONLABS-004	<sup>118</sup> 0.0427	<sup>117</sup> 0.0578	<sup>110</sup> 0.0703	<sup>97</sup> 0.0949	<sup>95</sup> 0.1853			
143	VISIONLABS-005	<sup>105</sup> 0.0369	<sup>103</sup> 0.0502	<sup>96</sup> 0.0626	<sup>90</sup> 0.0847	<sup>93</sup> 0.1815			
144	VISIONLABS-006	<sup>67</sup> 0.0188	<sup>68</sup> 0.0267	<sup>67</sup> 0.0336	<sup>73</sup> 0.0542	<sup>69</sup> 0.1478			

Table 16: **Identification-mode: Effect of N on FNIR at high threshold.** Values are threshold-based miss rates i.e. FNIR at FPIR = 0.001 for five enrollment population sizes, N. The right six columns apply for enrollment of one image. Missing entries usually apply because another algorithm from the same developer was run instead. Some developers are missing because less accurate algorithms were not run on galleries with  $N \geq 3\,000\,000$ . Throughout blue superscripts indicate the rank of the algorithm for that column.

MISSES BELOW THRESHOLD, T FNIR(N, T > 0, R > L)		ENROL MOST RECENT DATASET: FRVT 2018 MUGSHOTS				
#	ALGORITHM	N=0.64M	N=1.6M	N=3.0M	N=6.0M	N=12.0M
145	VISIONLABS-007	<sup>68</sup> 0.0188	<sup>67</sup> 0.0266	<sup>66</sup> 0.0335	<sup>72</sup> 0.0540	<sup>70</sup> 0.1479
146	VISIONLABS-008	<sup>35</sup> 0.0096	<sup>35</sup> 0.0131	<sup>35</sup> 0.0166	<sup>36</sup> 0.0291	<sup>32</sup> 0.1247
147	VISIONLABS-009	<sup>17</sup> 0.0034	<sup>17</sup> 0.0046	<sup>17</sup> 0.0060	<sup>17</sup> 0.0140	<sup>19</sup> 0.0881
148	VISIONLABS-010	<sup>20</sup> 0.0038	<sup>20</sup> 0.0051	<sup>20</sup> 0.0070	<sup>18</sup> 0.0149	<sup>21</sup> 0.0920
149	VOCORD-005	<sup>171</sup> 0.1179	<sup>173</sup> 0.1577	<sup>158</sup> 0.2183	<sup>152</sup> 0.3122	<sup>151</sup> 0.4490
150	VTS-001	<sup>37</sup> 0.0102	<sup>36</sup> 0.0133	<sup>38</sup> 0.0175	<sup>41</sup> 0.0322	<sup>51</sup> 0.1243
151	XFORWARDAI-000	<sup>41</sup> 0.0107	<sup>43</sup> 0.0151	<sup>42</sup> 0.0195	<sup>43</sup> 0.0324	<sup>31</sup> 0.1057
152	XFORWARDAI-001	<sup>18</sup> 0.0037	<sup>18</sup> 0.0049	<sup>18</sup> 0.0060	<sup>13</sup> 0.0120	<sup>17</sup> 0.0800
153	XFORWARDAI-002	<sup>12</sup> 0.0026	<sup>12</sup> 0.0030	<sup>12</sup> 0.0035	<sup>10</sup> 0.0078	<sup>12</sup> 0.0706
154	YITU-002	<sup>47</sup> 0.0129	<sup>47</sup> 0.0177	<sup>47</sup> 0.0228	<sup>47</sup> 0.0345	<sup>41</sup> 0.1133
155	YITU-003	<sup>53</sup> 0.0138	<sup>53</sup> 0.0185	<sup>50</sup> 0.0236	<sup>48</sup> 0.0353	<sup>44</sup> 0.1148
156	YITU-004	<sup>25</sup> 0.0067	<sup>24</sup> 0.0096	<sup>25</sup> 0.0129	<sup>22</sup> 0.0232	<sup>29</sup> 0.1046
157	YITU-005	<sup>27</sup> 0.0074	<sup>27</sup> 0.0101	<sup>26</sup> 0.0135	<sup>27</sup> 0.0255	<sup>32</sup> 0.1057

**Table 17: Identification-mode: Effect of N on FNIR at high threshold.** Values are threshold-based miss rates i.e. FNIR at FPIR = 0.001 for five enrollment population sizes, N. The right six columns apply for enrollment of one image. Missing entries usually apply because another algorithm from the same developer was run instead. Some developers are missing because less accurate algorithms were not run on galleries with  $N \geq 3\,000\,000$ . Throughout blue superscripts indicate the rank of the algorithm for that column.

MISSES AT GIVEN RANK FNIR(N, T = 0, r)		ENROL MOST RECENT																							
#	ALGORITHM	RANK 1					RANK 50																		
		N=0.64M	N=1.6M	N=3.0M	N=6.0M	N=12.0M	aN <sup>b</sup>	N=0.64M	N=1.6M	N=3.0M	N=6.0M	N=12.0M	aN <sup>b</sup>												
1	3DIVI-005	175	0.0137	173	0.0176	146	0.0210	141	0.0253	138	0.0302	112	0.0004 N <sup>0.271</sup> 120	158	0.0040	157	0.0049	136	0.0057	133	0.0068	130	0.0081	46	0.0002 N <sup>0.240</sup> 125
2	ACER-000	144	0.0081	151	0.0106	134	0.0128	133	0.0157	131	0.0195	52	0.0001 N <sup>0.299</sup> 144	111	0.0020	124	0.0026	115	0.0031	118	0.0037	112	0.0045	17	0.0000 N <sup>0.284</sup> 138
3	ALCHERA-003	141	0.0079	148	0.0104	132	0.0123	132	0.0147	129	0.0180	74	0.0002 N <sup>0.278</sup> 131	140	0.0027	139	0.0032	121	0.0035	119	0.0042	113	0.0048	50	0.0002 N <sup>0.199</sup> 115
4	ALLGOVISION-000	158	0.0101	159	0.0114	131	0.0127	131	0.0145	128	0.0166	136	0.0010 N <sup>0.171</sup> 65	177	0.0063	172	0.0067	141	0.0071	138	0.0075	129	0.0081	141	0.0020 N <sup>0.088</sup> 74
5	ALLGOVISION-001	134	0.0069	139	0.0090	127	0.0107	126	0.0128	125	0.0157	64	0.0002 N <sup>0.277</sup> 129	127	0.0023	128	0.0027	116	0.0031	112	0.0036	109	0.0043	39	0.0001 N <sup>0.211</sup> 120
6	ANKE-000	161	0.0102	166	0.0132	144	0.0155	138	0.0188	134	0.0225	98	0.0003 N <sup>0.270</sup> 119	149	0.0032	150	0.0040	132	0.0046	127	0.0056	121	0.0066	36	0.0001 N <sup>0.247</sup> 127
7	ANKE-002	75	0.0024	74	0.0028	74	0.0032	71	0.0037	66	0.0043	58	0.0002 N <sup>0.203</sup> 76	87	0.0016	80	0.0017	71	0.0018	65	0.0019	52	0.0006 N <sup>0.076</sup> 65		
8	AWARE-003	192	0.0238	193	0.0306	157	0.0361	152	0.0431	151	0.0506	134	0.0008 N <sup>0.288</sup> 114	171	0.0055	178	0.0075	151	0.0092	147	0.0113	148	0.0143	28	0.0001 N <sup>0.323</sup> 148
9	AWARE-005	193	0.0245	197	0.0311	158	0.0366	153	0.0434	142	0.0312	130	0.0056 N <sup>0.118</sup> 36	175	0.0062	184	0.0082	153	0.0101	150	0.0128	132	0.0089	107	0.0007 N <sup>0.169</sup> 110
10	AYONIX-002	226	0.2935	22	0.3414	168	0.3736	161	0.4101	157	0.4465	159	0.0440 N <sup>0.145</sup> 46	225	0.0950	227	0.1274	168	0.1524	168	0.1828	152	0.2150	144	0.023 N <sup>0.279</sup> 136
11	CAMVI-004	168	0.0124	200	0.0468	163	0.0719	160	0.2363	156	0.2367	140	0.0000 N <sup>0.155</sup> 158	198	0.0117	213	0.0464	164	0.0715	161	0.2361	157	0.2364	1	0.0000 N <sup>1.071</sup> 158
12	CIB-000	27	0.0014	24	0.0015	24	0.0017	27	0.0019	115	0.0131	24	0.0000 N <sup>0.635</sup> 157	37	0.0012	30	0.0012	29	0.0012	144	0.0122	2	0.0000 N <sup>0.647</sup> 157		
13	CLOUDWALK-HR-000	31	0.0015	21	0.0015	19	0.0015	16	0.0016	12	0.0017	130	0.0007 N <sup>0.084</sup> 9	75	0.0014	61	0.0014	52	0.0014	49	0.0014	36	0.0014	130	0.0012 N <sup>0.012</sup> 12
14	COGENT-000	160	0.0101	149	0.0105	128	0.0109	122	0.0115	117	0.0125	147	0.0038 N <sup>0.071</sup> 14	120	0.0021	118	0.0024	111	0.0028	115	0.0036	117	0.005	7	0.0000 N <sup>0.466</sup> 153
15	COGENT-001	159	0.0101	150	0.0105	129	0.0109	121	0.0115	116	0.0125	148	0.0038 N <sup>0.071</sup> 11	119	0.0021	117	0.0024	110	0.0028	114	0.0036	136	0.0095	6	0.0000 N <sup>0.466</sup> 154
16	COGENT-002	85	0.0029	88	0.0036	86	0.0041	85	0.0049	81	0.0059	38	0.0001 N <sup>0.244</sup> 106	71	0.0014	79	0.0015	74	0.0017	76	0.0019	51	0.0002 N <sup>0.144</sup> 104		
17	COGENT-003	91	0.0031	90	0.0038	96	0.0043	88	0.0051	84	0.0060	49	0.0001 N <sup>0.230</sup> 96	80	0.0015	82	0.0017	90	0.0018	87	0.0020	82	0.0022	59	0.0002 N <sup>0.143</sup> 103
18	COGENT-004	47	0.0018	49	0.0024	46	0.0025	46	0.0028	88	0.0002 N <sup>0.159</sup> 97	65	0.0013	58	0.0014	54	0.0014	51	0.0015	43	0.0015	36	0.0007 N <sup>0.050</sup> 51		
19	COGNITEC-000	186	0.0195	185	0.0252	158	0.0297	150	0.0352	146	0.0417	128	0.0006 N <sup>0.259</sup> 115	167	0.0050	171	0.0065	148	0.0077	145	0.0122	38	0.0001 N <sup>0.305</sup> 142		
20	COGNITEC-001	154	0.0090	159	0.0117	139	0.0139	136	0.0166	132	0.0199	90	0.0002 N <sup>0.271</sup> 122	145	0.0030	144	0.0034	129	0.0040	126	0.0046	117	0.0054	49	0.0002 N <sup>0.207</sup> 119
21	COGNITEC-002	116	0.0048	117	0.0057	107	0.0067	103	0.0079	103	0.0094	80	0.0002 N <sup>0.232</sup> 98	129	0.0024	125	0.0026	115	0.0028	109	0.0030	90	0.0034	81	0.0005 N <sup>0.117</sup> 90
22	COGNITEC-003	119	0.0053	118	0.0062	110	0.0072	108	0.0085	106	0.0100	96	0.0003 N <sup>0.222</sup> 88	142	0.0028	136	0.0030	118	0.0032	110	0.0035	103	0.0037	112	0.0008 N <sup>0.197</sup> 82
23	COGNITEC-004	81	0.0027	81	0.0032	81	0.0037	78	0.0045	78	0.0056	29	0.0001 N <sup>0.253</sup> 112	64	0.0013	62	0.0014	62	0.0015	60	0.0019	59	0.0002 N <sup>0.123</sup> 95		
24	COGNITEC-005	28	0.0014	31	0.0016	32	0.0018	31	0.0021	31	0.0024	53	0.0001 N <sup>0.169</sup> 63	27	0.0011	26	0.0011	24	0.0012	20	0.0012	19	0.0012	45	0.0007 N <sup>0.037</sup> 35
25	CYBERLINK-000	96	0.0034	92	0.0040	95	0.0046	90	0.0054	86	0.0063	28	0.0002 N <sup>0.209</sup> 82	117	0.0021	112	0.0022	104	0.0023	105	0.0025	93	0.0027	89	0.0006 N <sup>0.092</sup> 79
26	CYBERLINK-001	88	0.0030	86	0.0035	88	0.0042	87	0.0050	83	0.0060	39	0.0001 N <sup>0.243</sup> 105	89	0.0016	84	0.0018	81	0.0020	79	0.0022	71	0.0004 N <sup>0.110</sup> 86		
27	CYBERLINK-002	74	0.0024	69	0.0026	66	0.0028	62	0.0031	53	0.0035	12	0.0005 N <sup>0.121</sup> 37	112	0.0020	107	0.0021	100	0.0021	97	0.0022	83	0.0012 N <sup>0.036</sup> 34		
28	CYBERLINK-003	29	0.0015	28	0.0016	26	0.0017	21	0.0018	18	0.0020	109	0.0003 N <sup>0.110</sup> 30	29	0.0011	26	0.0012	24	0.0012	24	0.0013	22	0.0006 N <sup>0.047</sup> 47		
29	CYBERLINK-004	39	0.0016	33	0.0017	31	0.0018	29	0.0019	29	0.0021	124	0.0005 N <sup>0.088</sup> 25	72	0.0014	64	0.0014	54	0.0014	40	0.0015	38	0.0001 N <sup>0.010</sup> 22		
30	DAHUA-001	121	0.0053	122	0.0067	114	0.0079	113	0.0093	111	0.0112	66	0.0002 N <sup>0.256</sup> 113	139	0.0027	131	0.0029	110	0.0034	105	0.0038	84	0.0005 N <sup>0.121</sup> 93		
31	DAHUA-002	43	0.0017	39	0.0018	41	0.0021	38	0.0023	34	0.0027	75	0.0002 N <sup>0.156</sup> 51	57	0.0013	54	0.0013	49	0.0014	44	0.0014	38	0.0015	103	0.0007 N <sup>0.043</sup> 44
32	DAHUA-003	70	0.0010	19	0.0012	17	0.0014	15	0.0016	16	0.0018	20	0.0001 N <sup>0.199</sup> 75	12	0.0009	107	0.0009	100	0.0009	97	0.0009	87	0.0006 N <sup>0.027</sup> 30		
33	DEEPPGLINT-001	24	0.0014	19	0.0014	17	0.0015	17	0.0016	16	0.0018	116	0.0004 N <sup>0.089</sup> 19	55	0.0013	44	0.0013	42	0.0013	39	0.0013	126	0.0010 N <sup>0.107</sup> 19		
34	DEEPSSEA-001	95	0.0033	97	0.0043	97	0.0052	95	0.0065	95	0.0081	16	0.0001 N <sup>0.311</sup> 147	49	0.0012	47	0.0012	43	0.0013	31	0.0015	20	0.0020	45	0.0001 N <sup>0.157</sup> 108
35	DERMALOG-005	167	0.0114	144	0.0201	146	0.0289	149	0.0447	6	0.0000 N <sup>0.470</sup> 156	192	0.0094	193	0.0122	159	0.0171	154	0.0254	152	0.0406	8	0.0000 N <sup>0.305</sup> 155		
36	DERMALOG-006	136	0.0075	131	0.0081	122	0.0086	114	0.0093	107	0.0104	147	0.0017 N <sup>0.109</sup> 29	176	0.0062	170	0.0063	148	0.0064	135	0.0065	122	0.0068	144	0.0043 N <sup>0.28</sup> 31
37	DERMALOG-007	142	0.0080	126	0.0092	128	0.0102	124	0.0118	121	0.0140	126	0.0006 N <sup>0.190</sup> 72	169	0.0051	164	0.0054	135	0.0056	120	0.0063	142	0.0040 N <sup>0.168</sup> 66		
38	DERMALOG-008	73	0.0024	76	0.0034	76	0.0040	74	0.0048	53	0.0051	35	0.0001 N <sup>0.259</sup> 136	81	0.0015	75	0.0015	72	0.0016	69	0.0019	57	0.0004 N <sup>0.088</sup> 75		
39	GORILLA-002	177	0.0147	159	0.0197	150	0.0238	148	0.0288	144	0.0351	100	0.0003 N <sup>0.295</sup> 140	148	0.0032	152	0.0041</								

MISSES AT GIVEN RANK		ENROL MOST RECENT										$aN^b$	
FNIR(N, T= 0, r)		RANK 1					RANK 50					$aN^b$	
#	ALGORITHM	N=0.64M	N=1.6M	N=3.0M	N=6.0M	N=12.0M	$aN^b$	N=0.64M	N=1.6M	N=3.0M	N=6.0M	N=12.0M	$aN^b$
73	MICROSOFT-006	35.0016	46.0020	50.0025	60.0030	60.0038	10.0000 $N^{0.305}$ 145	4.0006	4.0007	4.0009	12.0010	20.0000 $N^{0.184}$ 112	
74	NEC-000	171.00131	171.00170	145.00203	148.00244	137.00294	108.0003 $N^{0.276}$ 128	144.0029	149.0038	133.0048	130.0059	125.0074	14.00000 $N^{0.191}$ 146
75	NEC-001	183.00180	180.00209	149.00233	144.00266	139.00304	141.0016 $N^{0.179}$ 69	196.0109	189.00113	154.00116	148.00121	145.00129	149.00051 $N^{0.056}$ 56
76	NEC-002	3.00009	5.00010	7.00011	8.00012	7.00013	78.0002 $N^{0.113}$ 34	5.00008	5.00008	4.00008	3.00008	77.00005 $N^{0.038}$ 37	
77	NEC-003	17.00013	13.00014	17.00015	12.00016	9.00016	119.0005 $N^{0.079}$ 16	38.00012	31.00012	28.00012	25.00012	22.00012	118.00009 $N^{0.119}$ 24
78	NEC-004	22.00014	17.00014	17.00015	17.00016	17.00017	127.0006 $N^{0.059}$ 11	57.0013	45.0013	41.0013	39.0013	28.0013	127.00010 $N^{0.116}$ 18
79	NEUROTECHNOLOGY-003	182.00179	181.00225	131.00263	147.00306	144.00361	133.0007 $N^{0.239}$ 104	161.0042	163.0057	144.0072	145.0090	142.00112	19.00000 $N^{0.334}$ 149
80	NEUROTECHNOLOGY-004	113.00046	110.00056	108.00064	108.00074	98.00088	91.0002 $N^{0.220}$ 87	121.0022	119.0025	112.0028	108.0031	100.0034	62.00003 $N^{0.154}$ 106
81	NEUROTECHNOLOGY-005	99.00035	96.00043	95.00049	92.00057	87.00068	68.0002 $N^{0.223}$ 90	118.0021	115.0023	105.0024	102.0025	94.00028	90.00006 $N^{0.092}$ 80
82	NEUROTECHNOLOGY-007	93.00032	91.00039	92.00044	89.00052	88.00062	60.0002 $N^{0.222}$ 89	111.0020	110.0022	103.0023	97.0024	88.0026	106.00007 $N^{0.067}$ 69
83	NEUROTECHNOLOGY-008	50.00019	53.00022	53.00025	56.00029	51.00034	40.0001 $N^{0.205}$ 80	62.0013	50.0013	46.0013	43.0014	39.00015	104.00007 $N^{0.043}$ 43
84	NEUROTECHNOLOGY-009	16.00013	18.00014	20.00016	22.00018	21.00021	51.0001 $N^{0.162}$ 59	25.0011	24.0011	23.0011	21.0012	18.0012	109.00007 $N^{0.029}$ 32
85	NTECHLAB-003	114.00046	116.00062	113.00076	118.00094	111.00114	22.0001 $N^{0.310}$ 146	69.0013	81.0016	89.0018	94.0022	89.0026	22.00001 $N^{0.237}$ 124
86	NTECHLAB-004	102.00037	105.00048	102.00058	99.00071	96.00085	24.0001 $N^{0.291}$ 137	31.0011	52.0013	64.0015	65.0017	74.0021	32.00001 $N^{0.198}$ 114
87	NTECHLAB-005	97.00035	103.00047	103.00058	108.00073	100.00092	14.0000 $N^{0.334}$ 152	9.0008	23.0011	31.0012	36.0015	63.0019	9.00000 $N^{0.285}$ 137
88	NTECHLAB-006	87.00030	95.00041	96.00050	94.00062	93.00078	13.0000 $N^{0.326}$ 151	6.00008	12.0009	22.0011	38.0013	49.0016	11.00000 $N^{0.253}$ 128
89	NTECHLAB-007	65.00022	69.00027	70.00031	70.00037	68.00044	28.0001 $N^{0.245}$ 108	36.0011	34.0012	37.0013	45.0014	44.00015	61.0003 $N^{0.107}$ 87
90	NTECHLAB-008	28.00014	35.00017	35.00020	42.00024	35.00027	19.0001 $N^{0.224}$ 92	21.0010	22.0010	20.0011	20.0011	19.0012	73.00004 $N^{0.065}$ 63
91	NTECHLAB-009	12.00012	12.00013	7.00014	11.00015	10.0018	67.0002 $N^{0.140}$ 43	17.0009	14.0009	15.0010	14.00010	13.00010	85.00005 $N^{0.041}$ 40
92	NTECHLAB-010	8.00011	7.00011	7.00012	7.00013	7.00014	102.0003 $N^{0.091}$ 25	25.0010	20.0010	15.0010	13.0010	11.0010	121.00009 $N^{0.005}$ 9
93	PARAVISION-003	80.0026	79.0031	78.0033	77.0042	75.0048	56.0002 $N^{0.210}$ 83	92.0016	91.0017	88.0018	84.0020	79.0021	79.00005 $N^{0.089}$ 76
94	PARAVISION-004	34.0015	30.0016	28.0017	29.0019	22.0021	108.0003 $N^{0.111}$ 31	58.0013	48.0013	43.0013	37.0013	32.0014	125.0010 $N^{0.020}$ 25
95	PARAVISION-005	30.0015	26.0015	21.0016	20.0018	17.0019	115.0004 $N^{0.094}$ 26	61.0013	51.0013	45.0013	38.0013	31.0014	129.0011 $N^{0.015}$ 16
96	PARAVISION-007	11.0011	9.00112	7.00112	8.00113	8.00115	104.0003 $N^{0.091}$ 24	25.0010	17.0010	16.0010	15.0010	14.0011	114.0008 $N^{0.018}$ 22
97	PIXELALL-002	104.00037	100.00045	98.00052	95.00062	91.00075	54.0002 $N^{0.238}$ 102	97.0017	103.0019	99.0021	98.0024	91.0027	54.00002 $N^{0.154}$ 107
98	PIXELALL-003	52.00019	52.00021	52.00024	51.00028	49.00032	61.0002 $N^{0.182}$ 71	70.0014	63.0014	55.0014	53.0015	46.0016	111.0007 $N^{0.045}$ 45
99	PIXELALL-004	44.00017	50.00020	49.00023	48.00026	44.00030	47.0001 $N^{0.192}$ 73	59.0013	53.0013	50.0014	47.0014	41.0015	98.00007 $N^{0.046}$ 46
100	PIXELALL-005	45.00018	45.00019	32.00020	36.00024	30.00024	121.0005 $N^{0.095}$ 27	84.0015	80.0016	70.0016	68.0016	61.0016	131.00012 $N^{0.018}$ 20
101	PTAKURATSATU-000	77.0025	78.00303	70.0036	71.0040	63.0040	99.0003 $N^{0.167}$ 61	81.0015	83.0016	91.0018	82.0020	69.0020	74.0004 $N^{0.096}$ 81
102	QUANTASOFT-001	225.00277	222.00277	16.00277	15.00277	15.00277	158.00217 $N^{0.217}$ 100	22.00116	224.00116	166.00116	154.00116	158.00116 $N^{0.000}$ 1	
103	RANKONE-002	178.00155	178.00194	148.00224	142.00262	140.00304	132.0007 $N^{0.230}$ 94	168.0048	168.0060	142.0071	142.0085	140.00102	44.00002 $N^{0.254}$ 131
104	RANKONE-003	179.00155	177.00194	142.00224	144.00262	14.00304	131.0007 $N^{0.230}$ 95	166.0048	169.0060	143.0071	143.0085	139.00102	45.00002 $N^{0.254}$ 130
105	RANKONE-005	137.00075	144.00094	130.00110	120.00132	124.00156	93.0003 $N^{0.251}$ 111	138.0026	138.0026	126.0036	121.0043	114.00050	40.00001 $N^{0.221}$ 121
106	RANKONE-007	84.0028	83.0034	82.0038	79.0045	77.0053	63.0002 $N^{0.211}$ 84	82.0015	84.0017	85.0018	79.0019	77.0021	64.00003 $N^{0.123}$ 94
107	RANKONE-009	55.00020	61.00024	62.00027	60.00032	60.00038	36.0001 $N^{0.219}$ 86	66.0013	60.0014	59.0015	54.0015	47.00016	88.0006 $N^{0.059}$ 59
108	RANKONE-010	59.00020	55.00022	54.00025	55.00029	50.00032	83.0002 $N^{0.164}$ 60	77.0014	68.0015	65.0015	58.0016	53.0017	93.0006 $N^{0.058}$ 58
109	RANKONE-011	21.00014	23.00015	25.00017	28.0018	22.0021	69.0002 $N^{0.150}$ 49	37.0011	27.0012	25.0012	22.0012	21.0012	117.0008 $N^{0.028}$ 28
110	REALNETWORKS-002	197.00299	193.00393	160.00470	155.00562	152.00580	138.0003 $N^{0.236}$ 101	170.0054	179.0076	152.0097	149.00126	146.00132	31.00001 $N^{0.320}$ 147
111	REALNETWORKS-003	184.00183	184.00242	153.00291	148.00352	148.00423	111.0004 $N^{0.287}$ 136	166.0041	162.0054	139.0064	140.00808	138.00101	25.00001 $N^{0.307}$ 143
112	REALNETWORKS-004	181.00175	182.00236	152.00284	148.00347	145.00416	109.0003 $N^{0.295}$ 139	157.0040	158.0050	137.0061	138.0078	137.0099	24.00001 $N^{0.315}$ 144
113	REALNETWORKS-005	56.00020	57.00023	60.00026	58.00030	58.00037	45.0001 $N^{0.207}$ 81	36.0012	36.0012	36.0012	36.0012	37.00015	72.00004 $N^{0.081}$ 71
114	REMARKAI-000	83.00027	85.00034	85.00040	80.00048	80.00058	28.0001 $N^{0.260}$ 117	78.0014	77.0015	73.0016	69.0018	68.0020	66.00003 $N^{0.108}$ 84
115	RENDIP-000	25.00014	27.00015	27.00019	28.00022	26.00022	62.0002 $N^{0.158}$ 54	36.0012	35.0012	30.0012	25.00012	25.00013	116.00008 $N^{0.029}$ 29
116	S1-000	60.00021	63.00024	65.00028	66.00032	59.00037	48.0001 $N^{0.203}$ 77	77.0014	74.00145	67.0015	62.00166	54.00017	97.00007 $N^{0.055}$ 55
117	SCANOVATE-000	105.00038	106.00050	104.00059	101.00073	90.00073	65.0002 $N^{0.235}$ 100	74.0014	78.0015	78.0017	89.00020	72.00020	53.00002 $N^{0.142}$ 102
118	SCANOVATE-001	107.00041	109.00053	105.00064	108.00079	105.00098	29.0001 $N^{0.299}$ 142	69.0013	76.0015	79.0017	90.0021	87.0024	34.00001 $N^{0.209}$ 118
119	SENSETIME-000	66.00022	59.00023	59.00026	54.00028	48.00032	111.0003 $N^{0.135}$ 41	91.0016	93.0017	86.0018	73.0018	66.0020	108.00007 $N^{0.060}$ 60
120	SENSETIME-001	64.00022	60.00023	59.00025	59.00029	59.00037	73.0002 $N^{0.177}$ 68	91.0016	82.0016	77.0017	72.0018	85.0024	63.0003 $N^{0.125}$ 96
121	SENSETIME-002	174.00136	165.00137	138.00137	129.00138	120.00139	153.00124 $N^{0.077}$ 2	202.0016	195.00136	156.00136	151.00136	142.00136	154.00135 $N^{0.001}$ 3
122	SENSETIME-003	6.00010	4.00010	4.00010	4.00011	4.00012	101.0003 $N^{0.085}$ 21	15.0009	13.0009	12.0009	12.00010	10.0010	113.00008 $N^{0.13}$ 14
123	SENSETIME-004	4.00010											

MISSES AT GIVEN RANK		ENROL MOST RECENT											
FNIR(N, T= 0, r)		RANK 1					RANK 50						
#	ALGORITHM	N=0.64M	N=1.6M	N=3.0M	N=6.0M	N=12.0M	aN <sup>b</sup>	N=0.64M	N=1.6M	N=3.0M	N=6.0M	N=12.0M	aN <sup>b</sup>
145	VISIONLABS-006	<sup>41</sup> 0.0016	<sup>41</sup> 0.0018	<sup>48</sup> 0.0022	<sup>53</sup> 0.0028	<sup>64</sup> 0.0041	<sup>8</sup> 0.0000 N <sup>0.314</sup> 148	<sup>41</sup> 0.0012	<sup>48</sup> 0.0013	<sup>60</sup> 0.0015	<sup>74</sup> 0.0019	<sup>92</sup> 0.0027	<sup>12</sup> 0.0000 N <sup>0.275</sup> 134
146	VISIONLABS-007	<sup>38</sup> 0.0016	<sup>36</sup> 0.0018	<sup>36</sup> 0.0020	<sup>41</sup> 0.0023	<sup>52</sup> 0.0034	<sup>17</sup> 0.0001 N <sup>0.248</sup> 109	<sup>40</sup> 0.0012	<sup>37</sup> 0.0012	<sup>34</sup> 0.0013	<sup>33</sup> 0.0013	<sup>67</sup> 0.0020	<sup>41</sup> 0.0001 N <sup>0.152</sup> 105
147	VISIONLABS-008	<sup>40</sup> 0.0019	<sup>48</sup> 0.0020	<sup>44</sup> 0.0021	<sup>47</sup> 0.0025	<sup>45</sup> 0.0030	<sup>70</sup> 0.0002 N <sup>0.169</sup> 62	<sup>90</sup> 0.0016	<sup>92</sup> 0.0017	<sup>81</sup> 0.0017	<sup>85</sup> 0.0020	<sup>84</sup> 0.0023	<sup>68</sup> 0.0003 N <sup>0.114</sup> 89
148	VISIONLABS-009	<sup>9</sup> 0.0011	<sup>8</sup> 0.0011	<sup>8</sup> 0.0012	<sup>9</sup> 0.0014	<sup>13</sup> 0.0017	<sup>41</sup> 0.0001 N <sup>0.160</sup> 58	<sup>20</sup> 0.0010	<sup>16</sup> 0.0010	<sup>17</sup> 0.0010	<sup>19</sup> 0.0011	<sup>35</sup> 0.0014	<sup>56</sup> 0.0002 N <sup>0.109</sup> 85
149	VISIONLABS-010	<sup>20</sup> 0.0014	<sup>15</sup> 0.0014	<sup>18</sup> 0.0015	<sup>18</sup> 0.0017	<sup>19</sup> 0.0021	<sup>77</sup> 0.0002 N <sup>0.137</sup> 42	<sup>39</sup> 0.0013	<sup>37</sup> 0.0013	<sup>44</sup> 0.0013	<sup>46</sup> 0.0014	<sup>52</sup> 0.0017	<sup>70</sup> 0.0004 N <sup>0.090</sup> 78
150	VOCORD-005	<sup>127</sup> 0.0060	<sup>126</sup> 0.0070	<sup>117</sup> 0.0082	<sup>117</sup> 0.0097	<sup>113</sup> 0.0117	<sup>92</sup> 0.0003 N <sup>0.232</sup> 99	<sup>152</sup> 0.0033	<sup>146</sup> 0.0035	<sup>128</sup> 0.0037	<sup>118</sup> 0.0040	<sup>110</sup> 0.0043	<sup>123</sup> 0.0010 N <sup>0.094</sup> 77
151	VTS-001	<sup>19</sup> 0.0014	<sup>25</sup> 0.0015	<sup>25</sup> 0.0017	<sup>29</sup> 0.0019	<sup>28</sup> 0.0023	<sup>42</sup> 0.0001 N <sup>0.179</sup> 70	<sup>19</sup> 0.0010	<sup>18</sup> 0.0010	<sup>18</sup> 0.0010	<sup>17</sup> 0.0011	<sup>16</sup> 0.0011	<sup>80</sup> 0.0005 N <sup>0.051</sup> 53
152	XFORWARDAI-000	<sup>63</sup> 0.0021	<sup>56</sup> 0.0023	<sup>51</sup> 0.0024	<sup>49</sup> 0.0027	<sup>42</sup> 0.0029	<sup>120</sup> 0.0005 N <sup>0.111</sup> 32	<sup>108</sup> 0.0019	<sup>102</sup> 0.0019	<sup>95</sup> 0.0019	<sup>86</sup> 0.0020	<sup>71</sup> 0.0020	<sup>136</sup> 0.0015 N <sup>0.041</sup> 21
153	XFORWARDAI-001	<sup>57</sup> 0.0020	<sup>51</sup> 0.0020	<sup>42</sup> 0.0021	<sup>36</sup> 0.0022	<sup>29</sup> 0.0024	<sup>135</sup> 0.0009 N <sup>0.058</sup> 10	<sup>10</sup> 0.0019	<sup>10</sup> 0.0019	<sup>93</sup> 0.0019	<sup>78</sup> 0.0019	<sup>64</sup> 0.0019	<sup>146</sup> 0.0018 N <sup>0.004</sup> 7
154	XFORWARDAI-002	<sup>53</sup> 0.0019	<sup>45</sup> 0.0020	<sup>39</sup> 0.0020	<sup>33</sup> 0.0021	<sup>24</sup> 0.0022	<sup>137</sup> 0.0011 N <sup>0.038</sup> 5	<sup>106</sup> 0.0019	<sup>99</sup> 0.0019	<sup>92</sup> 0.0019	<sup>77</sup> 0.0019	<sup>61</sup> 0.0019	<sup>139</sup> 0.0018 N <sup>0.003</sup> 6
155	YITU-002	<sup>36</sup> 0.0016	<sup>40</sup> 0.0018	<sup>42</sup> 0.0021	<sup>43</sup> 0.0024	<sup>42</sup> 0.0029	<sup>30</sup> 0.0001 N <sup>0.213</sup> 85	<sup>18</sup> 0.0009	<sup>21</sup> 0.0010	<sup>19</sup> 0.0010	<sup>18</sup> 0.0011	<sup>17</sup> 0.0012	<sup>69</sup> 0.0004 N <sup>0.073</sup> 88
156	YITU-003	<sup>79</sup> 0.0026	<sup>79</sup> 0.0029	<sup>71</sup> 0.0031	<sup>66</sup> 0.0035	<sup>62</sup> 0.0039	<sup>113</sup> 0.0004 N <sup>0.141</sup> 45	<sup>114</sup> 0.0020	<sup>109</sup> 0.0021	<sup>102</sup> 0.0022	<sup>96</sup> 0.0023	<sup>86</sup> 0.0024	<sup>124</sup> 0.0010 N <sup>0.054</sup> 54
157	YITU-004	<sup>10</sup> 0.0011	<sup>11</sup> 0.0013	<sup>16</sup> 0.0015	<sup>19</sup> 0.0017	<sup>22</sup> 0.0047	<sup>3</sup> 0.0000 N <sup>0.438</sup> 154	<sup>11</sup> 0.0008	<sup>9</sup> 0.0009	<sup>10</sup> 0.0009	<sup>9</sup> 0.0009	<sup>101</sup> 0.0036	<sup>5</sup> 0.0000 N <sup>0.395</sup> 151
158	YITU-005	<sup>69</sup> 0.0022	<sup>56</sup> 0.0023	<sup>55</sup> 0.0025	<sup>50</sup> 0.0027	<sup>46</sup> 0.0031	<sup>122</sup> 0.0005 N <sup>0.113</sup> 33	<sup>109</sup> 0.0020	<sup>104</sup> 0.0020	<sup>98</sup> 0.0020	<sup>88</sup> 0.0020	<sup>73</sup> 0.0020	<sup>138</sup> 0.0017 N <sup>0.012</sup> 13

**Table 20: Investigation-mode: Effect of N on FNIR on recent images** For five enrollment population sizes,  $N$ , with  $T = 0$  and  $FPIR = 1$ . The left five columns are rank 1 miss rates The right five columns are rank 50 miss rates Missing entries usually apply because another algorithm from the same developer was run instead. Some developers are missing because less accurate algorithms were not run on galleries with  $N > 1\,600\,000$ . Throughout blue superscripts indicate the rank of the algorithm for that column, and yellow highlighting indicates the most accurate value. Caution: The Power-low models are mostly intended to draw attention to the kind of behavior, not as a model to be used for prediction.

#	ALGORITHM	MISSES OUTSIDE RANK R		RESOURCE USAGE		ENROL MOST RECENT, N = 1.6M					
		FNIR(N, T=0, R)		TEMPLATE		R=1	R=5	R=10	R=20	R=50	WORK-10
		BYTES	MSEC								
1	3DIVI-003	39	512	126	625	21 <sup>0</sup> .0833	20 <sup>6</sup> .0444	20 <sup>6</sup> .0349	20 <sup>2</sup> .0270	20 <sup>2</sup> .0191	20 <sup>7</sup> .1.447
2	3DIVI-004	21 <sup>9</sup>	4096	12 <sup>2</sup>	628	17 <sup>2</sup> .0175	16 <sup>5</sup> .0091	16 <sup>3</sup> .0075	16 <sup>1</sup> .0061	15 <sup>6</sup> .0049	16 <sup>9</sup> .1.092
3	3DIVI-005	21 <sup>9</sup>	4096	13 <sup>3</sup>	653	17 <sup>2</sup> .0176	16 <sup>6</sup> .0091	16 <sup>1</sup> .0074	16 <sup>0</sup> .0061	15 <sup>7</sup> .0049	17 <sup>9</sup> .1.092
4	3DIVI-006	50	528	13 <sup>5</sup>	653	18 <sup>3</sup> .0240	18 <sup>9</sup> .0171	19 <sup>2</sup> .0160	19 <sup>3</sup> .0154	19 <sup>8</sup> .0148	18 <sup>8</sup> .1.162
5	ACER-000	35	512	29	201	13 <sup>1</sup> .0106	13 <sup>5</sup> .0051	13 <sup>2</sup> .0041	13 <sup>1</sup> .0034	12 <sup>4</sup> .0026	13 <sup>6</sup> .1.053
6	AIZE-001	13 <sup>2</sup>	2048	75	403	11 <sup>5</sup> .0056	11 <sup>5</sup> .0037	12 <sup>0</sup> .0033	12 <sup>1</sup> .0030	12 <sup>7</sup> .0027	11 <sup>5</sup> .1.035
7	ALCHERA-000	14 <sup>7</sup>	2048	42	263	16 <sup>8</sup> .0161	17 <sup>7</sup> .0124	18 <sup>7</sup> .0117	18 <sup>7</sup> .0111	18 <sup>8</sup> .0105	17 <sup>8</sup> .1.116
8	ALCHERA-001	11 <sup>9</sup>	2048	6 <sup>6</sup>	66	23 <sup>7</sup> .9869	23 <sup>7</sup> .9782	23 <sup>7</sup> .9735	23 <sup>7</sup> .9679	23 <sup>6</sup> .9590	23 <sup>9</sup> .9.811
9	ALCHERA-002	14 <sup>2</sup>	2048	14 <sup>1</sup>	115	21 <sup>2</sup> .0949	21 <sup>1</sup> .0555	20 <sup>9</sup> .0443	20 <sup>9</sup> .0354	20 <sup>4</sup> .0254	21 <sup>1</sup> .1.544
10	ALCHERA-003	12 <sup>7</sup>	2048	11 <sup>4</sup>	548	14 <sup>8</sup> .0104	13 <sup>8</sup> .0054	13 <sup>8</sup> .0045	13 <sup>8</sup> .0038	13 <sup>9</sup> .0032	14 <sup>6</sup> .1.055
11	ALLGOVISION-000	13 <sup>7</sup>	2048	8 <sup>3</sup>	425	15 <sup>5</sup> .0114	16 <sup>0</sup> .0084	16 <sup>6</sup> .0078	16 <sup>7</sup> .0073	17 <sup>2</sup> .0067	16 <sup>0</sup> .1.079
12	ALLGOVISION-001	11 <sup>8</sup>	2048	18 <sup>7</sup>	792	13 <sup>9</sup> .0090	13 <sup>3</sup> .0048	13 <sup>1</sup> .0040	13 <sup>0</sup> .0033	12 <sup>8</sup> .0027	13 <sup>3</sup> .1.048
13	ANKE-000	19 <sup>5</sup>	2072	8 <sup>5</sup>	431	16 <sup>3</sup> .0132	15 <sup>1</sup> .0073	15 <sup>1</sup> .0060	15 <sup>0</sup> .0050	15 <sup>0</sup> .0040	15 <sup>6</sup> .1.072
14	ANKE-001	19 <sup>6</sup>	2072	8 <sup>7</sup>	433	16 <sup>4</sup> .0132	15 <sup>2</sup> .0073	15 <sup>1</sup> .0061	15 <sup>1</sup> .0050	15 <sup>1</sup> .0040	15 <sup>7</sup> .1.073
15	ANKE-002	18 <sup>8</sup>	2056	12 <sup>9</sup>	641	7 <sup>4</sup> .0028	7 <sup>5</sup> .0020	7 <sup>5</sup> .0018	8 <sup>2</sup> .0018	8 <sup>6</sup> .0017	7 <sup>6</sup> .1.019
16	AWARE-003	19 <sup>7</sup>	2076	716	19 <sup>8</sup>	0.0306	18 <sup>7</sup> .0162	18 <sup>4</sup> .0127	18 <sup>1</sup> .0100	17 <sup>8</sup> .0075	18 <sup>7</sup> .1.163
17	AWARE-004	7 <sup>9</sup>	92	16 <sup>5</sup>	712	20 <sup>6</sup> .0679	20 <sup>3</sup> .0348	20 <sup>8</sup> .0274	20 <sup>0</sup> .0208	19 <sup>9</sup> .0145	20 <sup>3</sup> .1.354
18	AWARE-005	20 <sup>8</sup>	3100	19 <sup>4</sup>	827	19 <sup>3</sup> .0311	18 <sup>8</sup> .0167	18 <sup>6</sup> .0134	18 <sup>3</sup> .0107	18 <sup>4</sup> .0082	19 <sup>1</sup> .1.167
19	AWARE-006	3 <sup>1</sup>	124	19 <sup>0</sup>	818	20 <sup>8</sup> .0697	20 <sup>5</sup> .0369	20 <sup>1</sup> .0288	20 <sup>1</sup> .0223	19 <sup>9</sup> .0158	20 <sup>9</sup> .1.371
20	AYONIX-000	7 <sup>8</sup>	1036	1 <sup>0</sup>	10	23 <sup>1</sup> .0505	23 <sup>2</sup> .0350	23 <sup>2</sup> .0317	23 <sup>2</sup> .0284	23 <sup>2</sup> .0281	23 <sup>2</sup> .4.288
21	AYONIX-001	7 <sup>7</sup>	1036	3 <sup>12</sup>	3414	22 <sup>6</sup> .03414	22 <sup>6</sup> .0238	22 <sup>9</sup> .0197	22 <sup>7</sup> .01652	22 <sup>6</sup> .01274	22 <sup>7</sup> .3.226
22	AYONIX-002	7 <sup>5</sup>	1036	2 <sup>11</sup>	3414	22 <sup>7</sup> .03414	22 <sup>7</sup> .0238	22 <sup>7</sup> .0197	22 <sup>6</sup> .01652	22 <sup>7</sup> .01274	22 <sup>7</sup> .3.226
23	CAMVI-003	6 <sup>9</sup>	1024	16 <sup>1</sup>	707	20 <sup>5</sup> .0520	21 <sup>0</sup> .0517	21 <sup>1</sup> .0517	21 <sup>4</sup> .0517	21 <sup>4</sup> .0517	20 <sup>9</sup> .1.466
24	CAMVI-004	6 <sup>7</sup>	1024	17 <sup>0</sup>	718	20 <sup>0</sup> .0468	20 <sup>8</sup> .0465	21 <sup>0</sup> .0465	21 <sup>1</sup> .0464	21 <sup>3</sup> .0464	20 <sup>6</sup> .1.419
25	CAMVI-005	6 <sup>4</sup>	1024	17 <sup>9</sup>	769	20 <sup>6</sup> .0652	21 <sup>2</sup> .0648	21 <sup>5</sup> .0648	21 <sup>6</sup> .0648	21 <sup>8</sup> .0647	21 <sup>5</sup> .1.584
26	CIB-000	23 <sup>8</sup>	8196	14 <sup>1</sup>	674	24 <sup>0</sup> .0015	28 <sup>8</sup> .0013	27 <sup>2</sup> .0012	29 <sup>9</sup> .0012	30 <sup>0</sup> .0012	28 <sup>1</sup> .1.012
27	CLOUDWALK-HR-000	16 <sup>7</sup>	2048	22 <sup>3</sup>	908	24 <sup>0</sup> .0015	41 <sup>1</sup> .0014	45 <sup>0</sup> .0014	53 <sup>3</sup> .0014	61 <sup>0</sup> .0014	38 <sup>1</sup> .1.013
28	COGENT-000	4 <sup>7</sup>	525	11 <sup>5</sup>	551	14 <sup>9</sup> .0105	17 <sup>0</sup> .0096	17 <sup>0</sup> .0095	12 <sup>5</sup> .0032	11 <sup>8</sup> .0024	16 <sup>6</sup> .1.088
29	COGENT-001	46 <sup>5</sup>	525	11 <sup>6</sup>	552	15 <sup>0</sup> .0105	17 <sup>1</sup> .0096	17 <sup>4</sup> .0095	12 <sup>4</sup> .0032	11 <sup>7</sup> .0024	16 <sup>7</sup> .1.088
30	COGENT-002	80	1043	23 <sup>7</sup>	987	88 <sup>0</sup> .0036	84 <sup>8</sup> .0022	83 <sup>8</sup> .0020	80 <sup>8</sup> .0018	79 <sup>9</sup> .0015	88 <sup>1</sup> .1.021
31	COGENT-003	79	1043	23 <sup>5</sup>	960	90 <sup>0</sup> .0038	94 <sup>9</sup> .0024	91 <sup>9</sup> .0021	94 <sup>9</sup> .0019	87 <sup>9</sup> .0017	91 <sup>1</sup> .1.023
32	COGENT-004	180	2053	23 <sup>3</sup>	952	4 <sup>2</sup> .0020	49 <sup>0</sup> .0016	52 <sup>5</sup> .0015	57 <sup>5</sup> .0015	58 <sup>0</sup> .0014	48 <sup>1</sup> .1.015
33	COGNITEC-000	180	2052	19 <sup>7</sup>	176	18 <sup>5</sup> .0252	18 <sup>3</sup> .0136	18 <sup>1</sup> .0107	18 <sup>0</sup> .0085	17 <sup>1</sup> .0065	18 <sup>4</sup> .1.136
34	COGNITEC-001	17 <sup>7</sup>	2052	30 <sup>2</sup>	205	15 <sup>0</sup> .0117	14 <sup>5</sup> .0062	14 <sup>4</sup> .0051	14 <sup>6</sup> .0042	14 <sup>4</sup> .0034	14 <sup>5</sup> .1.062
35	COGNITEC-002	17 <sup>8</sup>	2052	35 <sup>227</sup>	227	11 <sup>4</sup> .0057	11 <sup>4</sup> .0037	11 <sup>5</sup> .0032	11 <sup>6</sup> .0029	12 <sup>5</sup> .0026	11 <sup>4</sup> .1.035
36	COGNITEC-003	17 <sup>7</sup>	2052	52 <sup>9</sup>	297	11 <sup>0</sup> .0062	12 <sup>2</sup> .0040	12 <sup>4</sup> .0036	12 <sup>9</sup> .0033	13 <sup>6</sup> .0030	12 <sup>1</sup> .1.039
37	COGNITEC-004	18 <sup>3</sup>	2052	26 <sup>8</sup>	192	81 <sup>0</sup> .0032	78 <sup>8</sup> .0020	69 <sup>8</sup> .0018	64 <sup>8</sup> .0015	62 <sup>8</sup> .0014	79 <sup>1</sup> .1.020
38	COGNITEC-005	17 <sup>7</sup>	2052	36 <sup>7</sup>	367	3 <sup>0</sup> .0016	24 <sup>0</sup> .0013	23 <sup>0</sup> .0012	23 <sup>0</sup> .0012	26 <sup>0</sup> .0011	29 <sup>1</sup> .1.012
39	CUBOX-000	12 <sup>6</sup>	2048	22 <sup>6</sup>	918	16 <sup>0</sup> .0014	33 <sup>0</sup> .0014	41 <sup>0</sup> .0014	47 <sup>0</sup> .0014	56 <sup>0</sup> .0014	32 <sup>1</sup> .1.012
40	CYBERLINK-000	18 <sup>1</sup>	2052	15 <sup>5</sup>	699	9 <sup>0</sup> .0040	10 <sup>3</sup> .0028	10 <sup>7</sup> .0026	11 <sup>0</sup> .0024	11 <sup>2</sup> .0022	10 <sup>2</sup> .1.027
41	CYBERLINK-001	17 <sup>1</sup>	2052	86 <sup>433</sup>	433	88 <sup>0</sup> .0035	90 <sup>0</sup> .0023	89 <sup>0</sup> .0021	84 <sup>8</sup> .0018	90 <sup>0</sup> .0017	87 <sup>1</sup> .1.022
42	CYBERLINK-002	23 <sup>3</sup>	4140	17 <sup>7</sup>	738	68 <sup>0</sup> .0026	86 <sup>0</sup> .0023	96 <sup>0</sup> .0022	103 <sup>0</sup> .0021	107 <sup>0</sup> .0021	83 <sup>1</sup> .1.021
43	CYBERLINK-003	23 <sup>2</sup>	6121	15 <sup>4</sup>	696	20 <sup>6</sup> .0016	27 <sup>0</sup> .0013	28 <sup>0</sup> .0013	27 <sup>0</sup> .0012	28 <sup>0</sup> .0012	29 <sup>1</sup> .1.012
44	CYBERLINK-004	23 <sup>5</sup>	6121	17 <sup>6</sup>	738	33 <sup>0</sup> .0017	44 <sup>0</sup> .0015	50 <sup>0</sup> .0015	54 <sup>0</sup> .0014	64 <sup>0</sup> .0014	42 <sup>1</sup> .014
45	DAHUA-000	11 <sup>1</sup>	2048	70 <sup>378</sup>	378	14 <sup>0</sup> .0093	148 <sup>0</sup> .0066	15 <sup>5</sup> .0061	158 <sup>0</sup> .0057	161 <sup>0</sup> .0054	146 <sup>1</sup> .062
46	DAHUA-001	15 <sup>2</sup>	2048	66 <sup>371</sup>	371	12 <sup>5</sup> .0067	123 <sup>0</sup> .0040	123 <sup>0</sup> .0036	127 <sup>0</sup> .0033	131 <sup>0</sup> .0029	123 <sup>1</sup> .0.40
47	DAHUA-002	15 <sup>9</sup>	2048	15 <sup>6</sup>	699	39 <sup>0</sup> .0018	43 <sup>0</sup> .0015	47 <sup>0</sup> .0014	51 <sup>0</sup> .0014	54 <sup>0</sup> .0013	48 <sup>1</sup> .1.014
48	DAHUA-003	14 <sup>8</sup>	2048	17 <sup>3</sup>	725	10 <sup>0</sup> .0012	8 <sup>0</sup> .0010	9 <sup>0</sup> .0009	10 <sup>0</sup> .0009	10 <sup>0</sup> .0009	7 <sup>1</sup> .1.009
49	DEEPLINT-001	21 <sup>6</sup>	4096	14 <sup>6</sup>	687	18 <sup>0</sup> .0014	31 <sup>0</sup> .0014	36 <sup>0</sup> .0013	38 <sup>0</sup> .0013	44 <sup>0</sup> .0013	31 <sup>1</sup> .1.012
50	DEEPESEA-001	10 <sup>8</sup>	2048	18 <sup>4</sup>	780	97 <sup>0</sup> .0043	85 <sup>0</sup> .0022	77 <sup>0</sup> .0018	69 <sup>0</sup> .0016	57 <sup>0</sup> .0014	88 <sup>1</sup> .0.22
51	DERMALOG-003	6 <sup>128</sup>	321	21 <sup>2</sup>	1259	21 <sup>5</sup> .0744	21 <sup>4</sup> .0603	21 <sup>3</sup> .0480	21 <sup>2</sup> .0347	21 <sup>1</sup> .0343	173 <sup>1</sup> .7.227
52	DERMALOG-004	4 <sup>128</sup>	3108	21 <sup>208</sup>	1251	21 <sup>4</sup> .0739	21 <sup>2</sup> .0598	21 <sup>2</sup> .0475	21 <sup>1</sup> .0343	21 <sup>1</sup> .0343	174 <sup>1</sup> .7.227
53	DERMALOG-005	7 <sup>128</sup>	108	532	16 <sup>7</sup>	0.0149	180 <sup>0</sup> .0129	183 <sup>0</sup> .0125	189 <sup>0</sup> .0123	193 <sup>0</sup> .0122	177 <sup>1</sup> .1.118
54	DERMALOG-006	13 <sup>256</sup>	106	514	13 <sup>0</sup>	0.0181	150 <sup>0</sup> .0069	154 <sup>0</sup> .0066	162 <sup>0</sup> .0065	170 <sup>0</sup> .0063	148 <sup>1</sup> .1.063
55	DERMALOG-007	5 <sup>128</sup>	81	413	14 <sup>2</sup>	0.0092	149 <sup>0</sup> .0066	150 <sup>0</sup> .0060	157 <sup>0</sup> .0057	164 <sup>0</sup> .0054	147 <sup>1</sup> .1.062
56	DERMALOG-008	38 <sup>512</sup>	65	370	7 <sup>0</sup>	0.0209	74 <sup>0</sup> .0020	75 <sup>0</sup> .0018	72 <sup>0</sup> .0017	75 <sup>0</sup> .0015	75 <sup>1</sup> .1.019
57	EYEDEA-003	76 <sup>1036</sup>	71	385	21 <sup>0</sup>	0.0800	20 <sup>7</sup> .0451	20 <sup>7</sup> .0362	20 <sup>3</sup> .0289	20 <sup>3</sup> .0211	20 <sup>8</sup> .1.448
58	F8-001	12 <sup>2048</sup>	206	851	16 <sup>1</sup>	0.0120	17 <sup>2</sup> .0105	17 <sup>1</sup> .0102	18 <sup>2</sup> .0100	18 <sup>6</sup> .0099	17 <sup>2</sup> .1.096
59	FINCORE-000	15 <sup>2048</sup>	97	477	15 <sup>2</sup>	0.0108	13 <sup>7</sup> .0052	13 <sup>4</sup> .0042	13 <sup>3</sup> .0034	126 <sup>0</sup> .0026	138 <sup>1</sup> .1.054
60	GLORY-000	30 <sup>418</sup>	15 <sup>1</sup>	60	22 <sup>2</sup>	0.1781	122 <sup>0</sup> .1391	22 <sup>2</sup> .1266	22 <sup>2</sup> .1154	22 <sup>2</sup> .1007	22 <sup>1</sup> .2.298
61	GLORY-001	10 <sup>1726</sup>	78	405	17 <sup>1</sup>	0.1268	21 <sup>7</sup> .0967	21 <sup>7</sup> .0869	21 <sup>8</sup> .0778	21 <sup>9</sup> .0673	21 <sup>7</sup> .1.903
62	GOR										

MISSES OUTSIDE RANK R			RESOURCE USAGE		ENROL MOST RECENT, N = 1.6M					
FNIR(N, T=0, R)			TEMPLATE		R=1	R=5	R=10	R=20	R=50	WORK-10
#	ALGORITHM		BYTES	MSEC						
73	IDEMIA-004		48	528	13 <sup>669</sup>	121 <sup>0.0066</sup>	11 <sup>0.0036</sup>	116 <sup>0.0032</sup>	115 <sup>0.0027</sup>	108 <sup>0.0021</sup>
74	IDEMIA-005		28 <sup>352</sup>	68 <sup>374</sup>	133 <sup>0.0081</sup>	12 <sup>0.0044</sup>	125 <sup>0.0036</sup>	128 <sup>0.0032</sup>	134 <sup>0.0030</sup>	129 <sup>1.044</sup>
75	IDEMIA-006		29 <sup>352</sup>	67 <sup>373</sup>	146 <sup>0.0096</sup>	136 <sup>0.0052</sup>	138 <sup>0.0042</sup>	142 <sup>0.0039</sup>	147 <sup>0.0037</sup>	135 <sup>1.052</sup>
76	IDEMIA-007		99 <sup>860</sup>	18 <sup>807</sup>	67 <sup>0.0026</sup>	39 <sup>0.0016</sup>	44 <sup>0.0014</sup>	35 <sup>0.0013</sup>	32 <sup>0.0012</sup>	54 <sup>1.015</sup>
77	IDEMIA-008		27 <sup>300</sup>	90 <sup>451</sup>	6 <sup>0.0111</sup>	7 <sup>0.0009</sup>	10 <sup>0.0009</sup>	11 <sup>0.0009</sup>	11 <sup>0.0009</sup>	5 <sup>1.009</sup>
78	IMAGUS-002		36 <sup>512</sup>	7 <sup>76</sup>	223 <sup>0.2203</sup>	22 <sup>0.1342</sup>	220 <sup>0.1090</sup>	219 <sup>0.0871</sup>	217 <sup>0.0632</sup>	222 <sup>2.308</sup>
79	IMAGUS-003		37 <sup>512</sup>	5 <sup>57</sup>	228 <sup>0.3559</sup>	228 <sup>0.2491</sup>	228 <sup>0.2132</sup>	228 <sup>0.1791</sup>	228 <sup>0.1397</sup>	228 <sup>3.363</sup>
80	IMAGUS-005		151 <sup>2048</sup>	186 <sup>788</sup>	44 <sup>0.0019</sup>	51 <sup>0.0016</sup>	51 <sup>0.0015</sup>	50 <sup>0.0014</sup>	50 <sup>0.0013</sup>	49 <sup>1.015</sup>
81	IMAGUS-006		140 <sup>2048</sup>	221 <sup>905</sup>	49 <sup>0.0020</sup>	54 <sup>0.0016</sup>	56 <sup>0.0015</sup>	58 <sup>0.0015</sup>	65 <sup>0.0014</sup>	51 <sup>1.015</sup>
82	IMPERIAL-000		16 <sup>2048</sup>	13 <sup>654</sup>	65 <sup>0.0024</sup>	6 <sup>0.0019</sup>	74 <sup>0.0018</sup>	81 <sup>0.0018</sup>	88 <sup>0.0017</sup>	66 <sup>1.018</sup>
83	INCODE-000		69 <sup>1024</sup>	24 <sup>190</sup>	201 <sup>0.0489</sup>	196 <sup>0.0261</sup>	196 <sup>0.0204</sup>	194 <sup>0.0160</sup>	191 <sup>0.0117</sup>	196 <sup>1.262</sup>
84	INCODE-001		13 <sup>2048</sup>	150 <sup>690</sup>	170 <sup>0.0166</sup>	16 <sup>0.0084</sup>	156 <sup>0.0067</sup>	153 <sup>0.0055</sup>	154 <sup>0.0043</sup>	162 <sup>1.086</sup>
85	INCODE-002		15 <sup>2048</sup>	49 <sup>291</sup>	174 <sup>0.0178</sup>	169 <sup>0.0090</sup>	158 <sup>0.0070</sup>	156 <sup>0.0056</sup>	155 <sup>0.0043</sup>	168 <sup>1.092</sup>
86	INCODE-003		131 <sup>2048</sup>	157 <sup>704</sup>	162 <sup>0.0129</sup>	147 <sup>0.0064</sup>	145 <sup>0.0051</sup>	144 <sup>0.0040</sup>	137 <sup>0.0031</sup>	150 <sup>1.066</sup>
87	INCODE-004		12 <sup>2048</sup>	10 <sup>508</sup>	87 <sup>0.0035</sup>	91 <sup>0.0024</sup>	93 <sup>0.0021</sup>	92 <sup>0.0020</sup>	97 <sup>0.0019</sup>	89 <sup>1.023</sup>
88	INCODE-005		16 <sup>2048</sup>	102 <sup>500</sup>	32 <sup>0.0017</sup>	32 <sup>0.0014</sup>	39 <sup>0.0014</sup>	38 <sup>0.0013</sup>	40 <sup>0.0013</sup>	34 <sup>1.013</sup>
89	INNOVATRICS-002		52 <sup>530</sup>	40 <sup>255</sup>	199 <sup>0.0451</sup>	20 <sup>0.0342</sup>	203 <sup>0.0322</sup>	205 <sup>0.0308</sup>	207 <sup>0.0297</sup>	202 <sup>1.321</sup>
90	INNOVATRICS-003		51 <sup>530</sup>	39 <sup>255</sup>	186 <sup>0.0263</sup>	178 <sup>0.0126</sup>	174 <sup>0.0095</sup>	169 <sup>0.0074</sup>	160 <sup>0.0053</sup>	181 <sup>1.129</sup>
91	INNOVATRICS-004		81 <sup>1076</sup>	7 <sup>406</sup>	161 <sup>0.0123</sup>	148 <sup>0.0063</sup>	145 <sup>0.0050</sup>	145 <sup>0.0040</sup>	140 <sup>0.0032</sup>	149 <sup>1.064</sup>
92	INNOVATRICS-005		55 <sup>538</sup>	202 <sup>842</sup>	66 <sup>0.0024</sup>	61 <sup>0.0018</sup>	64 <sup>0.0017</sup>	67 <sup>0.0016</sup>	66 <sup>0.0014</sup>	61 <sup>1.017</sup>
93	INNOVATRICS-007		53 <sup>538</sup>	18 <sup>785</sup>	34 <sup>0.0017</sup>	38 <sup>0.0014</sup>	34 <sup>0.0013</sup>	33 <sup>0.0013</sup>	38 <sup>0.0012</sup>	36 <sup>1.013</sup>
94	INTSYSMSU-000		166 <sup>2048</sup>	142 <sup>675</sup>	218 <sup>0.1457</sup>	229 <sup>0.1320</sup>	223 <sup>0.1272</sup>	225 <sup>0.1225</sup>	220 <sup>0.1163</sup>	220 <sup>2.203</sup>
95	IREX-000		20 <sup>3080</sup>	239 <sup>2379</sup>	98 <sup>0.0044</sup>	124 <sup>0.0043</sup>	137 <sup>0.0043</sup>	142 <sup>0.0043</sup>	133 <sup>0.0043</sup>	122 <sup>1.039</sup>
96	ISYSTEMS-002		11 <sup>2048</sup>	57 <sup>316</sup>	120 <sup>0.0064</sup>	124 <sup>0.0043</sup>	130 <sup>0.0039</sup>	139 <sup>0.0037</sup>	145 <sup>0.0034</sup>	125 <sup>1.041</sup>
97	ISYSTEMS-003		134 <sup>2048</sup>	207 <sup>856</sup>	108 <sup>0.0052</sup>	120 <sup>0.0039</sup>	126 <sup>0.0036</sup>	134 <sup>0.0034</sup>	141 <sup>0.0033</sup>	116 <sup>1.037</sup>
98	KAKAO-000		184 <sup>2052</sup>	200 <sup>840</sup>	200 <sup>0.0015</sup>	19 <sup>0.0011</sup>	17 <sup>0.0011</sup>	14 <sup>0.0010</sup>	15 <sup>0.0010</sup>	16 <sup>1.010</sup>
99	KEDACOM-001		25 <sup>292</sup>	110 <sup>537</sup>	129 <sup>0.0077</sup>	153 <sup>0.0074</sup>	159 <sup>0.0073</sup>	166 <sup>0.0072</sup>	174 <sup>0.0072</sup>	151 <sup>1.067</sup>
100	KNERON-000		10 <sup>2048</sup>	10 <sup>530</sup>	115 <sup>0.0059</sup>	141 <sup>0.0059</sup>	149 <sup>0.0059</sup>	159 <sup>0.0059</sup>	166 <sup>0.0059</sup>	137 <sup>1.053</sup>
101	KNERON-001		164 <sup>2048</sup>	96 <sup>468</sup>	189 <sup>0.0295</sup>	197 <sup>0.0295</sup>	202 <sup>0.0295</sup>	204 <sup>0.0295</sup>	205 <sup>0.0295</sup>	197 <sup>1.266</sup>
102	LINE-000		13 <sup>2048</sup>	98 <sup>482</sup>	540 <sup>0.0222</sup>	47 <sup>0.0015</sup>	42 <sup>0.0014</sup>	31 <sup>0.0013</sup>	29 <sup>0.0012</sup>	47 <sup>1.015</sup>
103	LOOKMAN-003		26 <sup>292</sup>	62 <sup>342</sup>	138 <sup>0.0088</sup>	157 <sup>0.0078</sup>	165 <sup>0.0076</sup>	171 <sup>0.0075</sup>	177 <sup>0.0074</sup>	154 <sup>1.071</sup>
104	LOOKMAN-004		56 <sup>548</sup>	58 <sup>325</sup>	140 <sup>0.0091</sup>	158 <sup>0.0079</sup>	164 <sup>0.0076</sup>	170 <sup>0.0075</sup>	170 <sup>0.0073</sup>	155 <sup>1.072</sup>
105	LOOKMAN-005		37 <sup>548</sup>	108 <sup>514</sup>	132 <sup>0.0080</sup>	158 <sup>0.0075</sup>	162 <sup>0.0074</sup>	168 <sup>0.0073</sup>	175 <sup>0.0072</sup>	152 <sup>1.068</sup>
106	MEGVII-001		21 <sup>4096</sup>	13 <sup>652</sup>	158 <sup>0.0118</sup>	169 <sup>0.0093</sup>	170 <sup>0.0088</sup>	177 <sup>0.0084</sup>	182 <sup>0.0080</sup>	164 <sup>1.086</sup>
107	MEGVII-002		220 <sup>4096</sup>	138 <sup>656</sup>	159 <sup>0.0118</sup>	169 <sup>0.0093</sup>	170 <sup>0.0088</sup>	177 <sup>0.0084</sup>	182 <sup>0.0080</sup>	164 <sup>1.087</sup>
108	MICROFOCUS-003		21 <sup>256</sup>	48 <sup>269</sup>	235 <sup>0.5942</sup>	239 <sup>0.4692</sup>	234 <sup>0.4204</sup>	234 <sup>0.3724</sup>	231 <sup>0.3095</sup>	234 <sup>5.361</sup>
109	MICROFOCUS-004		17 <sup>256</sup>	46 <sup>270</sup>	233 <sup>0.5763</sup>	233 <sup>0.4519</sup>	233 <sup>0.4026</sup>	233 <sup>0.3560</sup>	233 <sup>0.2957</sup>	233 <sup>5.199</sup>
110	MICROFOCUS-005		20 <sup>256</sup>	44 <sup>266</sup>	229 <sup>0.4242</sup>	229 <sup>0.3028</sup>	229 <sup>0.2606</sup>	229 <sup>0.2209</sup>	229 <sup>0.1724</sup>	239 <sup>3.861</sup>
111	MICROFOCUS-006		16 <sup>256</sup>	43 <sup>265</sup>	230 <sup>0.4268</sup>	230 <sup>0.3049</sup>	230 <sup>0.2623</sup>	231 <sup>0.2233</sup>	231 <sup>0.1746</sup>	230 <sup>3.880</sup>
112	MICROFOCUS-003		63 <sup>1024</sup>	7 <sup>404</sup>	29 <sup>0.0016</sup>	10 <sup>0.0010</sup>	6 <sup>0.0009</sup>	3 <sup>0.0008</sup>	0 <sup>0.0006</sup>	11 <sup>1.009</sup>
113	MICROSOFT-004		13 <sup>2048</sup>	18 <sup>773</sup>	222 <sup>0.0015</sup>	19 <sup>0.0009</sup>	17 <sup>0.0008</sup>	10 <sup>0.0007</sup>	10 <sup>0.0006</sup>	9 <sup>1.009</sup>
114	MICROSOFT-005		66 <sup>1024</sup>	140 <sup>673</sup>	42 <sup>0.0019</sup>	9 <sup>0.0100</sup>	5 <sup>0.0008</sup>	2 <sup>0.0008</sup>	3 <sup>0.0006</sup>	14 <sup>1.010</sup>
115	MICROSOFT-006		65 <sup>1024</sup>	15 <sup>695</sup>	46 <sup>0.0020</sup>	17 <sup>0.0011</sup>	12 <sup>0.0010</sup>	4 <sup>0.0008</sup>	4 <sup>0.0007</sup>	18 <sup>1.011</sup>
116	NEC-000		20 <sup>2592</sup>	8 <sup>82</sup>	171 <sup>0.0170</sup>	163 <sup>0.0086</sup>	155 <sup>0.0066</sup>	152 <sup>0.0052</sup>	149 <sup>0.0038</sup>	165 <sup>1.087</sup>
117	NEC-001		20 <sup>2592</sup>	9 <sup>88</sup>	180 <sup>0.0209</sup>	184 <sup>0.0141</sup>	185 <sup>0.0128</sup>	188 <sup>0.0119</sup>	180 <sup>0.0113</sup>	183 <sup>1.135</sup>
118	NEC-002		99 <sup>1616</sup>	134 <sup>653</sup>	5 <sup>0.0010</sup>	3 <sup>0.0009</sup>	4 <sup>0.0008</sup>	5 <sup>0.0008</sup>	5 <sup>0.0008</sup>	3 <sup>1.008</sup>
119	NEC-003		10 <sup>1712</sup>	14 <sup>690</sup>	130 <sup>0.0014</sup>	28 <sup>0.0012</sup>	24 <sup>0.0012</sup>	30 <sup>0.0012</sup>	31 <sup>0.0012</sup>	20 <sup>1.011</sup>
120	NEC-004		82 <sup>1104</sup>	236 <sup>667</sup>	17 <sup>0.0014</sup>	30 <sup>0.0013</sup>	37 <sup>0.0013</sup>	40 <sup>0.0013</sup>	45 <sup>0.0013</sup>	30 <sup>1.012</sup>
121	NEUROTECHNOLOGY-003		118 <sup>2048</sup>	113 <sup>547</sup>	181 <sup>0.0225</sup>	172 <sup>0.0126</sup>	177 <sup>0.0100</sup>	175 <sup>0.0078</sup>	165 <sup>0.0057</sup>	180 <sup>1.125</sup>
122	NEUROTECHNOLOGY-004		12 <sup>2048</sup>	115 <sup>543</sup>	110 <sup>0.0056</sup>	111 <sup>0.0036</sup>	118 <sup>0.0032</sup>	120 <sup>0.0029</sup>	119 <sup>0.0025</sup>	113 <sup>1.035</sup>
123	NEUROTECHNOLOGY-005		15 <sup>256</sup>	80 <sup>412</sup>	96 <sup>0.0043</sup>	10 <sup>0.0029</sup>	109 <sup>0.0027</sup>	105 <sup>0.0024</sup>	115 <sup>0.0023</sup>	105 <sup>1.028</sup>
124	NEUROTECHNOLOGY-006		19 <sup>256</sup>	17 <sup>746</sup>	175 <sup>0.0180</sup>	159 <sup>0.0079</sup>	148 <sup>0.0059</sup>	148 <sup>0.0046</sup>	144 <sup>0.0033</sup>	161 <sup>1.083</sup>
125	NEUROTECHNOLOGY-007		14 <sup>256</sup>	17 <sup>169</sup>	91 <sup>0.0039</sup>	100 <sup>0.0027</sup>	105 <sup>0.0025</sup>	107 <sup>0.0023</sup>	110 <sup>0.0022</sup>	98 <sup>1.026</sup>
126	NEUROTECHNOLOGY-008		45 <sup>514</sup>	18 <sup>804</sup>	53 <sup>0.0022</sup>	48 <sup>0.0015</sup>	48 <sup>0.0014</sup>	48 <sup>0.0014</sup>	50 <sup>0.0013</sup>	46 <sup>1.015</sup>
127	NEUROTECHNOLOGY-009		43 <sup>513</sup>	145 <sup>868</sup>	18 <sup>0.0014</sup>	20 <sup>0.0012</sup>	21 <sup>0.0012</sup>	22 <sup>0.0011</sup>	24 <sup>0.0011</sup>	19 <sup>1.011</sup>
128	NEWLAND-002		15 <sup>2048</sup>	21 <sup>868</sup>	20 <sup>0.0786</sup>	20 <sup>0.0480</sup>	20 <sup>0.0397</sup>	20 <sup>0.0332</sup>	20 <sup>0.0263</sup>	210 <sup>1.468</sup>
129	NOBLIS-001		163 <sup>2048</sup>	33 <sup>211</sup>	225 <sup>0.2492</sup>	225 <sup>0.1772</sup>	225 <sup>0.1542</sup>	225 <sup>0.1339</sup>	225 <sup>0.1112</sup>	225 <sup>2.679</sup>
130	NOBLIS-002		236 <sup>6144</sup>	10 <sup>535</sup>	221 <sup>0.1794</sup>	216 <sup>0.1108</sup>	218 <sup>0.0903</sup>	217 <sup>0.0722</sup>	210 <sup>0.0535</sup>	218 <sup>2.077</sup>
131	NTECHLAB-003		210 <sup>3484</sup>	196 <sup>831</sup>	116 <sup>0.0062</sup>	107 <sup>0.0029</sup>	102 <sup>0.0023</sup>	99 <sup>0.0019</sup>	81 <sup>0.0016</sup>	110 <sup>1.030</sup>
132	NTECHLAB-004		214 <sup>3484</sup>	22 <sup>929</sup>	105 <sup>0.0048</sup>	89 <sup>0.0023</sup>	77 <sup>0.0019</sup>	71 <sup>0.0016</sup>	52 <sup>0.0013</sup>	94 <sup>1.024</sup>
133	NTECHLAB-005		104 <sup>1940</sup>	169 <sup>717</sup>	103 <sup>0.0047</sup>	88 <sup>0.0022</sup>	68 <sup>0.0017</sup>	41 <sup>0.0013</sup>	22 <sup>0.0011</sup>	90 <sup>1.023</sup>
134	NTECHLAB-006		105 <sup>1940</sup>	20 <sup>841</sup>	95 <sup>0.0041</sup>	69 <sup>0.0019</sup>	53 <sup>0.0015</sup>	25 <sup>0.0012</sup>	12 <sup>0.0009</sup>	78 <sup>1.019</sup>
135	NTECHLAB-007		20 <sup>3348</sup>	19 <sup>834</sup>	69 <sup>0.0027</sup>	50 <sup>0.0017</sup>	46 <sup>0.0014</sup>	45 <sup>0.001</sup>		

MISSES OUTSIDE RANK R FNIR(N, T=0, R)		RESOURCE USAGE TEMPLATE		ENROL MOST RECENT, N = 1.6M FRVT 2018 MUGSHOTS					
#	ALGORITHM	BYTES	MSEC	R=1	R=5	R=10	R=20	R=50	WORK-10
145	PARAVISION-007	<sup>22</sup> 4096	<sup>16</sup> 706	<sup>9</sup> 0.0012	<sup>15</sup> 0.0011	<sup>16</sup> 0.0010	<sup>17</sup> 0.0010	<sup>15</sup> 0.0010	1.010
146	PIXELALL-002	<sup>20</sup> 2560	<sup>27</sup> 198	<sup>106</sup> 0.0045	<sup>106</sup> 0.0029	<sup>106</sup> 0.0025	<sup>108</sup> 0.0022	<sup>103</sup> 0.0019	<sup>106</sup> 1.028
147	PIXELALL-003	<sup>202</sup> 2560	<sup>171</sup> 719	<sup>52</sup> 0.0021	<sup>52</sup> 0.0016	<sup>55</sup> 0.0015	<sup>55</sup> 0.0014	<sup>63</sup> 0.0014	<sup>53</sup> 1.015
148	PIXELALL-004	<sup>20</sup> 2560	<sup>91</sup> 453	<sup>50</sup> 0.0020	<sup>46</sup> 0.0015	<sup>49</sup> 0.0015	<sup>52</sup> 0.0014	<sup>53</sup> 0.0013	<sup>45</sup> 1.014
149	PIXELALL-005	<sup>204</sup> 2560	<sup>204</sup> 845	<sup>43</sup> 0.0019	<sup>56</sup> 0.0017	<sup>58</sup> 0.0016	<sup>70</sup> 0.0016	<sup>80</sup> 0.0016	<sup>52</sup> 1.015
150	PTAKURATSATU-000	<sup>54</sup> 538	<sup>22</sup> 910	<sup>78</sup> 0.0030	<sup>81</sup> 0.0021	<sup>82</sup> 0.0019	<sup>78</sup> 0.0018	<sup>83</sup> 0.0016	<sup>80</sup> 1.020
151	QNAP-000	<sup>158</sup> 2048	<sup>92</sup> 457	<sup>130</sup> 0.0078	<sup>126</sup> 0.0044	<sup>127</sup> 0.0037	<sup>128</sup> 0.0033	<sup>130</sup> 0.0028	<sup>127</sup> 1.043
152	QUANTASOFT-001	<sup>13</sup> 2048	<sup>74</sup> 396	<sup>222</sup> 0.2177	<sup>224</sup> 0.1643	<sup>224</sup> 0.1468	<sup>224</sup> 0.1312	<sup>224</sup> 0.1116	<sup>224</sup> 2.539
153	RANKONE-002	<sup>8</sup> 133	<sup>12</sup> 113	<sup>178</sup> 0.0194	<sup>174</sup> 0.0112	<sup>173</sup> 0.0093	<sup>172</sup> 0.0077	<sup>168</sup> 0.0060	<sup>174</sup> 1.111
154	RANKONE-003	<sup>10</sup> 133	<sup>13</sup> 114	<sup>177</sup> 0.0194	<sup>177</sup> 0.0112	<sup>172</sup> 0.0093	<sup>173</sup> 0.0077	<sup>169</sup> 0.0060	<sup>173</sup> 1.111
155	RANKONE-004	<sup>1</sup> 85	<sup>4</sup> 36	<sup>198</sup> 0.0415	<sup>195</sup> 0.0226	<sup>195</sup> 0.0177	<sup>191</sup> 0.0141	<sup>187</sup> 0.0102	<sup>195</sup> 1.225
156	RANKONE-005	<sup>9</sup> 133	<sup>10</sup> 94	<sup>144</sup> 0.0094	<sup>139</sup> 0.0054	<sup>139</sup> 0.0046	<sup>141</sup> 0.0039	<sup>138</sup> 0.0032	<sup>139</sup> 1.054
157	RANKONE-006	<sup>12</sup> 165	<sup>41</sup> 261	<sup>107</sup> 0.0050	<sup>110</sup> 0.0030	<sup>110</sup> 0.0027	<sup>108</sup> 0.0024	<sup>106</sup> 0.0021	<sup>109</sup> 1.030
158	RANKONE-007	<sup>11</sup> 165	<sup>48</sup> 278	<sup>83</sup> 0.0034	<sup>89</sup> 0.0023	<sup>90</sup> 0.0021	<sup>86</sup> 0.0018	<sup>84</sup> 0.0017	<sup>86</sup> 1.022
159	RANKONE-009	<sup>22</sup> 260	<sup>25</sup> 191	<sup>61</sup> 0.0024	<sup>59</sup> 0.0016	<sup>57</sup> 0.0015	<sup>60</sup> 0.0015	<sup>60</sup> 0.0014	<sup>55</sup> 1.015
160	RANKONE-010	<sup>24</sup> 261	<sup>28</sup> 200	<sup>55</sup> 0.0022	<sup>59</sup> 0.0018	<sup>61</sup> 0.0016	<sup>66</sup> 0.0015	<sup>68</sup> 0.0015	<sup>58</sup> 1.016
161	RANKONE-011	<sup>23</sup> 261	<sup>119</sup> 567	<sup>23</sup> 0.0015	<sup>24</sup> 0.0012	<sup>22</sup> 0.0012	<sup>24</sup> 0.0012	<sup>21</sup> 0.0012	<sup>21</sup> 1.011
162	REALNETWORKS-000	<sup>225</sup> 4100	<sup>37</sup> 244	<sup>196</sup> 0.0402	<sup>193</sup> 0.0195	<sup>189</sup> 0.0149	<sup>186</sup> 0.0111	<sup>181</sup> 0.0077	<sup>193</sup> 1.201
163	REALNETWORKS-001	<sup>22</sup> 4104	<sup>36</sup> 243	<sup>197</sup> 0.0402	<sup>194</sup> 0.0195	<sup>190</sup> 0.0149	<sup>188</sup> 0.0111	<sup>184</sup> 0.0077	<sup>194</sup> 1.201
164	REALNETWORKS-002	<sup>228</sup> 4104	<sup>38</sup> 245	<sup>193</sup> 0.0393	<sup>192</sup> 0.0189	<sup>188</sup> 0.0142	<sup>184</sup> 0.0108	<sup>179</sup> 0.0076	<sup>192</sup> 1.195
165	REALNETWORKS-003	<sup>108</sup> 1848	<sup>20</sup> 178	<sup>184</sup> 0.0242	<sup>174</sup> 0.0117	<sup>171</sup> 0.0090	<sup>168</sup> 0.0070	<sup>162</sup> 0.0054	<sup>178</sup> 1.120
166	REALNETWORKS-004	<sup>102</sup> 1848	<sup>21</sup> 185	<sup>182</sup> 0.0236	<sup>175</sup> 0.0112	<sup>169</sup> 0.0087	<sup>163</sup> 0.0068	<sup>158</sup> 0.0050	<sup>175</sup> 1.116
167	REALNETWORKS-005	<sup>186</sup> 2056	<sup>60</sup> 337	<sup>52</sup> 0.0023	<sup>48</sup> 0.0016	<sup>43</sup> 0.0014	<sup>46</sup> 0.0013	<sup>50</sup> 0.0012	<sup>50</sup> 1.015
168	REMARKAI-000	<sup>12</sup> 2048	<sup>151</sup> 691	<sup>85</sup> 0.0034	<sup>89</sup> 0.0021	<sup>76</sup> 0.0019	<sup>73</sup> 0.0017	<sup>77</sup> 0.0015	<sup>81</sup> 1.020
169	REMARKAI-000	<sup>130</sup> 2048	<sup>123</sup> 615	<sup>137</sup> 0.0086	<sup>128</sup> 0.0044	<sup>121</sup> 0.0036	<sup>123</sup> 0.0031	<sup>120</sup> 0.0025	<sup>130</sup> 1.045
170	REMARKAI-002	<sup>11</sup> 2048	<sup>88</sup> 434	<sup>135</sup> 0.0081	<sup>124</sup> 0.0040	<sup>114</sup> 0.0031	<sup>111</sup> 0.0026	<sup>105</sup> 0.0021	<sup>124</sup> 1.041
171	RENDIP-000	<sup>161</sup> 2048	<sup>218</sup> 894	<sup>27</sup> 0.0015	<sup>26</sup> 0.0013	<sup>25</sup> 0.0012	<sup>28</sup> 0.0012	<sup>33</sup> 0.0012	<sup>27</sup> 1.012
172	S1-000	<sup>22</sup> 4096	<sup>210</sup> 865	<sup>63</sup> 0.0024	<sup>59</sup> 0.0018	<sup>62</sup> 0.0017	<sup>68</sup> 0.0016	<sup>74</sup> 0.0015	<sup>60</sup> 1.017
173	SCANOVATE-000	<sup>113</sup> 2048	<sup>164</sup> 712	<sup>106</sup> 0.0050	<sup>99</sup> 0.0026	<sup>92</sup> 0.0022	<sup>83</sup> 0.0018	<sup>78</sup> 0.0015	<sup>101</sup> 1.026
174	SCANOVATE-001	<sup>14</sup> 2048	<sup>14</sup> 675	<sup>105</sup> 0.0053	<sup>107</sup> 0.0027	<sup>100</sup> 0.0022	<sup>87</sup> 0.0018	<sup>76</sup> 0.0015	<sup>104</sup> 1.028
175	SENSETIME-000	<sup>230</sup> 4104	<sup>67</sup> 715	<sup>59</sup> 0.0023	<sup>26</sup> 0.0020	<sup>80</sup> 0.0019	<sup>83</sup> 0.0018	<sup>93</sup> 0.0017	<sup>71</sup> 1.018
176	SENSETIME-001	<sup>228</sup> 4104	<sup>13</sup> 656	<sup>60</sup> 0.0023	<sup>27</sup> 0.0020	<sup>78</sup> 0.0019	<sup>77</sup> 0.0017	<sup>82</sup> 0.0016	<sup>69</sup> 1.018
177	SENSETIME-002	<sup>187</sup> 2056	<sup>131</sup> 650	<sup>165</sup> 0.0137	<sup>182</sup> 0.0136	<sup>187</sup> 0.0136	<sup>198</sup> 0.0136	<sup>195</sup> 0.0136	<sup>179</sup> 1.122
178	SENSETIME-003	<sup>18</sup> 2056	<sup>23</sup> 940	<sup>40</sup> 0.0010	<sup>10</sup> 0.0010	<sup>11</sup> 0.0010	<sup>12</sup> 0.0009	<sup>13</sup> 0.0009	<sup>6</sup> 1.009
179	SENSETIME-004	<sup>71</sup> 1032	<sup>163</sup> 710	<sup>30</sup> 0.0010	<sup>4</sup> 0.0009	<sup>7</sup> 0.0009	<sup>8</sup> 0.0009	<sup>8</sup> 0.0009	<sup>4</sup> 1.008
180	SENSETIME-005	<sup>71</sup> 1032	<sup>238</sup> 1007	<sup>20</sup> 0.0009	<sup>2</sup> 0.0008	<sup>2</sup> 0.0008	<sup>6</sup> 0.0008	<sup>6</sup> 0.0008	<sup>2</sup> 1.008
181	SENSETIME-006	<sup>72</sup> 1032	<sup>23</sup> 956	<sup>10</sup> 0.0009	<sup>1</sup> 0.0008	<sup>3</sup> 0.0008	<sup>7</sup> 0.0008	<sup>7</sup> 0.0008	<sup>2</sup> 1.008
182	SHAMAN-003	<sup>122</sup> 2048	<sup>158</sup> 704	<sup>213</sup> 0.1243	<sup>216</sup> 0.0823	<sup>216</sup> 0.0708	<sup>213</sup> 0.0616	<sup>215</sup> 0.0518	<sup>216</sup> 1.789
183	SHAMAN-004	<sup>111</sup> 2048	<sup>130</sup> 642	<sup>224</sup> 0.2221	<sup>222</sup> 0.1473	<sup>221</sup> 0.1241	<sup>222</sup> 0.1049	<sup>220</sup> 0.0825	<sup>223</sup> 2.411
184	SHAMAN-006	<sup>138</sup> 2048	<sup>159</sup> 706	<sup>195</sup> 0.0398	<sup>202</sup> 0.0344	<sup>205</sup> 0.0332	<sup>207</sup> 0.0323	<sup>210</sup> 0.0315	<sup>201</sup> 1.316
185	SHAMAN-007	<sup>16</sup> 2048	<sup>16</sup> 709	<sup>194</sup> 0.0396	<sup>204</sup> 0.0342	<sup>204</sup> 0.0331	<sup>206</sup> 0.0322	<sup>207</sup> 0.0314	<sup>199</sup> 1.315
186	SIAT-001	<sup>178</sup> 2052	<sup>203</sup> 842	<sup>37</sup> 0.0018	<sup>37</sup> 0.0014	<sup>29</sup> 0.0013	<sup>26</sup> 0.0012	<sup>25</sup> 0.0011	<sup>37</sup> 1.013
187	SIAT-002	<sup>17</sup> 2052	<sup>22</sup> 906	<sup>38</sup> 0.0018	<sup>36</sup> 0.0014	<sup>36</sup> 0.0013	<sup>37</sup> 0.0013	<sup>40</sup> 0.0012	<sup>40</sup> 1.013
188	SMILART-004	<sup>31</sup> 512	<sup>16</sup> 167	<sup>236</sup> 0.9648	<sup>236</sup> 0.9641	<sup>236</sup> 0.9640	<sup>236</sup> 0.9639	<sup>236</sup> 0.9638	<sup>239</sup> 9.678
189	SMILART-005	<sup>143</sup> 2048	<sup>94</sup> 464						<sup>239</sup> 10.000
190	STAQU-000	<sup>216</sup> 4096	<sup>193</sup> 827	<sup>127</sup> 0.0071	<sup>144</sup> 0.0060	<sup>146</sup> 0.0057	<sup>154</sup> 0.0055	<sup>159</sup> 0.0053	<sup>141</sup> 1.056
191	SYNESIS-003	<sup>120</sup> 2048	<sup>31</sup> 215	<sup>169</sup> 0.0162	<sup>186</sup> 0.0160	<sup>191</sup> 0.0160	<sup>193</sup> 0.0160	<sup>200</sup> 0.0160	<sup>185</sup> 1.144
192	SYNESIS-003	<sup>21</sup> 4096	<sup>11</sup> 103	<sup>219</sup> 0.1700	<sup>219</sup> 0.1172	<sup>219</sup> 0.1047	<sup>220</sup> 0.0953	<sup>221</sup> 0.0869	<sup>219</sup> 2.120
193	SYNESIS-005	<sup>229</sup> 4104	<sup>181</sup> 772	<sup>136</sup> 0.0085	<sup>162</sup> 0.0085	<sup>167</sup> 0.0085	<sup>173</sup> 0.0085	<sup>185</sup> 0.0085	<sup>159</sup> 1.076
194	TECH5-001	<sup>91</sup> 1536	<sup>218</sup> 898	<sup>93</sup> 0.0040	<sup>92</sup> 0.0024	<sup>92</sup> 0.0021	<sup>88</sup> 0.0018	<sup>89</sup> 0.0017	<sup>93</sup> 1.024
195	TECH5-002	<sup>44</sup> 513	<sup>232</sup> 941	<sup>70</sup> 0.0027	<sup>40</sup> 0.0014	<sup>26</sup> 0.0012	<sup>21</sup> 0.0011	<sup>19</sup> 0.0010	<sup>44</sup> 1.014
196	TEVIAN-003	<sup>141</sup> 2048	<sup>58</sup> 300	<sup>166</sup> 0.0147	<sup>158</sup> 0.0074	<sup>147</sup> 0.0059	<sup>148</sup> 0.0047	<sup>148</sup> 0.0037	<sup>158</sup> 1.075
197	TEVIAN-004	<sup>149</sup> 2048	<sup>53</sup> 299	<sup>153</sup> 0.0113	<sup>140</sup> 0.0057	<sup>140</sup> 0.0047	<sup>137</sup> 0.0037	<sup>133</sup> 0.0030	<sup>142</sup> 1.058
198	TEVIAN-005	<sup>168</sup> 2048	<sup>84</sup> 416	<sup>128</sup> 0.0073	<sup>118</sup> 0.0038	<sup>113</sup> 0.0031	<sup>114</sup> 0.0027	<sup>110</sup> 0.0023	<sup>120</sup> 1.038
199	TEVIAN-006	<sup>73</sup> 1032	<sup>121</sup> 599	<sup>64</sup> 0.0024	<sup>62</sup> 0.0018	<sup>70</sup> 0.0018	<sup>75</sup> 0.0017	<sup>85</sup> 0.0017	<sup>62</sup> 1.017
200	TIGER-000	<sup>171</sup> 2052	<sup>84</sup> 428	<sup>204</sup> 0.0616	<sup>193</sup> 0.0310	<sup>198</sup> 0.0236	<sup>199</sup> 0.0178	<sup>192</sup> 0.0120	<sup>200</sup> 1.315
201	TIGER-002	<sup>188</sup> 2052	<sup>93</sup> 464	<sup>112</sup> 0.0056	<sup>108</sup> 0.0029	<sup>104</sup> 0.0024	<sup>99</sup> 0.0019	<sup>72</sup> 0.0015	<sup>107</sup> 1.030
202	TIGER-003	<sup>177</sup> 2052	<sup>95</sup> 464	<sup>111</sup> 0.0056	<sup>109</sup> 0.0029	<sup>103</sup> 0.0024	<sup>91</sup> 0.0019	<sup>73</sup> 0.0015	<sup>108</sup> 1.030
203	TONGYITRANS-000	<sup>19</sup> 2070	<sup>23</sup> 190	<sup>123</sup> 0.0069	<sup>117</sup> 0.0038	<sup>119</sup> 0.0032	<sup>119</sup> 0.0029	<sup>122</sup> 0.0026	<sup>118</sup> 1.038
204	TONGYITRANS-001	<sup>192</sup> 2070	<sup>22</sup> 189	<sup>124</sup> 0.0069	<sup>117</sup> 0.0038	<sup>117</sup> 0.0032	<sup>118</sup> 0.0029	<sup>122</sup> 0.0026	<sup>119</sup> 1.038
205	TOSHIBA-000	<sup>96</sup> 1548	<sup>22</sup> 930	<sup>99</sup> 0.0045	<sup>98</sup> 0.0026	<sup>98</sup> 0.0022	<sup>99</sup> 0.0020	<sup>99</sup> 0.0018	<sup>99</sup> 1.026
206	TOSHIBA-001	<sup>190</sup> 2060	<sup>229</sup> 931	<sup>104</sup> 0.0048	<sup>102</sup> 0.0027	<sup>101</sup> 0.0023	<sup>101</sup> 0.0020	<sup>95</sup> 0.0018	<sup>103</sup> 1.027
207	TRUEFACE-000	<sup>108</sup> 2000	<sup>63</sup> 365	<sup>82</sup> 0.0033	<sup>103</sup> 0.0028	<sup>111</sup> 0.0028	<sup>112</sup> 0.0026	<sup>120</sup> 0.0026	<sup>100</sup> 1.026
208	VD-000	<sup>70</sup> 1028	<sup>59</sup> 337	<sup>232</sup> 0.4737	<sup>231</sup> 0.3204	<sup>231</sup> 0.2695	<sup>230</sup> 0.2215	<sup>229</sup> 0.1678	<sup>231</sup> 4.058
209	VD-001	<sup>172</sup> 2052	<sup>15</sup> 695	<sup>188</sup> 0.0276	<sup>191</sup> 0.0181	<sup>193</sup> 0.0162	<sup>192</sup> 0.0146	<sup>194</sup> 0.0130	<sup>191</sup> 1.174
210	VD-002	<sup>1</sup>							

MISSES OUTSIDE RANK R FNIR(N, T=0, R)		RESOURCE USAGE		ENROL MOST RECENT, N = 1.6M FRVT 2018 MUGSHOTS						
#	ALGORITHM	BYTES	MSEC	R=1	R=5	R=10	R=20	R=50	WORK-10	
217	VIGILANTSOLUTIONS-007	<sup>92</sup> 1544	<sup>124</sup> 618	<sup>84</sup> 0.0034	<sup>72</sup> 0.0020	<sup>67</sup> 0.0017	<sup>63</sup> 0.0015	<sup>49</sup> 0.0013	<sup>77</sup> 1.019	
218	VIGILANTSOLUTIONS-008	<sup>95</sup> 1544	<sup>77</sup> 405	<sup>77</sup> 0.0029	<sup>66</sup> 0.0018	<sup>59</sup> 0.0016	<sup>56</sup> 0.0015	<sup>41</sup> 0.0013	<sup>67</sup> 1.018	
219	VISIONLABS-004	<sup>18</sup> 256	<sup>56</sup> 315	<sup>71</sup> 0.0027	<sup>60</sup> 0.0018	<sup>60</sup> 0.0016	<sup>61</sup> 0.0015	<sup>59</sup> 0.0014	<sup>64</sup> 1.017	
220	VISIONLABS-005	<sup>34</sup> 512	<sup>34</sup> 300	<sup>62</sup> 0.0024	<sup>57</sup> 0.0017	<sup>54</sup> 0.0015	<sup>45</sup> 0.0014	<sup>40</sup> 0.0013	<sup>56</sup> 1.016	
221	VISIONLABS-006	<sup>41</sup> 512	<sup>50</sup> 292	<sup>41</sup> 0.0018	<sup>42</sup> 0.0015	<sup>40</sup> 0.0014	<sup>42</sup> 0.0013	<sup>42</sup> 0.0013	<sup>41</sup> 1.014	
222	VISIONLABS-007	<sup>34</sup> 512	<sup>51</sup> 293	<sup>36</sup> 0.0018	<sup>39</sup> 0.0014	<sup>32</sup> 0.0013	<sup>32</sup> 0.0013	<sup>37</sup> 0.0012	<sup>39</sup> 1.013	
223	VISIONLABS-008	<sup>40</sup> 512	<sup>47</sup> 277	<sup>48</sup> 0.0020	<sup>68</sup> 0.0018	<sup>71</sup> 0.0018	<sup>79</sup> 0.0018	<sup>92</sup> 0.0017	<sup>59</sup> 1.017	
224	VISIONLABS-009	<sup>42</sup> 512	<sup>101</sup> 494	<sup>8</sup> 0.0011	<sup>13</sup> 0.0011	<sup>14</sup> 0.0010	<sup>16</sup> 0.0010	<sup>16</sup> 0.0010	<sup>12</sup> 1.010	
225	VISIONLABS-010	<sup>34</sup> 512	<sup>174</sup> 732	<sup>15</sup> 0.0014	<sup>29</sup> 0.0013	<sup>30</sup> 0.0013	<sup>34</sup> 0.0013	<sup>39</sup> 0.0013	<sup>26</sup> 1.012	
226	VOCORD-003	<sup>60</sup> 896	<sup>166</sup> 714	<sup>117</sup> 0.0062	<sup>112</sup> 0.0035	<sup>112</sup> 0.0030	<sup>112</sup> 0.0026	<sup>116</sup> 0.0023	<sup>112</sup> 1.035	
227	VOCORD-004	<sup>6</sup> 896	<sup>11</sup> 538	<sup>131</sup> 0.0079	<sup>13</sup> 0.0049	<sup>136</sup> 0.0043	<sup>146</sup> 0.0038	<sup>143</sup> 0.0034	<sup>132</sup> 1.048	
228	VOCORD-005	<sup>58</sup> 768	<sup>191</sup> 822	<sup>126</sup> 0.0070	<sup>131</sup> 0.0046	<sup>133</sup> 0.0041	<sup>139</sup> 0.0038	<sup>146</sup> 0.0035	<sup>128</sup> 1.044	
229	VOCORD-006	<sup>239</sup> 10240	<sup>194</sup> 825	<sup>239</sup> 1.0000	<sup>238</sup> 1.0000	<sup>238</sup> 1.0000	<sup>238</sup> 1.0000	<sup>238</sup> 1.0000	<sup>238</sup> 10.000	
230	VTS-000	<sup>116</sup> 2048	<sup>100</sup> 492	<sup>234</sup> 0.5937	<sup>238</sup> 0.5936	<sup>238</sup> 0.5936	<sup>238</sup> 0.5936	<sup>238</sup> 0.5936	<sup>238</sup> 6.343	
231	VTS-001	<sup>137</sup> 2048	<sup>21</sup> 891	<sup>25</sup> 0.0015	<sup>18</sup> 0.0012	<sup>18</sup> 0.0011	<sup>18</sup> 0.0011	<sup>17</sup> 0.0010	<sup>17</sup> 1.011	
232	XFORWARDAI-000	<sup>146</sup> 2048	<sup>179</sup> 768	<sup>56</sup> 0.0023	<sup>77</sup> 0.0020	<sup>84</sup> 0.0020	<sup>96</sup> 0.0019	<sup>102</sup> 0.0019	<sup>72</sup> 1.018	
233	XFORWARDAI-001	<sup>107</sup> 2048	<sup>144</sup> 681	<sup>51</sup> 0.0020	<sup>71</sup> 0.0019	<sup>81</sup> 0.0019	<sup>93</sup> 0.0019	<sup>101</sup> 0.0019	<sup>65</sup> 1.018	
234	XFORWARDAI-002	<sup>221</sup> 4096	<sup>230</sup> 635	<sup>45</sup> 0.0020	<sup>68</sup> 0.0019	<sup>79</sup> 0.0019	<sup>92</sup> 0.0019	<sup>99</sup> 0.0019	<sup>63</sup> 1.017	
235	YISHENG-001	<sup>212</sup> 3704	<sup>72</sup> 387	<sup>187</sup> 0.0265	<sup>181</sup> 0.0130	<sup>178</sup> 0.0102	<sup>176</sup> 0.0080	<sup>167</sup> 0.0059	<sup>182</sup> 1.134	
236	YITU-002	<sup>231</sup> 4138	<sup>212</sup> 870	<sup>40</sup> 0.0018	<sup>21</sup> 0.0012	<sup>19</sup> 0.0011	<sup>19</sup> 0.0011	<sup>21</sup> 0.0010	<sup>25</sup> 1.012	
237	YITU-003	<sup>232</sup> 4138	<sup>213</sup> 871	<sup>76</sup> 0.0029	<sup>87</sup> 0.0023	<sup>95</sup> 0.0022	<sup>104</sup> 0.0021	<sup>109</sup> 0.0021	<sup>84</sup> 1.021	
238	YITU-004	<sup>193</sup> 2070	<sup>22</sup> 910	<sup>111</sup> 0.0013	<sup>3</sup> 0.0009	<sup>8</sup> 0.0009	<sup>9</sup> 0.0009	<sup>7</sup> 0.0009	<sup>8</sup> 1.009	
239	YITU-005	<sup>194</sup> 2070	<sup>209</sup> 861	<sup>58</sup> 0.0023	<sup>79</sup> 0.0021	<sup>86</sup> 0.0020	<sup>99</sup> 0.0020	<sup>104</sup> 0.0020	<sup>74</sup> 1.019	

**Table 24: Rank-based accuracy for the FRVT 2018 mugshot sets.** In columns 3 and 4 are template size and template generation duration. Thereafter values are rank-based FNIR with  $T = 0$  and FPIR = 1. This is appropriate to investigational uses but not those with higher volumes where candidates from all searches would need review. The next column is a workload statistic, a small value shows an algorithm front-loads mates into the first 10 candidates. Throughout, blue superscripts indicate the rank of the algorithm for that column, and the best value is highlighted in yellow.

MISSES BELOW THRESHOLD, T		ENROL RECENT MUGSHOT, N = 1.6M												ENROL APPLICATION PORTRAIT, N = 1.6M																	
#	ALGORITHM	ENROL: MUGSHOT			ENROL: MUGSHOT			ENROL: MUGSHOT			ENROL: VISA			ENROL: BORDER			ENROL: BORDER 10+YR			ENROL: KIOSK											
		FPIR=0.0003	FPIR=0.001	FPIR=0.01	FPIR=0.0003	FPIR=0.001	FPIR=0.01	FPIR=0.0003	FPIR=0.001	FPIR=0.01	FPIR=0.0001	FPIR=0.001	FPIR=0.01	FPIR=0.0001	FPIR=0.001	FPIR=0.01	FPIR=0.0001	FPIR=0.001	FPIR=0.01	FPIR=0.0001	FPIR=0.001	FPIR=0.01									
1	3DIVI-003	194	0.482	207	0.400	211	0.282	196	0.685	207	0.626	209	0.497				141	0.605	141	0.445				116	0.821	128	0.717				
2	3DIVI-004	167	0.256	181	0.169	185	0.093	169	0.400	18	0.343	191	0.237				123	0.277	122	0.172				96	0.607	118	0.485				
3	3DIVI-005	166	0.255	178	0.166	184	0.093	168	0.395	185	0.339	190	0.234	109	0.998	110	0.996	117	0.990	146	0.864	148	0.846		95	0.597	109	0.484			
4	3DIVI-006	165	0.253	180	0.168	187	0.096	172	0.403	185	0.342	192	0.238				124	0.283	122	0.174				99	0.615	111	0.490				
5	ACER-000	155	0.208	171	0.146	174	0.074	154	0.300	165	0.246	166	0.157	66	0.987	71	0.981	83	0.955	118	0.201	122	0.114		84	0.490	96	0.363			
6	AIZE-001	113	0.127	134	0.077	132	0.034	124	0.187	124	0.143	123	0.087	86	0.995	91	0.994	107	0.983	94	0.101	96	0.052	45	0.364	48	0.216				
7	ALCHERA-000	160	0.231	168	0.138	169	0.070	143	0.259	151	0.216	160	0.146	119	0.999	125	0.999	144	0.996	113	0.176	120	0.111		69	0.387	80	0.289			
8	ALCHERA-001	234	1.000	234	0.999	236	0.999	225	1.000	235	1.000						227	1.000	235	1.000				161	1.000	159	1.000				
9	ALCHERA-002	213	0.807	214	0.486	214	0.302	195	0.685	204	0.442	147	1.000	147	1.000	163	0.999	145	0.827	148	0.770				113	0.811	128	0.705			
10	ALCHERA-003	189	0.450	172	0.155	171	0.070	151	0.304	16	0.239	165	0.152	143	1.000	134	0.999	149	0.997	112	0.172	118	0.097		81	0.464	95	0.362			
11	ALLGOVISION-000	121	0.138	146	0.088	151	0.045	131	0.202	140	0.166	147	0.106	74	0.993	86	0.990	106	0.982	97	0.117	102	0.066		90	0.526	108	0.396			
12	ALLGOVISION-001	130	0.155	152	0.102	157	0.053	148	0.275	155	0.221	159	0.141	78	0.993	77	0.986	72	0.933	107	0.150	109	0.081		85	0.491	102	0.389			
13	ANKE-000	141	0.184	156	0.117	166	0.063	141	0.256	154	0.220	163	0.151	83	0.995	92	0.994	115	0.990	201	1.000	217	1.000		188	1.000	176	1.000			
14	ANKE-001	139	0.183	160	0.119	167	0.063	142	0.256	153	0.220	164	0.151	87	0.995	97	0.994	126	0.992	186	1.000	186	1.000		205	1.000	208	1.000			
15	ANKE-002	72	0.062	78	0.032	77	0.014	63	0.103	67	0.079	69	0.050	46	0.975	48	0.948	50	0.795	51	0.034	50	0.018		43	0.245	50	0.190			
16	AWARE-003	138	0.174	164	0.128	177	0.082	164	0.351	179	0.298	184	0.204	63	0.987	75	0.984	101	0.977	132	0.428	135	0.378		91	0.530	104	0.443			
17	AWARE-004	181	0.355	194	0.269	202	0.175	189	0.619	200	0.509	202	0.375	146	1.000	148	1.000	16	0.999	129	0.397	131	0.279		114	0.816	128	0.631			
18	AWARE-005	203	0.608	202	0.364	129	0.085	159	0.342	166	0.253	168	0.163	140	1.000	152	1.000	165	0.999	122	0.255	124	0.122		123	0.916	127	0.714			
19	AWARE-006	193	0.475	195	0.276	205	0.175	188	0.466	195	0.398	195	0.283	130	1.000	143	0.999	161	0.999	127	0.368	128	0.254		106	0.749	117	0.623			
20	AYONIX-000	216	0.846	223	0.811	228	0.724	213	0.956	222	0.939	224	0.892	116	0.998	117	0.998	142	0.995	150	0.954	150	0.891		134	0.982	142	0.959			
21	AYONIX-001	217	0.875	225	0.824	224	0.701	206	0.946	217	0.920	220	0.845	138	1.000	141	0.999	148	0.996	154	0.999	154	0.998		131	0.969	138	0.926			
22	AYONIX-002	218	0.876	224	0.824	227	0.702	209	0.946	218	0.920	219	0.845	139	1.000	139	0.999	146	0.996	147	0.915	146	0.821		130	0.969	138	0.926			
23	CAMVI-003	92	0.094	129	0.071	16	0.058	162	0.152	117	0.132	148	0.108	52	0.979	56	0.970	70	0.940	96	0.114	118	0.100		72	0.402	99	0.377			
24	CAMVI-004	101	0.107	130	0.072	160	0.054	138	0.240	119	0.136	137	0.100	131	1.000	137	1.000	152	0.998	93	0.100	108	0.081		110	0.787	112	0.507			
25	CAMVI-005	122	0.139	150	0.099	126	0.076	128	0.451	147	0.179	154	0.132	135	1.000	146	1.000	158	0.998	108	0.156	121	0.112		142	0.999	148	0.983			
26	CIB-000	50	0.044	33	0.012	20	0.005	45	0.077	32	0.045	31	0.025	163	1.000	158	1.000	172	1.000	29	0.017	27	0.008	22	0.141	21	0.068	121	0.894	113	0.521
27	CLOUDWALK-HR-000	5	0.004	6	0.002	9	0.002	4	0.015	6	0.013	9	0.012	10	0.188	1	0.133	2	0.095	5	0.005	7	0.003	3	0.033	4	0.099	2	0.075		
28	COGENT-000	125	0.143	106	0.053	123	0.029	115	0.175	120	0.140	139	0.100	90	0.996	103	0.995	121	0.991												
29	COGENT-001	126	0.143	107	0.053	124	0.029	112	0.175	121	0.140	141	0.100	91	0.996	102	0.995	123	0.991												
30	COGENT-002	136	0.159	94	0.044	89	0.017	81	0.124	91	0.098	94	0.063	113	0.998	114	0.998	137	0.994												
31	COGENT-003	153	0.203	98	0.046	82	0.016	79	0.121	85	0.095	92	0.061	114	0.999	115	0.998	140	0.995												
32	COGENT-004	156	0.209	79	0.033	37	0.006	36	0.067	38	0.051	39	0.031	108	0.998	112	0.997	144	0.995	36	0.022	35	0.012	20	0.126	21	0.072	79	0.456	47	0.178
33	COGNITEC-000	159	0.226	176	0.161	186	0.095	176	0.439	180	0.303	182	0.200	89	0.996	88	0.992	91	0.971												
34	COGNITEC-001	151	0.192	151	0.102	158	0.053	22	0.997	159	0.230	156	0.135	197	1.000	224	1.000	87	0.965												
35	COGNITEC-002	109	0.122	109	0.053	114	0.025	220	0.990	146	0.178	144	0.101	194	1.000	157	1.000	84	0.956												
36	COGNITEC-003	96	0.099	105	0.053	116	0.025	135	0.222	138	0.162	138	0.100	238	1.000	159	1.000	29	0.946												
37	COGNITEC-004	66	0.055	77	0.031	78	0.014	84	0.127	89	0.097	84	0.058	85	0.995	83	0.990	69	0.919	82	0.068	83	0.038	44	0.316	47	0.196	52	0.288	61	0.218
38	COGNITEC-005	67	0.055	25	0.010	23	0.004	29	0.058	30	0.041	25	0.022	192	1.000	214	1.000	63	0.878	58	0.041	20	0.028	26	0.157	30	0.092	29	0.179	35	0.145
39	CUBOX-000	8	0.005	11	0.003	12	0.002	12	0.019	13	0.014	4	0.276	2	0.168	1	0.104	2	0.004	2	0.003	2	0.028	1	0.014	1	0.073	1	0.062		
40	CYBERLINK-000	120	0.137	115	0.056																										

MISSES BELOW THRESHOLD, T		ENROL RECENT MUGSHOT, N = 1.6M												ENROL APPLICATION PORTRAIT, N = 1.6M														
#	ALGORITHM	ENROL: MUGSHOT			ENROL: MUGSHOT			ENROL: WEBCAM			ENROL: MUGSHOT			PROBE: PROFILE			ENROL: VISA		ENROL: BORDER		ENROL: BORDER 10+YR		ENROL: VISA					
		FPIR=0.0003	FPIR=0.001	FPIR=0.01	FPIR=0.0003	FPIR=0.001	FPIR=0.01	FPIR=0.0003	FPIR=0.001	FPIR=0.01	FPIR=0.0003	FPIR=0.001	FPIR=0.01	FPIR=0.0003	FPIR=0.001	FPIR=0.01	FPIR=0.001	FPIR=0.01	FPIR=0.001	FPIR=0.01	FPIR=0.001	FPIR=0.01	FPIR=0.001	FPIR=0.01				
47	DAHUA-002	31.026	42.015	40.006	30.060	34.046	35.029	19.0681	23.0638	30.0522	26.017	29.008	23.013	23.0159	25.0125	23.0159	25.0125	23.0159	25.0125	23.0159	25.0125	23.0159	25.0125	23.0159	25.0125			
48	DAHUA-003	30.025	38.014	33.005	26.054	29.041	29.024	16.0647	19.0579	24.0447	21.0013	19.006	13.0081	14.0043	16.0134	15.0109	16.0134	15.0109	16.0134	15.0109	16.0134	15.0109	16.0134	15.0109	16.0134	15.0109		
49	DEEPLINT-001	13.010	13.003	13.002	7.018	7.014	5.010	168.1000	144.1.000	26.0503	8.0006	12.0004	8.0006	8.0006	12.0004	22.0159	20.0097	22.0159	20.0097	22.0159	20.0097	22.0159	20.0097	22.0159	20.0097			
50	DEEPSA-001	81.073	97.046	103.022	87.129	92.101	87.059	69.0988	76.0985	96.0973	86.077	88.041	86.077	88.041	86.077	88.041	62.0326	70.0251	62.0326	70.0251	62.0326	70.0251	62.0326	70.0251	62.0326	70.0251		
51	DERMALOG-003	199.0550	213.0482	217.0360	199.0715	209.0655	213.0526	96.0997	106.0995	125.0991	144.0677	144.0554	119.0870	130.0791	119.0870	130.0791	118.0856	131.0751	118.0856	131.0751	118.0856	131.0751	118.0856	131.0751	118.0856	131.0751		
52	DERMALOG-004	201.0554	212.0480	216.0358	198.0711	210.0657	211.0526	92.0996	85.0990	84.0950	125.0300	125.0267	125.0300	125.0267	98.0614	106.0459	98.0614	106.0459	98.0614	106.0459	98.0614	106.0459	98.0614	106.0459				
53	DERMALOG-005	150.0189	145.0088	144.0043	12.0201	131.0154	134.0096	93.0996	84.0990	84.0950	75.0059	76.0031	94.0557	82.0299	94.0557	82.0299	61.0318	65.0230	61.0318	65.0230	61.0318	65.0230	61.0318	65.0230	61.0318	65.0230		
54	DERMALOG-006	95.0098	104.0052	118.0026	94.0137	95.0105	98.0067	70.0989	70.0981	74.0933	75.0059	76.0031	75.0059	76.0031	75.0059	76.0031	61.0318	65.0230	61.0318	65.0230	61.0318	65.0230	61.0318	65.0230	61.0318	65.0230		
55	DERMALOG-007	147.0188	143.0086	142.0040	120.0200	120.0152	131.0093	93.0996	84.0990	84.0950	92.009	92.0052	92.009	92.0052	92.009	92.0052	94.0557	82.0299	94.0557	82.0299	94.0557	82.0299	94.0557	82.0299	94.0557	82.0299		
56	DERMALOG-008	170.268	96.0045	87.0017	136.0231	82.0094	79.0054	154.0000	178.0000	173.0000	72.0057	68.0025	48.0382	48.0158	127.0940	127.0678	127.0940	127.0678	127.0940	127.0678	127.0940	127.0678	127.0940	127.0678				
57	EYEDEA-003	19.509	204.0388	20.0265	19.0625	20.0543	203.0404	95.0997	98.0994	11.0990	138.0570	13.0392	111.0792	122.0658	111.0792	122.0658	111.0792	122.0658	111.0792	122.0658	111.0792	122.0658	111.0792	122.0658	111.0792	122.0658		
58	F8-001	191.0458	177.0166	133.0036	120.0999	124.0998	143.0095	120.0999	124.0998	143.0095	114.0187	119.0108	51.0598	53.0418	80.0458	92.0349	80.0458	92.0349	80.0458	92.0349	80.0458	92.0349	80.0458	92.0349	80.0458	92.0349		
59	FINCORE-000	146.0187	167.0134	17.0071	147.0267	152.0217	157.0140	142.0000	154.0000	139.0095	114.0187	119.0108	51.0598	53.0418	80.0458	92.0349	80.0458	92.0349	80.0458	92.0349	80.0458	92.0349	80.0458	92.0349	80.0458	92.0349		
60	GLORY-000	188.0441	203.0367	213.0295	187.0586	203.0547	207.0470	82.0995	100.0995	129.0993	134.0453	136.0381	117.0839	130.0795	117.0839	130.0795	115.0819	132.0753	115.0819	132.0753	115.0819	132.0753	115.0819	132.0753	115.0819	132.0753		
61	GLORY-001	180.0355	196.0305	206.0236	186.0582	201.0537	205.0448	79.0994	89.0993	119.0991	131.0408	133.0336	115.0819	132.0753	115.0819	132.0753	115.0819	132.0753	115.0819	132.0753	115.0819	132.0753	115.0819	132.0753	115.0819	132.0753		
62	GORILLA-001	211.0747	208.0406	207.0246	188.0590	196.0453	197.0314	156.0100	173.0100	183.0100	135.0468	132.0299	126.01000	126.01000	126.01000	126.01000	126.01000	126.01000	126.01000	126.01000	126.01000	126.01000	126.01000	126.01000	126.01000			
63	GORILLA-002	169.0266	184.0188	191.0106	161.0342	173.0268	174.0170	153.0100	163.0100	171.0100	121.0250	120.0137	120.0137	120.0137	120.0137	120.0137	120.0137	120.0137	120.0137	120.0137	120.0137	120.0137	120.0137	120.0137	120.0137			
64	GORILLA-003	209.0694	198.0318	201.0157	194.0684	194.0434	193.0247	200.0100	217.0100	170.0100	130.0407	128.0213	111.007	111.0044	111.007	111.0044	111.007	111.0044	111.007	111.0044	111.007	111.0044	111.007	111.0044	111.007	111.0044		
65	GORILLA-004	118.0135	148.0089	145.0043	128.0202	137.0160	142.0101	44.0972	50.0959	65.0903	102.0135	105.0072	60.0315	62.0223	60.0315	62.0223	60.0315	62.0223	60.0315	62.0223	60.0315	62.0223	60.0315	62.0223	60.0315	62.0223		
66	GORILLA-005	90.0086	119.0058	119.0026	111.0179	12.0142	125.0088	23.0770	26.0700	31.0553	90.0088	87.0040	78.0445	91.0359	78.0445	91.0359	78.0445	91.0359	78.0445	91.0359	78.0445	91.0359	78.0445	91.0359	78.0445	91.0359		
67	HIK-003	135.0159	153.0103	161.0057	123.0190	133.0158	146.0105	54.0980	54.0969	70.0925	105.0142	107.0080	120.0879	120.0743	120.0879	120.0743	120.0879	120.0743	120.0879	120.0743	120.0879	120.0743	120.0879	120.0743	120.0879	120.0743		
68	HIK-004	132.0156	149.0099	159.0054	118.0182	130.0153	143.0101	59.0983	61.0976	80.0947	103.0137	105.0077	125.0436	125.0258	125.0436	125.0258	125.0436	125.0258	125.0436	125.0258	125.0436	125.0258	125.0436	125.0258	125.0436	125.0258		
69	HIK-005	98.0102	91.0044	92.0019	66.0077	68.0048	136.0000	142.0999	154.0998	81.0068	81.0068	81.0068	81.0068	81.0068	81.0068	81.0068	81.0068	81.0068	81.0068	81.0068	81.0068	81.0068	81.0068	81.0068				
70	HIK-006	124.0142	99.0047	94.0020	71.0086	74.0052	151.0000	172.0000	169.0000	57.0041	157.0000	128.0999	135.0995	59.0042	61.0020	44.0245	44.0168	44.0245	44.0168	44.0245	44.0168	44.0245	44.0168	44.0245	44.0168	44.0245	44.0168	44.0245
71	HYPERVERGE-001	11.0009	16.0004	17.0002	20.0039	22.0031	21.0020	3.0275	5.0220	7.0146	11.0007	11.0004	9.0053	11.0027	11.0007	11.0004	11.0007	11.0004	11.0007	11.0004	11.0007	11.0004	11.0007	11.0004	11.0007	11.0004		
72	IDEMIA-003	200.0552	100.0047	99.0021	233.0000	137.0165	117.0079	19.0000	106.0976	60.0973	88.0968	99.0123	99.0061	109.0766	115.0630	109.0766	115.0630	108.0766	115.0630	108.0766	115.0630	108.0766	115.0630	108.0766	115.0630	108.0766	115.0630	
73	IDEMIA-004	65.0055	87.0037	97.0021	97.0144	106.0118	116.0079	49.0976	60.0973	88.0968	99.0123	99.0061	108.0766	115.0630	108.0766	115.0630	108.0766	115.0630	108.0766	115.0630	108.0766	115.0630	108.0766	115.0630	108.0766	115.0630		
74	IDEMIA-005	79.0066	93.0044	117.0026	117.0181	128.0150	143.0102	53.0979	65.0978	95.0973	100.0130	104.0070	120.0879	120.0743	120.0879	120.0743	120.0879	120.0743	120.0879	120.0743	120.0879	120.0743	120.0879	120.0743	120.0879	120.0743		
75	IDEMIA-006	77.0065	90.0043	115.0025	146.0266	15.0026	167.0161	62.0984	72.0982	104.0980	106.0144	110.0090	106.0144	106.0144	110.0090	106.0144	106.0144	110.0090	106.0144	106.0144	110.0090	106.0144	106.0144	110.0090	106.0144			
7																												

MISSSES BELOW THRESHOLD, T		ENROL RECENT MUGSHOT, N = 1.6M												ENROL APPLICATION PORTRAIT, N = 1.6M												
		ENROL: MUGSHOT			ENROL: MUGSHOT			ENROL: MUGSHOT			ENROL: VISA			ENROL: BORDER			ENROL: BORDER 10+YR			ENROL: KIOSK						
#	ALGORITHM	FPIR=0.0003	FPIR=0.001	FPIR=0.01	FPIR=0.0003	FPIR=0.001	FPIR=0.01	FPIR=0.0003	FPIR=0.001	FPIR=0.01	FPIR=0.0001	FPIR=0.01	FPIR=0.01	FPIR=0.0001	FPIR=0.01	FPIR=0.01	FPIR=0.0001	FPIR=0.01	FPIR=0.001	FPIR=0.01	FPIR=0.0001	FPIR=0.01	FPIR=0.001	FPIR=0.01		
93	INNOVATRICS-007	25 0.24	36 0.013	34 0.005	33 0.065	39 0.051	40 0.032	28 0.806	27 0.743	32 0.567	27 0.017	29 0.009	15 0.93	18 0.053	15 0.154	24 0.120	143 0.999	153 0.989	143 0.999	150 0.988	143 0.999	150 0.988	143 0.999	150 0.988		
94	INTSYSMSU-000	20 0.999	23 0.998	23 0.990	25 1.000	22 1.000	22 0.998	141 1.000	150 1.000	153 0.998	153 0.999	153 0.999	153 0.999	153 0.999	153 0.999	153 0.999	153 0.999	153 0.999	153 0.999	153 0.999	153 0.999	153 0.999	153 0.999			
95	IREX-000	86 0.068	75 0.028	50 0.008	60 0.099	50 0.060	48 0.032	69 0.988	49 0.957	44 0.680	62 0.044	34 0.011	43 0.302	20 0.062	27 0.170	31 0.135	20 0.062	27 0.170	31 0.135	20 0.062	27 0.170	31 0.135	20 0.062	27 0.170	31 0.135	
96	ISYSTEMS-002	131 0.155	136 0.078	129 0.032	105 0.161	113 0.126	119 0.080	112 0.998	113 0.998	128 0.993	143 0.999	143 0.999	143 0.999	143 0.999	143 0.999	143 0.999	143 0.999	143 0.999	143 0.999	143 0.999	143 0.999	143 0.999	143 0.999	143 0.999		
97	ISYSTEMS-003	154 0.204	129 0.059	112 0.024	93 0.135	98 0.107	101 0.068	148 1.000	151 1.000	151 0.997	151 0.997	151 0.997	151 0.997	151 0.997	151 0.997	151 0.997	151 0.997	151 0.997	151 0.997	151 0.997	151 0.997	151 0.997	151 0.997	151 0.997		
98	KAKAO-000	34 0.028	44 0.015	42 0.006	41 0.071	47 0.056	48 0.034	10 0.539	13 0.468	19 0.327	31 0.019	30 0.010	21 0.141	25 0.075	21 0.158	23 0.120	21 0.158	23 0.120	21 0.158	23 0.120	21 0.158	23 0.120	21 0.158	23 0.120		
99	KEDACOM-001	49 0.041	61 0.023	76 0.013	57 0.096	61 0.072	79 0.054	79 0.989	78 0.986	97 0.973	71 0.055	89 0.043	56 0.305	74 0.264	56 0.305	74 0.264	56 0.305	74 0.264	56 0.305	74 0.264	56 0.305	74 0.264	56 0.305	74 0.264	56 0.305	
100	KNERON-000							136 0.099																		
101	KNERON-001																									
102	LINE-000	73 0.062	76 0.031	75 0.012	91 0.132	86 0.095	80 0.054				186 1.000	63 0.046	62 0.021	41 0.278	44 0.151	172 1.000	75 0.268									
103	LOOKMAN-003	78 0.066	92 0.044	113 0.025	90 0.131	101 0.112	128 0.082					89 0.084	100 0.061				63 0.355	88 0.304								
104	LOOKMAN-004	82 0.074	95 0.045	110 0.024	80 0.123	97 0.105	111 0.075	51 0.979	62 0.977	98 0.974																
105	LOOKMAN-005	61 0.050	75 0.030	85 0.017	61 0.102	73 0.086	91 0.063	58 0.980	64 0.978	94 0.973	78 0.062	91 0.047											57 0.308	77 0.273		
106	MEGVII-001	157 0.210	131 0.072	135 0.037	76 0.119	90 0.097	89 0.061																			
107	MEGVII-002	168 0.258	137 0.077	137 0.037	77 0.120	88 0.096	86 0.059	118 0.999	123 0.998	62 0.872																
108	MICROFOCUS-003	224 0.958	228 0.931	231 0.866	219 0.988	226 0.979	226 0.948										152 0.982	152 0.945					138 0.991	145 0.977		
109	MICROFOCUS-004	239 0.999	237 0.999	237 0.999	218 0.984	224 0.975	222 0.940										151 0.974	151 0.935					139 0.989	144 0.976		
110	MICROFOCUS-005	219 0.883	226 0.835	229 0.736	211 0.951	220 0.928	222 0.865										149 0.935	149 0.848					135 0.985	143 0.965		
111	MICROFOCUS-006	228 0.983	239 0.978	232 0.963	210 0.950	219 0.923	223 0.858										148 0.923	147 0.843					136 0.971	140 0.939		
112	MICROSOFT-003	59 0.049	71 0.028	70 0.012	72 0.117	80 0.091	83 0.056										53 0.036	59 0.019					42 0.233	46 0.176		
113	MICROSOFT-004	56 0.046	66 0.026	65 0.011	69 0.111	75 0.087	77 0.053										49 0.033	55 0.018					36 0.222	44 0.170		
114	MICROSOFT-005	56 0.047	66 0.026	64 0.010	53 0.090	59 0.070	58 0.041	126 0.999	20 0.587	20 0.354	38 0.027	39 0.013					30 0.180	32 0.134								
115	MICROSOFT-006	29 0.025	36 0.012	39 0.006	24 0.048	27 0.037	36 0.024	3 0.452	10 0.386	14 0.281	46 0.032	45 0.015											25 0.178	32 0.138		
116	NEC-000	108 0.113	138 0.079	152 0.047	110 0.171	122 0.140	129 0.093	58 0.983	66 0.979	90 0.969													81 0.474	100 0.377		
117	NEC-001	128 0.148	155 0.106	165 0.060	137 0.238	149 0.197	155 0.133	77 0.991	79 0.986	92 0.972	101 0.133	110 0.082											82 0.468	101 0.378		
118	NEC-002	19 0.018	101 0.003	8 0.002	14 0.029	13 0.020	11 0.013	131 1.000	138 0.999	137 0.995	14 0.008	16 0.005											105 0.676	84 0.292		
119	NEC-003	7 0.005	8 0.002	10 0.002	11 0.021	11 0.017	10 0.013	33 0.902	34 0.824	37 0.628	16 0.008	17 0.006	6 0.036	7 0.023									101 0.668	73 0.261		
120	NEC-004	1 0.003	3 0.002	2 0.002	3 0.015	4 0.013	7 0.010	17 0.654	2 0.622	33 0.575	3 0.004	6 0.004	1 0.019	1 0.012									9 0.100	6 0.088		
121	NEUROTECHNOLOGY-003	231 0.999	219 0.636	189 0.099	201 0.773	172 0.266	169 0.164	229 1.000	182 1.000	212 1.000																
122	NEUROTECHNOLOGY-004	107 0.120	125 0.063	121 0.028	98 0.146	103 0.117	107 0.073	91 0.996	90 0.994	116 0.990																
123	NEUROTECHNOLOGY-005	106 0.117	113 0.054	104 0.022	140 0.252	115 0.130	110 0.074	116 0.999	116 0.998	113 0.989																
124	NEUROTECHNOLOGY-006	229 0.987	197 0.249	194 0.121	234 1.000	191 0.418	188 0.206																			
125	NEUROTECHNOLOGY-007	164 0.252	124 0.062	101 0.021	222 0.996	143 0.173	100 0.068	171 1.000	156 1.000	150 0.997	126 0.339	82 0.036											168 1.000	151 0.989		
126	NEUROTECHNOLOGY-008	21 0.797	106 0.053	74 0.012	67 0.110	69 0.080	66 0.047	161 1.000	161 1.000	179 1.000	36 0.035	51 0.017	42 0.293	43 0.149								36 0.203	37 0.152			
127	NEUROTECHNOLOGY-009	32 0.027	45 0.015	38 0.006	34 0.066	42 0.052	41 0.032	18 0.661	21 0.588	23 0.436	32 0.020	31 0.010	25 0.153	28 0.082									24 0.165	27 0.129		
128	NEWLAND-002	196 0.523	219 0.438	212 0.294	183 0.535	197 0.466	199 0.335	129 0.999	130 0.999	156 0.998																
129	NOBLIS-001	238 1.000	235 1.000	235 0.991	237 1.000	233 1.000	234 1.000	150 1.000	174 1.000	181 1.000																
130	NOBLIS-002	230 1.000	231 0.997	221 0.488	230 1.000	239 1.000	238 1.000	167 1.000	167 1.000	187 1.000																
131	NTECHLAB-003	88 0.080	111 0.054	122 0.028	99 0.148	104 0.118	112 0.075	30 0.873	36 0.837	52 0.752																
132	NTECHLAB-004	73 0.063	89 0.041	99 0.021	89 0.131	96 0.105	97 0.065	27 0.868	37 0.833	50 0.746	70 0.053	73 0.030											40 0.263	60 0.214		
133	NTECHLAB-005	74 0.062	89 0.042	100 0.021	88 0.130	94 0.102	99 0.063	27 0.816	30 0.771	42 0.661	89 0.073	85 0.039											50 0.294	64 0.227		
134	NTECHLAB-006	68 0.056	83 0.037	90 0.018	78 0.121	83 0.094	88 0.059	25 0.802	29 0.754	38 0.635	73 0.057	77 0.032											48 0.260	58 0.207		
135	NTECHLAB-007	48 0.040	69 0.026	71 0.012	49 0.085	55 0.067	56 0.041	29 0.796	28 0.750	39 0.642	47 0.032	52 0.017											39 0.223	45 0.176		
136	NTECHLAB-008	27 0.024	39 0.014	44 0.007	28 0.057	33 0.045	36 0.029	13 0.601	18 0.529	22 0.391	50 0.033	56 0.018											31 0.183	33 0.140		
137	NTECHLAB-009	12 0.010	15 0.005	19 0.003	13 0.028	14 0.022	11 0.014	27 0.522	10 0.430	16 0.311	24 0.015	24 0.008	18 0.109	19 0.061								17 0.142	16 0.114			
138	NTECHLAB-010	9 0.005	9 0.003	6 0.002	8 0.018	8 0.015	8 0.011	7 0.334	7 0.252	10 0.169	9 0.															

Table 27: **Threshold-based accuracy.** Values are  $FNIR(N, T, L)$  with  $N = 1.6$  million with thresholds set to produce  $FPIR = 0.0003, 0.001$ , and  $0.01$  in non-mate searches. Throughout blue superscripts indicate the rank of the algorithm for that column. Caution: The Power-low models are mostly intended to draw attention to the kind of behavior, not as a model to be used for prediction.

2021/09/21  
09:55:08

FNIR(N, K, I) = False neg. identification rate  
FPIR(N, T) = False pos. identification rate

$N =$  Num. enrolled subjects  
 $R =$  Num. candidates examined

### Threshold

$T \geq 0 \rightarrow$  Identification

MISSES BELOW THRESHOLD, T		ENROL RECENT MUGSHOT, N = 1.6M												ENROL APPLICATION PORTRAIT, N = 1.6M																			
#	ALGORITHM	ENROL: MUGSHOT			ENROL: MUGSHOT			ENROL: MUGSHOT			ENROL: VISA			ENROL: BORDER			ENROL: BORDER 10+YR			ENROL: KIOSK													
		FPIR=0.0003	FPIR=0.001	FPIR=0.01	FPIR=0.0003	FPIR=0.001	FPIR=0.01	FPIR=0.0003	FPIR=0.001	FPIR=0.01	FPIR=0.0001	FPIR=0.001	FPIR=0.01	FPIR=0.001	FPIR=0.001	FPIR=0.01	FPIR=0.001	FPIR=0.01	FPIR=0.001	FPIR=0.01	FPIR=0.001	FPIR=0.01	FPIR=0.001	FPIR=0.01									
139	PARAVISION-000	173	0.278	147	0.089	150	0.045	177	0.447	141	0.170	140	0.100	166	1.000	133	0.999	148	0.997	136	0.470	140	0.443	126	0.926	131	0.779						
140	PARAVISION-001	123	0.140	101	0.049	96	0.020	132	0.207	114	0.128	109	0.074	170	1.000	126	0.999	133	0.994	133	0.444	139	0.428	105	0.739	116	0.573						
141	PARAVISION-002	89	0.085	102	0.050	106	0.022	103	0.152	107	0.119	114	0.076	73	0.992	73	0.983	51	0.748	87	0.080	90	0.043	86	0.497	76	0.268						
142	PARAVISION-003	76	0.063	81	0.035	81	0.016	81	0.124	81	0.096	88	0.060	100	0.997	96	0.994	49	0.733	74	0.058	81	0.034	55	0.296	66	0.232						
143	PARAVISION-004	28	0.025	28	0.010	28	0.004	25	0.049	28	0.038	28	0.024	152	1.000	173	1.000	56	0.797	30	0.018	33	0.011	122	0.908	59	0.211						
144	PARAVISION-005	18	0.014	15	0.004	16	0.002	15	0.031	15	0.024	16	0.016	98	0.997	67	0.980	11	0.181	19	0.011	28	0.008	14	0.132	21	0.120						
145	PARAVISION-007	57	0.048	14	0.004	11	0.002	184	0.560	16	0.025	15	0.015	155	1.000	176	1.000	182	1.000	18	0.009	18	0.006	19	0.113	8	0.024	238	1.000	229	1.000		
146	PIXELALL-002	206	0.664	154	0.105	12	0.030	210	0.974	18	0.388	121	0.083	163	1.000	171	1.000	139	0.602	99	0.047	157	1.000	153	1.000	93	0.554	71	0.255				
147	PIXELALL-003	58	0.049	58	0.022	57	0.009	62	0.102	62	0.073	61	0.043	145	1.000	155	0.998	56	0.037	60	0.020	139	0.994	141	0.942	150	1.000	144	1.000	147	0.983		
148	PIXELALL-004	108	0.120	51	0.018	49	0.007	202	0.783	68	0.079	51	0.037	160	1.000	162	0.999	67	0.051	49	0.015	150	1.000	144	1.000	147	0.983	152	1.000	148	0.979		
149	PIXELALL-005	84	0.079	32	0.012	28	0.005	170	0.456	37	0.050	33	0.027	170	1.000	169	0.999	39	0.027	48	0.017	34	0.203	22	0.071	144	1.000	147	0.983				
150	PTAKURATSATU-000	70	0.057	82	0.037	86	0.017	108	0.165	112	0.124	106	0.071	42	0.947	46	0.924	61	0.868	64	0.046	62	0.022	36	0.206	38	0.120	41	0.232	48	0.179		
151	QNAP-000	227	0.972	165	0.129	156	0.052	228	0.998	161	0.238	150	0.117	173	1.000	181	1.000	184	1.000	115	0.191	103	0.068	50	0.539	52	0.263	141	0.998	149	0.985		
152	QUANTASOFT-001	70	0.713	220	0.639	222	0.493																										
153	RANKONE-002	143	0.184	159	0.118	172	0.071	156	0.308	168	0.261	179	0.190																				
154	RANKONE-003	142	0.184	158	0.118	171	0.071	153	0.300	167	0.255	177	0.187																				
155	RANKONE-004	163	0.250	185	0.193	19	0.124	181	0.482	193	0.426	198	0.324																				
156	RANKONE-005	94	0.096	121	0.059	130	0.033	133	0.212	144	0.173	151	0.119	129	0.999	118	0.998	134	0.994														
157	RANKONE-006	71	0.061	84	0.037	93	0.020	60	0.022	67	0.011	75	0.118	84	0.095	91	0.061	48	0.975	53	0.967	69	0.924										
158	RANKONE-007	39	0.034	60	0.022	67	0.011	75	0.118	84	0.095	91	0.061	48	0.975	53	0.967	76	0.062	72	0.029			63	0.328	57	0.206						
159	RANKONE-009	36	0.031	48	0.018	39	0.008	38	0.098	69	0.076	63	0.045	57	0.983	55	0.969	69	0.859	76	0.062	72	0.029										
160	RANKONE-010	23	0.023	37	0.014	47	0.007	44	0.077	48	0.058	50	0.036	34	0.905	32	0.802	41	0.652	69	0.052	69	0.027	37	0.208	39	0.119	46	0.259	50	0.194		
161	RANKONE-011	103	0.109	23	0.009	24	0.004	47	0.079	35	0.048	37	0.029					55	0.037	53	0.017	30	0.182	32	0.092	133	0.977	107	0.465				
162	REALNETWORKS-000	183	0.374	190	0.234	198	0.138	175	0.433	183	0.191	187	0.209																				
163	REALNETWORKS-001	184	0.374	191	0.234	199	0.138	174	0.433	184	0.191	188	0.209																				
164	REALNETWORKS-002	182	0.370	189	0.231	19	0.137	177	0.416	185	0.315	189	0.209																				
165	REALNETWORKS-003	171	0.273	175	0.159	181	0.090	169	0.342	171	0.266	175	0.172	122	0.999	122	0.998	110	0.987	110	0.164	115	0.103	87	0.500	97	0.364						
166	REALNETWORKS-004	166	0.242	174	0.158	180	0.090	167	0.353	167	0.263	172	0.169	134	1.000	135	0.999	12	0.992	111	0.170	116	0.103	97	0.613	98	0.370						
167	REALNETWORKS-005	63	0.052	70	0.028	73	0.012	56	0.094	63	0.074	65	0.047	60	0.984	57	0.971	64	0.896	54	0.037	49	0.017	38	0.223	40	0.123	37	0.215	41	0.165		
168	REMARKAI-000	112	0.125	114	0.055	106	0.023	111	0.173	108	0.120	103	0.070	129	0.999	132	0.999	130	0.995	83	0.069	79	0.033			103	0.717	96	0.315				
169	REMARKAI-000	152	0.197	163	0.128	164	0.059	145	0.263	150	0.203	153	0.123																				
170	REMARKAI-002	148	0.188	162	0.124	163	0.059	129	0.248	148	0.196	152	0.122	77	0.993	87	0.991	103	0.980														
171	RENDIP-000	24	0.023	31	0.012	32	0.005	122	0.189	49	0.059	47	0.034	41	0.945	43	0.894	49	0.744	34	0.022	38	0.013	32	0.185	29	0.089	25	0.167	28	0.130		
172	S1-000	119	0.137	72	0.028	66	0.011	86	0.129	72	0.085	67	0.048	172	1.000	173	1.000	34	0.596	66	0.047	57	0.018	107	1.000	39	0.123	219	1.000	121	0.632		
173	SCANOVATE-000	99	0.103	128	0.067	126	0.030	152	0.296	164	0.240	162	0.150	37	0.931	42	0.893	59	0.803	119	0.215	12	0.118			71	0.400	86	0.299				
174	SCANOVATE-001	114	0.128	139	0.081	138	0.037	151	0.281	158	0.227	158	0.140	38	0.935	45	0.911	58	0.834	116	0.192	117	0.103			74	0.404	82	0.290				
175	SENSETIME-000	43	0.036	56	0.021	59	0.009	49	0.078	52	0.063	54	0.040	183	1.000	238	1.000	111	0.988														
176	SENSETIME-001	44	0.036	59	0.022	61	0.010	48	0.080	53	0.064	59	0.041																				
177	SENSETIME-002	45	0.037	40	0.015	81	0.014	10	0.012	20	0.009	14	0.007	97	0.997	93	0.994	102	0.979	45	0.032	50	0.017			89	0.523	40	0.160				
178	SENSETIME-003	4	0.004	4	0.002	4	0.001	10	0.014	10	0.012	20	0.009	14	0.607	14	0.477	17	0.31														

MISSES BELOW THRESHOLD, T			ENROL RECENT MUGSHOT, N = 1.6M												ENROL APPLICATION PORTRAIT, N = 1.6M									
#	ALGORITHM	FPIR=0.0003	ENROL: MUGSHOT			ENROL: MUGSHOT			ENROL: MUGSHOT			ENROL: PROFILE			ENROL: VISA		ENROL: BORDER		ENROL: VISA					
			PROBE: MUGSHOT			PROBE: WEBCAM			PROBE: PROFILE			PROBE: BORDER		PROBE: BORDER 10+YR		PROBE: KIOSK								
185	SHAMAN-007	140 0.183	170 0.141	182 0.092	150 0.280	165 0.240	173 0.169								43 0.031	46 0.014								
186	SIAT-001	117 0.132	46 0.018	47 0.007	193 0.641	188 0.365	208 0.348								128 0.372	134 0.356					125 0.923	43 0.169		
187	SIAT-002	186 0.417	57 0.022	48 0.007	209 0.942	198 0.478	206 0.460																	
188	SMILART-004	226 0.970	229 0.968	233 0.965	218 0.977	225 0.976	227 0.973																	
189	SMILART-005																							
190	STAQU-000	178 0.334	122 0.062	102 0.022	204 0.848	195 0.443	90 0.061	149 1.000	153 1.000	164 0.999	137 0.535	86 0.039	53 0.961	46 0.183	151 1.000	152 0.999								
191	SYNESIS-003	104 0.111	126 0.065	127 0.032	101 0.155	111 0.123	115 0.078	45 0.973	51 0.960	66 0.911	85 0.075	84 0.039									59 0.314	68 0.235		
192	SYNESIS-003	205 0.648	216 0.582	219 0.443	197 0.708	208 0.646	210 0.524																	
193	SYNESIS-005	60 0.050	62 0.025	69 0.011	51 0.088	66 0.072	62 0.043	84 0.995	74 0.984	54 0.795	48 0.032	45 0.016									36 0.214	39 0.158		
194	TECH5-001	214 0.807	116 0.057	89 0.018	221 0.994	221 0.935	82 0.055	185 1.000	180 1.000	178 1.000	120 0.244	71 0.028									140 0.994	137 0.817		
195	TECH5-002	64 0.053	69 0.027	72 0.012	56 0.094	55 0.040	31 0.874	33 0.805	36 0.627	57 0.039	58 0.019	35 0.205	35 0.111	27 0.440								51 0.182		
196	TEVIAN-003	161 0.239	182 0.177	188 0.096	162 0.346	178 0.298	181 0.198																	
197	TEVIAN-004	137 0.170	137 0.117	168 0.063	134 0.216	145 0.176	149 0.115																	
198	TEVIAN-005	116 0.129	144 0.087	149 0.045	118 0.180	122 0.144	126 0.089	67 0.988	82 0.962	56 0.796														
199	TEVIAN-006	26 0.024	26 0.010	31 0.005	22 0.041	23 0.032	23 0.021	11 0.562	9 0.425	15 0.291	24 0.016	27 0.009	14 0.093	16 0.050	128 0.951	190 0.117								
200	TIGER-000	192 0.462	206 0.390	208 0.261	187 0.565	197 0.500	201 0.366																	
201	TIGER-002	134 0.158	141 0.086	141 0.039	130 0.202	135 0.158	133 0.095	128 0.999	130 0.999	99 0.975														
202	TIGER-003	133 0.158	140 0.086	146 0.039	129 0.202	134 0.158	132 0.095																	
203	TONGYITRANS-000	102 0.107	133 0.074	139 0.038	96 0.141	100 0.112	102 0.069																	
204	TONGYITRANS-001	111 0.124	127 0.066	128 0.032	89 0.128	95 0.101	93 0.062																	
205	TOSHIBA-000	110 0.123	123 0.062	129 0.027	109 0.150	105 0.118	108 0.074	99 0.997	104 0.995	112 0.988														
206	TOSHIBA-001	158 0.225	118 0.058	91 0.019	92 0.133	81 0.092	81 0.054																	
207	TRUEFACE-000	54 0.046	50 0.018	59 0.008	46 0.079	51 0.062	52 0.039	88 0.995	39 0.882	28 0.499	42 0.030	47 0.016	33 0.194	36 0.111	33 0.188	34 0.145								
208	VD-000	223 0.950	227 0.917	230 0.827	219 0.968	222 0.946	225 0.871																	
209	VD-001	172 0.278	186 0.201	193 0.116	157 0.331	177 0.281	178 0.188																	
210	VD-002	127 0.144	137 0.079	134 0.036	121 0.188	127 0.148	127 0.092	107 0.998	107 0.996	109 0.987	91 0.095	94 0.048	46 0.367	49 0.220	67 0.372	78 0.280								
211	VERIDAS-001	86 0.080	86 0.037	89 0.016	69 0.106	71 0.082	70 0.051	76 0.993	81 0.987	76 0.938	60 0.044	67 0.023	39 0.266	41 0.146	51 0.264	55 0.204								
212	VERIDAS-002	87 0.080	85 0.037	84 0.016	66 0.106	70 0.082	71 0.051	75 0.993	80 0.987	77 0.938	61 0.044	66 0.023	40 0.266	42 0.146	50 0.264	56 0.204								
213	VIGILANTSOLUTIONS-003	195 0.482	209 0.408	210 0.282	209 0.730	211 0.660	212 0.526	124 0.999	127 0.999	139 0.995														
214	VIGILANTSOLUTIONS-004	204 0.624	215 0.549	218 0.422	205 0.858	211 0.817	217 0.709	111 0.998	109 0.996	122 0.991														
215	VIGILANTSOLUTIONS-005	222 0.936	205 0.388	147 0.043							162 1.000	171 1.000	180 1.000											
216	VIGILANTSOLUTIONS-006	225 0.959	200 0.353	146 0.043							167 1.000	162 1.000	188 1.000											
217	VIGILANTSOLUTIONS-007	83 0.076	74 0.028	69 0.011	70 0.113	76 0.088	76 0.053	104 0.997	108 0.996	124 0.991	88 0.081	92 0.047	47 0.371	50 0.242	70 0.391	85 0.295								
218	VIGILANTSOLUTIONS-008	62 0.051	35 0.021	69 0.010	64 0.105	63 0.077	64 0.046	132 1.000	129 0.999	120 0.991	95 0.104	97 0.054	49 0.398	51 0.259	88 0.511	91 0.316								
219	VISIONLABS-004	91 0.091	117 0.058	111 0.024	123 0.199	132 0.159	135 0.097	39 0.944	41 0.890	46 0.742														
220	VISIONLABS-005	88 0.080	103 0.050	99 0.020	111 0.183	124 0.147	124 0.087	40 0.945	40 0.888	47 0.736														
221	VISIONLABS-006	52 0.044	68 0.027	63 0.010	71 0.117	72 0.090	73 0.051	21 0.764	24 0.672	29 0.511														
222	VISIONLABS-007	51 0.044	67 0.027	62 0.010	73 0.117	75 0.090	72 0.051	22 0.764	25 0.672	28 0.511	44 0.031	41 0.014									32 0.185	36 0.145		
223	VISIONLABS-008	33 0.028	35 0.013	35 0.006	38 0.068	41 0.051	43 0.032	12 0.574	15 0.481	18 0.317	25 0.017	23 0.008									18 0.151	20 0.119		
224	VISIONLABS-009	16 0.012	17 0.005	14 0.002	16 0.032	17 0.025	17 0.017	36 0.930	31 0.799	12 0.196	17 0.008	15 0.004									1 0.113	11 0.093		
225	VISIONLABS-010	17 0.014	20 0.005	18 0.002	17 0.034	19 0.027	19 0.019				9 0.169	12 0.008	9 0.004	10 0.055	10 0.027	10 0.109	8 0.089							
226	VOCORD-003	179 0.354	161 0.122	157 0.048	124 0.195	132 0.155	130 0.093	117 0.999	119 0.998	118 0.991	109 0.157	118 0.105									73 0.404	81 0.289		
227	VOCORD-004	215 0.826	201 0.355	154 0.051	170 0.401	142 0.173	128 0.093	169 1.000	153 1.000	161 0.999	117 0.193	101 0.065									35 0.991	133 0.776		
228	VOCORD-005	208 0.689	173 0.158	147 0.044	108 0.161	111 0.130	118 0.080	121 0.999	111 0.997	89 0.968	104 0.138	112 0.090									6 0.381	79 0.287		
229	VOCORD-006	237 1.000	238 1.000	239 1.000	231 1.000	233 1.000	232 1.000	182 1.000	228 1.000	201 1.000	165 1.000	168 1.000									228 1.000	230 1.000		
230	VTS-000	202 0.605	217 0.598	223 0.595	199 0.624	208 0.619	214 0.613	127 0.999	136 0.999	159 0.998	142 0.613	144 0.609	52 0.760	54 0.739	107 0.761	130 0.749								

Table 29: **Threshold-based accuracy.** Values are FNIR( $N, T, L$ ) with  $N = 1.6$  million with thresholds set to produce FPIR = 0.0003, 0.001, and 0.01 in non-mate searches. Throughout blue superscripts indicate the rank of the algorithm for that column. Caution: The Power-low models are mostly intended to draw attention to the kind of behavior, not as a model to be used for prediction.

2021 / 09 / 21

09:55:08

FNIR( $N, R, T$ ) = False neg. identification rateFPIR( $N, T$ ) = False pos. identification rate

MISSES BELOW THRESHOLD, T		ENROL RECENT MUGSHOT, N = 1.6M												ENROL APPLICATION PORTRAIT, N = 1.6M																
#	ALGORITHM	ENROL: MUGSHOT			ENROL: MUGSHOT			ENROL: MUGSHOT			ENROL: WEBCAM			PROBE: PROFILE			ENROL: VISA		ENROL: BORDER		ENROL: BORDER 10+YR		ENROL: VISA		ENROL: BORDER		ENROL: BORDER 10+YR		ENROL: KIOSK	
		FPIR=0.0003	FPIR=0.001	FPIR=0.01	FPIR=0.0003	FPIR=0.001	FPIR=0.01	FPIR=0.0003	FPIR=0.001	FPIR=0.01	FPIR=0.0003	FPIR=0.001	FPIR=0.01	FPIR=0.0003	FPIR=0.001	FPIR=0.01	FPIR=0.0001	FPIR=0.01	FPIR=0.001	FPIR=0.01	FPIR=0.0001	FPIR=0.01	FPIR=0.0001	FPIR=0.01	FPIR=0.0001	FPIR=0.01	FPIR=0.0001	FPIR=0.01		
231	VTS-001	<sup>41</sup> 0.035	<sup>36</sup> 0.013	<sup>36</sup> 0.006	<sup>37</sup> 0.067	<sup>40</sup> 0.051	<sup>38</sup> 0.031	<sup>106</sup> 0.998	<sup>94</sup> 0.994	<sup>2</sup> 0.510	<sup>35</sup> 0.022	<sup>30</sup> 0.012	<sup>23</sup> 0.141	<sup>20</sup> 0.079	<sup>34</sup> 0.192	<sup>26</sup> 0.126														
232	XFORWARDAI-000	<sup>35</sup> 0.029	<sup>42</sup> 0.015	<sup>43</sup> 0.006	<sup>40</sup> 0.070	<sup>45</sup> 0.053	<sup>49</sup> 0.034	<sup>20</sup> 0.698	<sup>11</sup> 0.440	<sup>13</sup> 0.250	<sup>33</sup> 0.021	<sup>32</sup> 0.011	<sup>27</sup> 0.159	<sup>27</sup> 0.082	<sup>26</sup> 0.169	<sup>29</sup> 0.134														
233	XFORWARDAI-001	<sup>14</sup> 0.010	<sup>18</sup> 0.005	<sup>20</sup> 0.003	<sup>19</sup> 0.036	<sup>21</sup> 0.028	<sup>20</sup> 0.020	<sup>28</sup> 0.838	<sup>12</sup> 0.448	<sup>8</sup> 0.143	<sup>15</sup> 0.008	<sup>14</sup> 0.005	<sup>12</sup> 0.062	<sup>12</sup> 0.030	<sup>13</sup> 0.123	<sup>14</sup> 0.102														
234	XFORWARDAI-002	<sup>10</sup> 0.007	<sup>12</sup> 0.003	<sup>15</sup> 0.002	<sup>10</sup> 0.018	<sup>10</sup> 0.016	<sup>12</sup> 0.014	<sup>47</sup> 0.975	<sup>16</sup> 0.525	<sup>1</sup> 0.095	<sup>6</sup> 0.005	<sup>5</sup> 0.003	<sup>7</sup> 0.041	<sup>5</sup> 0.018	<sup>5</sup> 0.099	<sup>7</sup> 0.089														
235	YISHENG-001	<sup>190</sup> 0.452	<sup>199</sup> 0.346	<sup>20</sup> 0.206	<sup>21</sup> 0.983	<sup>21</sup> 0.808	<sup>194</sup> 0.269				<sup>143</sup> 0.666	<sup>138</sup> 0.396					<sup>124</sup> 0.919	<sup>121</sup> 0.695												
236	YITU-002	<sup>37</sup> 0.031	<sup>47</sup> 0.018	<sup>49</sup> 0.008	<sup>31</sup> 0.063	<sup>36</sup> 0.049	<sup>34</sup> 0.028																							
237	YITU-003	<sup>38</sup> 0.032	<sup>53</sup> 0.019	<sup>50</sup> 0.009	<sup>35</sup> 0.067	<sup>43</sup> 0.052	<sup>46</sup> 0.033																							
238	YITU-004	<sup>20</sup> 0.019	<sup>24</sup> 0.010	<sup>25</sup> 0.004	<sup>18</sup> 0.035	<sup>18</sup> 0.027	<sup>18</sup> 0.017	<sup>43</sup> 0.948	<sup>47</sup> 0.936	<sup>67</sup> 0.913																				
239	YITU-005	<sup>22</sup> 0.022	<sup>27</sup> 0.010	<sup>30</sup> 0.005	<sup>21</sup> 0.039	<sup>24</sup> 0.032	<sup>26</sup> 0.023																							

Table 30: **Threshold-based accuracy.** Values are FNIR(N, R, T) with N = 1.6 million with thresholds set to produce FPIR = 0.0003, 0.001, and 0.01 in non-mate searches. Throughout blue superscripts indicate the rank of the algorithm for that column. Caution: The Power-low models are mostly intended to draw attention to the kind of behavior, not as a model to be used for prediction.

# Appendices

## Appendix A Accuracy on large-population FRVT 2018 mugshots

---

2021/09/21  
09:55:08

FNIR(N, R, T) = False neg. identification rate  
FPTR(N, T) = False pos. identification rate

N = Num. enrolled subjects  
R = Num. candidates examined  
T = Threshold  
T = 0 → Investigation  
T > 0 → Identification

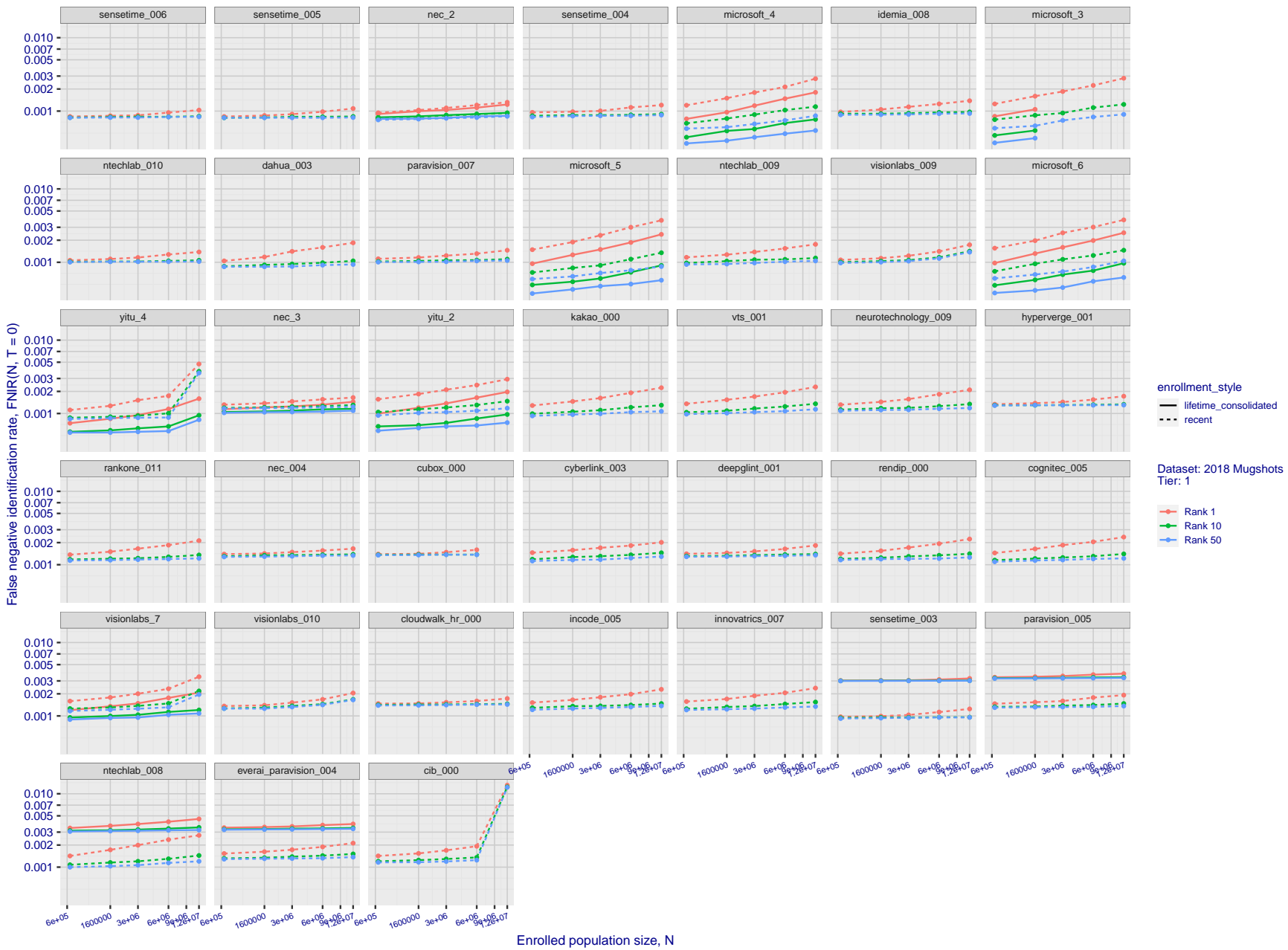


Figure 20: [FRVT-2018 Mugshot Dataset] Rank-based identification miss rates vs. number of enrolled subjects. The figure shows false negative identification rates,  $\text{FNIR}(N, R)$ , across various gallery sizes and ranks 1, 10 and 50. The threshold is set to zero, so this metric rewards even weak scoring rank 1 mates. This also means  $\text{FPIR} = 1$ , so any search without an enrolled mate will return non-mated candidates. For clarity, results are sorted and reported into tiers spanning multiple pages, the tiering criteria being rank 1 hit rate on a gallery size of 640 000.

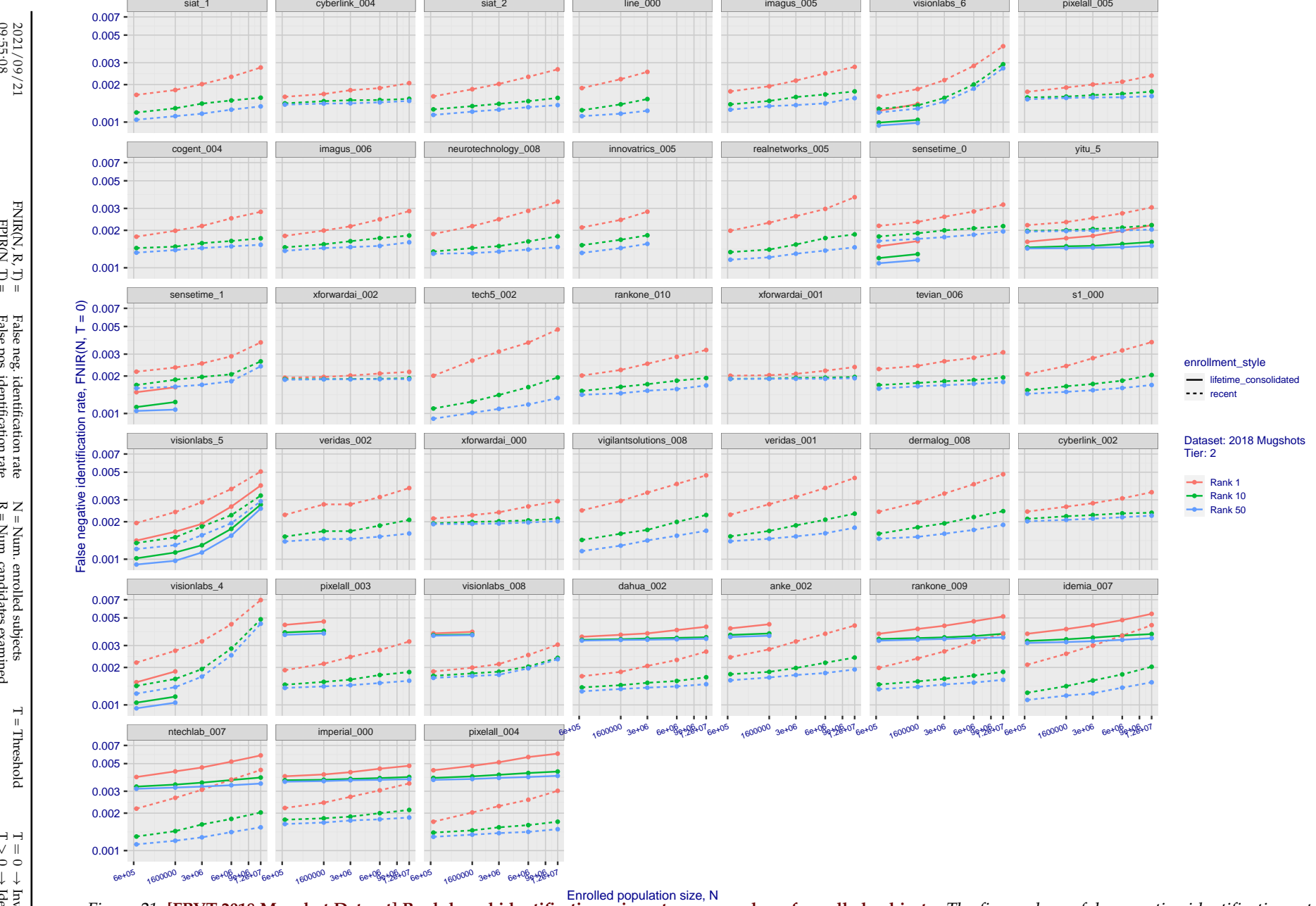


Figure 21: [FRVT-2018 Mugshot Dataset] Rank-based identification miss rates vs. number of enrolled subjects. The figure shows false negative identification rates,  $\text{FNIR}(N, R)$ , across various gallery sizes and ranks 1, 10 and 50. The threshold is set to zero, so this metric rewards even weak scoring rank 1 mates. This also means  $\text{FPIR} = 1$ , so any search without an enrolled mate will return non-mated candidates. For clarity, results are sorted and reported into tiers spanning multiple pages, the tiering criteria being rank 1 hit rate on a gallery size of 640 000.

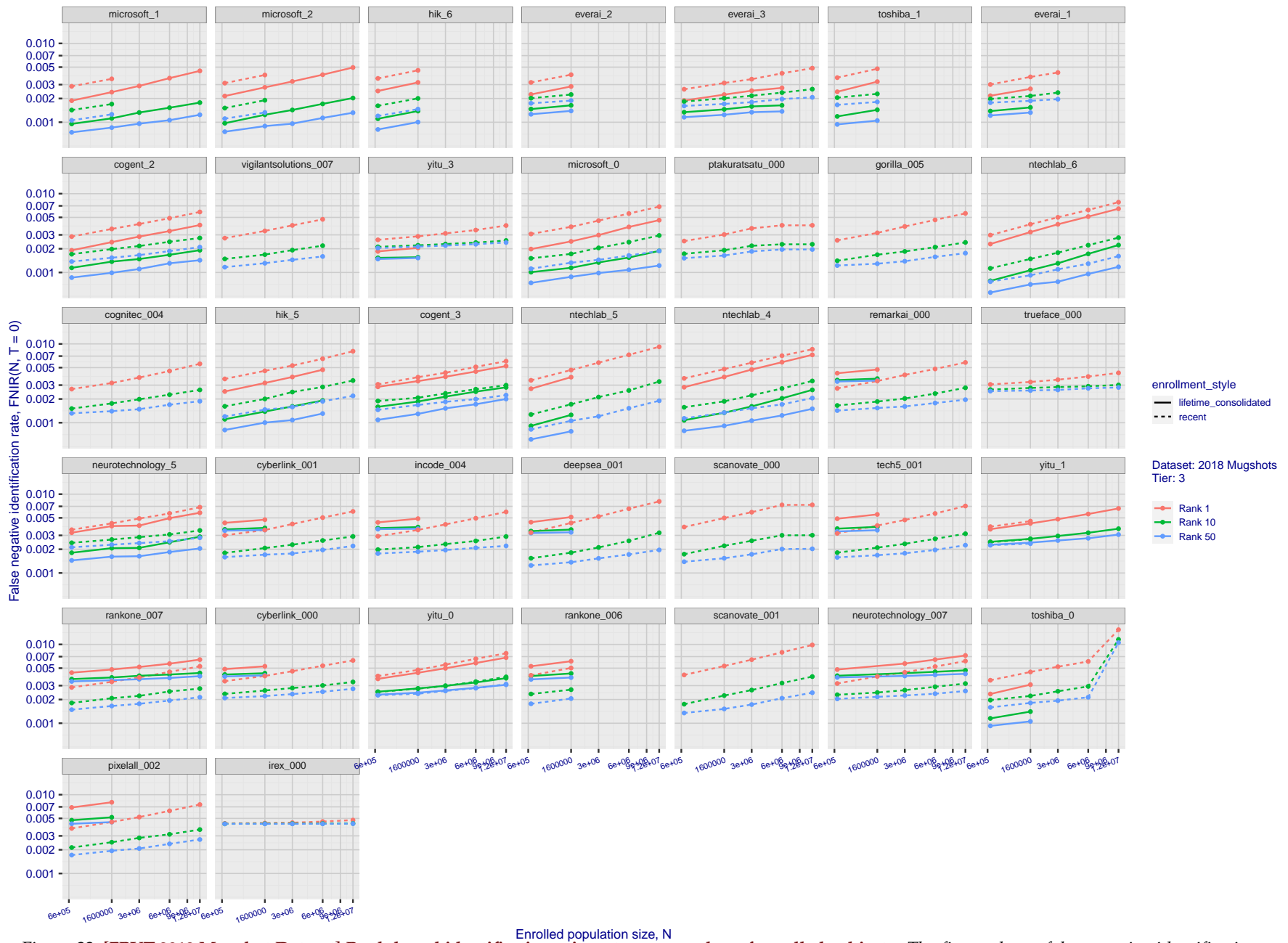


Figure 22: [FRVT-2018 Mugshot Dataset] Rank-based identification miss rates vs. number of enrolled subjects. The figure shows false negative identification rates,  $\text{FNIR}(N, R)$ , across various gallery sizes and ranks 1, 10 and 50. The threshold is set to zero, so this metric rewards even weak scoring rank 1 mates. This also means  $\text{FPIR} = 1$ , so any search without an enrolled mate will return non-mated candidates. For clarity, results are sorted and reported into tiers spanning multiple pages, the tiering criteria being rank 1 hit rate on a gallery size of 640 000.

2021/09/21  
09:55:08  
  
 $\text{FNIR}(N, R, T) = \text{False neg. identification rate}$   
 $\text{FPIR}(N, T) = \text{False pos. identification rate}$   
 $N = \text{Num. enrolled subjects}$   
 $R = \text{Num. candidates examined}$   
 $T = \text{Threshold}$   
 $T = 0 \rightarrow \text{Investigation}$   
 $T > 0 \rightarrow \text{Identification}$

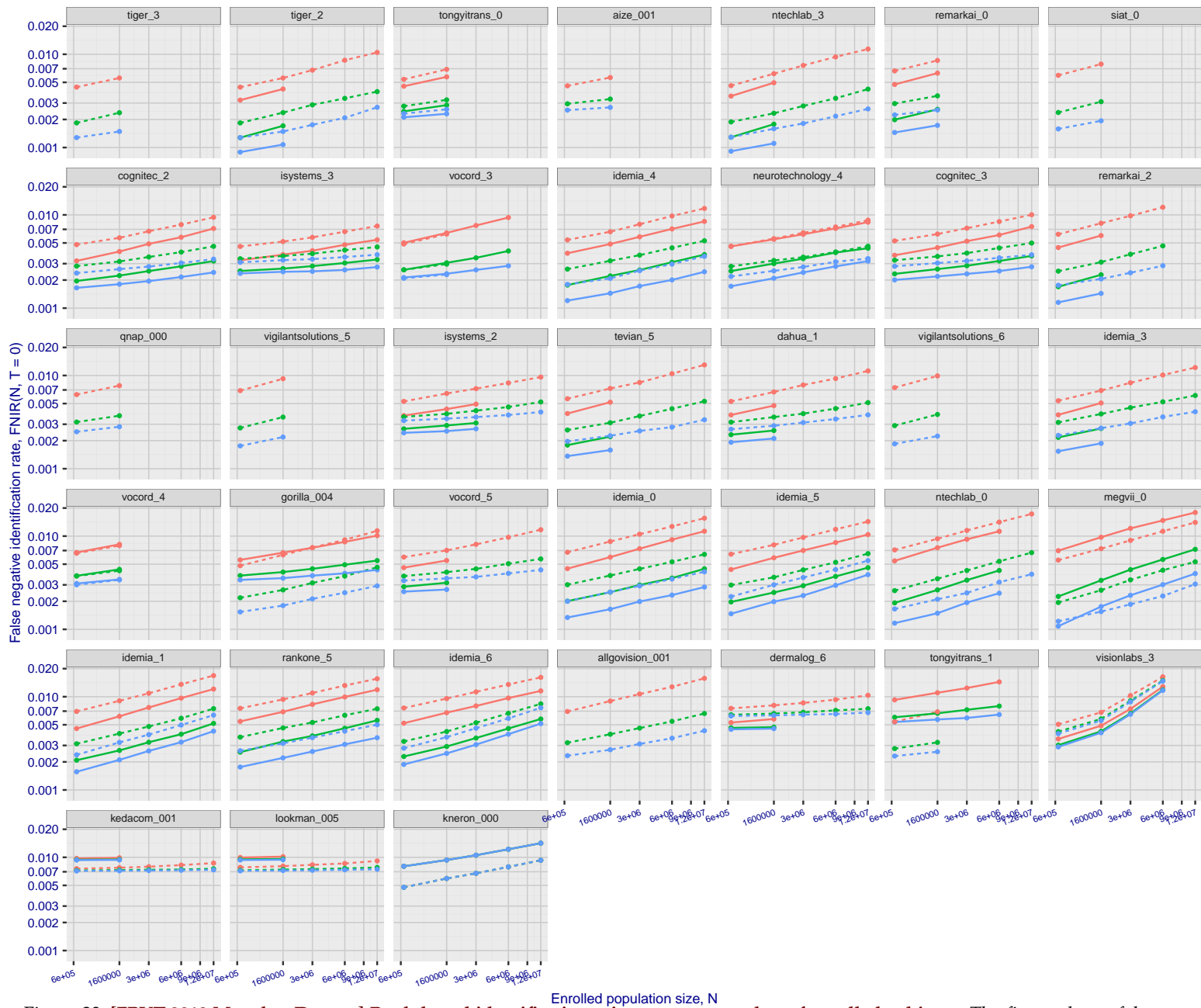
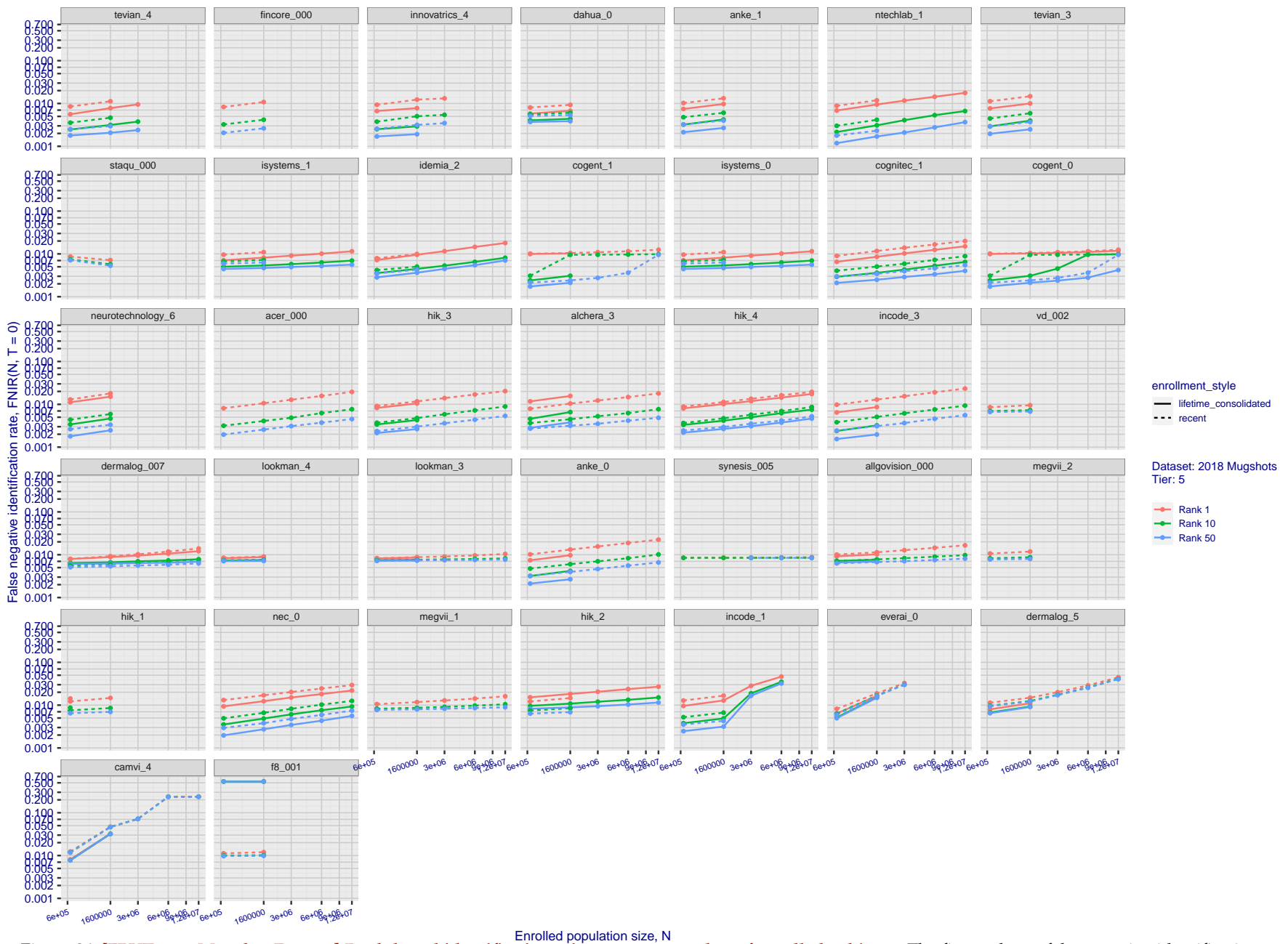


Figure 23: [FRVT-2018 Mugshot Dataset] Rank-based identification miss rates vs. number of enrolled subjects. The figure shows false negative identification rates,  $\text{FNIR}(N, R)$ , across various gallery sizes and ranks 1, 10 and 50. The threshold is set to zero, so this metric rewards even weak scoring rank 1 mates. This also means  $\text{FPIR} = 1$ , so any search without an enrolled mate will return non-mated candidates. For clarity, results are sorted and reported into tiers spanning multiple pages, the tiering criteria being rank 1 hit rate on a gallery size of 640 000.



**Figure 24: [FRVT-2018 Mugshot Dataset] Rank-based identification miss rates vs. number of enrolled subjects.** The figure shows false negative identification rates,  $\text{FNIR}(N, R)$ , across various gallery sizes and ranks 1, 10 and 50. The threshold is set to zero, so this metric rewards even weak scoring rank 1 mates. This also means  $\text{FPIR} = 1$ , so any search without an enrolled mate will return non-mated candidates. For clarity, results are sorted and reported into tiers spanning multiple pages, the tiering criteria being rank 1 hit rate on a gallery size of 640 000.

2021/09/21

09:55:08

FNIR(N, R, T) = False neg. identification rate

FPPIR(N, T) = False pos. identification rate

N = Num. enrolled subjects

T = Threshold

T = 0 → Investigation

T &gt; 0 → Identification

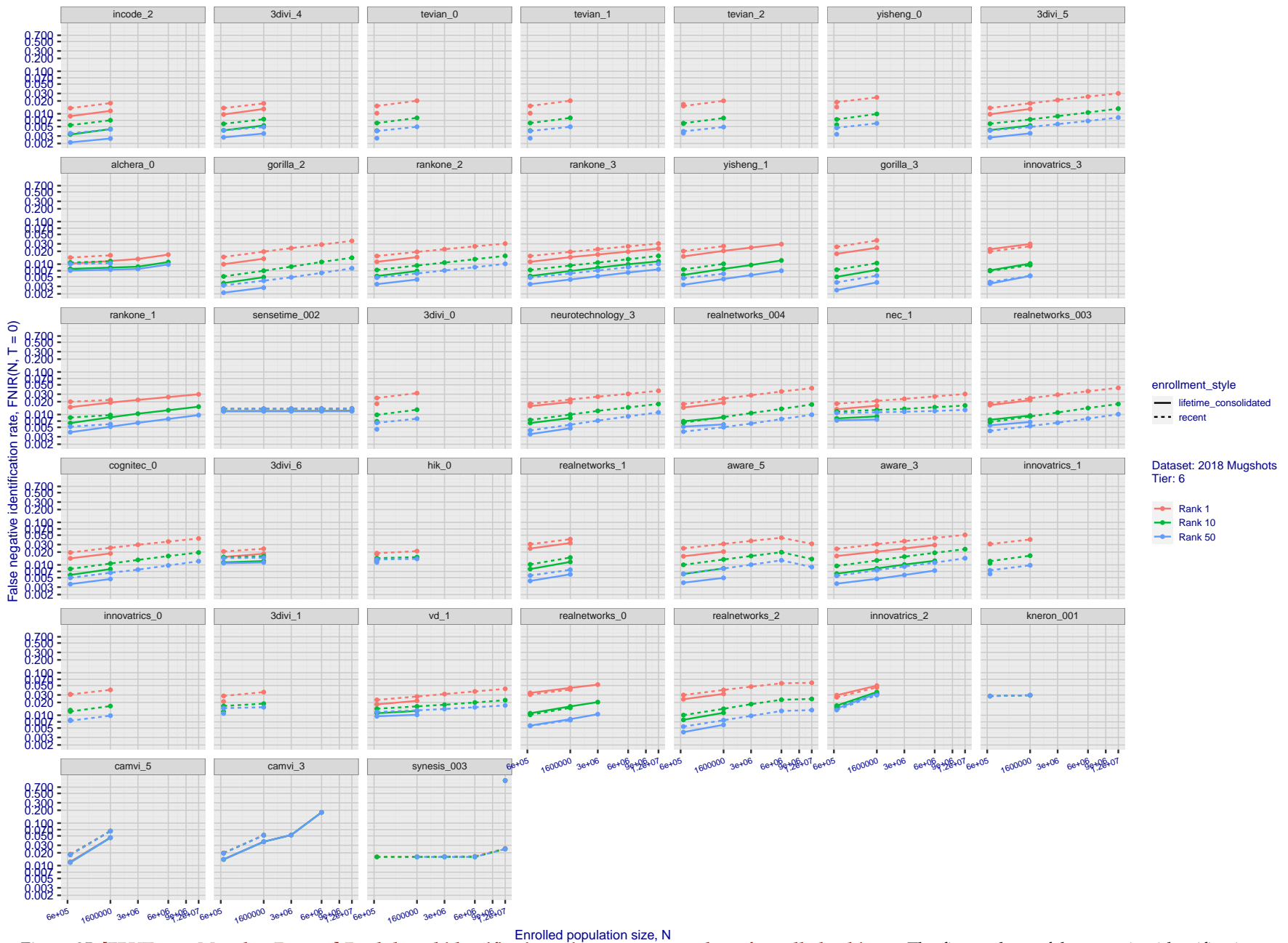


**Figure 25: [FRVT-2018 Mugshot Dataset] Rank-based identification miss rates vs. number of enrolled subjects.** The figure shows false negative identification rates,  $\text{FNIR}(N, R)$ , across various gallery sizes and ranks 1, 10 and 50. The threshold is set to zero, so this metric rewards even weak scoring rank 1 mates. This also means  $\text{FPIR} = 1$ , so any search without an enrolled mate will return non-mated candidates. For clarity, results are sorted and reported into tiers spanning multiple pages, the tiering criteria being rank 1 hit rate on a gallery size of 640 000.

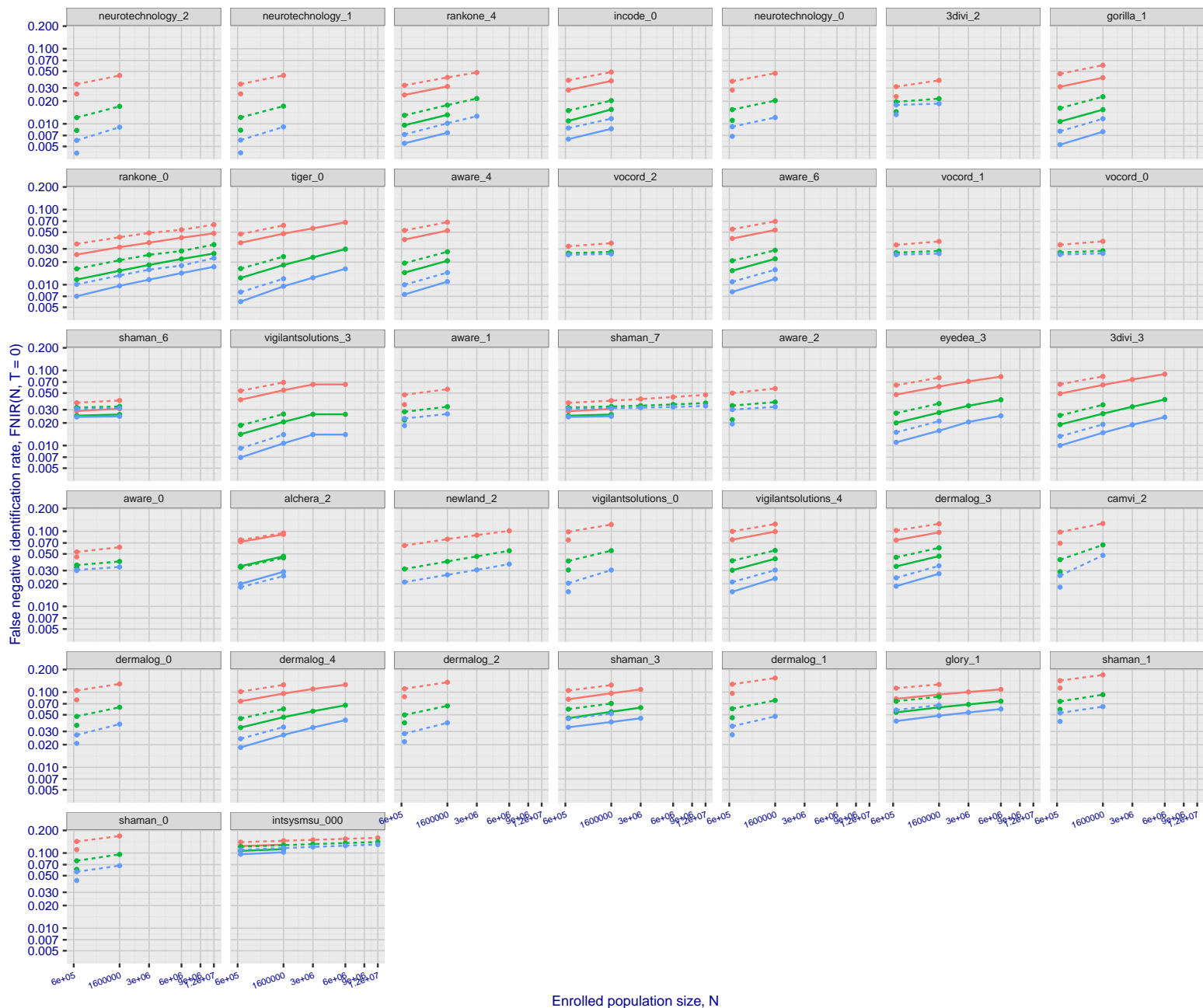


Figure 26: [FRVT-2018 Mugshot Dataset] Rank-based identification miss rates vs. number of enrolled subjects. The figure shows false negative identification rates,  $\text{FNIR}(N, R)$ , across various gallery sizes and ranks 1, 10 and 50. The threshold is set to zero, so this metric rewards even weak scoring rank 1 mates. This also means  $\text{FPIR} = 1$ , so any search without an enrolled mate will return non-mated candidates. For clarity, results are sorted and reported into tiers spanning multiple pages, the tiering criteria being rank 1 hit rate on a gallery size of 640 000.

2021 / 09 / 21

09:55:08

 $\text{FNIR}(N, R, T) =$   
False neg. identification rate $N = \text{Num. enrolled subjects}$   
 $R = \text{Num. candidates examined}$  $T = \text{Threshold}$  $T = 0 \rightarrow \text{Investigation}$   
 $T > 0 \rightarrow \text{Identification}$

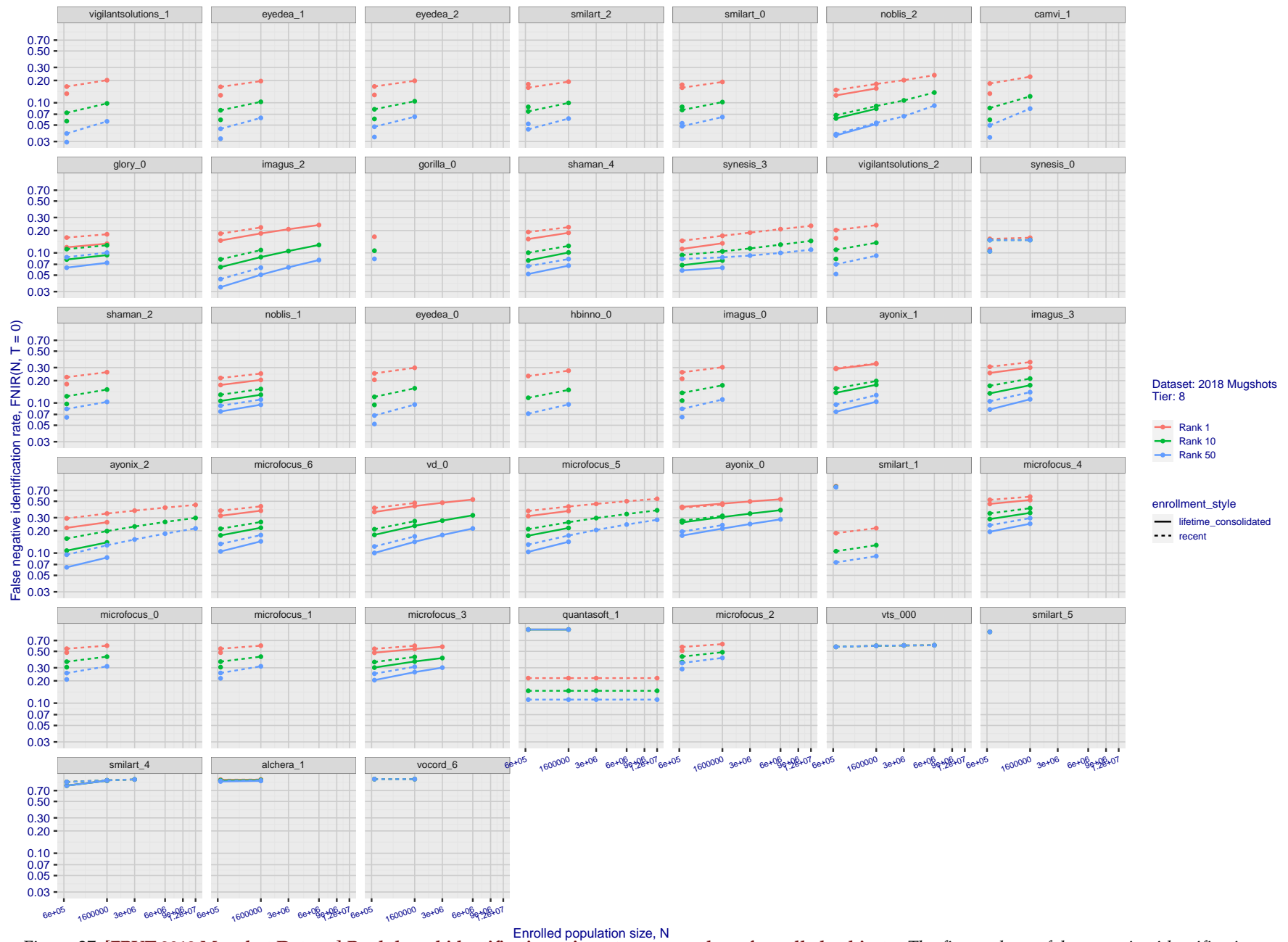


Figure 27: [FRVT-2018 Mugshot Dataset] Rank-based identification miss rates vs. number of enrolled subjects. The figure shows false negative identification rates,  $\text{FNIR}(N, R)$ , across various gallery sizes and ranks 1, 10 and 50. The threshold is set to zero, so this metric rewards even weak scoring rank 1 mates. This also means  $\text{FPIR} = 1$ , so any search without an enrolled mate will return non-mated candidates. For clarity, results are sorted and reported into tiers spanning multiple pages, the tiering criteria being rank 1 hit rate on a gallery size of 640 000.

2021/09/21

09:55:08

FNIR( $N, R, T = 0$ ) = False neg. identification rate $N = \text{Num. enrolled subjects}$ 

T = Threshold

 $T = 0 \rightarrow \text{Investigation}$  $T > 0 \rightarrow \text{Identification}$

---

2021/09/21  
09:55:08

FNIR(N, R, T) = False neg. identification rate  
FPTR(N, T) = False pos. identification rate

N = Num. enrolled subjects  
R = Num. candidates examined

T = Threshold  
T > 0 → Identification

T = 0 → Investigation

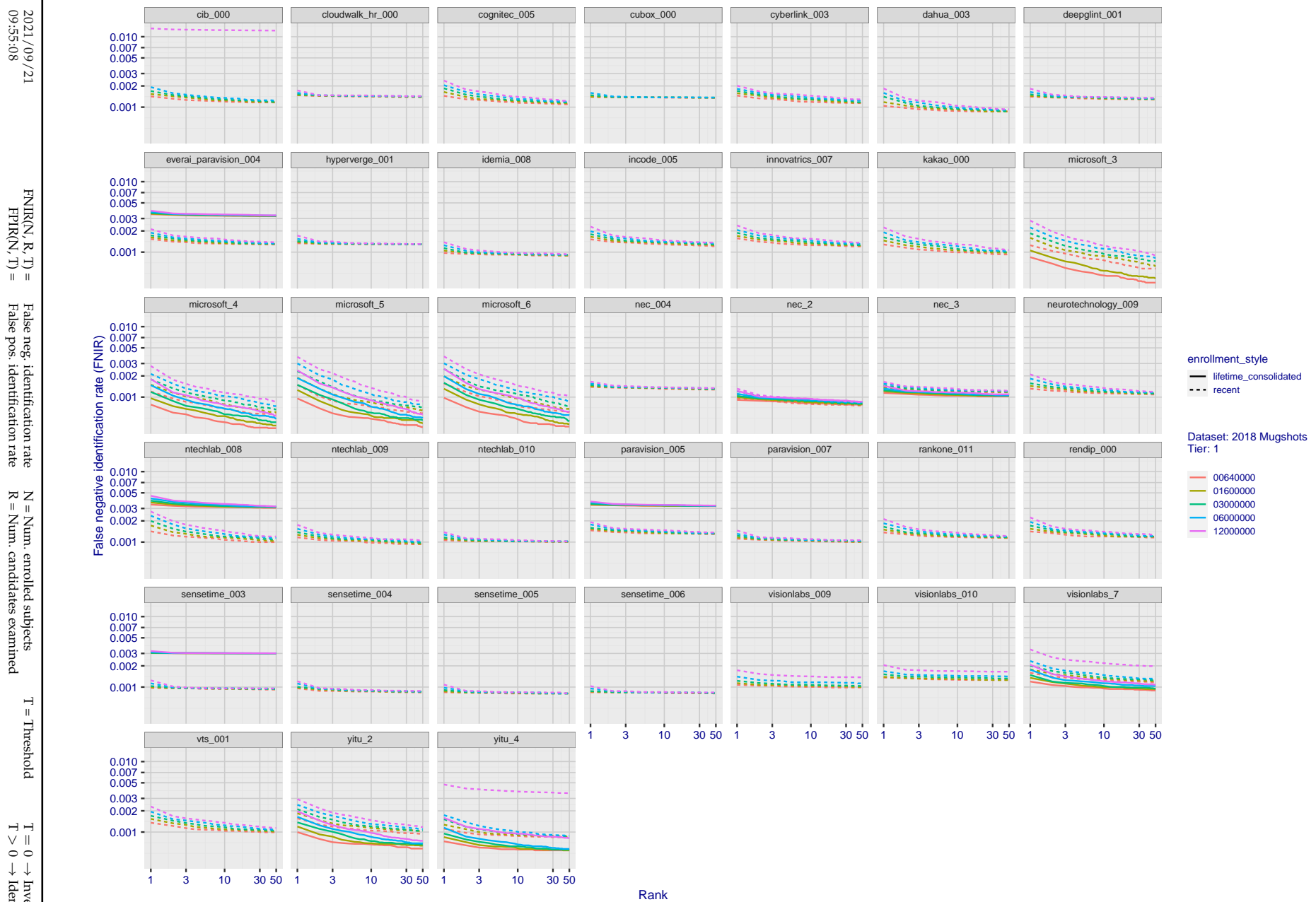


**Figure 28: [FRVT-2018 Mugshot Dataset] Rank-based identification miss rates vs. rank.** The figure shows false negative identification rates (FNIR) for ranks up to 50. This metric is appropriate to investigational applications where human reviewers will adjudicate sorted candidate lists. Note that with threshold set to zero, FPIR = 1, i.e. any search without an enrolled mate will return non-mated candidates. Results are sorted and reported into tiers for clarity, with the tiering criteria being rank 1 hit rate on a gallery size of N = 640 000 subjects.

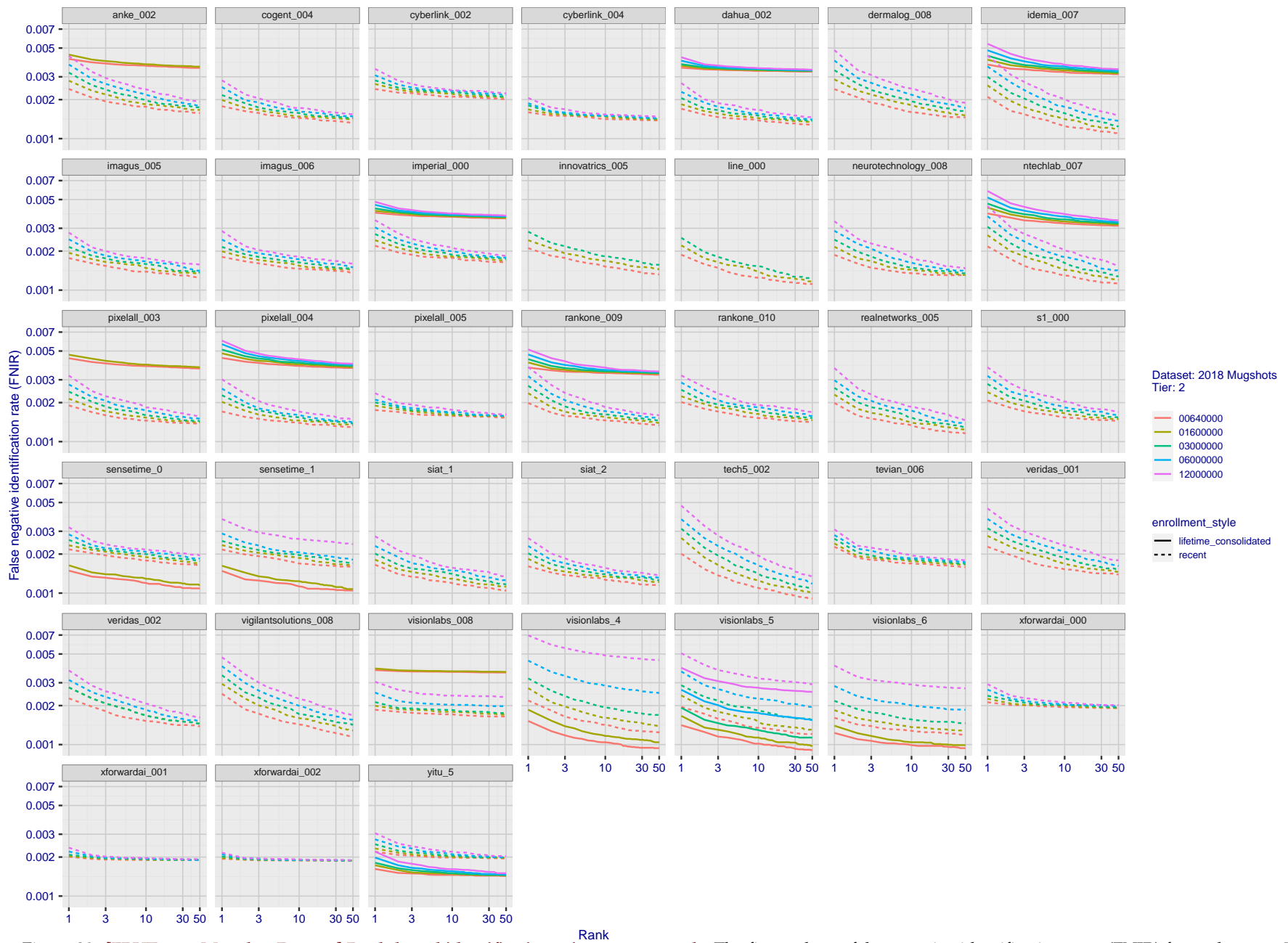
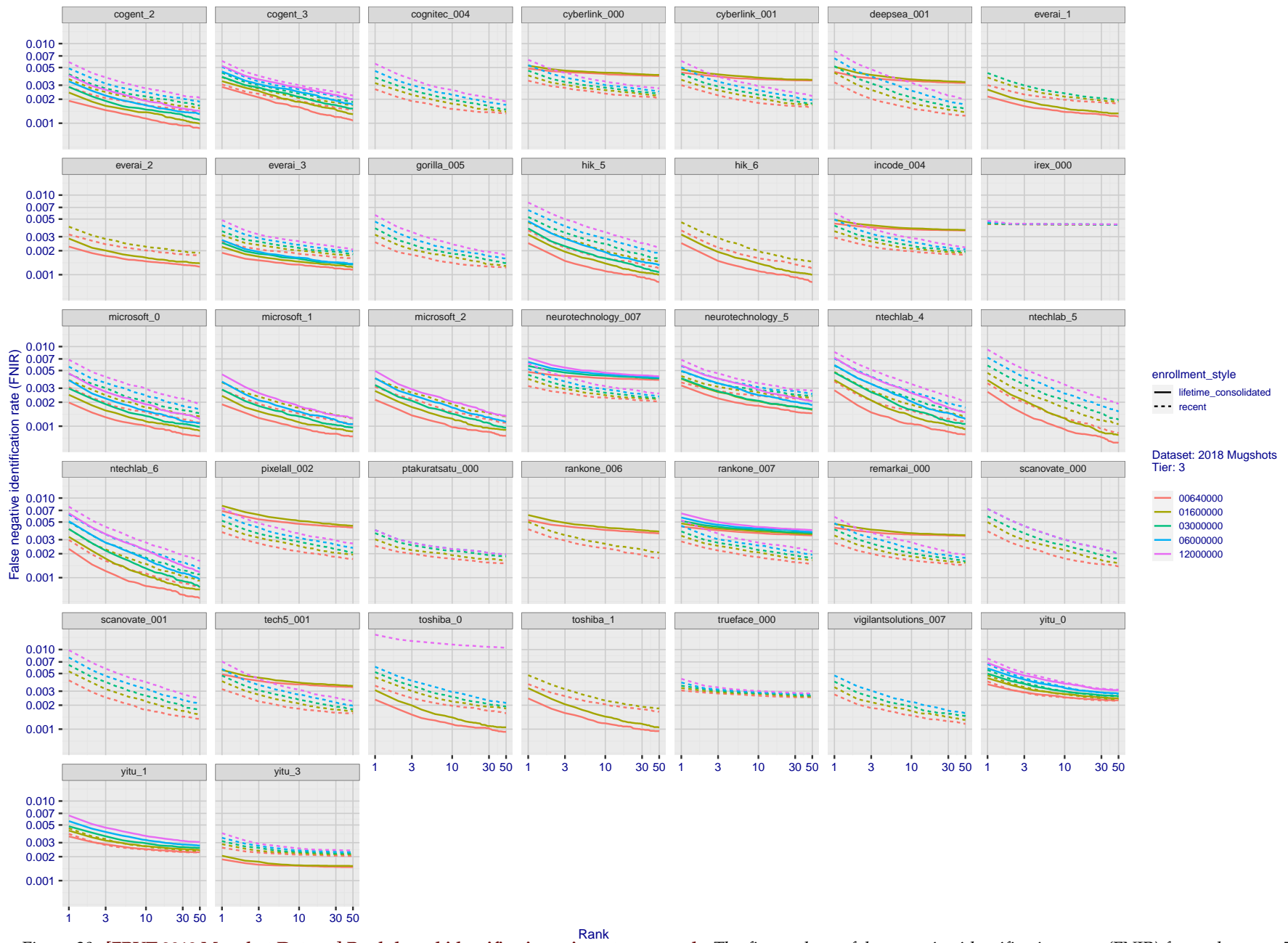
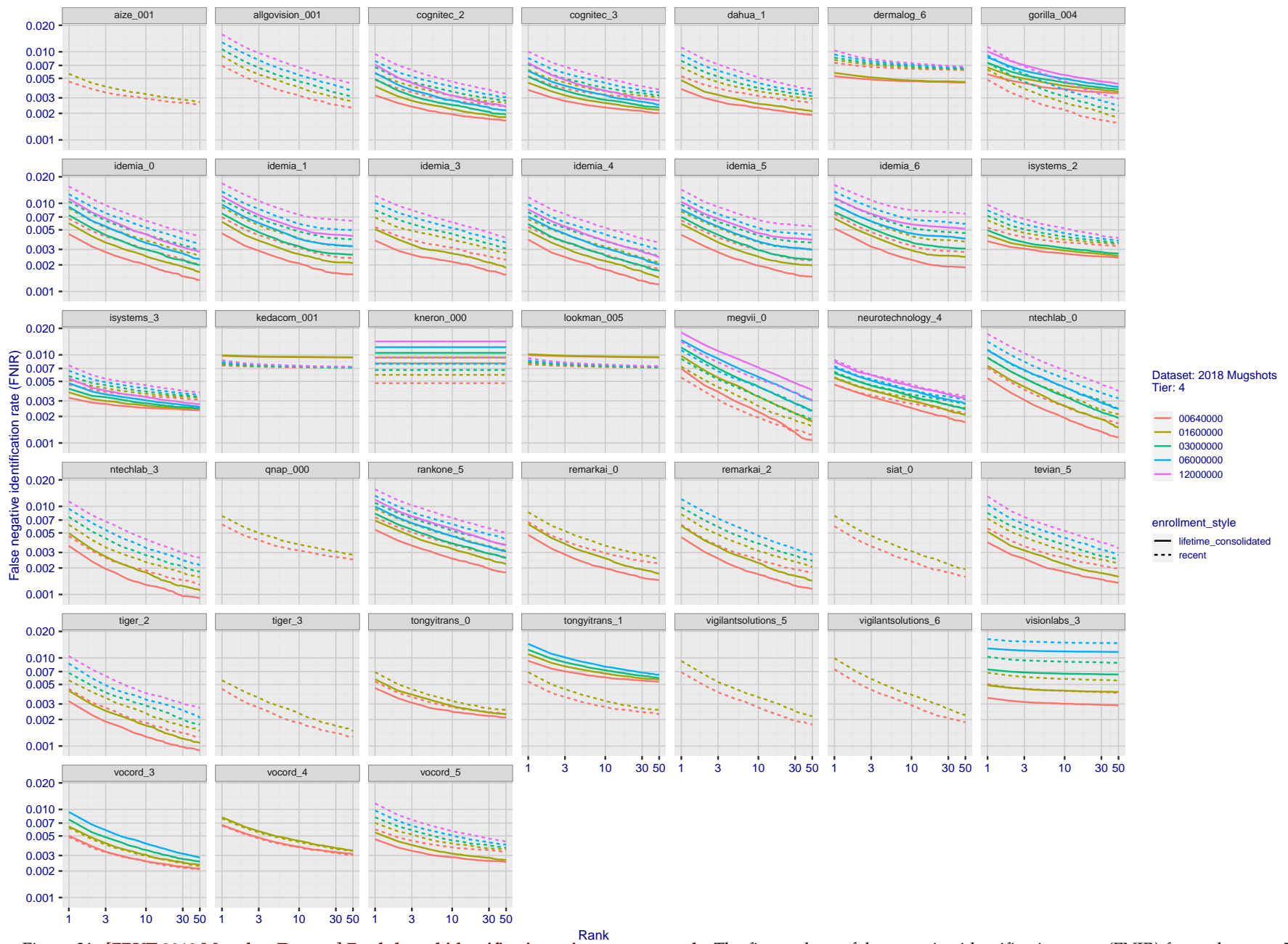


Figure 29: [FRVT-2018 Mugshot Dataset] Rank-based identification miss rates vs. rank. The figure shows false negative identification rates (FNIR) for ranks up to 50. This metric is appropriate to investigational applications where human reviewers will adjudicate sorted candidate lists. Note that with threshold set to zero, FPIR = 1, i.e. any search without an enrolled mate will return non-mated candidates. Results are sorted and reported into tiers for clarity, with the tiering criteria being rank 1 hit rate on a gallery size of  $N = 640\,000$  subjects.



**Figure 30: [FRVT-2018 Mugshot Dataset] Rank-based identification miss rates vs. rank.** The figure shows false negative identification rates (FNIR) for ranks up to 50. This metric is appropriate to investigational applications where human reviewers will adjudicate sorted candidate lists. Note that with threshold set to zero, FPIR = 1, i.e. any search without an enrolled mate will return non-mated candidates. Results are sorted and reported into tiers for clarity, with the tiering criteria being rank 1 hit rate on a gallery size of N = 640 000 subjects.



**Figure 31: [FRVT-2018 Mugshot Dataset] Rank-based identification miss rates vs. rank.** The figure shows false negative identification rates (FNIR) for ranks up to 50. This metric is appropriate to investigational applications where human reviewers will adjudicate sorted candidate lists. Note that with threshold set to zero, FPIR = 1, i.e. any search without an enrolled mate will return non-mated candidates. Results are sorted and reported into tiers for clarity, with the tiering criteria being rank 1 hit rate on a gallery size of N = 640 000 subjects.

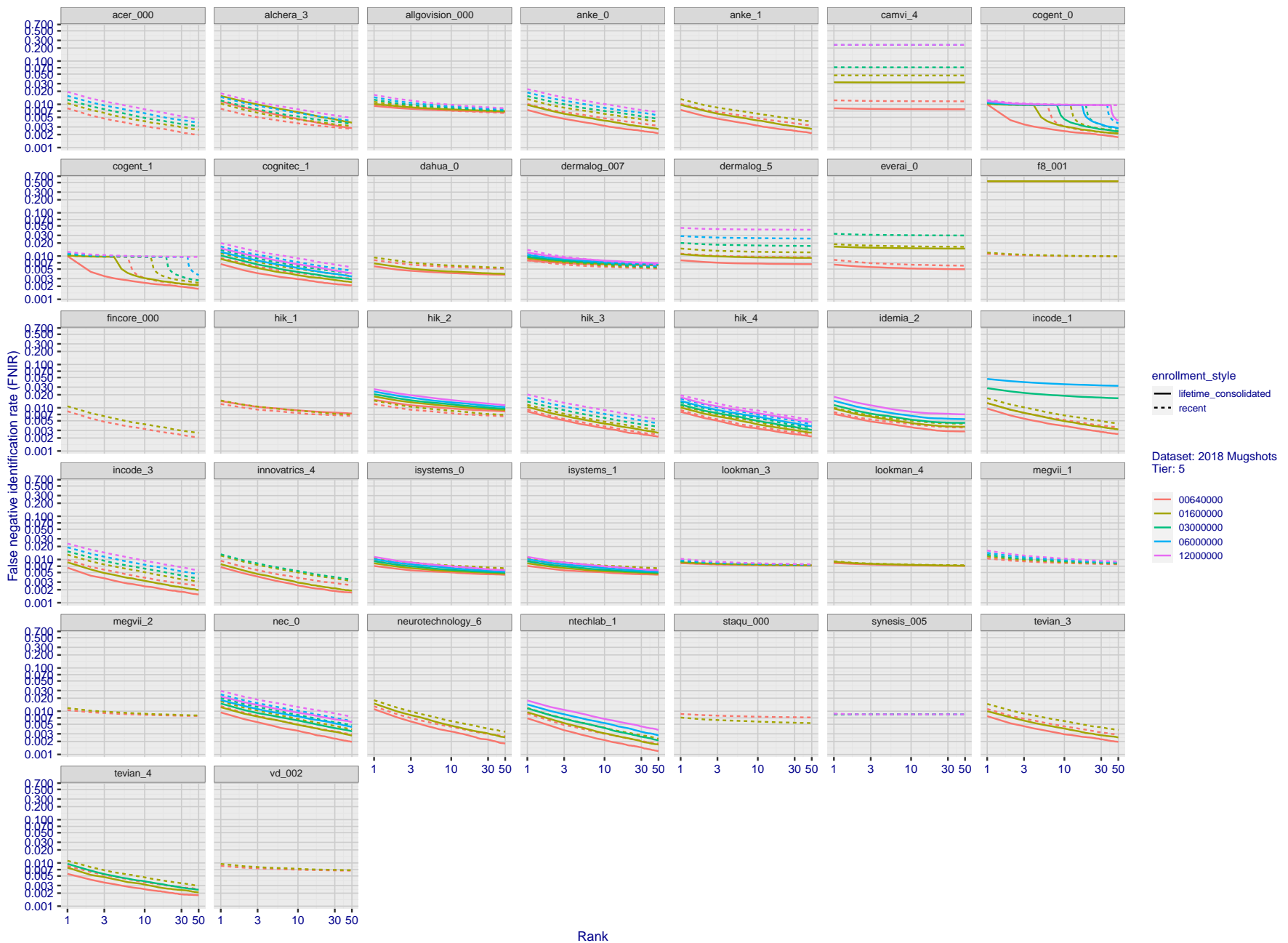


**Figure 32: [FRVT-2018 Mugshot Dataset] Rank-based identification miss rates vs. rank.** The figure shows false negative identification rates (FNIR) for ranks up to 50. This metric is appropriate to investigational applications where human reviewers will adjudicate sorted candidate lists. Note that with threshold set to zero, FPFR = 1, i.e. any search without an enrolled mate will return non-mated candidates. Results are sorted and reported into tiers for clarity, with the tiering criteria being rank 1 hit rate on a gallery size of N = 640 000 subjects.

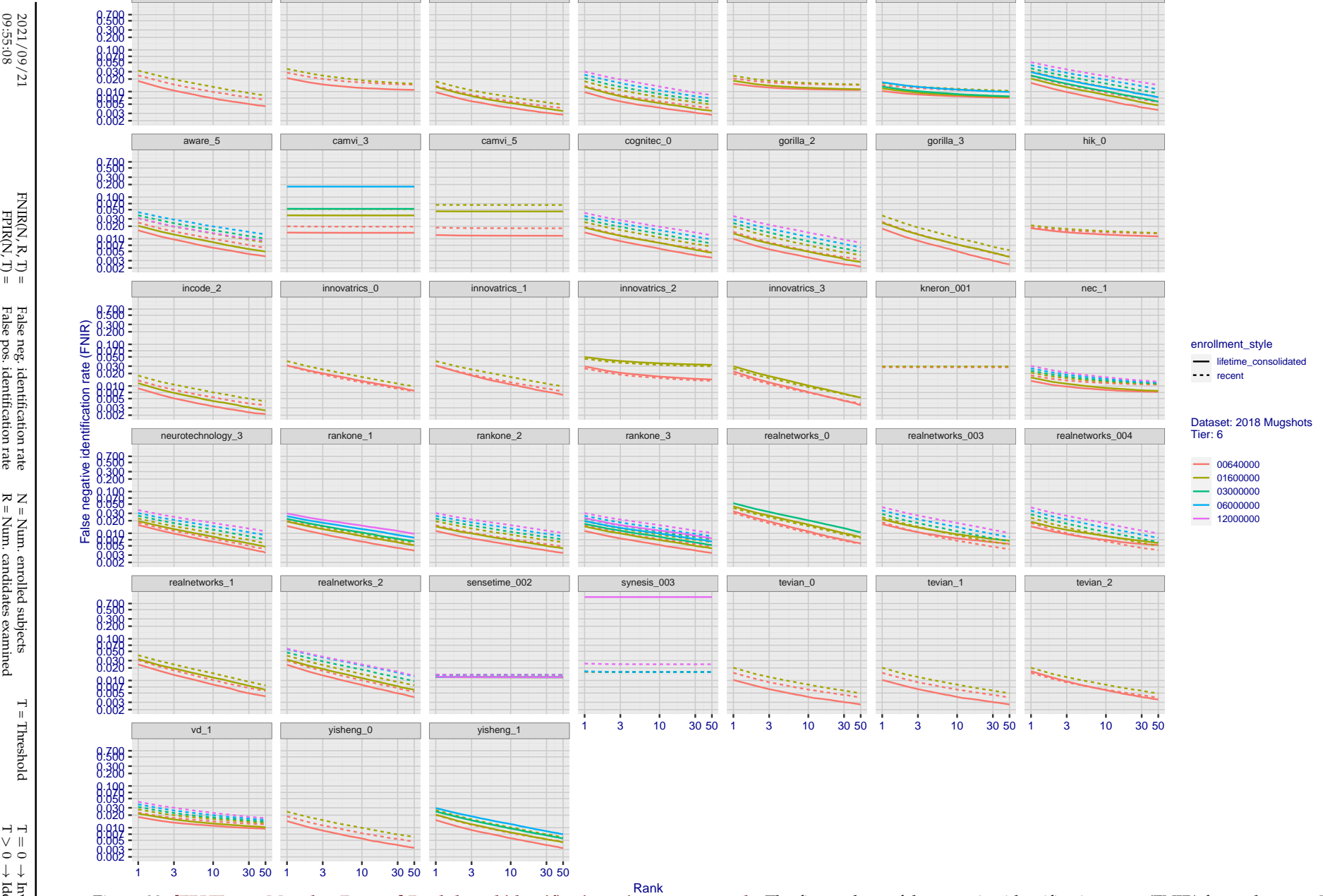


**Figure 33: [FRVT-2018 Mugshot Dataset] Rank-based identification miss rates vs. rank.** The figure shows false negative identification rates (FNIR) for ranks up to 50. This metric is appropriate to investigational applications where human reviewers will adjudicate sorted candidate lists. Note that with threshold set to zero, FPIR = 1, i.e. any search without an enrolled mate will return non-mated candidates. Results are sorted and reported into tiers for clarity, with the tiering criteria being rank 1 hit rate on a gallery size of N = 640 000 subjects.

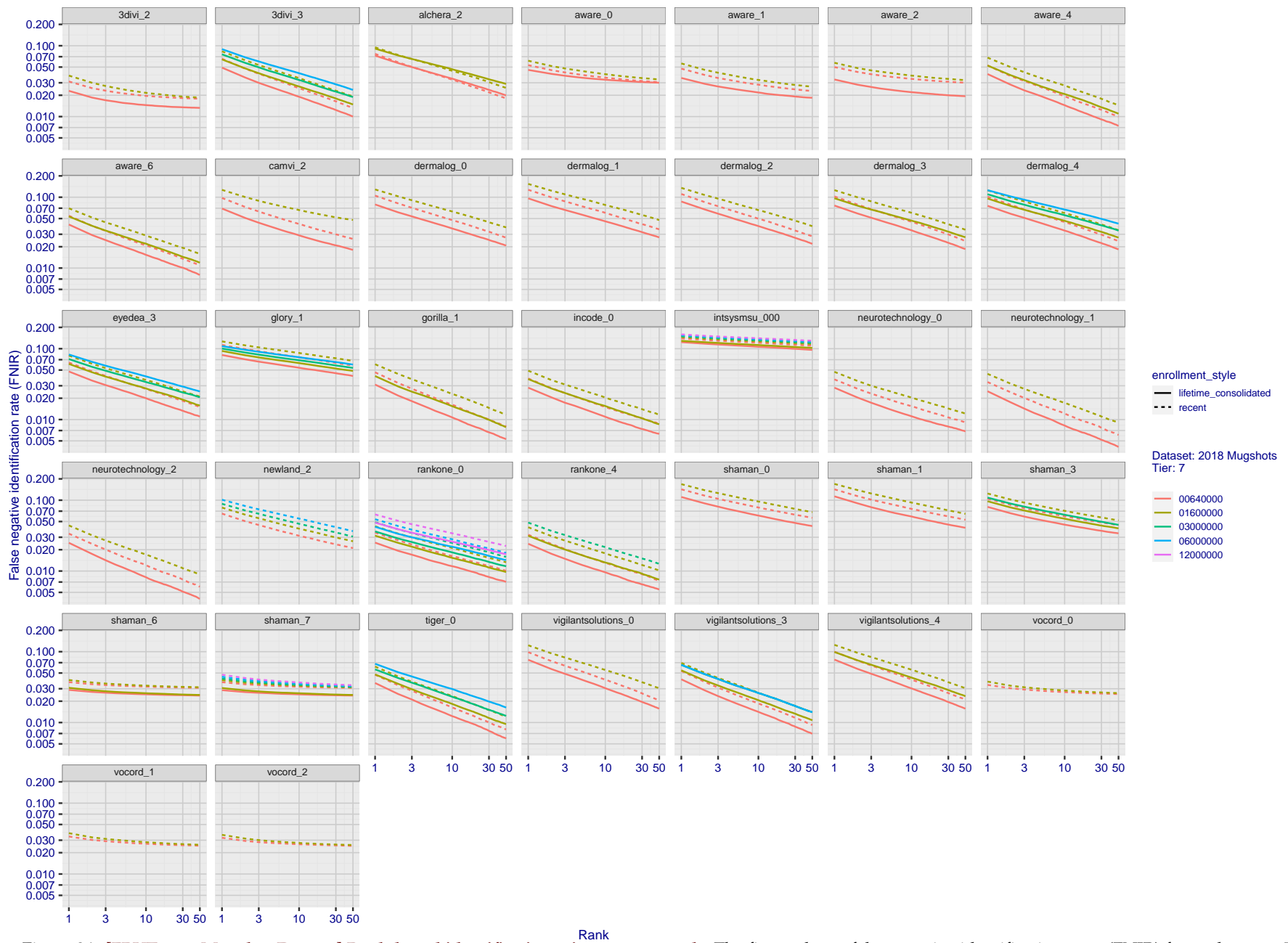


Figure 34: [FRVT-2018 Mugshot Dataset] Rank-based identification miss rates vs. rank. The figure shows false negative identification rates (FNIR) for ranks up to 50. This metric is appropriate to investigational applications where human reviewers will adjudicate sorted candidate lists. Note that with threshold set to zero, FPIR = 1, i.e. any search without an enrolled mate will return non-mated candidates. Results are sorted and reported into tiers for clarity, with the tiering criteria being rank 1 hit rate on a gallery size of  $N = 640\,000$  subjects.

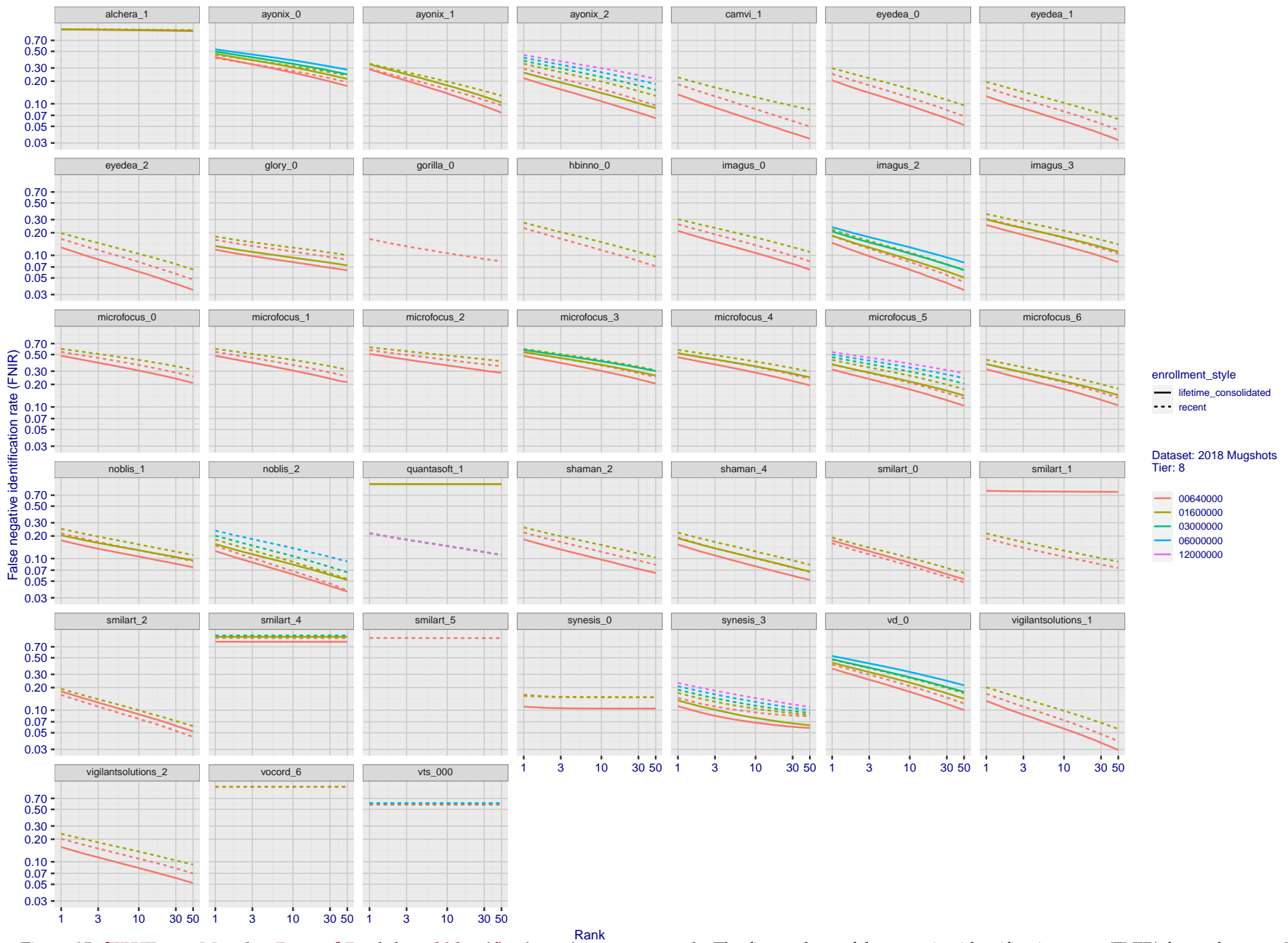


Figure 35: [FRVT-2018 Mugshot Dataset] Rank-based identification miss rates vs. rank. The figure shows false negative identification rates (FNIR) for ranks up to 50. This metric is appropriate to investigational applications where human reviewers will adjudicate sorted candidate lists. Note that with threshold set to zero, FPIR = 1, i.e. any search without an enrolled mate will return non-mated candidates. Results are sorted and reported into tiers for clarity, with the tiering criteria being rank 1 hit rate on a gallery size of N = 640 000 subjects.

2021/09/21 09:55:08	$\text{FNIR}(N, R, T) =$ $\text{FPTR}(N, T) =$	False neg. identification rate False pos. identification rate	$N =$ Num. enrolled subjects $R =$ Num. candidates examined	$T =$ Threshold $T > 0 \rightarrow$ Identification	$T = 0 \rightarrow$ Investigation
------------------------	---	--	--	---	-----------------------------------

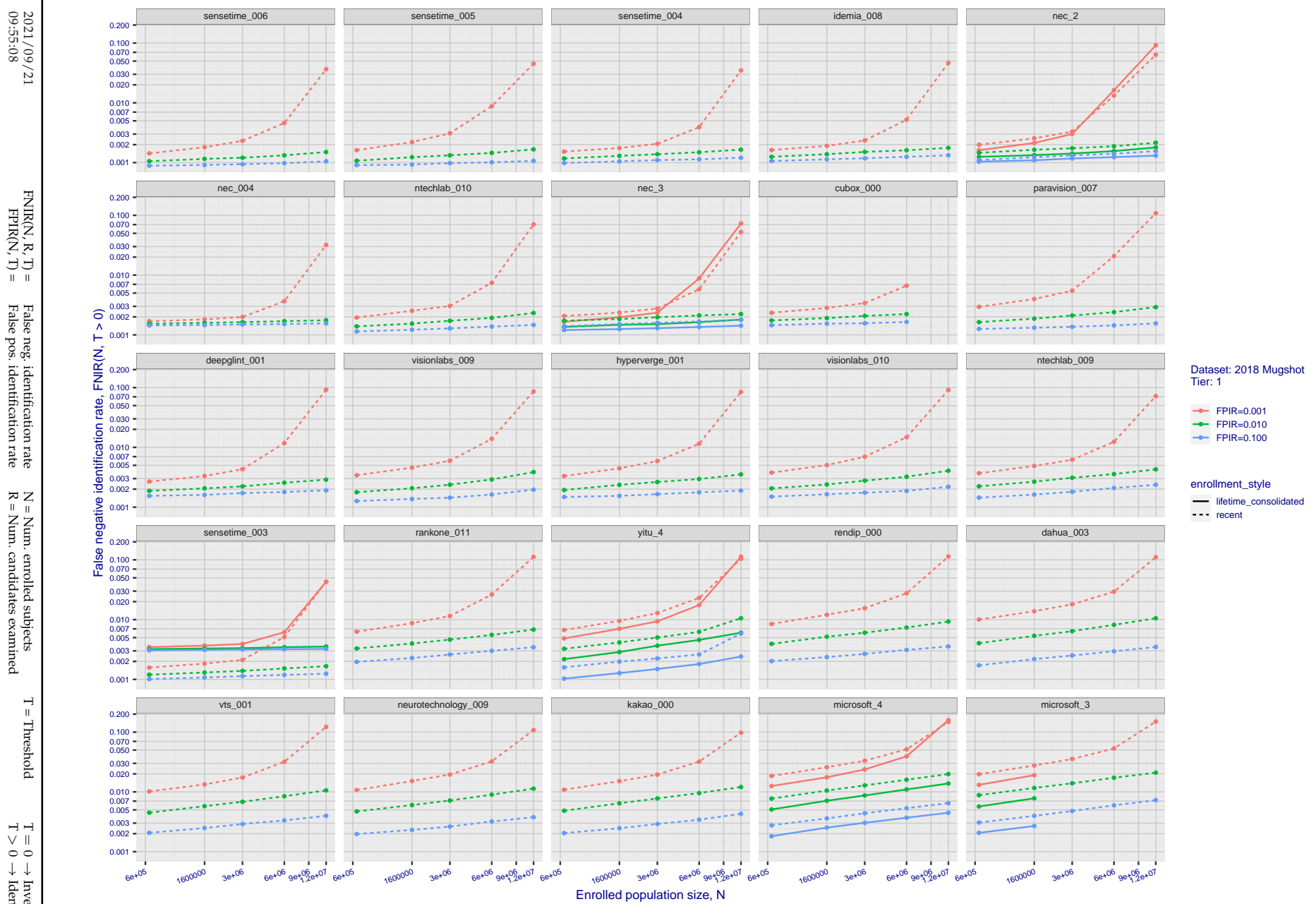


Figure 36: [FRVT-2018 Mugshot Dataset] Threshold-based identification miss rates vs. number of enrolled subjects. The figure shows  $\text{FNIR}(N, T)$  across various gallery sizes when the threshold is set to achieve the given FPIRs. The rank criterion is irrelevant at high thresholds as mates are always at rank 1. The results are computed from the trials listed in rows 1-10 of Table 1. Less accurate algorithms were not run on large  $N$ , so results are missing. For clarity, results are sorted and reported into tiers spanning multiple pages. The tiering criteria is complicated: First paging by  $\text{FNIR}(N_b, 1, 0)$ , then sorting by median  $\text{FNIR}(N_b, T)$ ,  $N_b = 640\,000$ .

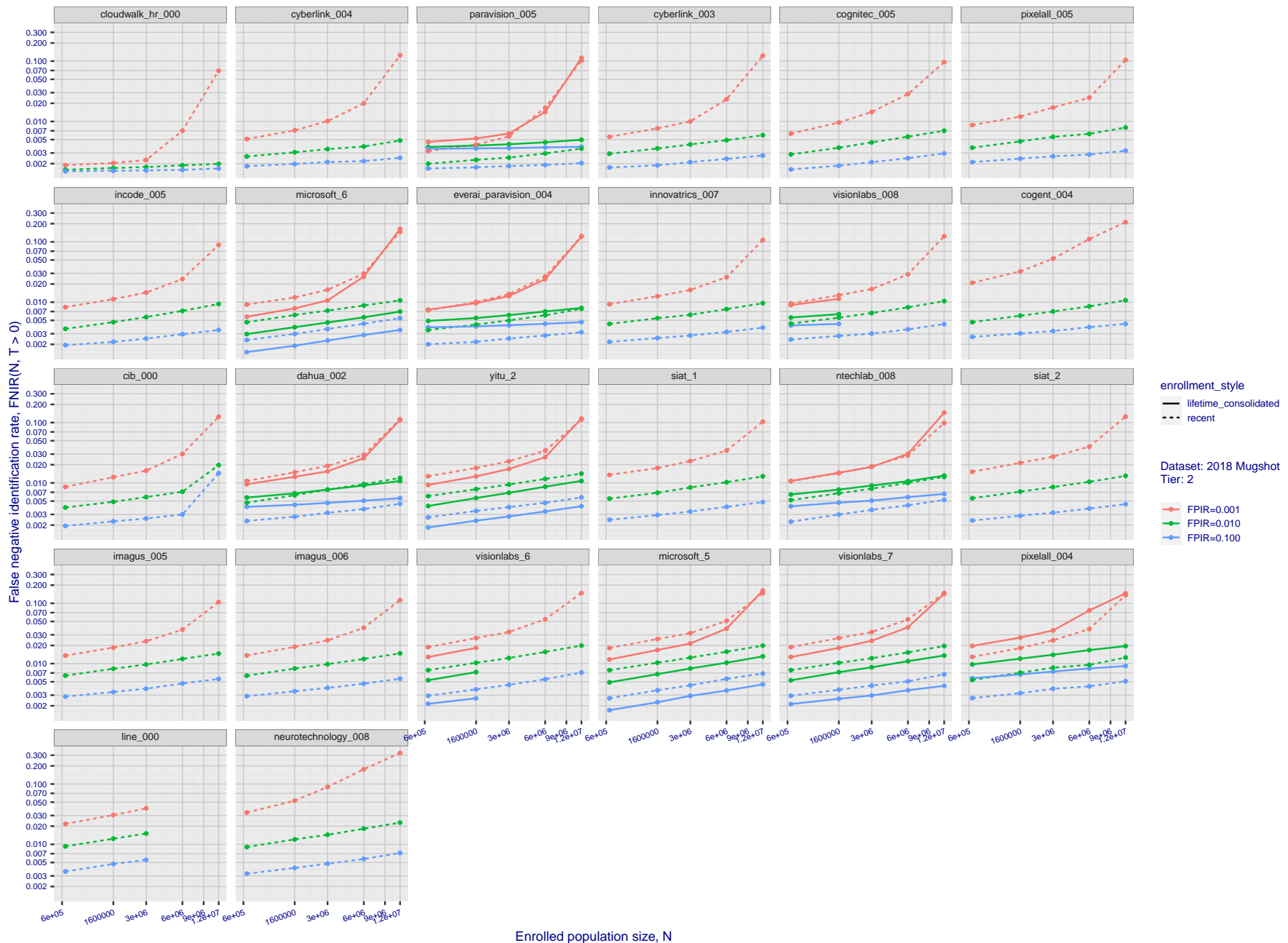


Figure 37: [FRVT-2018 Mugshot Dataset] Threshold-based identification miss rates vs. number of enrolled subjects. The figure shows  $\text{FNIR}(N, T)$  across various gallery sizes when the threshold is set to achieve the given FPIRs. The rank criterion is irrelevant at high thresholds as mates are always at rank 1. The results are computed from the trials listed in rows 1-10 of Table 1. Less accurate algorithms were not run on large  $N$ , so results are missing. For clarity, results are sorted and reported into tiers spanning multiple pages. The tiering criteria is complicated: First paging by  $\text{FNIR}(N_b, 1, 0)$ , then sorting by median  $\text{FNIR}(N_b, T)$ ,  $N_b = 640\,000$ .

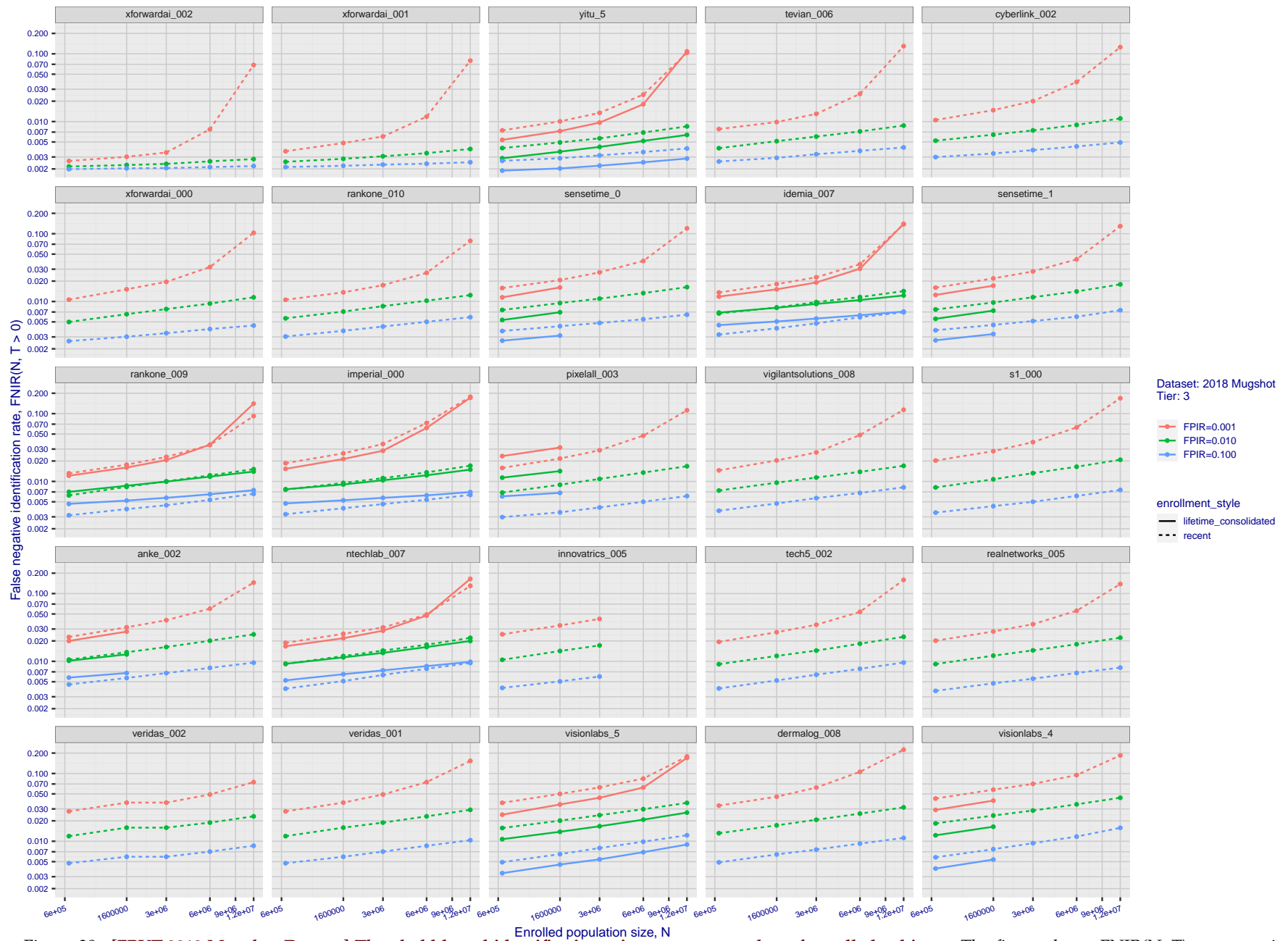
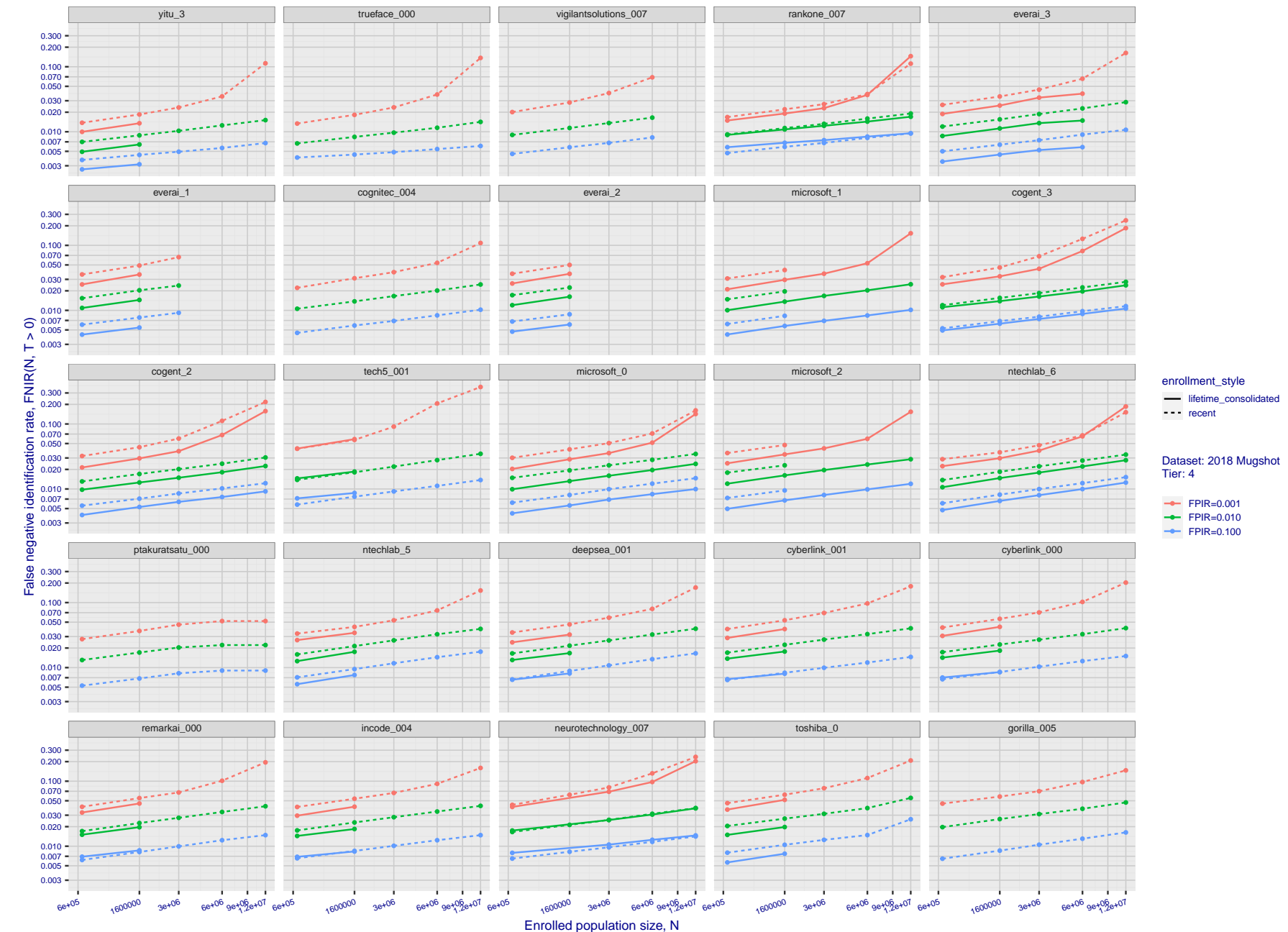
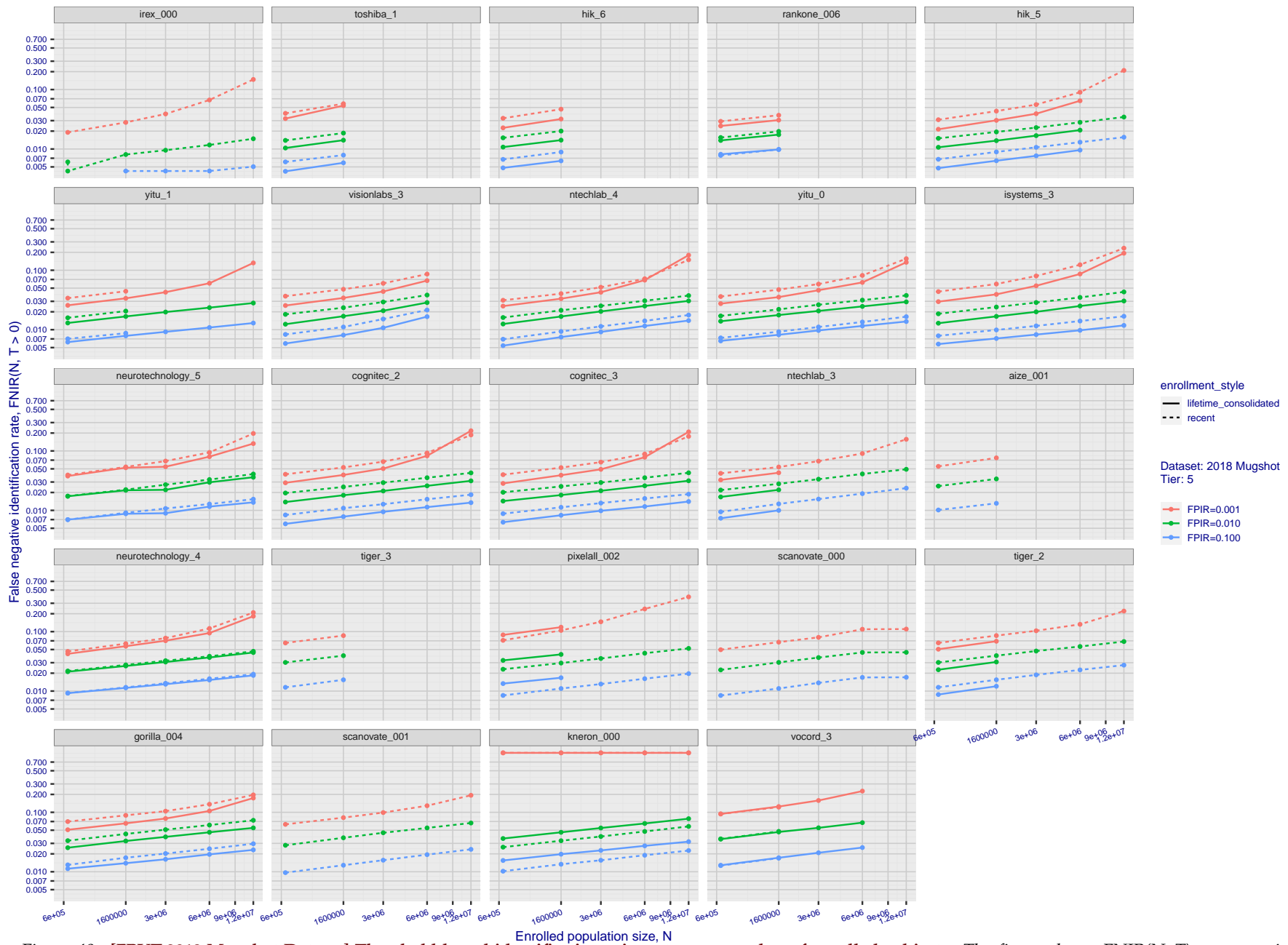


Figure 38: [FRVT-2018 Mugshot Dataset] Threshold-based identification miss rates vs. number of enrolled subjects. The figure shows FNIR( $N, T$ ) across various gallery sizes when the threshold is set to achieve the given FPIRs. The rank criterion is irrelevant at high thresholds as mates are always at rank 1. The results are computed from the trials listed in rows 1-10 of Table 1. Less accurate algorithms were not run on large  $N$ , so results are missing. For clarity, results are sorted and reported into tiers spanning multiple pages. The tiering criteria is complicated: First paging by FNIR( $N_b, 1, 0$ ), then sorting by median FNIR( $N_b, T$ ),  $N_b = 640\,000$ .



**Figure 39: [FRVT-2018 Mugshot Dataset] Threshold-based identification miss rates vs. number of enrolled subjects.** The figure shows  $\text{FNIR}(N, T)$  across various gallery sizes when the threshold is set to achieve the given FPIRs. The rank criterion is irrelevant at high thresholds as mates are always at rank 1. The results are computed from the trials listed in rows 1-10 of Table 1. Less accurate algorithms were not run on large  $N$ , so results are missing. For clarity, results are sorted and reported into tiers spanning multiple pages. The tiering criteria is complicated: First paging by  $\text{FNIR}(N_b, 1, 0)$ , then sorting by median  $\text{FNIR}(N_b, T)$ ,  $N_b = 640\,000$ .

2021 / 09 / 21  
09:55:08FNIR( $N, R, T$ ) = False neg. identification rate  
FPIR( $N, T$ ) = False pos. identification rate $N$  = Num. enrolled subjects  
 $R$  = Num. candidates examined $T$  = Threshold $T = 0 \rightarrow$  Investigation  
 $T > 0 \rightarrow$  Identification



**Figure 40: [FRVT-2018 Mugshot Dataset] Threshold-based identification miss rates vs. number of enrolled subjects.** The figure shows FNIR( $N, T$ ) across various gallery sizes when the threshold is set to achieve the given FPIRs. The rank criterion is irrelevant at high thresholds as mates are always at rank 1. The results are computed from the trials listed in rows 1-10 of Table 1. Less accurate algorithms were not run on large  $N$ , so results are missing. For clarity, results are sorted and reported into tiers spanning multiple pages. The tiering criteria is complicated: First paging by FNIR( $N_b, 1, 0$ ), then sorting by median FNIR( $N_b, T$ ),  $N_b = 640\,000$ .

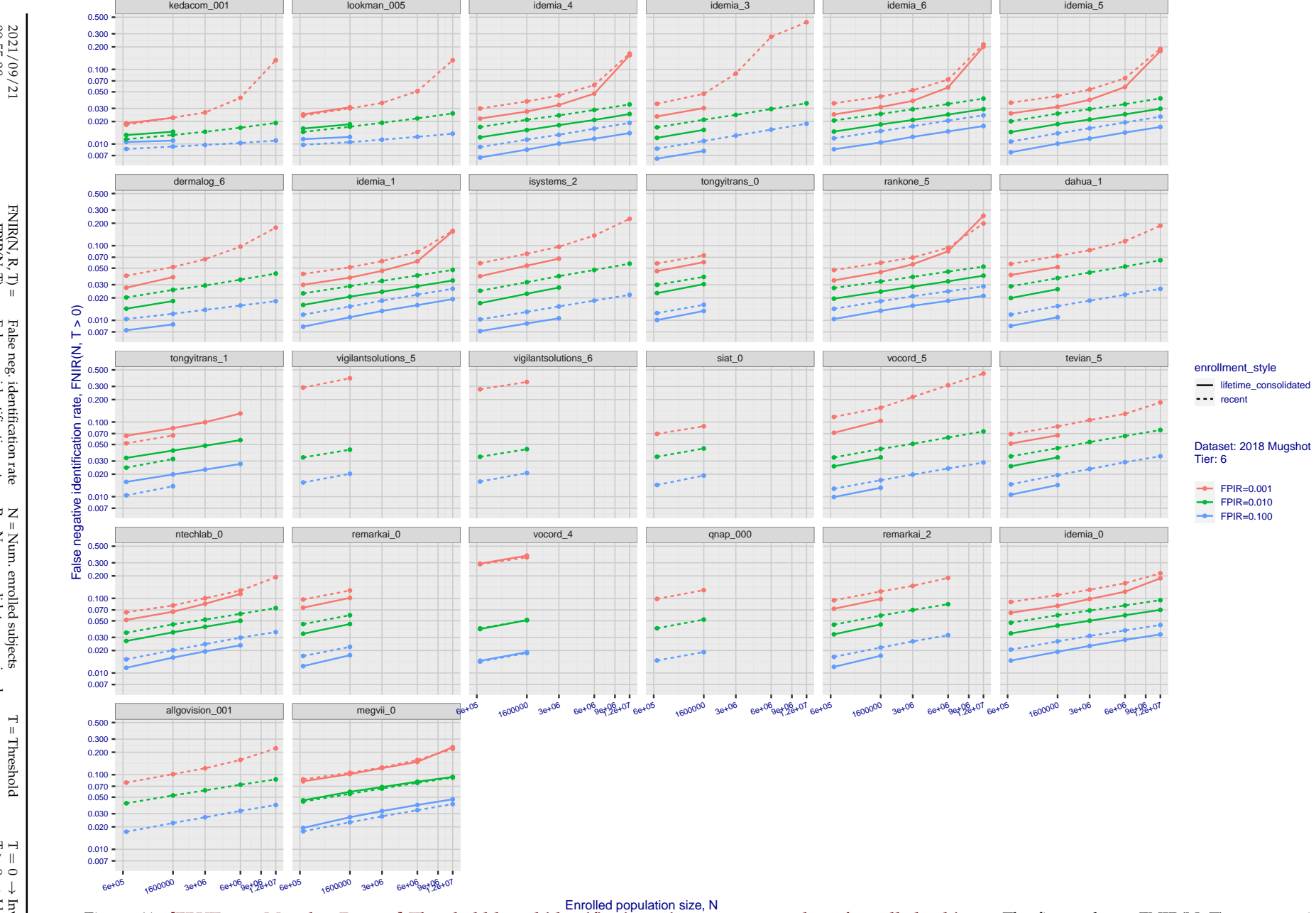


Figure 41: [FRVT-2018 Mugshot Dataset] Threshold-based identification miss rates vs. number of enrolled subjects. The figure shows  $\text{FNIR}(N, T)$  across various gallery sizes when the threshold is set to achieve the given FPIRs. The rank criterion is irrelevant at high thresholds as mates are always at rank 1. The results are computed from the trials listed in rows 1-10 of Table 1. Less accurate algorithms were not run on large  $N$ , so results are missing. For clarity, results are sorted and reported into tiers spanning multiple pages. The tiering criteria is complicated: First paging by  $\text{FNIR}(N_b, 1, 0)$ , then sorting by median  $\text{FNIR}(N_b, T)$ ,  $N_b = 640\,000$ .

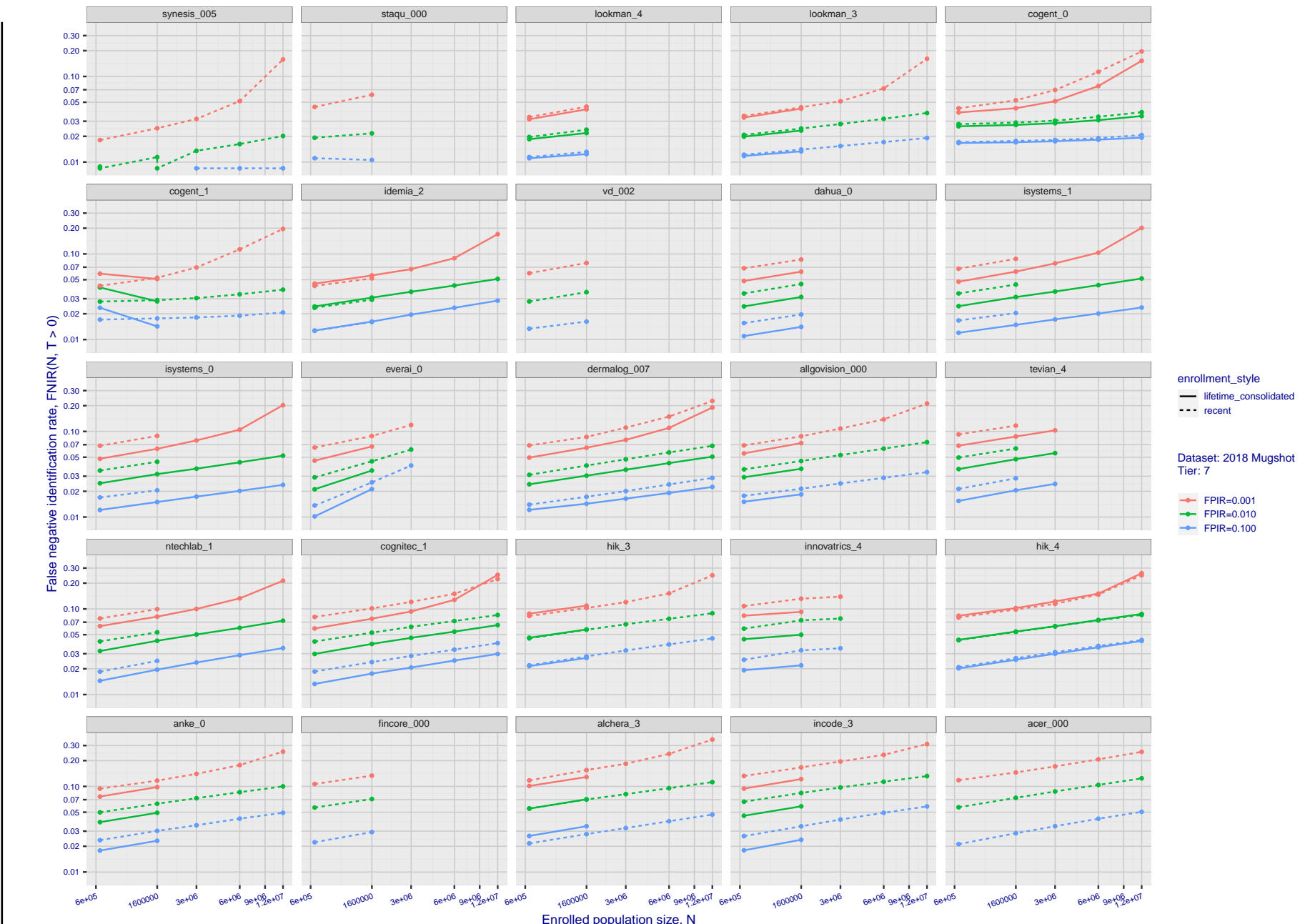


Figure 42: [FRVT-2018 Mugshot Dataset] Threshold-based identification miss rates vs. number of enrolled subjects. The figure shows  $\text{FNIR}(N, T)$  across various gallery sizes when the threshold is set to achieve the given FPIRs. The rank criterion is irrelevant at high thresholds as mates are always at rank 1. The results are computed from the trials listed in rows 1-10 of Table 1. Less accurate algorithms were not run on large  $N$ , so results are missing. For clarity, results are sorted and reported into tiers spanning multiple pages. The tiering criteria is complicated: First paging by  $\text{FNIR}(N_b, 1, 0)$ , then sorting by median  $\text{FNIR}(N_b, T)$ ,  $N_b = 640\,000$ .

2021/09/2  
09:55:08

$\text{FNIR}(N, K, T) = \text{False neg. identification rate}$   
 $\text{FPIR}(N, T) = \text{False pos. identification rate}$

$N = \text{Num. enrolled subjects}$   
 $R = \text{Num. candidates examined}$

$N =$  Num. enroled subjects  
 $R =$  Num. candidates examined       $I =$  Inclusion

$I = 0 \rightarrow$  Investigation  
 $T > 0 \rightarrow$  Identification

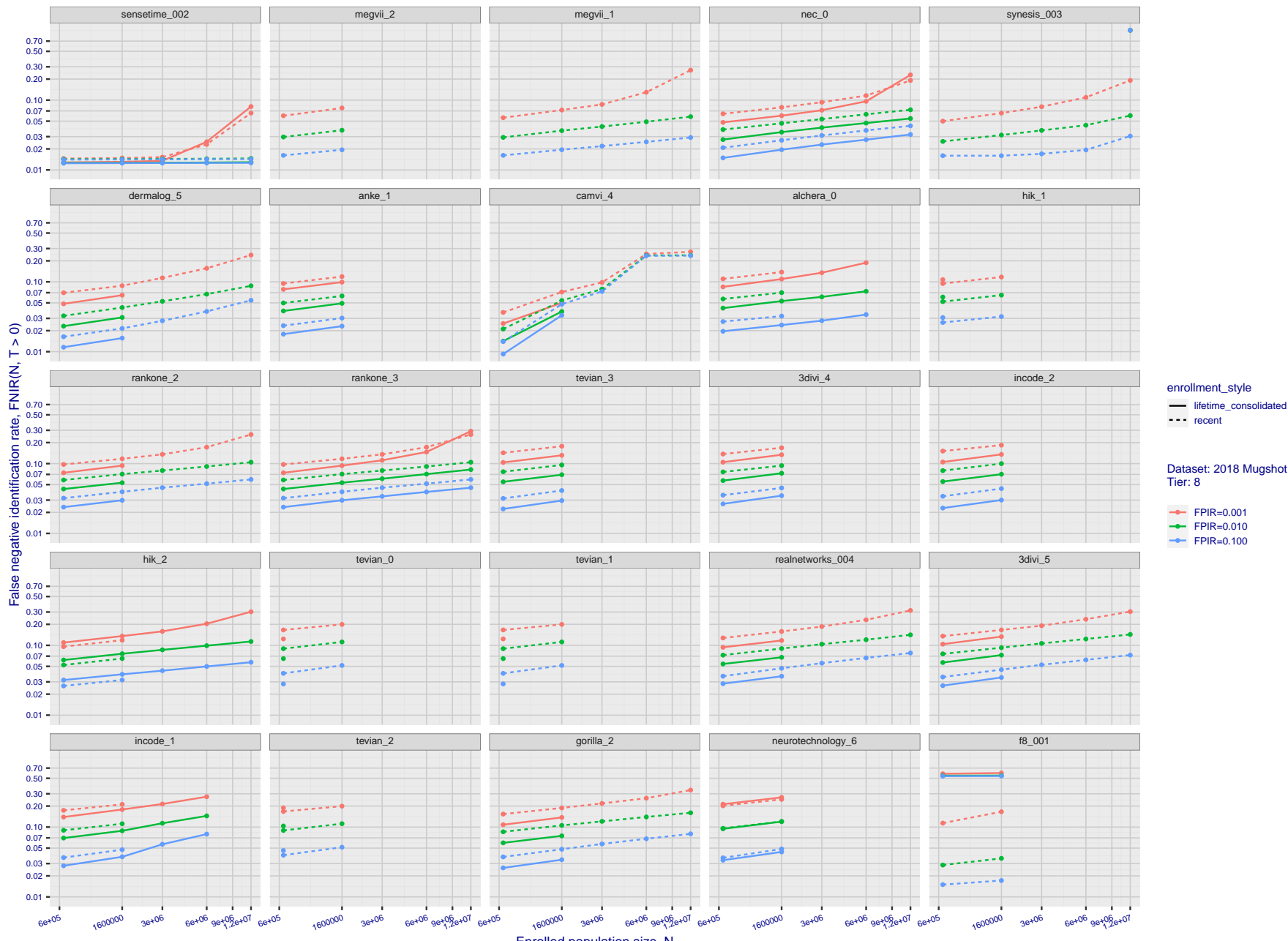


**Figure 43: [FRVT-2018 Mugshot Dataset] Threshold-based identification miss rates vs. number of enrolled subjects.** The figure shows FNIR( $N, T$ ) across various gallery sizes when the threshold is set to achieve the given FPIRs. The rank criterion is irrelevant at high thresholds as mates are always at rank 1. The results are computed from the trials listed in rows 1-10 of Table 1. Less accurate algorithms were not run on large  $N$ , so results are missing. For clarity, results are sorted and reported into tiers spanning multiple pages. The tiering criteria is complicated: First paging by FNIR( $N_b, 1, 0$ ), then sorting by median FNIR( $N_b, T$ ),  $N_b = 640\,000$ .

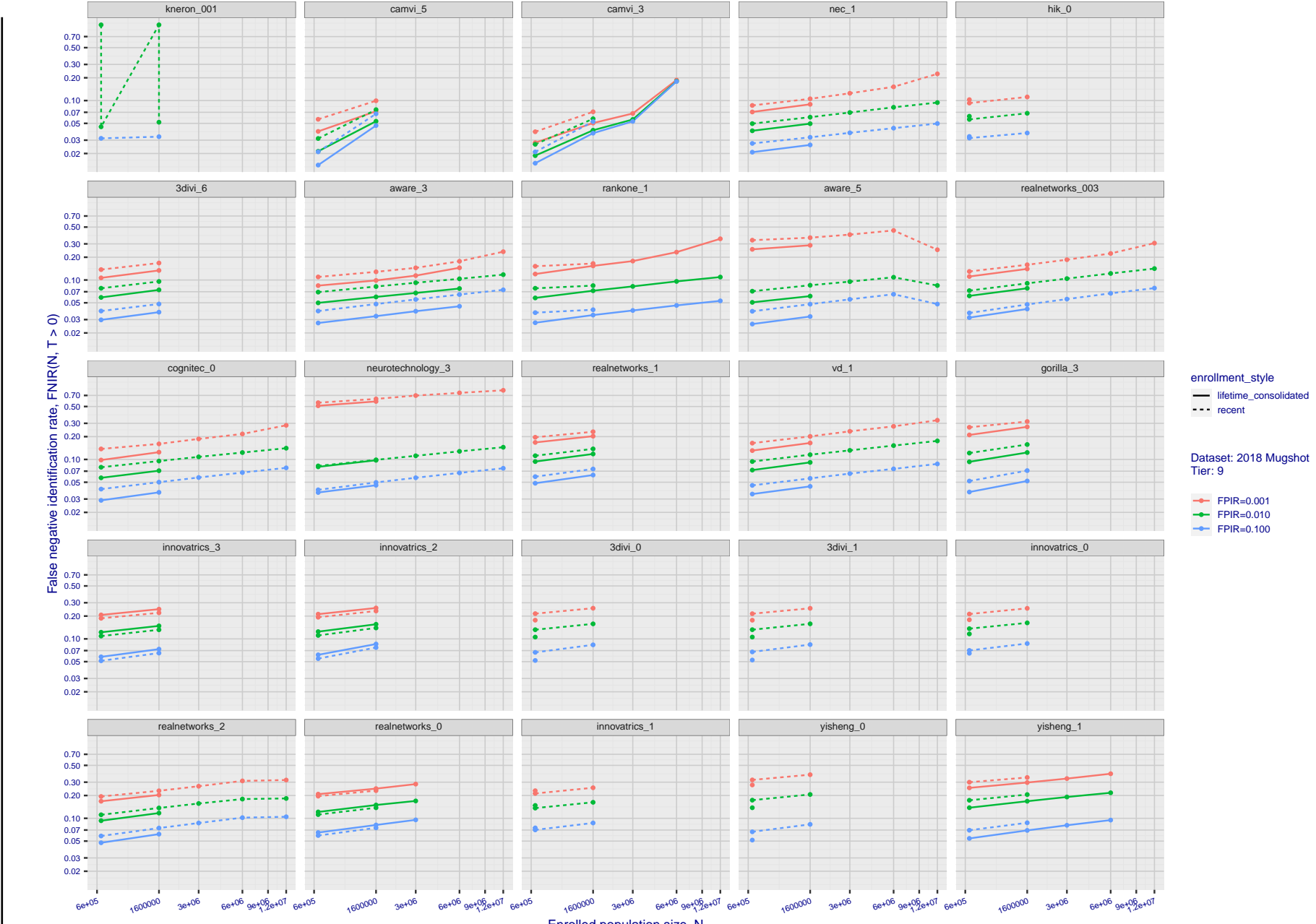


Figure 44: [FRVT-2018 Mugshot Dataset] Threshold-based identification miss rates vs. number of enrolled subjects. The figure shows FNIR( $N, T$ ) across various gallery sizes when the threshold is set to achieve the given FPIRs. The rank criterion is irrelevant at high thresholds as mates are always at rank 1. The results are computed from the trials listed in rows 1-10 of Table 1. Less accurate algorithms were not run on large  $N$ , so results are missing. For clarity, results are sorted and reported into tiers spanning multiple pages. The tiering criteria is complicated: First paging by  $\text{FNIR}(N_b, 1, 0)$ , then sorting by median  $\text{FNIR}(N_b, T)$ ,  $N_b = 640\,000$ .



Figure 45: [FRVT-2018 Mugshot Dataset] Threshold-based identification miss rates vs. number of enrolled subjects. The figure shows FNIR( $N, T$ ) across various gallery sizes when the threshold is set to achieve the given FPIRs. The rank criterion is irrelevant at high thresholds as mates are always at rank 1. The results are computed from the trials listed in rows 1-10 of Table 1. Less accurate algorithms were not run on large  $N$ , so results are missing. For clarity, results are sorted and reported into tiers spanning multiple pages. The tiering criteria is complicated: First paging by  $\text{FNIR}(N_b, 1, 0)$ , then sorting by median  $\text{FNIR}(N_b, T)$ ,  $N_b = 640\,000$ .

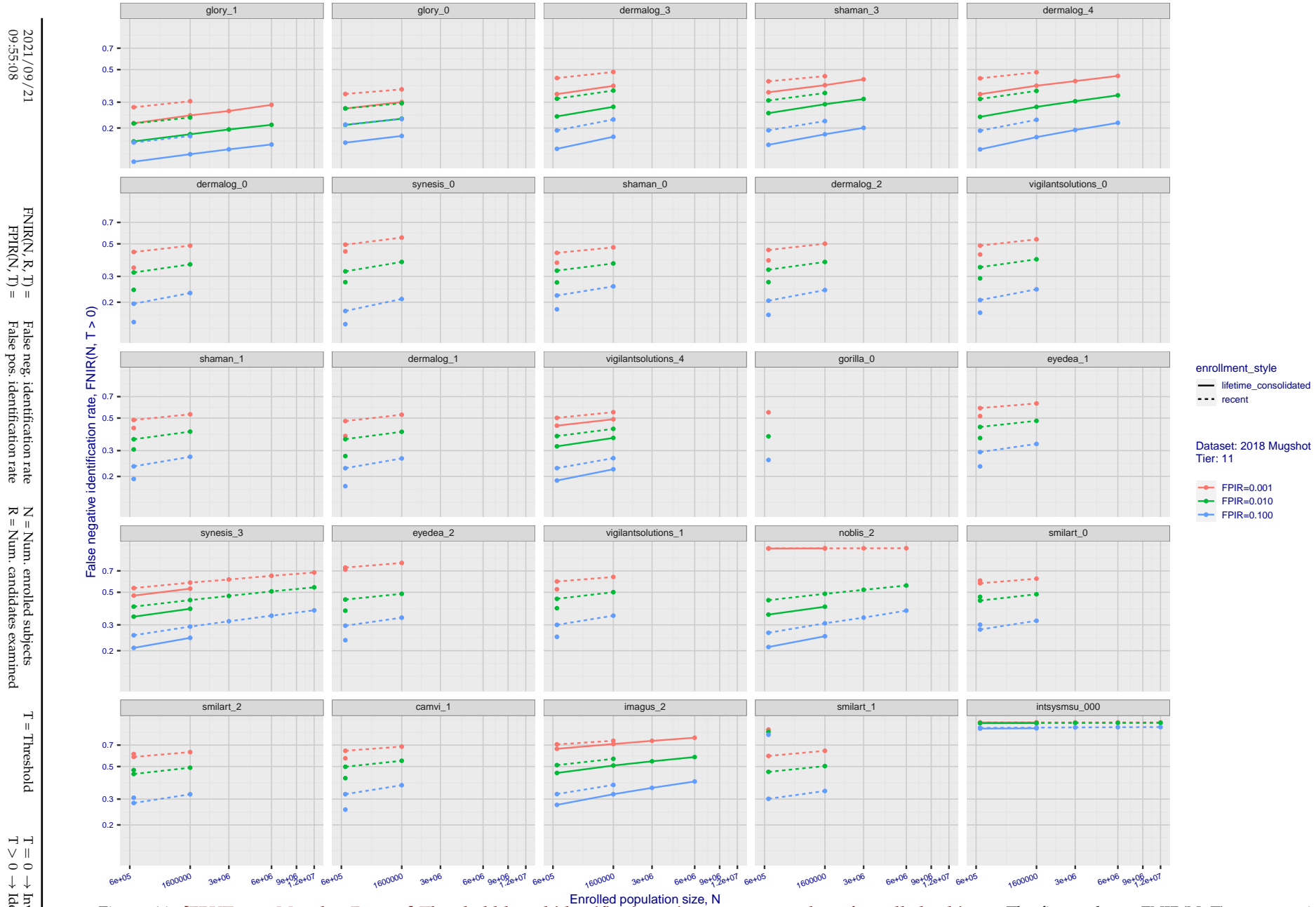


Figure 46: [FRVT-2018 Mugshot Dataset] Threshold-based identification miss rates vs. number of enrolled subjects. The figure shows FNIR( $N, T$ ) across various gallery sizes when the threshold is set to achieve the given FPIRs. The rank criterion is irrelevant at high thresholds as mates are always at rank 1. The results are computed from the trials listed in rows 1-10 of Table 1. Less accurate algorithms were not run on large  $N$ , so results are missing. For clarity, results are sorted and reported into tiers spanning multiple pages. The tiering criteria is complicated: First paging by  $\text{FNIR}(N_b, 1, 0)$ , then sorting by median  $\text{FNIR}(N_b, T)$ ,  $N_b = 640\,000$ .

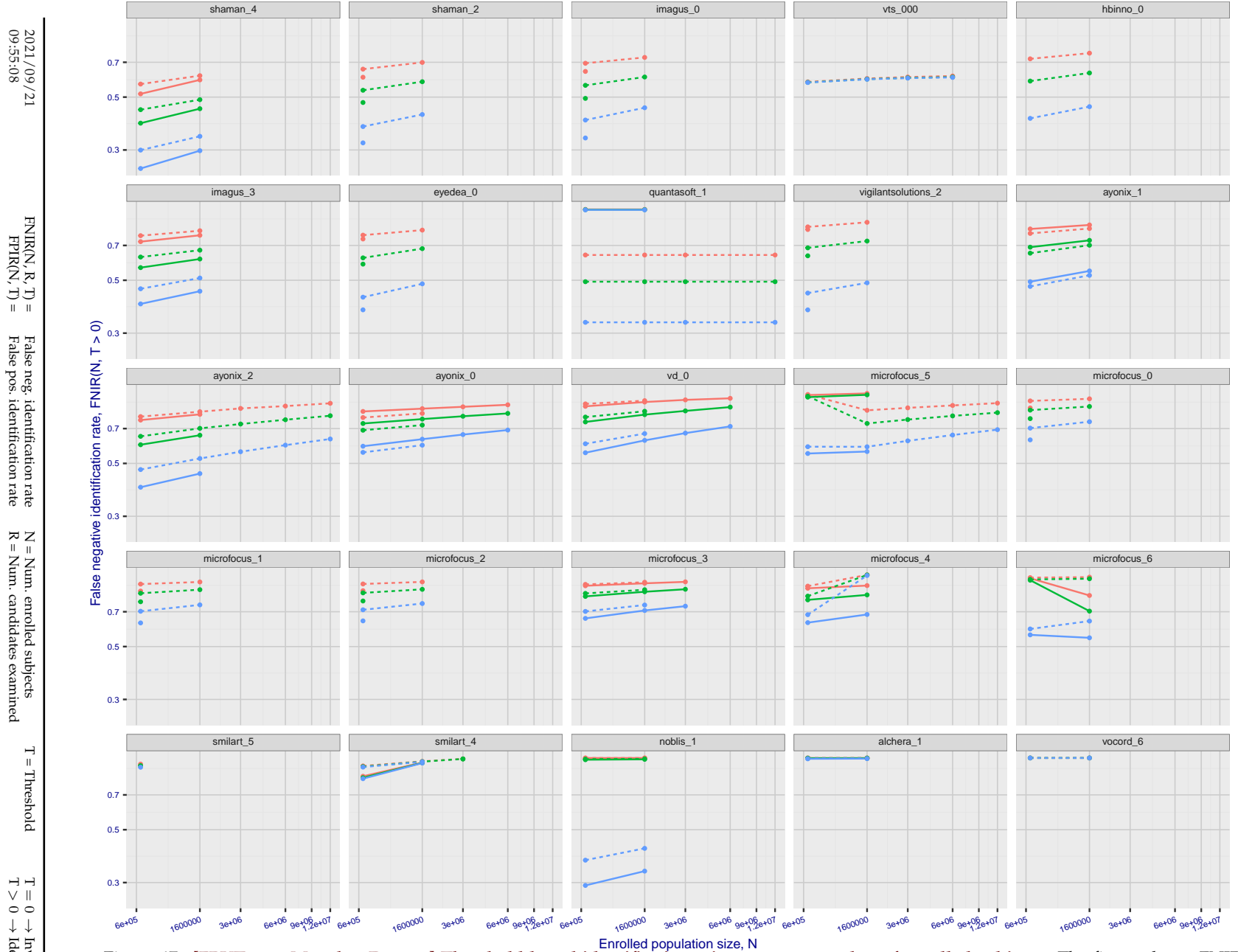


Figure 47: [FRVT-2018 Mugshot Dataset] Threshold-based identification miss rates vs. number of enrolled subjects. The figure shows  $\text{FNIR}(N, T)$  across various gallery sizes when the threshold is set to achieve the given FPIRs. The rank criterion is irrelevant at high thresholds as mates are always at rank 1. The results are computed from the trials listed in rows 1-10 of Table 1. Less accurate algorithms were not run on large  $N$ , so results are missing. For clarity, results are sorted and reported into tiers spanning multiple pages. The tiering criteria is complicated: First paging by  $\text{FNIR}(N_b, 1, 0)$ , then sorting by median  $\text{FNIR}(N_b, T)$ ,  $N_b = 640\,000$ .

---

2021/09/21  
09:55:08

FNIR(N, R, T) = False neg. identification rate  
FPTR(N, T) = False pos. identification rate

N = Num. enrolled subjects  
R = Num. candidates examined

T = Threshold  
T > 0 → Identification

T = 0 → Investigation

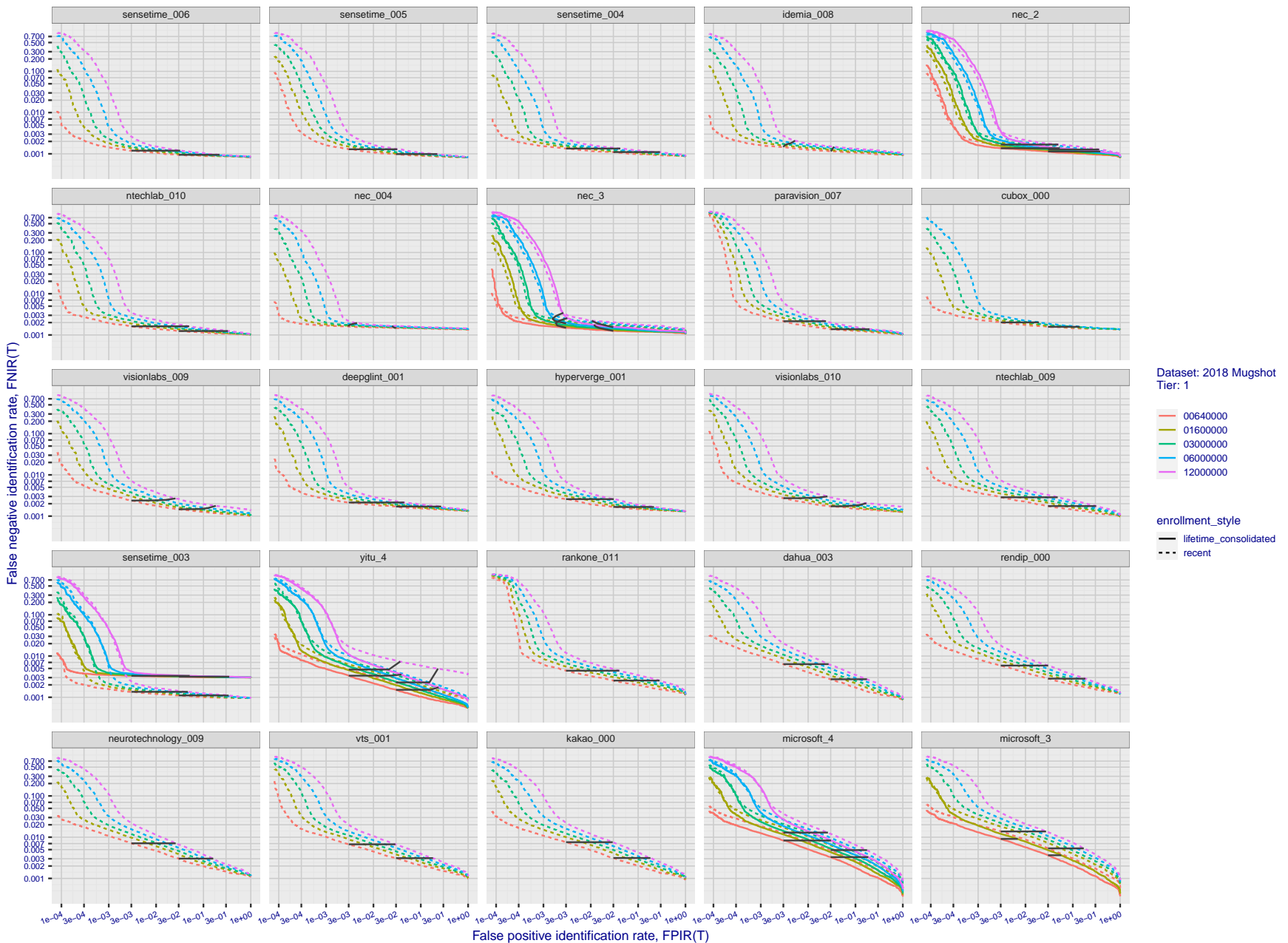
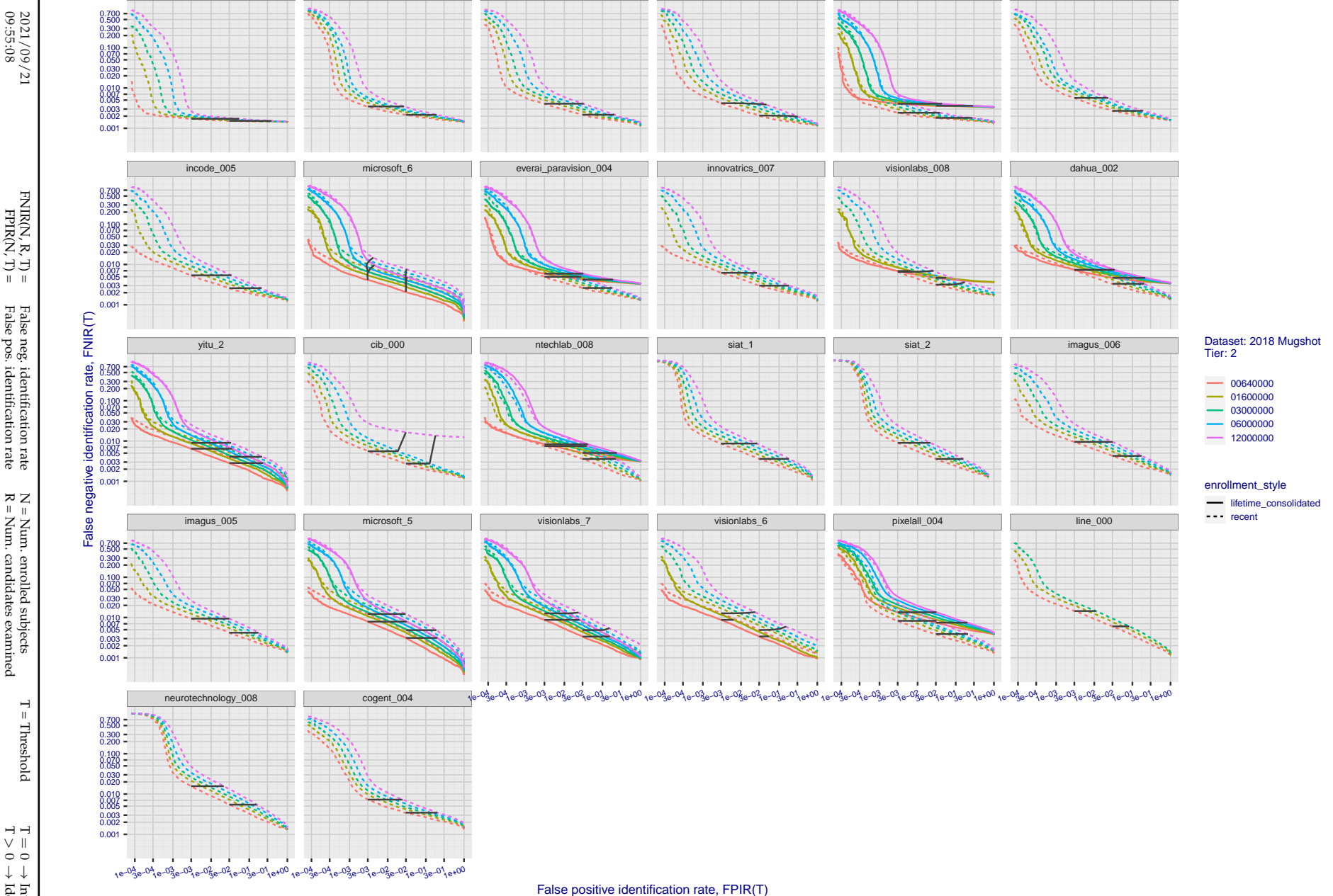
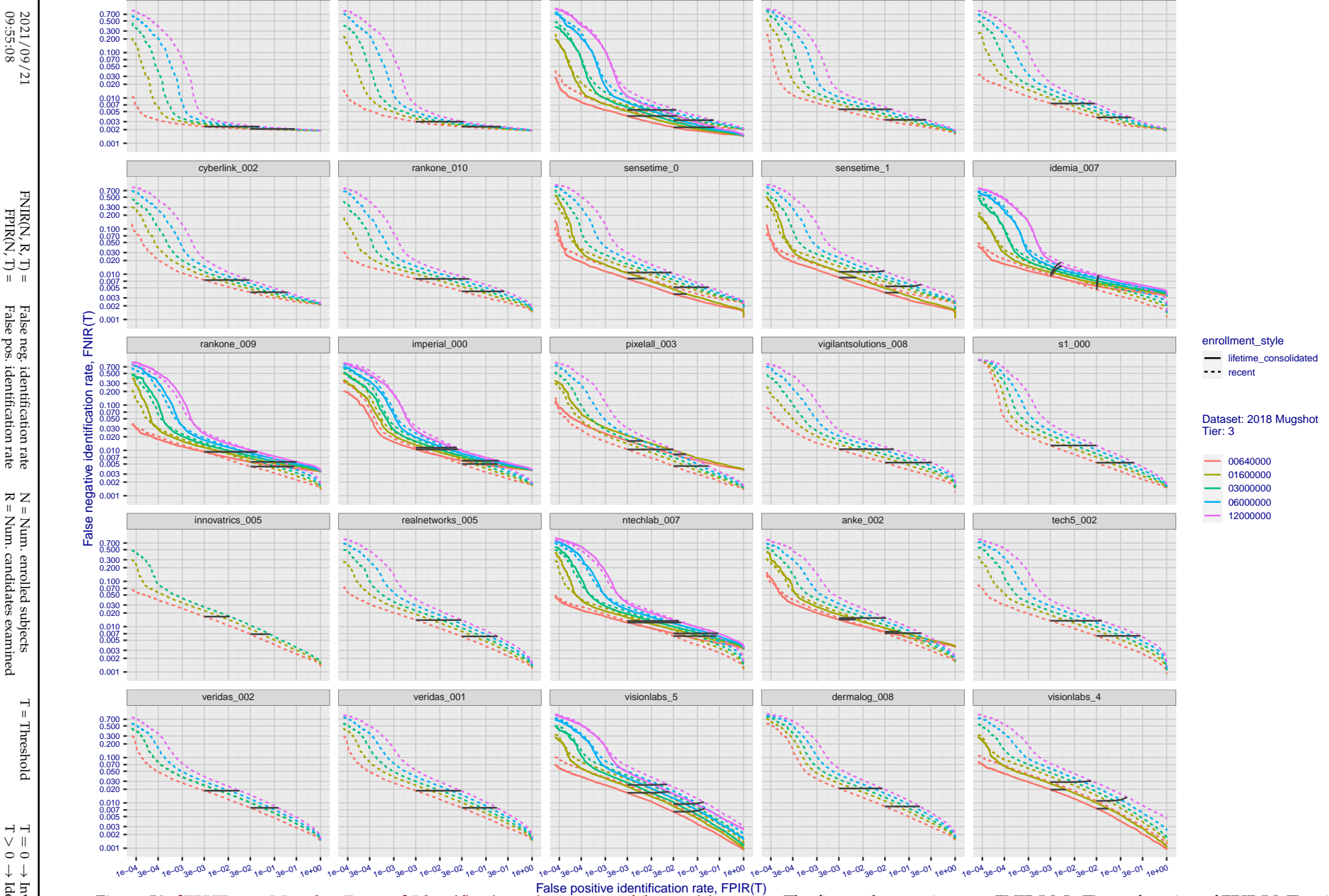


Figure 48: [FRVT-2018 Mugshot Dataset] Identification miss rates vs. false positive rates. The figure shows miss rates  $\text{FNIR}(N, L, T)$  as a function of  $\text{FPIR}(N, T)$ , with  $N$  ranging from 640 000 to 12 000 000 as noted in rows 1-10 of Table 1. These error tradeoff characteristics are useful for applications where a threshold must be elevated to limit false positives, such as when human reviewer labor is not matched to the volume of searches. Dark lines join points of equal threshold: If horizontal,  $\text{FPIR}(T)$  rises with  $N$ , and mate scores are independent of  $N$ . Other algorithms adjust scores in an attempt to make  $\text{FPIR}$  independent of  $N$ .



**Figure 49: [FRVT-2018 Mugshot Dataset] Identification miss rates vs. false positive rates.** The figure shows miss rates  $\text{FNIR}(N, L, T)$  as a function of  $\text{FPIR}(N, T)$ , with  $N$  ranging from 640 000 to 12 000 000 as noted in rows 1-10 of Table 1. These error tradeoff characteristics are useful for applications where a threshold must be elevated to limit false positives, such as when human reviewer labor is not matched to the volume of searches. Dark lines join points of equal threshold: If horizontal,  $\text{FPIR}(T)$  rises with  $N$ , and mate scores are independent of  $N$ . Other algorithms adjust scores in an attempt to make  $\text{FPIR}$  independent of  $N$ .



**Figure 50: [FRVT-2018 Mugshot Dataset] Identification miss rates vs. false positive rates.** The figure shows miss rates  $\text{FNIR}(N, L, T)$  as a function of  $\text{FPIR}(N, T)$ , with  $N$  ranging from 640 000 to 12 000 000 as noted in rows 1-10 of Table 1. These error tradeoff characteristics are useful for applications where a threshold must be elevated to limit false positives, such as when human reviewer labor is not matched to the volume of searches. Dark lines join points of equal threshold: If horizontal,  $\text{FPIR}(T)$  rises with  $N$ , and mate scores are independent of  $N$ . Other algorithms adjust scores in an attempt to make  $\text{FPIR}$  independent of  $N$ .

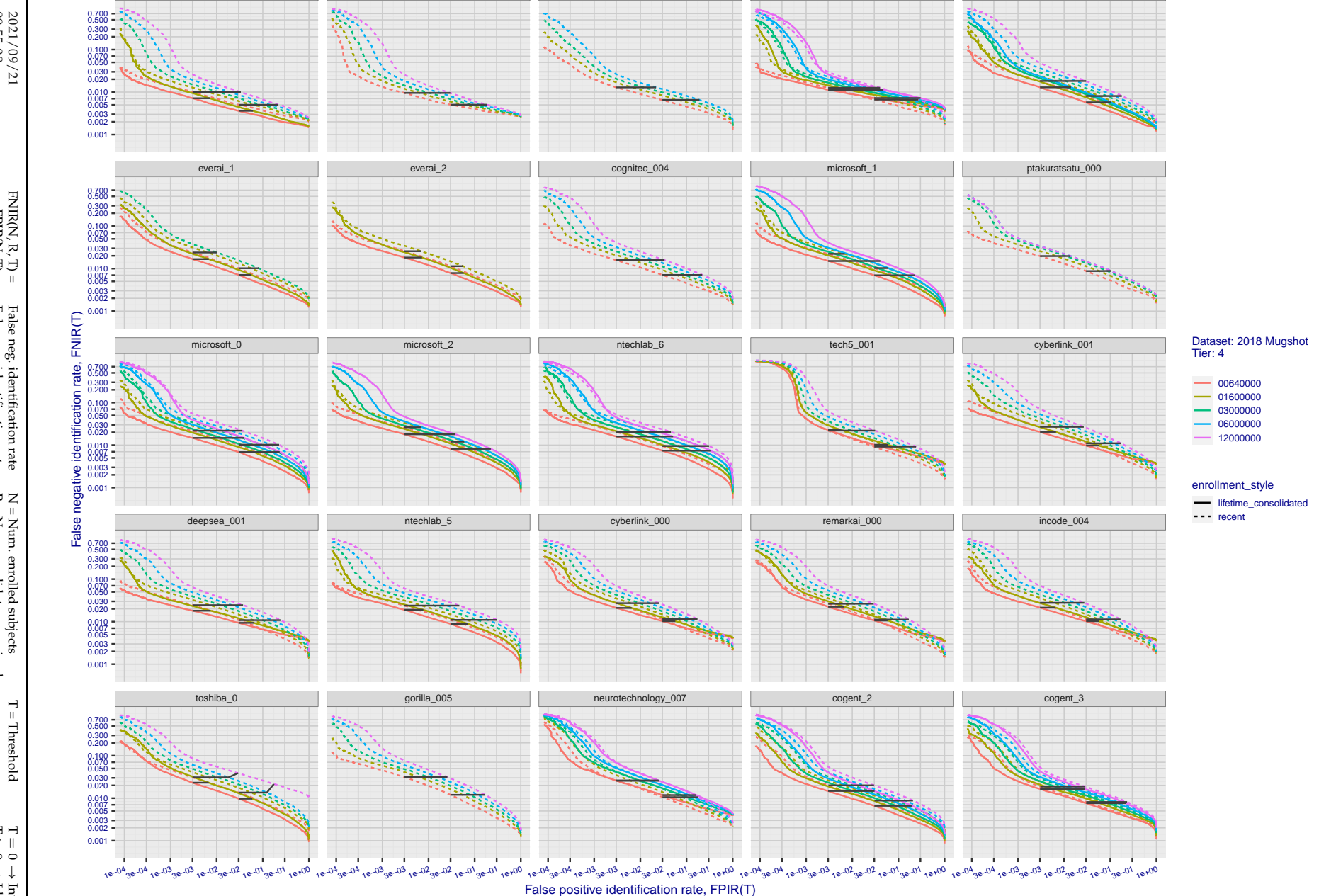


**Figure 51: [FRVT-2018 Mugshot Dataset] Identification miss rates vs. false positive rates.** The figure shows miss rates  $\text{FNIR}(N, L, T)$  as a function of  $\text{FPIR}(N, T)$ , with  $N$  ranging from 640 000 to 12 000 000 as noted in rows 1-10 of Table 1. These error tradeoff characteristics are useful for applications where a threshold must be elevated to limit false positives, such as when human reviewer labor is not matched to the volume of searches. Dark lines join points of equal threshold: If horizontal,  $\text{FPIR}(T)$  rises with  $N$ , and mate scores are independent of  $N$ . Other algorithms adjust scores in an attempt to make  $\text{FPIR}$  independent of  $N$ .

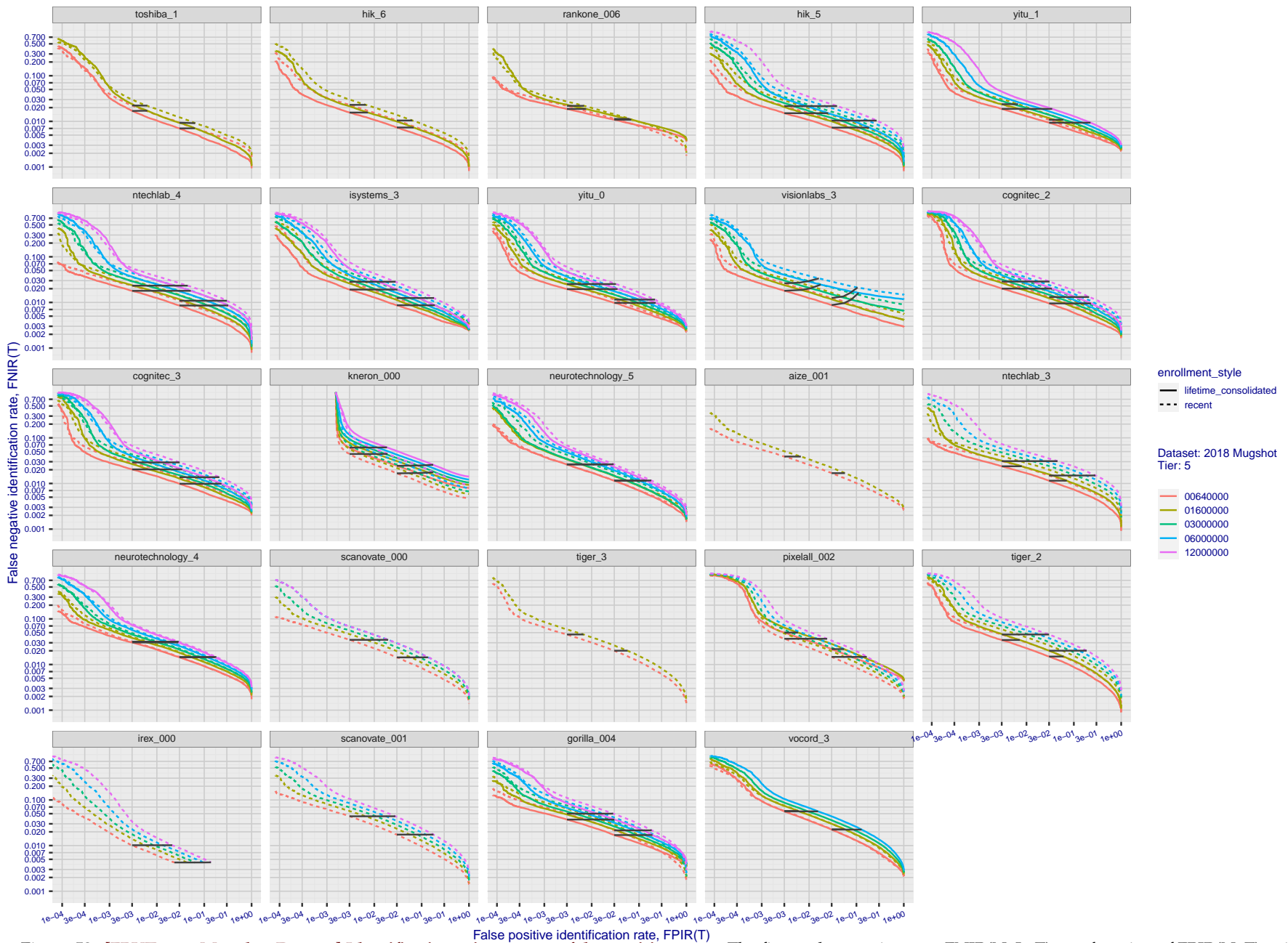
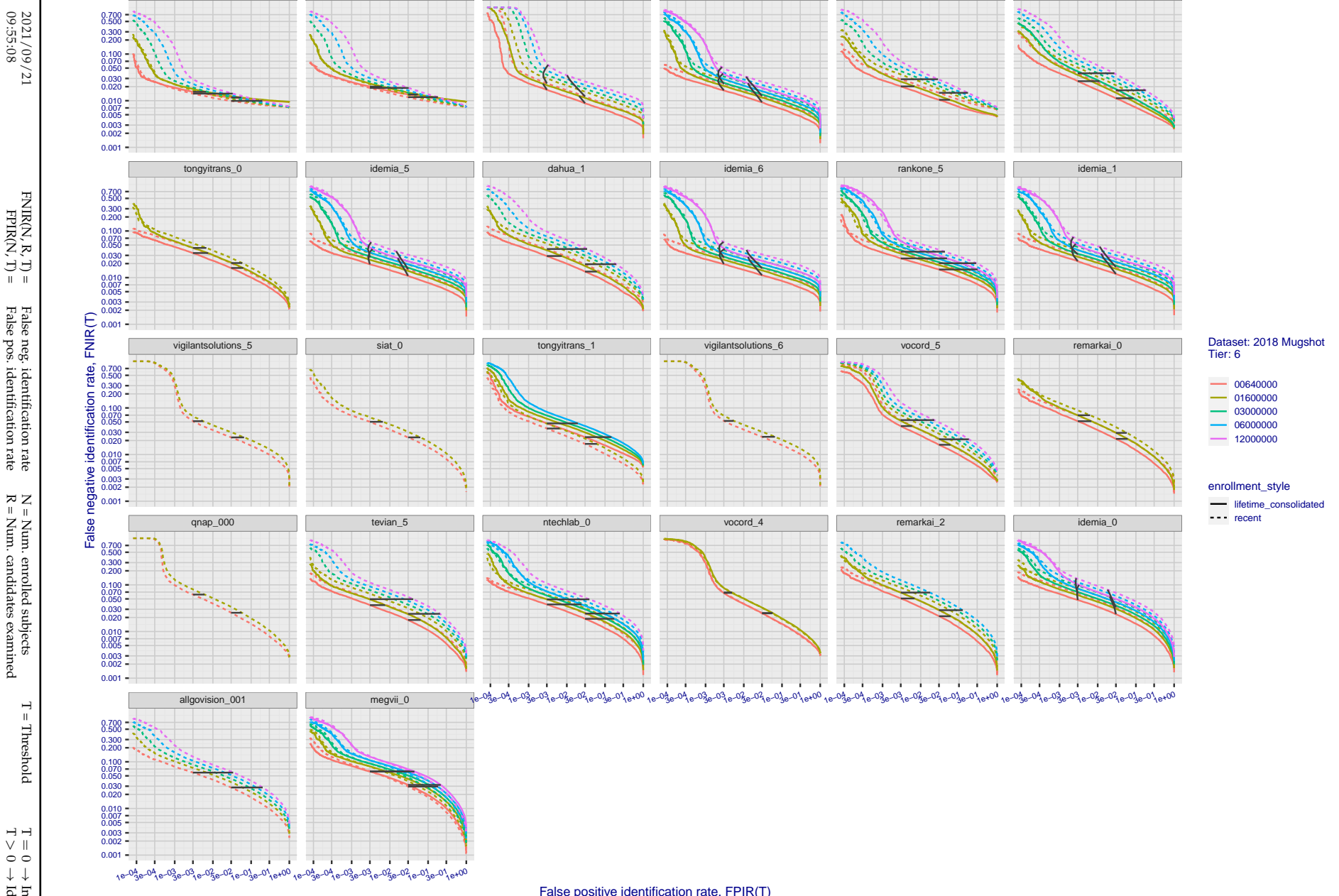
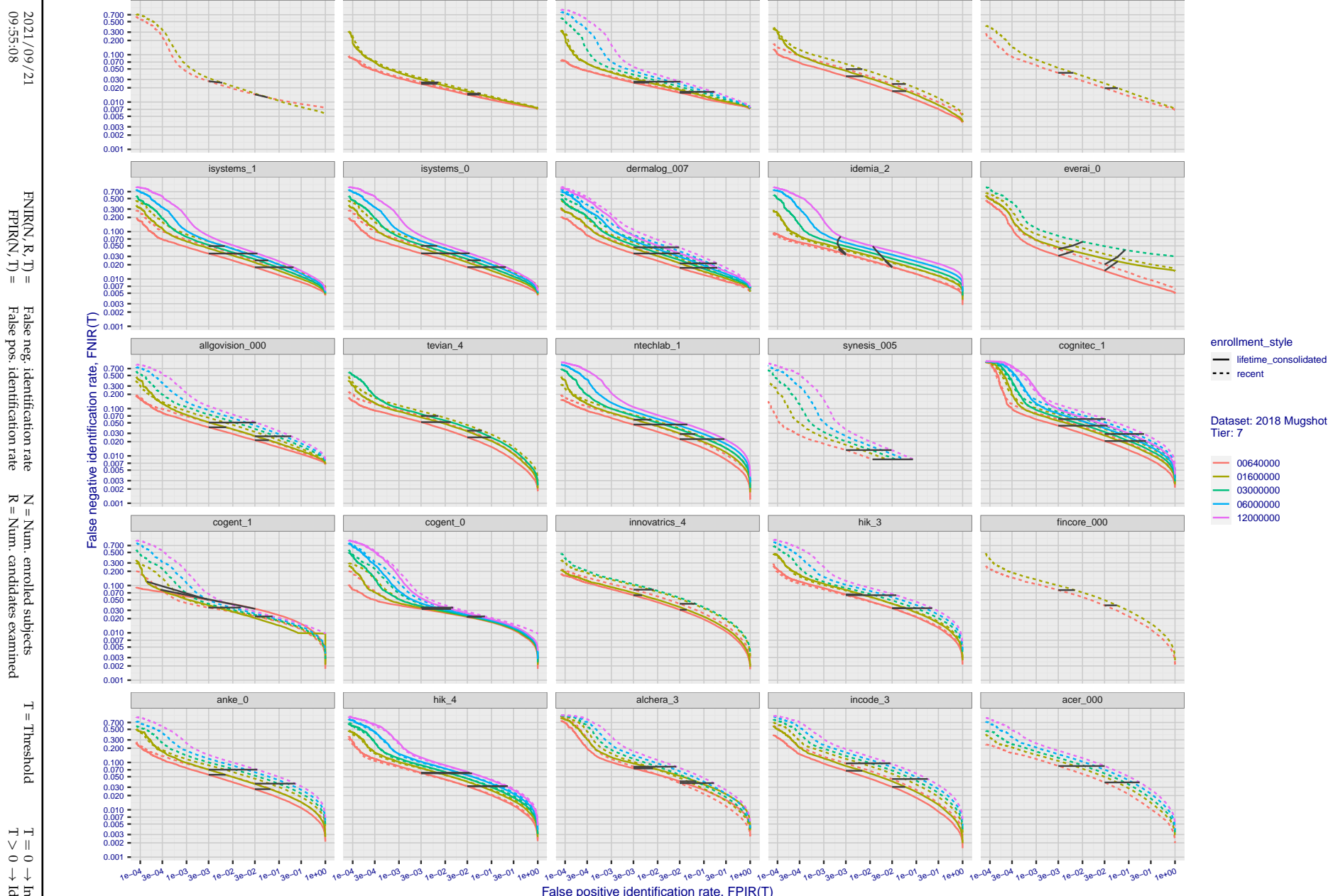


Figure 52: [FRVT-2018 Mugshot Dataset] Identification miss rates vs. false positive rates. The figure shows miss rates  $\text{FNIR}(N, L, T)$  as a function of  $\text{FPIR}(N, T)$ , with  $N$  ranging from 640 000 to 12 000 000 as noted in rows 1-10 of Table 1. These error tradeoff characteristics are useful for applications where a threshold must be elevated to limit false positives, such as when human reviewer labor is not matched to the volume of searches. Dark lines join points of equal threshold: If horizontal,  $\text{FPIR}(T)$  rises with  $N$ , and mate scores are independent of  $N$ . Other algorithms adjust scores in an attempt to make  $\text{FPIR}$  independent of  $N$ .



**Figure 53: [FRVT-2018 Mugshot Dataset] Identification miss rates vs. false positive rates.** The figure shows miss rates  $\text{FNIR}(N, L, T)$  as a function of  $\text{FPIR}(N, T)$ , with  $N$  ranging from 64 000 to 12 000 000 as noted in rows 1-10 of Table 1. These error tradeoff characteristics are useful for applications where a threshold must be elevated to limit false positives, such as when human reviewer labor is not matched to the volume of searches. Dark lines join points of equal  $N$ . Other algorithms adjust scores in an attempt to make  $\text{FPIR}$  independent of  $N$ .



**Figure 54: [FRVT-2018 Mugshot Dataset] Identification miss rates vs. false positive rates.** The figure shows miss rates  $\text{FNIR}(N, L, T)$  as a function of  $\text{FPIR}(N, T)$ , with  $N$  ranging from 640 000 to 12 000 000 as noted in rows 1-10 of Table 1. These error tradeoff characteristics are useful for applications where a threshold must be elevated to limit false positives, such as when human reviewer labor is not matched to the volume of searches. Dark lines join points of equal threshold: If horizontal,  $\text{FPIR}(T)$  rises with  $N$ , and mate scores are independent of  $N$ . Other algorithms adjust scores in an attempt to make  $\text{FPIR}$  independent of  $N$ .

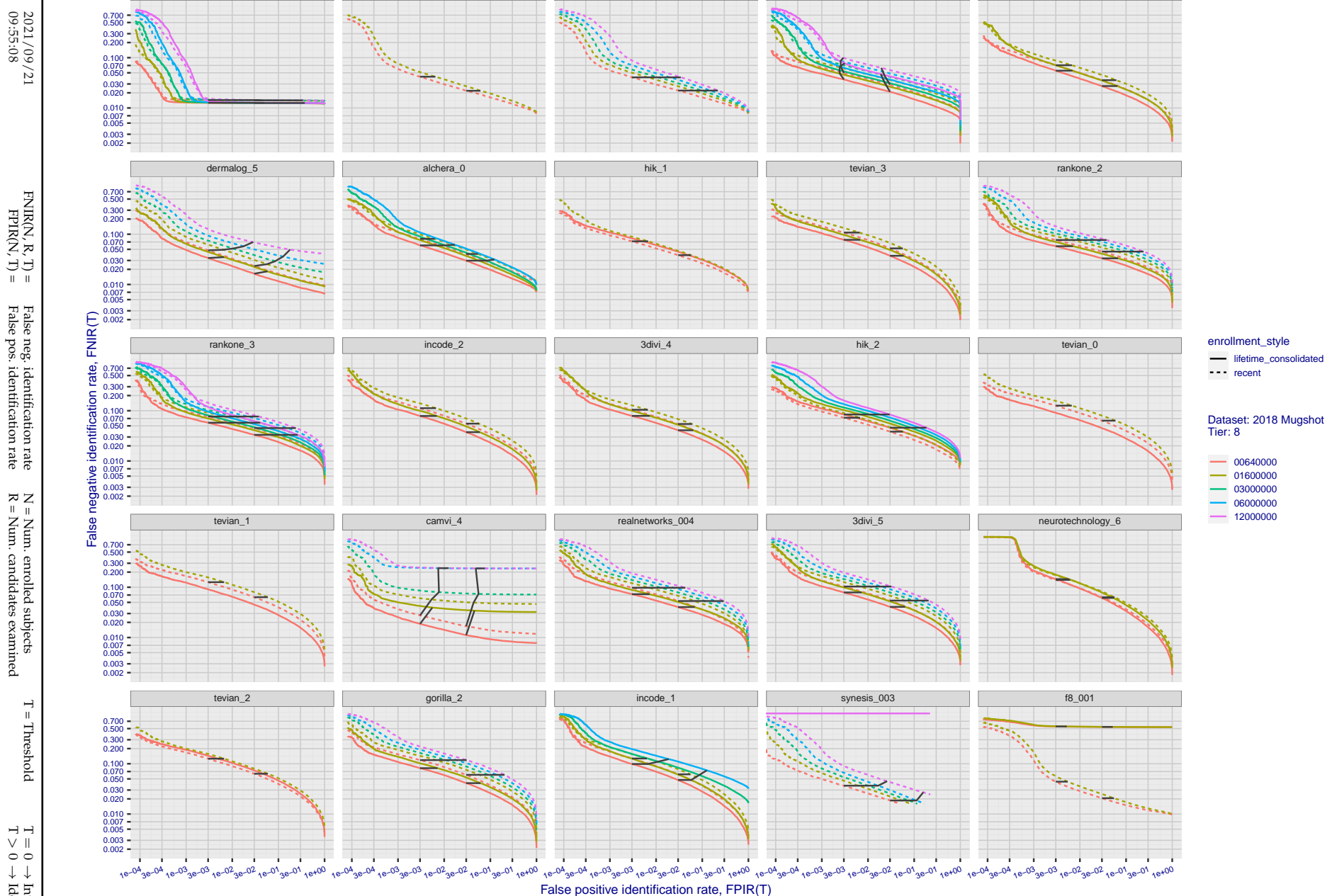


**Figure 55: [FRVT-2018 Mugshot Dataset] Identification miss rates vs. false positive rates.** The figure shows miss rates  $\text{FNIR}(N, L, T)$  as a function of  $\text{FPIR}(N, T)$ , with  $N$  ranging from 640 000 to 12 000 000 as noted in rows 1-10 of Table 1. These error tradeoff characteristics are useful for applications where a threshold must be elevated to limit false positives, such as when human reviewer labor is not matched to the volume of searches. Dark lines join points of equal threshold: If horizontal,  $\text{FPIR}(T)$  rises with  $N$ , and mate scores are independent of  $N$ . Other algorithms adjust scores in an attempt to make  $\text{FPIR}$  independent of  $N$ .

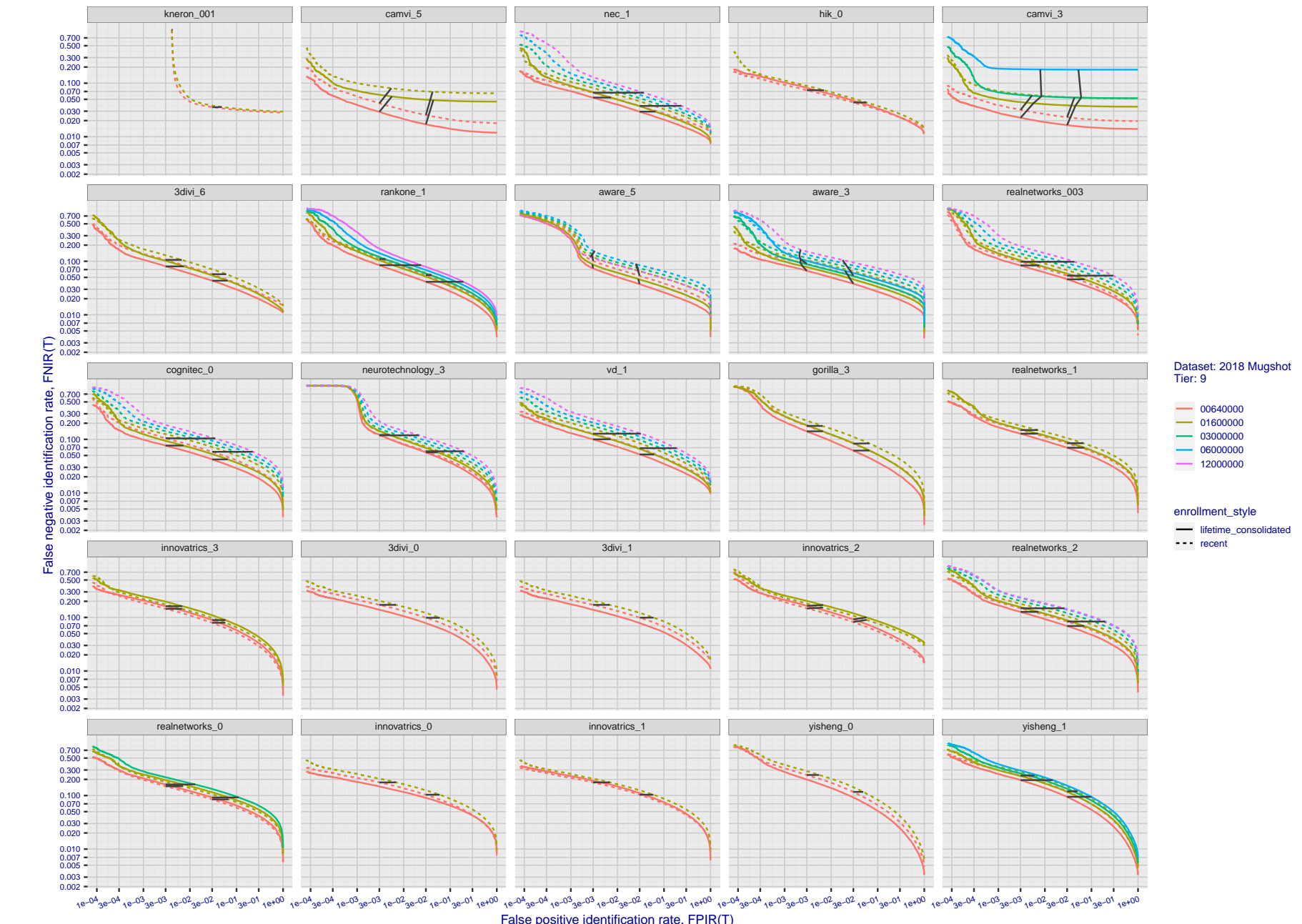


**Figure 56: [FRVT-2018 Mugshot Dataset] Identification miss rates vs. false positive rates.** The figure shows miss rates  $\text{FNIR}(N, L, T)$  as a function of  $\text{FPIR}(N, T)$ , with  $N$  ranging from 64 000 to 12 000 000 as noted in rows 1-10 of Table 1. These error tradeoff characteristics are useful for applications where a threshold must be elevated to limit false positives, such as when human reviewer labor is not matched to the volume of searches. Dark lines join points of equal threshold: If horizontal,  $\text{FPIR}(T)$  rises with  $N$ , and mate scores are independent of  $N$ . Other algorithms adjust scores in an attempt to make  $\text{FPIR}$  independent of  $N$ .

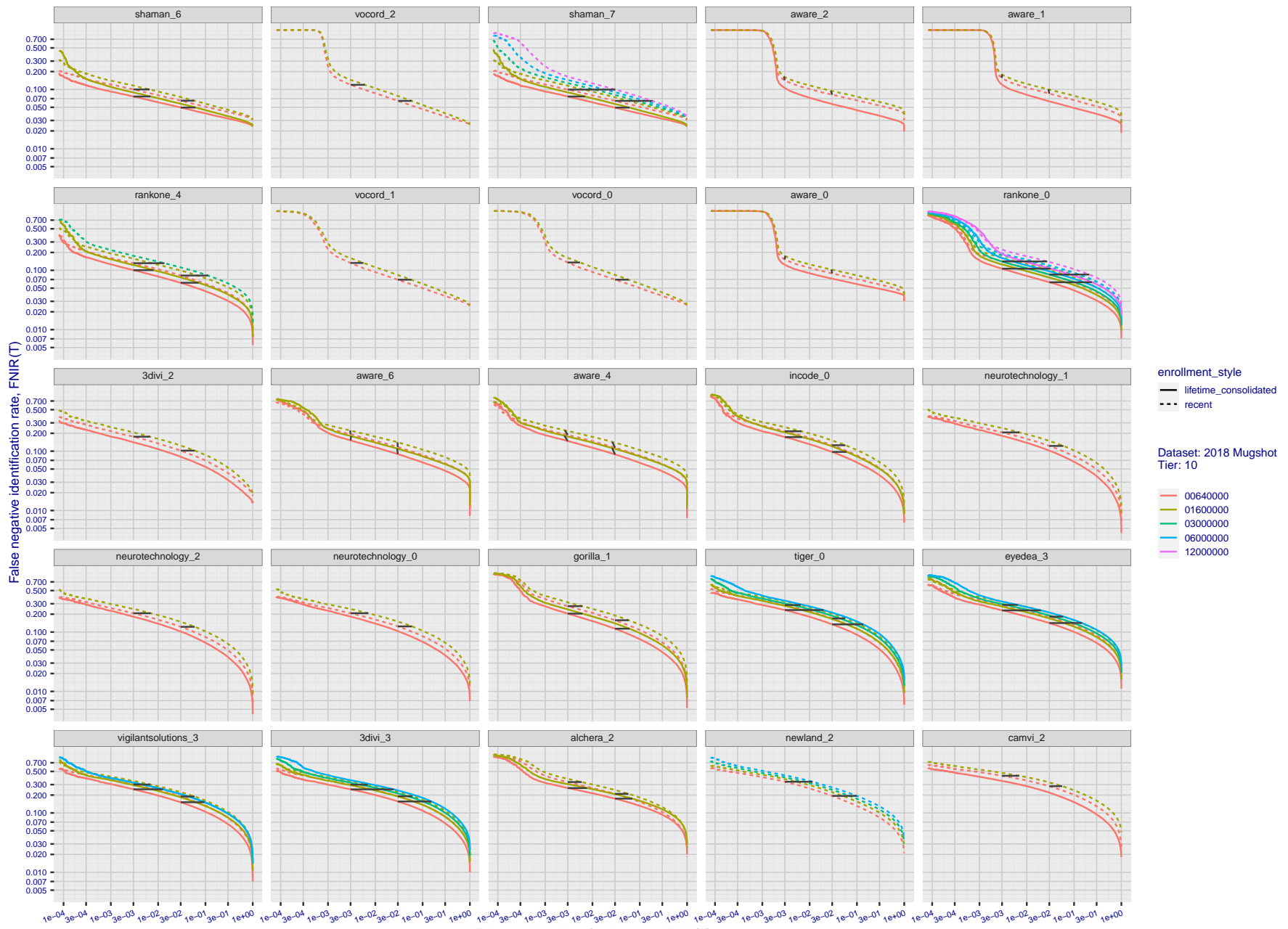


**Figure 57: [FRVT-2018 Mugshot Dataset] Identification miss rates vs. false positive rates.** The figure shows miss rates  $\text{FNIR}(N, L, T)$  as a function of  $\text{FPIR}(N, T)$ , with  $N$  ranging from 640 000 to 12 000 000 as noted in rows 1-10 of Table 1. These error tradeoff characteristics are useful for applications where a threshold must be elevated to limit false positives, such as when human reviewer labor is not matched to the volume of searches. Dark lines join points of equal threshold: If horizontal,  $\text{FPIR}(T)$  rises with  $N$ , and mate scores are independent of  $N$ . Other algorithms adjust scores in an attempt to make  $\text{FPIR}$  independent of  $N$ .

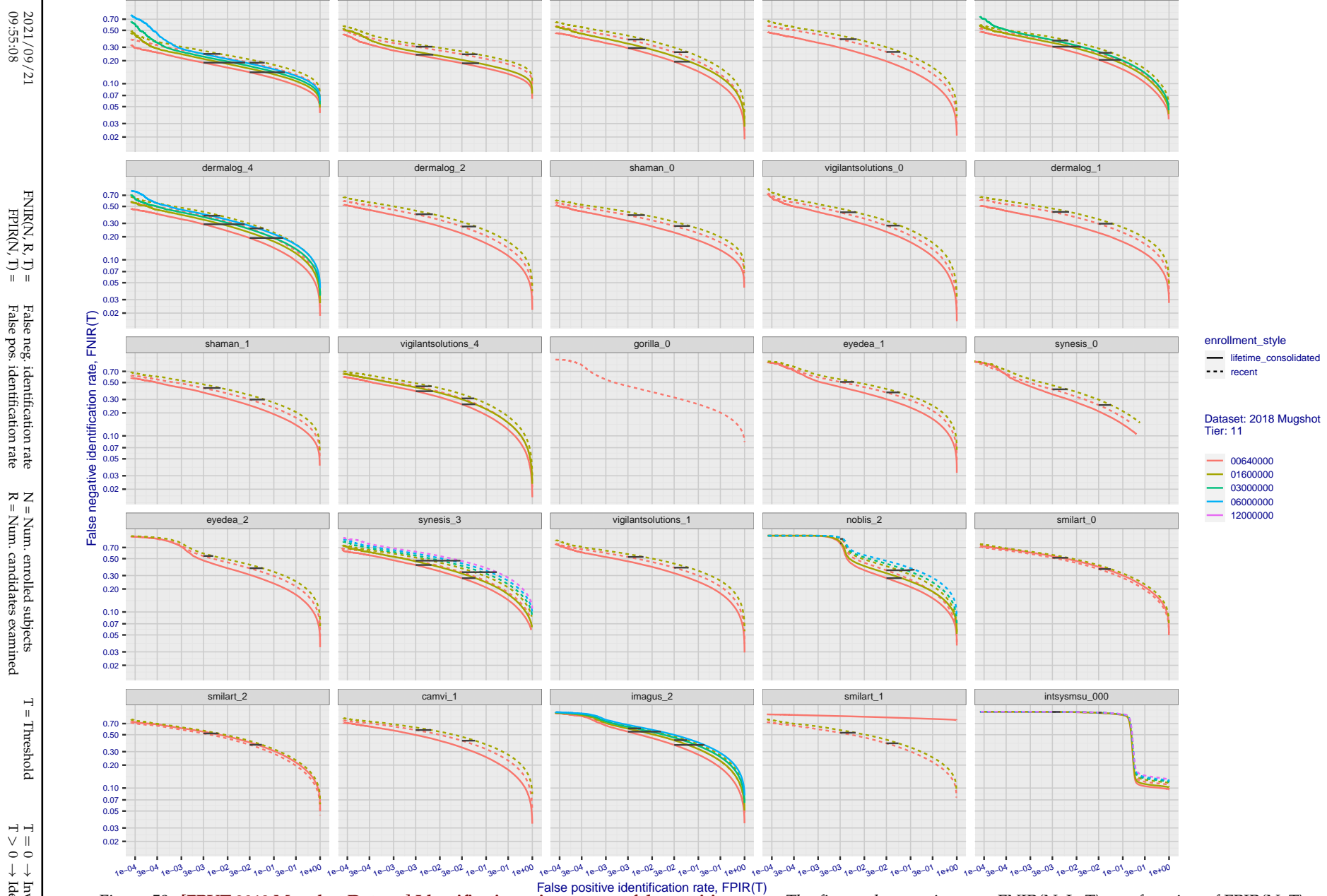


**Figure 58: [FRVT-2018 Mugshot Dataset] Identification miss rates vs. false positive rates.** The figure shows miss rates  $\text{FNIR}(N, L, T)$  as a function of  $\text{FPIR}(N, T)$ , with  $N$  ranging from 640 000 to 12 000 000 as noted in rows 1-10 of Table 1. These error tradeoff characteristics are useful for applications where a threshold must be elevated to limit false positives, such as when human reviewer labor is not matched to the volume of searches. Dark lines join points of equal threshold: If horizontal,  $\text{FPIR}(T)$  rises with  $N$ , and mate scores are independent of  $N$ . Other algorithms adjust scores in an attempt to make  $\text{FPIR}$  independent of  $N$ .

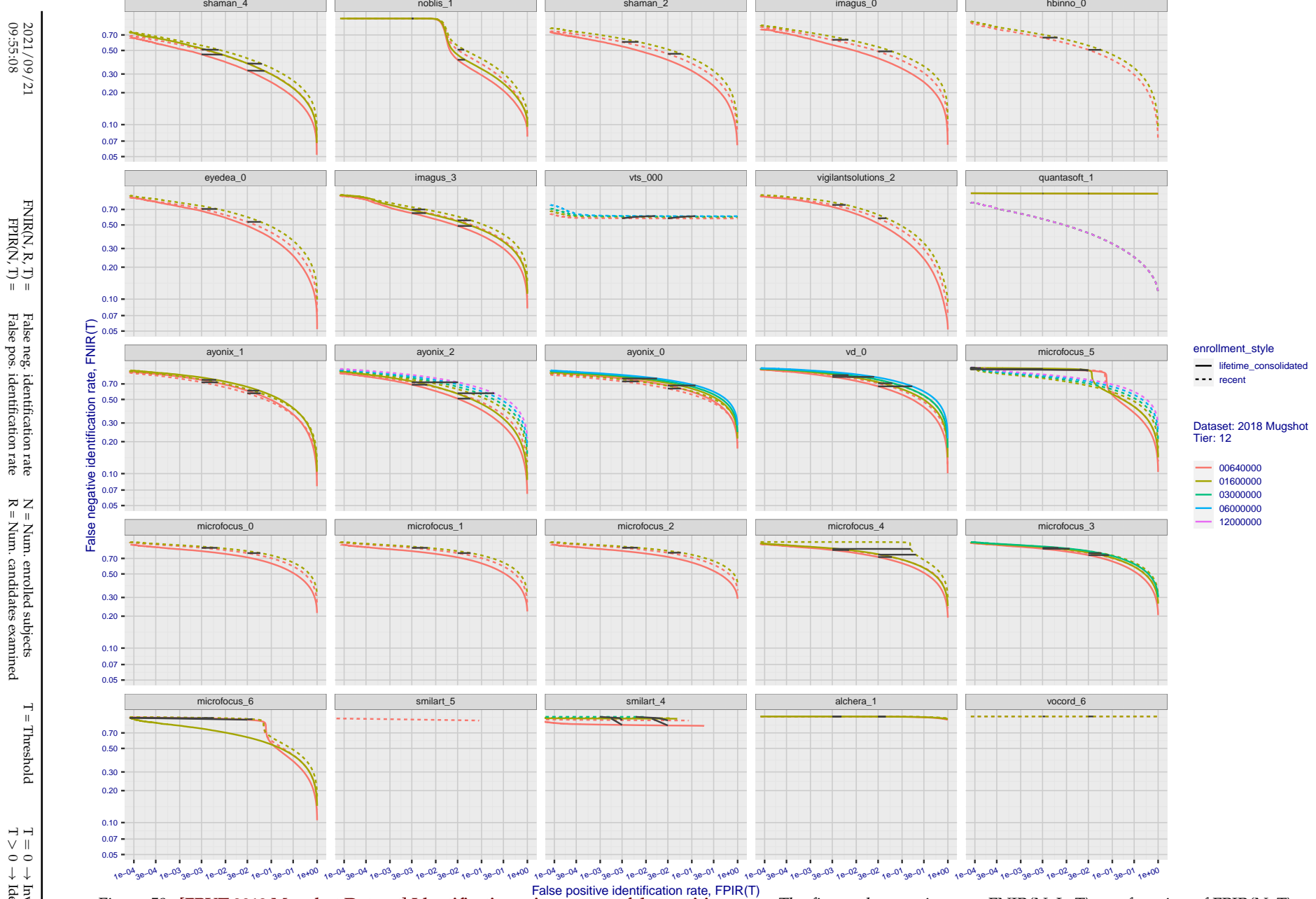


Figure 59: [FRVT-2018 Mugshot Dataset] Identification miss rates vs. false positive rates. The figure shows miss rates  $\text{FNIR}(N, L, T)$  as a function of  $\text{FPIR}(N, T)$ , with  $N$  ranging from 640 000 to 12 000 000 as noted in rows 1-10 of Table 1. These error tradeoff characteristics are useful for applications where a threshold must be elevated to limit false positives, such as when human reviewer labor is not matched to the volume of searches. Dark lines join points of equal threshold: If horizontal,  $\text{FPIR}(T)$  rises with  $N$ , and mate scores are independent of  $N$ . Other algorithms adjust scores in an attempt to make  $\text{FPIR}$  independent of  $N$ .

## Appendix B Effect of time-lapse: Accuracy after face ageing

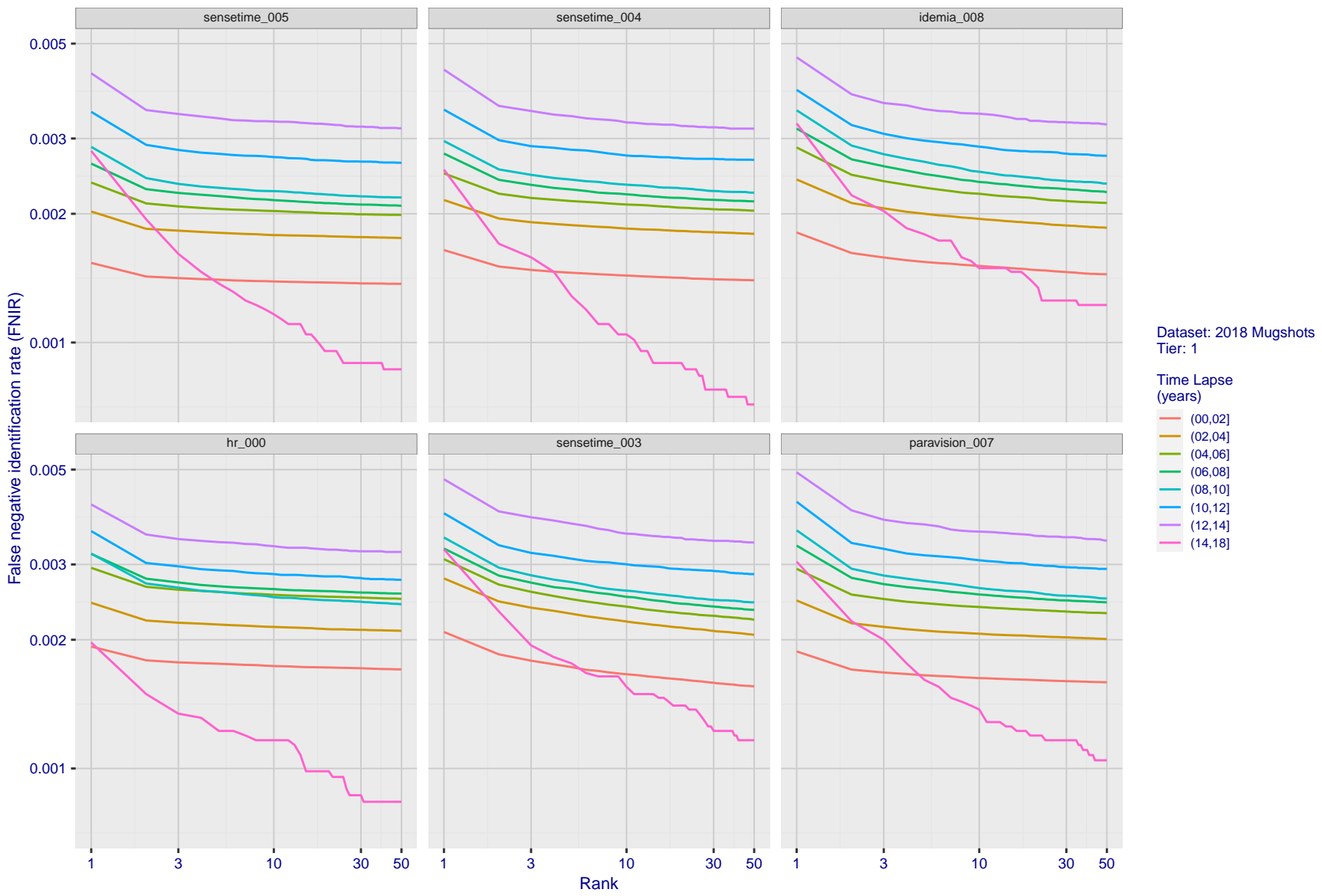
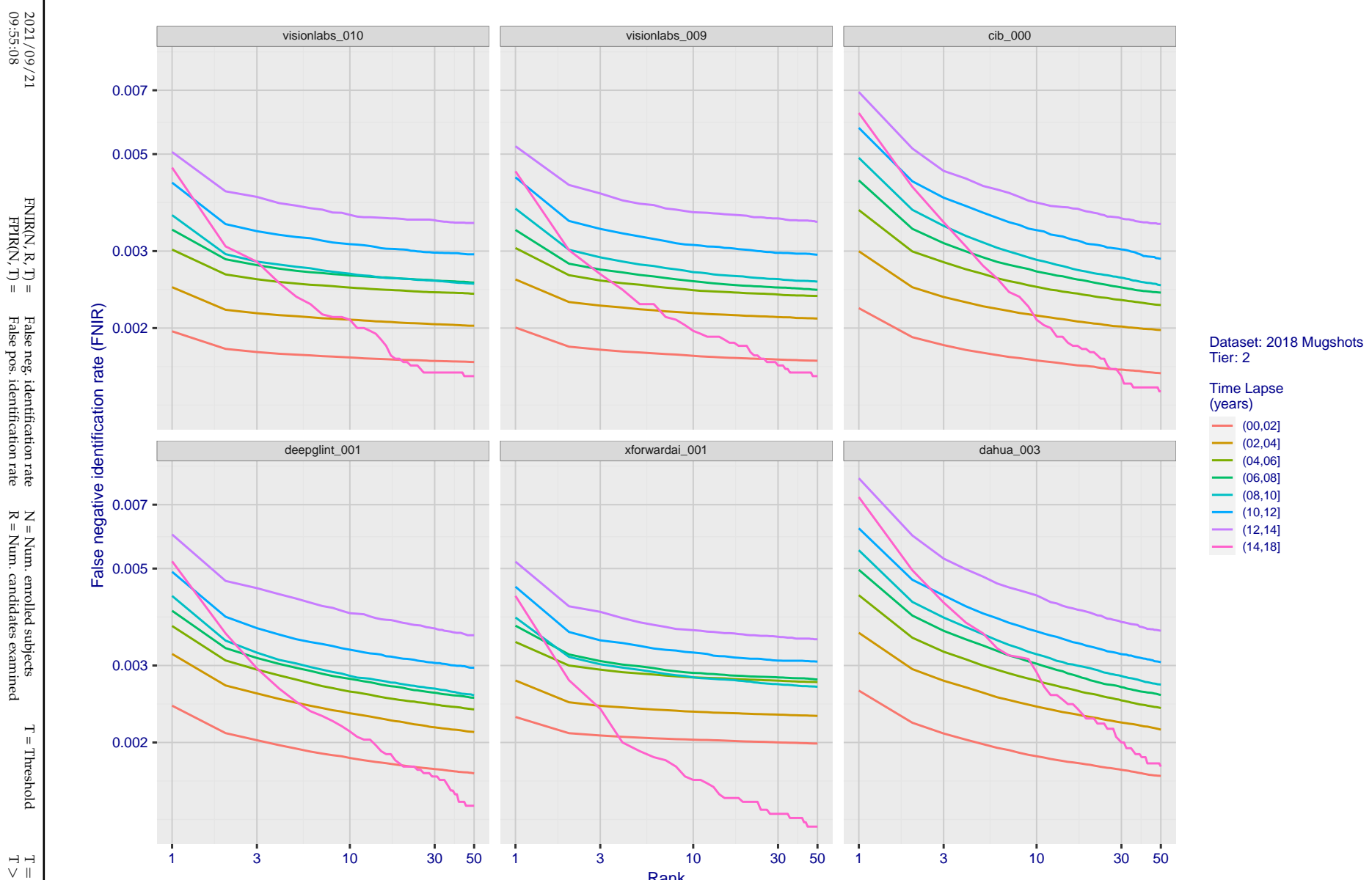


Figure 60: [FRVT-2018 Mugshot Ageing Dataset] Identification miss rates vs. rank by time-elapsed. The oldest image of each individual is enrolled. Thereafter, all more recent images are searched. Miss rates are computed over all searches noted in row 17 of Table 1 and binned by number of years between search and initial enrollment.



**Figure 61: [FRVT-2018 Mugshot Ageing Dataset] Identification miss rates vs. rank by time-elapsed.** The oldest image of each individual is enrolled. Thereafter, all more recent images are searched. Miss rates are computed over all searches noted in row 17 of Table 1 and binned by number of years between search and initial enrollment.

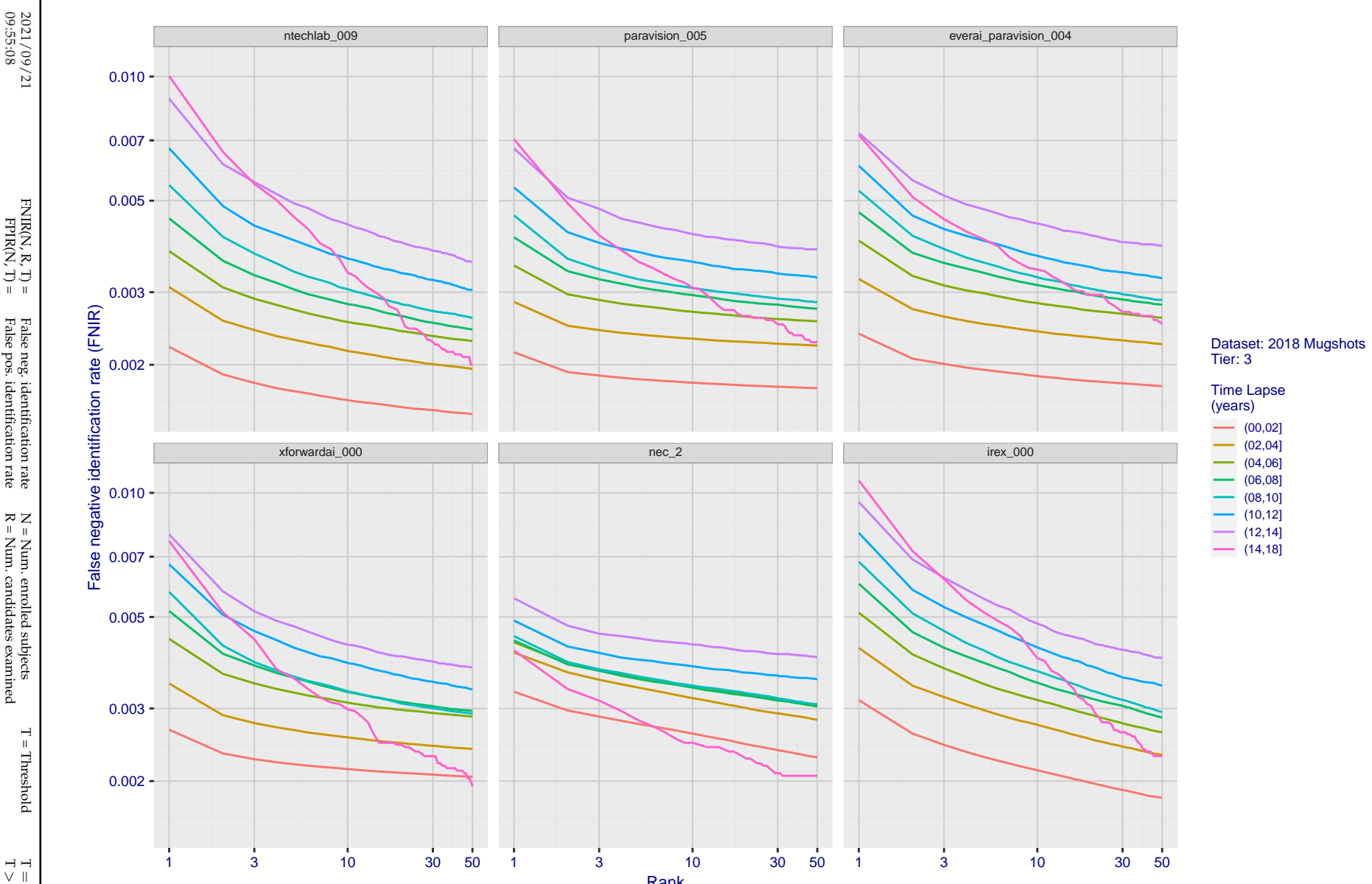


Figure 62: [FRVT-2018 Mugshot Ageing Dataset] Identification miss rates vs. rank by time-elapsed. The oldest image of each individual is enrolled. Thereafter, all more recent images are searched. Miss rates are computed over all searches noted in row 17 of Table 1 and binned by number of years between search and initial enrollment.

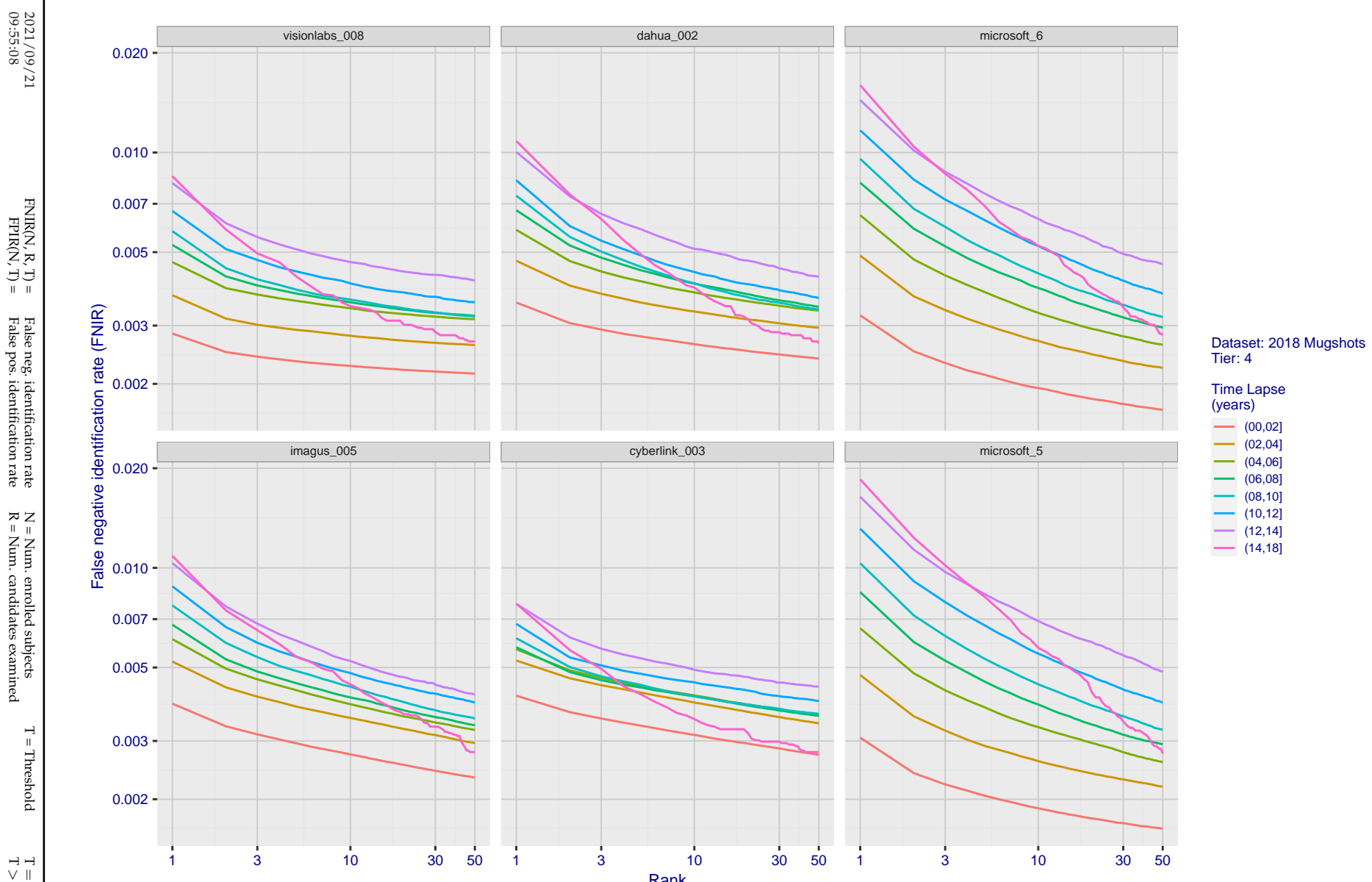
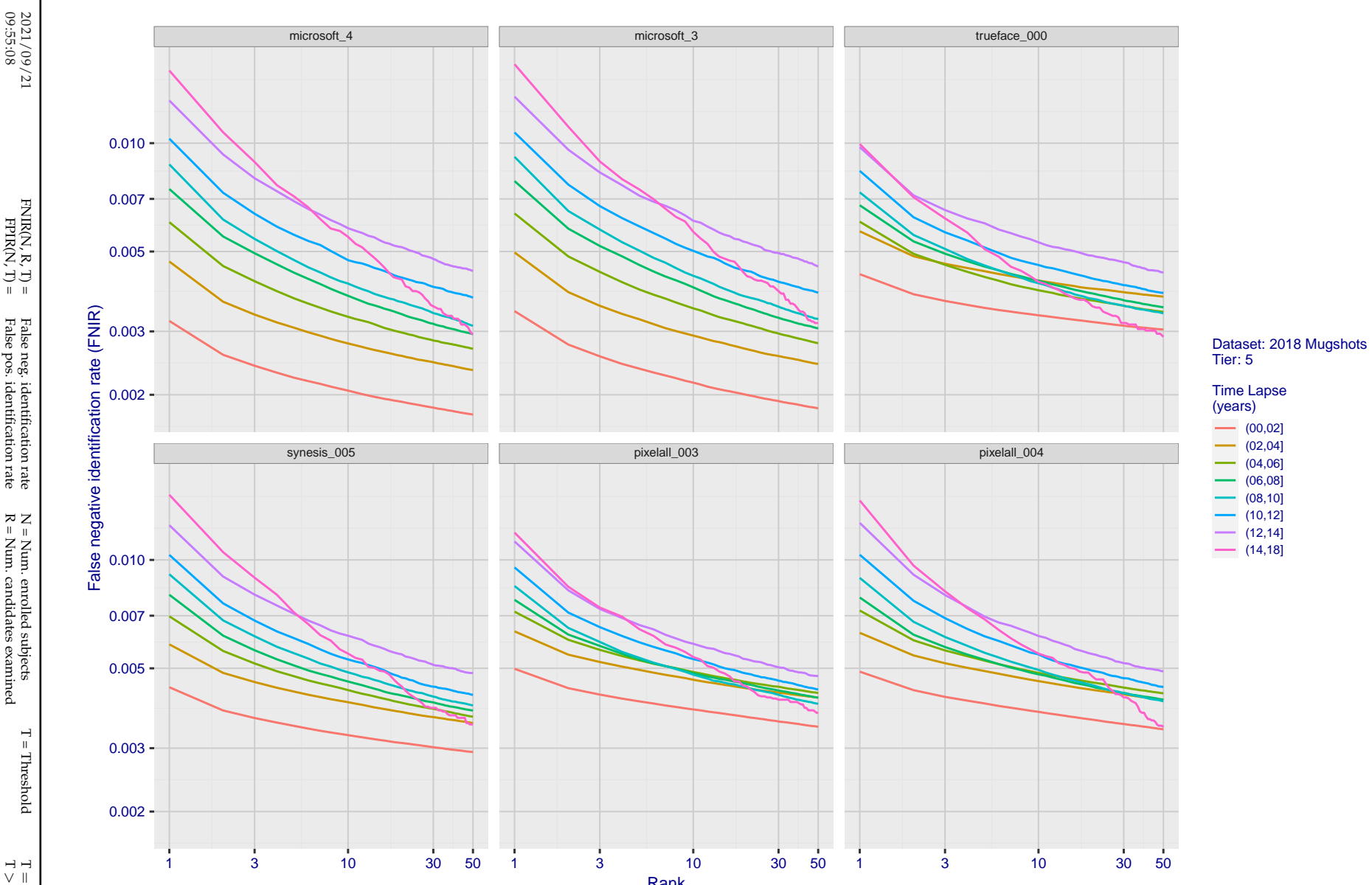


Figure 63: [FRVT-2018 Mugshot Ageing Dataset] Identification miss rates vs. rank by time-elapsed. The oldest image of each individual is enrolled. Thereafter, all more recent images are searched. Miss rates are computed over all searches noted in row 17 of Table 1 and binned by number of years between search and initial enrollment.



**Figure 64: [FRVT-2018 Mugshot Ageing Dataset] Identification miss rates vs. rank by time-elapsed.** The oldest image of each individual is enrolled. Thereafter, all more recent images are searched. Miss rates are computed over all searches noted in row 17 of Table 1 and binned by number of years between search and initial enrollment.

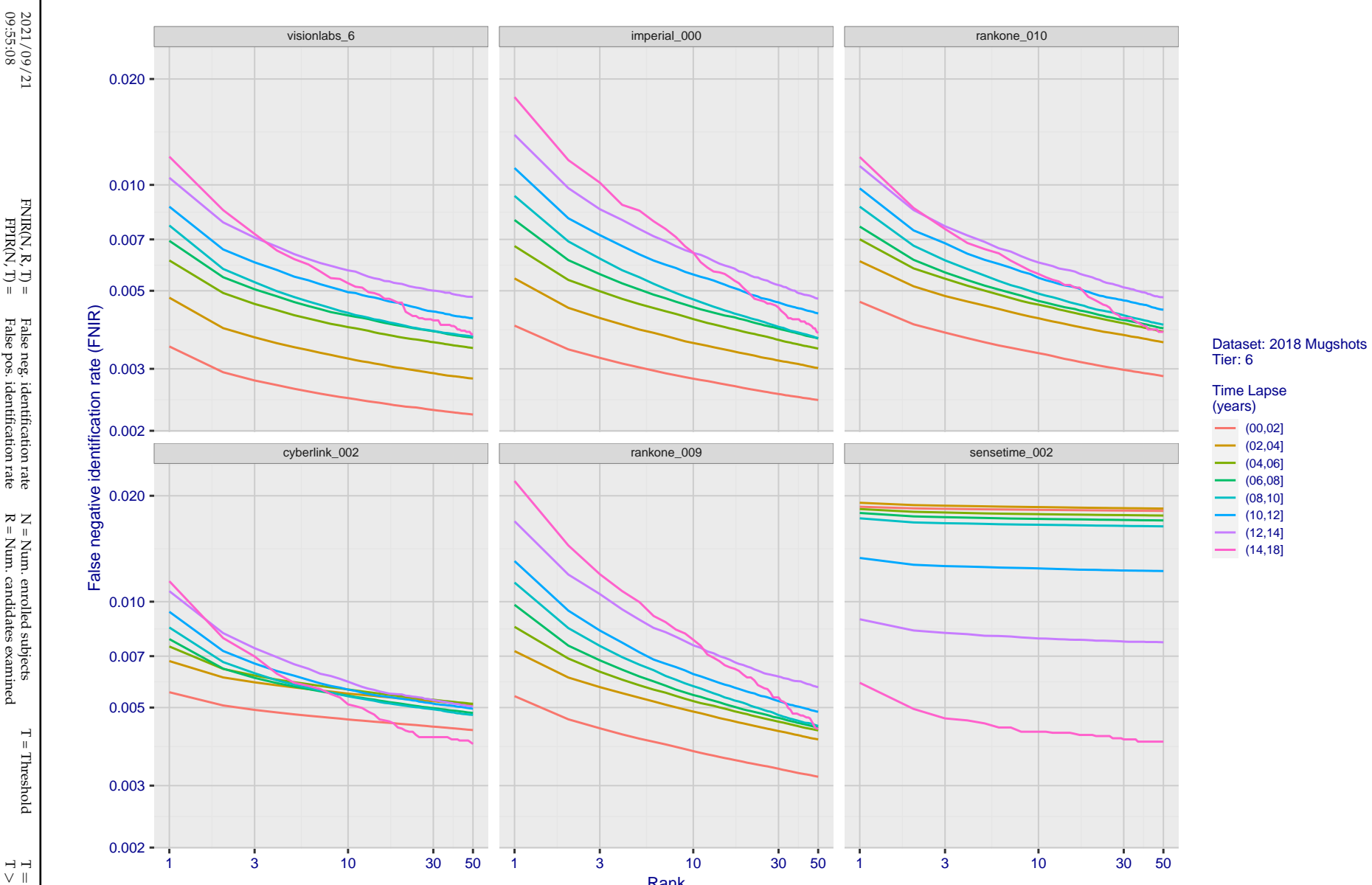


Figure 65: [FRVT-2018 Mugshot Ageing Dataset] Identification miss rates vs. rank by time-elapsed. The oldest image of each individual is enrolled. Thereafter, all more recent images are searched. Miss rates are computed over all searches noted in row 17 of Table 1 and binned by number of years between search and initial enrollment.

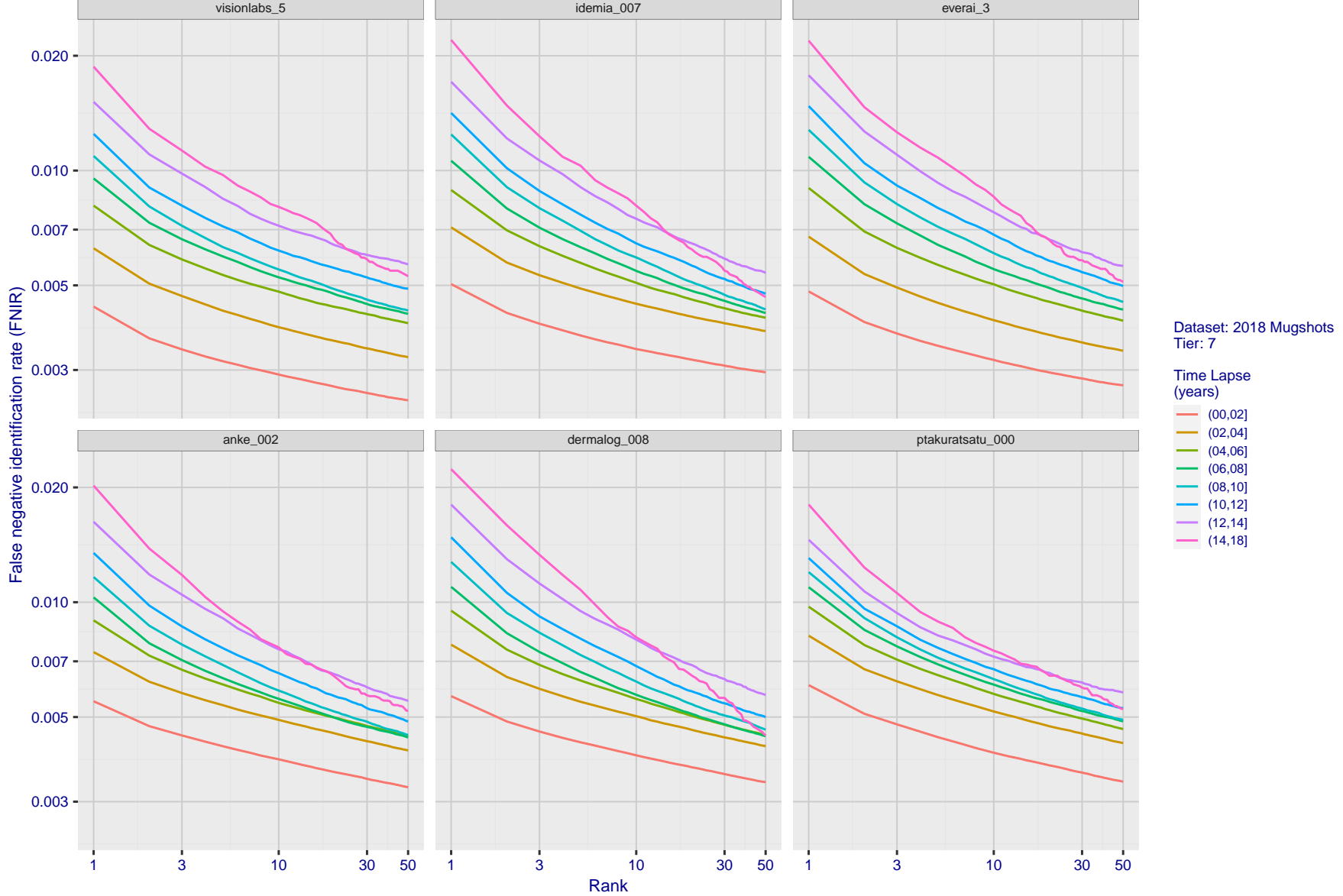


Figure 66: [FRVT-2018 Mugshot Ageing Dataset] Identification miss rates vs. rank by time-elapsed. The oldest image of each individual is enrolled. Thereafter, all more recent images are searched. Miss rates are computed over all searches noted in row 17 of Table 1 and binned by number of years between search and initial enrollment.

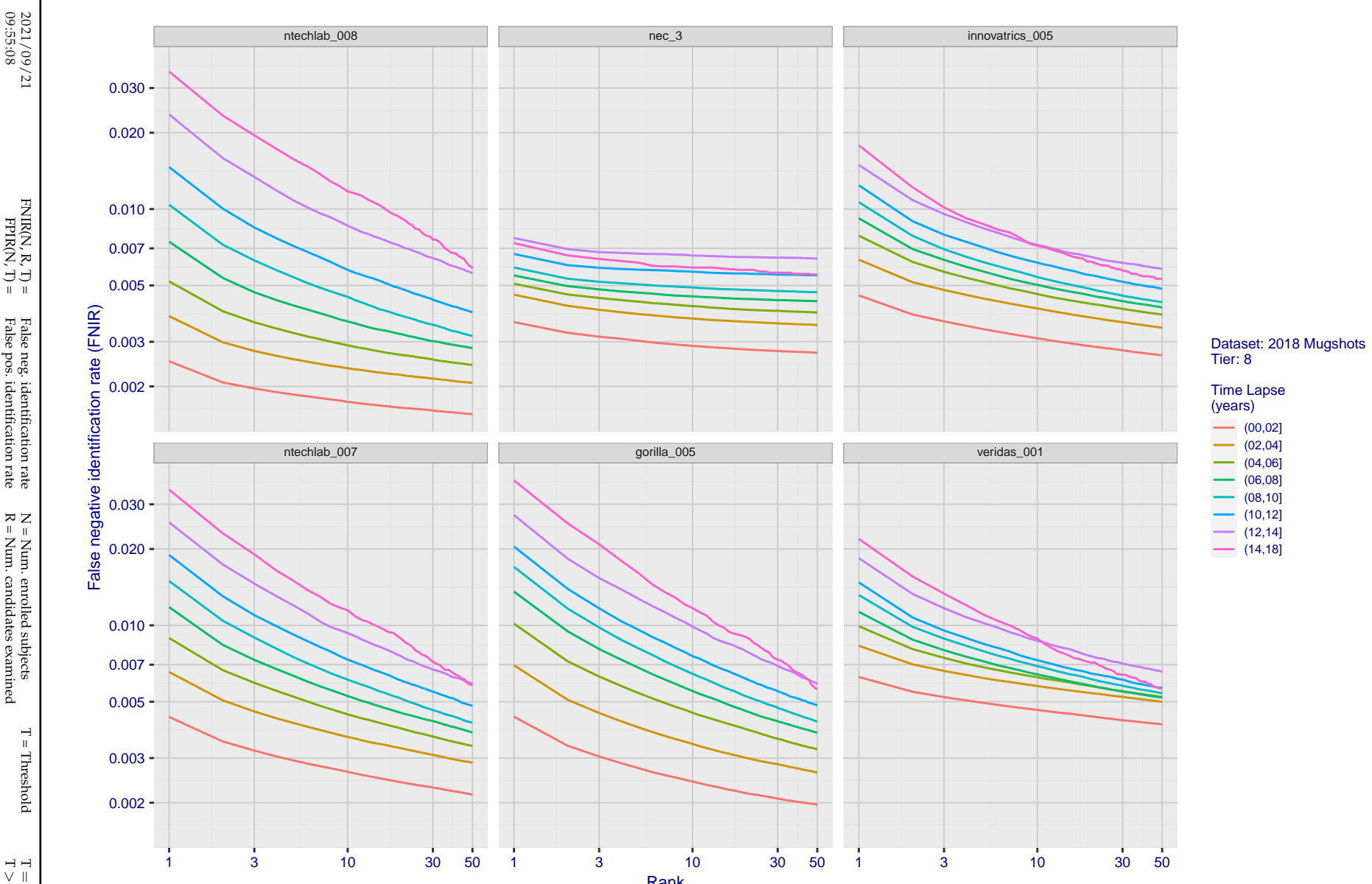


Figure 67: [FRVT-2018 Mugshot Ageing Dataset] Identification miss rates vs. rank by time-elapsed. The oldest image of each individual is enrolled. Thereafter, all more recent images are searched. Miss rates are computed over all searches noted in row 17 of Table 1 and binned by number of years between search and initial enrollment.

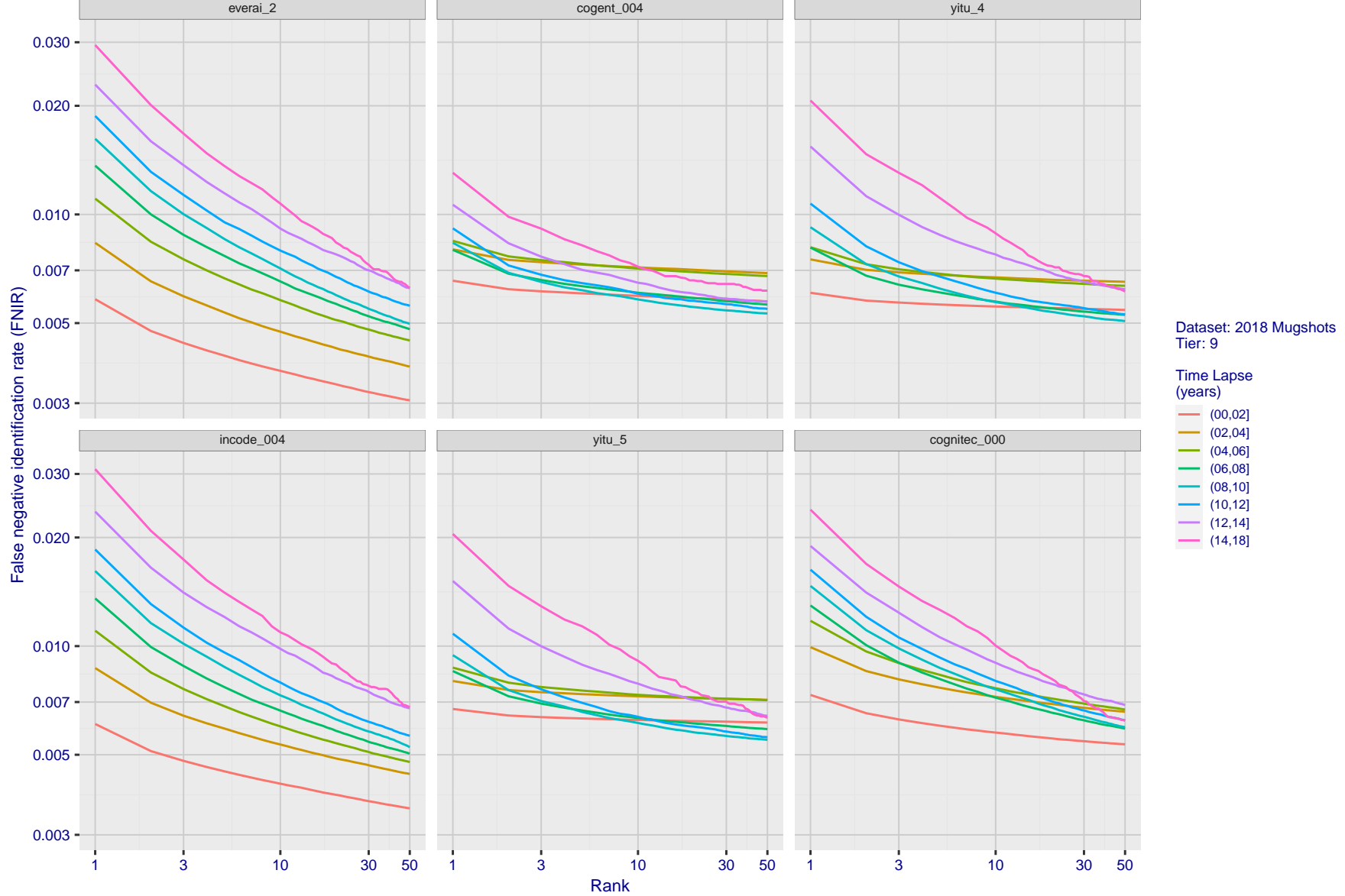


Figure 68: [FRVT-2018 Mugshot Ageing Dataset] Identification miss rates vs. rank by time-elapsed. The oldest image of each individual is enrolled. Thereafter, all more recent images are searched. Miss rates are computed over all searches noted in row 17 of Table 1 and binned by number of years between search and initial enrollment.

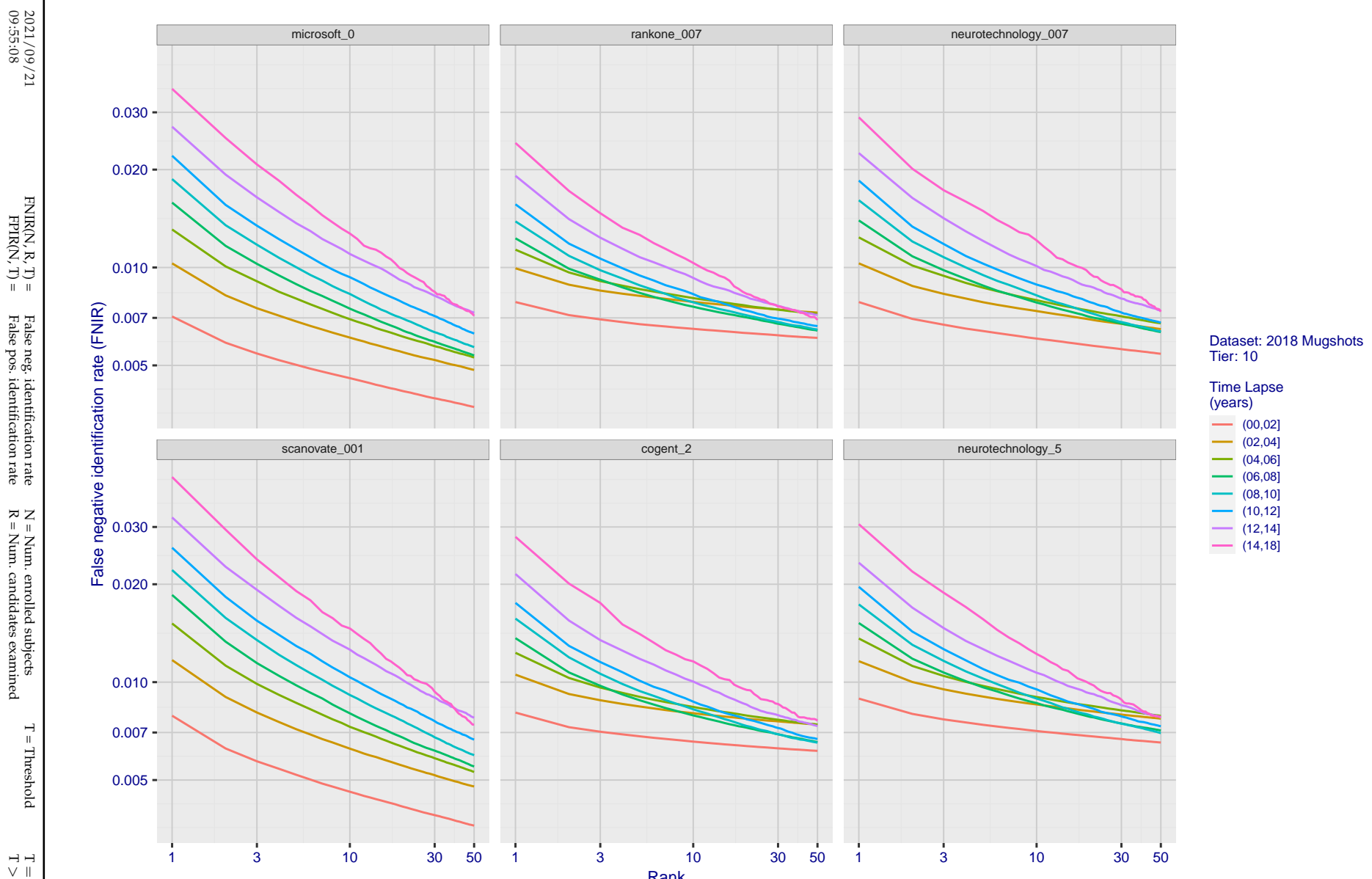
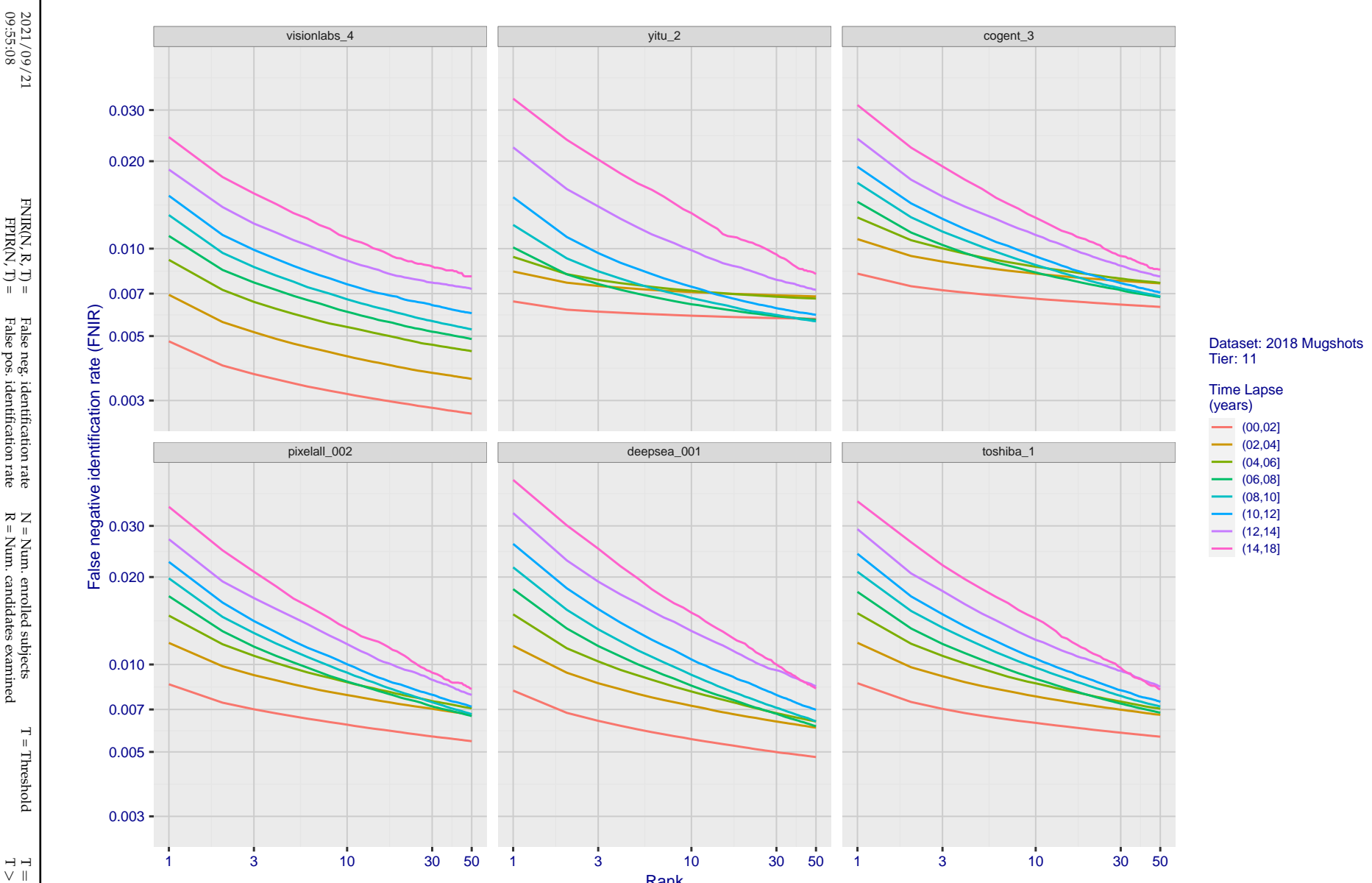
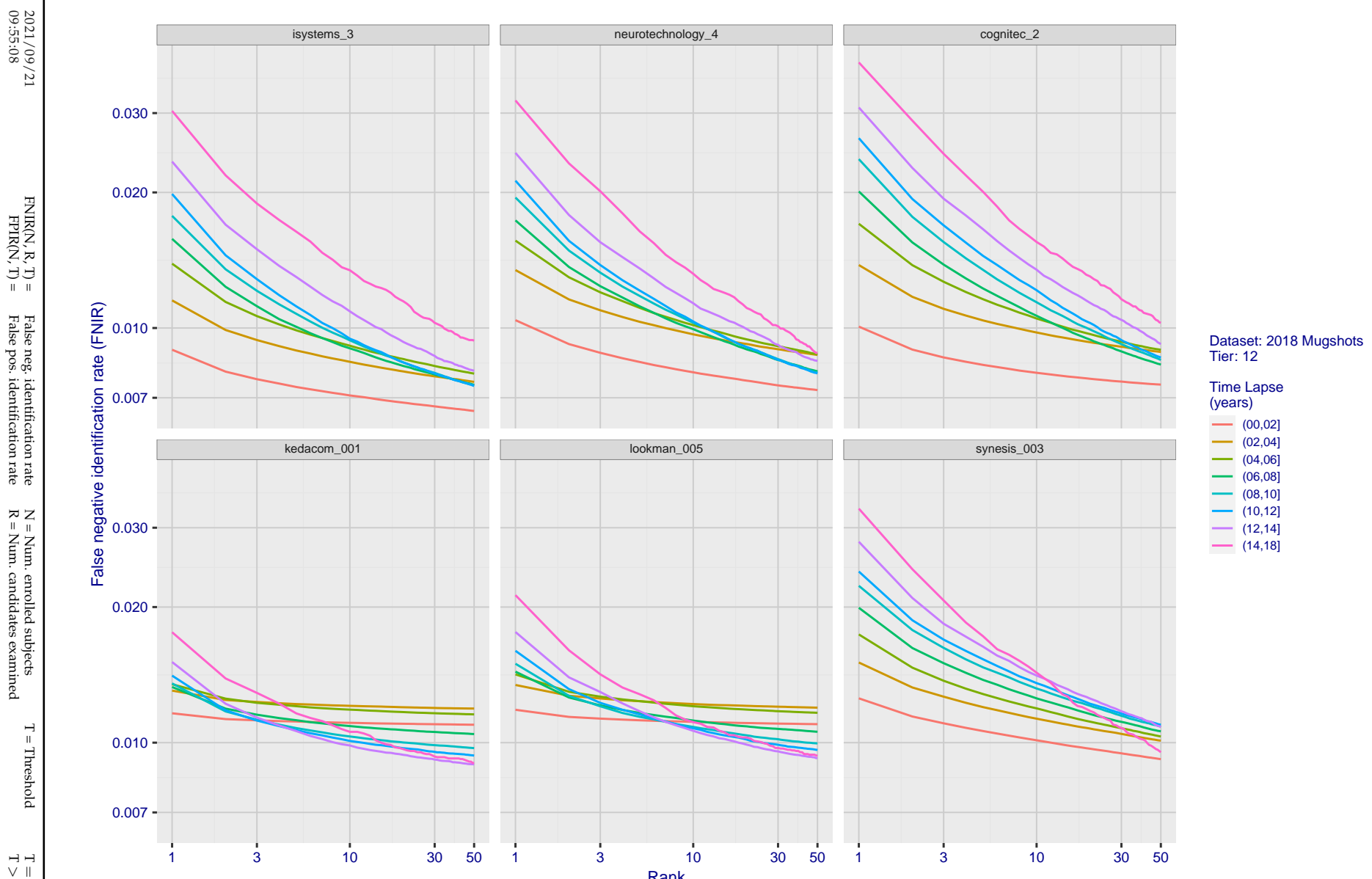


Figure 69: [FRVT-2018 Mugshot Ageing Dataset] Identification miss rates vs. rank by time elapsed. The oldest image of each individual is enrolled. Thereafter, all more recent images are searched. Miss rates are computed over all searches noted in row 17 of Table 1 and binned by number of years between search and initial enrollment.



**Figure 70: [FRVT-2018 Mugshot Ageing Dataset] Identification miss rates vs. rank by time-elapsed.** The oldest image of each individual is enrolled. Thereafter, all more recent images are searched. Miss rates are computed over all searches noted in row 17 of Table 1 and binned by number of years between search and initial enrollment.



**Figure 71: [FRVT-2018 Mugshot Ageing Dataset] Identification miss rates vs. rank by time-elapsed.** The oldest image of each individual is enrolled. Thereafter, all more recent images are searched. Miss rates are computed over all searches noted in row 17 of Table 1 and binned by number of years between search and initial enrollment.

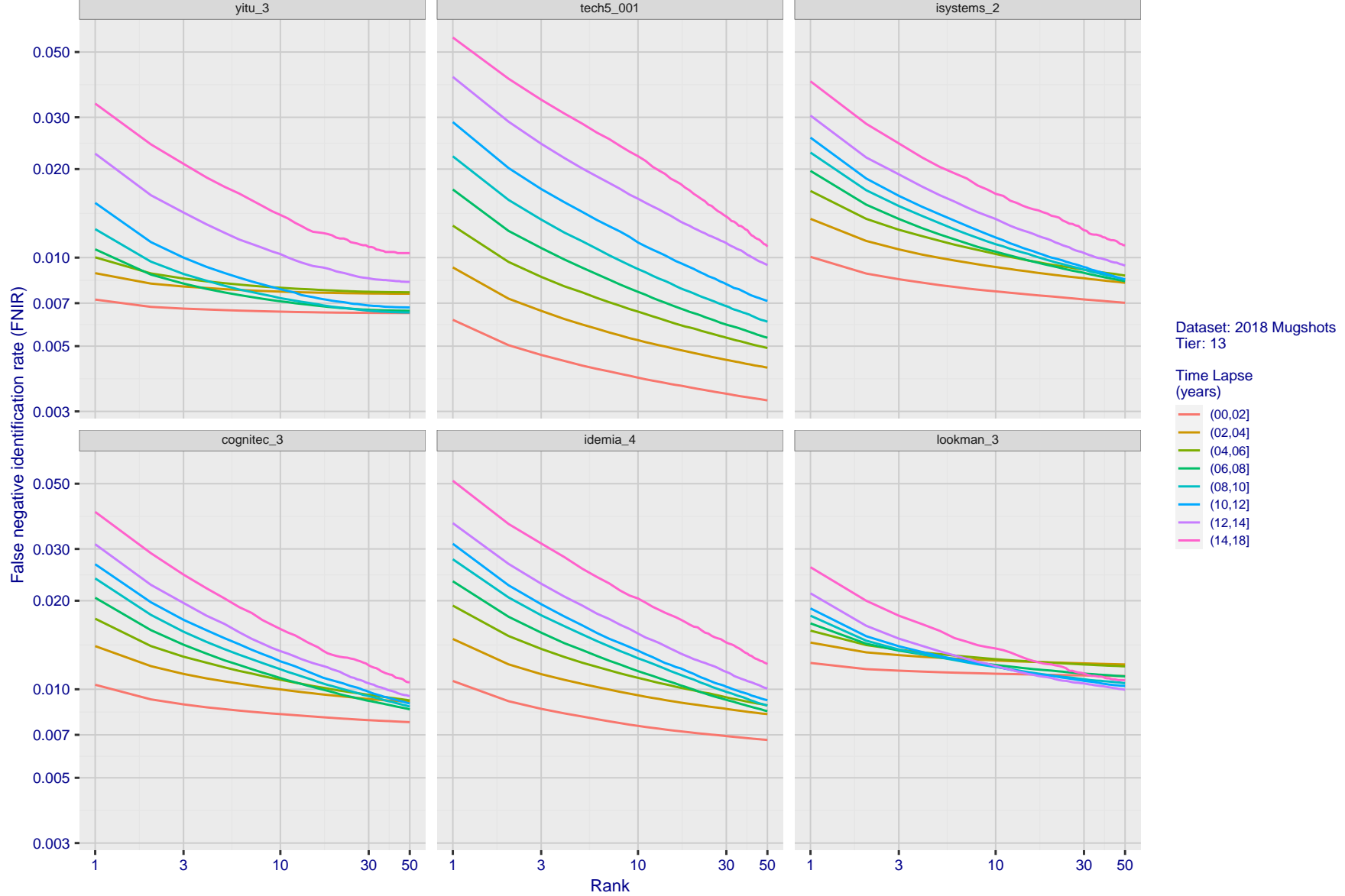


**Figure 72: [FRVT-2018 Mugshot Ageing Dataset] Identification miss rates vs. rank by time-elapsed.** The oldest image of each individual is enrolled. Thereafter, all more recent images are searched. Miss rates are computed over all searches noted in row 17 of Table 1 and binned by number of years between search and initial enrollment.

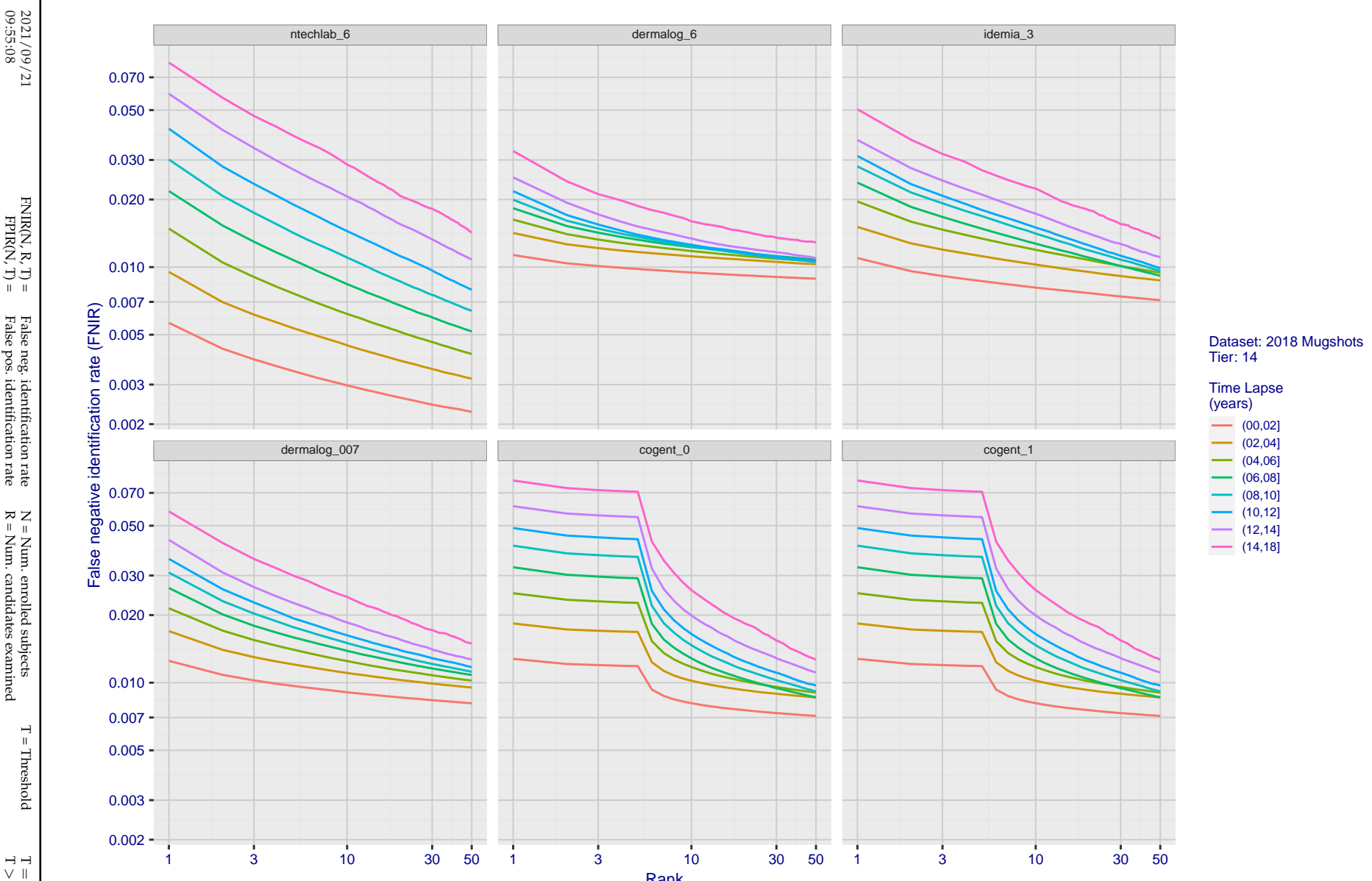


Figure 73: [FRVT-2018 Mugshot Ageing Dataset] Identification miss rates vs. rank by time elapsed. The oldest image of each individual is enrolled. Thereafter, all more recent images are searched. Miss rates are computed over all searches noted in row 17 of Table 1 and binned by number of years between search and initial enrollment.

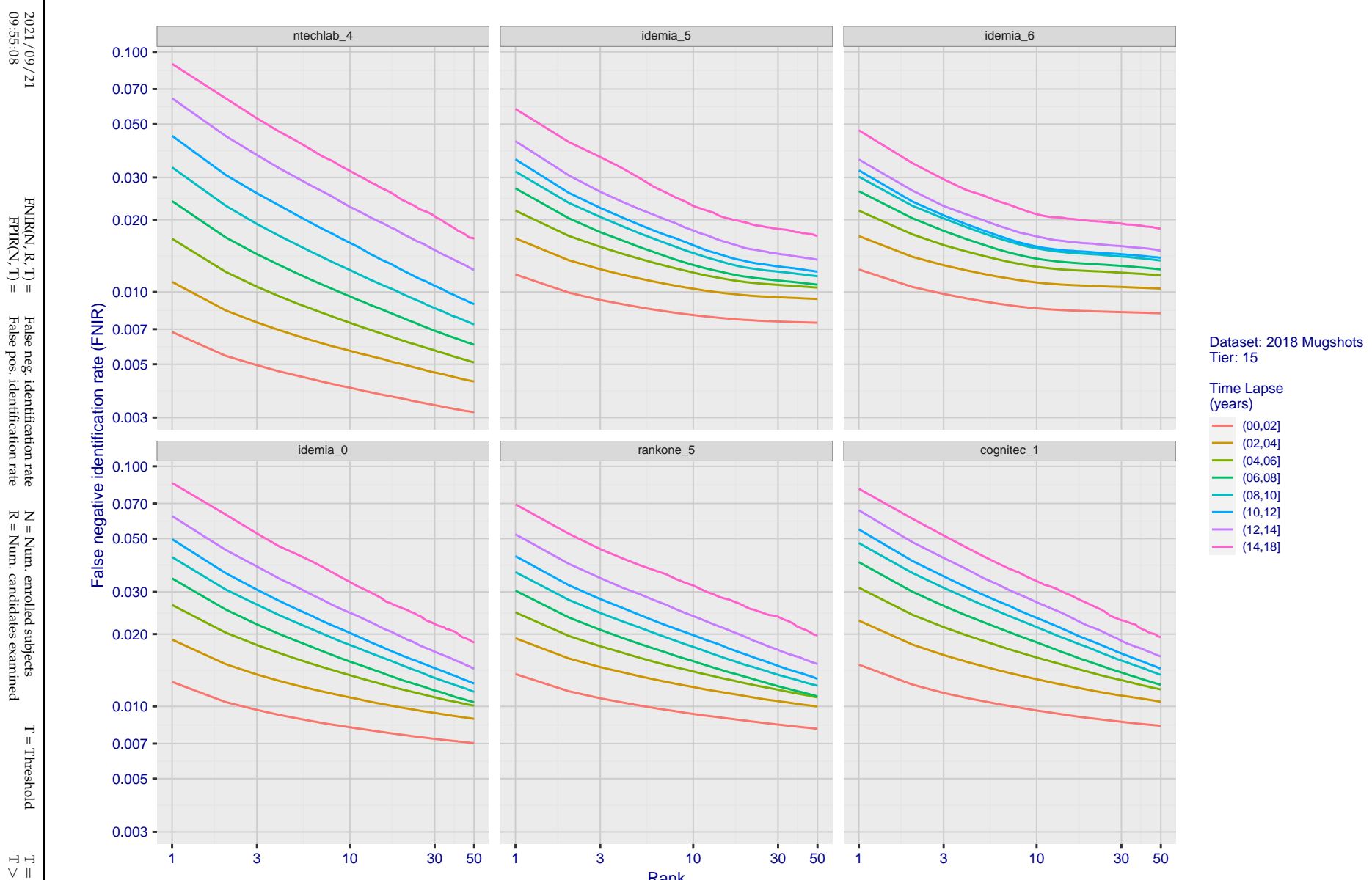


Figure 74: [FRVT-2018 Mugshot Ageing Dataset] Identification miss rates vs. rank by time elapsed. The oldest image of each individual is enrolled. Thereafter, all more recent images are searched. Miss rates are computed over all searches noted in row 17 of Table 1 and binned by number of years between search and initial enrollment.

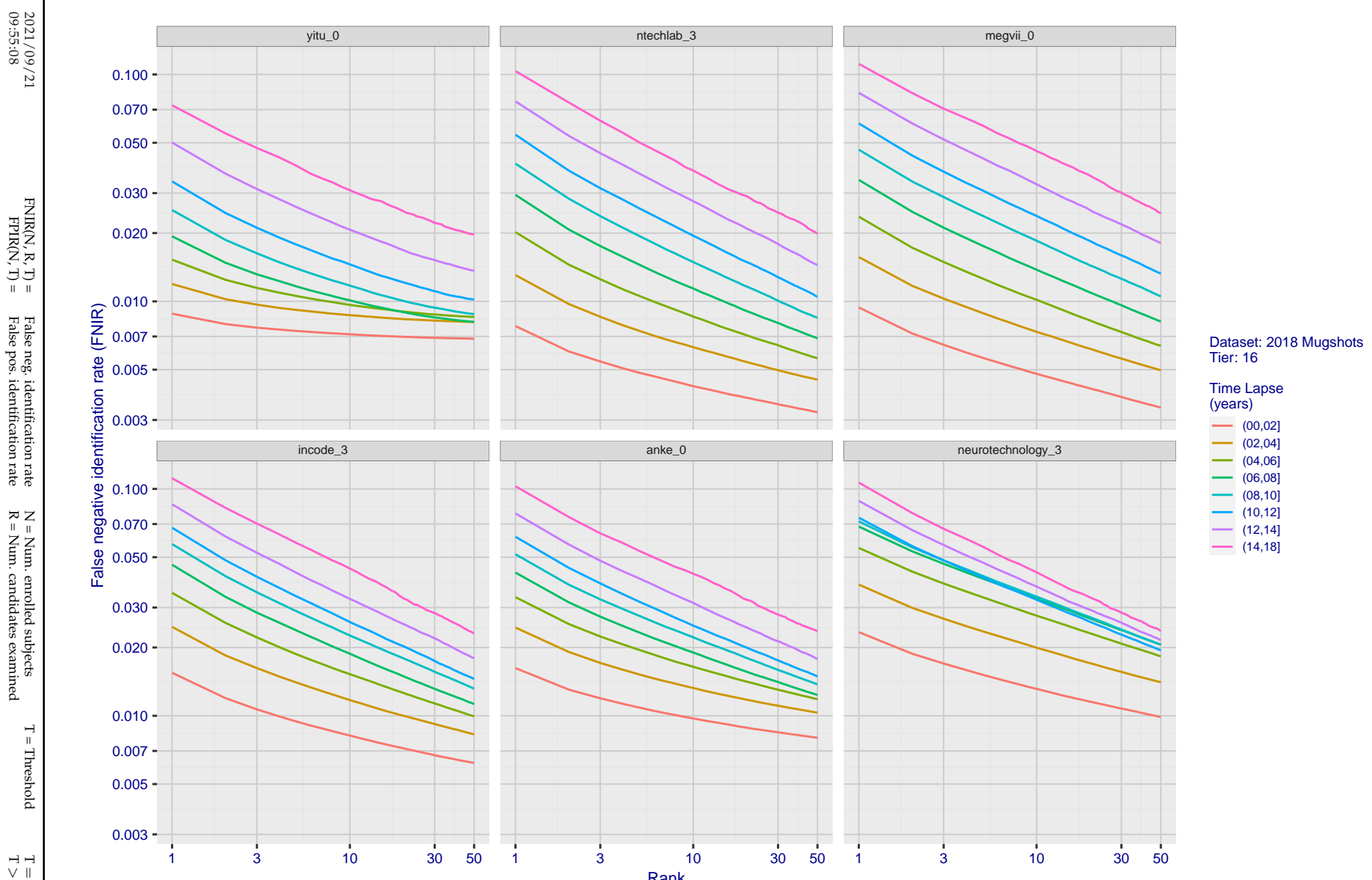
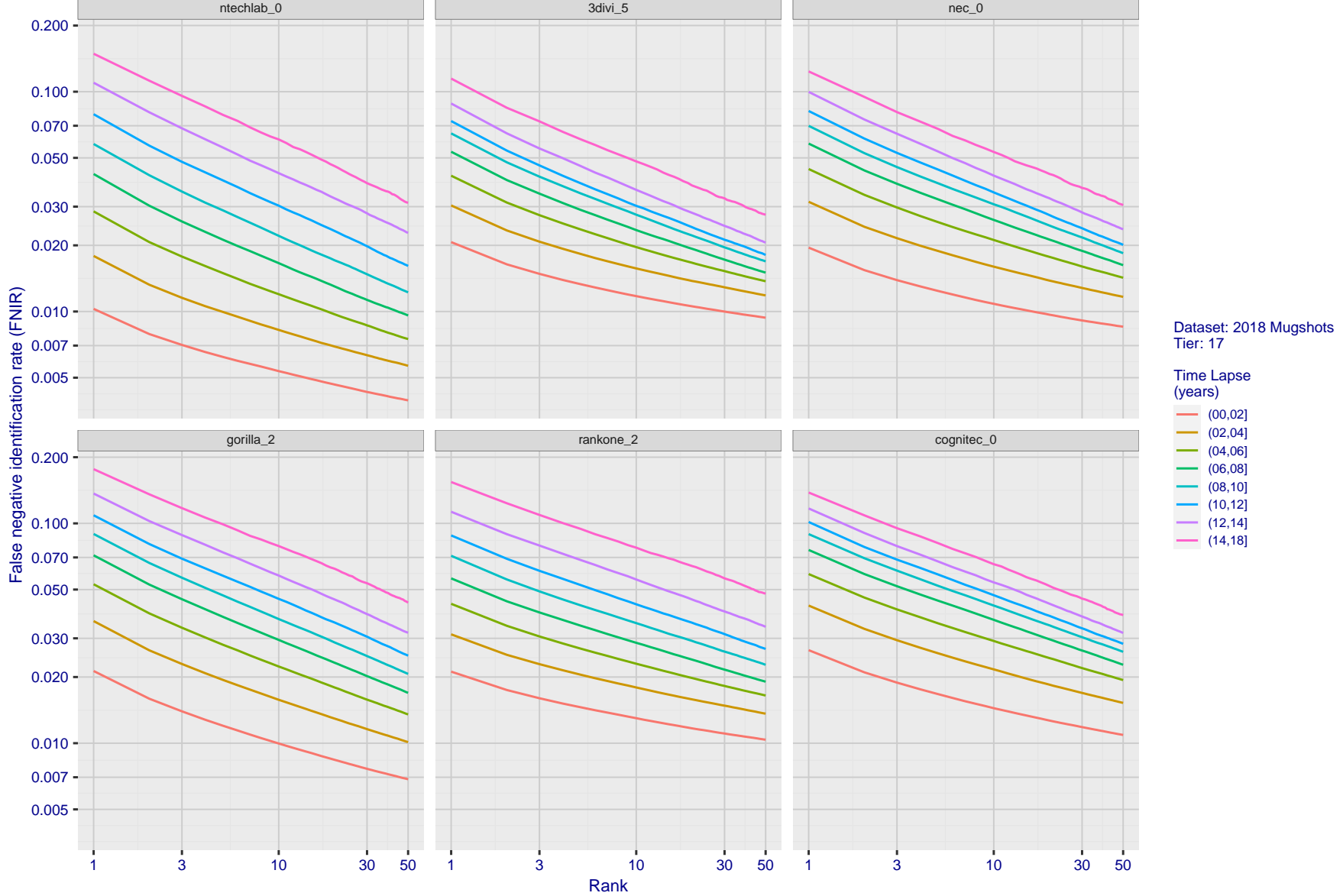
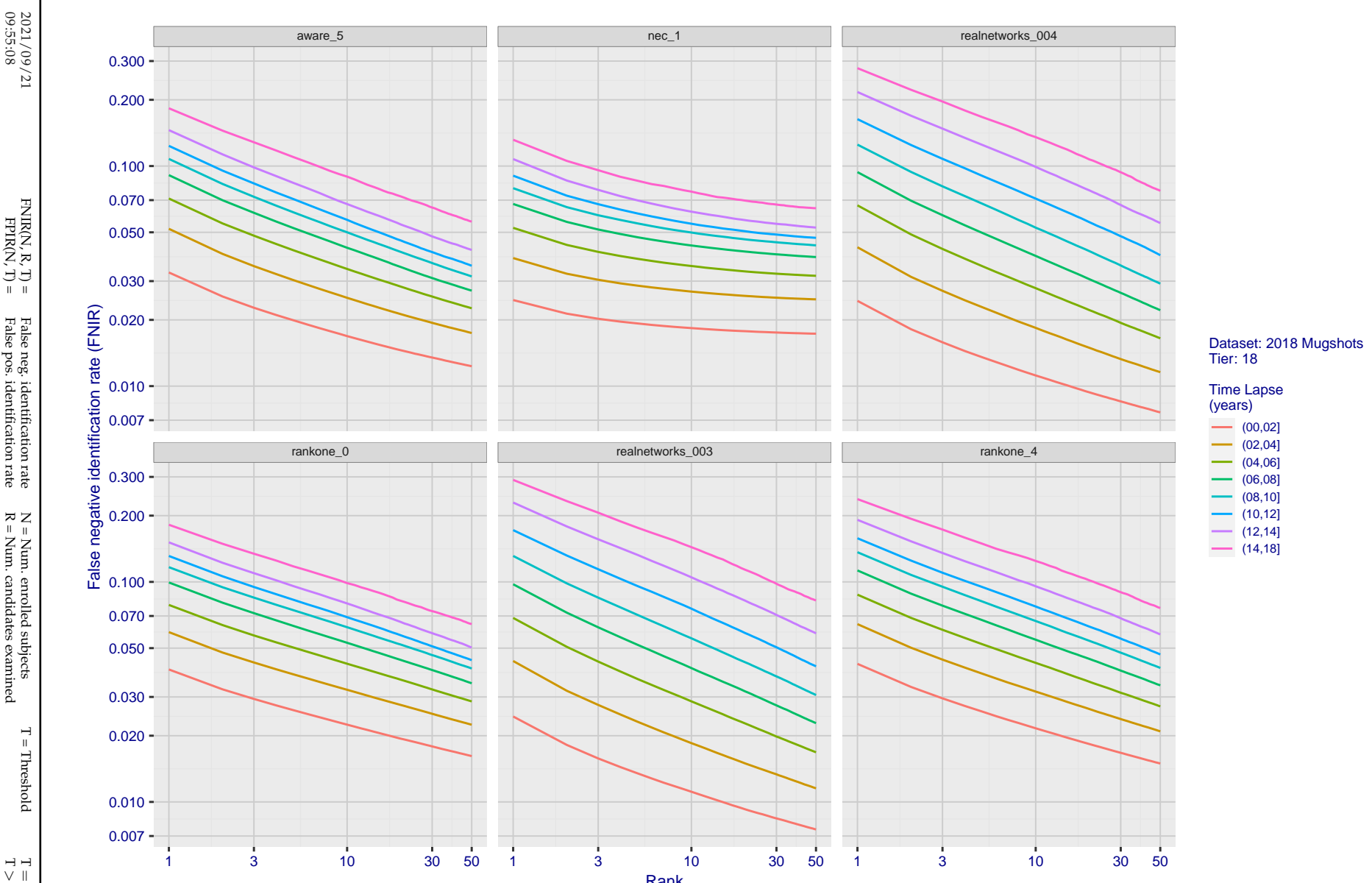


Figure 75: [FRVT-2018 Mugshot Ageing Dataset] Identification miss rates vs. rank by time-elapsed. The oldest image of each individual is enrolled. Thereafter, all more recent images are searched. Miss rates are computed over all searches noted in row 17 of Table 1 and binned by number of years between search and initial enrollment.



**Figure 76: [FRVT-2018 Mugshot Ageing Dataset] Identification miss rates vs. rank by time-elapsed.** The oldest image of each individual is enrolled. Thereafter, all more recent images are searched. Miss rates are computed over all searches noted in row 17 of Table 1 and binned by number of years between search and initial enrollment.



**Figure 77: [FRVT-2018 Mugshot Ageing Dataset] Identification miss rates vs. rank by time-elapsed.** The oldest image of each individual is enrolled. Thereafter, all more recent images are searched. Miss rates are computed over all searches noted in row 17 of Table 1 and binned by number of years between search and initial enrollment.

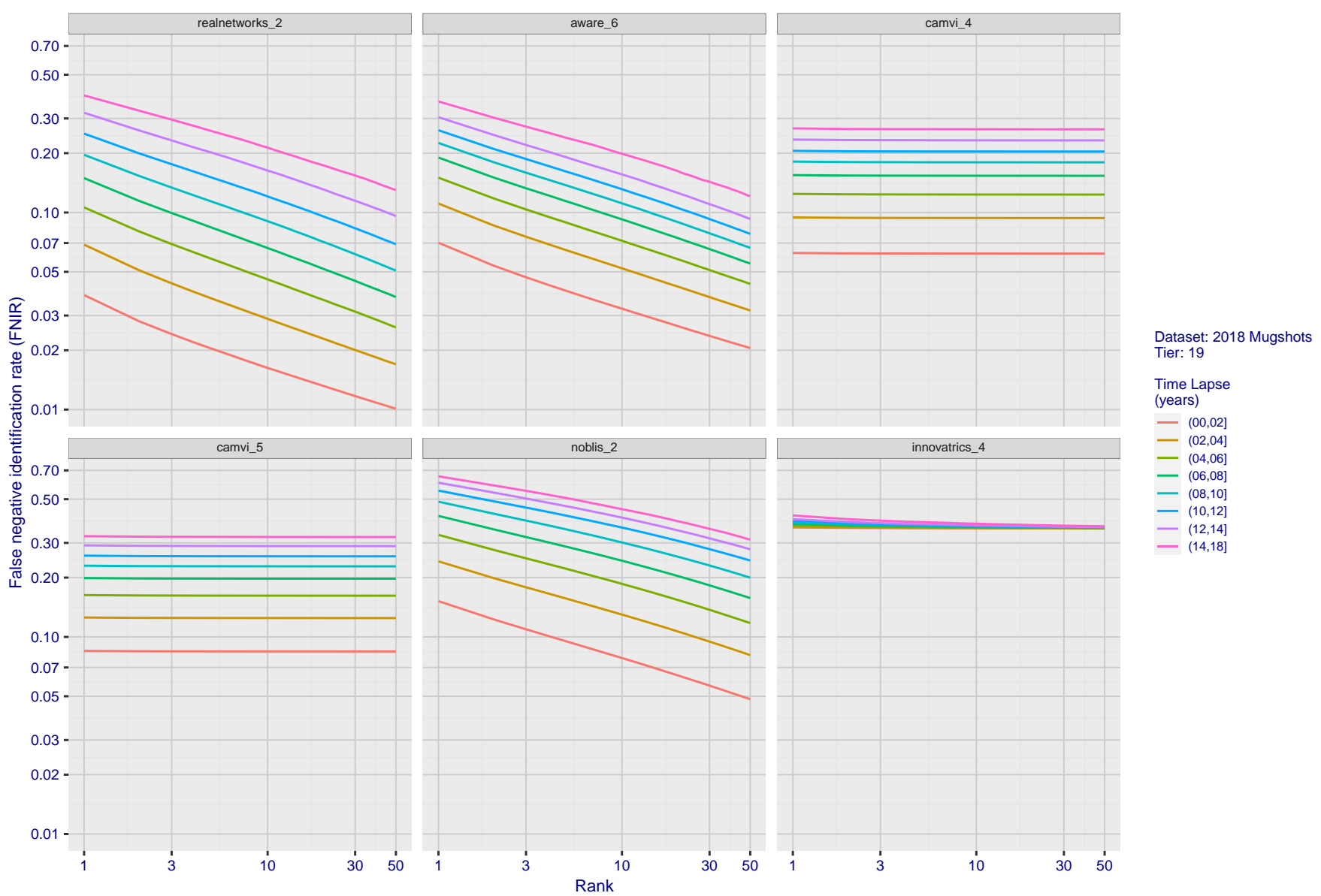
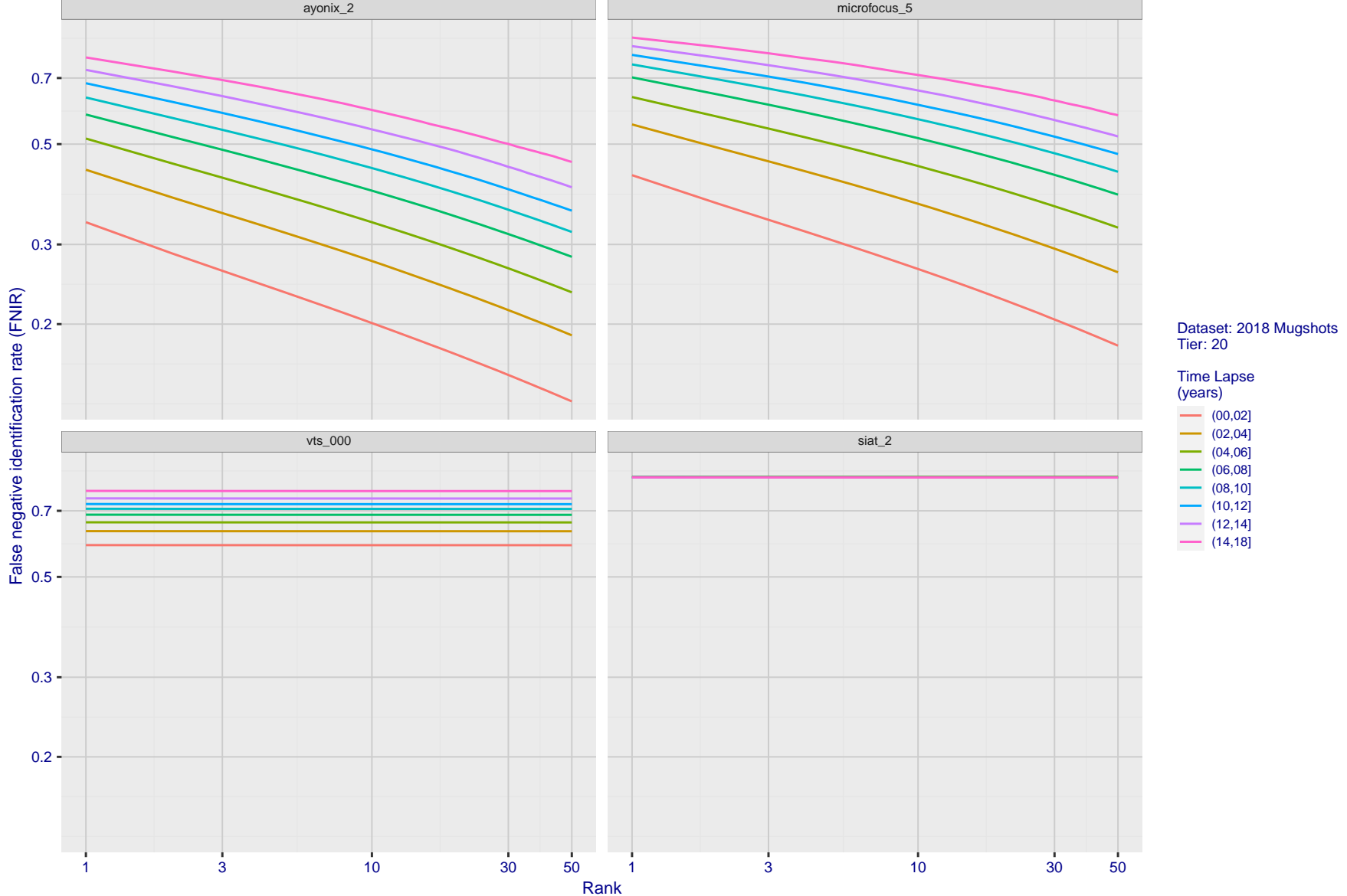


Figure 78: [FRVT-2018 Mugshot Ageing Dataset] Identification miss rates vs. rank by time-elapsed. The oldest image of each individual is enrolled. Thereafter, all more recent images are searched. Miss rates are computed over all searches noted in row 17 of Table 1 and binned by number of years between search and initial enrollment.



**Figure 79: [FRVT-2018 Mugshot Ageing Dataset] Identification miss rates vs. rank by time-elapsed.** The oldest image of each individual is enrolled. Thereafter, all more recent images are searched. Miss rates are computed over all searches noted in row 17 of Table 1 and binned by number of years between search and initial enrollment.

---

2021/09/21  
09:55:08

FNIR(N, R, T) = False neg. identification rate  
FPTR(N, T) = False pos. identification rate

N = Num. enrolled subjects  
R = Num. candidates examined  
T = Threshold  
T = 0 → Investigation  
T > 0 → Identification

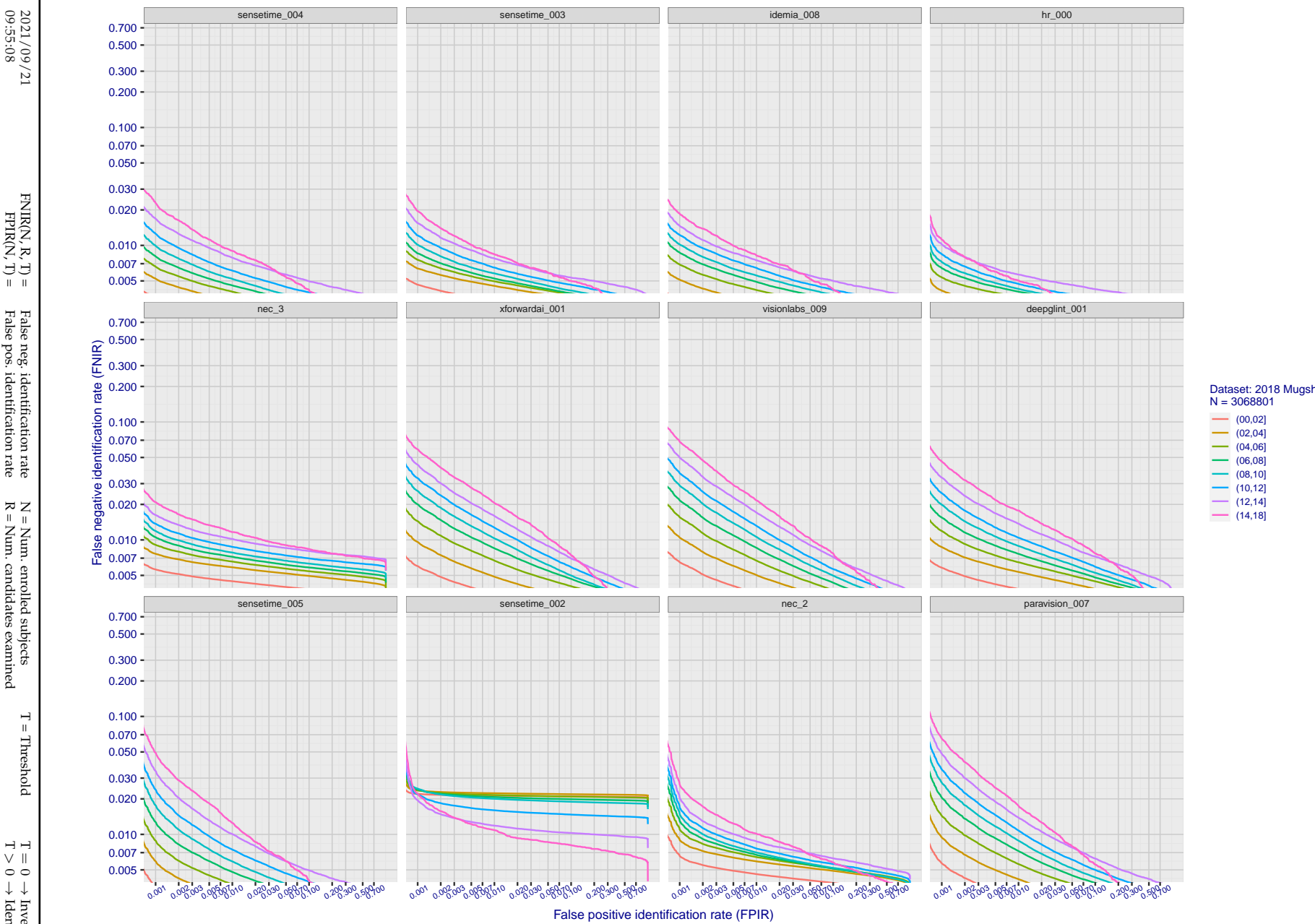


**Figure 80: [FRVT-2018 Mugshot Ageing Dataset] Identification miss rates vs. FPIR by time-elapsed.** The oldest image of each individual is enrolled. Thereafter, all more recent images are searched. Miss rates are computed over all searches noted in row 17 of Table 1 and binned by number of years between search and initial enrollment. FPIR is computed from the same FRVT 2018 non-mates noted in row 3 of Table 1 with  $N = 3000\,000$ .

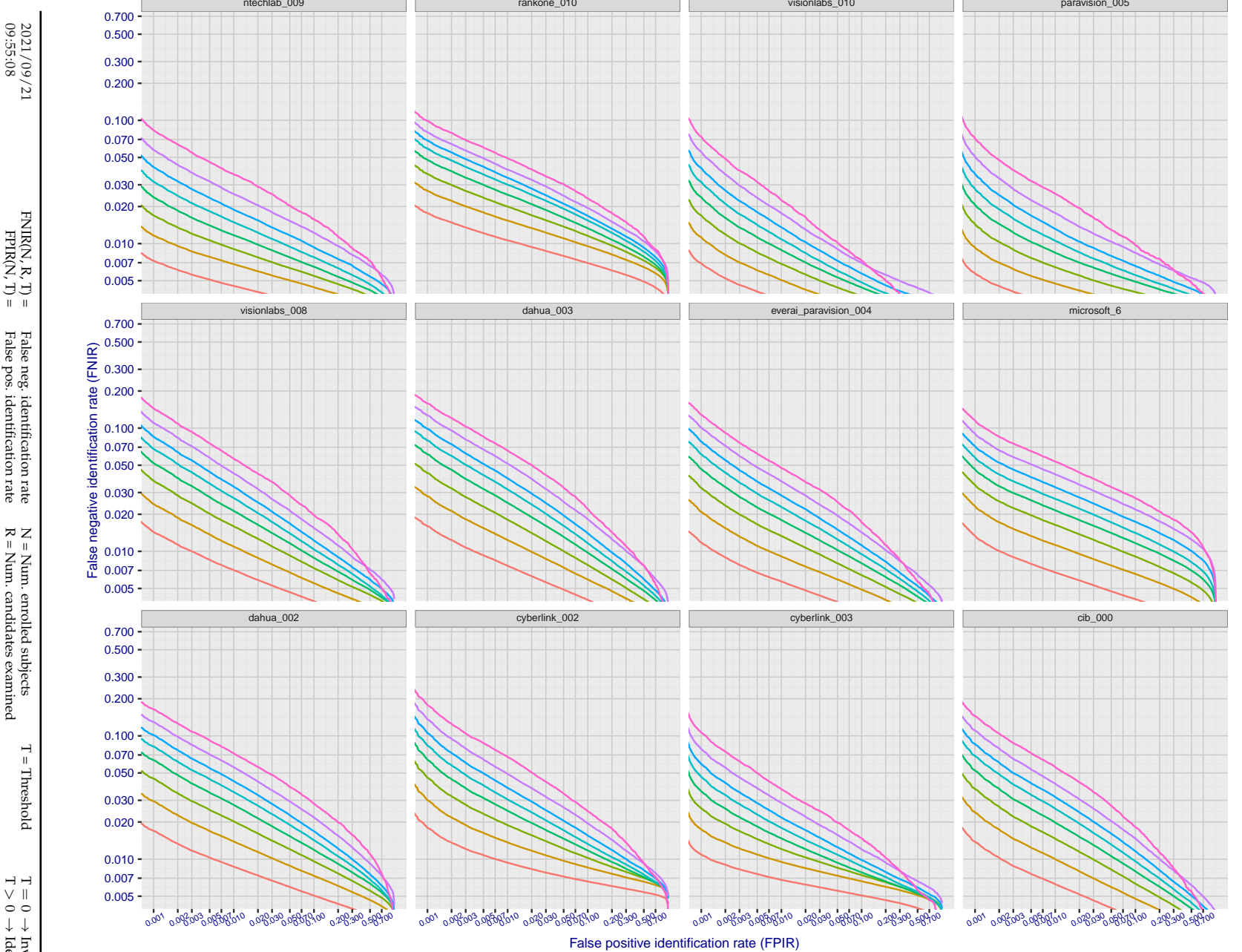
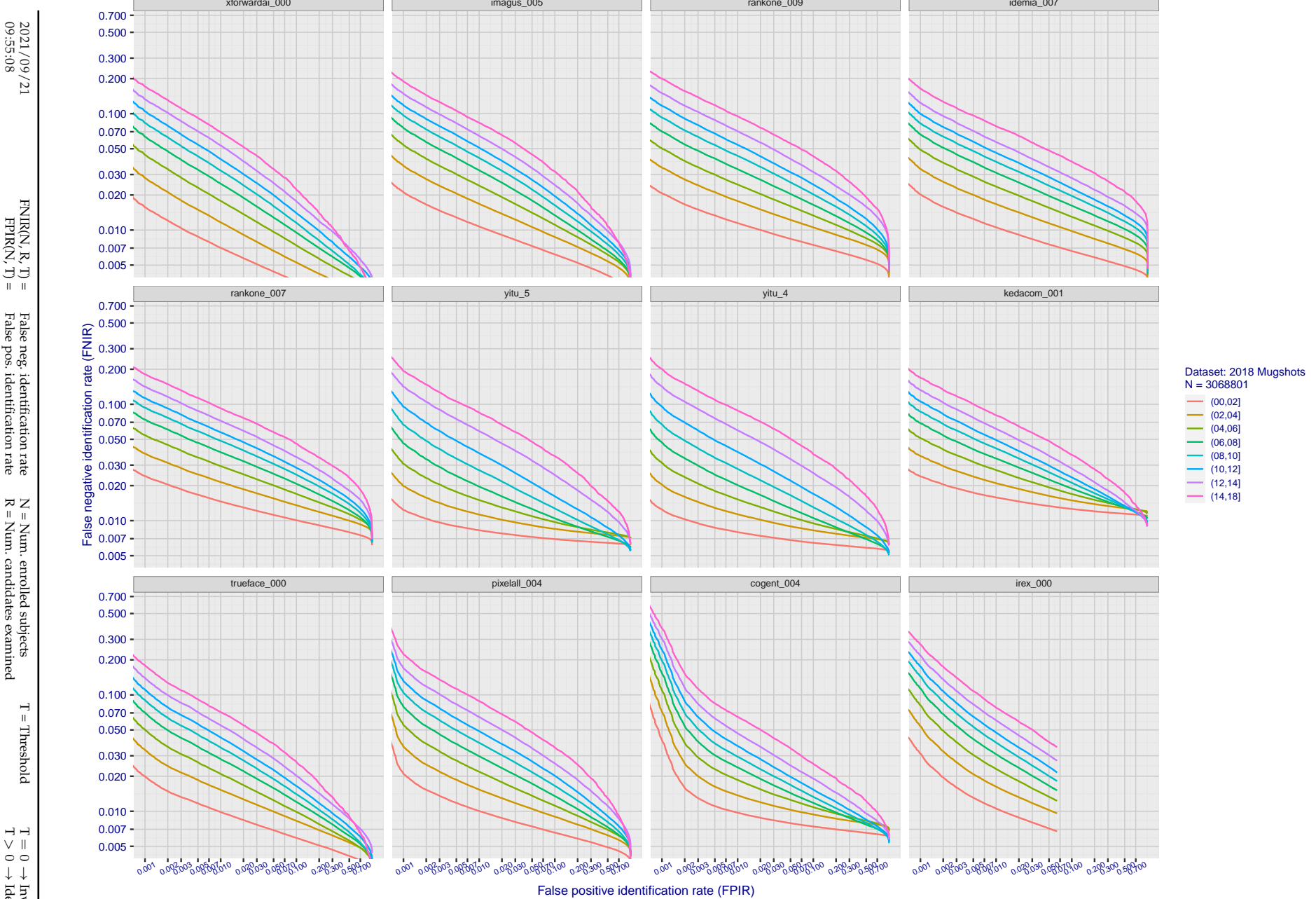
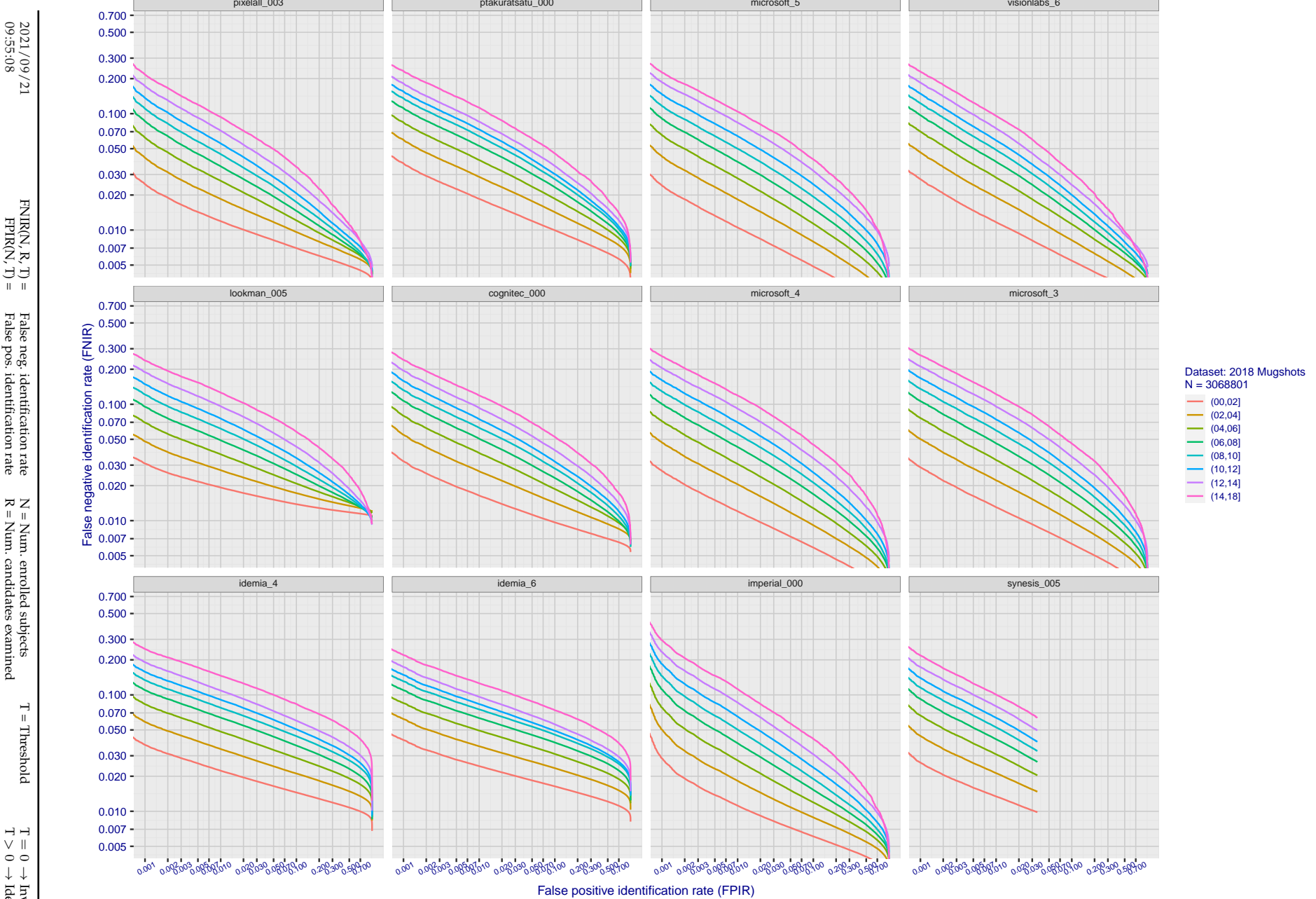


Figure 81: [FRVT-2018 Mugshot Ageing Dataset] Identification miss rates vs. FPIR by time-elapsed. The oldest image of each individual is enrolled. Thereafter, all more recent images are searched. Miss rates are computed over all searches noted in row 17 of Table 1 and binned by number of years between search and initial enrollment. FPIR is computed from the same FRVT 2018 non-mates noted in row 3 of Table 1 with  $N = 3\,000\,000$ .



**Figure 82: [FRVT-2018 Mugshot Ageing Dataset] Identification miss rates vs. FPIR by time-elapsed.** The oldest image of each individual is enrolled. Thereafter, all more recent images are searched. Miss rates are computed over all searches noted in row 17 of Table 1 and binned by number of years between search and initial enrollment. FPIR is computed from the same FRVT 2018 non-mates noted in row 3 of Table 1 with  $N = 3\,000\,000$ .



**Figure 83: [FRVT-2018 Mugshot Ageing Dataset] Identification miss rates vs. FPIR by time-elapsed.** The oldest image of each individual is enrolled. Thereafter, all more recent images are searched. Miss rates are computed over all searches noted in row 17 of Table 1 and binned by number of years between search and initial enrollment. FPIR is computed from the same FRVT 2018 non-mates noted in row 3 of Table 1 with  $N = 3\,000\,000$ .

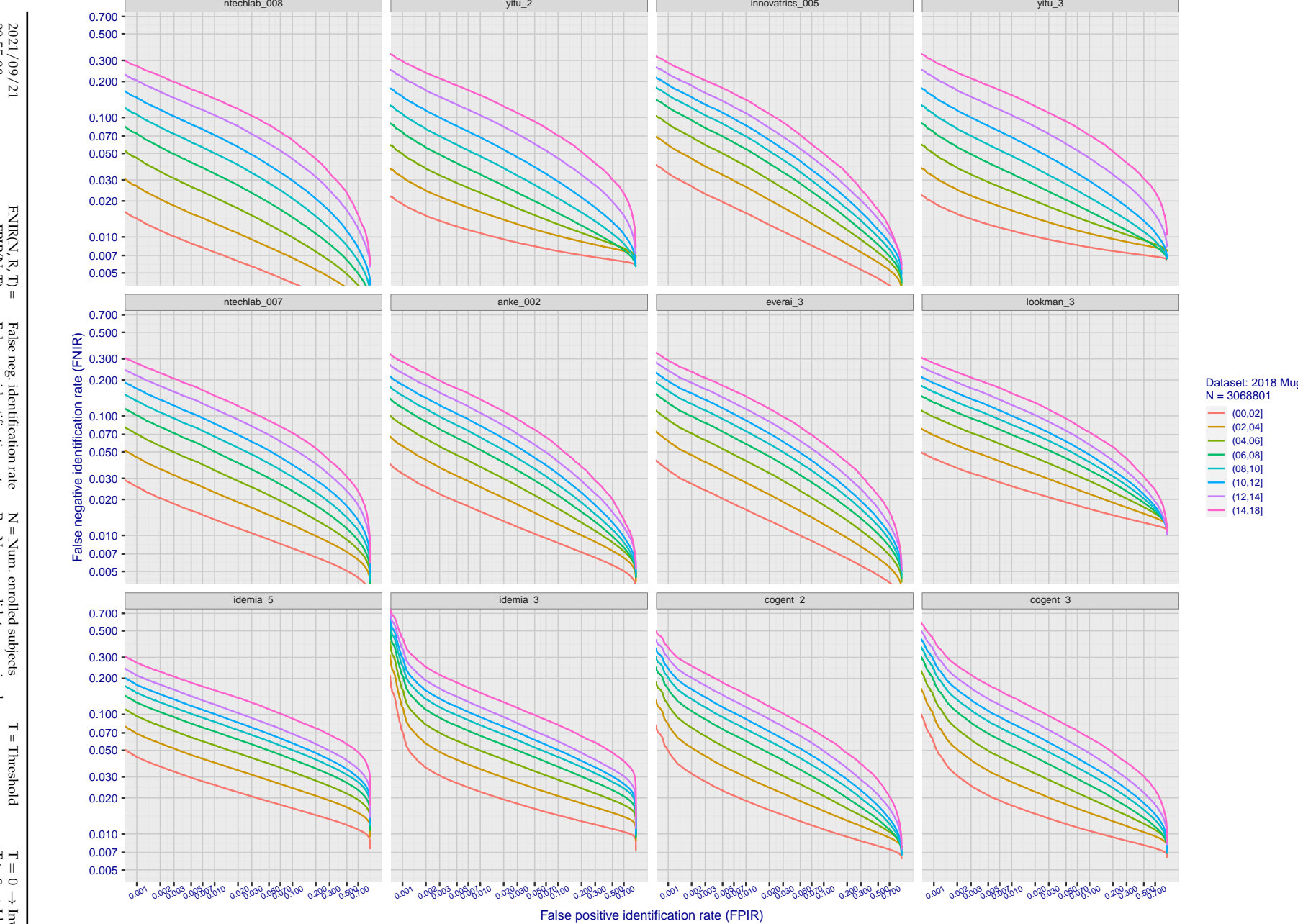


**Figure 84: [FRVT-2018 Mugshot Ageing Dataset] Identification miss rates vs. FPIR by time-elapsed.** The oldest image of each individual is enrolled. Thereafter, all more recent images are searched. Miss rates are computed over all searches noted in row 17 of Table 1 and binned by number of years between search and initial enrollment. FPIR is computed from the same FRVT 2018 non-mates noted in row 3 of Table 1 with N = 3 000 000.

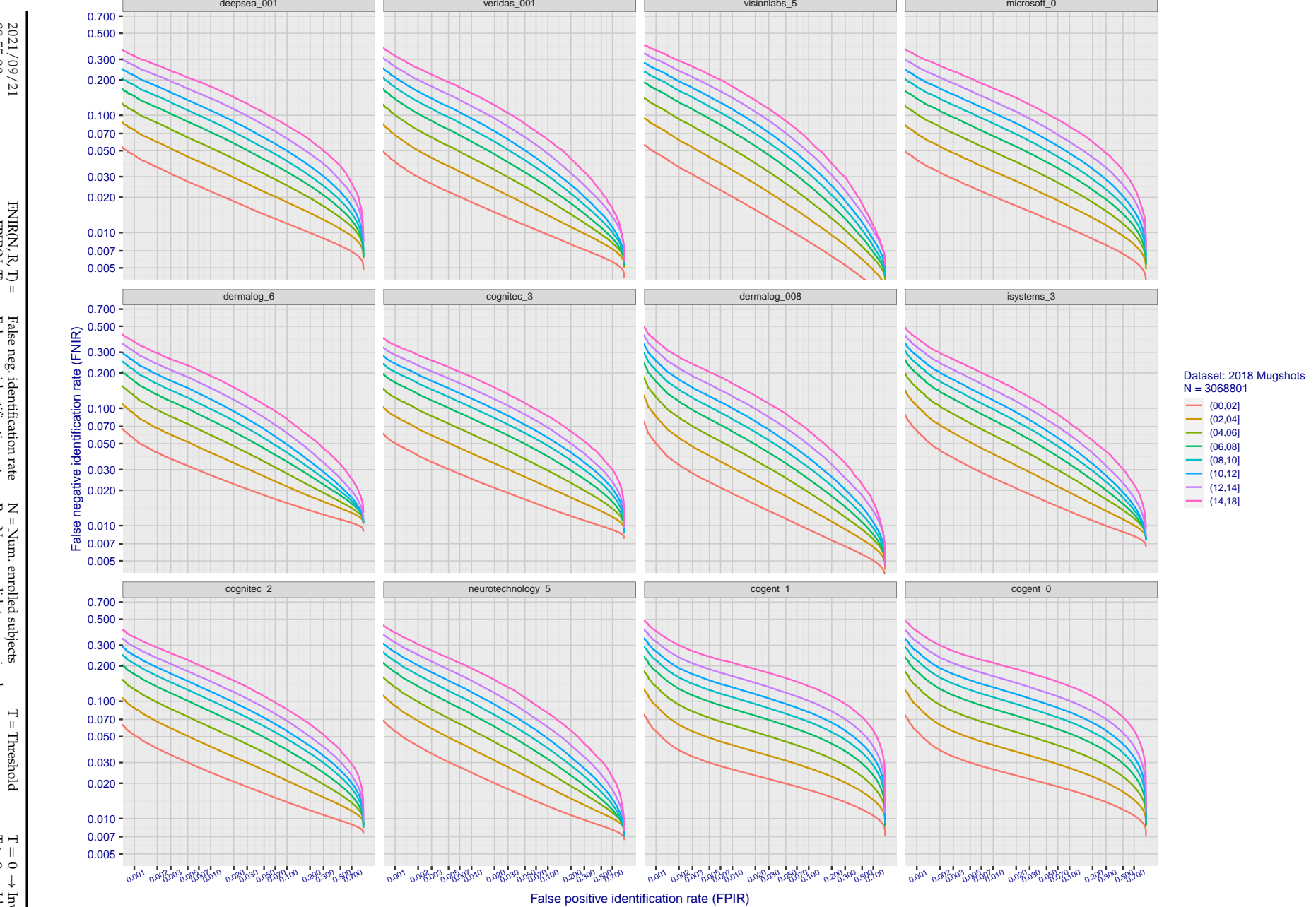


**Figure 85: [FRVT-2018 Mugshot Ageing Dataset] Identification miss rates vs. FPIR by time-elapsed.** The oldest image of each individual is enrolled. Thereafter, all more recent images are searched. Miss rates are computed over all searches noted in row 17 of Table 1 and binned by number of years between search and initial enrollment. FPIR is computed from the same FRVT 2018 non-mates noted in row 3 of Table 1 with  $N = 3\,000\,000$ .

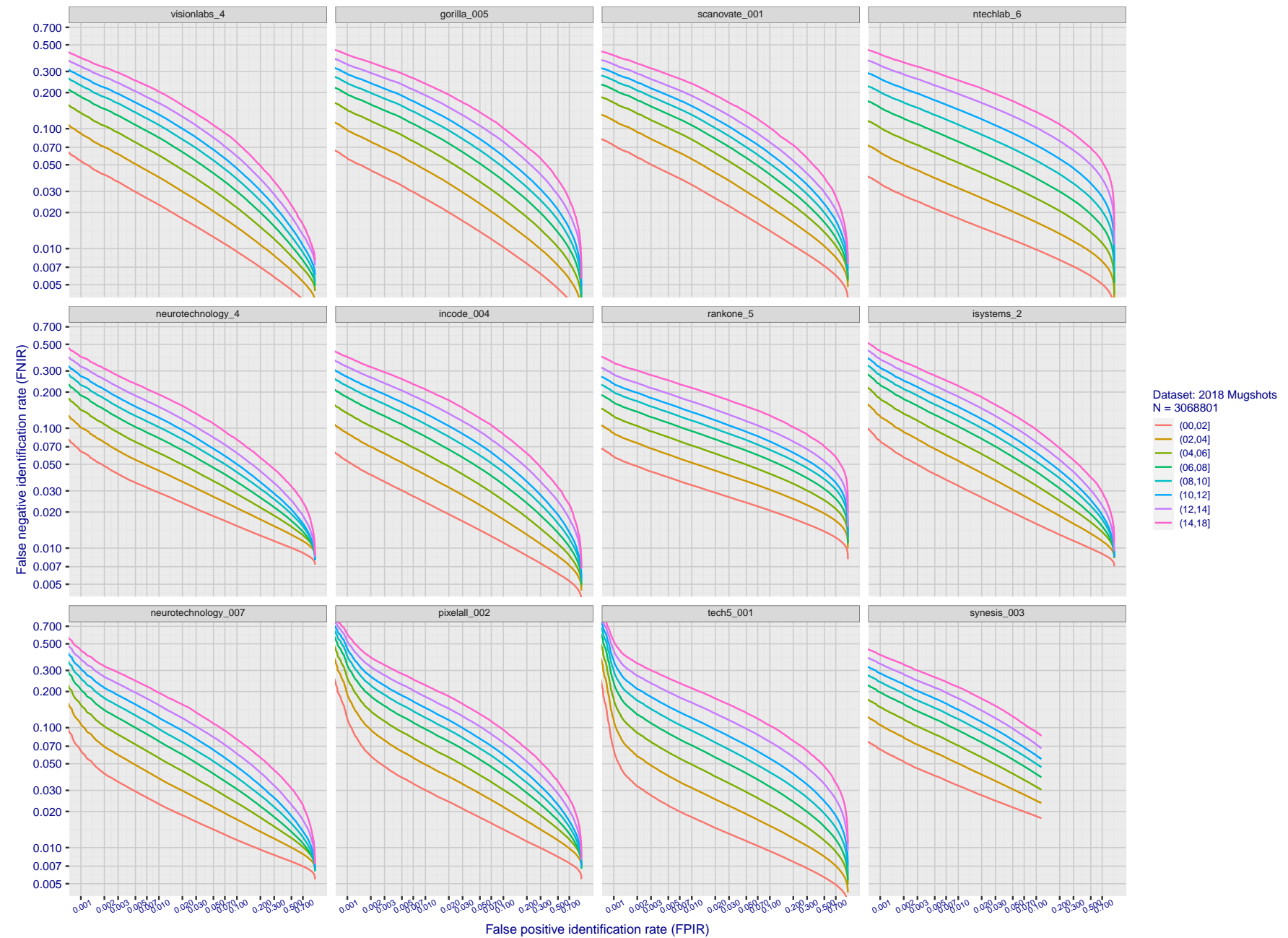


**Figure 86: [FRVT-2018 Mugshot Ageing Dataset] Identification miss rates vs. FPIR by time-elapsed.** The oldest image of each individual is enrolled. Thereafter, all more recent images are searched. Miss rates are computed over all searches noted in row 17 of Table 1 and binned by number of years between search and initial enrollment. FPIR is computed from the same FRVT 2018 non-mates noted in row 3 of Table 1 with  $N = 3\,000\,000$ .

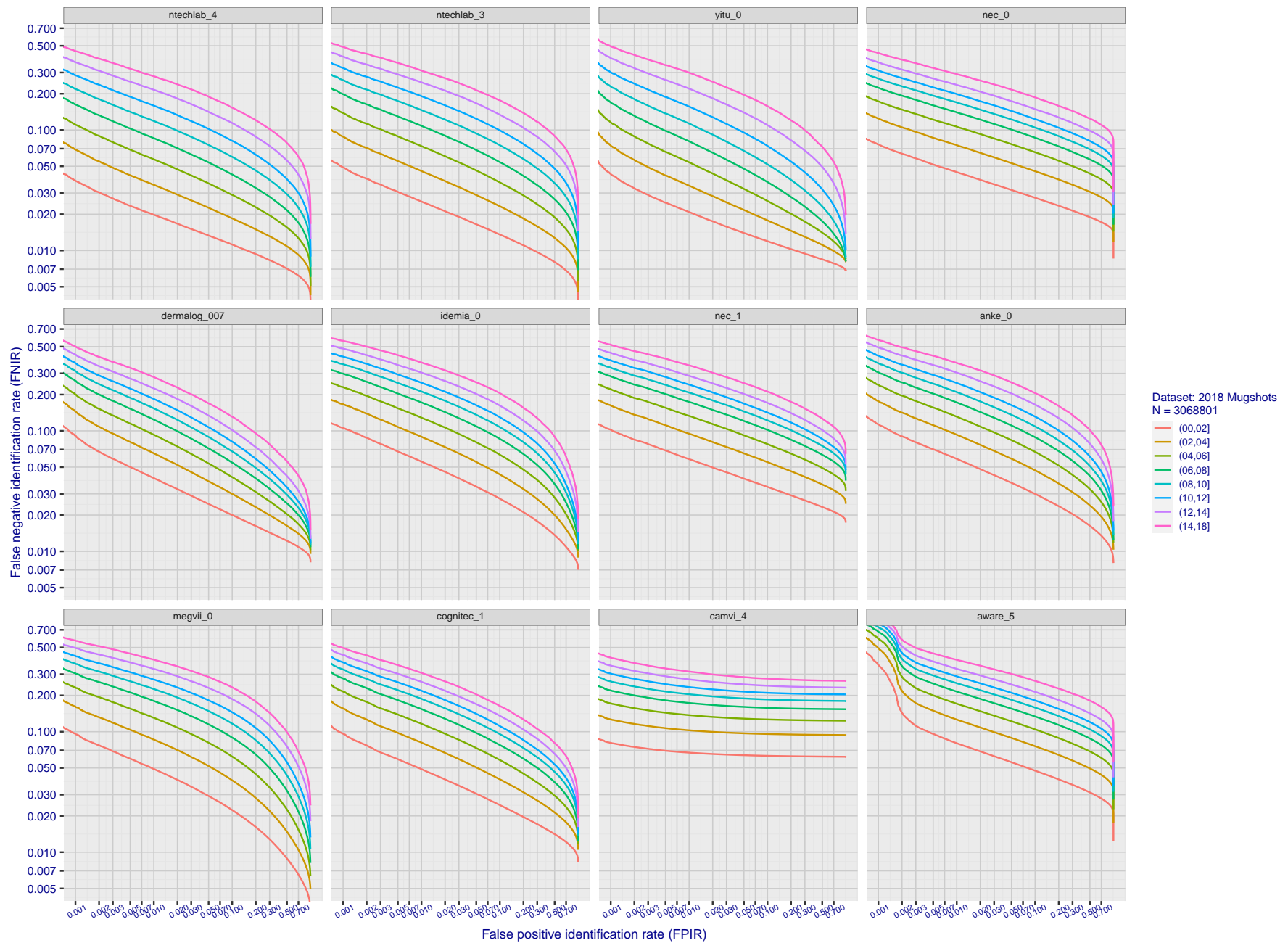


**Figure 87: [FRVT-2018 Mugshot Ageing Dataset] Identification miss rates vs. FPIR by time-elapsed.** The oldest image of each individual is enrolled. Thereafter, all more recent images are searched. Miss rates are computed over all searches noted in row 17 of Table 1 and binned by number of years between search and initial enrollment. FPIR is computed from the same FRVT 2018 non-mates noted in row 3 of Table 1 with  $N = 3\,000\,000$ .

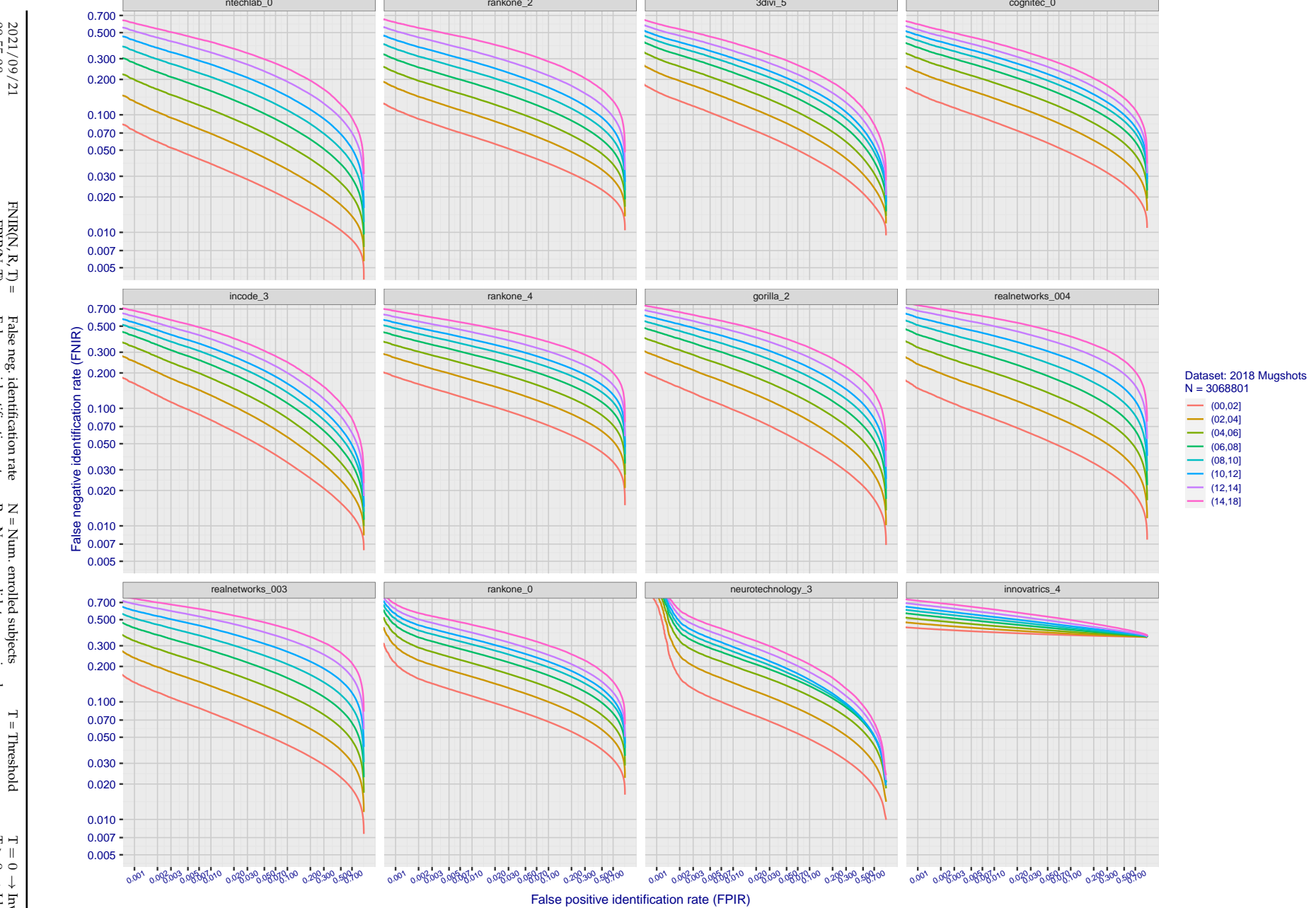


**Figure 88: [FRVT-2018 Mugshot Ageing Dataset] Identification miss rates vs. FPIR by time-elapsed.** The oldest image of each individual is enrolled. Thereafter, all more recent images are searched. Miss rates are computed over all searches noted in row 17 of Table 1 and binned by number of years between search and initial enrollment. FPIR is computed from the same FRVT 2018 non-mates noted in row 3 of Table 1 with  $N = 3\,000\,000$ .

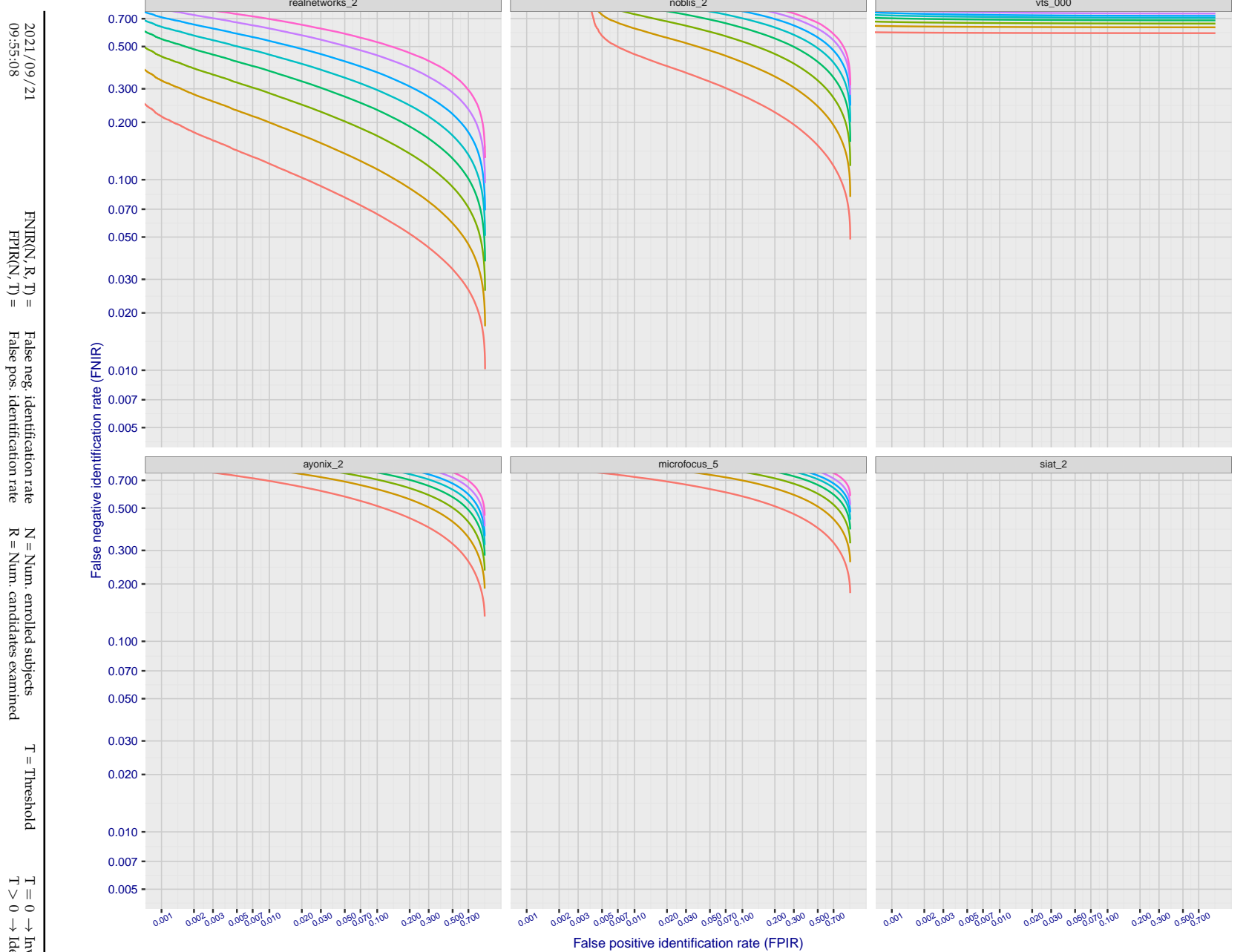


**Figure 89: [FRVT-2018 Mugshot Ageing Dataset] Identification miss rates vs. FPIR by time-elapsed.** The oldest image of each individual is enrolled. Thereafter, all more recent images are searched. Miss rates are computed over all searches noted in row 17 of Table 1 and binned by number of years between search and initial enrollment. FPIR is computed from the same FRVT 2018 non-mates noted in row 3 of Table 1 with  $N = 3000000$ .

---

2021/09/21  
09:55:08

FNIR(N, R, T) = False neg. identification rate  
FPTR(N, T) = False pos. identification rate

N = Num. enrolled subjects  
R = Num. candidates examined

T = Threshold  
T = 0 → Investigation  
T > 0 → Identification

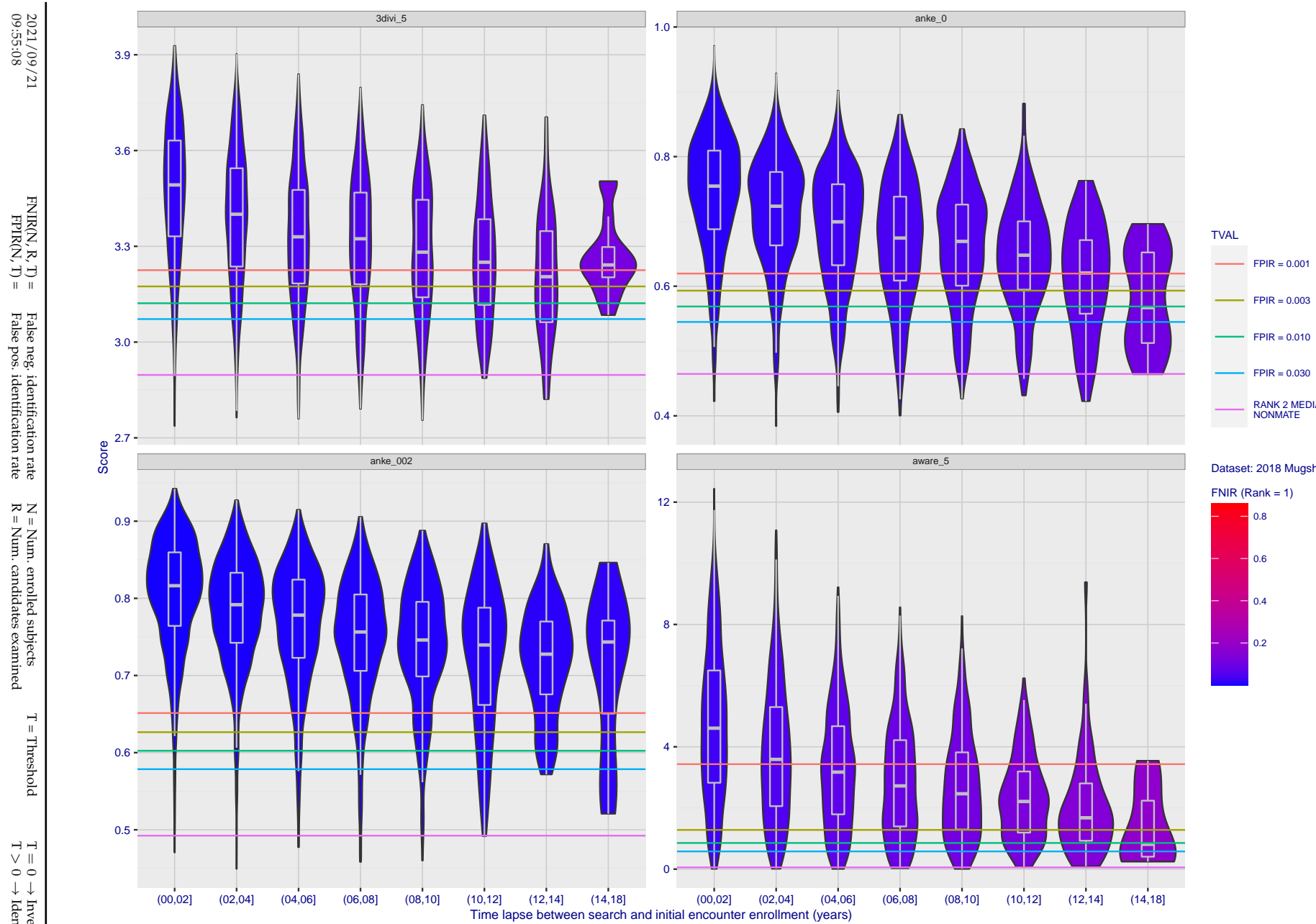


Figure 90: [FRVT-2018 Mugshot Ageing Dataset] Native mate scores vs. time-elapsed. The oldest image of each individual is enrolled. Thereafter, all more recent images are searched. Mated score distributions are computed over all searches noted in row 17 of Table 1 binned by number of years between search and initial enrollment.

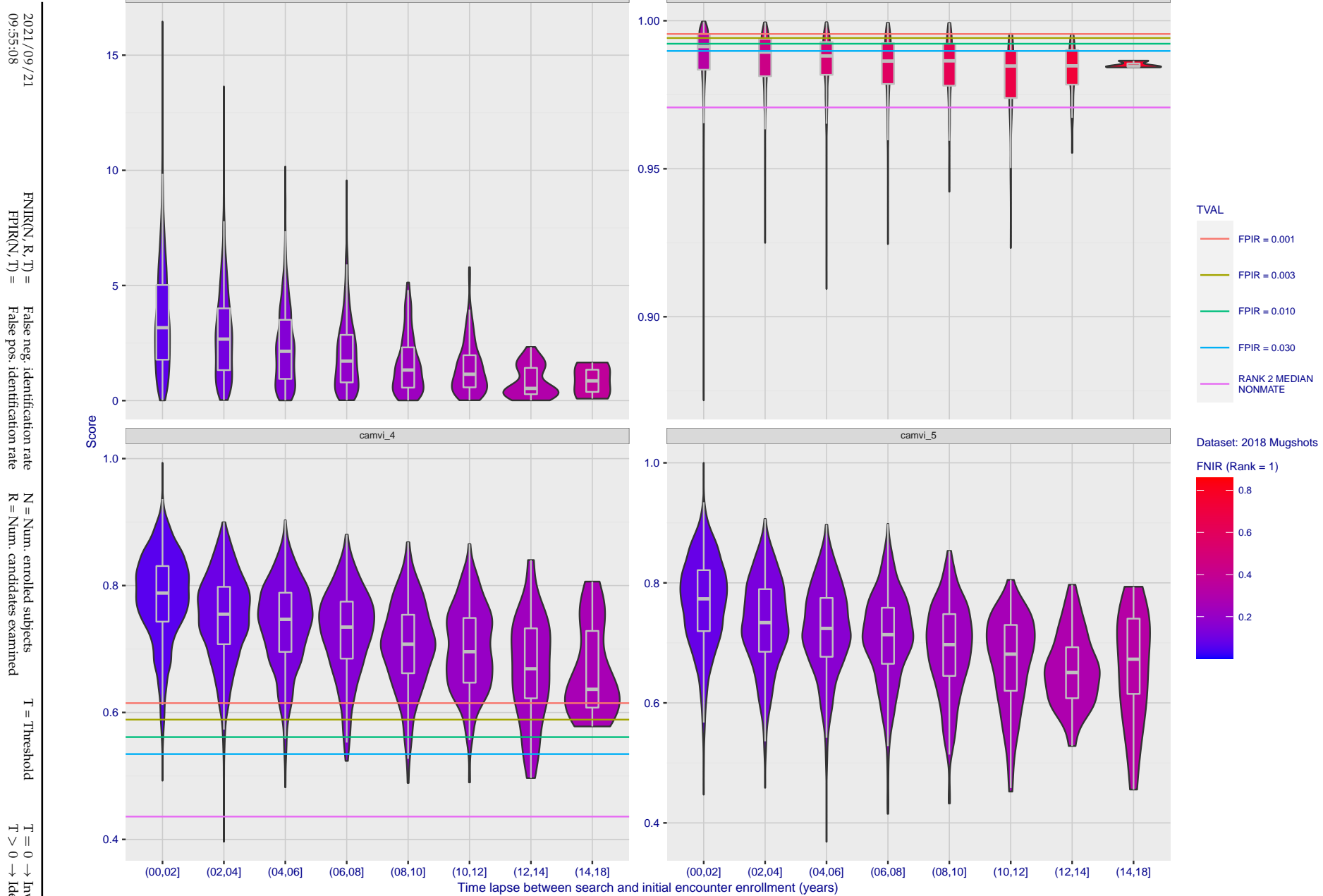


Figure 91: [FRVT-2018 Mugshot Ageing Dataset] Native mate scores vs. time-elapsed. The oldest image of each individual is enrolled. Thereafter, all more recent images are searched. Mated score distributions are computed over all searches noted in row 17 of Table 1 binned by number of years between search and initial enrollment.

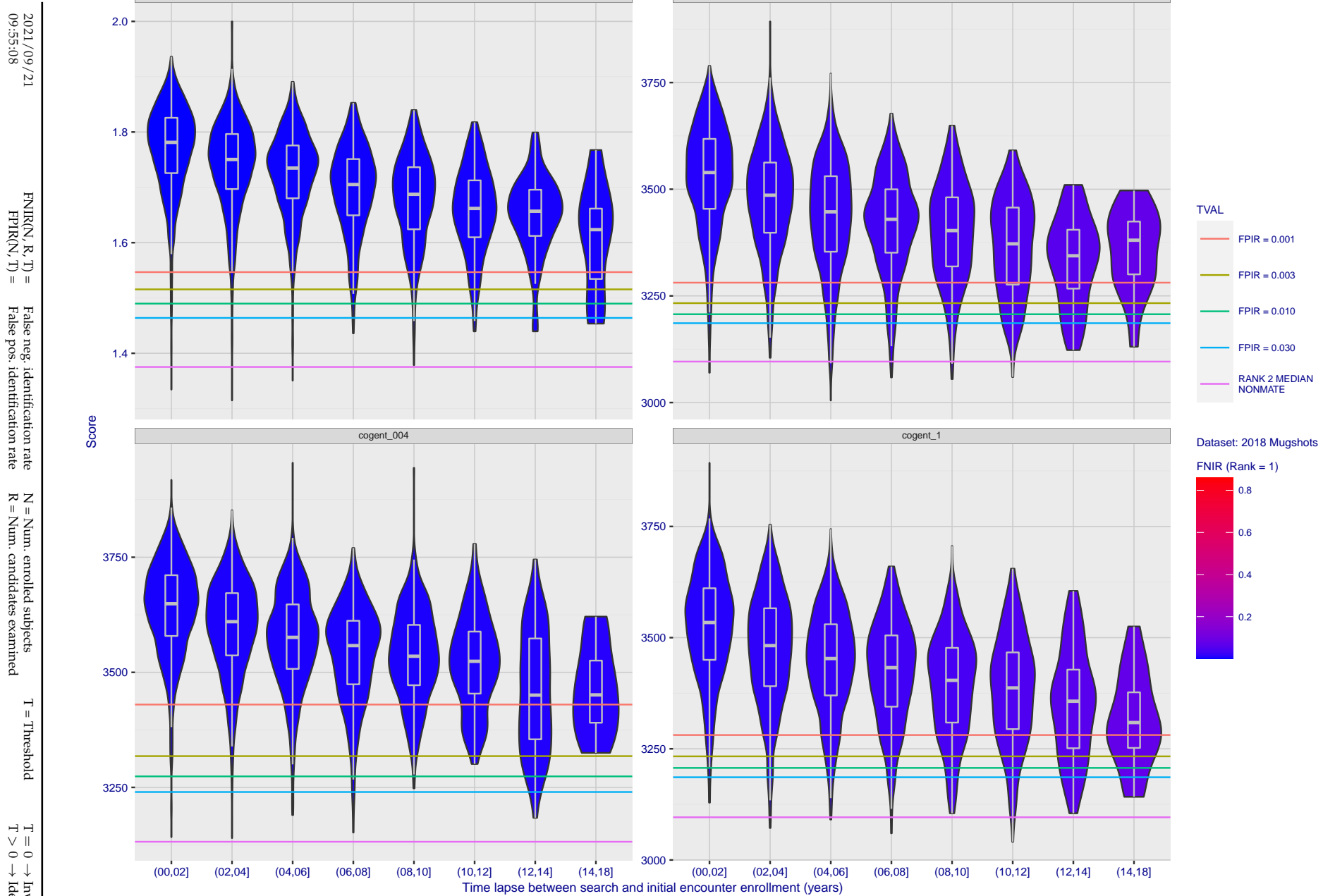
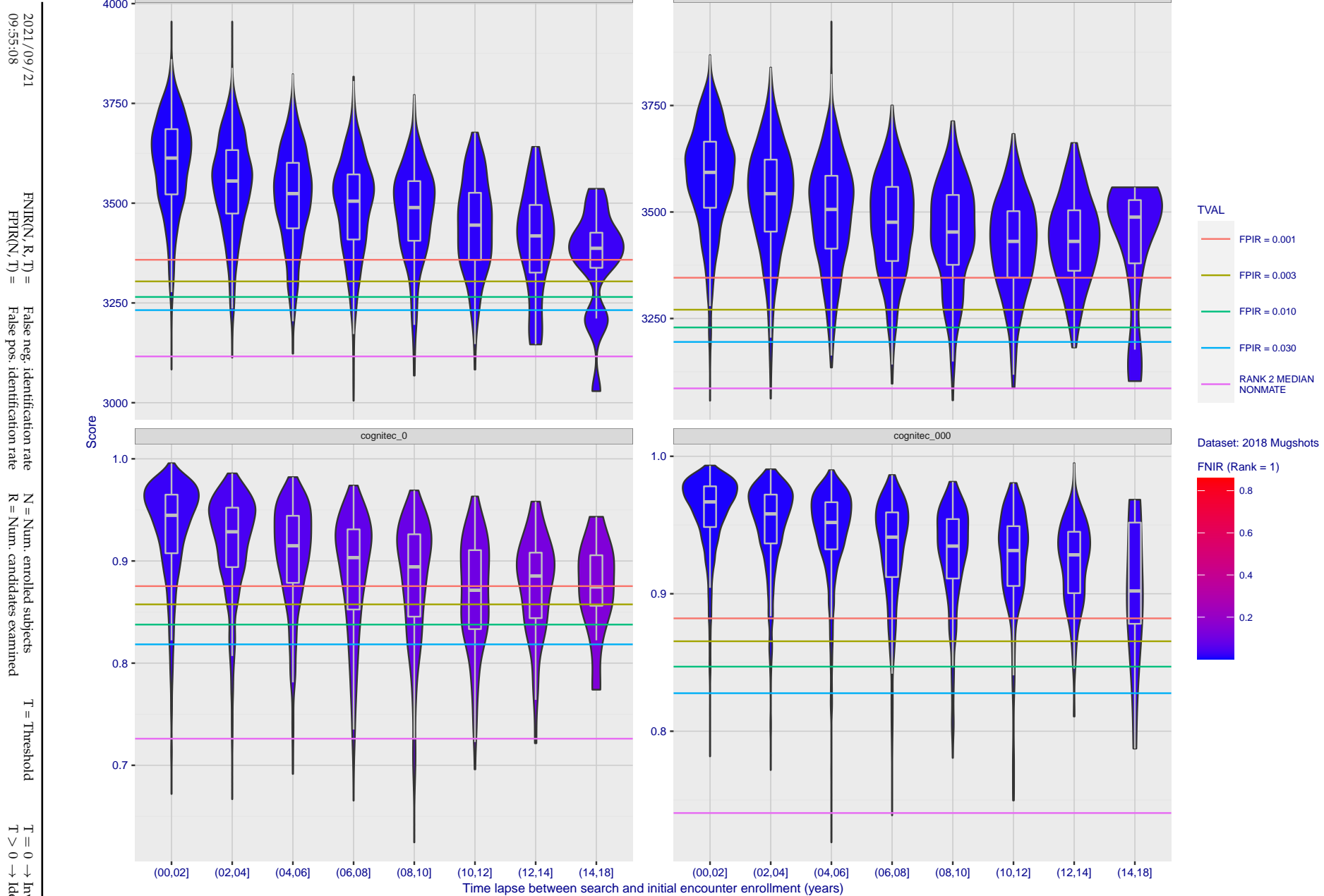


Figure 92: [FRVT-2018 Mugshot Ageing Dataset] Native mate scores vs. time-elapsed. The oldest image of each individual is enrolled. Thereafter, all more recent images are searched. Mated score distributions are computed over all searches noted in row 17 of Table 1 binned by number of years between search and initial enrollment.



**Figure 93: [FRVT-2018 Mugshot Ageing Dataset] Native mate scores vs. time-elapsed.** The oldest image of each individual is enrolled. Thereafter, all more recent images are searched. Mated score distributions are computed over all searches noted in row 17 of Table 1 binned by number of years between search and initial enrollment.

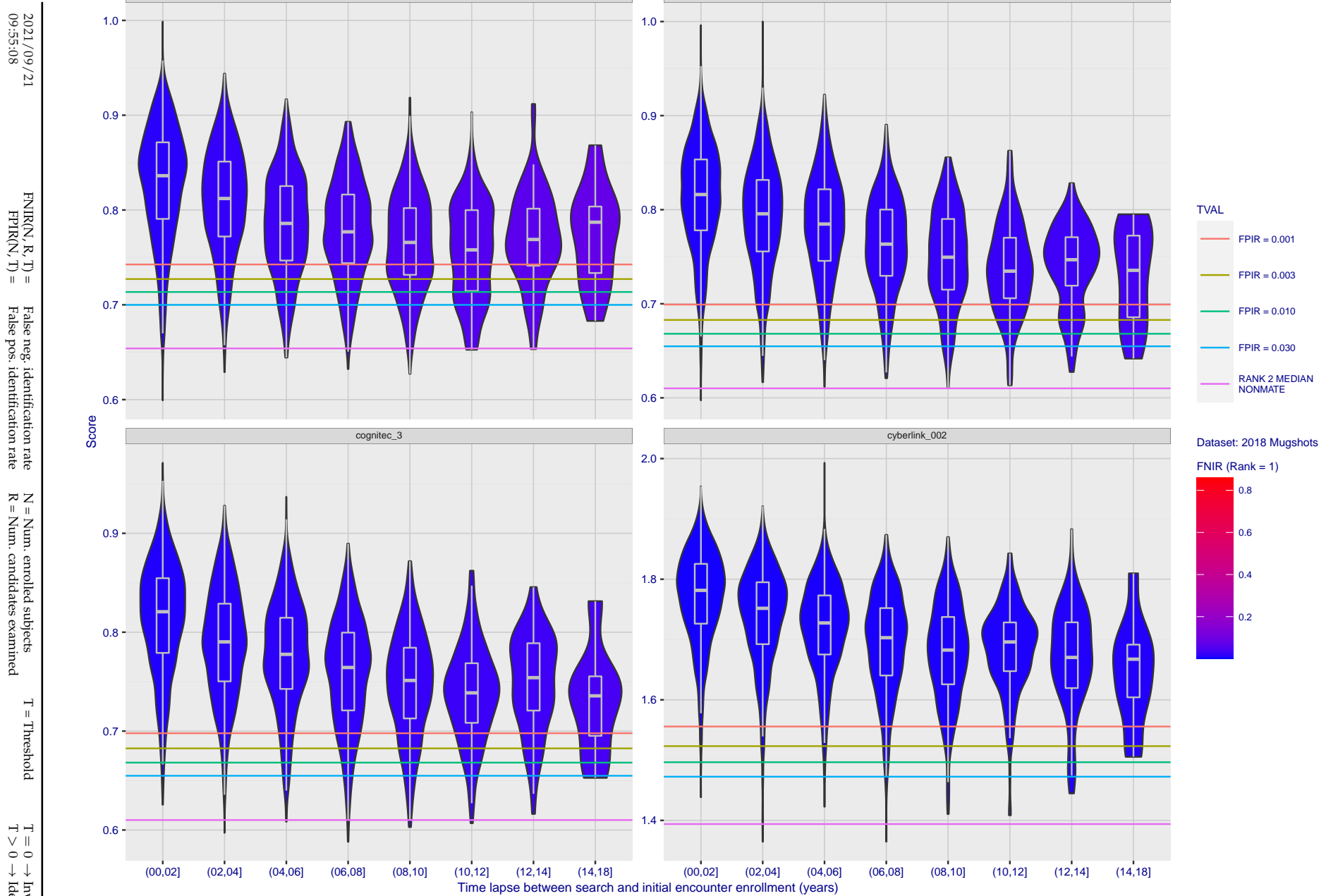
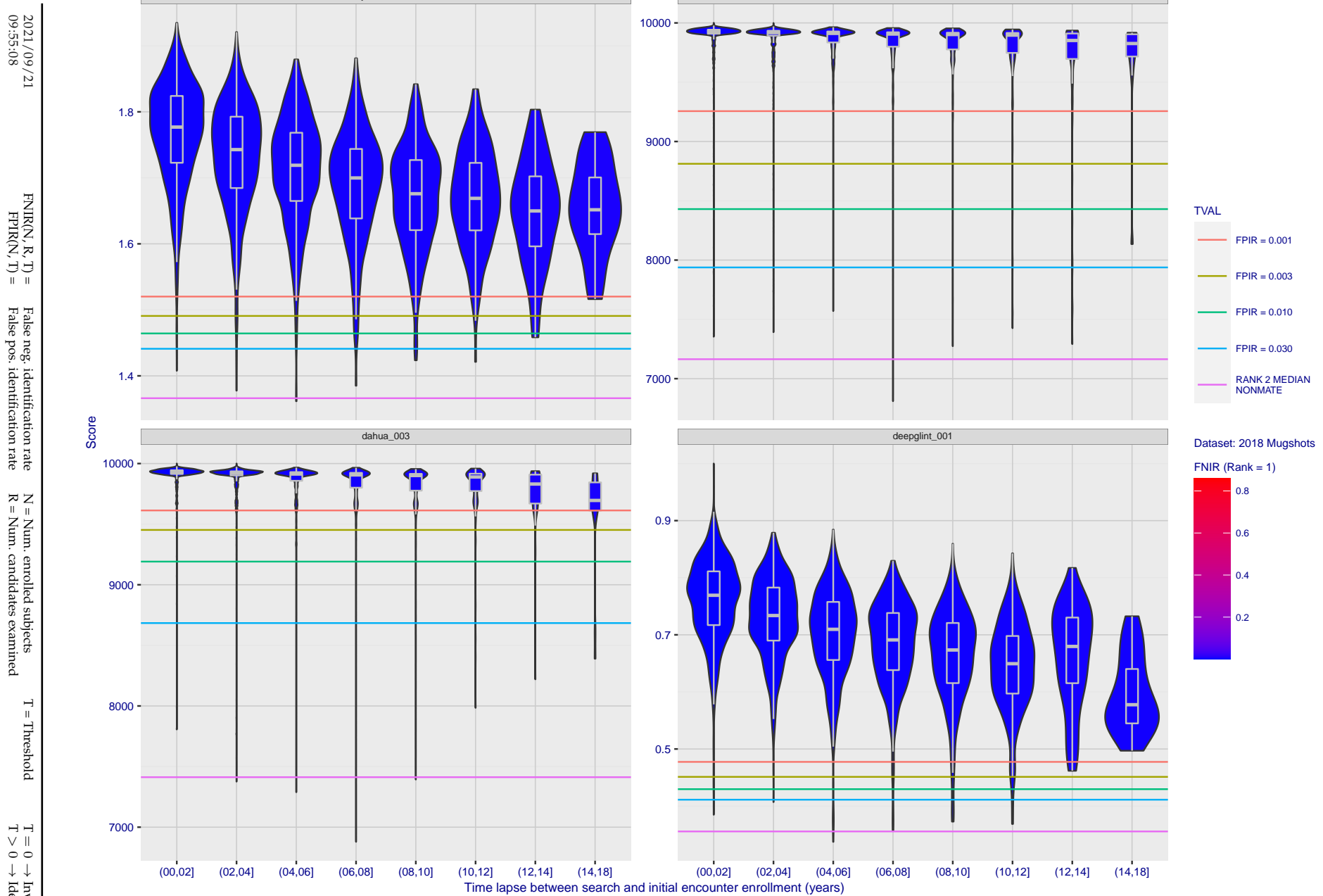


Figure 94: [FRVT-2018 Mugshot Ageing Dataset] Native mate scores vs. time-elapsed. The oldest image of each individual is enrolled. Thereafter, all more recent images are searched. Mated score distributions are computed over all searches noted in row 17 of Table 1 binned by number of years between search and initial enrollment.



**Figure 95: [FRVT-2018 Mugshot Ageing Dataset] Native mate scores vs. time-elapsed.** The oldest image of each individual is enrolled. Thereafter, all more recent images are searched. Mated score distributions are computed over all searches noted in row 17 of Table 1 binned by number of years between search and initial enrollment.

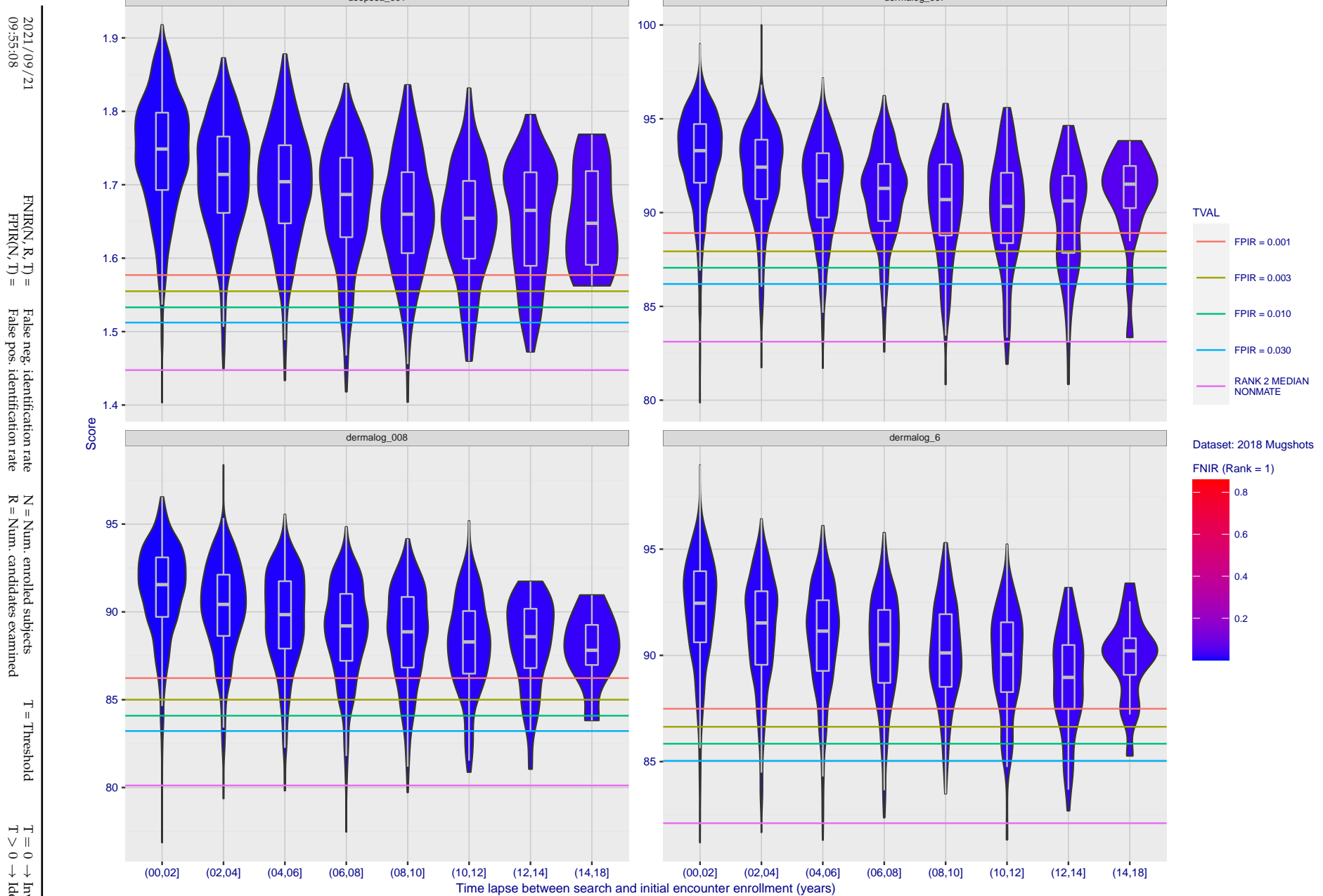
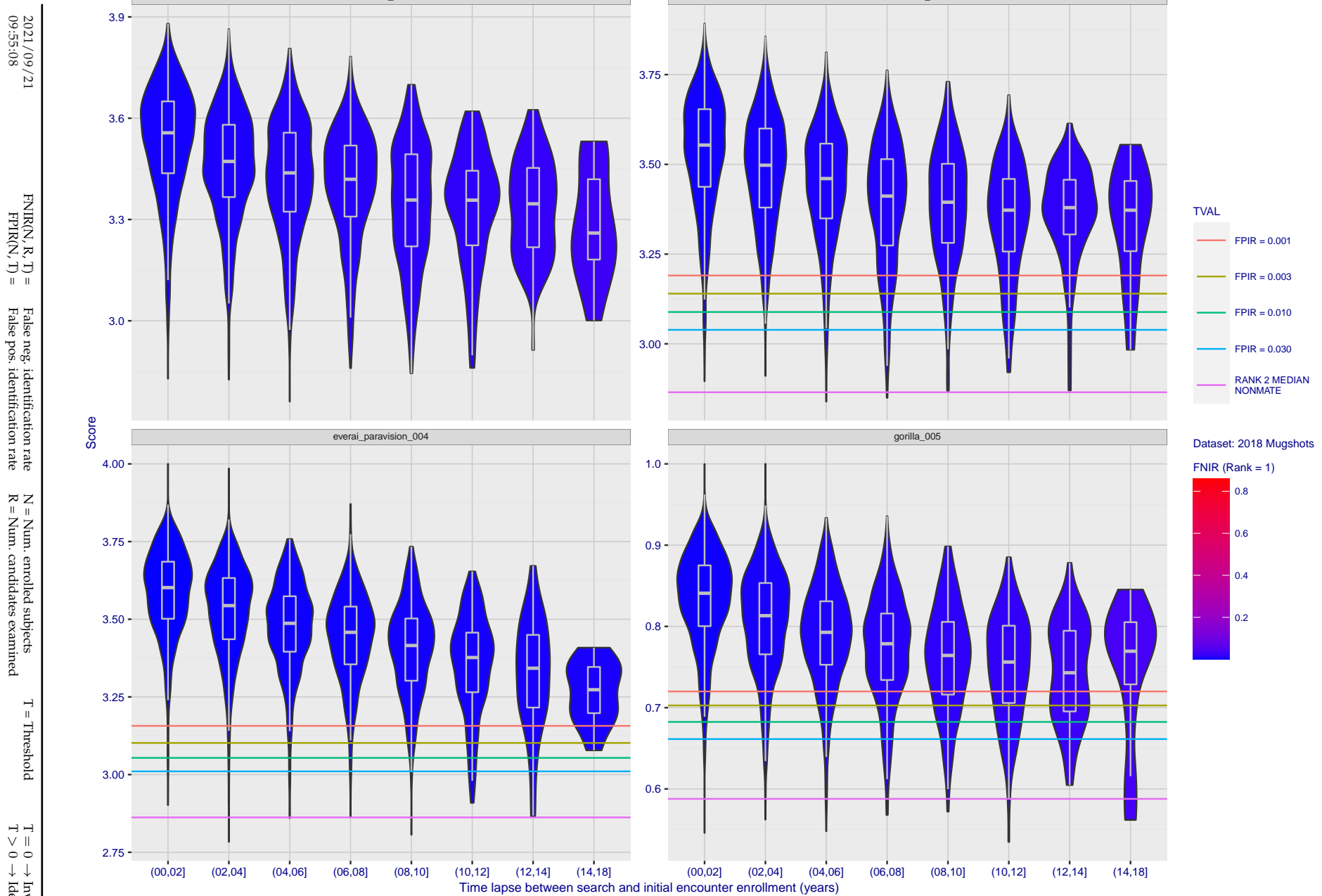


Figure 96: [FRVT-2018 Mugshot Ageing Dataset] Native mate scores vs. time-elapsed. The oldest image of each individual is enrolled. Thereafter, all more recent images are searched. Mated score distributions are computed over all searches noted in row 17 of Table 1 binned by number of years between search and initial enrollment.



**Figure 97: [FRVT-2018 Mugshot Ageing Dataset] Native mate scores vs. time-elapsed.** The oldest image of each individual is enrolled. Thereafter, all more recent images are searched. Mated score distributions are computed over all searches noted in row 17 of Table 1 binned by number of years between search and initial enrollment.

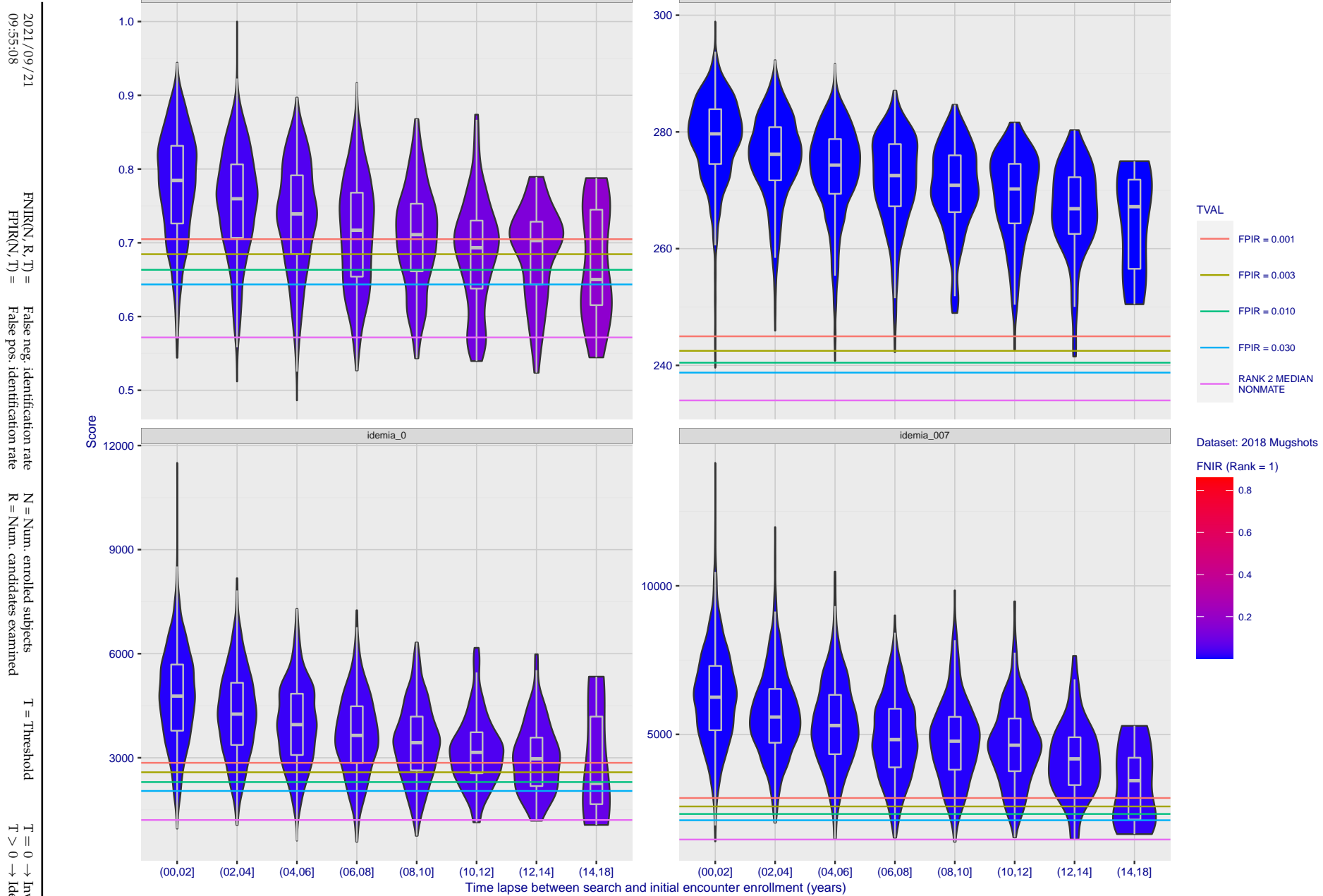


Figure 98: [FRVT-2018 Mugshot Ageing Dataset] Native mate scores vs. time-elapsed. The oldest image of each individual is enrolled. Thereafter, all more recent images are searched. Mated score distributions are computed over all searches noted in row 17 of Table 1 binned by number of years between search and initial enrollment.

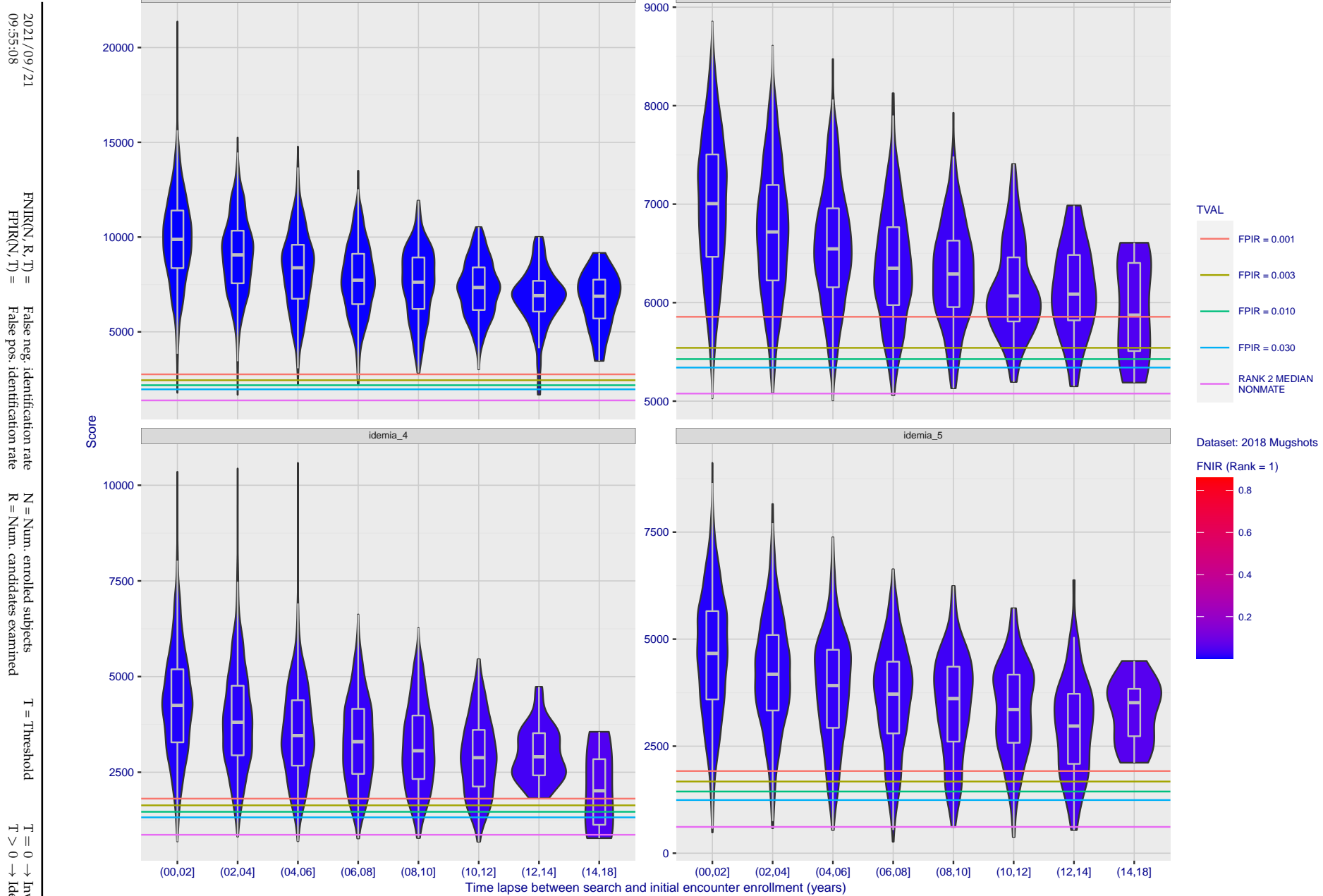


Figure 99: [FRVT-2018 Mugshot Ageing Dataset] Native mate scores vs. time-elapsed. The oldest image of each individual is enrolled. Thereafter, all more recent images are searched. Mated score distributions are computed over all searches noted in row 17 of Table 1 binned by number of years between search and initial enrollment.

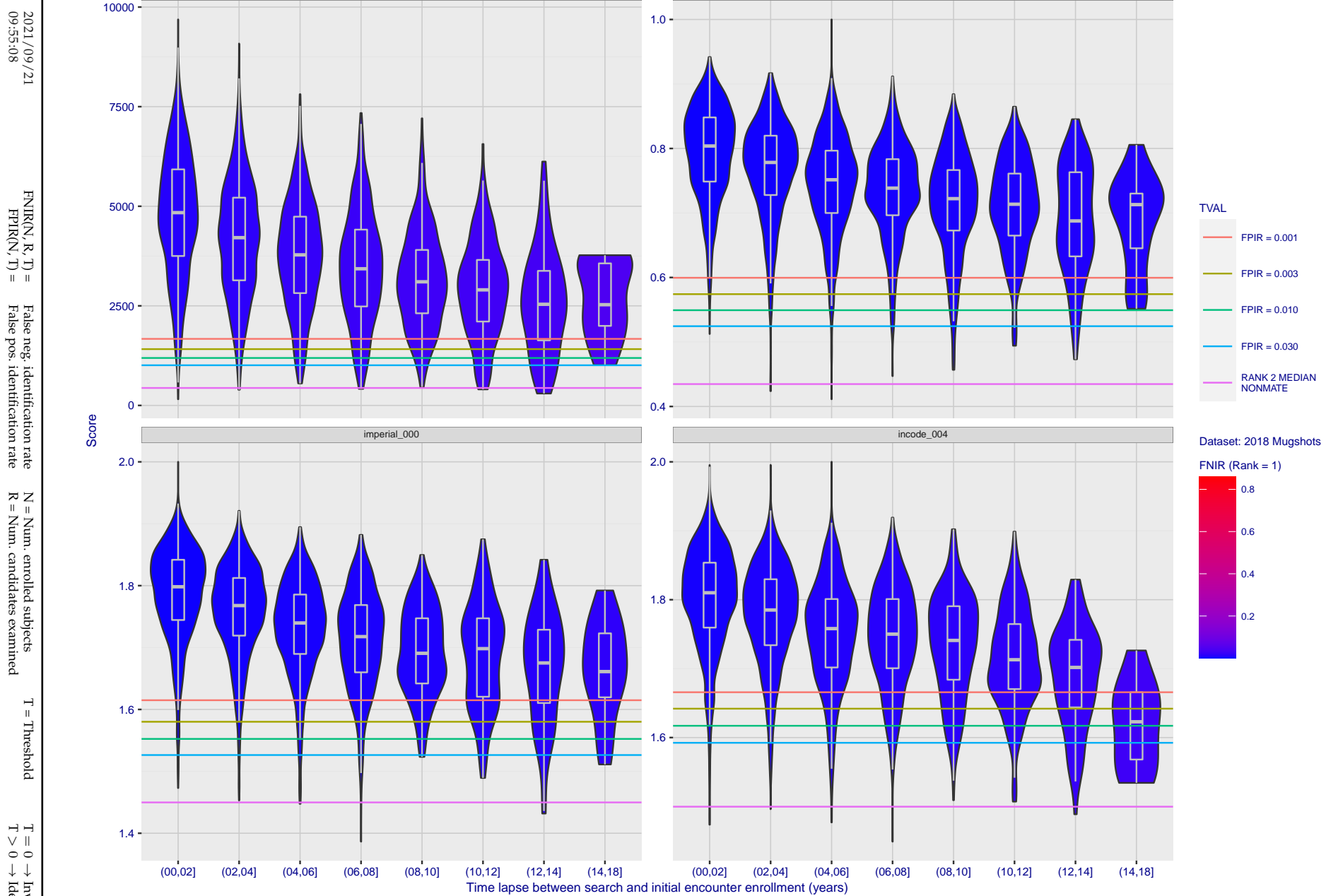


Figure 100: [FRVT-2018 Mugshot Ageing Dataset] Native mate scores vs. time-elapsed. The oldest image of each individual is enrolled. Thereafter, all more recent images are searched. Mated score distributions are computed over all searches noted in row 17 of Table 1 binned by number of years between search and initial enrollment.

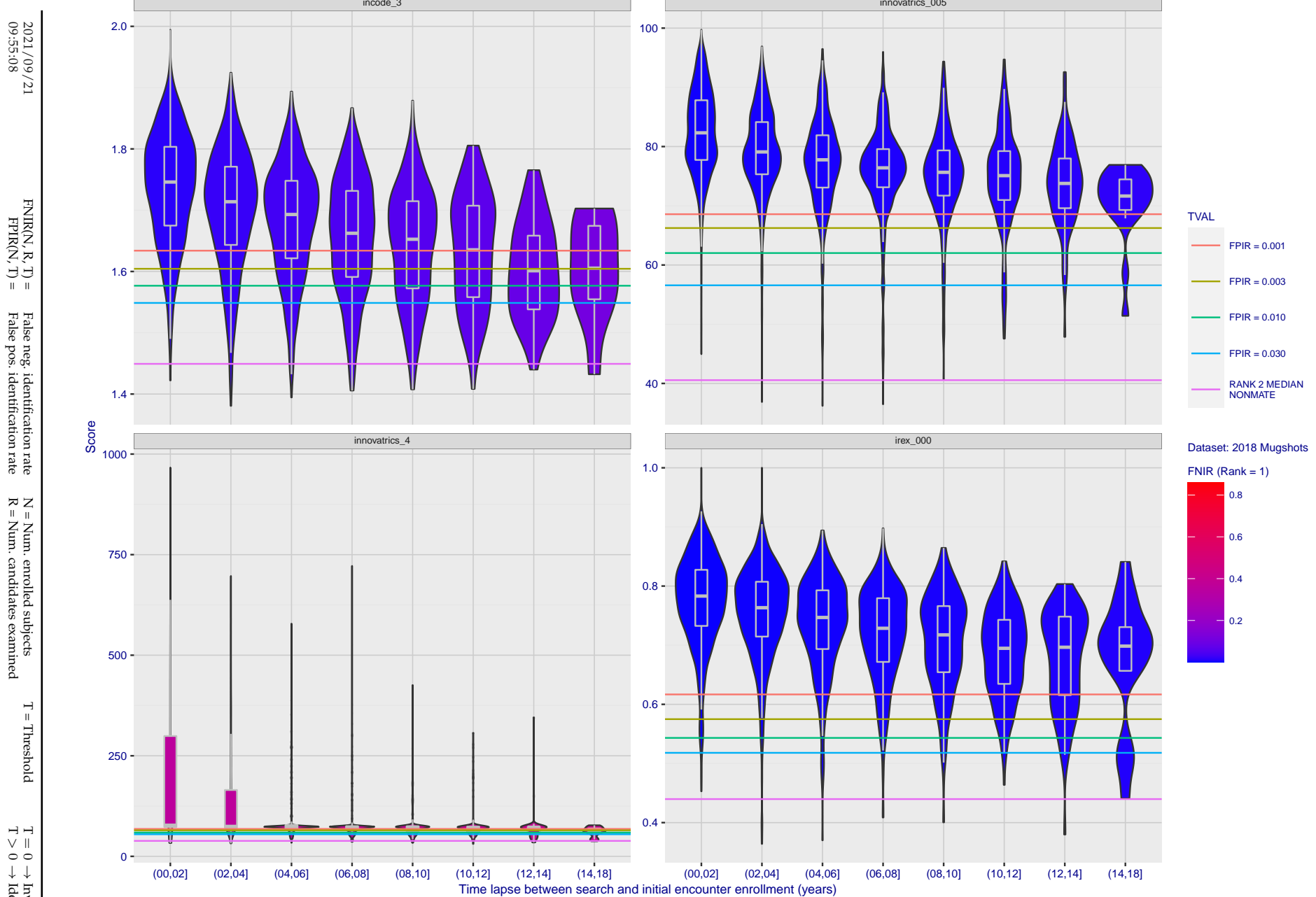


Figure 101: [FRVT-2018 Mugshot Ageing Dataset] Native mate scores vs. time-elapsed. The oldest image of each individual is enrolled. Thereafter, all more recent images are searched. Mated score distributions are computed over all searches noted in row 17 of Table 1 binned by number of years between search and initial enrollment.

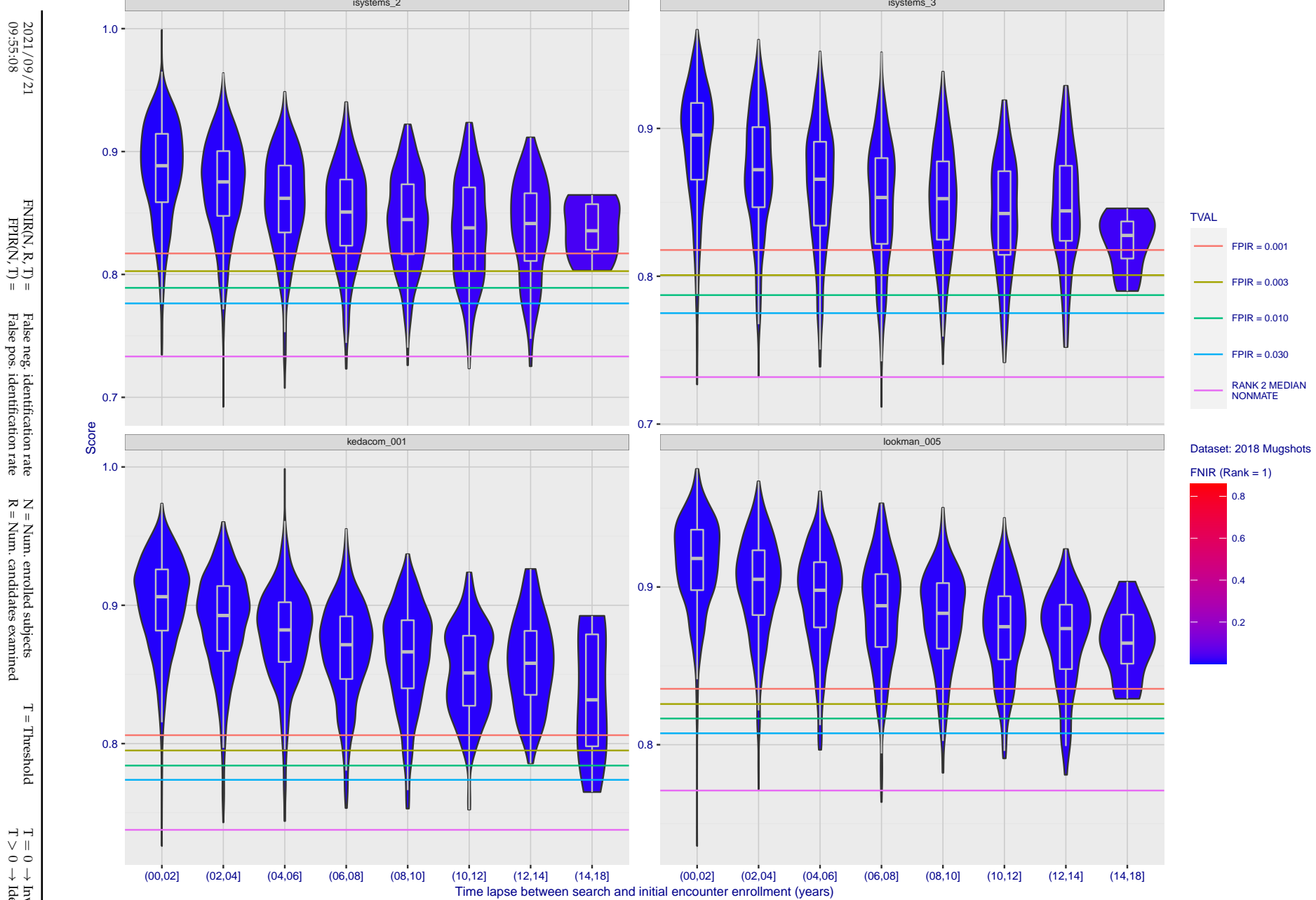


Figure 102: [FRVT-2018 Mugshot Ageing Dataset] Native mate scores vs. time-elapsed. The oldest image of each individual is enrolled. Thereafter, all more recent images are searched. Mated score distributions are computed over all searches noted in row 17 of Table 1 binned by number of years between search and initial enrollment.

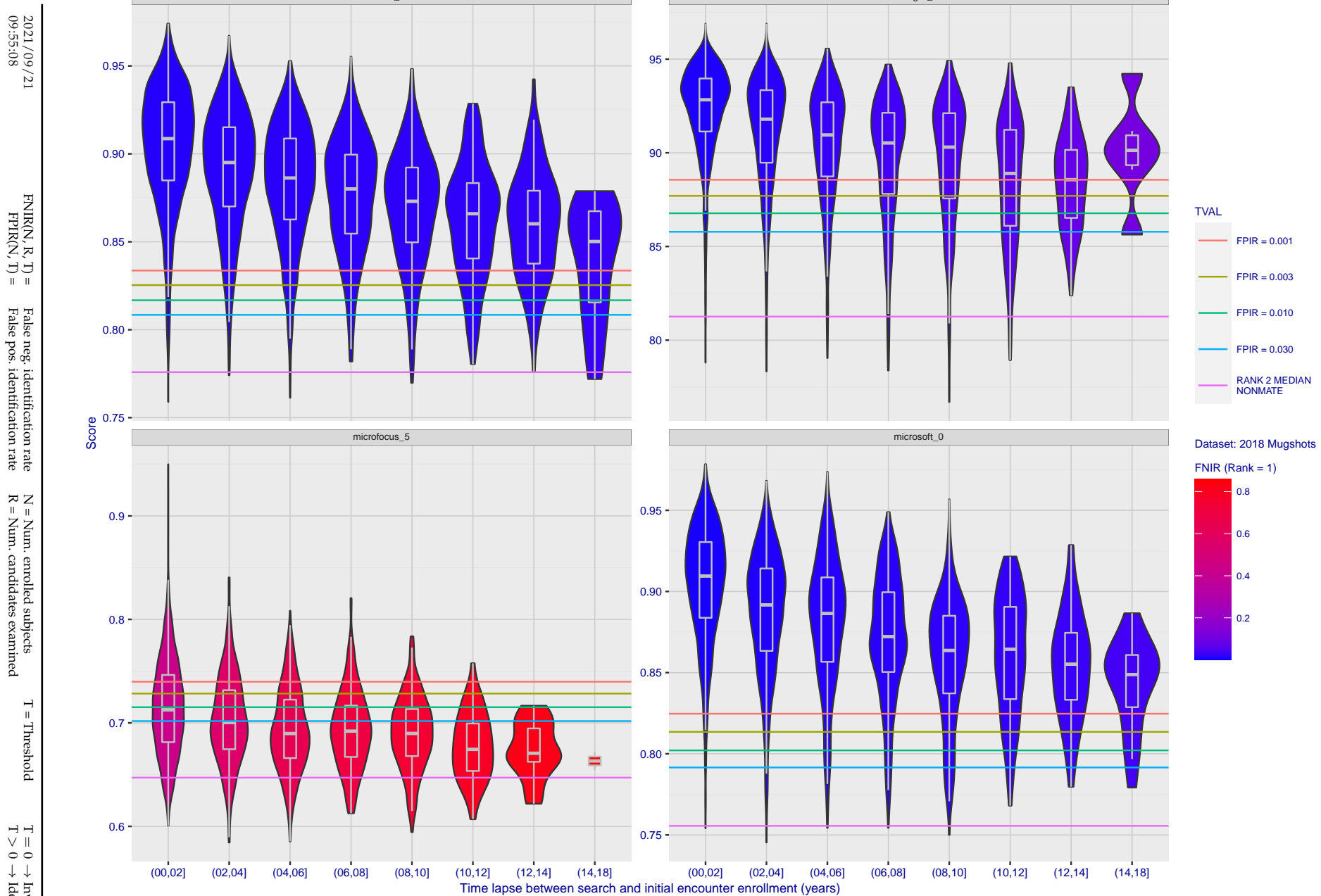


Figure 103: [FRVT-2018 Mugshot Ageing Dataset] Native mate scores vs. time-elapsed. The oldest image of each individual is enrolled. Thereafter, all more recent images are searched. Mated score distributions are computed over all searches noted in row 17 of Table 1 binned by number of years between search and initial enrollment.

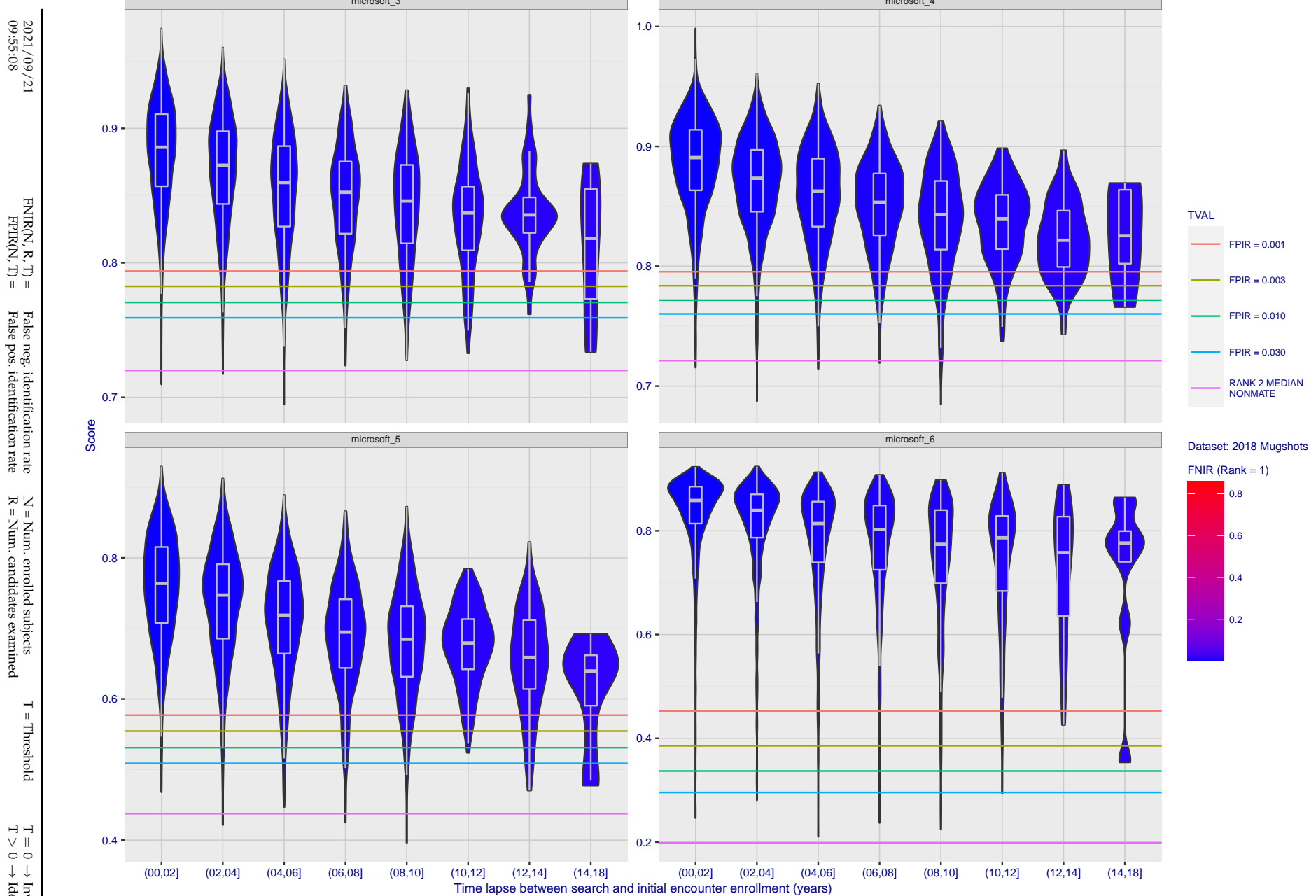


Figure 104: [FRVT-2018 Mugshot Ageing Dataset] Native mate scores vs. time-elapsed. The oldest image of each individual is enrolled. Thereafter, all more recent images are searched. Mated score distributions are computed over all searches noted in row 17 of Table 1 binned by number of years between search and initial enrollment.

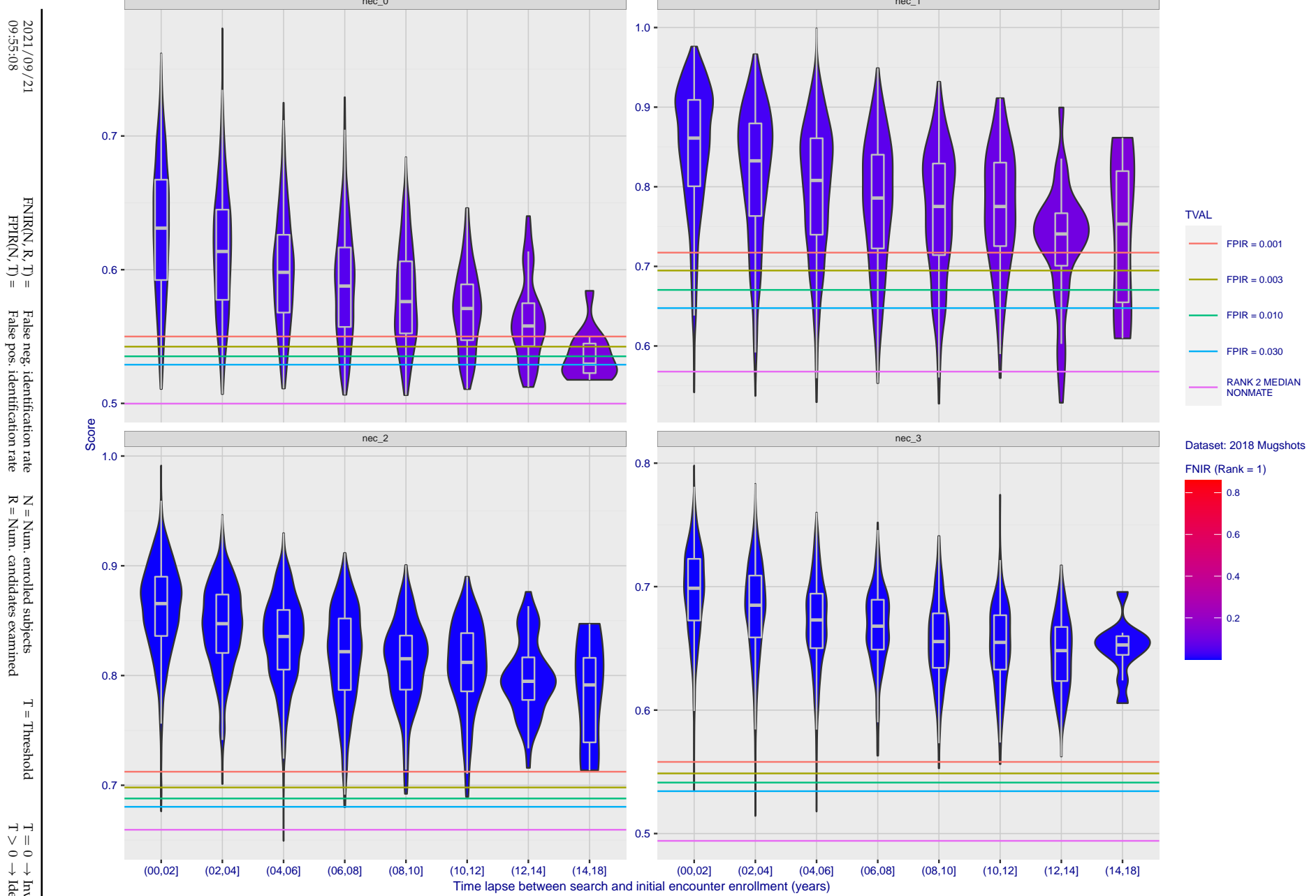


Figure 105: [FRVT-2018 Mugshot Ageing Dataset] Native mate scores vs. time-elapsed. The oldest image of each individual is enrolled. Thereafter, all more recent images are searched. Mated score distributions are computed over all searches noted in row 17 of Table 1 binned by number of years between search and initial enrollment.

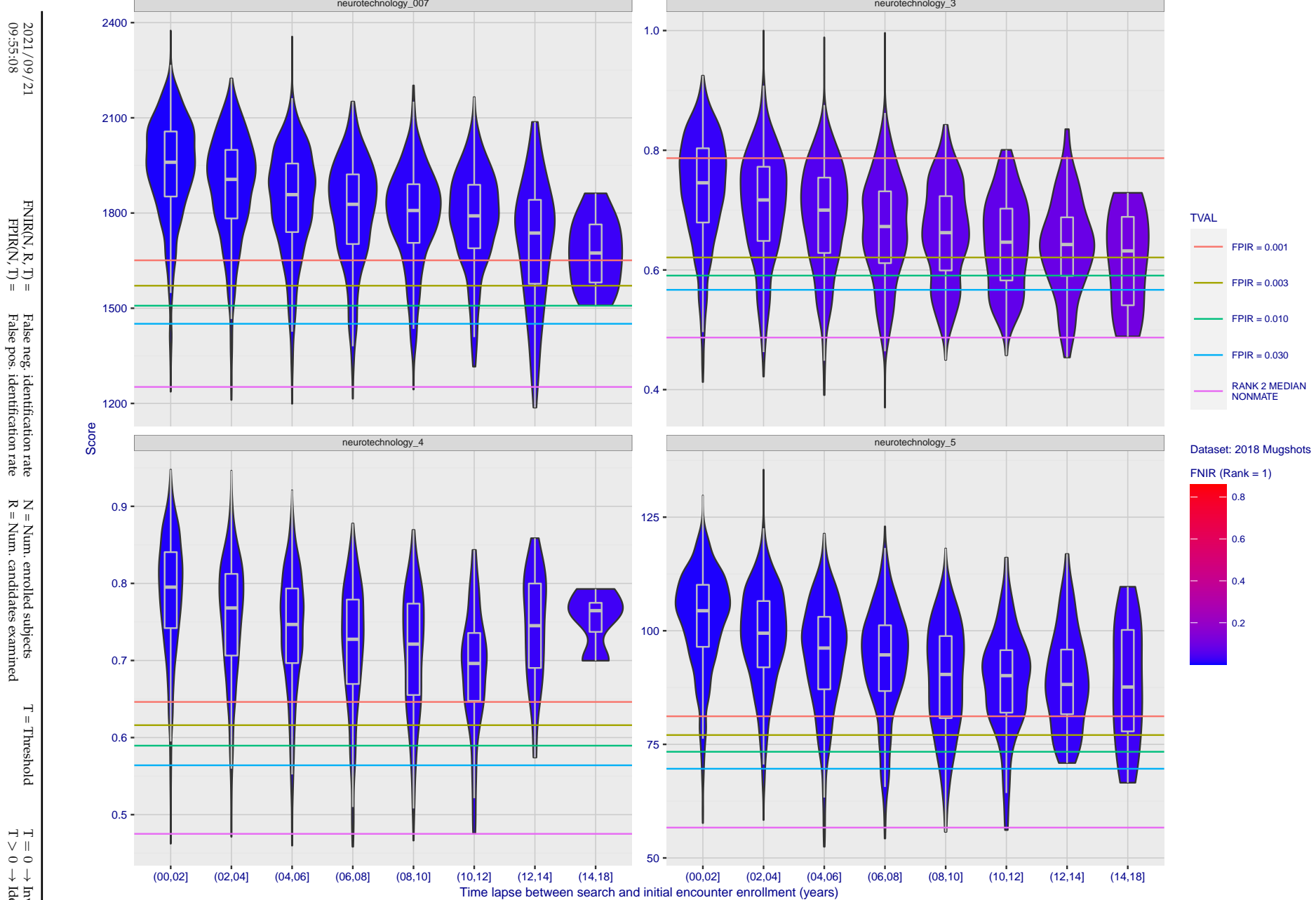


Figure 106: [FRVT-2018 Mugshot Ageing Dataset] Native mate scores vs. time-elapsed. The oldest image of each individual is enrolled. Thereafter, all more recent images are searched. Mated score distributions are computed over all searches noted in row 17 of Table 1 binned by number of years between search and initial enrollment.

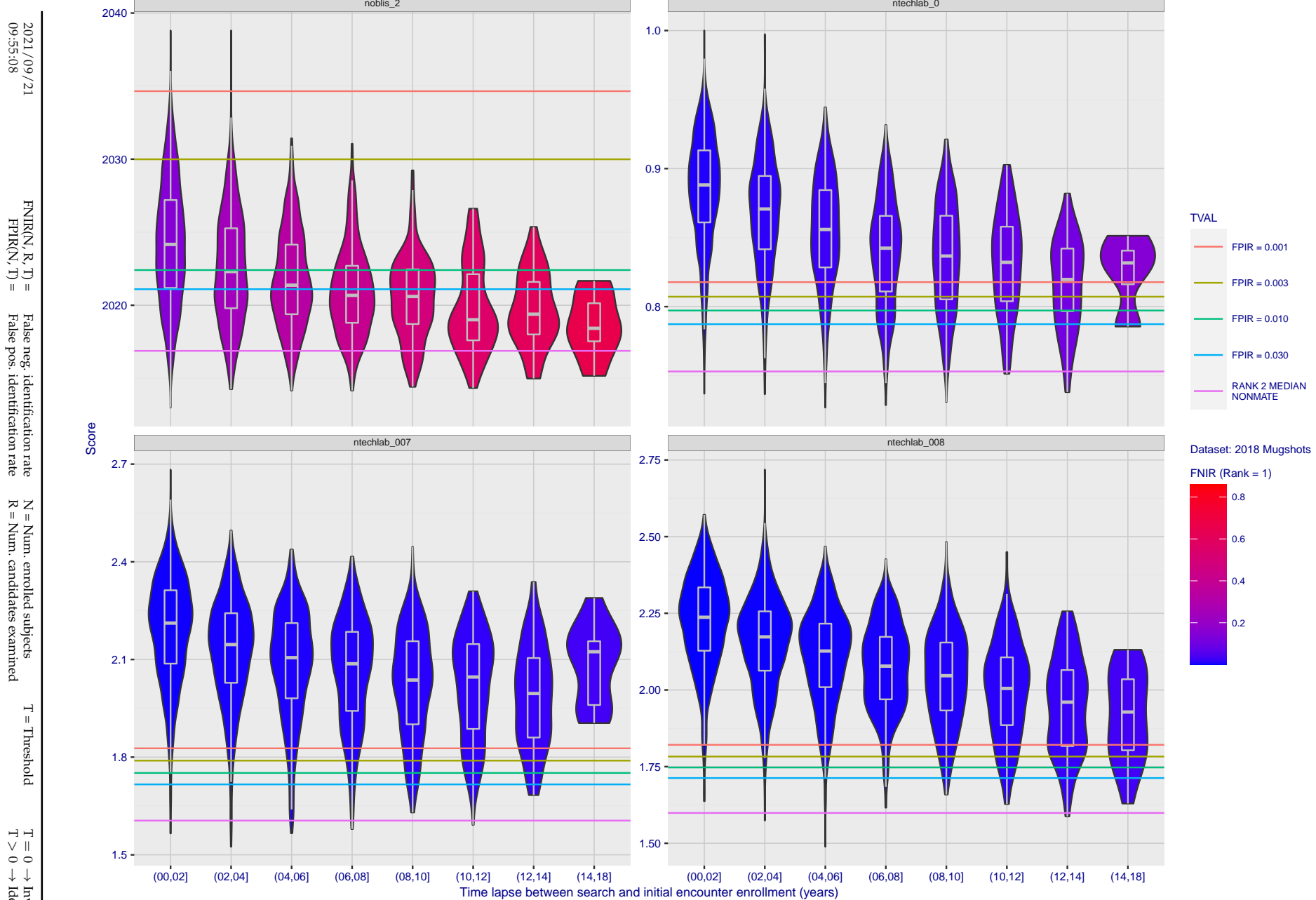


Figure 107: [FRVT-2018 Mugshot Ageing Dataset] Native mate scores vs. time-elapsed. The oldest image of each individual is enrolled. Thereafter, all more recent images are searched. Mated score distributions are computed over all searches noted in row 17 of Table 1 binned by number of years between search and initial enrollment.

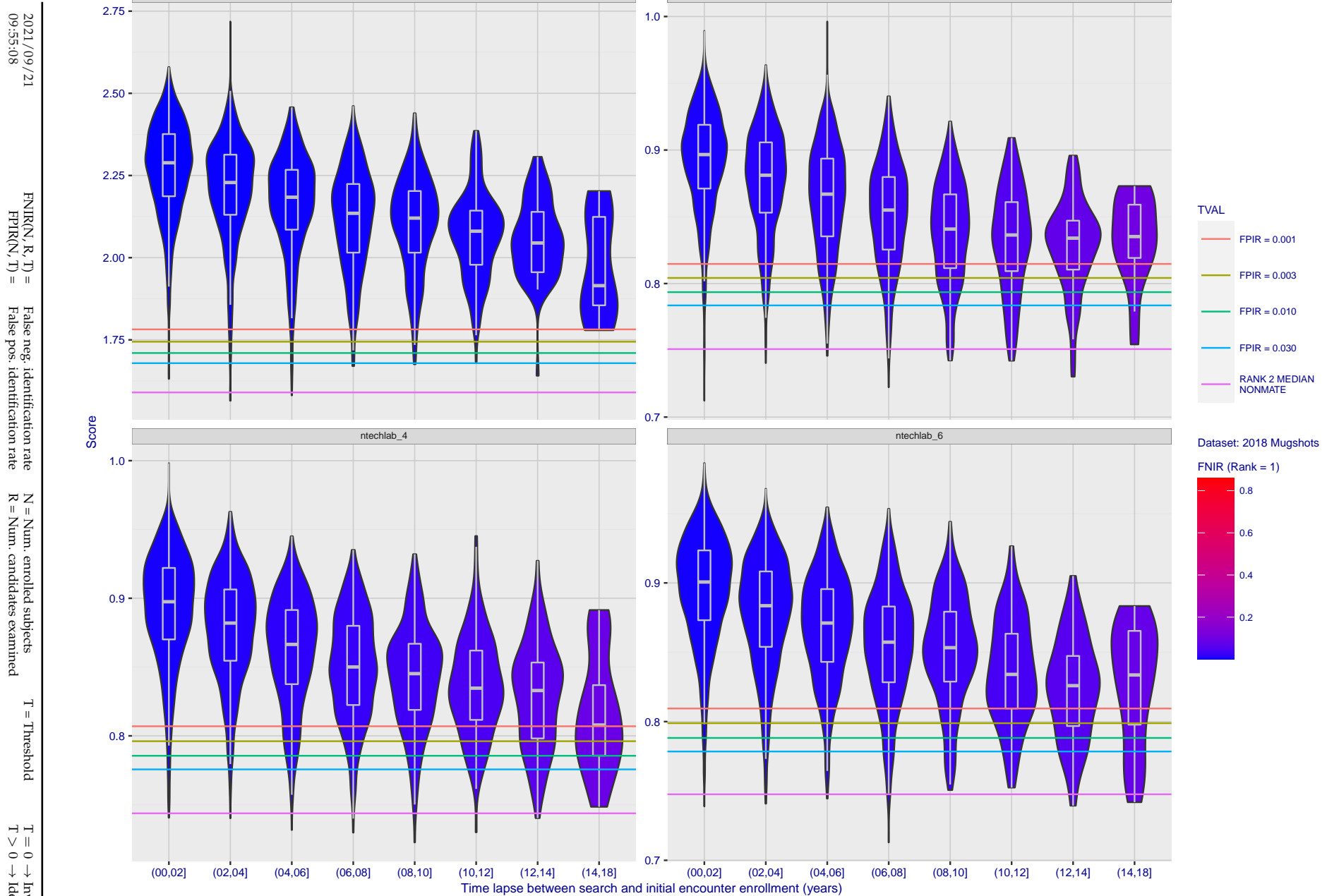


Figure 108: [FRVT-2018 Mugshot Ageing Dataset] Native mate scores vs. time-elapsed. The oldest image of each individual is enrolled. Thereafter, all more recent images are searched. Mated score distributions are computed over all searches noted in row 17 of Table 1 binned by number of years between search and initial enrollment.

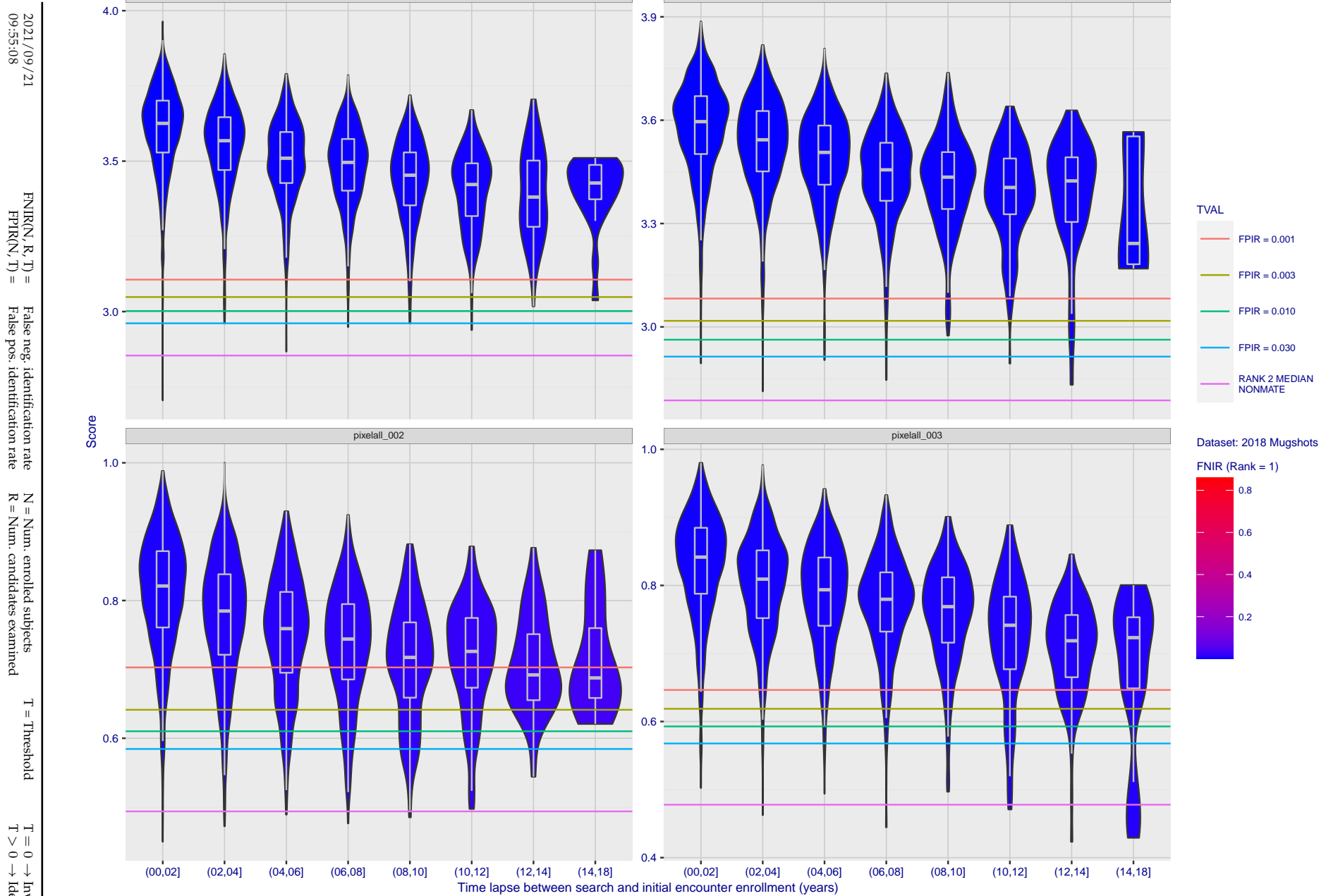
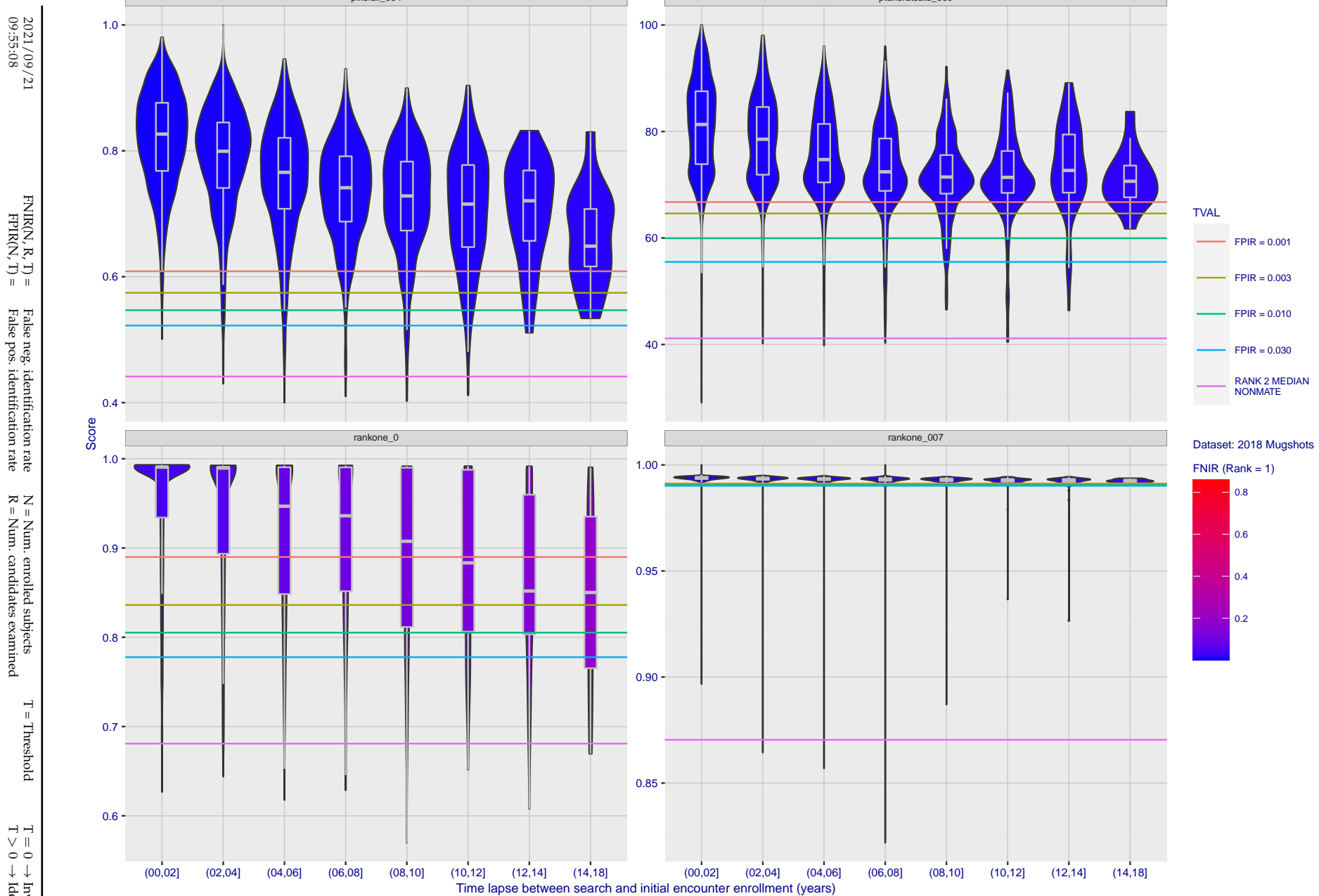


Figure 109: [FRVT-2018 Mugshot Ageing Dataset] Native mate scores vs. time-elapsed. The oldest image of each individual is enrolled. Thereafter, all more recent images are searched. Mated score distributions are computed over all searches noted in row 17 of Table 1 binned by number of years between search and initial enrollment.



**Figure 110: [FRVT-2018 Mugshot Ageing Dataset] Native mate scores vs. time-elapsed.** The oldest image of each individual is enrolled. Thereafter, all more recent images are searched. Mated score distributions are computed over all searches noted in row 17 of Table 1 binned by number of years between search and initial enrollment.

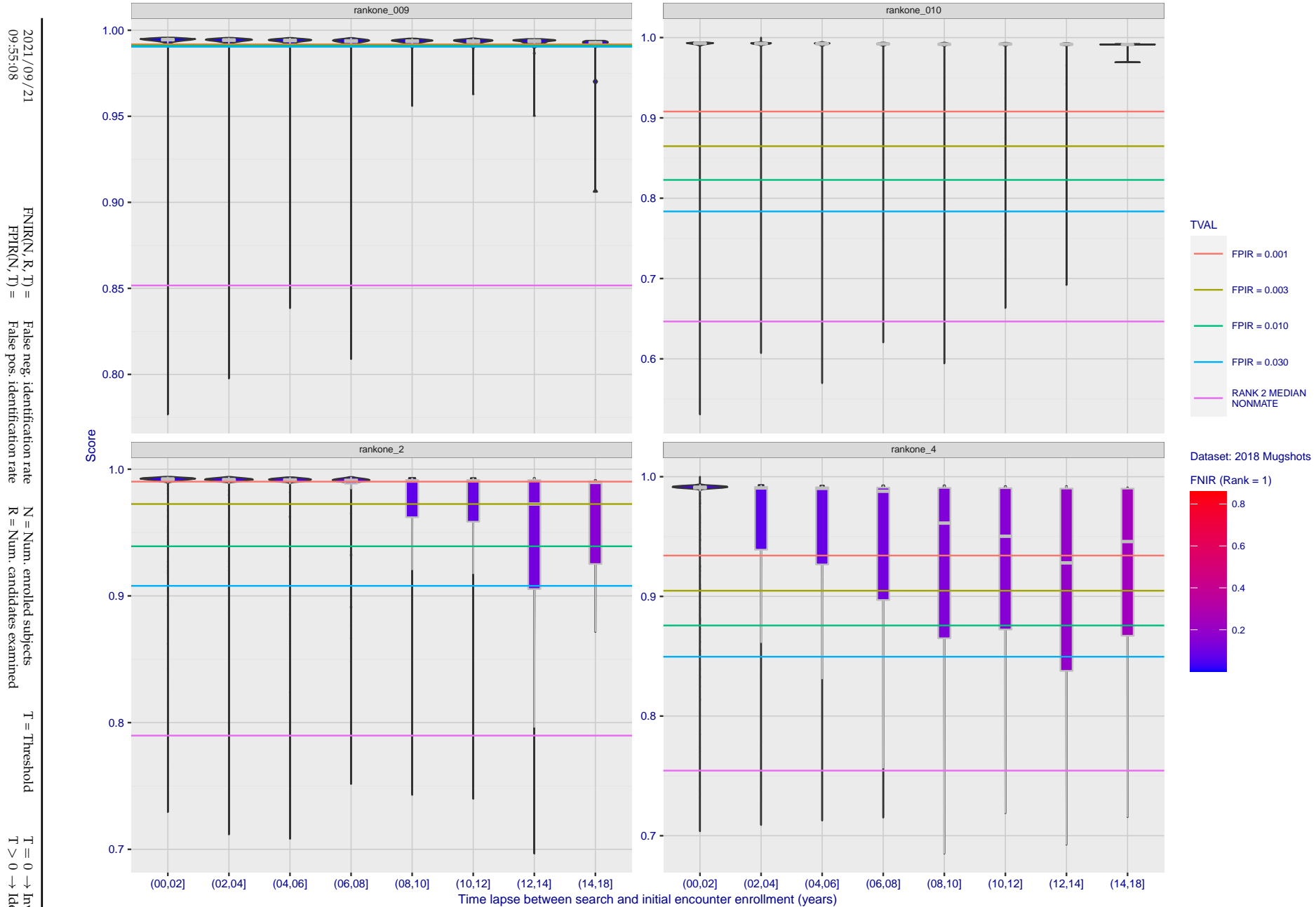
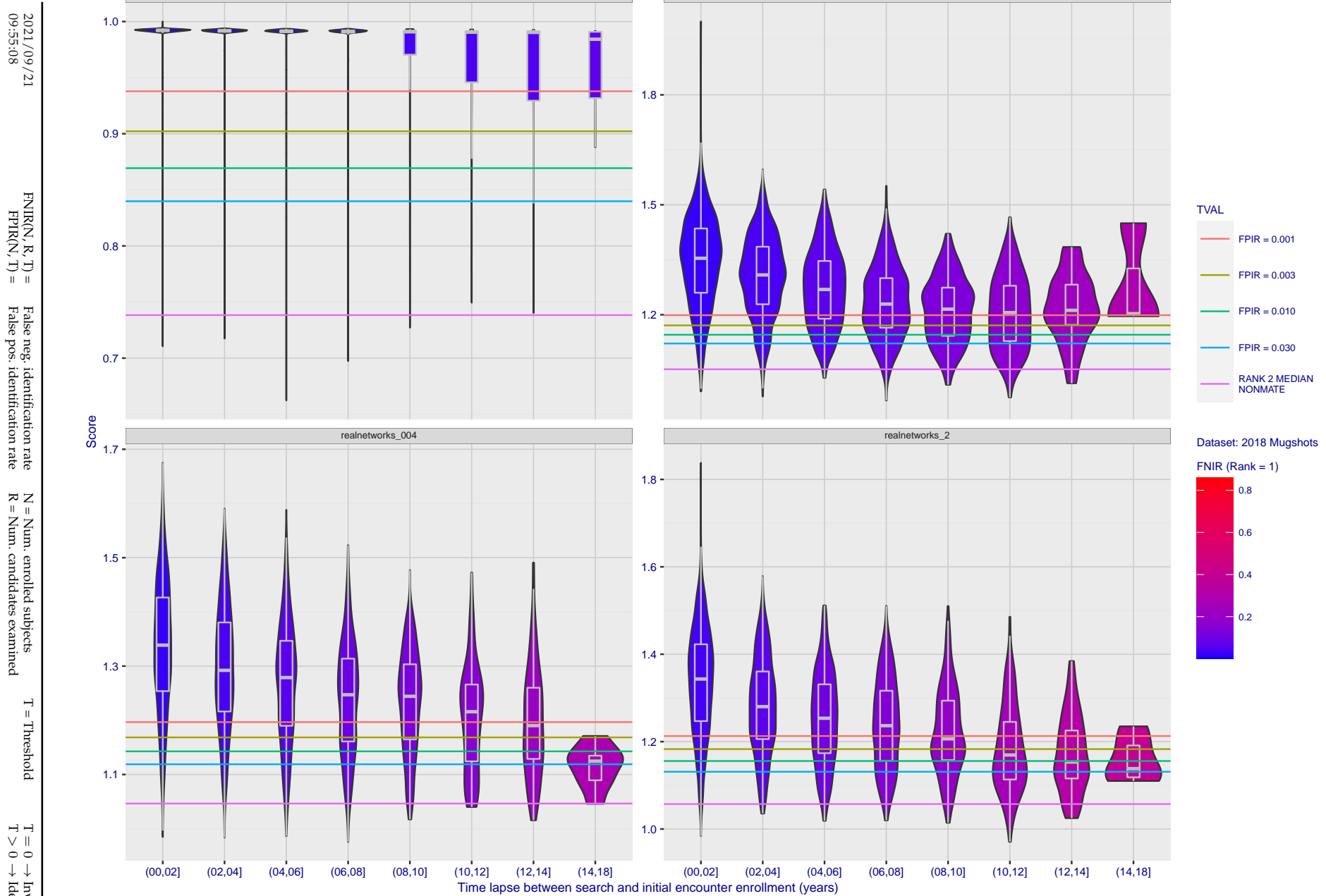


Figure 111: [FRVT-2018 Mugshot Ageing Dataset] Native mate scores vs. time-elapsed. The oldest image of each individual is enrolled. Thereafter, all more recent images are searched. Mated score distributions are computed over all searches noted in row 17 of Table 1 binned by number of years between search and initial enrollment.



**Figure 112: [FRVT-2018 Mugshot Ageing Dataset] Native mate scores vs. time-elapsed.** The oldest image of each individual is enrolled. Thereafter, all more recent images are searched. Mated score distributions are computed over all searches noted in row 17 of Table 1 binned by number of years between search and initial enrollment.

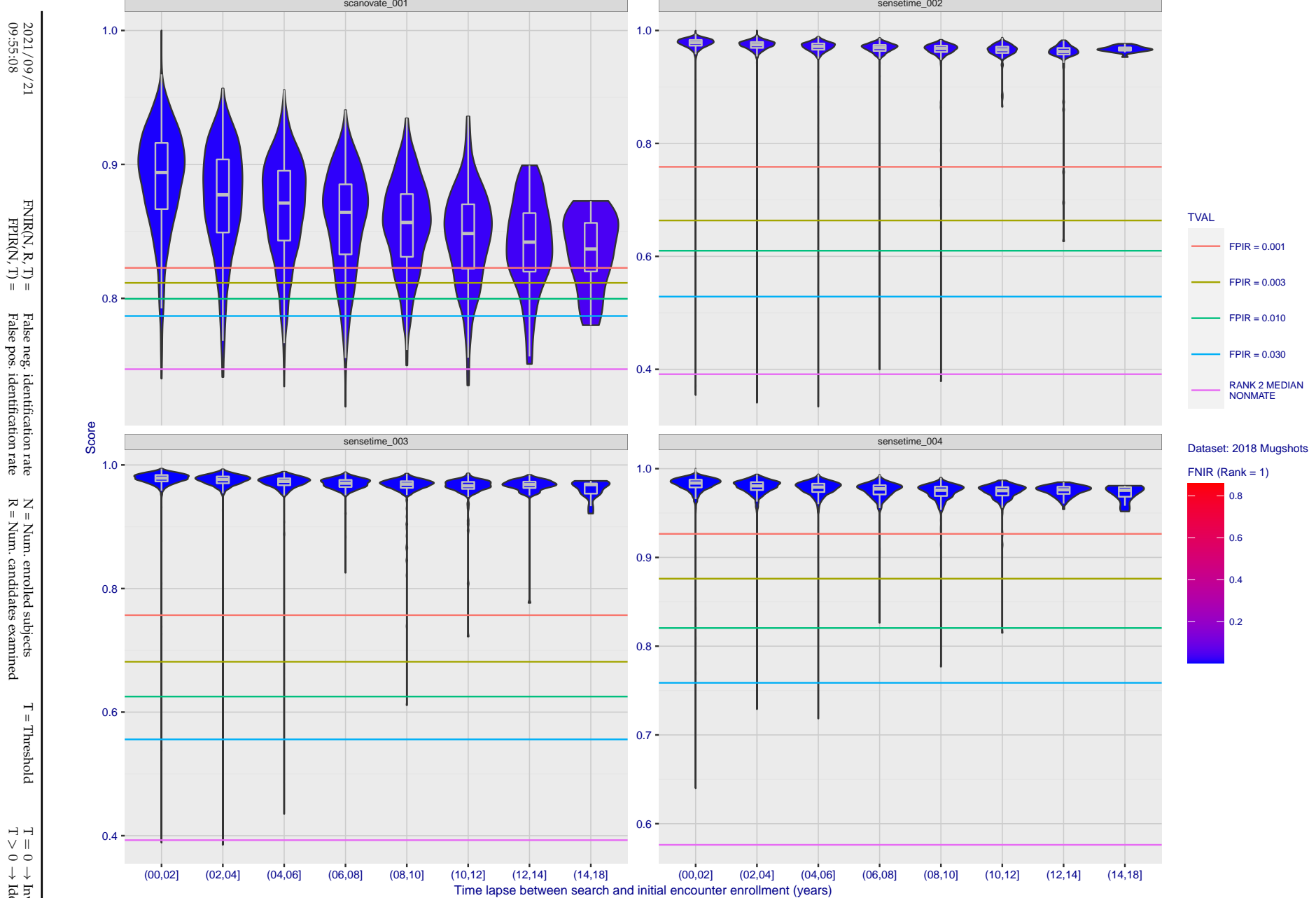


Figure 113: [FRVT-2018 Mugshot Ageing Dataset] Native mate scores vs. time-elapsed. The oldest image of each individual is enrolled. Thereafter, all more recent images are searched. Mated score distributions are computed over all searches noted in row 17 of Table 1 binned by number of years between search and initial enrollment.

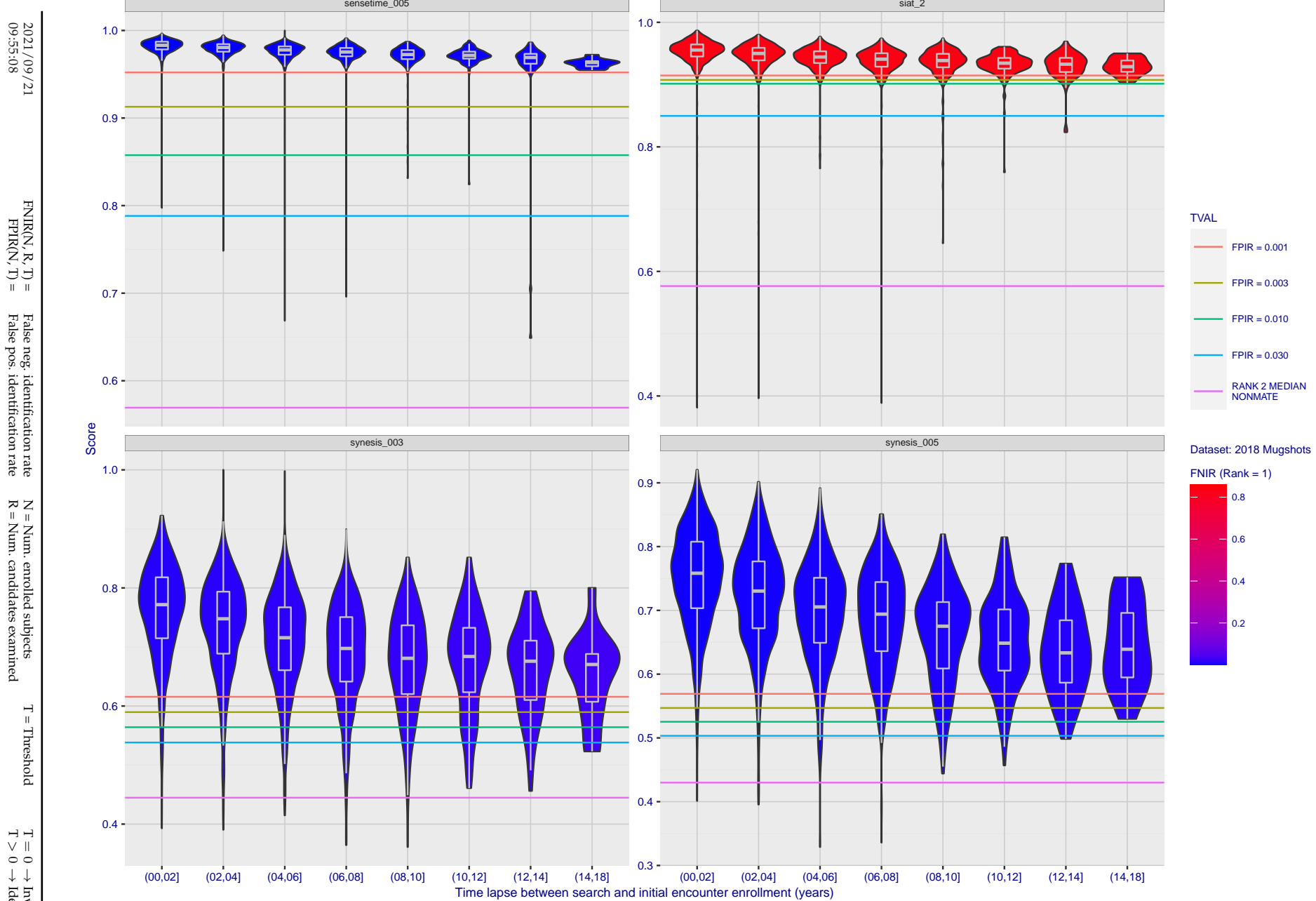


Figure 114: [FRVT-2018 Mugshot Ageing Dataset] Native mate scores vs. time-elapsed. The oldest image of each individual is enrolled. Thereafter, all more recent images are searched. Mated score distributions are computed over all searches noted in row 17 of Table 1 binned by number of years between search and initial enrollment.

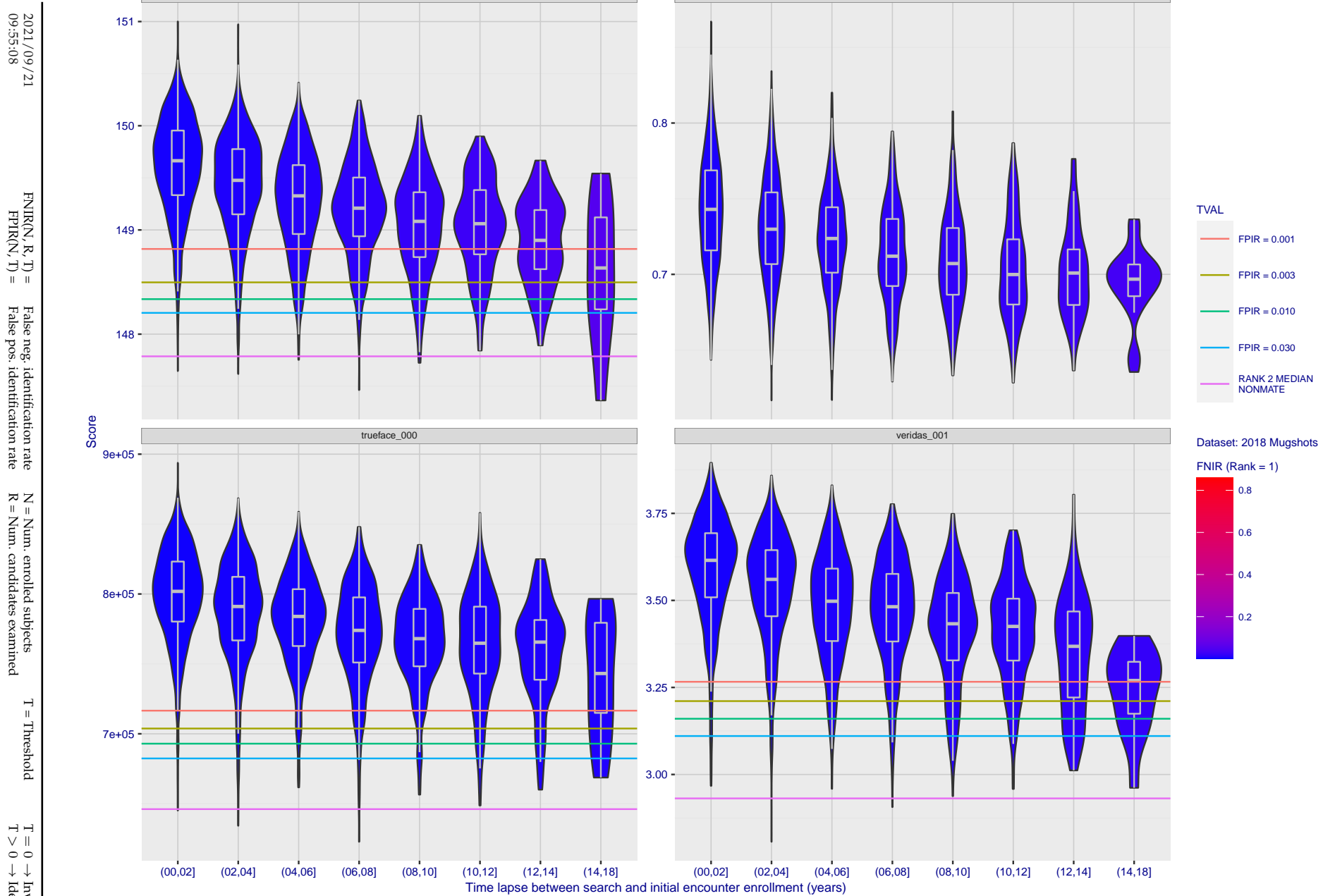
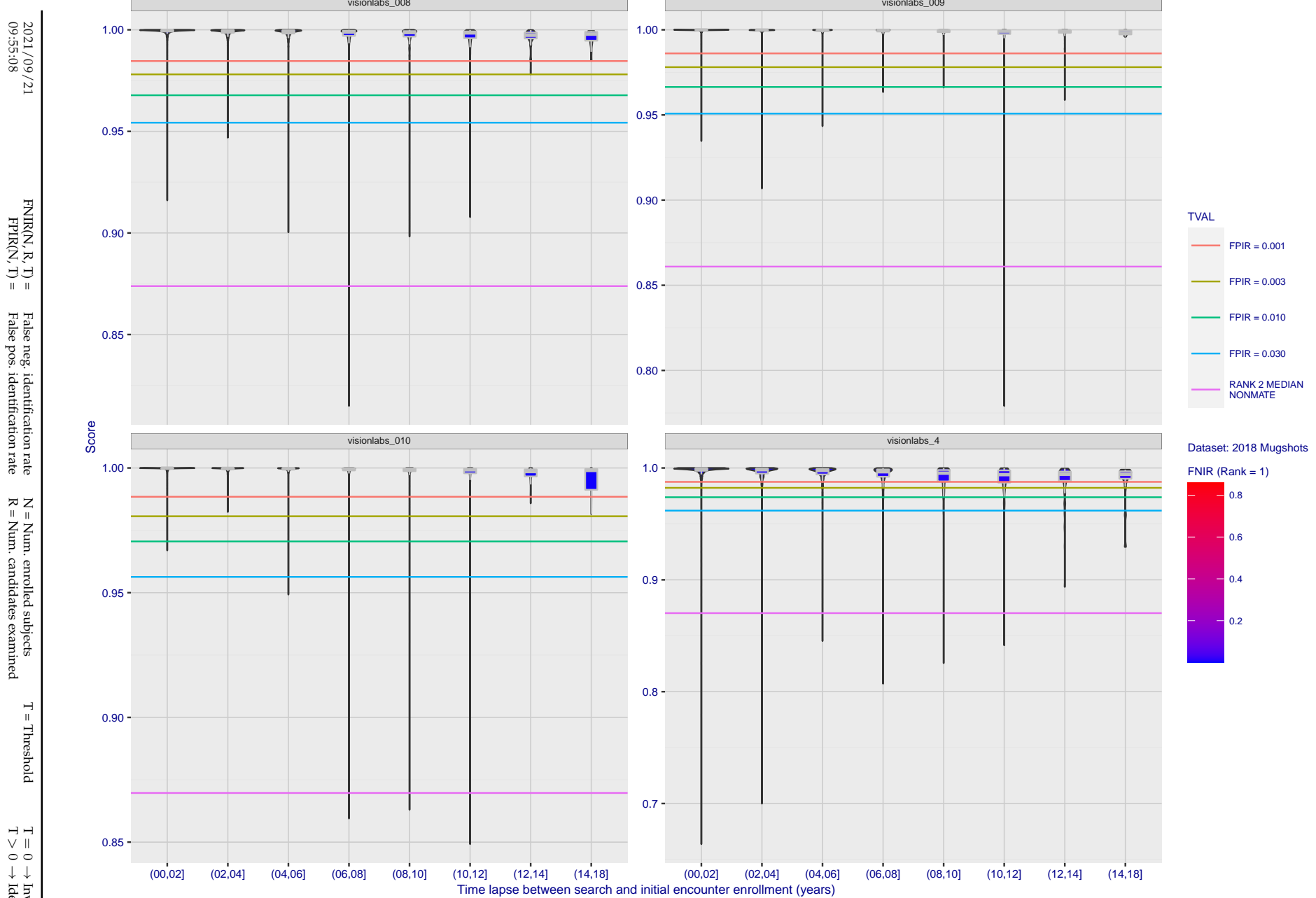
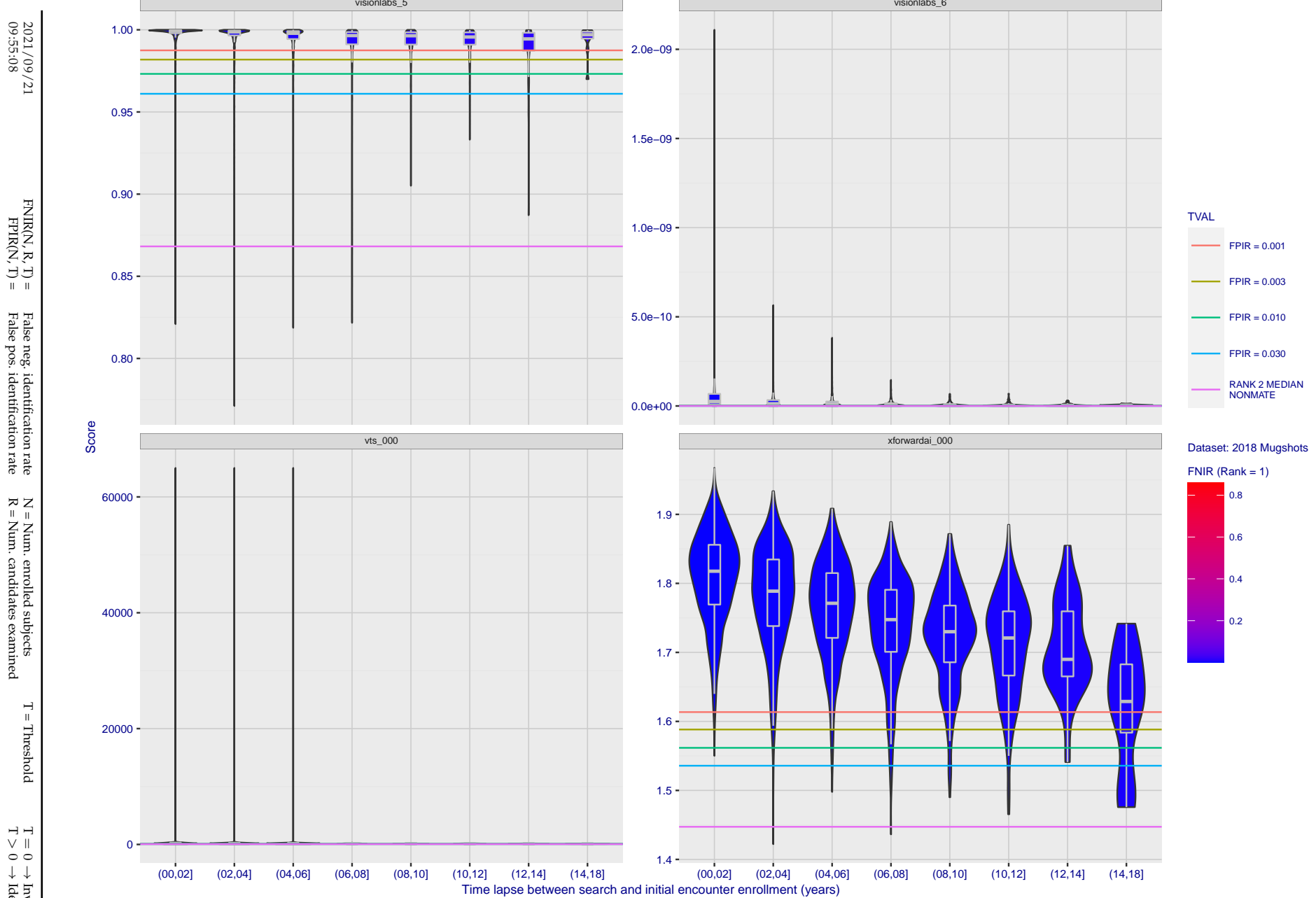


Figure 115: [FRVT-2018 Mugshot Ageing Dataset] Native mate scores vs. time-elapsed. The oldest image of each individual is enrolled. Thereafter, all more recent images are searched. Mated score distributions are computed over all searches noted in row 17 of Table 1 binned by number of years between search and initial enrollment.



**Figure 116: [FRVT-2018 Mugshot Ageing Dataset] Native mate scores vs. time-elapsed.** The oldest image of each individual is enrolled. Thereafter, all more recent images are searched. Mated score distributions are computed over all searches noted in row 17 of Table 1 binned by number of years between search and initial enrollment.



**Figure 117: [FRVT-2018 Mugshot Ageing Dataset] Native mate scores vs. time-elapsed.** The oldest image of each individual is enrolled. Thereafter, all more recent images are searched. Mated score distributions are computed over all searches noted in row 17 of Table 1 binned by number of years between search and initial enrollment.

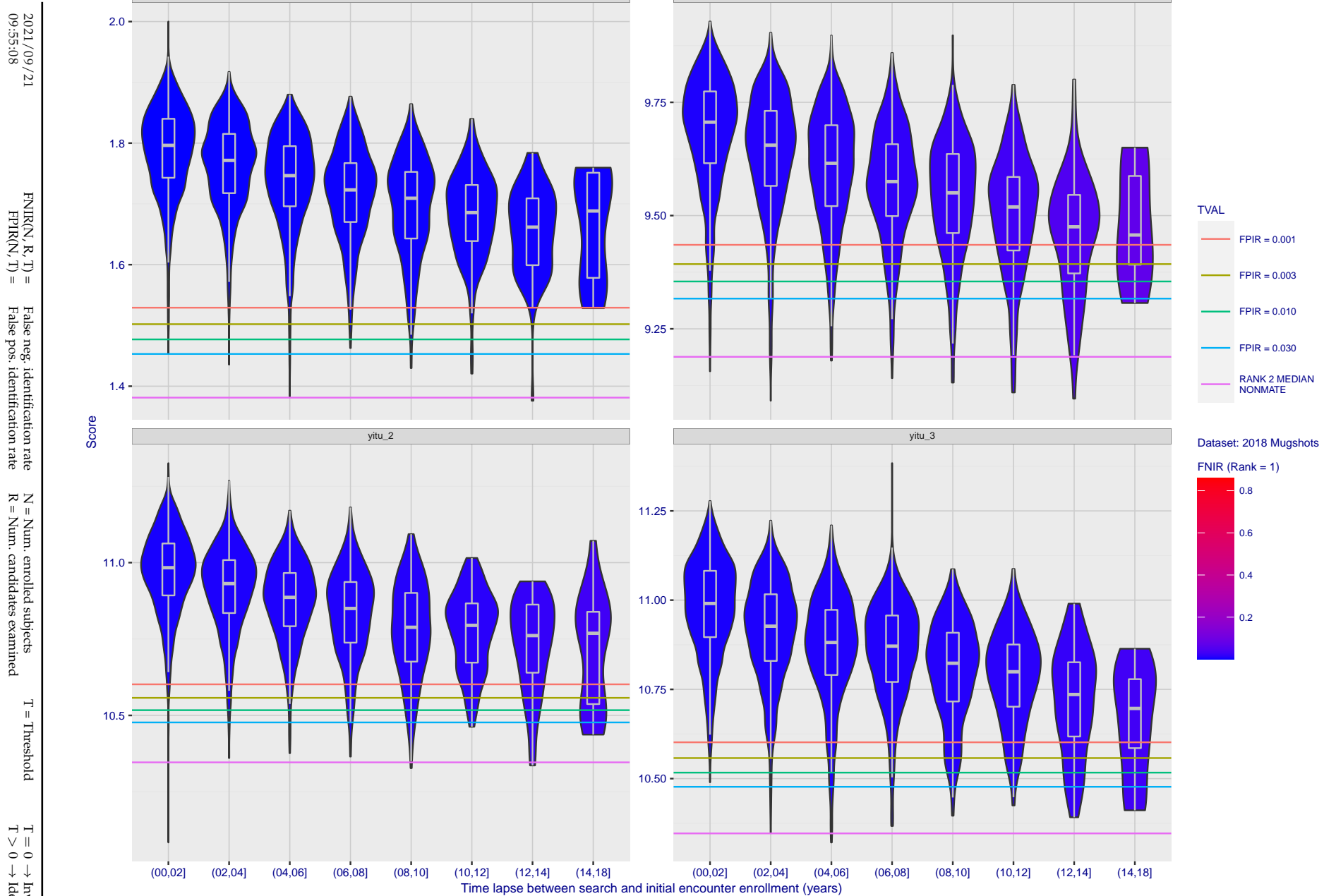


**Figure 118: [FRVT-2018 Mugshot Ageing Dataset] Native mate scores vs. time-elapsed.** The oldest image of each individual is enrolled. Thereafter, all more recent images are searched. Mated score distributions are computed over all searches noted in row 17 of Table 1 binned by number of years between search and initial enrollment.

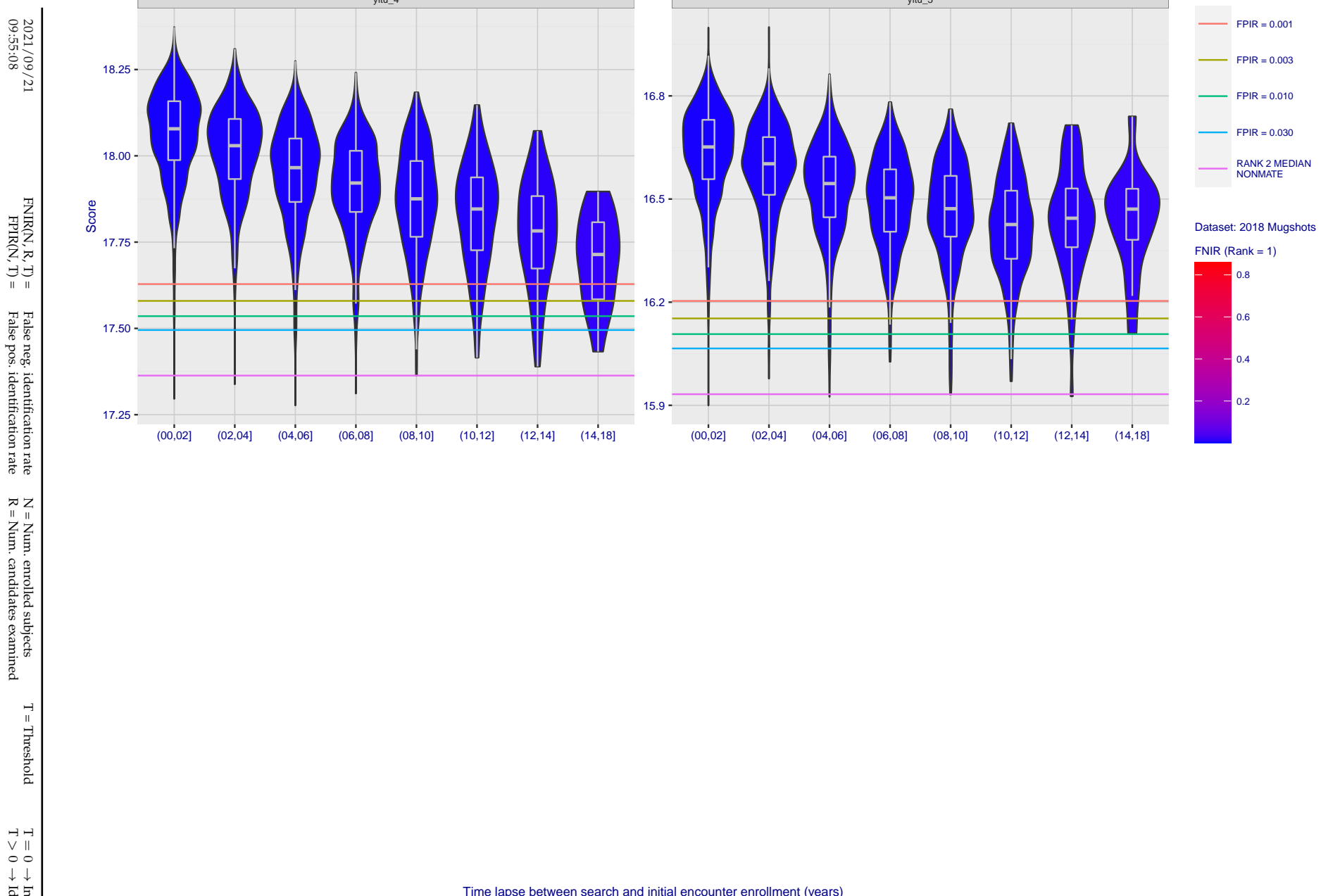


Figure 119: [FRVT-2018 Mugshot Ageing Dataset] Native mate scores vs. time-elapsed. The oldest image of each individual is enrolled. Thereafter, all more recent images are searched. Mated score distributions are computed over all searches noted in row 17 of Table 1 binned by number of years between search and initial enrollment.

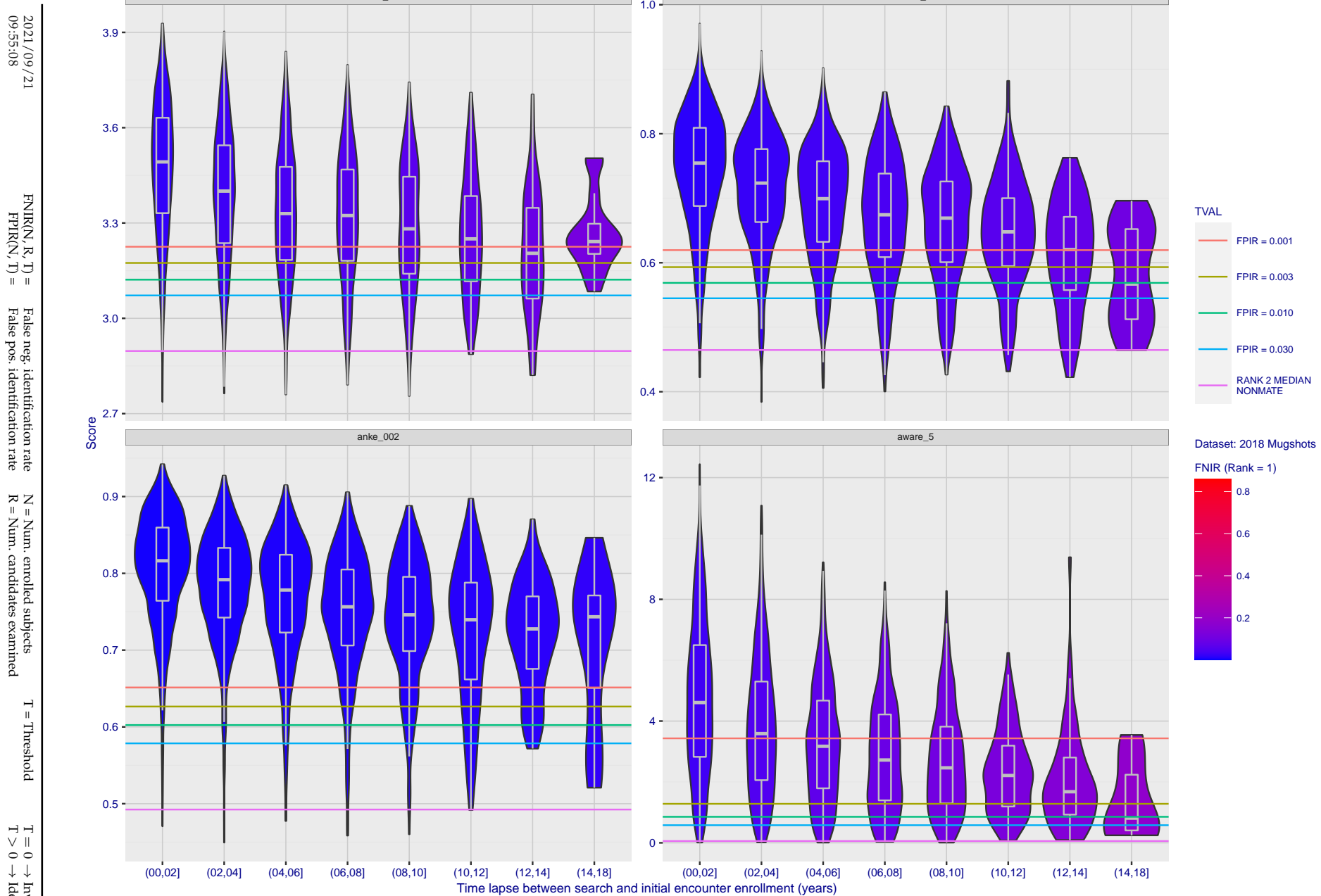


Figure 120: [FRVT-2018 Mugshot Ageing Dataset] Native mate scores vs. time-elapsed. The oldest image of each individual is enrolled. Thereafter, all more recent images are searched. Mated score distributions are computed over all searches noted in row 17 of Table 1 binned by number of years between search and initial enrollment.

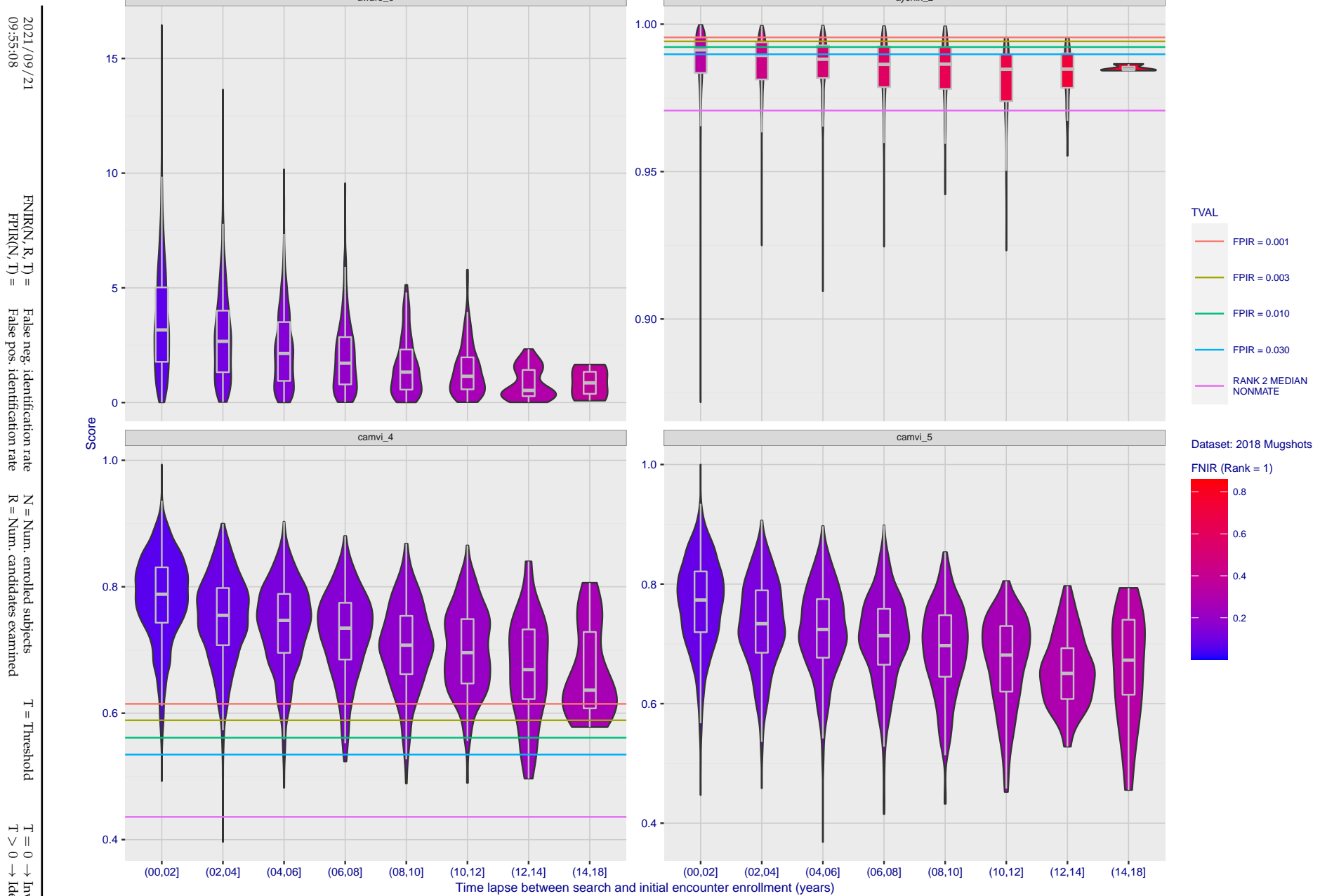


Figure 121: [FRVT-2018 Mugshot Ageing Dataset] Native mate scores vs. time-elapsed. The oldest image of each individual is enrolled. Thereafter, all more recent images are searched. Mated score distributions are computed over all searches noted in row 17 of Table 1 binned by number of years between search and initial enrollment.

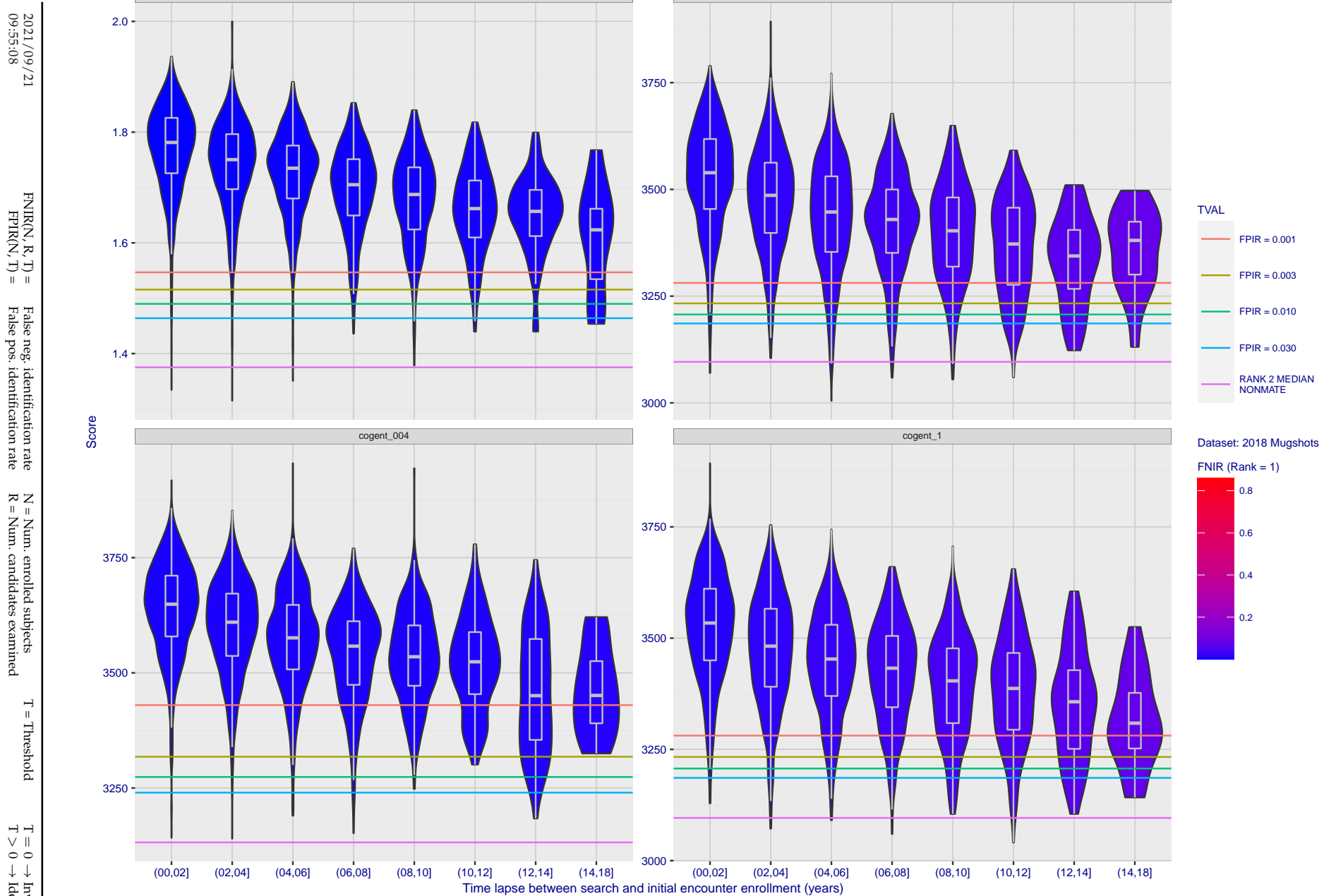
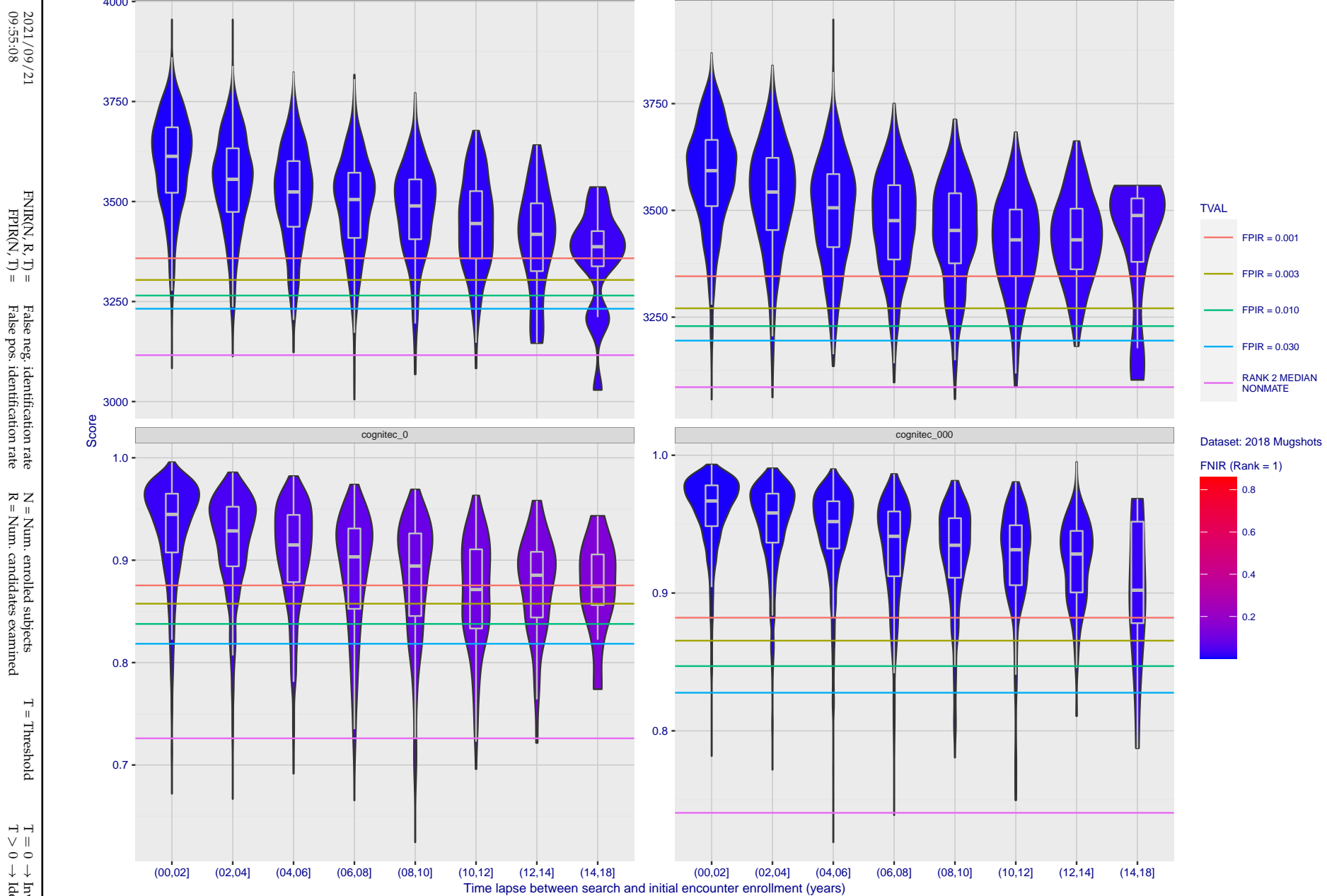


Figure 122: [FRVT-2018 Mugshot Ageing Dataset] Native mate scores vs. time-elapsed. The oldest image of each individual is enrolled. Thereafter, all more recent images are searched. Mated score distributions are computed over all searches noted in row 17 of Table 1 binned by number of years between search and initial enrollment.



**Figure 123: [FRVT-2018 Mugshot Ageing Dataset] Native mate scores vs. time-elapsed.** The oldest image of each individual is enrolled. Thereafter, all more recent images are searched. Mated score distributions are computed over all searches noted in row 17 of Table 1 binned by number of years between search and initial enrollment.

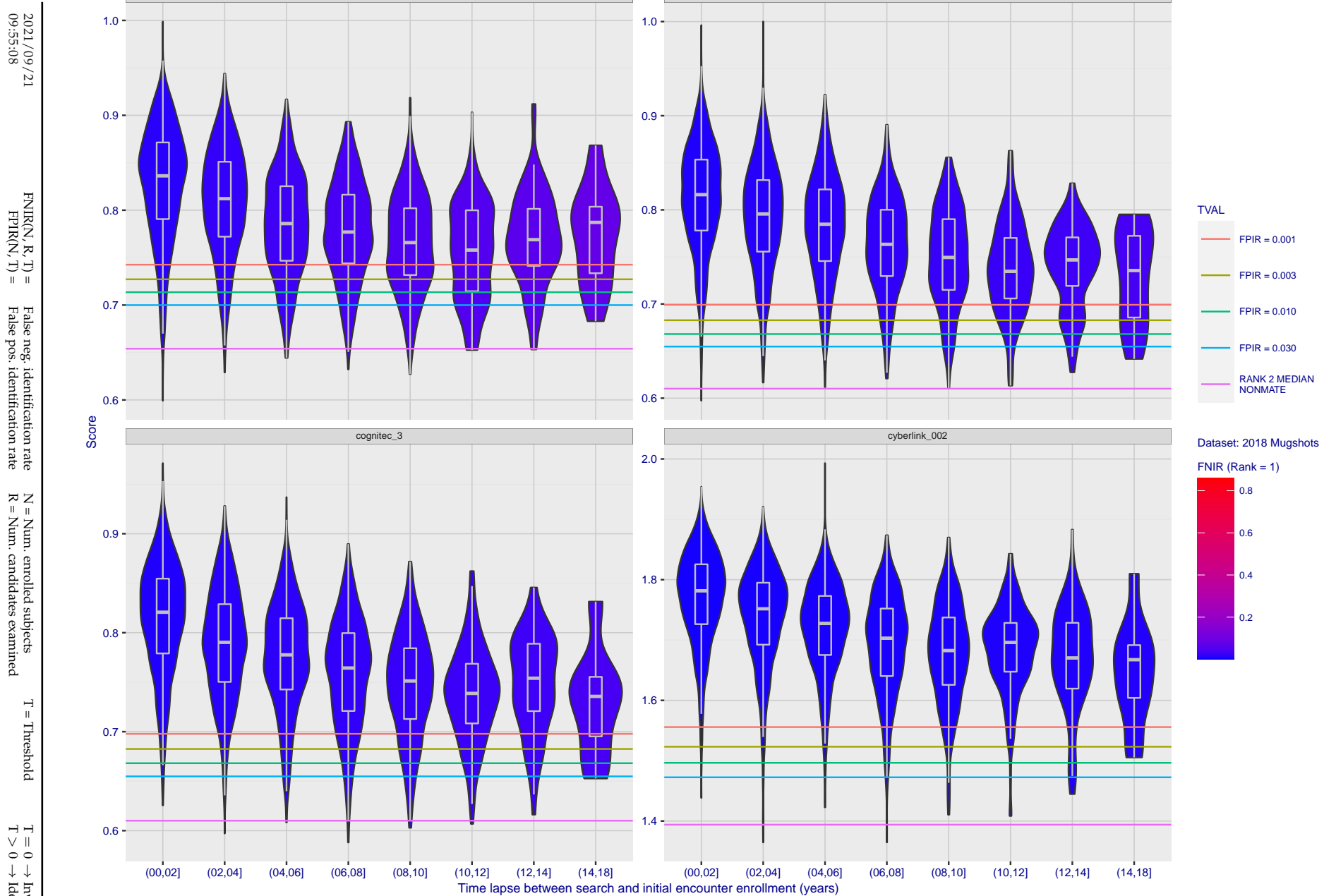
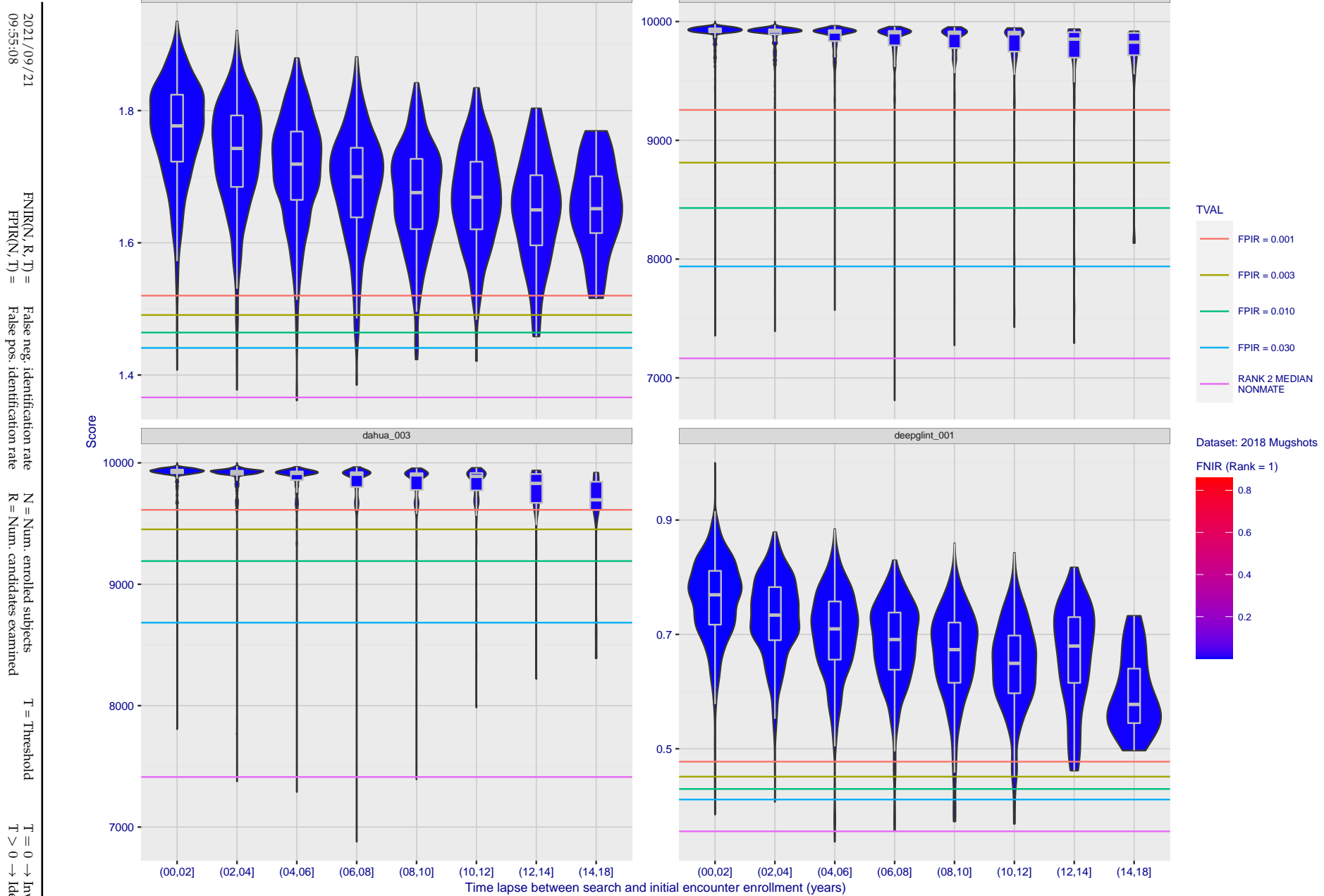


Figure 124: [FRVT-2018 Mugshot Ageing Dataset] Native mate scores vs. time-elapsed. The oldest image of each individual is enrolled. Thereafter, all more recent images are searched. Mated score distributions are computed over all searches noted in row 17 of Table 1 binned by number of years between search and initial enrollment.



**Figure 125: [FRVT-2018 Mugshot Ageing Dataset] Native mate scores vs. time-elapsed.** The oldest image of each individual is enrolled. Thereafter, all more recent images are searched. Mated score distributions are computed over all searches noted in row 17 of Table 1 binned by number of years between search and initial enrollment.

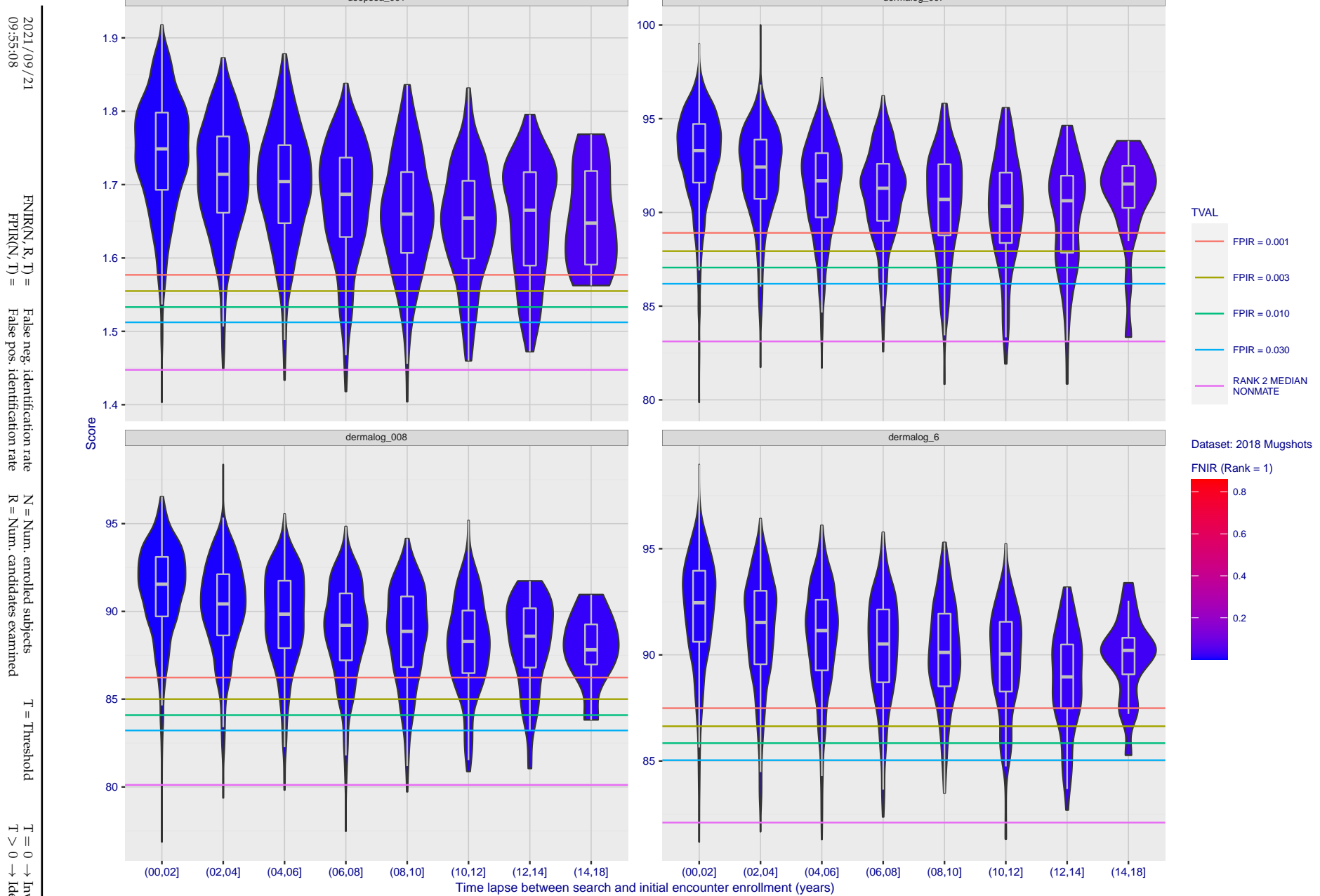


Figure 126: [FRVT-2018 Mugshot Ageing Dataset] Native mate scores vs. time-elapsed. The oldest image of each individual is enrolled. Thereafter, all more recent images are searched. Mated score distributions are computed over all searches noted in row 17 of Table 1 binned by number of years between search and initial enrollment.

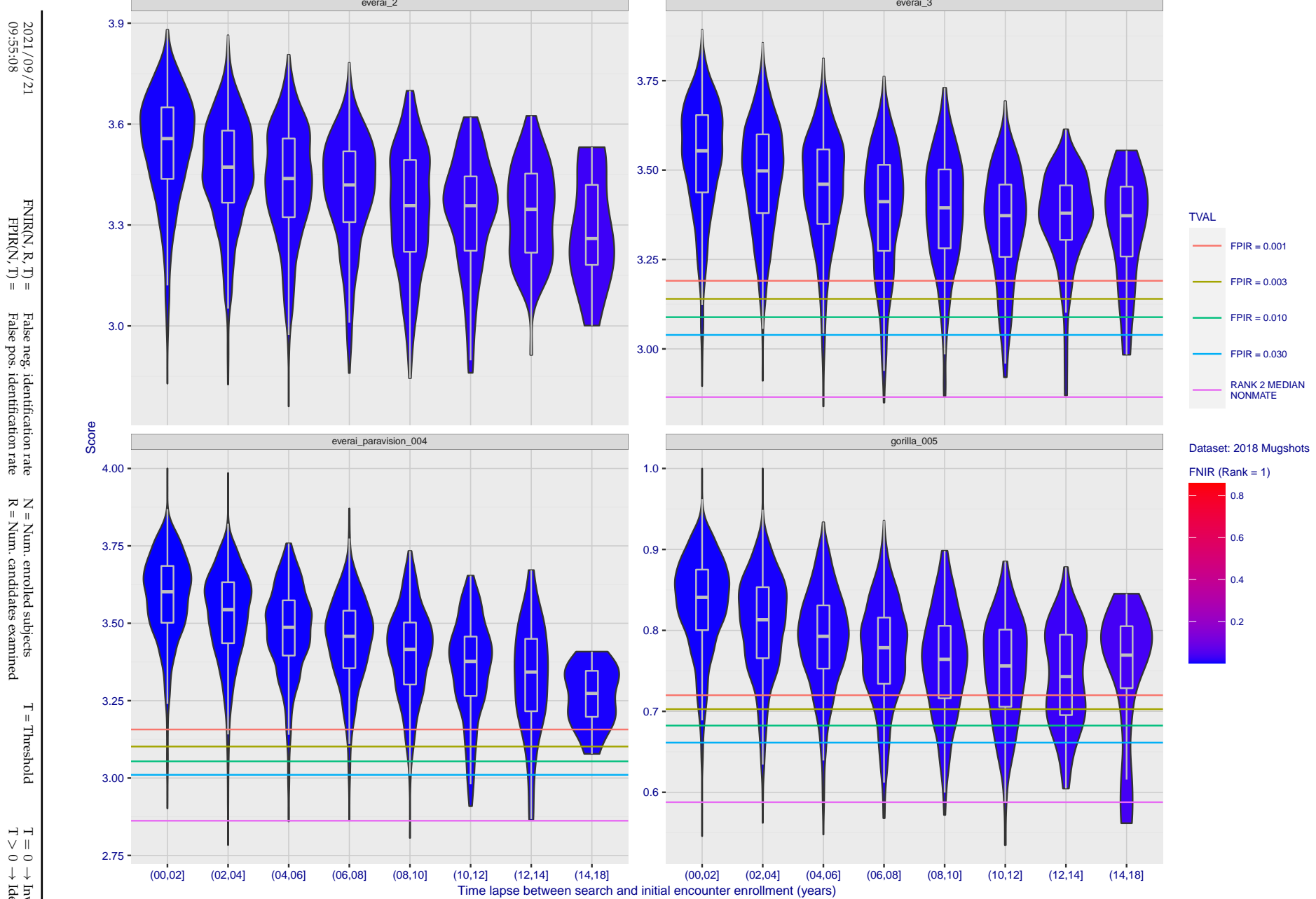


Figure 127: [FRVT-2018 Mugshot Ageing Dataset] Native mate scores vs. time-elapsed. The oldest image of each individual is enrolled. Thereafter, all more recent images are searched. Mated score distributions are computed over all searches noted in row 17 of Table 1 binned by number of years between search and initial enrollment.

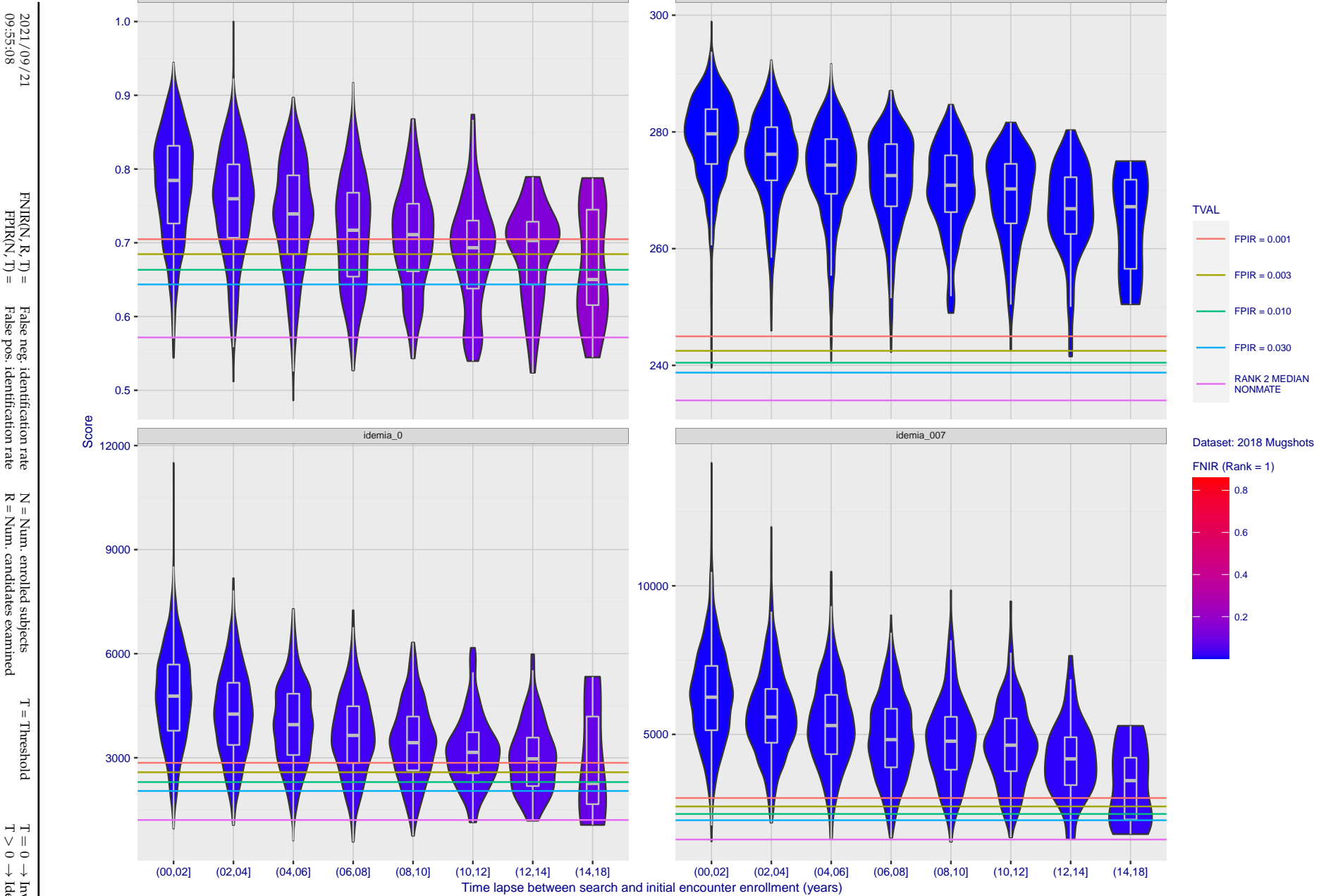


Figure 128: [FRVT-2018 Mugshot Ageing Dataset] Native mate scores vs. time-elapsed. The oldest image of each individual is enrolled. Thereafter, all more recent images are searched. Mated score distributions are computed over all searches noted in row 17 of Table 1 binned by number of years between search and initial enrollment.

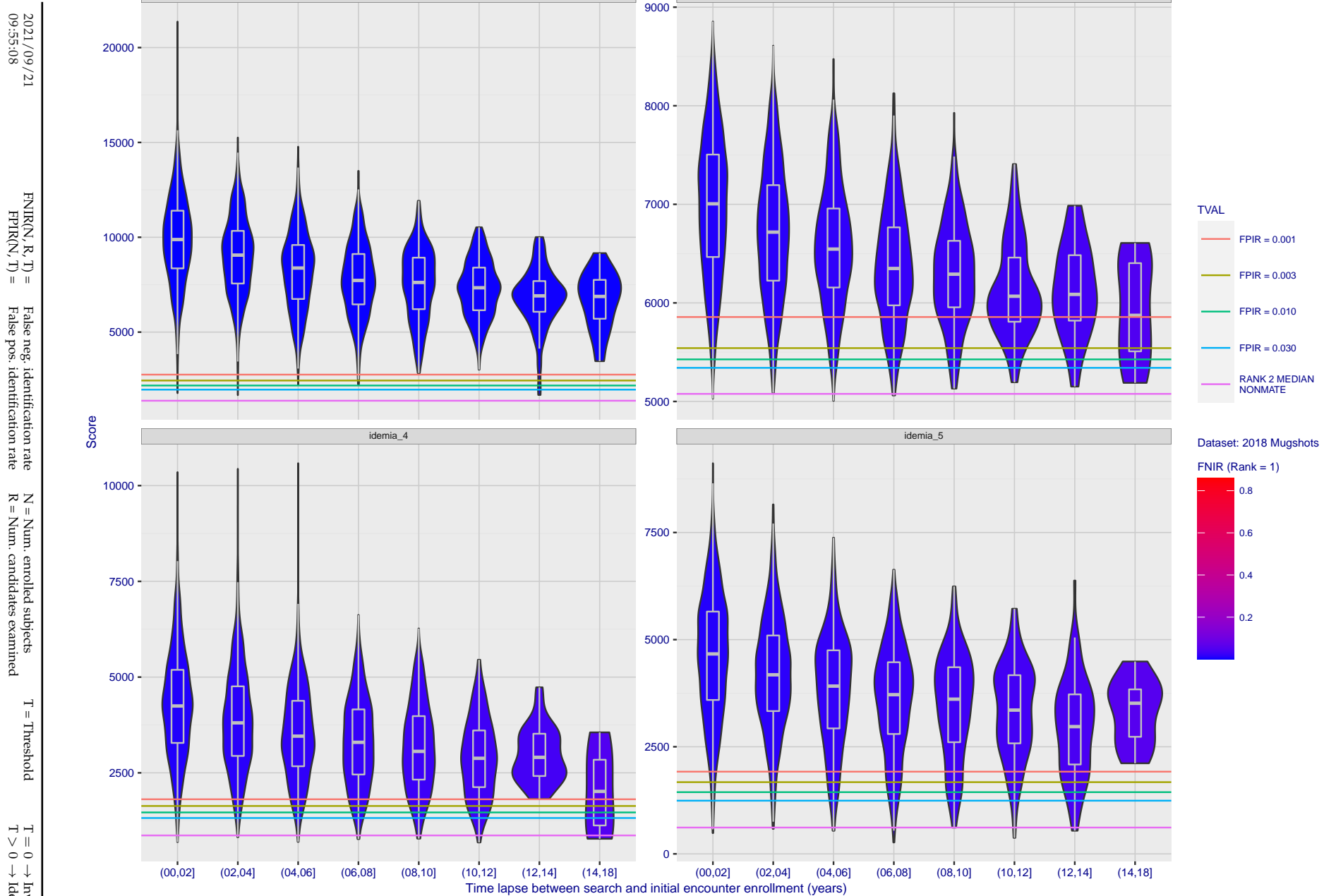


Figure 129: [FRVT-2018 Mugshot Ageing Dataset] Native mate scores vs. time-elapsed. The oldest image of each individual is enrolled. Thereafter, all more recent images are searched. Mated score distributions are computed over all searches noted in row 17 of Table 1 binned by number of years between search and initial enrollment.

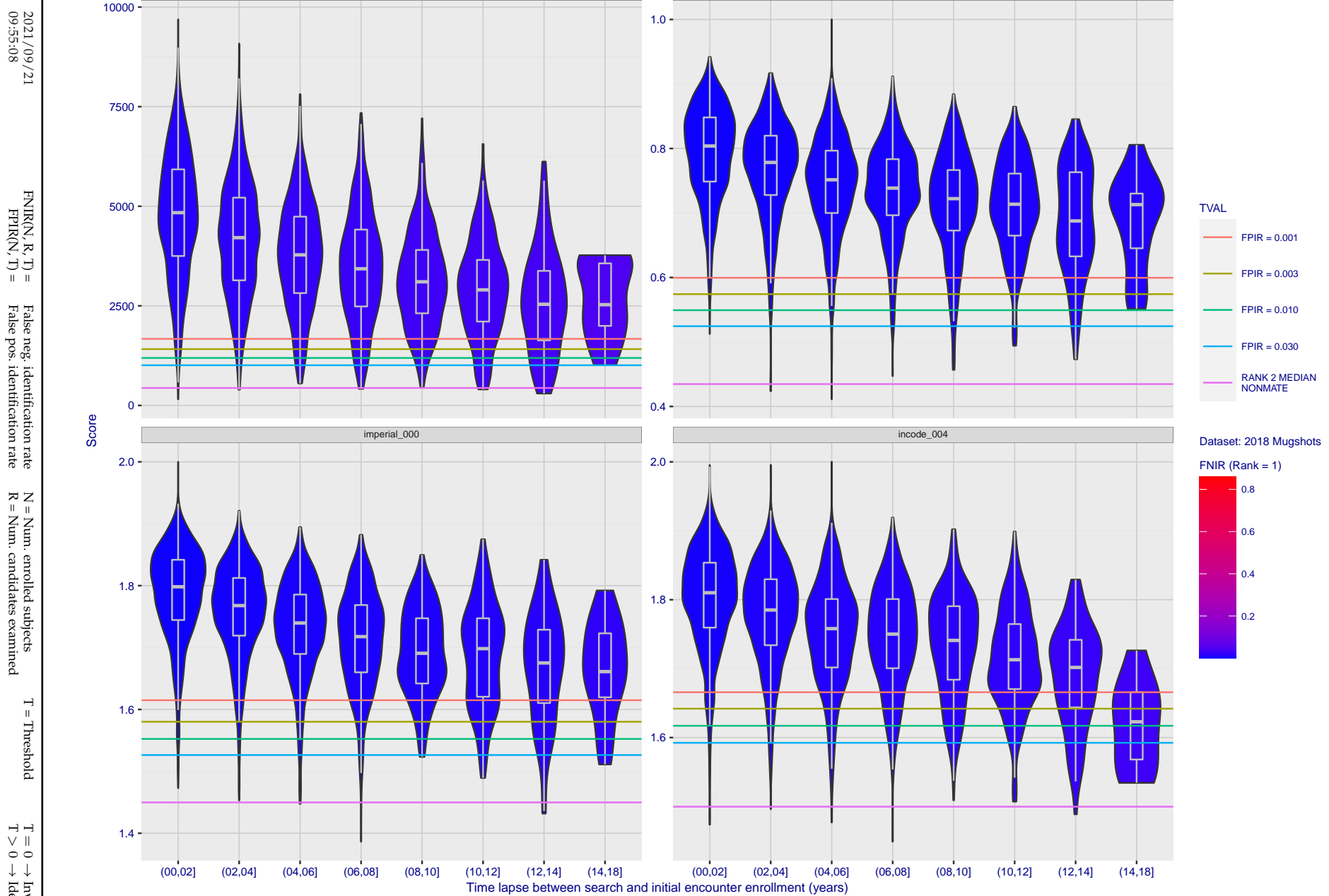


Figure 130: [FRVT-2018 Mugshot Ageing Dataset] Native mate scores vs. time-elapsed. The oldest image of each individual is enrolled. Thereafter, all more recent images are searched. Mated score distributions are computed over all searches noted in row 17 of Table 1 binned by number of years between search and initial enrollment.

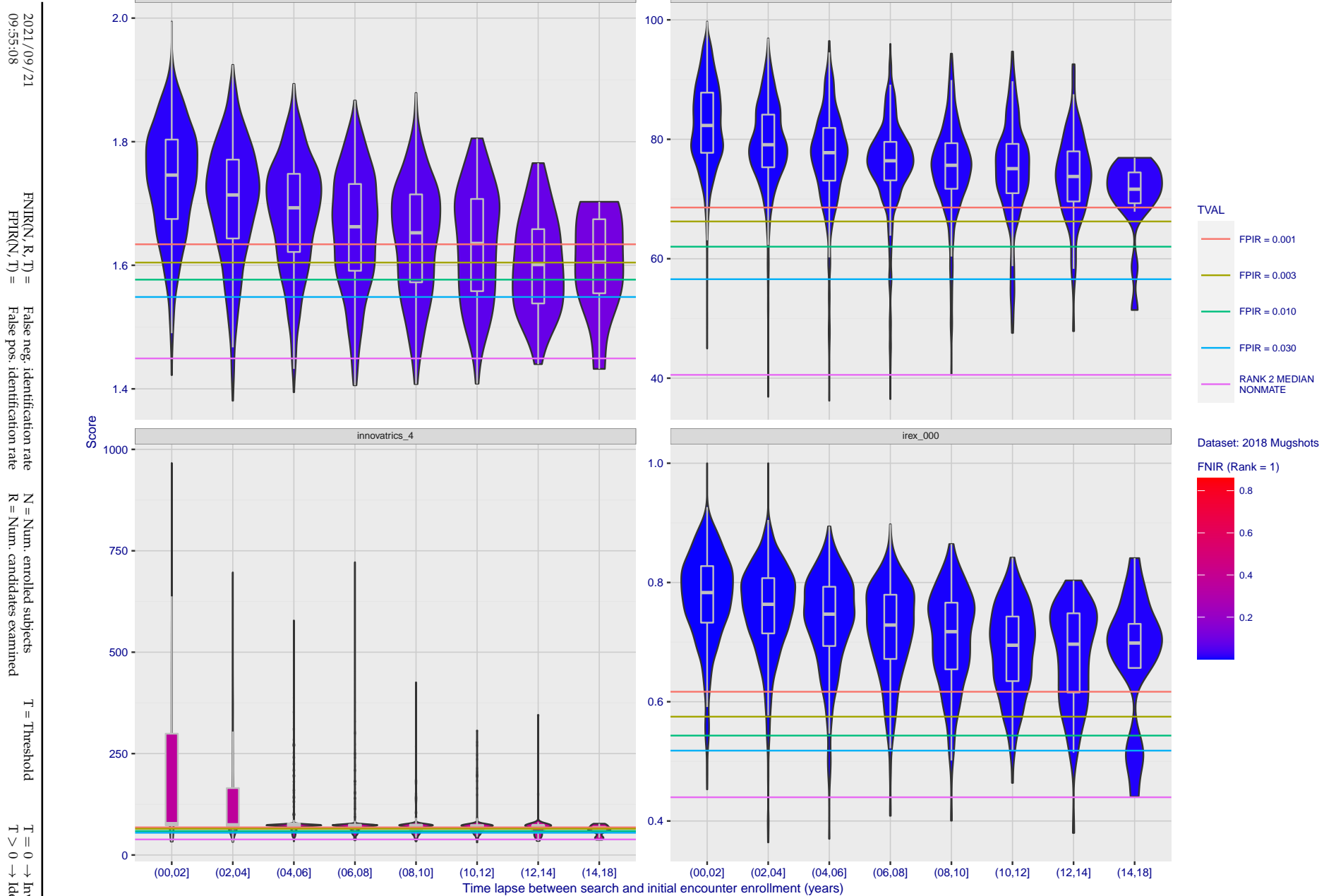
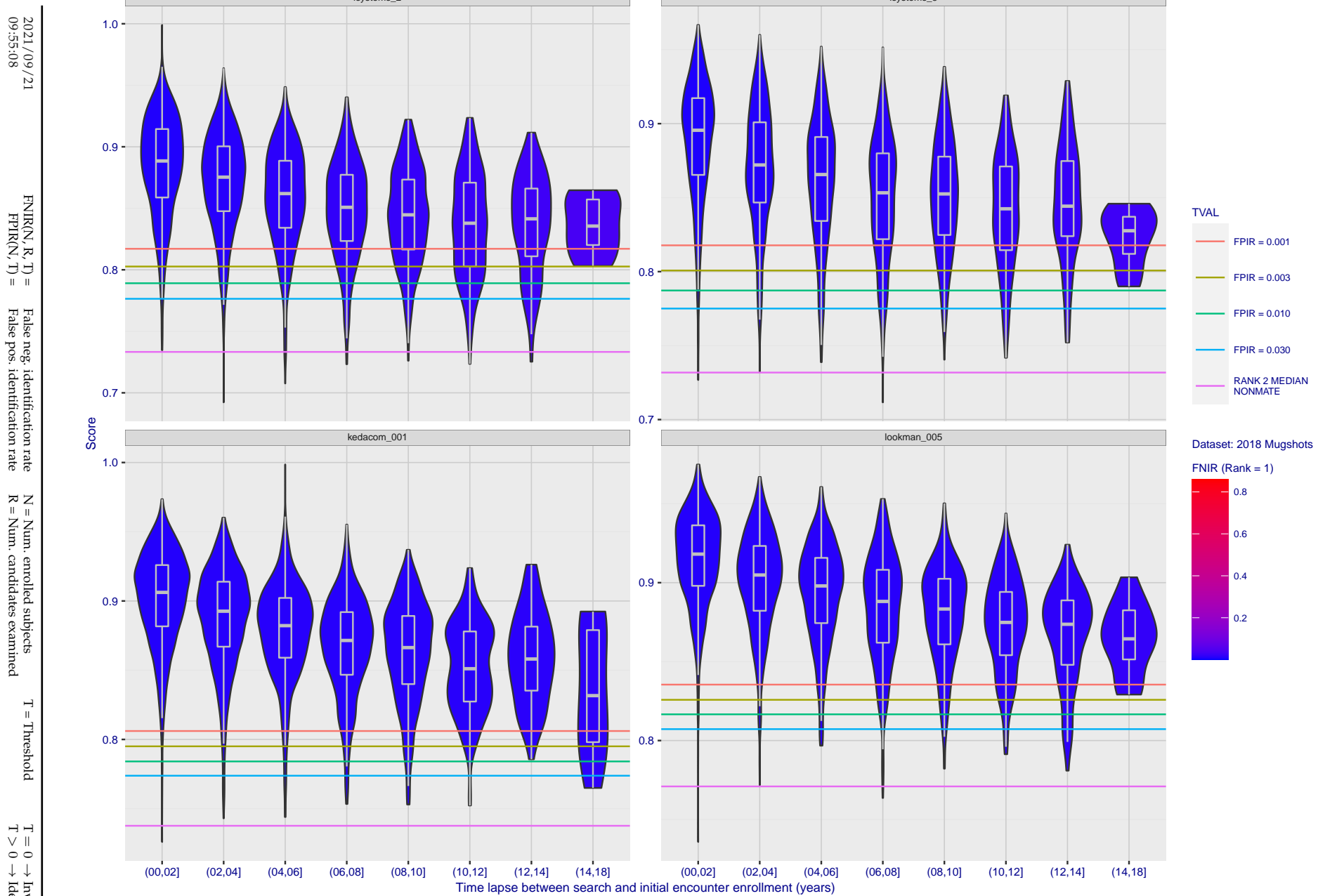


Figure 131: [FRVT-2018 Mugshot Ageing Dataset] Native mate scores vs. time-elapsed. The oldest image of each individual is enrolled. Thereafter, all more recent images are searched. Mated score distributions are computed over all searches noted in row 17 of Table 1 binned by number of years between search and initial enrollment.



**Figure 132: [FRVT-2018 Mugshot Ageing Dataset] Native mate scores vs. time-elapsed.** The oldest image of each individual is enrolled. Thereafter, all more recent images are searched. Mated score distributions are computed over all searches noted in row 17 of Table 1 binned by number of years between search and initial enrollment.

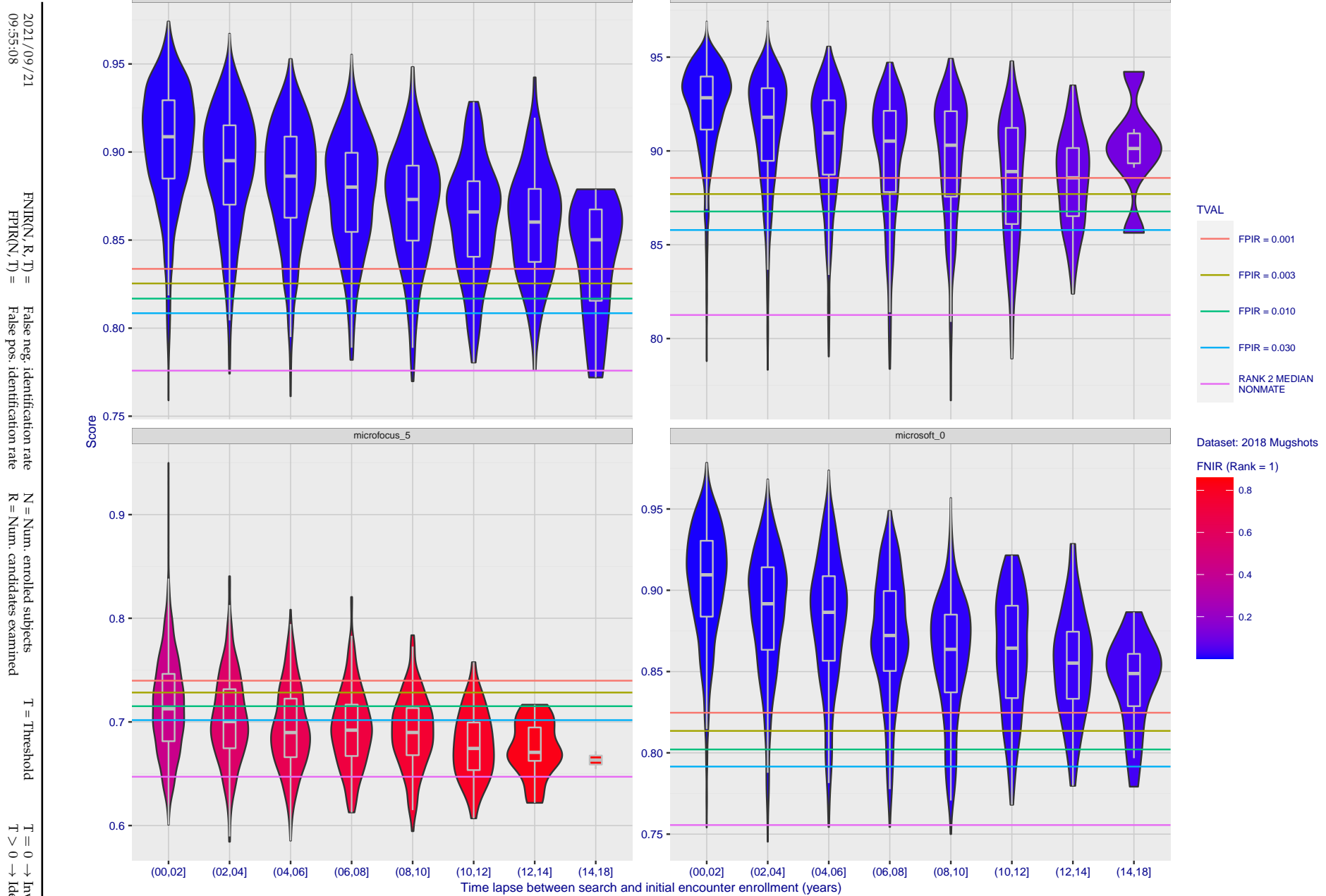
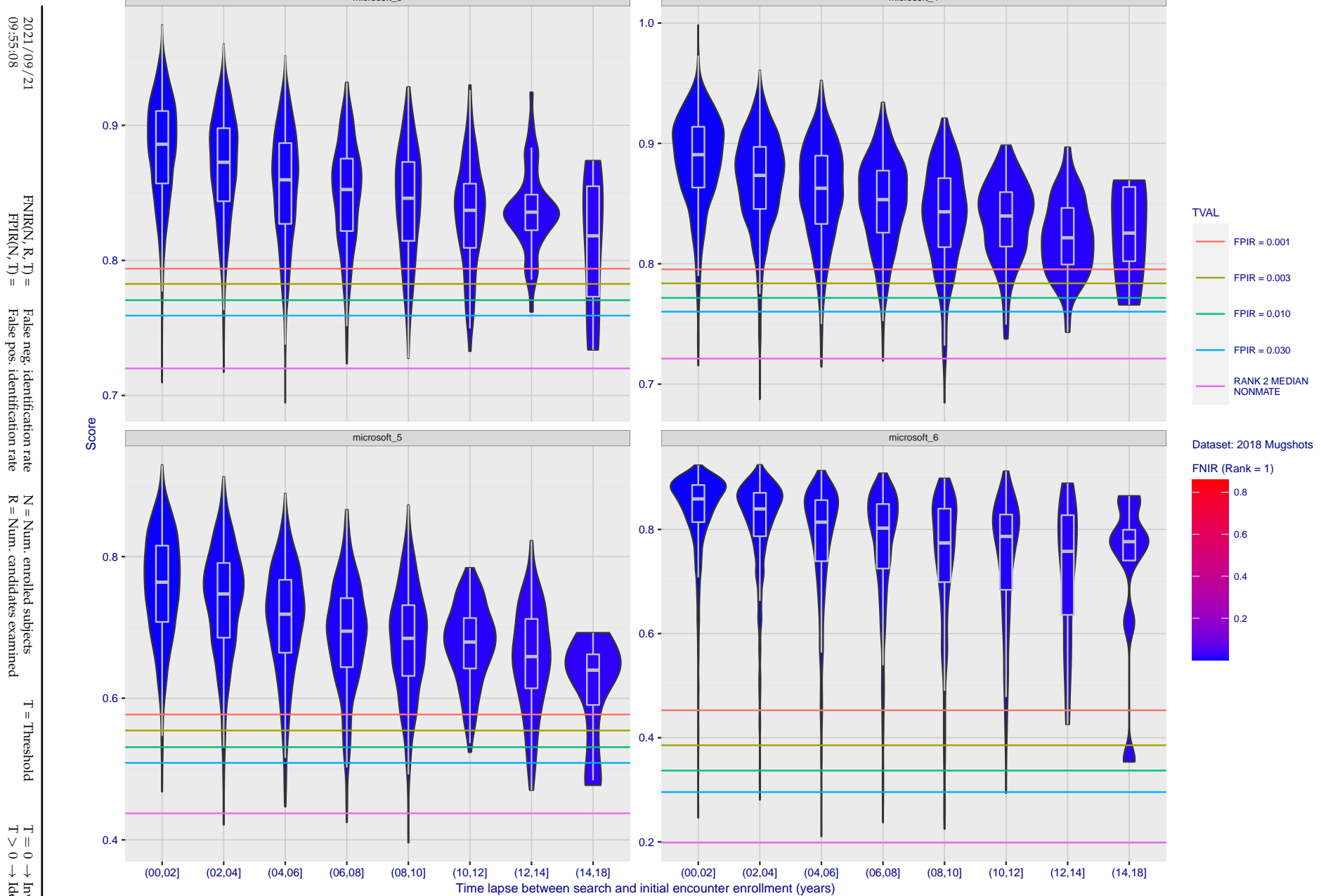


Figure 133: [FRVT-2018 Mugshot Ageing Dataset] Native mate scores vs. time-elapsed. The oldest image of each individual is enrolled. Thereafter, all more recent images are searched. Mated score distributions are computed over all searches noted in row 17 of Table 1 binned by number of years between search and initial enrollment.



**Figure 134: [FRVT-2018 Mugshot Ageing Dataset] Native mate scores vs. time-elapsed.** The oldest image of each individual is enrolled. Thereafter, all more recent images are searched. Mated score distributions are computed over all searches noted in row 17 of Table 1 binned by number of years between search and initial enrollment.

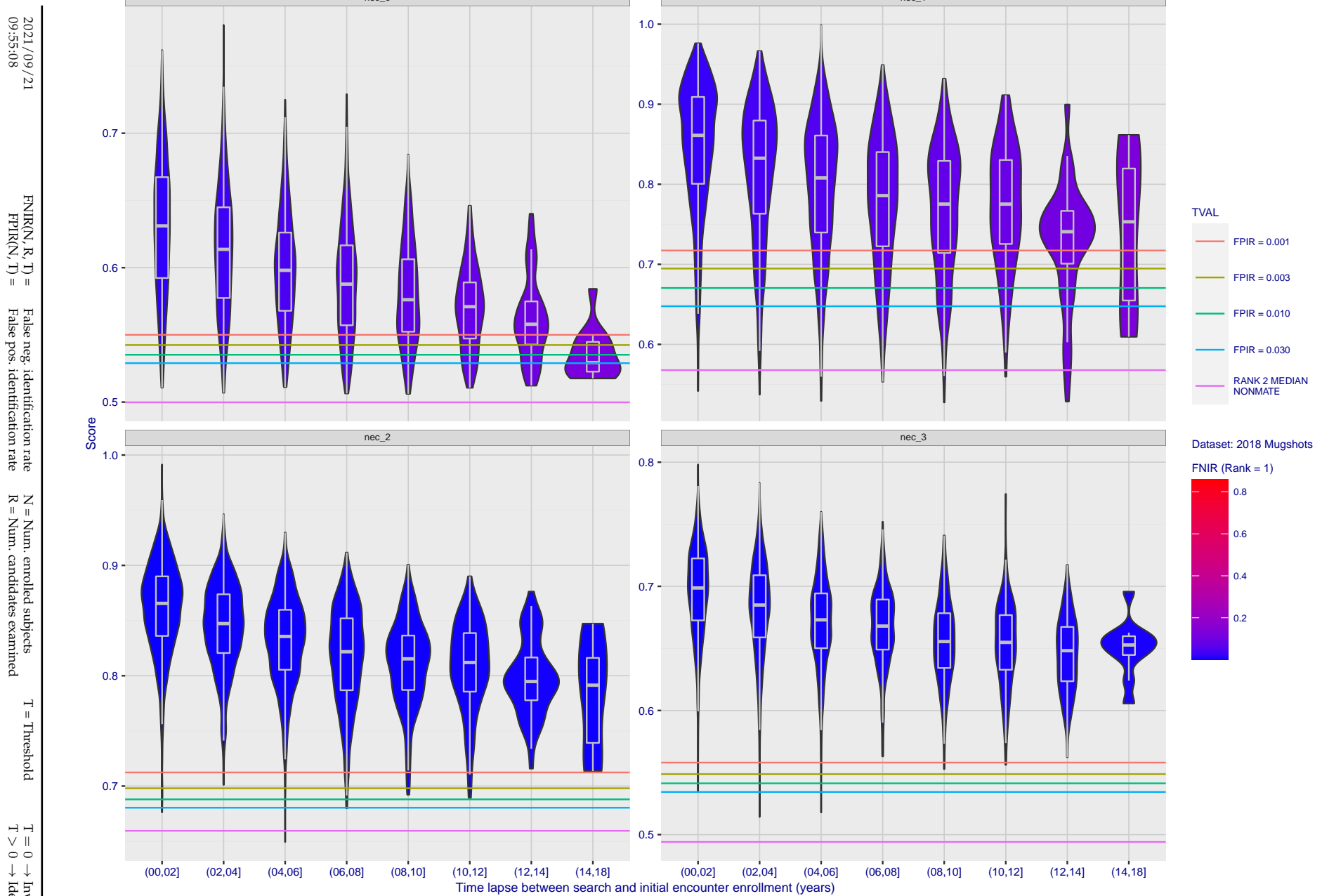


Figure 135: [FRVT-2018 Mugshot Ageing Dataset] Native mate scores vs. time-elapsed. The oldest image of each individual is enrolled. Thereafter, all more recent images are searched. Mated score distributions are computed over all searches noted in row 17 of Table 1 binned by number of years between search and initial enrollment.

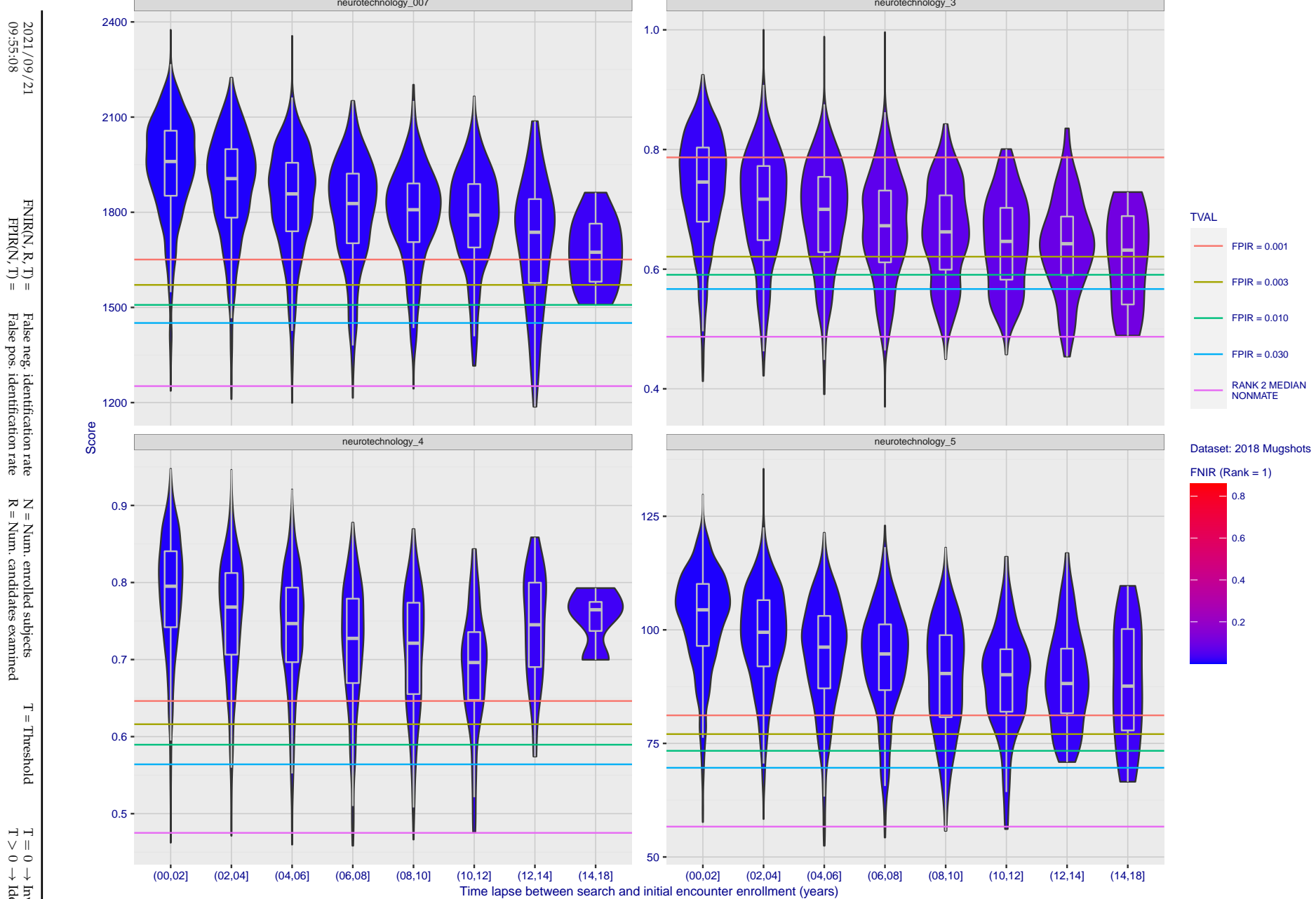


Figure 136: [FRVT-2018 Mugshot Ageing Dataset] Native mate scores vs. time-elapsed. The oldest image of each individual is enrolled. Thereafter, all more recent images are searched. Mated score distributions are computed over all searches noted in row 17 of Table 1 binned by number of years between search and initial enrollment.

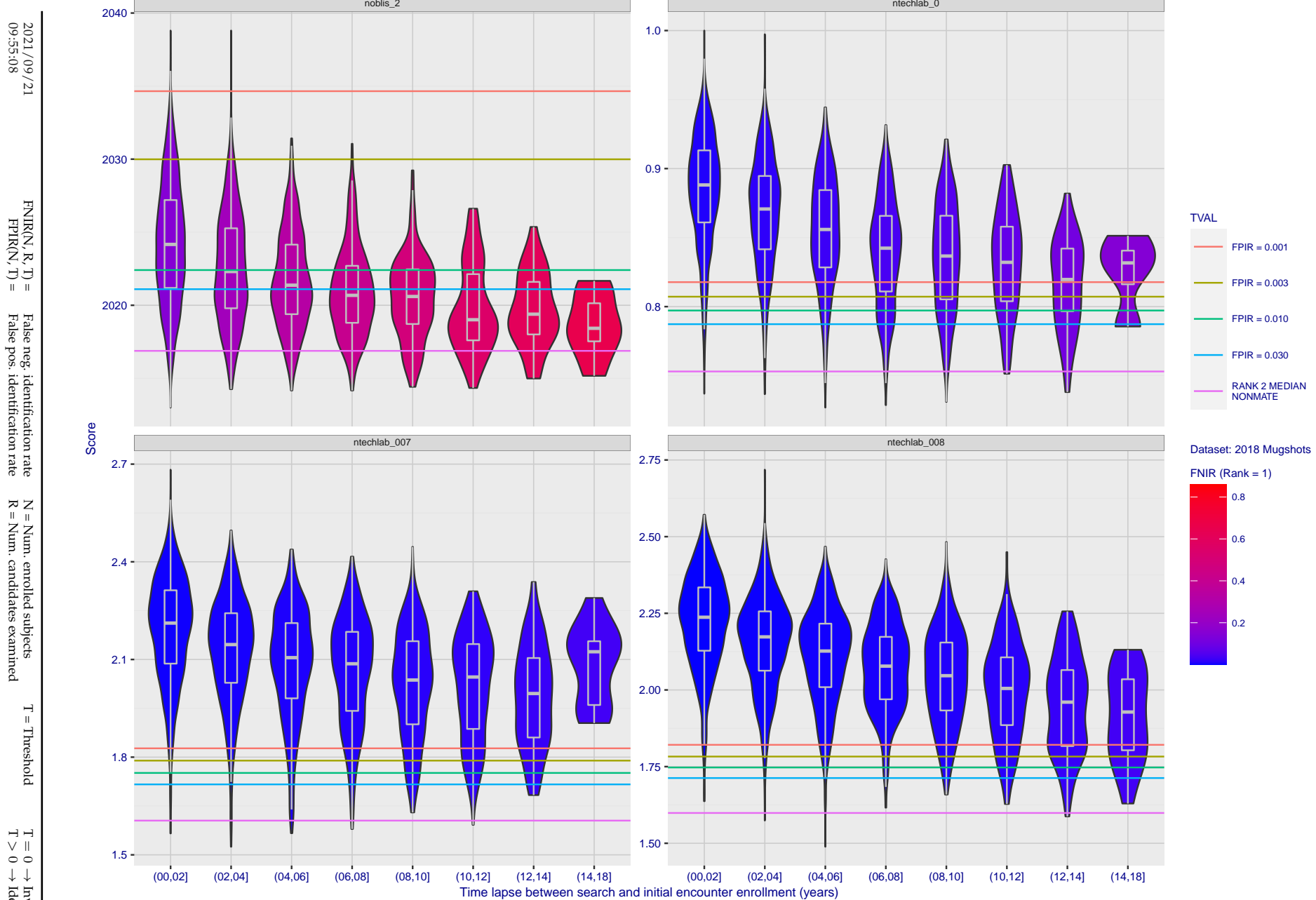
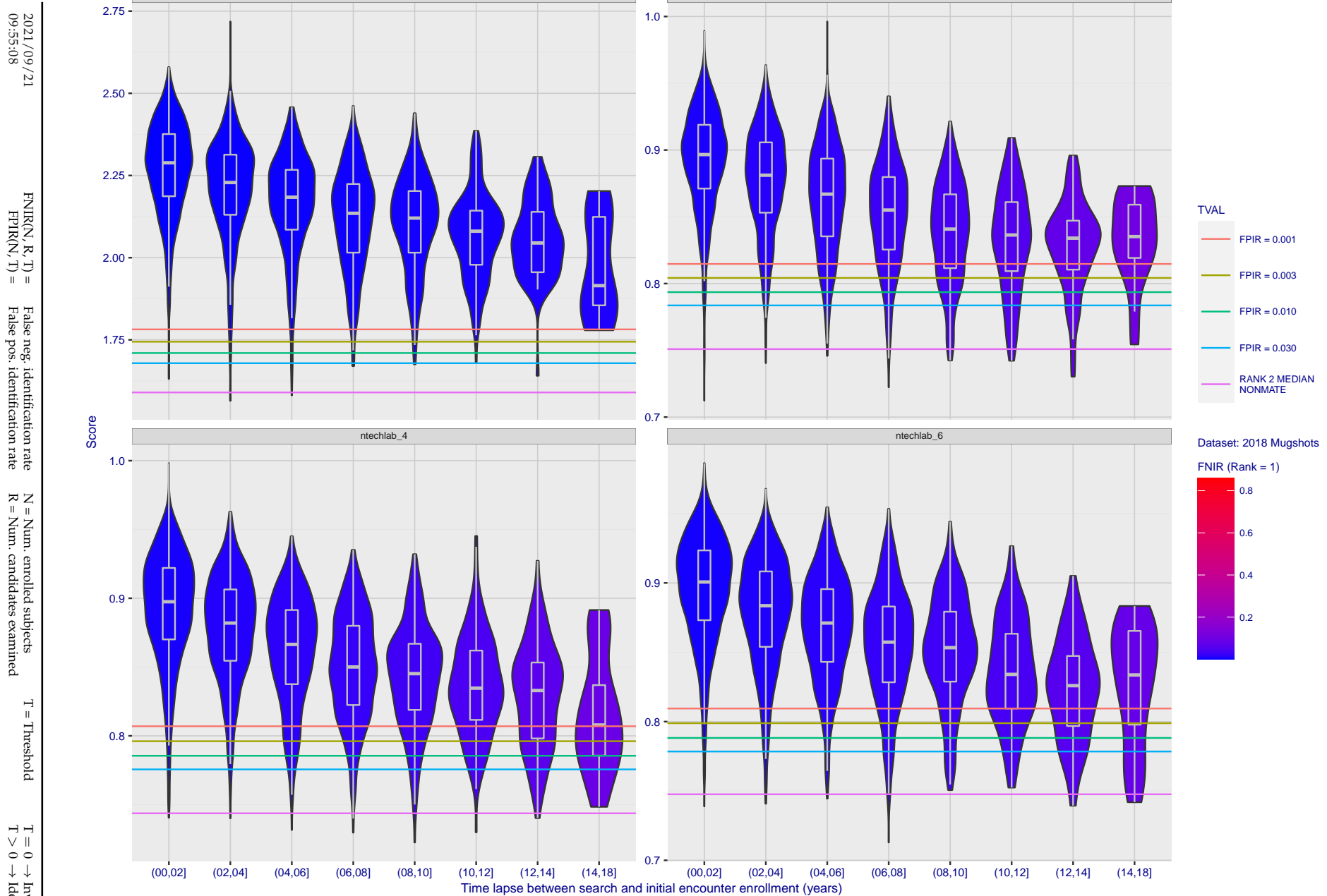


Figure 137: [FRVT-2018 Mugshot Ageing Dataset] Native mate scores vs. time-elapsed. The oldest image of each individual is enrolled. Thereafter, all more recent images are searched. Mated score distributions are computed over all searches noted in row 17 of Table 1 binned by number of years between search and initial enrollment.



**Figure 138: [FRVT-2018 Mugshot Ageing Dataset] Native mate scores vs. time-elapsed.** The oldest image of each individual is enrolled. Thereafter, all more recent images are searched. Mated score distributions are computed over all searches noted in row 17 of Table 1 binned by number of years between search and initial enrollment.

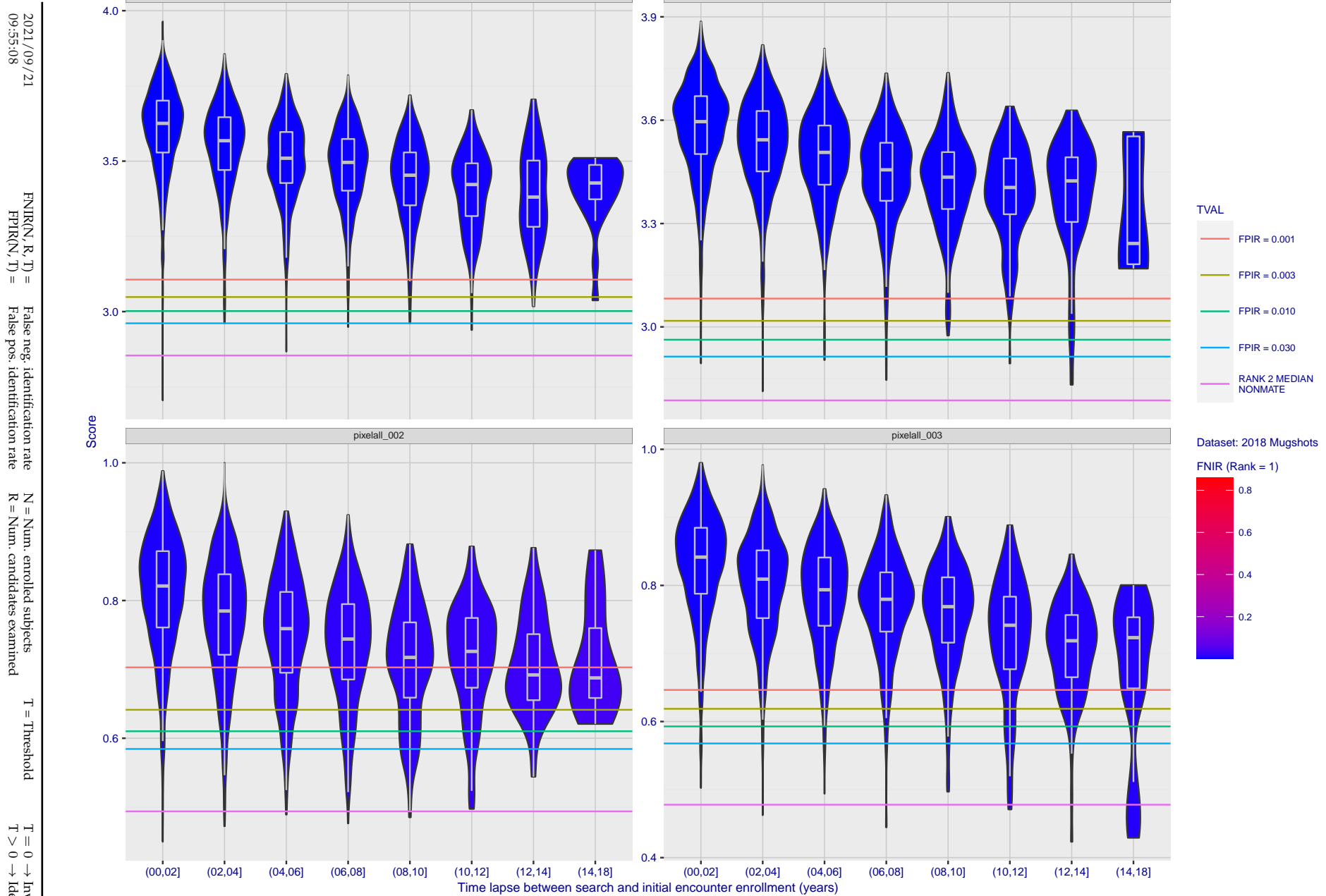


Figure 139: [FRVT-2018 Mugshot Ageing Dataset] Native mate scores vs. time-elapsed. The oldest image of each individual is enrolled. Thereafter, all more recent images are searched. Mated score distributions are computed over all searches noted in row 17 of Table 1 binned by number of years between search and initial enrollment.

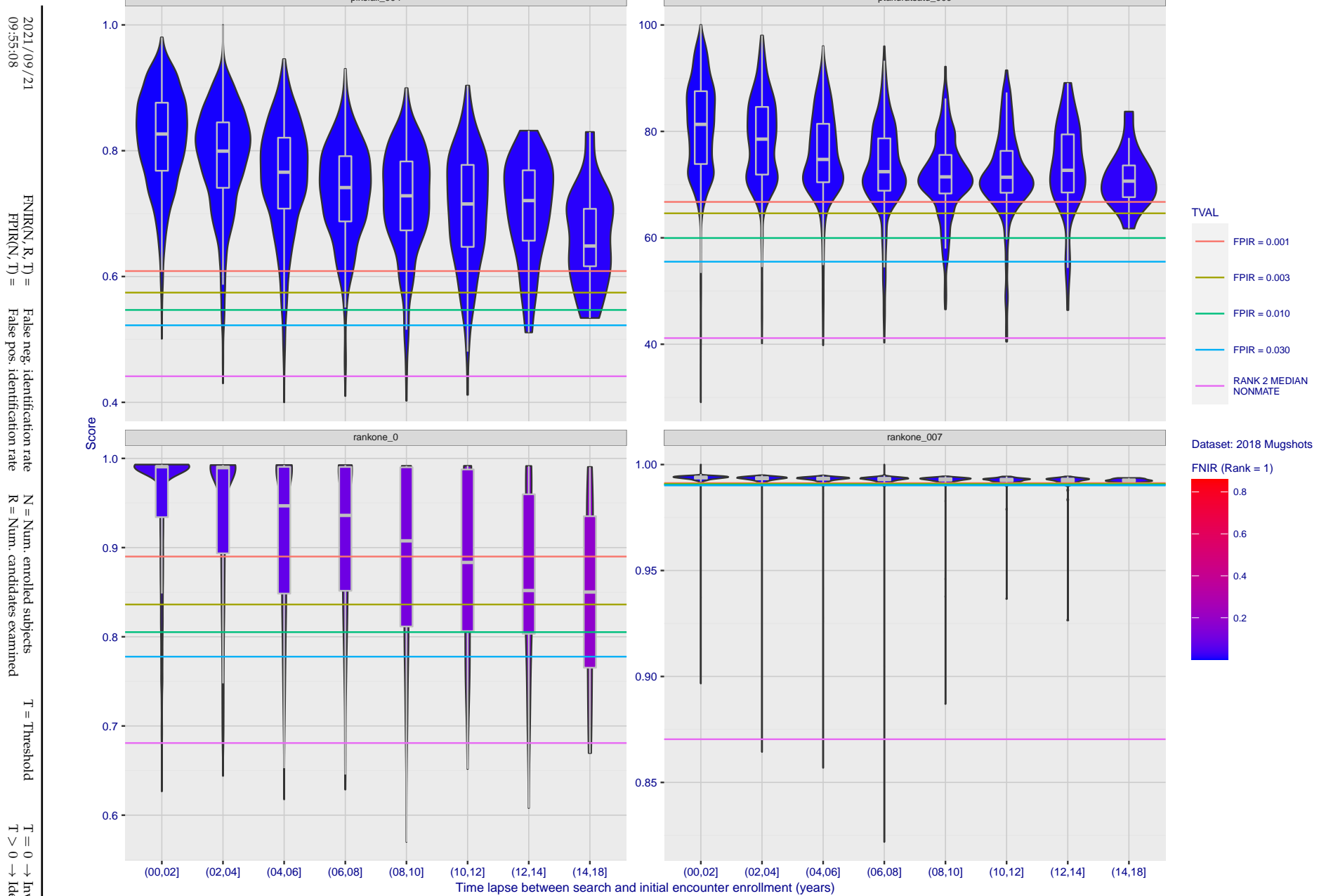


Figure 140: [FRVT-2018 Mugshot Ageing Dataset] Native mate scores vs. time-elapsed. The oldest image of each individual is enrolled. Thereafter, all more recent images are searched. Mated score distributions are computed over all searches noted in row 17 of Table 1 binned by number of years between search and initial enrollment.

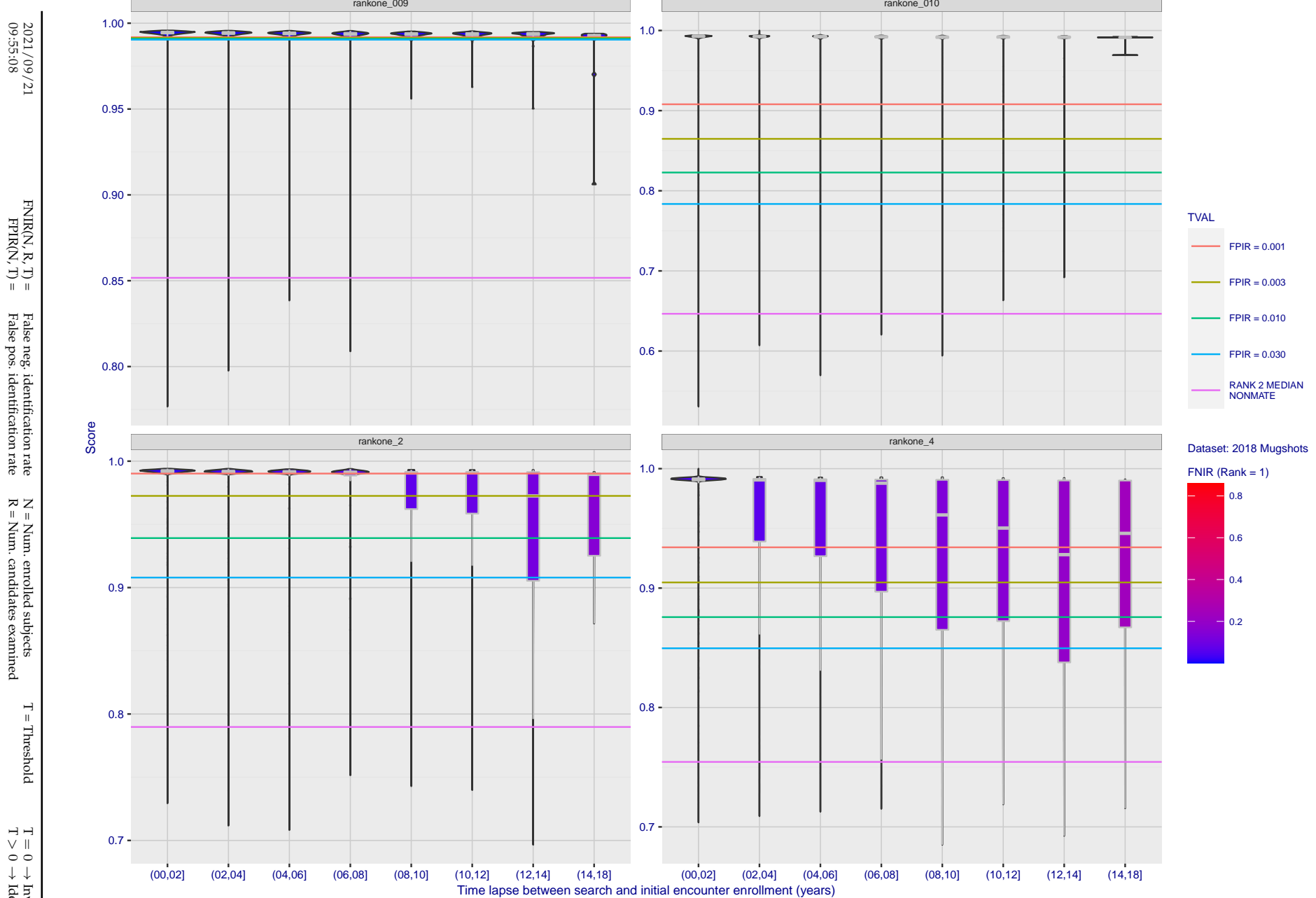


Figure 141: [FRVT-2018 Mugshot Ageing Dataset] Native mate scores vs. time-elapsed. The oldest image of each individual is enrolled. Thereafter, all more recent images are searched. Mated score distributions are computed over all searches noted in row 17 of Table 1 binned by number of years between search and initial enrollment.

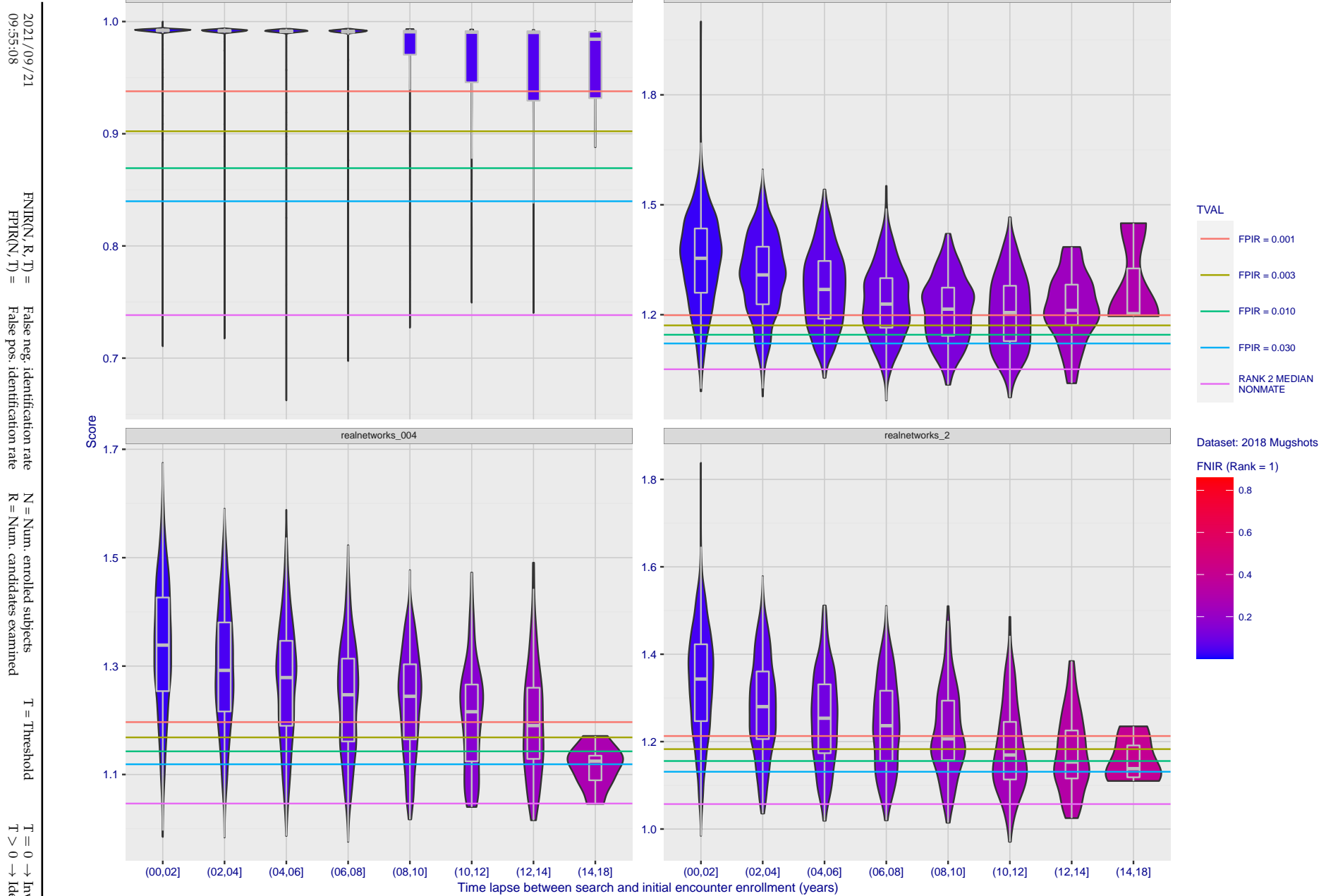


Figure 142: [FRVT-2018 Mugshot Ageing Dataset] Native mate scores vs. time-elapsed. The oldest image of each individual is enrolled. Thereafter, all more recent images are searched. Mated score distributions are computed over all searches noted in row 17 of Table 1 binned by number of years between search and initial enrollment.

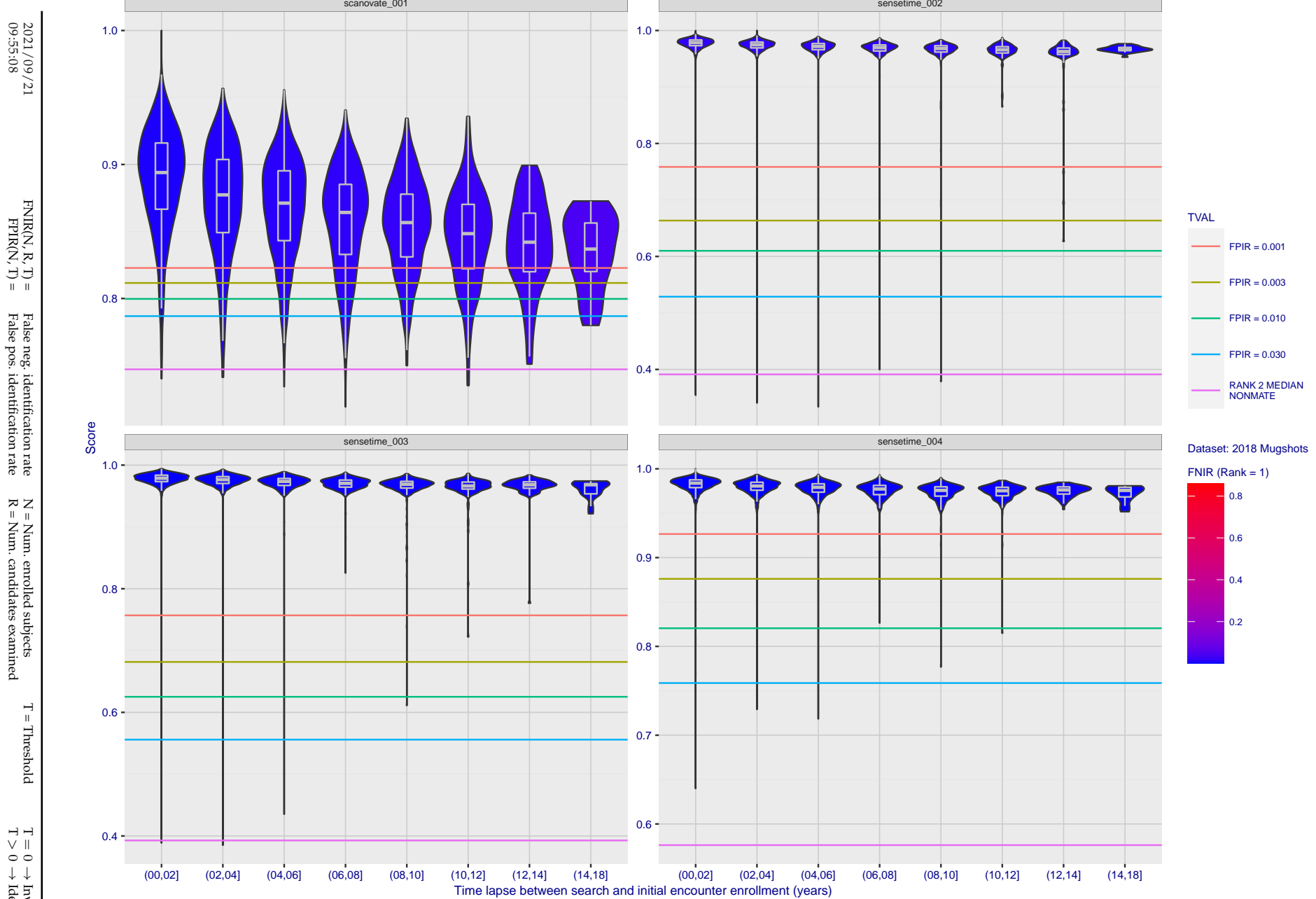


Figure 143: [FRVT-2018 Mugshot Ageing Dataset] Native mate scores vs. time-elapsed. The oldest image of each individual is enrolled. Thereafter, all more recent images are searched. Mated score distributions are computed over all searches noted in row 17 of Table 1 binned by number of years between search and initial enrollment.

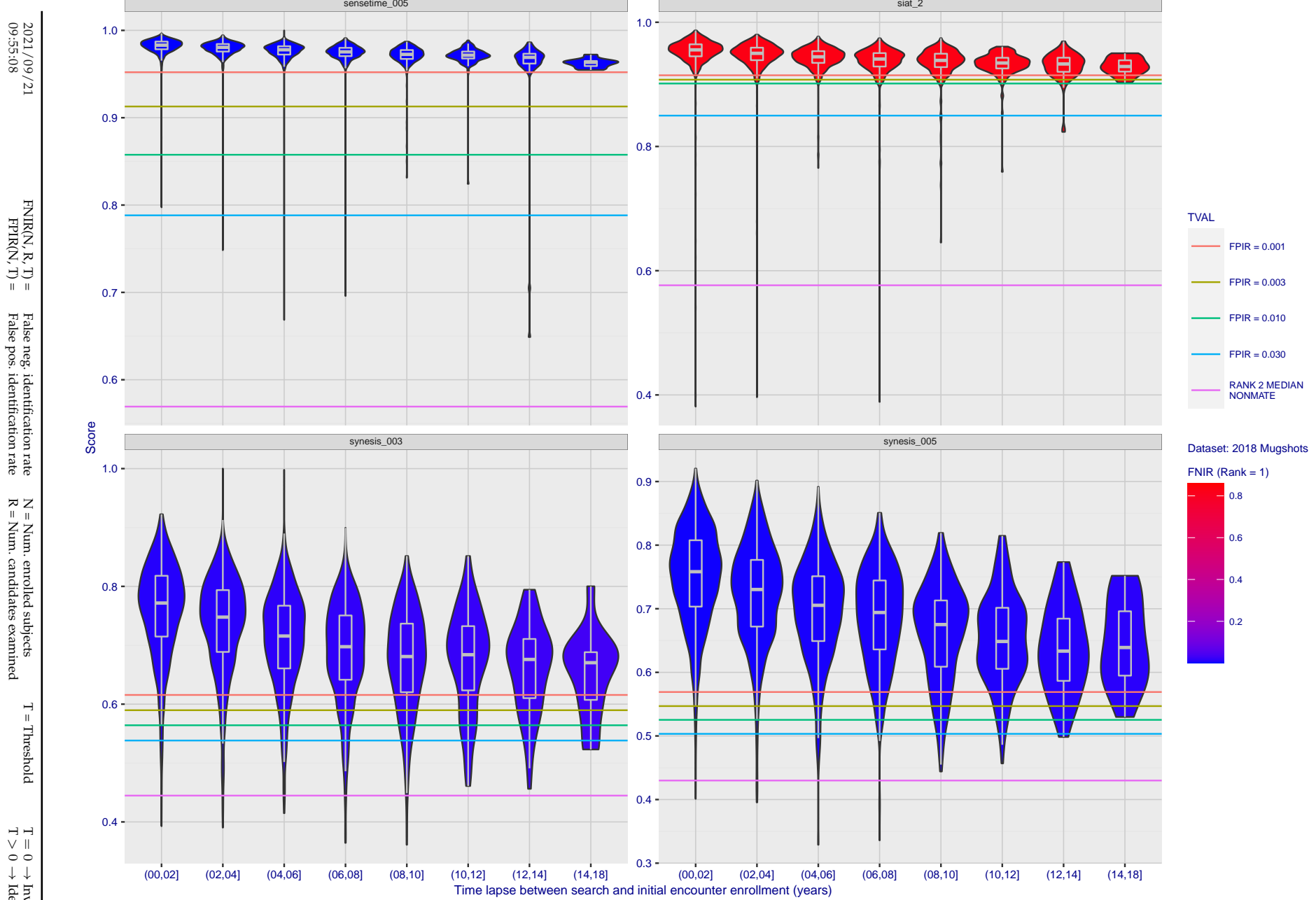
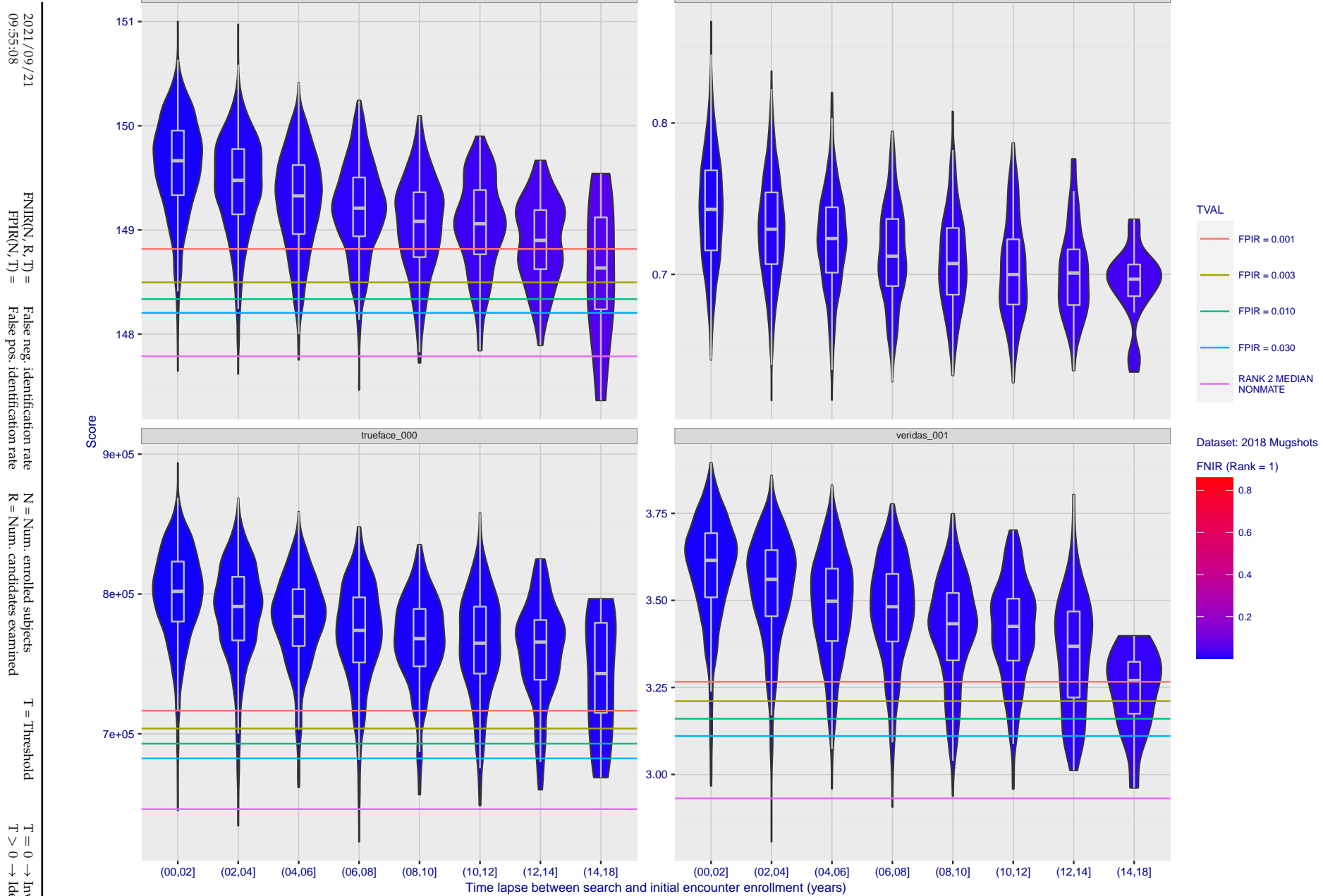
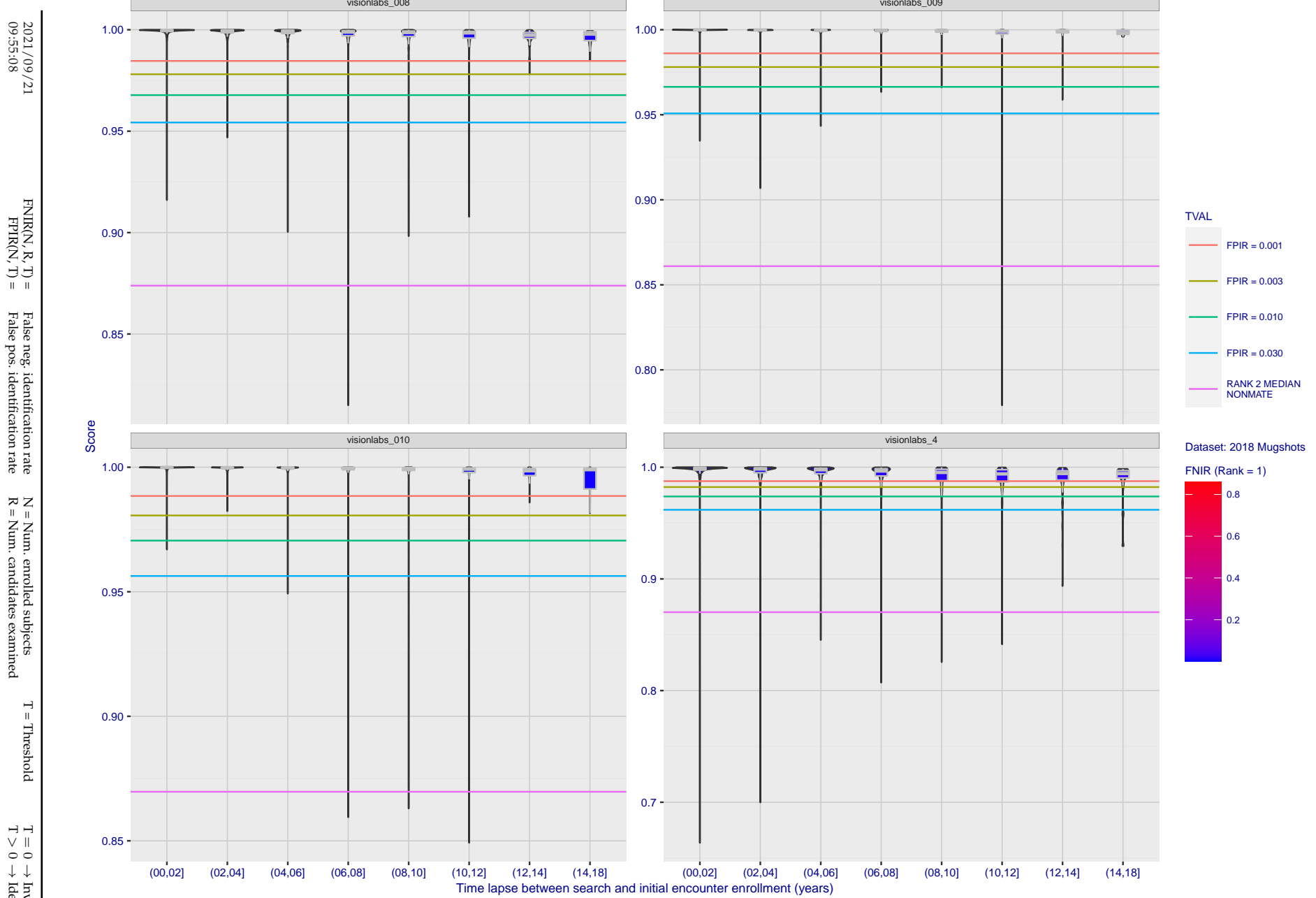


Figure 144: [FRVT-2018 Mugshot Ageing Dataset] Native mate scores vs. time-elapsed. The oldest image of each individual is enrolled. Thereafter, all more recent images are searched. Mated score distributions are computed over all searches noted in row 17 of Table 1 binned by number of years between search and initial enrollment.



**Figure 145: [FRVT-2018 Mugshot Ageing Dataset] Native mate scores vs. time-elapsed.** The oldest image of each individual is enrolled. Thereafter, all more recent images are searched. Mated score distributions are computed over all searches noted in row 17 of Table 1 binned by number of years between search and initial enrollment.



**Figure 146: [FRVT-2018 Mugshot Ageing Dataset] Native mate scores vs. time-elapsed.** The oldest image of each individual is enrolled. Thereafter, all more recent images are searched. Mated score distributions are computed over all searches noted in row 17 of Table 1 binned by number of years between search and initial enrollment.

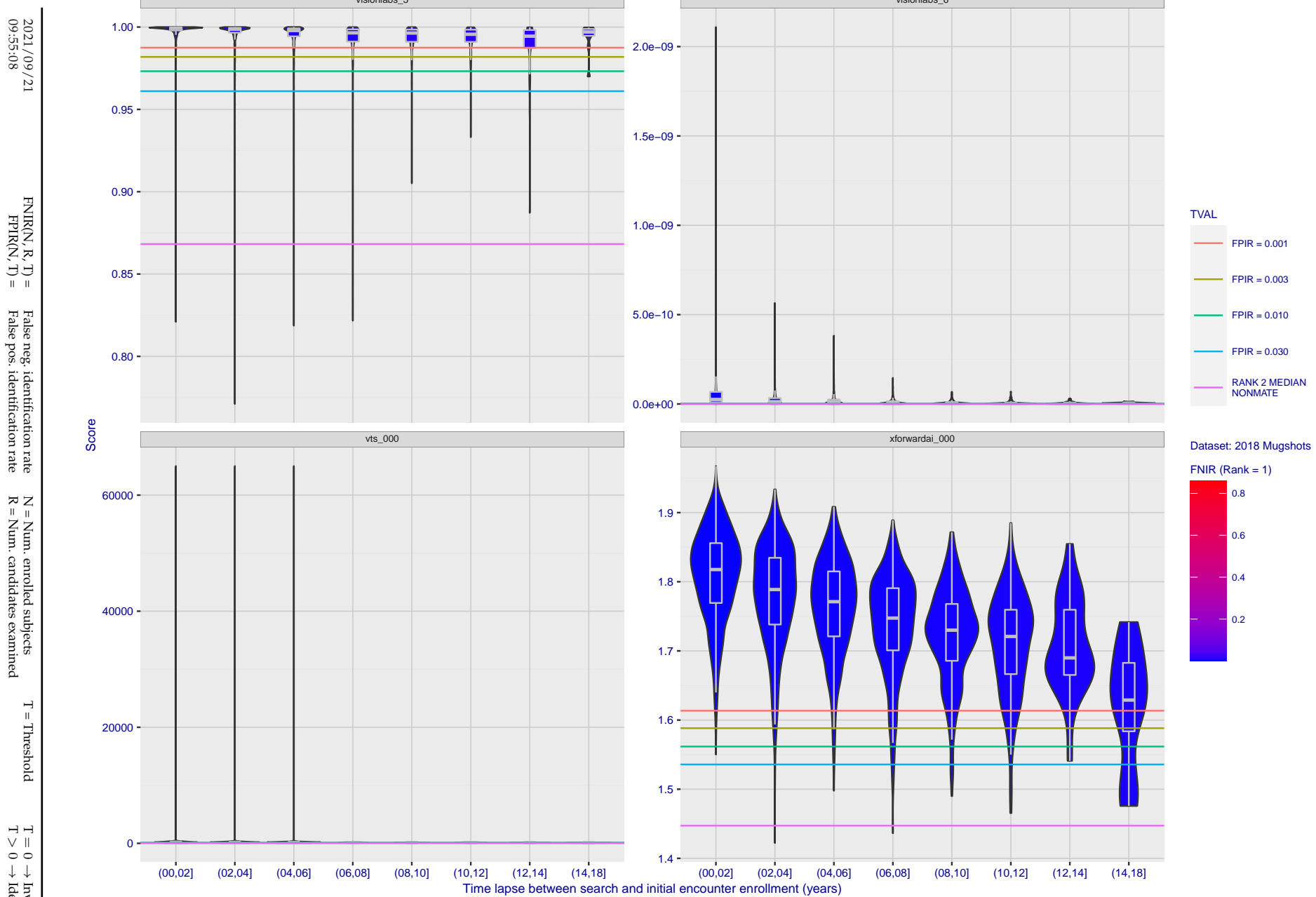


Figure 147: [FRVT-2018 Mugshot Ageing Dataset] Native mate scores vs. time-elapsed. The oldest image of each individual is enrolled. Thereafter, all more recent images are searched. Mated score distributions are computed over all searches noted in row 17 of Table 1 binned by number of years between search and initial enrollment.

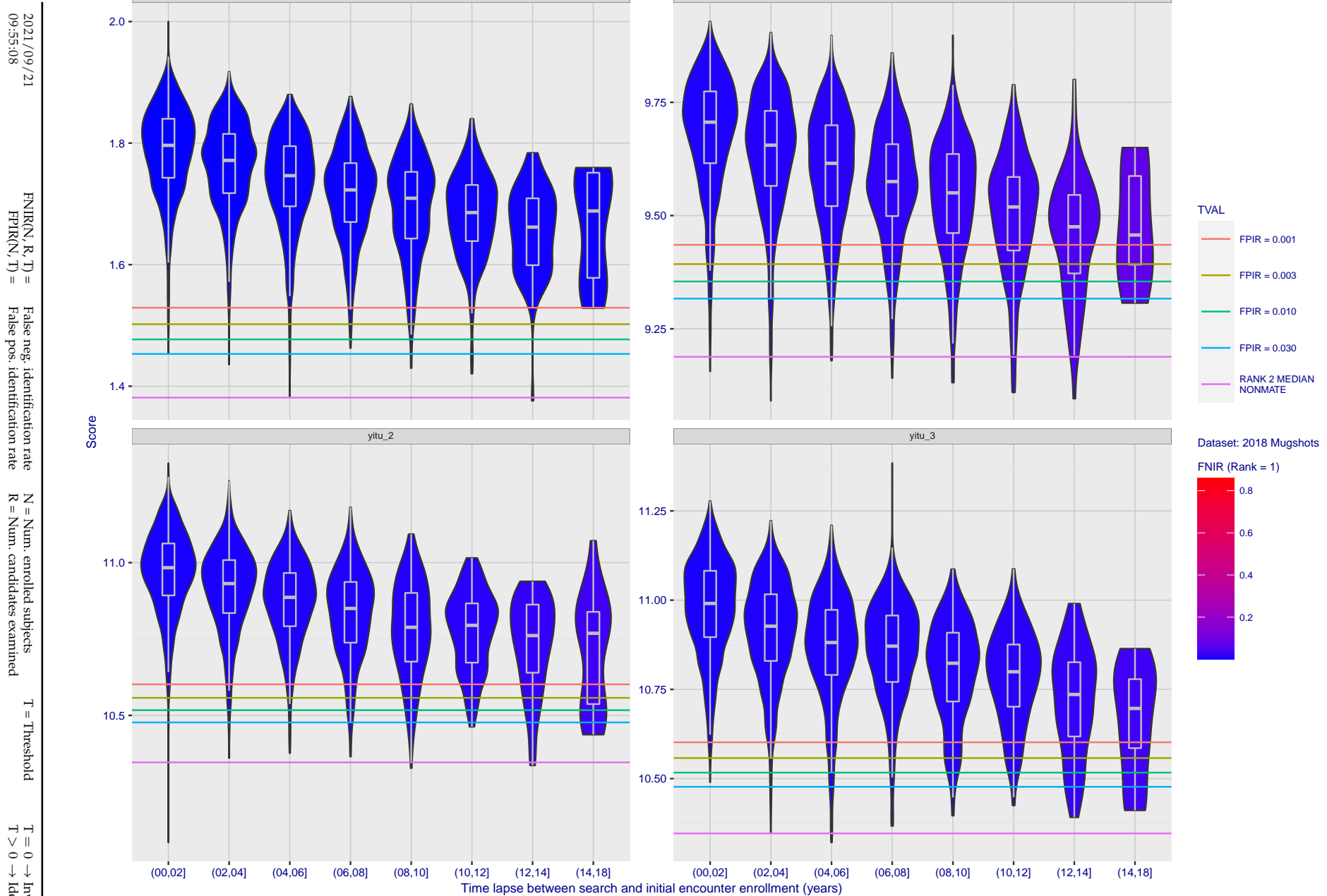
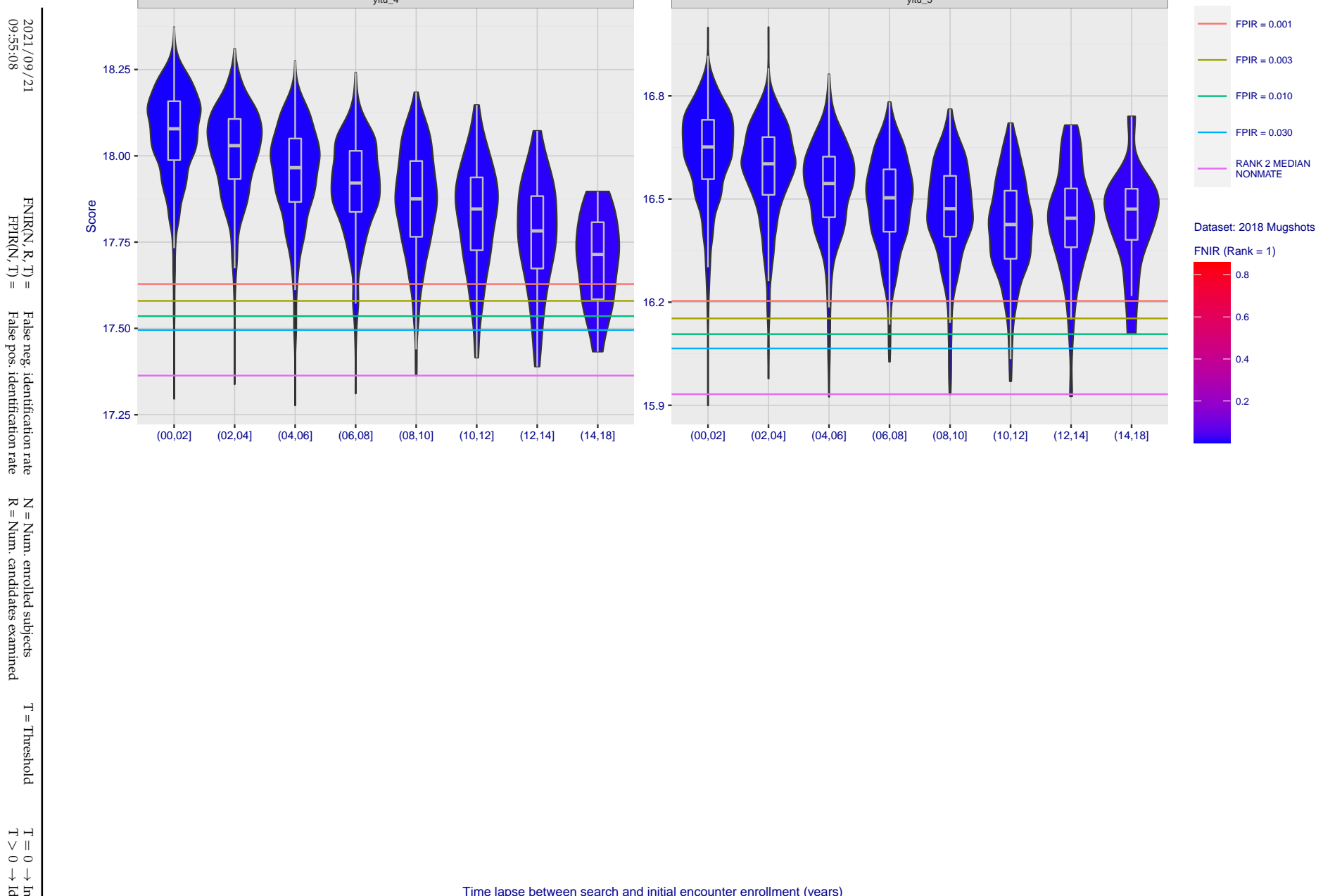


Figure 148: [FRVT-2018 Mugshot Ageing Dataset] Native mate scores vs. time-elapsed. The oldest image of each individual is enrolled. Thereafter, all more recent images are searched. Mated score distributions are computed over all searches noted in row 17 of Table 1 binned by number of years between search and initial enrollment.



**Figure 149: [FRVT-2018 Mugshot Ageing Dataset] Native mate scores vs. time-elapsed.** The oldest image of each individual is enrolled. Thereafter, all more recent images are searched. Mated score distributions are computed over all searches noted in row 17 of Table 1 binned by number of years between search and initial enrollment.

## Appendix C Effect of enrolling multiple images

2021/09/21  
09:55:08  
  
 $FNIR(N, R, T) =$   
False neg. identification rate  
 $FPFR(N, T) =$   
False pos. identification rate  
  
 $N =$  Num. enrolled subjects  
 $R =$  Num. candidates examined  
  
 $T =$  Threshold  
 $T = 0 \rightarrow$  Investigation  
 $T > 0 \rightarrow$  Identification

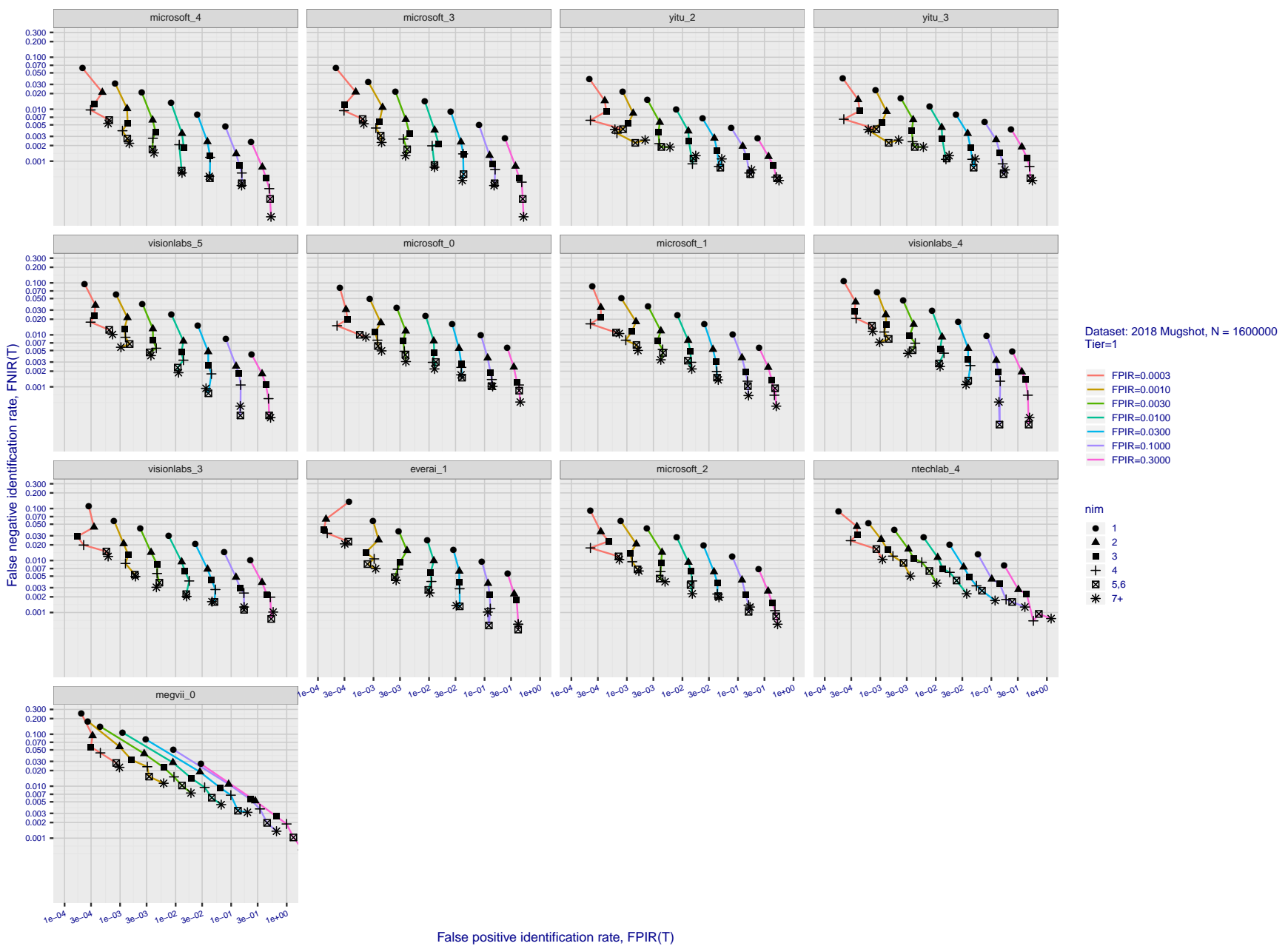


Figure 150: [FRVT-2018 Mugshot Dataset] Effect of enrolling multiple images for each identity. The plot shows an identification miss rates vs. false positive rates, at seven operating thresholds. The enrolled population size is fixed. The images are enrolled with lifetime-consolidation - see section 2.3.

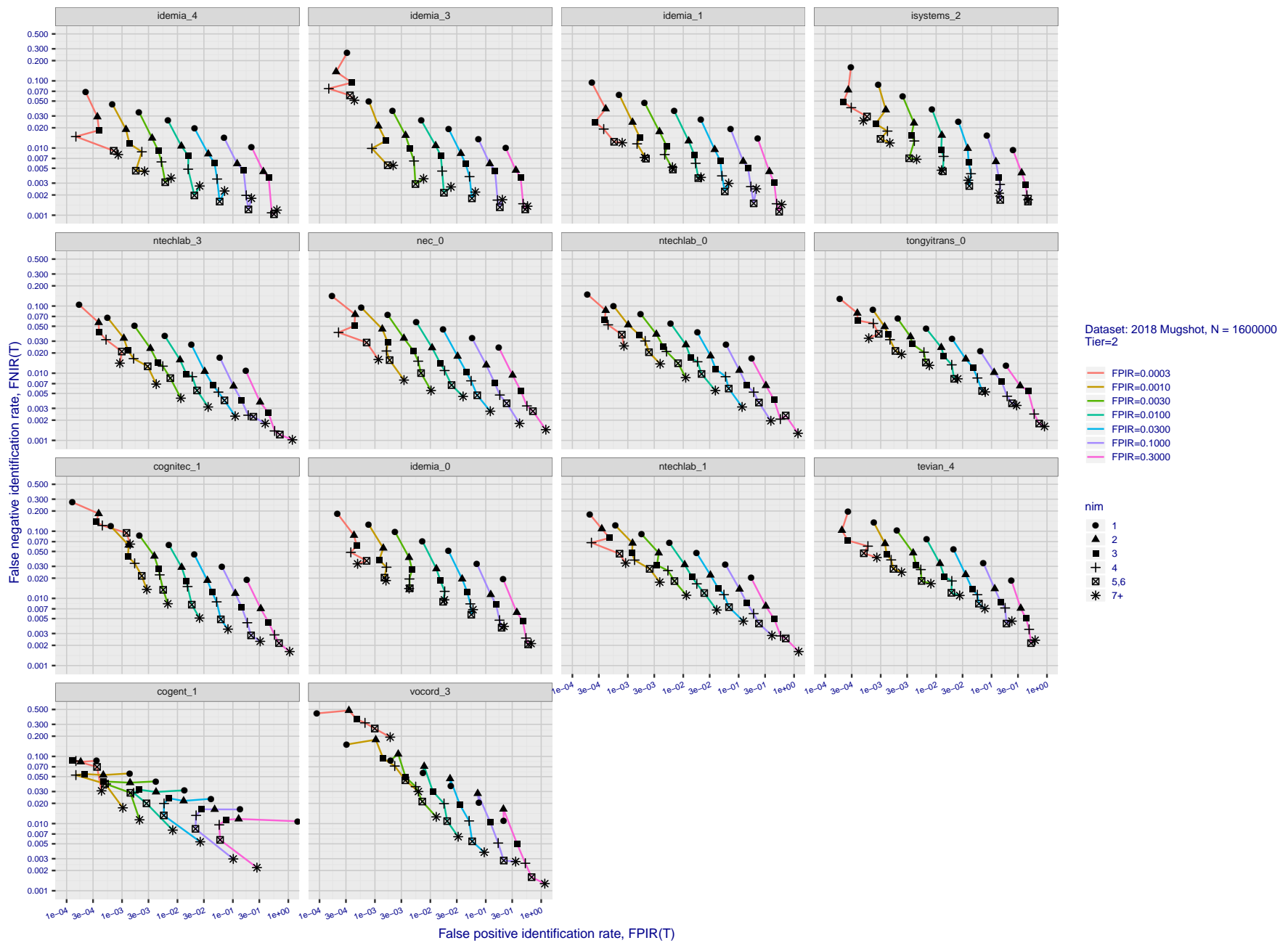


Figure 151: [FRVT-2018 Mugshot Dataset] Effect of enrolling multiple images for each identity. The plot shows an identification miss rates vs. false positive rates, at seven operating thresholds. The enrolled population size is fixed. The images are enrolled with lifetime-consolidation - see section 2.3.

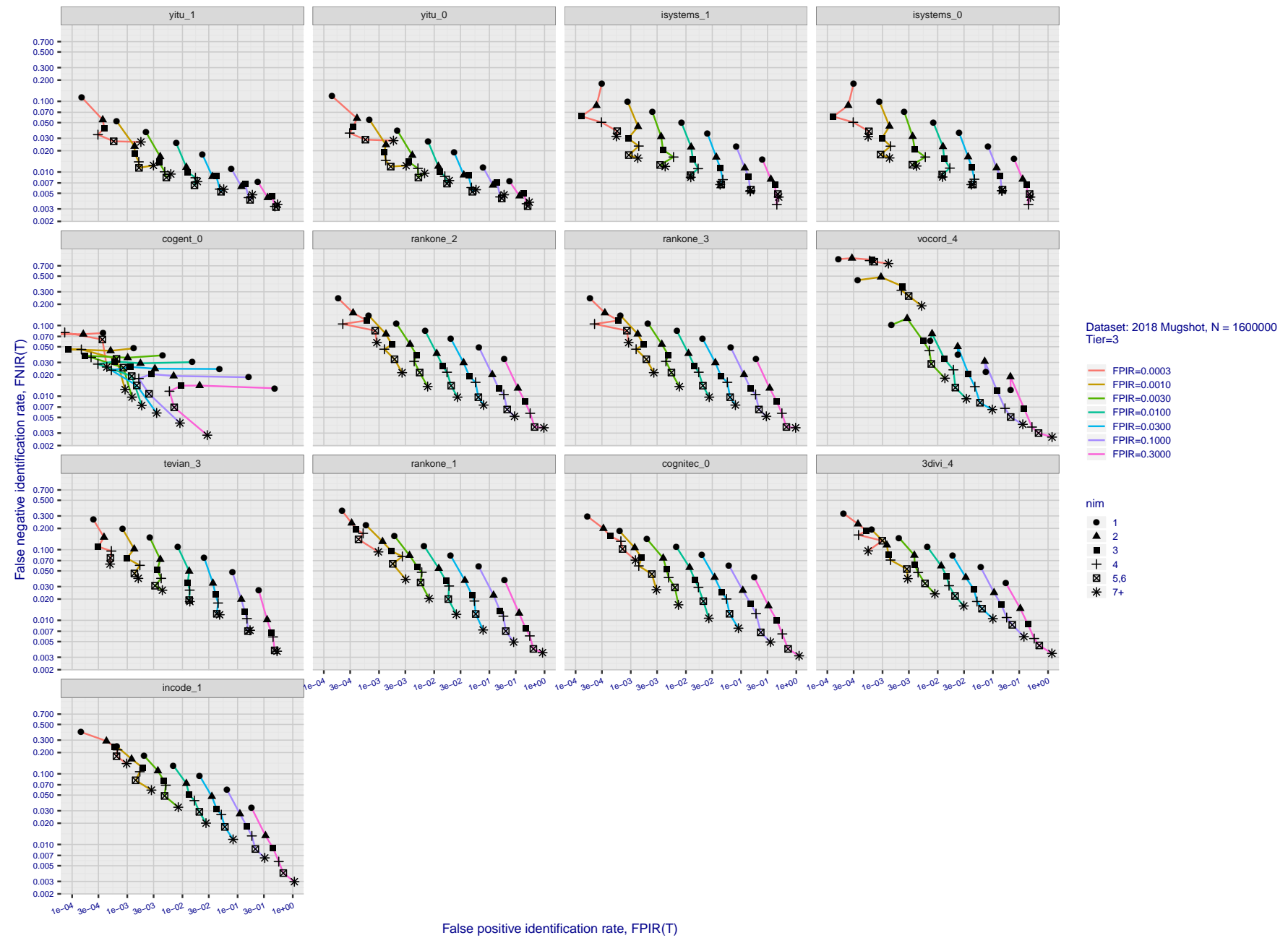


Figure 152: [FRVT-2018 Mugshot Dataset] Effect of enrolling multiple images for each identity. The plot shows an identification miss rates vs. false positive rates, at seven operating thresholds. The enrolled population size is fixed. The images are enrolled with lifetime-consolidation - see section 2.3.

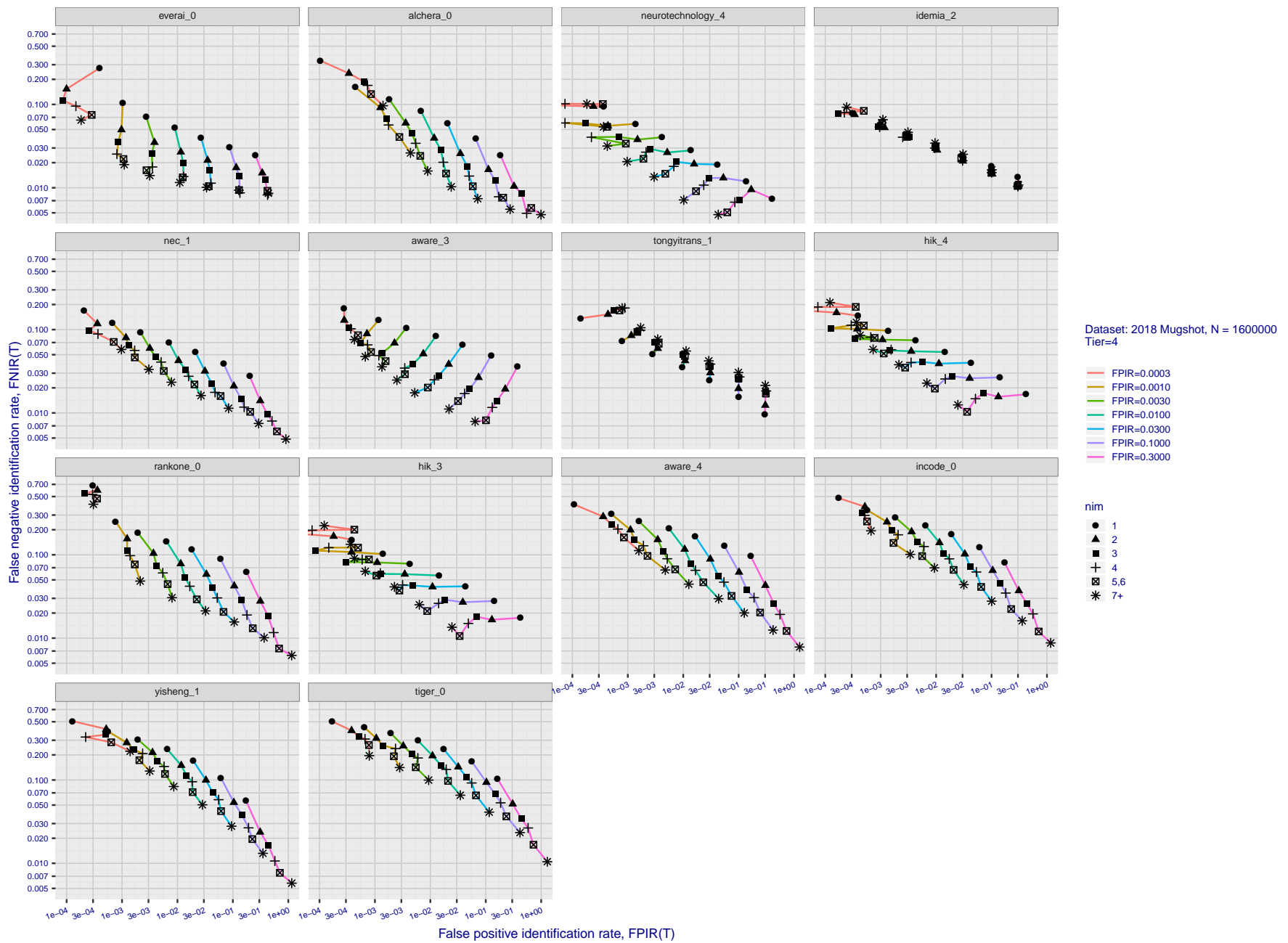


Figure 153: [FRVT-2018 Mugshot Dataset] Effect of enrolling multiple images for each identity. The plot shows an identification miss rates vs. false positive rates, at seven operating thresholds. The enrolled population size is fixed. The images are enrolled with lifetime-consolidation - see section 2.3.

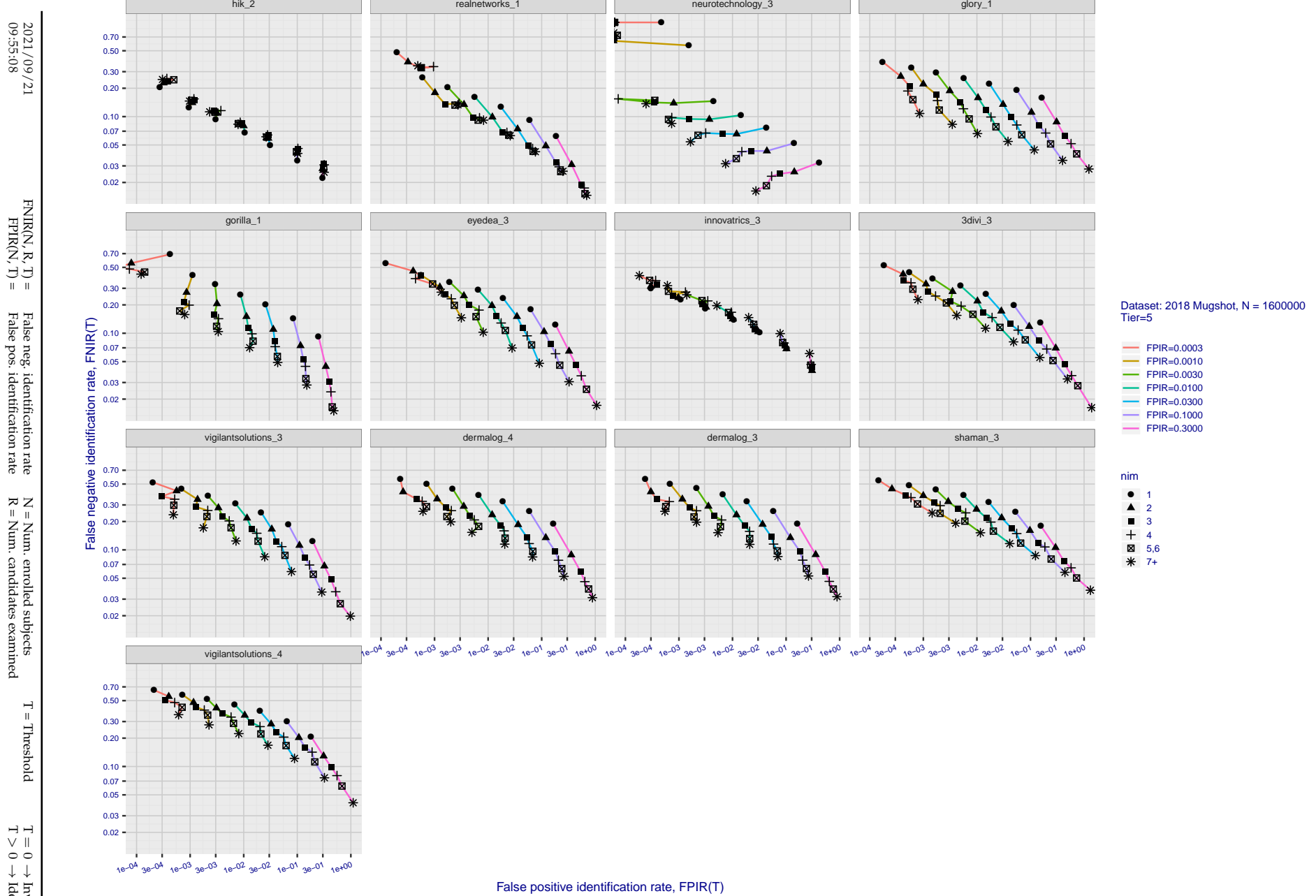


Figure 154: [FRVT-2018 Mugshot Dataset] Effect of enrolling multiple images for each identity. The plot shows an identification miss rates vs. false positive rates, at seven operating thresholds. The enrolled population size is fixed. The images are enrolled with lifetime-consolidation - see section 2.3.

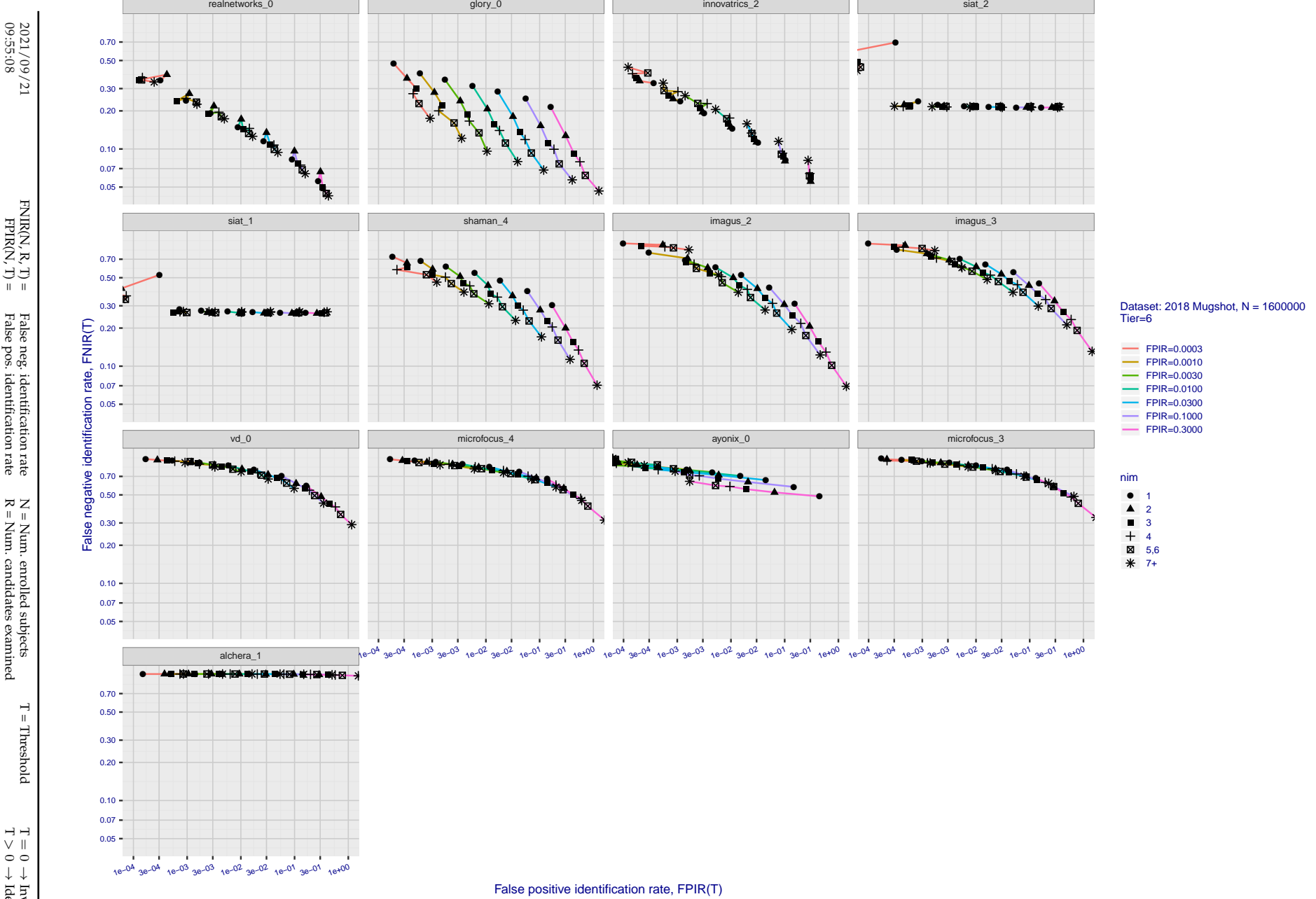


Figure 155: [FRVT-2018 Mugshot Dataset] Effect of enrolling multiple images for each identity. The plot shows an identification miss rates vs. false positive rates, at seven operating thresholds. The enrolled population size is fixed. The images are enrolled with lifetime-consolidation - see section 2.3.

## Appendix D Accuracy with poor quality webcam images

2021/09/21 09:55:08	$FNIR(N, R, T) =$ $FPIR(N, T) =$	False neg. identification rate False pos. identification rate	$N =$ Num. enrolled subjects $R =$ Num. candidates examined	$T =$ Threshold $T > 0 \rightarrow$ Identification	$T = 0 \rightarrow$ Investigation
------------------------	-------------------------------------	--	--	---	-----------------------------------

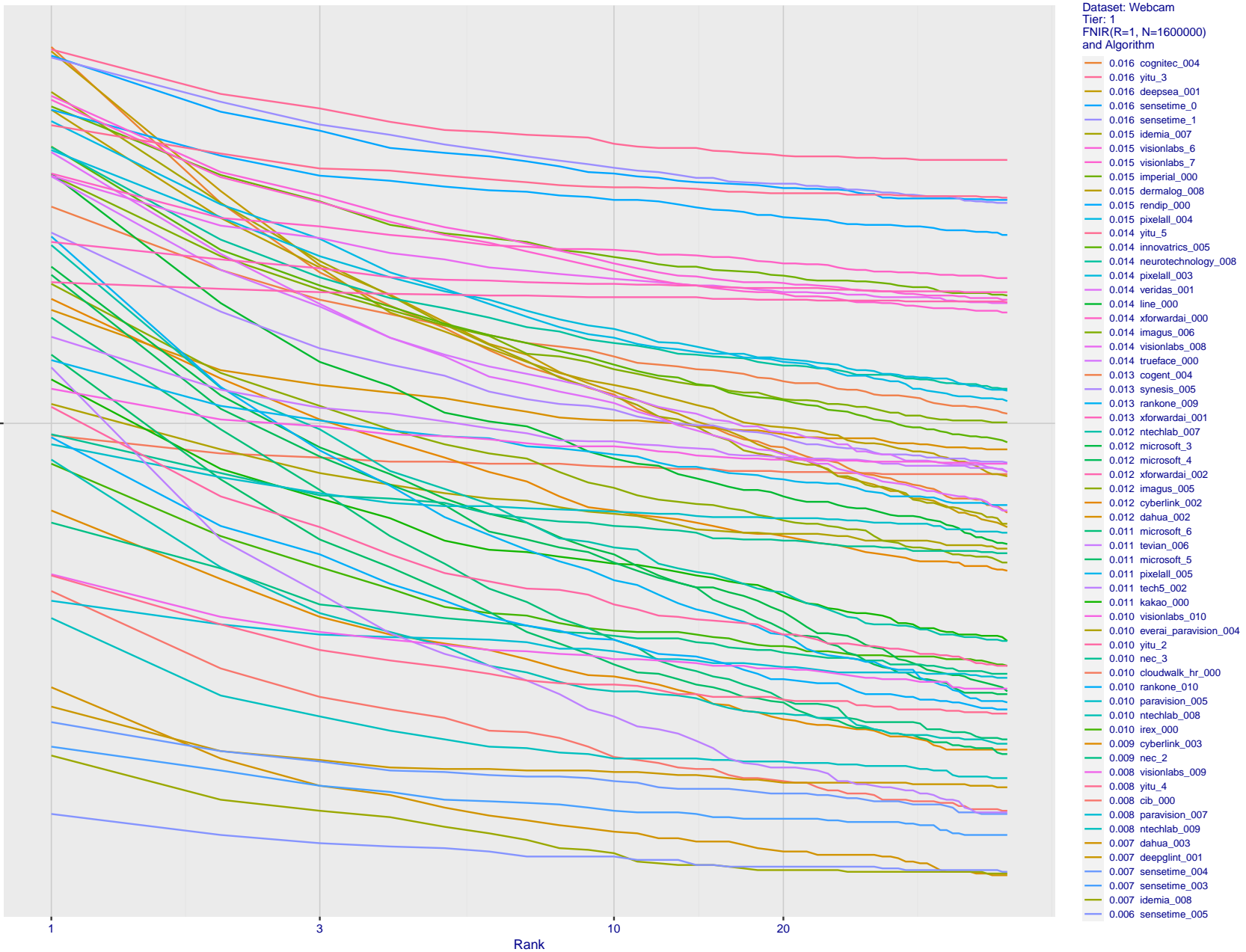


Figure 156: [Webcam Dataset] Identification miss rates vs. rank. The results apply to cross-domain recognition in which webcams are searched against enrolled mugshots. The FNIR values are higher than those for mugshot-mugshot identification due to low image resolution, lighting and less constrained subject pose in webcam images - see Figure 6.

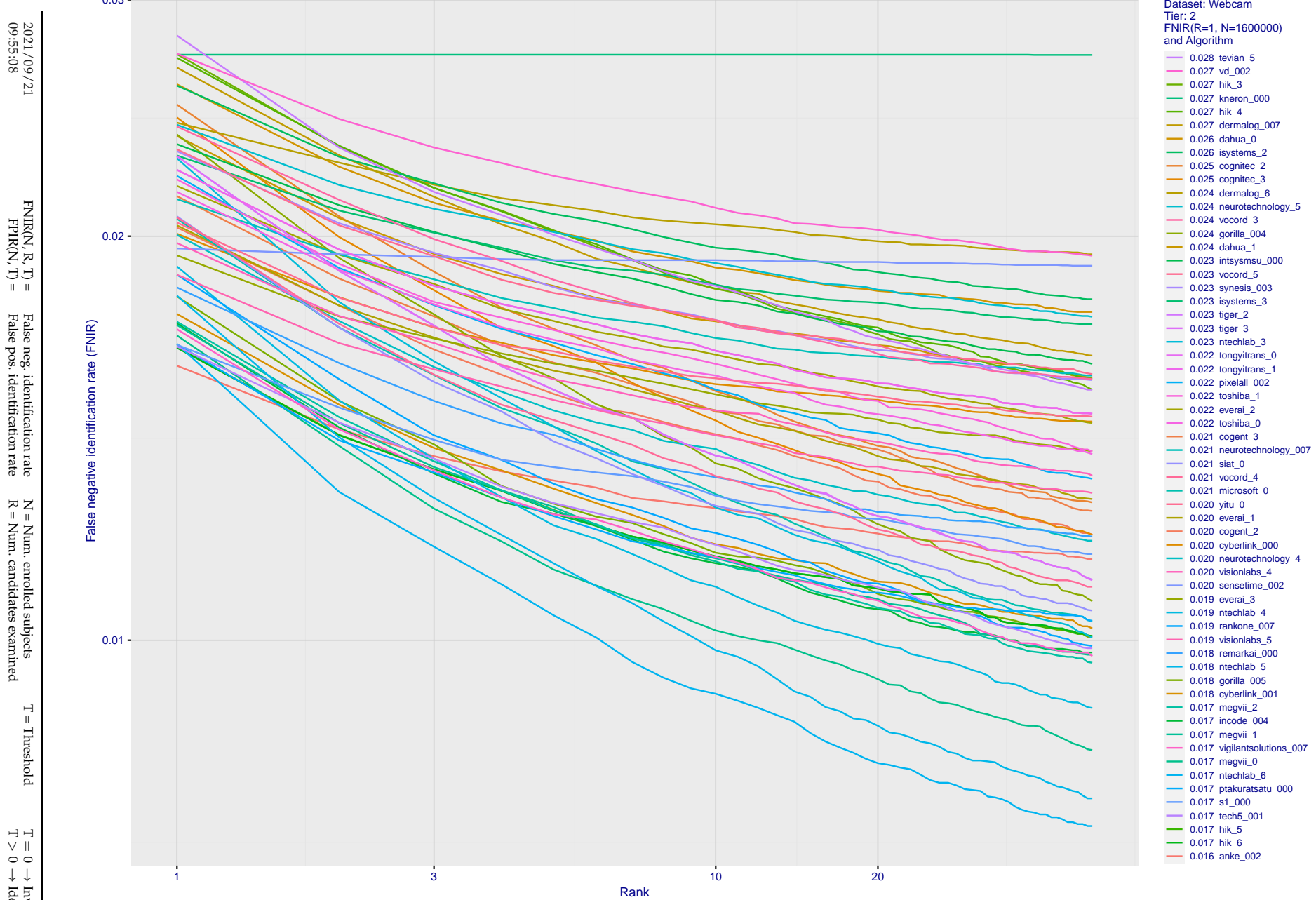


Figure 157: [Webcam Dataset] Identification miss rates vs. rank. The results apply to cross-domain recognition in which webcams are searched against enrolled mugshots. The FNIR values are higher than those for mugshot-mugshot identification due to low image resolution, lighting and less constrained subject pose in webcam images - see Figure 6.

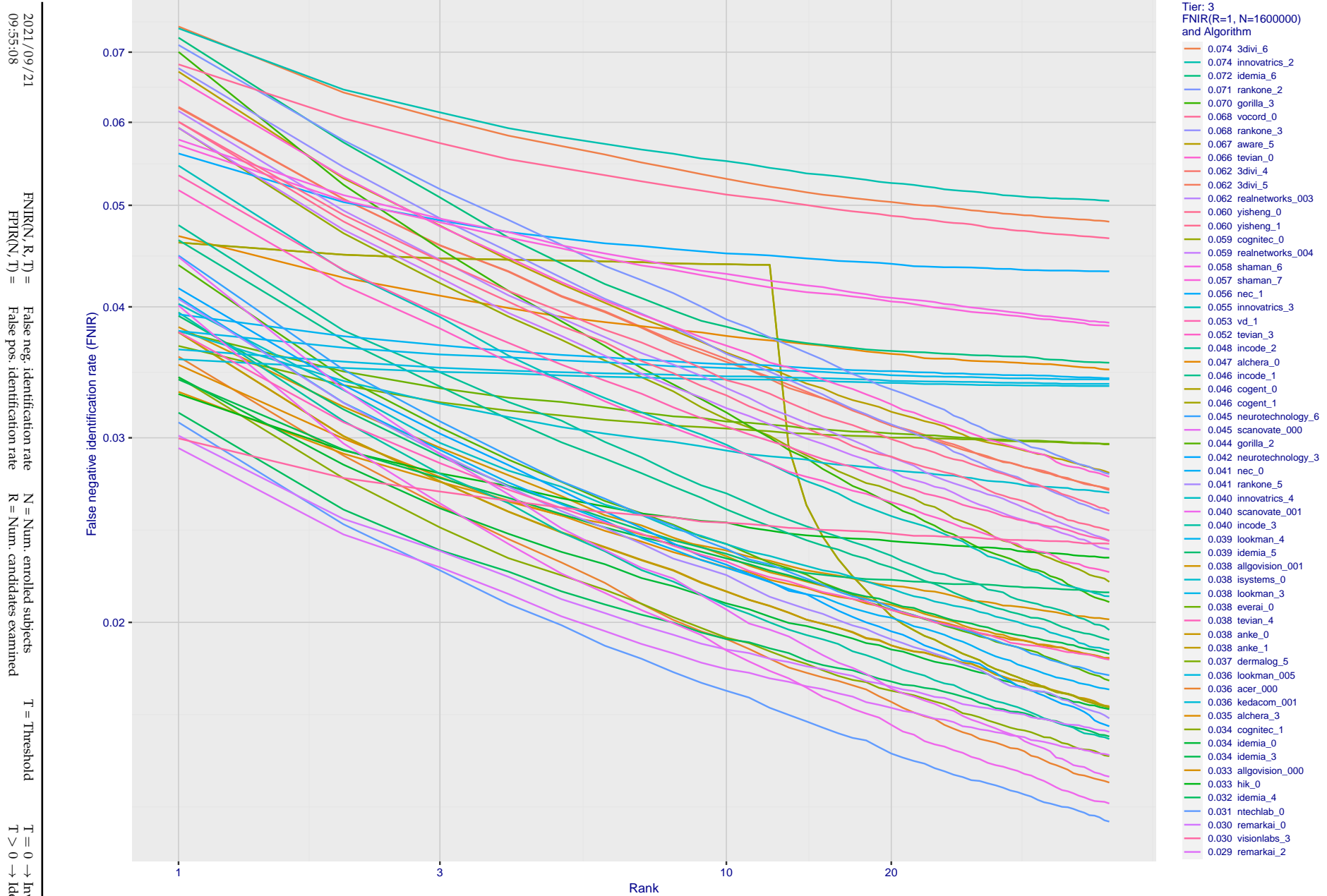


Figure 158: [Webcam Dataset] Identification miss rates vs. rank. The results apply to cross-domain recognition in which webcams are searched against enrolled mugshots. The FNIR values are higher than those for mugshot-mugshot identification due to low image resolution, lighting and less constrained subject pose in webcam images - see Figure 6.

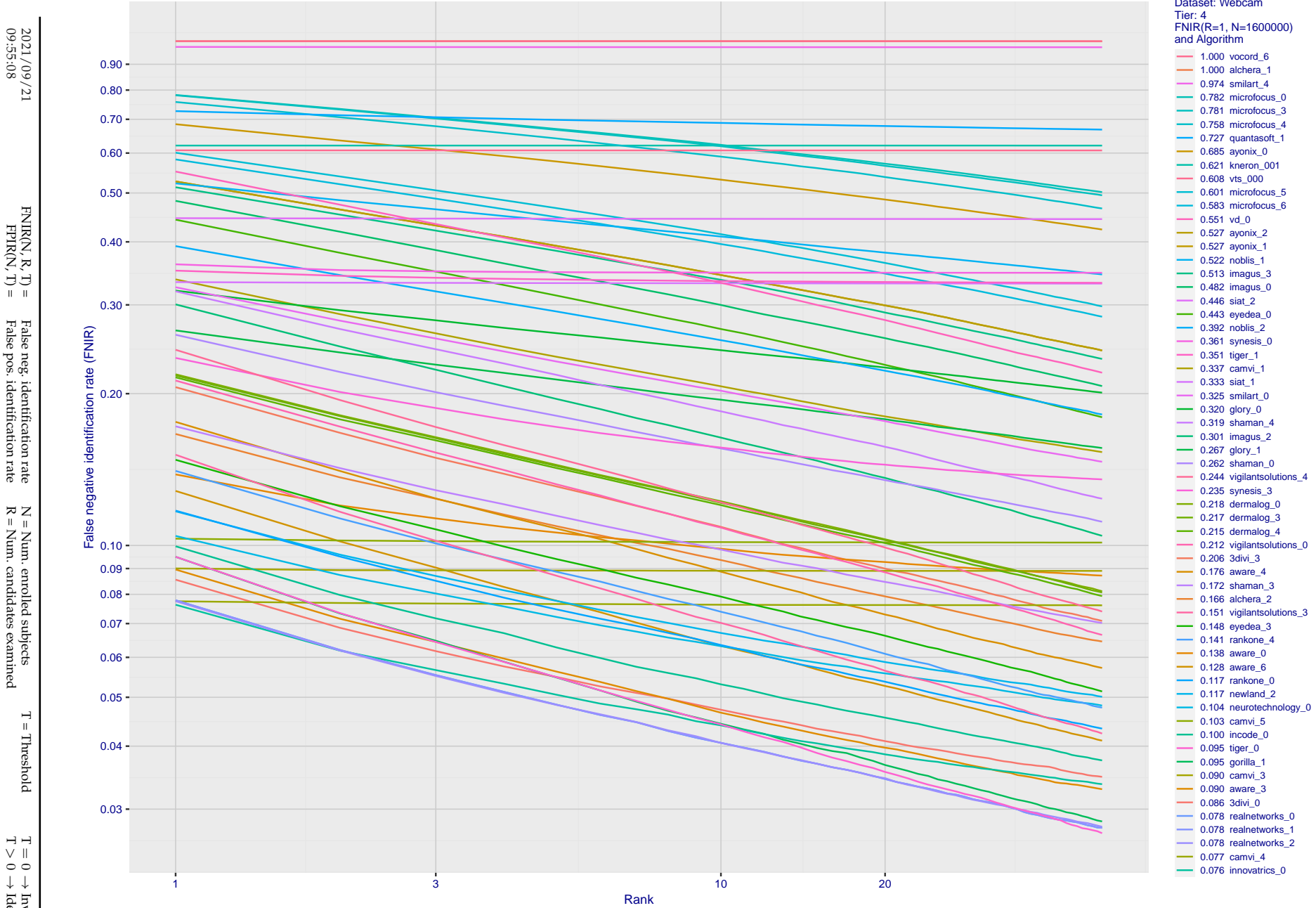


Figure 159: [Webcam Dataset] Identification miss rates vs. rank. The results apply to cross-domain recognition in which webcams are searched against enrolled mugshots. The FNIR values are higher than those for mugshot-mugshot identification due to low image resolution, lighting and less constrained subject pose in webcam images - see Figure 6.

---

2021/09/21  
09:55:08

FNIR(N, R, T) = False neg. identification rate  
FPTR(N, T) = False pos. identification rate

N = Num. enrolled subjects  
R = Num. candidates examined  
T = Threshold  
T = 0 → Investigation  
T > 0 → Identification

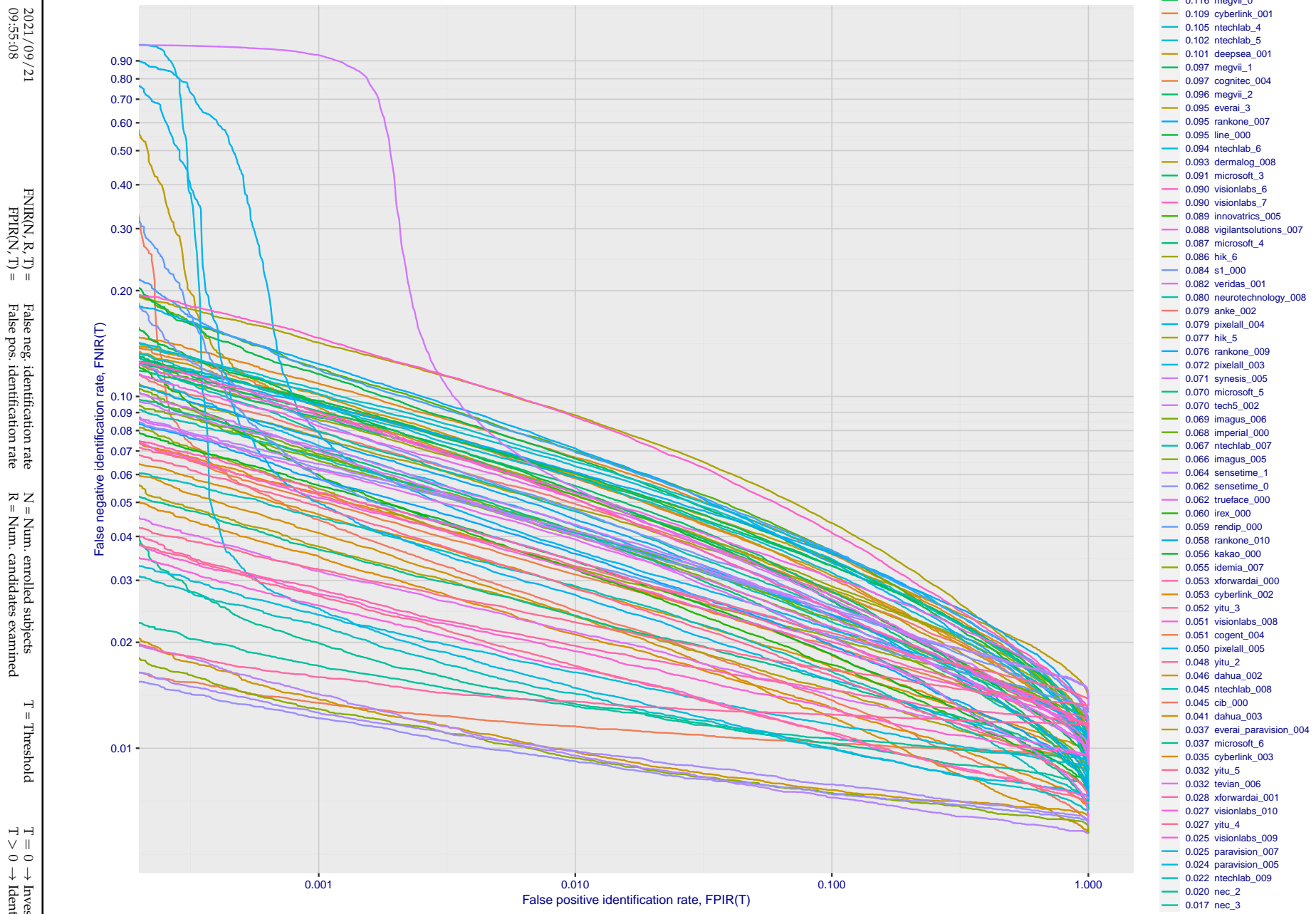


Figure 160: [Webcam Dataset] Identification miss rates vs. false positive rates. The results apply to cross-domain recognition in which webcams are searched against enrolled mugshots. The FNIR values are higher than those for mugshot-mugshot identification due to low image resolution, lighting and less constrained subject pose in webcam images - see Figure 6.

2021/09/21  
09:55:08  
 $\text{FNIR}(N, R, T) =$   
 $\text{False neg. identification rate}$   
 $\text{FPIR}(N, T) =$   
 $\text{False pos. identification rate}$   
 $N = \text{Num. enrolled subjects}$   
 $R = \text{Num. candidates examined}$   
 $T = \text{Threshold}$   
 $T = 0 \rightarrow \text{Investigation}$   
 $T > 0 \rightarrow \text{Identification}$

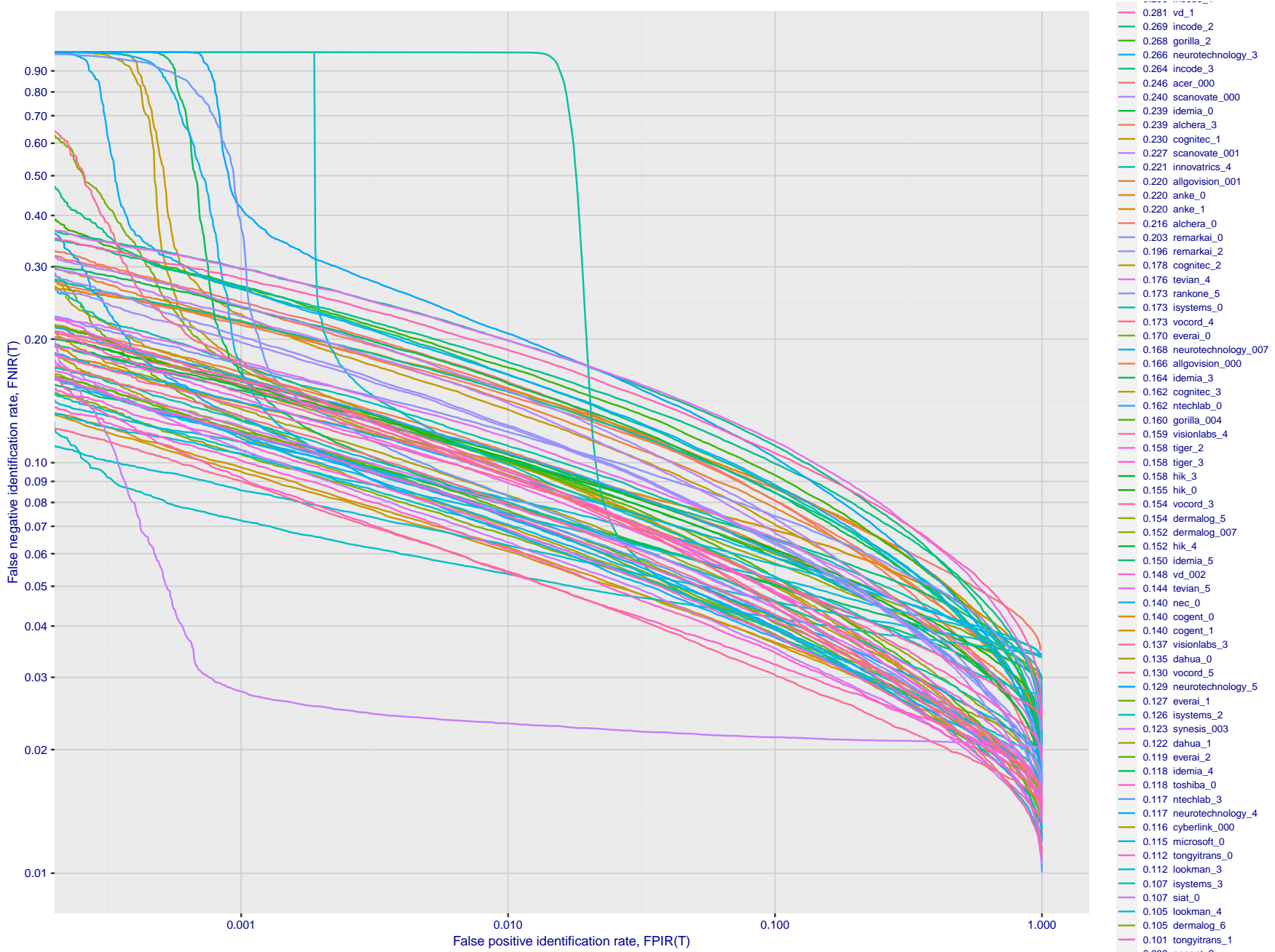


Figure 161: [Webcam Dataset] Identification miss rates vs. false positive rates. The results apply to cross-domain recognition in which webcams are searched against enrolled mugshots. The FNIR values are higher than those for mugshot-mugshot identification due to low image resolution, lighting and less constrained subject pose in webcam images - see Figure 6.

- 0.281 vd\_1
- 0.269 incode\_2
- 0.268 gorilla\_2
- 0.266 neurotechnology\_3
- 0.264 incode\_3
- 0.246 acer\_000
- 0.240 scanovate\_000
- 0.239 idemia\_0
- 0.239 alchera\_3
- 0.230 cognitec\_1
- 0.227 scanovate\_001
- 0.221 innovatrics\_4
- 0.220 allgovision\_001
- 0.220 anke\_0
- 0.220 anke\_1
- 0.216 alchera\_0
- 0.203 remarkai\_0
- 0.196 remarkai\_2
- 0.178 cognitec\_2
- 0.176 tevian\_4
- 0.173 rankone\_5
- 0.173 isystems\_0
- 0.173 vocord\_4
- 0.170 everai\_0
- 0.168 neurotechnology\_007
- 0.166 allgovision\_000
- 0.164 idemia\_3
- 0.162 cognitec\_3
- 0.162 nteclab\_0
- 0.160 gorilla\_004
- 0.159 visionlabs\_4
- 0.158 tiger\_2
- 0.158 tiger\_3
- 0.158 hik\_3
- 0.155 hik\_0
- 0.154 vocord\_3
- 0.154 dermalog\_5
- 0.152 dermalog\_007
- 0.152 hik\_4
- 0.150 idemia\_5
- 0.148 vd\_002
- 0.144 tevian\_5
- 0.140 nec\_0
- 0.140 cogent\_0
- 0.140 cogent\_1
- 0.137 visionlabs\_3
- 0.135 dahua\_0
- 0.130 vocord\_5
- 0.129 neurotechnology\_5
- 0.127 everai\_1
- 0.126 isystems\_2
- 0.123 synesis\_003
- 0.122 dahua\_1
- 0.119 everai\_2
- 0.118 idemia\_4
- 0.118 toshiba\_0
- 0.117 nteclab\_3
- 0.117 neurotechnology\_4
- 0.116 cyberlink\_000
- 0.115 microsoft\_0
- 0.112 tongyitrans\_0
- 0.112 lookman\_3
- 0.107 isystems\_3
- 0.107 siat\_0
- 0.105 lookman\_4
- 0.105 dermalog\_6
- 0.101 tongyitrans\_1
- 0.099 accent\_3

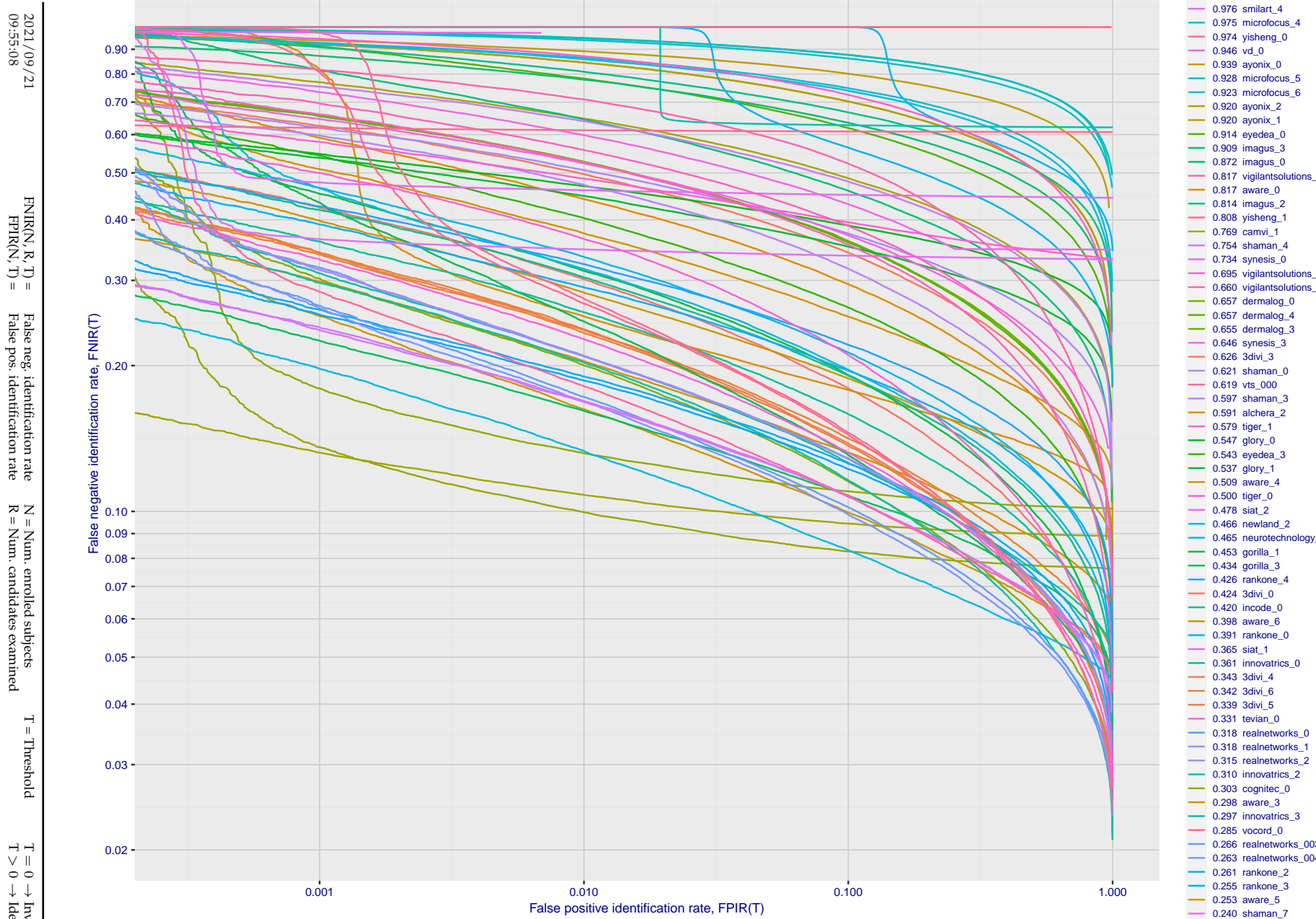
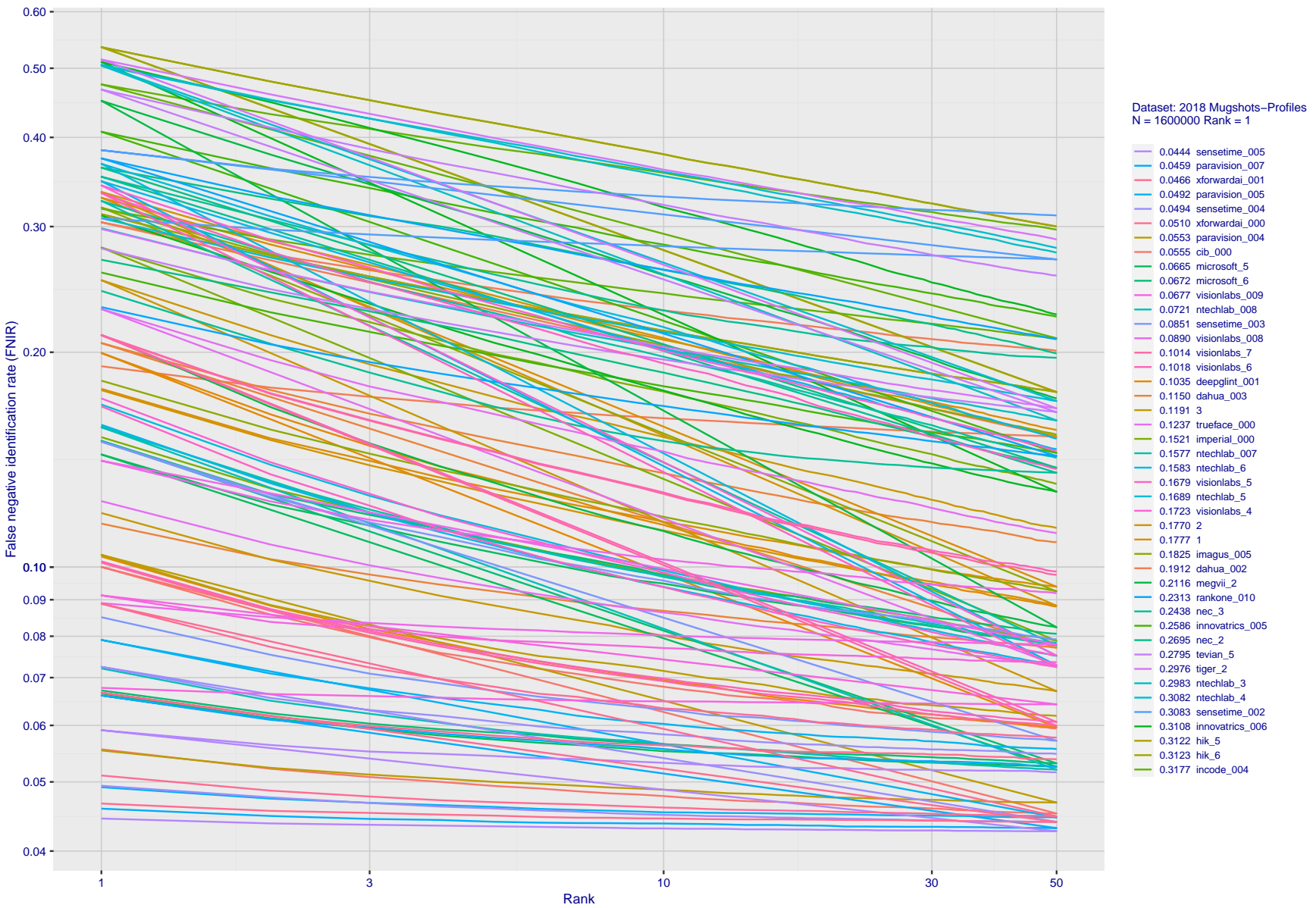


Figure 162: [Webcam Dataset] Identification miss rates vs. false positive rates. The results apply to cross-domain recognition in which webcams are searched against enrolled mugshots. The FNIR values are higher than those for mugshot-mugshot identification due to low image resolution, lighting and less constrained subject pose in webcam images - see Figure 6.

## Appendix E Accuracy for profile-view to frontal recognition

Figures 163 - 165 gives accuracy results for searching 100 000 mated and 100 000 non-mated profile-view images against the same FRVT 2018 frontal enrollment dataset,  $N = 1\,600\,000$ , used in the main mugshot trials. This experiment corresponds to row-13 of Table 1. An example of profile-view image is given in Figure 7.



**Figure 163: [Mugshot and profile-view dataset] Rank-based accuracy.** For some of the more accurate Phase 3 algorithms the figure plots error tradeoff characteristics for frontal and profile-view searches into an enrolled set of  $N = 1600000$  frontal images. Note that some algorithms fail on profile-view images with  $\text{FNIR} \rightarrow 1$  - this evaluation did not ask developers to provide profile-view capability. Some algorithms, on the other hand, give  $\text{FNIR}$  approaching that for frontal-view searches using c. 2010 algorithms. The best result is that 91% of profile-view searches yield the correct mate at rank 1, and better than 94% in the top-50 candidates.

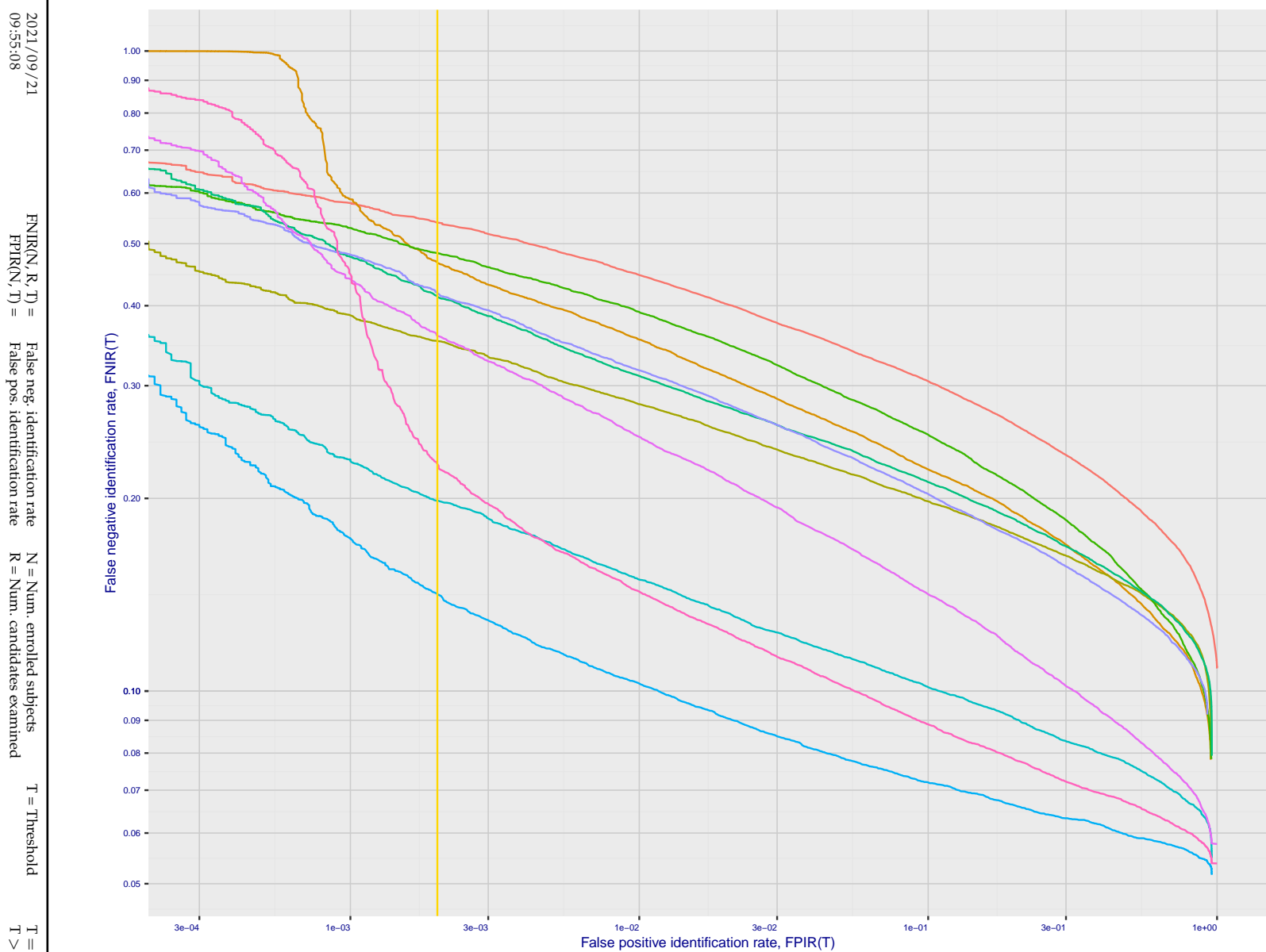


Figure 164: [Mugshot and profile-view dataset] Threshold-based accuracy. For some of the more accurate Phase 3 algorithms the figure plots error tradeoff characteristics for frontal and profile-view searches into an enrolled set of  $N = 1\,600\,000$  frontal images. Note that some algorithms fail on profile-view images with  $\text{FNIR} \rightarrow 1$  - this evaluation did not ask developers to provide profile-view capability. Some algorithms, on the other hand, give  $\text{FNIR}$  approaching that for frontal-view searches using c. 2010 algorithms.

2021/09/21

FNIR(N, R, T) = False neg. identification rate  
FPIR(N, T) = False pos. identification rateN = Num. enrolled subjects  
R = Num. candidates examined

T = Threshold

T = 0 → Investigation  
T > 0 → Identification

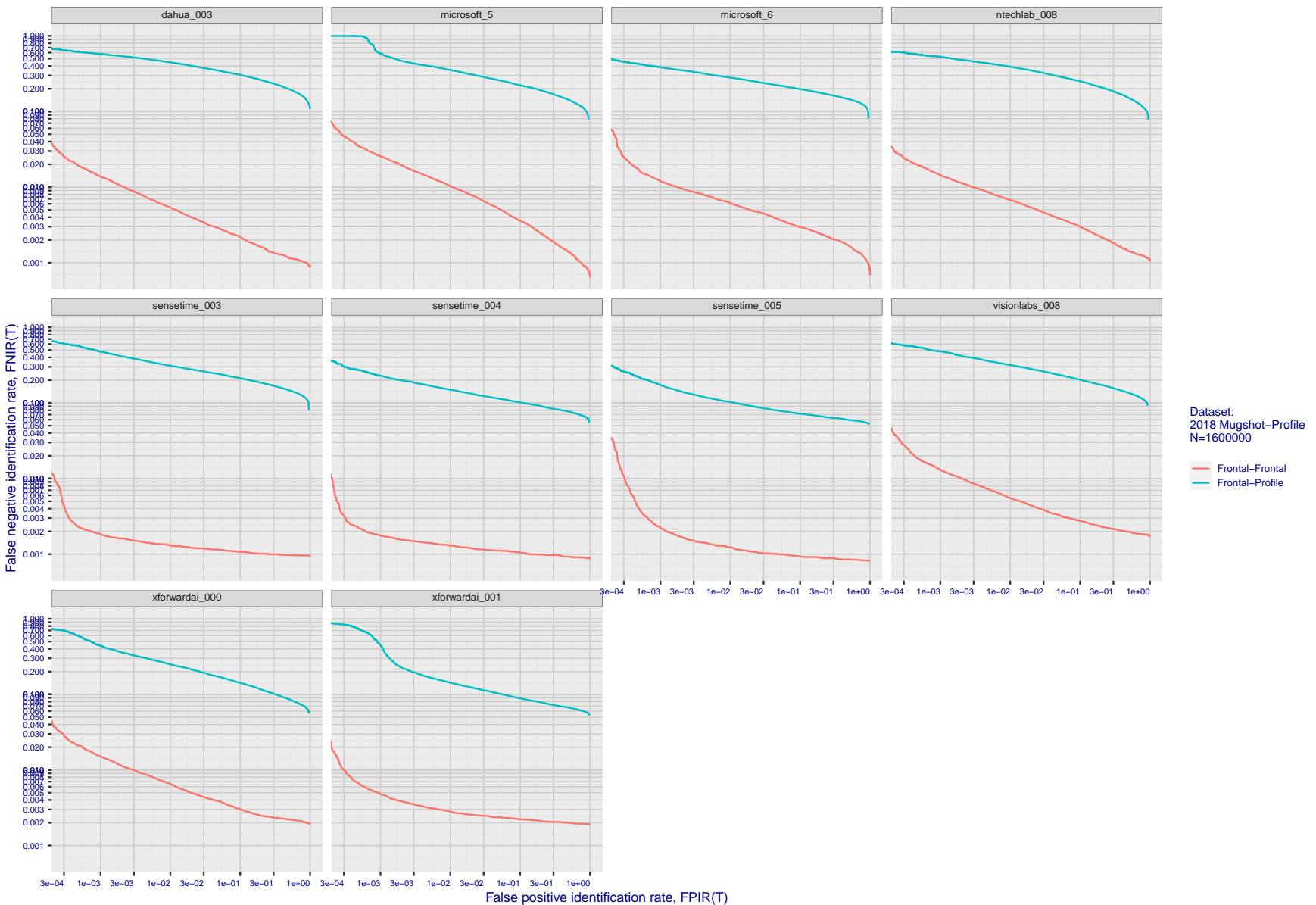


**Figure 165: [Mugshot and profile-view dataset] Speed-accuracy tradeoff.** For some of the more accurate Phase 3 algorithms the figure plots error tradeoff characteristics for frontal and profile-view searches into an enrolled set of  $N = 1\,600\,000$  frontal images. Some algorithms fail on profile-view images with  $\text{FNIR} \rightarrow 1$  - this evaluation did not ask developers to provide profile-view capability. Some algorithms, on the other hand, give  $\text{FNIR}$  approaching that for frontal-view searches using c. 2010 algorithms. Blue lines connect points of equal threshold from which it is evident that some algorithms would give markedly higher false positive outcomes if profile-view images were searched in a system configured for frontal searches. This would be a vulnerability in an access control system.

2021 / 09 / 21

09:55:08

FNIR( $N, R, T$ ) = False neg. identification rate  
FPIR( $N, T$ ) = False pos. identification rateN = Num. enrolled subjects  
R = Num. candidates examined

T = Threshold

T = 0 → Investigation  
T > 0 → Identification

## Appendix F Search duration

As in and prior tests, this section documents search speeds spanning three orders of magnitude. In applications where search volumes are high enough, this will have implications for hardware requirements especially for large N or when search duration is appreciably larger than the time it takes to prepare a template from the search image(s). Further, given very large (and growing) operational databases, the scalability of algorithms is important. It has been reported previously [8] that search duration can scale sublinearly with enrolled population size N. Further there has been considerable recent research on indexing, exact [13] and approximate nearest neighbor search [1,13] and fast-search [14,16].

Figure 166 charts the search duration measurements presented earlier in Tables 2 - 4.

- ▷ Most algorithms scale linearly. For those in that category, there is a wide range in speed with search durations ranging from 82 milliseconds for a 12 million gallery (for NEC-3) to more than 40 seconds (for Yitu-3, Toshiba-2) and even higher for less accurate algorithms.
- ▷ Some developers (Camvi, Dermalog, EverAI, Innovatrics, and Visionlabs) provide algorithms whose template search durations grow approximately logarithmically i.e.  $T(N) \sim \log N$  with the constant  $a$  varying between implementations. In the figure this model is fit using the point  $T(1) = 0$ , and  $T(640\,000)$ . This very sublinear behaviour affords extremely fast search times in very large galleries. One caveat for the sublinear algorithms is that their fast-search data structures can require considerable computation time - on the order of hours - for N in the millions, and this scales mildly super-linearly, i.e.  $O(N^b)$ ,  $b > 1$ . There are exceptions: the Camvi algorithms take minutes; and Innovatrics' scale sublinearly.

2021/09/21 FNIR(N, R, T) = False neg. identification rate  
09:55:08 FPIRN(T) = False pos. identification rate  
N = Num. enrolled subjects  
R = Num. candidates examined  
T = Threshold  
T = 0 → Investigation  
T > 0 → Identification

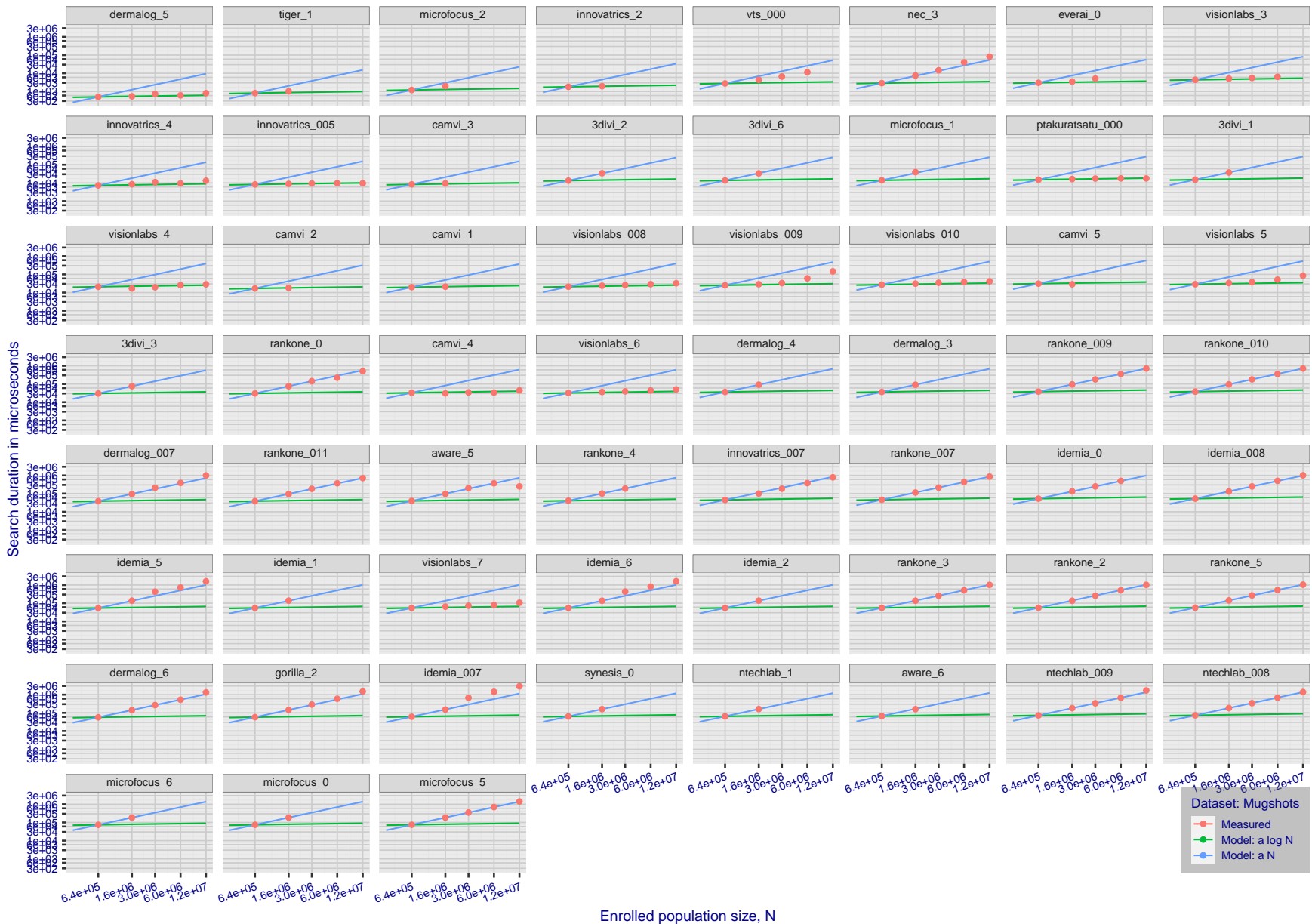


**Figure 166: [Mugshot Dataset] Search duration vs. enrolled population size.** In red are the actual point durations measured on a single c. 2016 core. The blue shows linear growth from  $N = 640\,000$ . The green line shows logarithmic growth from that point to  $N = 1\,600\,000$ . Note the sublinear growth from algorithms from Camvi, Dermalog, EverAI, Innovatrics, and Visionlabs. The tiger\_1 algorithm is also sublinear, but inaccurate and inoperable at  $N \geq 3000000$ . This capability sometimes comes at the additional expense of converting a linear gallery data structure into whatever fast-search data structure is used. Note that search times are sometimes dominated by the template generation times shown in Table 21.

2021/09/21  
09:55:08FNIR(N, R, T) = False neg. identification rate  
FPFR(N, T) = False pos. identification rateN = Num. enrolled subjects  
R = Num. candidates examined

T = Threshold

T = 0 → Investigation  
 $T > 0 \rightarrow$  Identification

2021 / 09 / 21  
09:55:08FNIR(N, R, T) = False neg. identification rate  
FPIR(N, T) = False pos. identification rateN = Num. enrolled subjects  
R = Num. candidates examined

T = Threshold

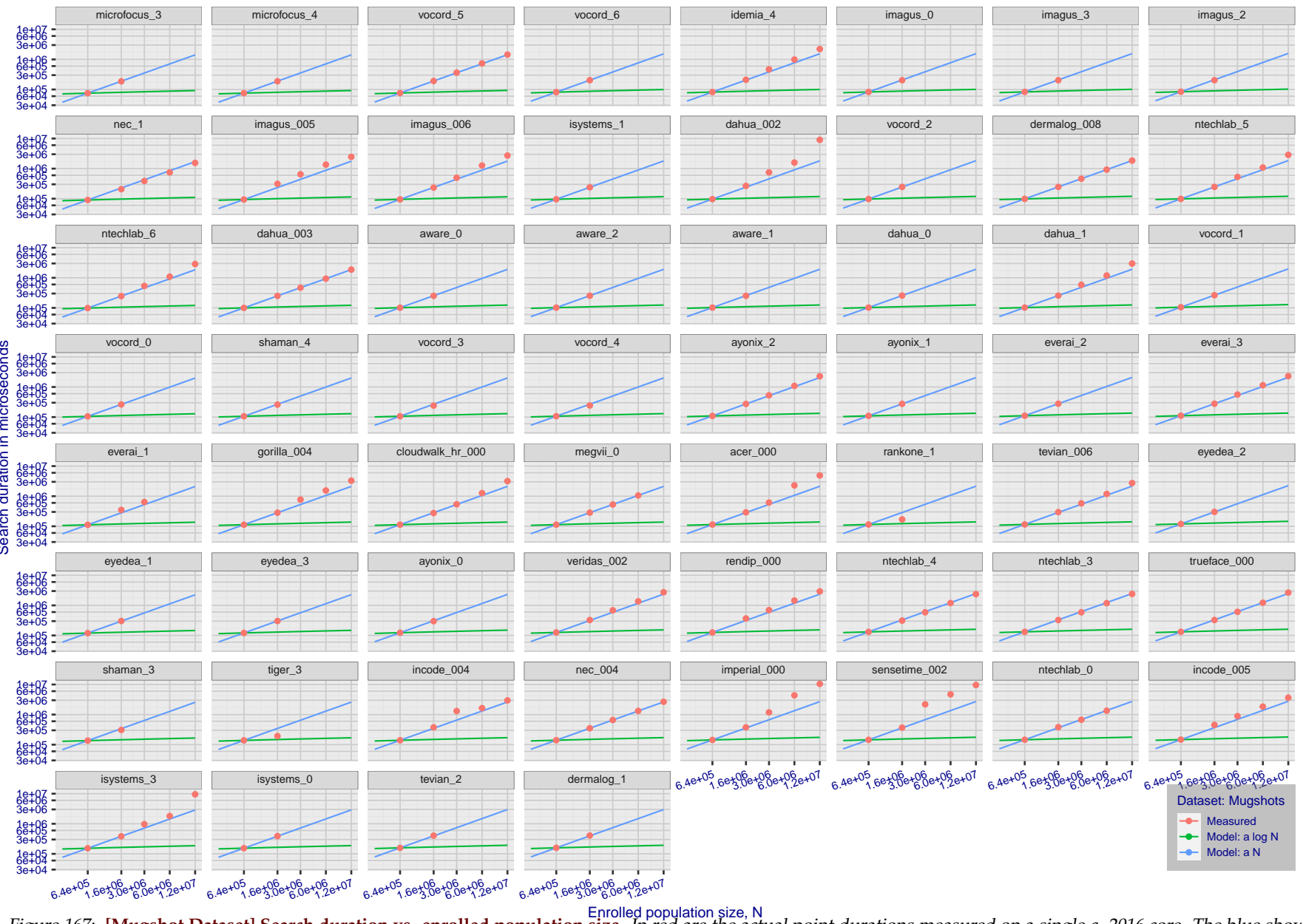
T = 0 → Investigation  
T > 0 → Identification

Figure 167: [Mugshot Dataset] Search duration vs. enrolled population size. In red are the actual point durations measured on a single c. 2016 core. The blue shows linear growth from  $N = 640\,000$ . The green line shows logarithmic growth from that point to  $N = 1\,600\,000$ . Note the sublinear growth from algorithms from Camvi, Dermalog, EverAI, Innovatrics, and Visionlabs. The tiger\_1 algorithm is also sublinear, but inaccurate and inoperable at  $N \geq 3000000$ . This capability sometimes comes at the additional expense of converting a linear gallery data structure into whatever fast-search data structure is used. Note that search times are sometimes dominated by the template generation times shown in Table 21.

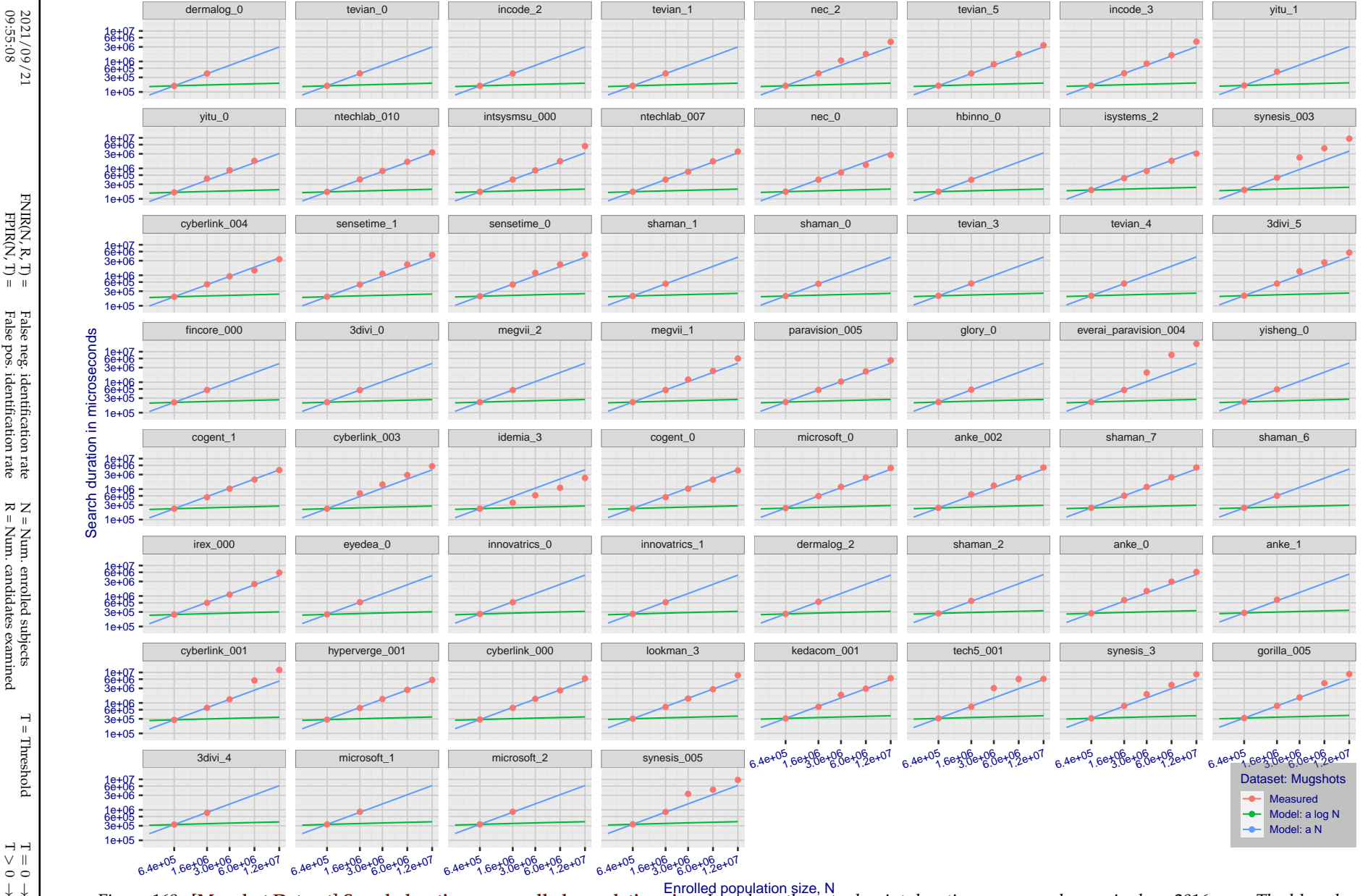


Figure 168: [Mugshot Dataset] Search duration vs. enrolled population size. In red are the actual point durations measured on a single c. 2016 core. The blue shows linear growth from  $N = 640\,000$ . The green line shows logarithmic growth from that point to  $N = 1\,600\,000$ . Note the sublinear growth from algorithms from Camvi, Dermalog, EverAI, Innovatrics, and Visionlabs. The tiger\_1 algorithm is also sublinear, but inaccurate and inoperable at  $N \geq 3000000$ . This capability sometimes comes at the additional expense of converting a linear gallery data structure into whatever fast-search data structure is used. Note that search times are sometimes dominated by the template generation times shown in Table 21.

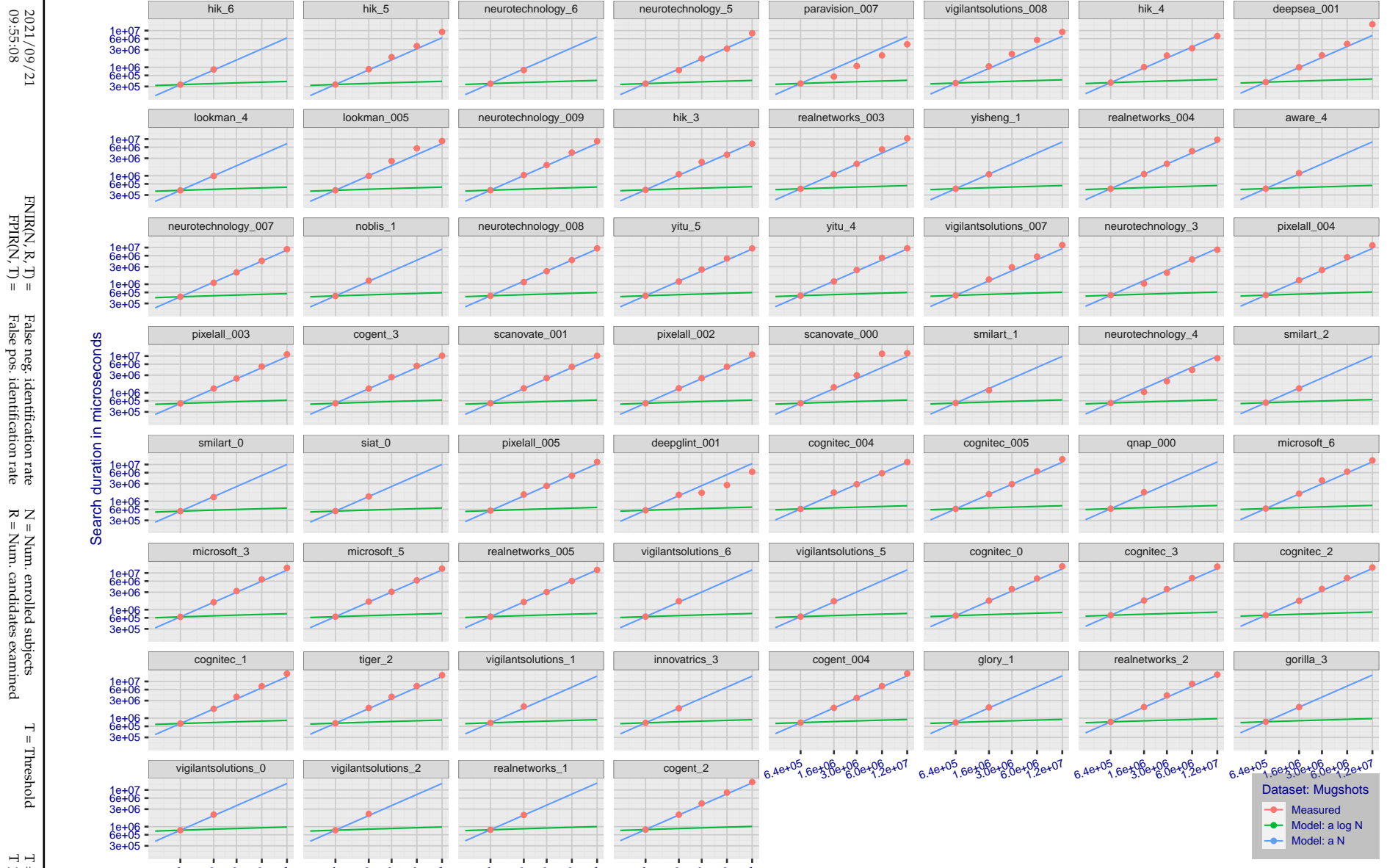


Figure 169: [Mugshot Dataset] Search duration vs. enrolled population size. In red are the actual point durations measured on a single c. 2016 core. The blue shows linear growth from  $N = 640\,000$ . The green line shows logarithmic growth from that point to  $N = 1\,600\,000$ . Note the sublinear growth from algorithms from Camvi, Dermalog, EverAI, Innovatrics, and Visionlabs. The tiger\_1 algorithm is also sublinear, but inaccurate and inoperable at  $N \geq 3000000$ . This capability sometimes comes at the additional expense of converting a linear gallery data structure into whatever fast-search data structure is used. Note that search times are sometimes dominated by the template generation times shown in Table 21.

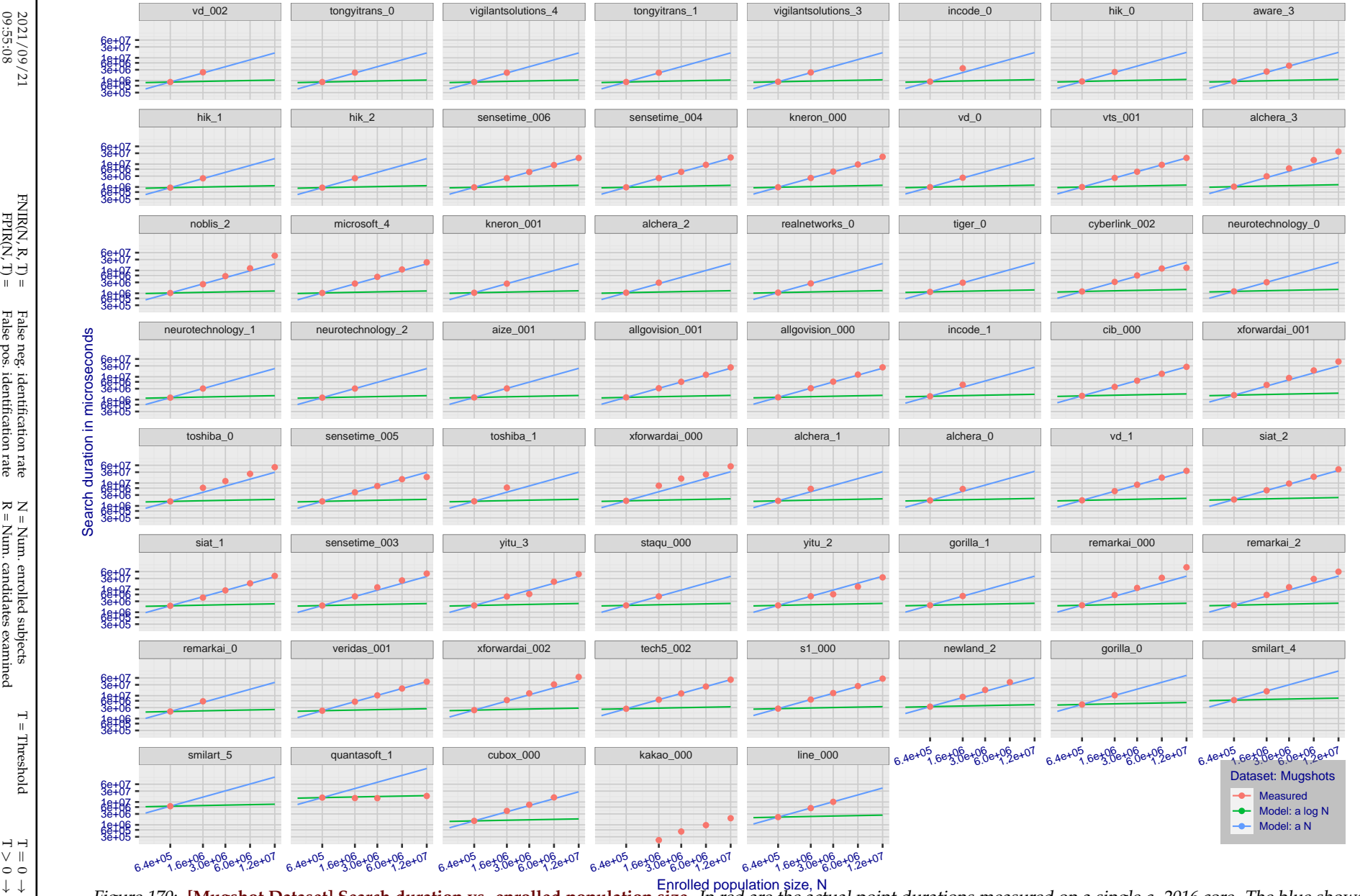


Figure 170: [Mugshot Dataset] Search duration vs. enrolled population size. In red are the actual point durations measured on a single c. 2016 core. The blue shows linear growth from  $N = 640\,000$ . The green line shows logarithmic growth from that point to  $N = 1\,600\,000$ . Note the sublinear growth from algorithms from Camvi, Dermalog, EverAI, Innovatrics, and Visionlabs. The tiger\_1 algorithm is also sublinear, but inaccurate and inoperable at  $N \geq 3000000$ . This capability sometimes comes at the additional expense of converting a linear gallery data structure into whatever fast-search data structure is used. Note that search times are sometimes dominated by the template generation times shown in Table 21.

2021/09/21  
09:55:08FNIR(N, R, T) = False neg. identification rate  
FPFR(N, T) = False pos. identification rateN = Num. enrolled subjects  
R = Num. candidates examined

T = Threshold

T = 0 → Investigation  
 $T > 0 \rightarrow$  Identification

## Appendix G Gallery Insertion Timing

2021/09/21  
09:55:08FNIR(N, R, T) = False neg. identification rate  
FPIR(N, T) = False pos. identification rateN = Num. enrolled subjects  
R = Num. candidates examinedT = Threshold  
T = 0 → Investigation

T &gt; 0 → Identification

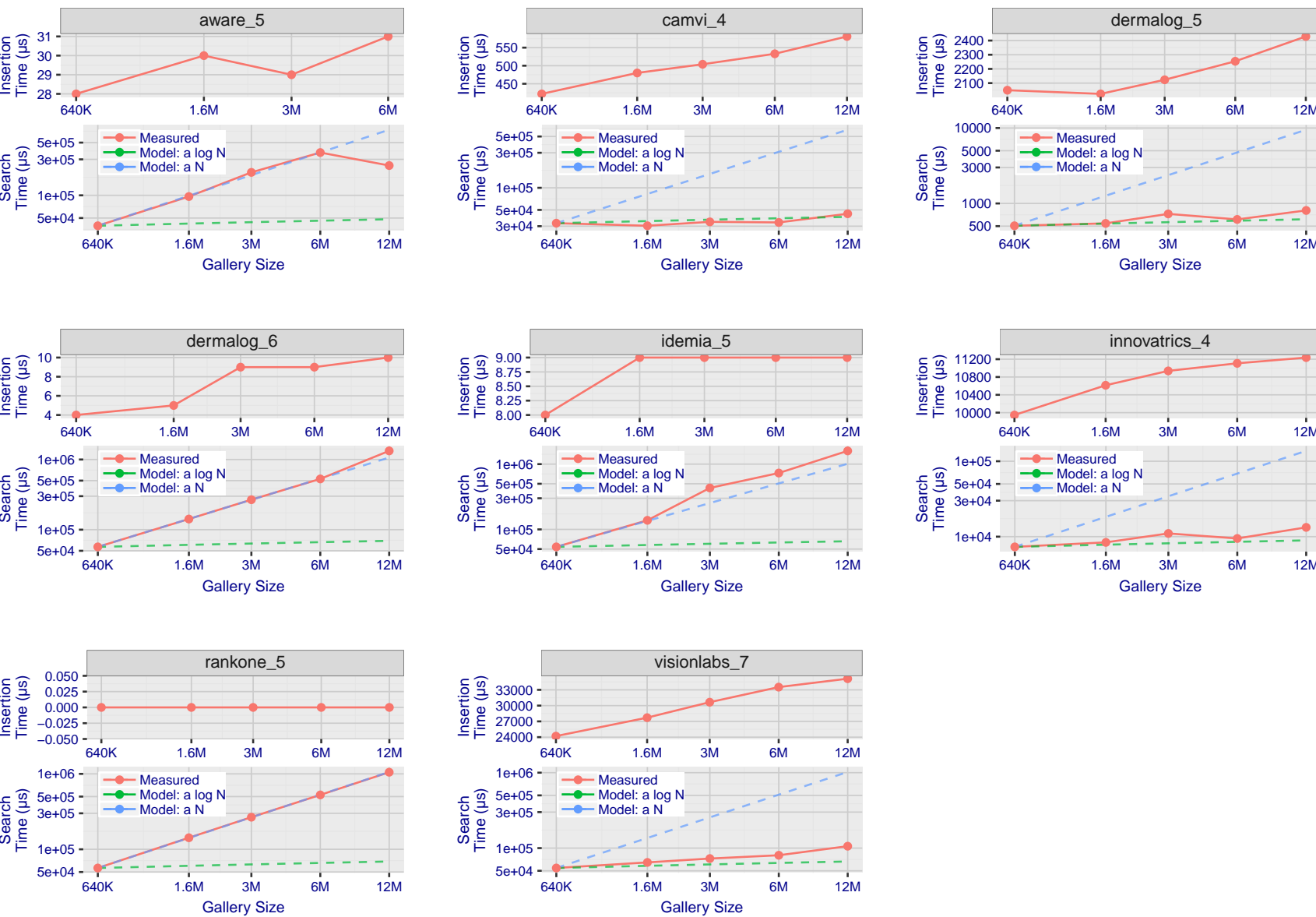


Figure 171: [Mugshot Dataset] Gallery insertion duration vs. enrolled population size. This chart plots the time it takes to insert a single template into a finalized gallery, illustrated over increasing gallery sizes. For reference, search times on finalized galleries of corresponding sizes are plotted right underneath. Gallery insertion time plots were generated on algorithms that 1) successfully implemented gallery insertion with no errors and 2) that were run on galleries with  $N$  up to 12 000 000. Generally, only the more accurate algorithms were run on galleries with  $N$  up to 12 000 000.

2021/09/21  
09:55:08FNIR(N, R, T) = False neg. identification rate  
FPFR(N, T) = False pos. identification rateN = Num. enrolled subjects  
R = Num. candidates examinedT = Threshold  
T = 0 → Investigation

T &gt; 0 → Identification

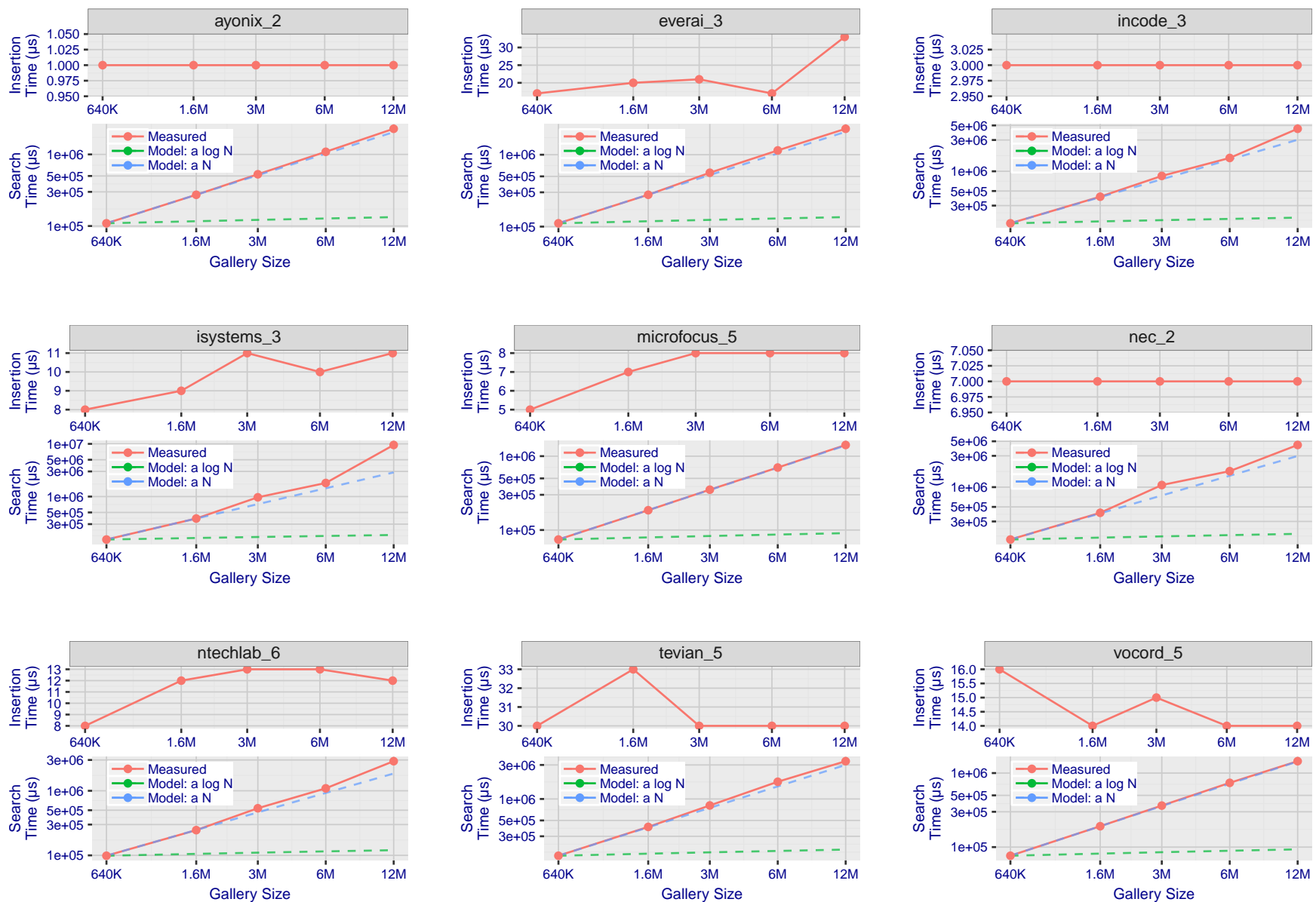


Figure 172: [Mugshot Dataset] Gallery insertion duration vs. enrolled population size. This chart plots the time it takes to insert a single template into a finalized gallery, illustrated over increasing gallery sizes. For reference, search times on finalized galleries of corresponding sizes are plotted right underneath. Gallery insertion time plots were generated on algorithms that 1) successfully implemented gallery insertion with no errors and 2) that were run on galleries with  $N$  up to 12 000 000. Generally, only the more accurate algorithms were run on galleries with  $N$  up to 12 000 000.

2021/09/21  
09:55:08FNIR(N, R, T) = False neg. identification rate  
FPIR(N, T) = False pos. identification rateN = Num. enrolled subjects  
R = Num. candidates examined

T = Threshold

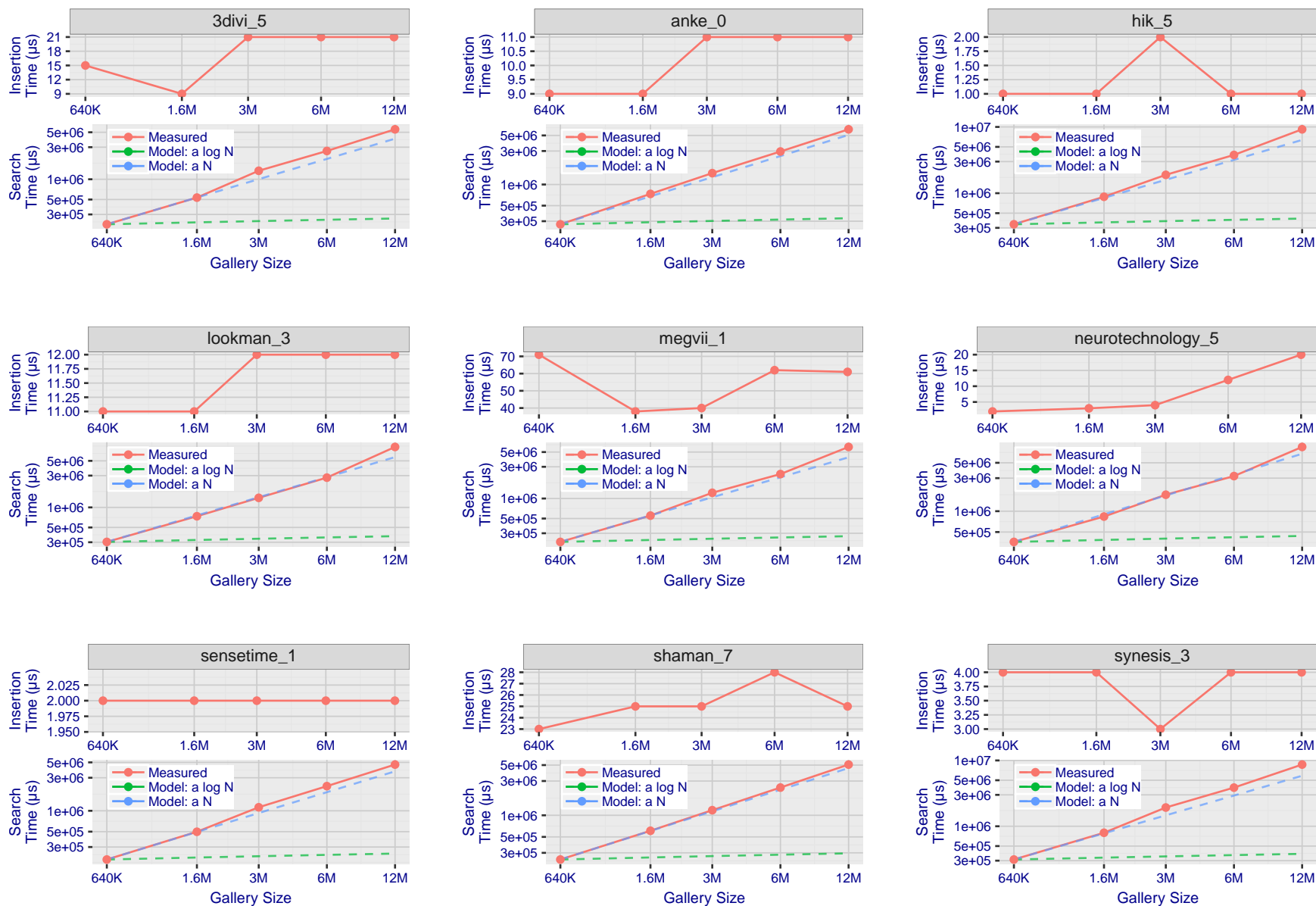
T = 0 → Investigation  
 $T > 0 \rightarrow$  Identification

Figure 173: [Mugshot Dataset] Gallery insertion duration vs. enrolled population size. This chart plots the time it takes to insert a single template into a finalized gallery, illustrated over increasing gallery sizes. For reference, search times on finalized galleries of corresponding sizes are plotted right underneath. Gallery insertion time plots were generated on algorithms that 1) successfully implemented gallery insertion with no errors and 2) that were run on galleries with  $N$  up to 12 000 000. Generally, only the more accurate algorithms were run on galleries with  $N$  up to 12 000 000.

2021/09/21  
09:55:08FNIR(N, R, T) = False neg. identification rate  
FPTR(N, T) = False pos. identification rateN = Num. enrolled subjects  
R = Num. candidates examinedT = Threshold  
T = 0 → Investigation

T &gt; 0 → Identification

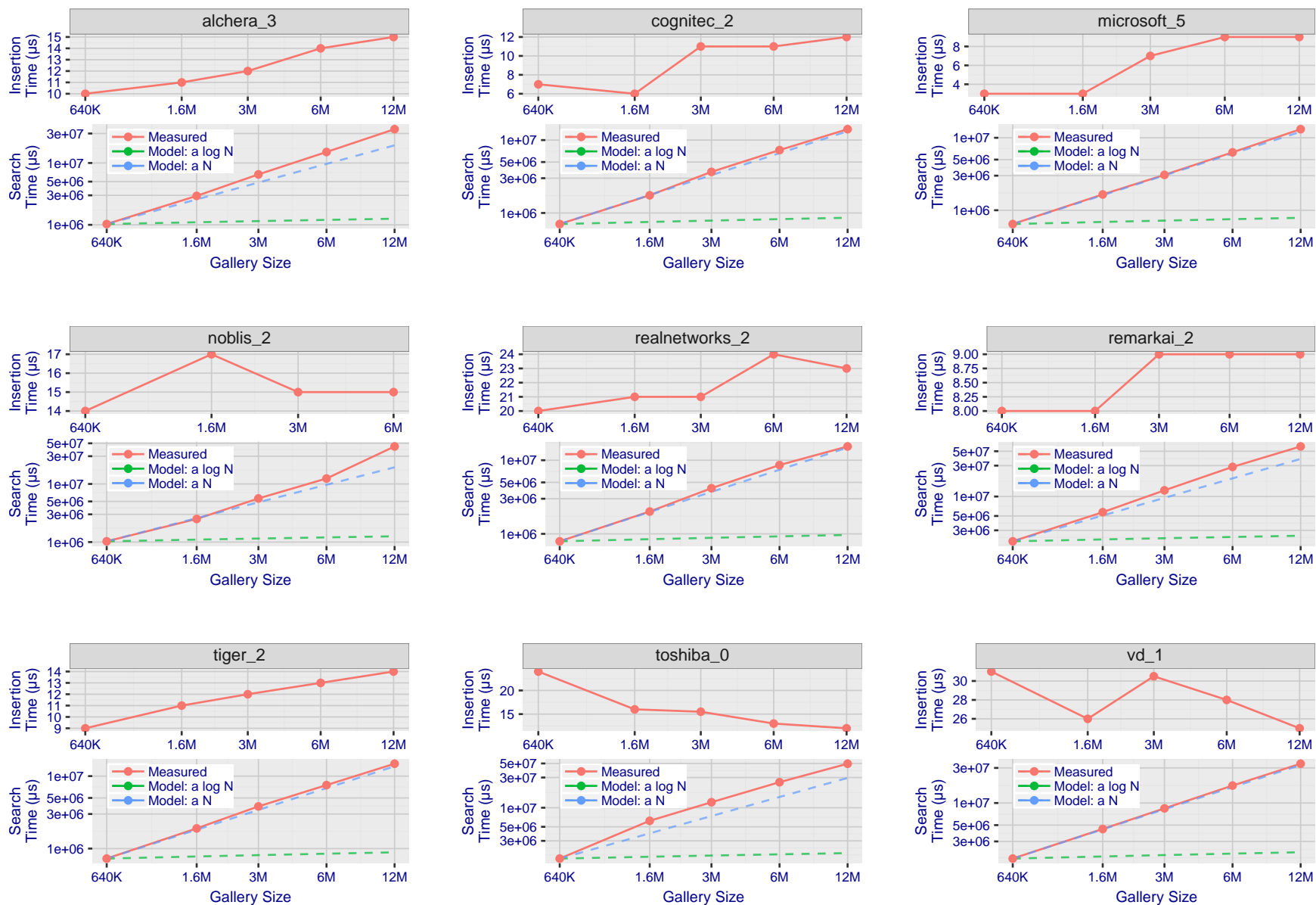


Figure 174: [Mugshot Dataset] Gallery insertion duration vs. enrolled population size. This chart plots the time it takes to insert a single template into a finalized gallery, illustrated over increasing gallery sizes. For reference, search times on finalized galleries of corresponding sizes are plotted right underneath. Gallery insertion time plots were generated on algorithms that 1) successfully implemented gallery insertion with no errors and 2) that were run on galleries with  $N$  up to 12 000 000. Generally, only the more accurate algorithms were run on galleries with  $N$  up to 12 000 000.

## References

- [1] Artem Babenko and Victor Lempitsky. Efficient indexing of billion-scale datasets of deep descriptors. In *The IEEE Conference on Computer Vision and Pattern Recognition (CVPR)*, June 2016.
- [2] L. Best-Rowden and A. K. Jain. Longitudinal study of automatic face recognition. *IEEE Transactions on Pattern Analysis and Machine Intelligence*, 40(1):148–162, Jan 2018.
- [3] Blumstein, Cohen, Roth, and Visher, editors. *Random parameter stochastic models of criminal careers*. National Academy of Sciences Press, 1986.
- [4] Thomas P. Bonczar and Lauren E. Glaze. Probation and parole in the united statesm 2007, statistical tables. Technical report, Bureau of Justice Statistics, December 2008.
- [5] White D., Kemp R. I., Jenkins R., Matheson M, and Burton A. M. Passport officers' errors in face matching. *PLoS ONE*, 9(8), 2014. e103510. doi:10.1371/journal.pone.0103510.
- [6] P. Grother, G. W. Quinn, and P. J. Phillips. Evaluation of 2d still-image face recognition algorithms. NIST Interagency Report 7709, National Institute of Standards and Technology, 8 2010. <http://face.nist.gov/mbe> as MBE2010 FRVT2010.
- [7] P. J. Grother, R. J. Micheals, and P. J. Phillips. Performance metrics for the frvt 2002 evaluation. In *Proceedings of Audio and Video Based Person Authentication Conference (AVBPA)*, June 2003.
- [8] Patrick Grother and Mei Ngan. Interagency report 8009, performance of face identification algorithms. *Face Recognition Vendor Test (FRVT)*, May 2014.
- [9] Patrick Grother, George Quinn, and Mei Ngan. Face in video evaluation (five) face recognition of non-cooperative subjects. Interagency Report 8173, National Institute of Standards and Technology, March 2017. <https://doi.org/10.6028/NIST.IR.8173>.
- [10] Patrick Grother, George W. Quinn, and Mei Ngan. Face recognition vendor test - still face image and video concept, evaluation plan and api. Technical report, National Institute of Standards and Technology, 7 2013. [http://biometrics.nist.gov/cs.links/face/frvt/frvt2012/NIST\\_FRVT2012.api\\_Aug15.pdf](http://biometrics.nist.gov/cs.links/face/frvt/frvt2012/NIST_FRVT2012.api_Aug15.pdf).
- [11] K. He, X. Zhang, S. Ren, and J. Sun. Deep residual learning for image recognition. In *2016 IEEE Conference on Computer Vision and Pattern Recognition (CVPR)*, pages 770–778, June 2016.
- [12] Gary B. Huang, Manu Ramesh, Tamara Berg, and Erik Learned-Miller. Labeled faces in the wild: A database for studying face recognition in unconstrained environments. Technical Report 07-49, University of Massachusetts, Amherst, October 2007.
- [13] Masato Ishii, Hitoshi Imaoka, and Atsushi Sato. Fast k-nearest neighbor search for face identification using bounds of residual score. In *2017 12th IEEE International Conference on Automatic Face & Gesture Recognition (FG 2017)*, pages 194–199, Los Alamitos, CA, USA, May 2017. IEEE Computer Society.
- [14] Jeff Johnson, Matthijs Douze, and Hervé Jégou. Billion-scale similarity search with gpus. *CoRR*, abs/1702.08734, 2017.

- [15] Ira Kemelmacher-Shlizerman, Steven M. Seitz, Daniel Miller, and Evan Brossard. The megaface benchmark: 1 million faces for recognition at scale. *CoRR*, abs/1512.00596, 2015.
- [16] Yury A. Malkov and D. A. Yashunin. Efficient and robust approximate nearest neighbor search using hierarchical navigable small world graphs. *CoRR*, abs/1603.09320, 2016.
- [17] Joyce A. Martin, Brady E. Hamilton, Michelle J.K. Osterman, Anne K. Driscoll, , and Patrick Drake. National vital statistics reports. Technical Report 8, Centers for Disease Control and Prevention, National Center for Health Statistics, National Vital Statistics System, Division of Vital Statistics, November 2018.
- [18] O. M. Parkhi, A. Vedaldi, and A. Zisserman. Deep face recognition. In *British Machine Vision Conference*, 2015.
- [19] P. Jonathon Phillips, Amy N. Yates, Ying Hu, Carina A. Hahn, Eilidh Noyes, Kelsey Jackson, Jacqueline G. Cava-zos, Géraldine Jeckeln, Rajeev Ranjan, Swami Sankaranarayanan, Jun-Cheng Chen, Carlos D. Castillo, Rama Chellappa, David White, and Alice J. O'Toole. Face recognition accuracy of forensic examiners, superrecognitioners, and face recognition algorithms. *Proceedings of the National Academy of Sciences*, 115(24):6171–6176, 2018.
- [20] Florian Schroff, Dmitry Kalenichenko, and James Philbin. Facenet: A unified embedding for face recognition and clustering. *CoRR*, abs/1503.03832, 2015.
- [21] Jeroen Smits and Christiaan Monden. Twinning across the developing world. *PLOS ONE*, 6(9):1–5, 09 2011.
- [22] Yaniv Taigman, Ming Yang, Marc'Aurelio Ranzato, and Lior Wolf. Deepface: Closing the gap to human-level performance in face verification. In *Proceedings of the 2014 IEEE Conference on Computer Vision and Pattern Recognition, CVPR '14*, pages 1701–1708, Washington, DC, USA, 2014. IEEE Computer Society.
- [23] A. Towler, R. I. Kemp, and D White. *Unfamiliar face matching systems in applied settings*. Nova Science, 2017.
- [24] Working Group 3. Ed. M. Werner. *ISO/IEC 19794-5 Information Technology - Biometric Data Interchange Formats - Part 5: Face image data*. JTC1 :: SC37, 2 edition, 2011. <http://webstore.ansi.org>.
- [25] David White, James D. Dunn, Alexandra C. Schmid, and Richard I. Kemp. Error rates in users of automatic face recognition software. *PLoS ONE*, 10:1–14, October 2015.
- [26] Bradford Wing and R. Michael McCabe. Special publication 500-271: American national standard for information systems data format for the interchange of fingerprint, facial, and other biometric information part 1. Technical report, NIST, September 2015. ANSI/NIST ITL 1-2015.
- [27] Andreas Wolf. Portrait quality - (reference facial images for mrtd). Technical report, ICAO, April 2018.
- [28] D. Yadav, N. Kohli, P. Pandey, R. Singh, M. Vatsa, and A. Noore. Effect of illicit drug abuse on face recognition. In *2016 IEEE Winter Conference on Applications of Computer Vision (WACV)*, pages 1–7, Los Alamitos, CA, USA, mar 2016. IEEE Computer Society.